

Diss. ETH N° 21911

# **Design, Synthesis, and Evaluation of Novel Partially Fluorinated Alkyl Groups**

A dissertation submitted to

**ETH Zurich**

For the degree of

**Doctor of Sciences**

Presented by

**Quentin Alban Huchet**

Diplôme d'Ingénieur INSA Rouen

Born December 13<sup>th</sup> 1986

Citizen of France

Accepted on the recommendation of

Prof. Dr. Erick M. Carreira, examiner

Prof. Dr. Karl-Heinz Altmann, co-examiner

Prof. Dr. Klaus Müller, co-examiner

2014



# Acknowledgements

I am particularly grateful to my supervisor, Prof. Dr. Erick M. Carreira, for giving me the priceless opportunity to conduct my doctoral studies in his research group. I would like to thank him for his trust in me and my project, and for his continued support. Under his guidance, I benefited from the freedom to elaborate and implement my own ideas, which contributed greatly to my chemical education.

I would like to express my gratitude to Prof. Dr. Klaus Müller, whose mentoring throughout this project helped me improve as a medicinal chemist. His visionary ideas, the numerous illuminating discussions we shared, and his true passion for science were a constant source of motivation and inspiration to me.

I am thankful to Prof. Dr. Karl-Heinz Altmann for taking on the co-examination of my thesis. After having worked under the supervision of his talented and passionate disciple, Dr. Frédéric Cachoux, I was truly delighted by his immediate acceptance.

I would also like to thank several collaborators at F. Hoffmann-La Roche, who contributed greatly to this research project. Therefore, many thanks go to Dr. Bernd Kuhn, Dr. Holger Fischer, Dr. Manfred Kansy, Dr. Achim Grenz, Björn Wagner, and Daniel Zimmerli for taking care of the precious compounds I synthesized during my doctoral studies.

Obviously, none of this work would have been possible without the excellent infrastructure and technical staff of ETH Zurich and the LOC (Laboratorium für Organische Chemie). In this regard, I am particularly thankful to Dr. Bernd Schweizer and Dr. Nils Trapp, who carefully carried out the X-ray measurements. The MS-team, with Louis Bertschi, Oswald Greter, and Rolf Häfliger are not to be forgotten, as well as the NMR service and the very helpful Schalter-team.

In the course of my studies, I had the privilege to supervise highly talented and passionate undergraduate students and therefore would like to acknowledge Raffael Vorberg, Cornelius Gropp, Gregor Simm, Pascal Engl, Natalja Früh, Oliver Engl, and Patrick Lancuba for their contribution.

I am deeply grateful to Dr. Sébastien Goudreau with whom I shared countless insightful and constructive discussions. His constant input and friendly support inside and outside the laboratory were instrumental in the success of this project.

Special thanks go to Dr. Riccardo Cribiú who taught me so much about science and more. He initiated me to various overlooked aspects of chemistry, which contributed to make my stay in the laboratory a lively and unforgettable experience.

I was fortunate to supervise and collaborate with Raffael Vorberg who shared my passion for fluorine chemistry. His dedication to work and creativity led to significant synthetic improvements that largely benefited to this work.

Many thanks go to Stefan Ruider with whom I had the pleasure to share numerous, constructive discussions on various aspects that go beyond science. Our common interests led us to build a relationship that I hope will persist after I leave the group.

As a former member of my laboratory, I would also like to thank Dr. Lukas Kreis who introduced me to the group, and taught me all about computer system administration. I am also grateful for his valuable opinions that helped me envision the next steps.

I should also acknowledge Guido Möller and Simon Breitler for sharing the burden of keeping the group's computers up and running. Special thanks go to my friend and colleague Nicolás Armanino who not only took care of the electronic lab journal, but also shared with me some of the most enjoyable moments I spent out of work.

I am grateful to all my proofreaders: Camille Le Chapelain, Guido Möller, Dr. Riccardo Cribiú, Raffael Vorberg, and Jovana Milić who dedicated a significant amount of time to correcting this thesis. Their critical feedback led to a substantial improvement of this manuscript.

Évidemment, je ne saurais oublier mes collègues et amis compatriotes français au sein du groupe. Ainsi, je remercie chaleureusement Dr. Carine Guérot, Camille Le Chapelain, Dr. Damien Barbaras, Dr. Thomas Fessard et Adrien Joliton pour leur contribution directe ou indirecte à mon épanouissement dans cet environnement si particulier.

Last but not least, I am particularly indebted to Jovana Milić, probably the most passionate and talented student I have ever met. Her vision and support not only allowed me to sustain the effort throughout my studies, but also enlightened my perception of fundamental problems.

# Publications and Presentations

## Publications

Huchet, Q. A.; Kuhn, B.; Wagner, B.; Fischer, H.; Kansy, M.; Zimmerli, D.; Carreira, E. M.; Müller, K. *Journal of Fluorine Chemistry* **2013**, *152*, 119–128. “*On the Polarity of Partially Fluorinated Methyl Groups.*”

Koller, R.; Huchet, Q. A.; Battaglia, P.; Welch, J. M.; Togni, A. *Chemical Communications* **2009**, 5993–5995. “*Acid-Mediated Formation of Trifluoromethylsulfonates from Sulfonic Acids and a Hypervalent Iodine Trifluoromethylating Agent.*”

## Presentations

December 2013      **6<sup>th</sup> SSCI Symposium (Zurich, Switzerland)**  
*On the Polarity of Partially Fluorinated Methyl Groups.*  
**Poster Presentation**

February 2011      **F. Hoffmann-La Roche Meeting (Basel, Switzerland)**  
*Design, Synthesis, and Exploration of Novel Small Fluorine-Containing Groups.*  
**Oral Presentation**



*“Fluorine leaves nobody indifferent; it inflames emotions, be that affections or aversions. As a substituent, it is rarely boring, always good for a surprise, but often completely unpredictable.”*

Prof. Dr. Manfred Schlosser





---

# Table of Contents

Acknowledgements .....	i
Publications and Presentations.....	iii
Abstract (English) .....	xi
Abstract (Français).....	xii
<b>1 Introduction.....</b>	<b>1</b>
<b>1.1 A Brief Historical Overview of Fluoroorganic Chemistry.....</b>	<b>1</b>
1.1.1 Taming the Beast.....	1
1.1.2 The Birth of Fluorine Industry .....	2
1.1.3 Historical Fluorine-Containing Pharmaceuticals .....	2
<b>1.2 Fundamental Atomic Properties of Fluorine.....</b>	<b>3</b>
<b>1.3 Effects of Fluorine Substitution on Biological Properties.....</b>	<b>5</b>
1.3.1 Drug-Target Binding Affinity .....	5
1.3.2 Absorption .....	11
1.3.3 Metabolism .....	13
<b>1.4 Impact of Fluorine in Pharmaceuticals.....</b>	<b>16</b>
<b>1.5 Aim of the Present Work.....</b>	<b>17</b>
<b>2 Partially Fluorinated Methyl Groups.....</b>	<b>19</b>
<b>2.1 Introduction.....</b>	<b>19</b>
<b>2.2 Study on the Polarity of Partially Fluorinated Methyl Groups.....</b>	<b>20</b>
2.2.1 Preliminary Observations.....	20
2.2.2 The <i>n</i> -Propylbenzene Case .....	22
<b>2.3 Design and Synthesis of a Prototypical Set of Model Compounds .....</b>	<b>27</b>
2.3.1 A Suitable Model.....	27
2.3.2 Access to 3-Substituted Indole Derivatives.....	29
<b>2.4 Physicochemical and Pharmacological Properties .....</b>	<b>33</b>
2.4.1 Lipophilicity .....	33
2.4.2 Metabolic Stability .....	35

<b>2.5</b>	<b>Influence of Conformation on Polarity</b> .....	<b>39</b>
2.5.1	Introduction.....	39
2.5.2	Conformational Preference of 3-Substituted Indole Derivatives.....	39
2.5.3	Calculation of Conformationally Dependent Dipole Moments.....	41
2.5.4	Solvation Energy: Qualitative Approximation of Polarity.....	41
2.5.5	Conclusion.....	43
<b>2.6</b>	<b>Study on the Polarity of Conformationally Restricted Model Compounds</b> .....	<b>43</b>
2.6.1	The Cyclohexyl Ring: Conformational Lock and Molecular Spacer.....	43
2.6.2	Synthesis of Cyclohexyl-Containing Indole Derivatives.....	44
2.6.3	Lipophilicity Measurements.....	46
2.6.4	X-ray Crystal Structures.....	48
2.6.5	Theoretical Examination: 1,4-Dimethylcyclohexane.....	51
<b>2.7</b>	<b>Conclusion</b> .....	<b>55</b>
<b>3</b>	<b>Vicinal and Multi-Vicinal Fluoroalkyl Groups</b> .....	<b>57</b>
<b>3.1</b>	<b>Introduction</b> .....	<b>57</b>
<b>3.2</b>	<b>Study on the Polarity of Vicinal and Multi-Vicinal Fluoroalkyl Groups</b> .....	<b>58</b>
3.2.1	Molecular Dipole Moment.....	58
3.2.2	Solvation Energy.....	60
3.2.3	Impact of the Fluorine <i>Gauche</i> Effect on Physicochemical Properties.....	63
3.2.4	The <i>bis</i> -Vicinal Trifluoro Motif.....	67
<b>3.3</b>	<b>Design and Synthesis of a Prototypical Set of Model Compounds</b> .....	<b>69</b>
3.3.1	The Appropriate Candidates.....	69
3.3.2	Retrosynthetic Analysis.....	69
3.3.3	Synthetic Access.....	73
<b>3.4</b>	<b>Physicochemical and Pharmacological Properties</b> .....	<b>80</b>
3.4.1	Lipophilicity.....	80
3.4.2	Aqueous Solubility.....	82
3.4.3	Metabolic Stability.....	85
<b>3.5</b>	<b>Conclusion</b> .....	<b>87</b>
<b>4</b>	<b>Partially Fluorinated Alkyl Ethers</b> .....	<b>89</b>

---

<b>4.1</b>	<b>Introduction.....</b>	<b>89</b>
<b>4.2</b>	<b>Study on the Polarity of Partially Fluorinated Alkyl Ethers.....</b>	<b>91</b>
4.2.1	Preliminary Observations.....	91
4.2.2	Deciphering the Trend.....	92
4.2.3	Towards Lipophilicity-Lowering Alkyl Ethers.....	98
<b>4.3</b>	<b>Design and Synthesis of a Prototypical Set of Model Compounds.....</b>	<b>99</b>
4.3.1	The Appropriate Candidates.....	99
4.3.2	Retrosynthetic Analysis.....	100
4.3.3	Synthetic Access.....	103
<b>4.4</b>	<b>Physicochemical and Pharmacological Properties.....</b>	<b>112</b>
4.4.1	Basic Set of Model Compounds.....	112
4.4.2	Extended Set of Model Compounds.....	116
<b>4.5</b>	<b>Conclusion.....</b>	<b>121</b>
<b>5</b>	<b>Conclusion and Outlook.....</b>	<b>123</b>
	<b>Experimental Section.....</b>	<b>125</b>
•	Materials and Methods.....	125
•	Synthetic Procedures.....	129
	<b>Appendix.....</b>	<b>235</b>
•	NMR Spectra.....	235
•	X-ray Crystallographic Data.....	299
	<b>Abbreviations.....</b>	<b>359</b>
	<b>References.....</b>	<b>363</b>
	<b>Curriculum Vitae.....</b>	<b>371</b>



## Abstract

Despite its countless applications in modern drug discovery, fluorine still suffers from persistent prejudices that hamper its utilisation for particular purposes, among which tuning lipophilicity is a prominent paradigm. It has been shown in the course of this work that inclusion of fluorine atoms into saturated alkyl units not only lowers lipophilicity, but also leads to highly desirable pharmacological properties. In view of gaining valuable insight into the effects of fluorination on lipophilicity, some relevant indole-based model compounds bearing partially fluorinated alkyl substituents in key positions have thus been designed, synthesized, and evaluated.

The first part of this work was dedicated to studying 3-substituted indole derivatives, with a particular emphasis on partially fluorinated propyl scaffolds. In this regard, the evaluation of model compounds **Ia–d** confirmed the lipophilicity trend observed for the analogous series of partially fluorinated propylbenzene derivatives, i.e.  $CH_3 > CF_3 \gg CHF_2 \geq CH_2F$  (Figure I, left). Furthermore, compound **Ie** revealed that modifying the arrangement of fluorine atoms along the alkyl chain could impart lower lipophilicity, along with higher solubility and metabolic stability.

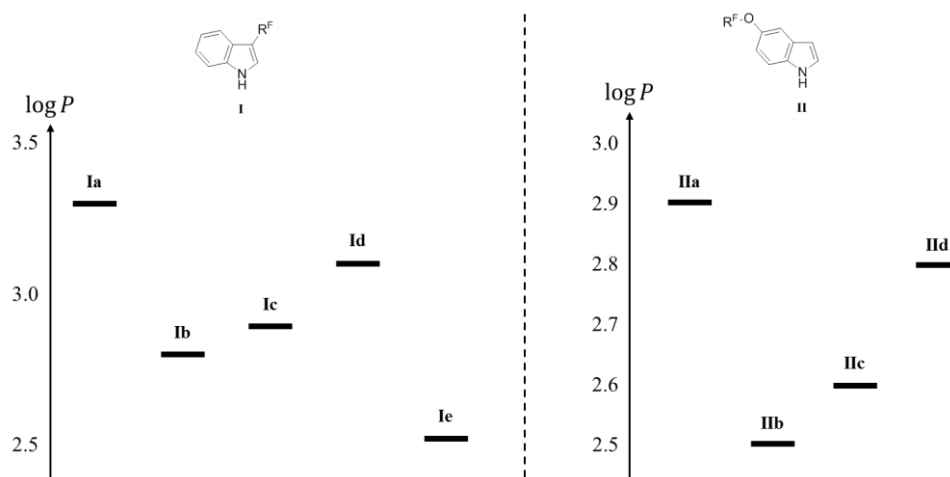


**Figure I.** Experimental lipophilicity trends determined for series **I** and **II** of indole-based model compounds. **a** –  $R^F = CH_2CH_2CH_3$ ; **b** –  $R^F = CH_2CH_2CH_2F$ ; **c** –  $R^F = CH_2CH_2CHF_2$ ; **d** –  $R^F = CH_2CH_2CF_3$ ; **e** –  $R^F = CH_2CHFCH_2F$ .

The second part of this project focused on 5-substituted indole derivatives and aimed at probing the potential of partially fluorinated aryl ethers. Interestingly, unlike the reported methyl or ethyl ether analogs, partially fluorinated propyl ethers **IIa–d** exhibited a lipophilicity trend conspicuously similar to that of compounds **Ia–d** (Figure I, right).

## Abstract

Malgré ses innombrables applications en recherche pharmaceutique moderne, le fluor souffre toujours de préjugés qui freinent son utilisation en vue d'applications spécifiques telles que la modulation de la lipophilie. Au cours de nos recherches, nous avons pu montrer que l'incorporation d'atomes de fluor à des groupes alkyles saturés permet non seulement de réduire la lipophilie, mais confère aussi des propriétés pharmacologiques intéressantes. Afin d'avoir un meilleur aperçu des effets de la fluoration sur la lipophilie, nous avons donc conçu, synthétisé et évalué un set de composés indoliques modèles substitués en des positions clés.

La première partie de ce travail de recherche fut dédiée à l'étude de dérivés indoliques substitués en position 3, avec un accent particulier mis sur les chaînes alkyles fluorées. Ainsi, l'évaluation des composés modèles **Ia–d** a confirmé la variation de lipophilie relevée dans le cas de la série analogue dérivée du propylbenzène, soit  $CH_3 > CF_3 \gg CHF_2 \geq CH_2F$  (Figure I, gauche). De plus, le composé **Ie** a permis de montrer que modifier l'arrangement des atomes de fluor sur la chaîne alkyle pouvait résulter en une lipophilie sensiblement réduite, additionnée d'une solubilité et d'une stabilité métabolique accrues.

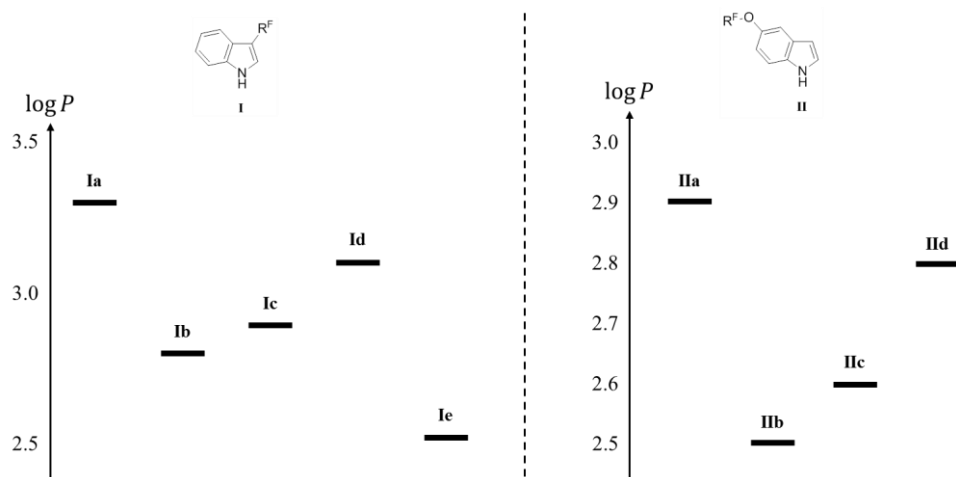


**Figure I.** Variation de lipophilie déterminée pour les séries de composés modèles **I** et **II**. **a** –  $R^F = CH_2CH_2CH_3$ ; **b** –  $R^F = CH_2CH_2CH_2F$ ; **c** –  $R^F = CH_2CH_2CHF_2$ ; **d** –  $R^F = CH_2CH_2CF_3$ ; **e** –  $R^F = CH_2CHFCH_2F$ .

Dans une seconde partie, nous nous sommes concentrés sur les composés indoliques substitués en position 5, avec pour intention d'évaluer le potentiel des éthers fluorés aromatiques. Curieusement, et contrairement aux éthers de méthyle et d'éthyle, les éthers de propyle fluorés **IIa–d** ont révélé une variation de lipophilie similaire à celle observée pour les composés **Ia–d** (Figure 1, droite).

# 1 Introduction

## 1.1 A Brief Historical Overview of Fluoroorganic Chemistry

### 1.1.1 Taming the Beast

Of all halogens, fluorine is the most abundant in the Earth's crust. However, due to its intrinsic properties, the bulk of the element is bound in insoluble form as fluorine-containing minerals, thus rendering the halogen largely unavailable to living organisms.<sup>1</sup> This is probably the reason why, unlike any other element, its isolation and characterization proved to be a tedious process.

About five centuries ago, Georgius Agricola first reported the use of fluorite, a natural occurrence of calcium fluoride, as an additive that helped melt ores and slags during smelting.<sup>2</sup> More than two centuries later, the first definite preparation of hydrofluoric acid was reported by Andreas Sigismund Marggraf. This finding became a milestone on the way to the isolation of elemental fluorine.<sup>3</sup> Nevertheless, segregating this peculiar element proved to be a perilous scientific endeavour.

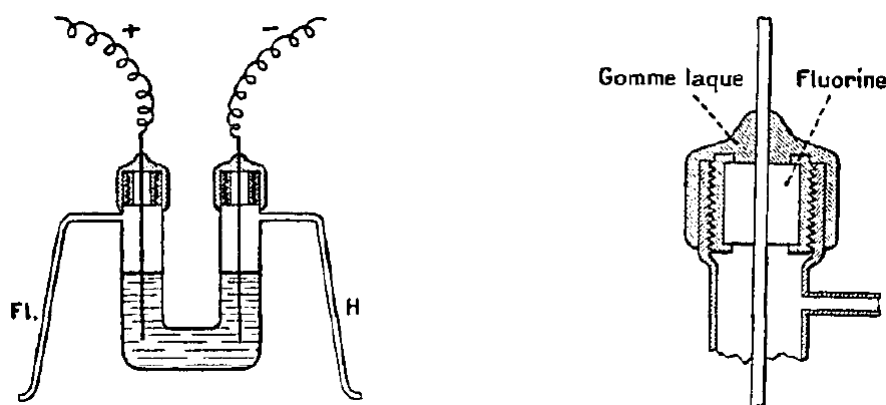


**Figure 1.** Experimental setting employed for the first isolation of elemental fluorine, as reported by Henri Moissan.<sup>4</sup> Fl. – fluorine; H – hydrogen; Gomme laque – shellac; Fluorine – fluorite.

Indeed, although the French physicist André-Marie Ampère suggested in the early 19<sup>th</sup> century that hydrofluoric acid was a compound of hydrogen with an unknown element, analogous to chlorine,<sup>5</sup> it took another century to the scientific community to report the first isolation of fluorine. As a matter of fact, due to the exceptional danger of generating fluorine, all efforts in that direction were considerably slowed down.

Eventually, thanks to his scientific ingenuity and great personal courage, Henri Moissan claimed the first isolation of elemental fluorine in 1886.<sup>4</sup> He thus reported to the French Academy that the electrolysis of a solution of potassium bifluoride and hydrogen fluoride, placed in a specifically designed container, allowed him to liberate a gas whose characteristics led him to conclude that he was in presence of elemental fluorine (Figure 1). After “taming the beast”, Moissan’s historic effort was rewarded with the Nobel Prize in Chemistry in 1906, only two months before his death. At that time, he could not imagine the impact his discovery would have on the century to come.<sup>6</sup>

### 1.1.2 The Birth of Fluorine Industry

Although Moissan offered to chemists a reliable process that is still in use for the industrial production of fluorine gas, further development of fluorine chemistry was extremely sluggish, pursued by a handful of experts capable of handling the violent gas, using specially designed laboratory equipment. Interestingly, industrial-scale production of fluorochemicals dates back to late 1930s, when the need for elemental fluorine culminated with the necessity for production of fissile U-235 from heavier U-238 via centrifugation.<sup>6</sup>

Due to the very corrosive nature of uranium hexafluoride, its production and use required the development of special inert fluorine-based materials, in particular polymers such as Teflon<sup>®</sup>. During that time, many methodological breakthroughs occurred, including the development of electrophilic fluorinating agents, electrochemical fluorination, and strategies to tame the violent reactivity of fluorine gas. These discoveries paved the way to fine synthetic fluoroorganic chemistry, and marked the beginning of a new era dominated by fluorine-containing building blocks.<sup>7</sup>

### 1.1.3 Historical Fluorine-Containing Pharmaceuticals

In the late 1940–1950s, the idea of synthesizing fluorinated analogs of naturally occurring molecules was rather implausible. The prevailing wisdom of that time clearly suggested that fluorine was an abiotic element, and its application was limited to military needs and special materials. It is therefore not astonishing that the discovery of Fludrocortisone (**1**), the first fluorine-containing pharmaceutical product, was the result of a systematic study of a series of 9 $\alpha$ -halogenated cortisone derivatives, which initially did not include the fluorinated analog.

In 1953, Fried and Sabo noticed the relationship between the bioactivity of 9 $\alpha$ -halocortisones and the size of the halogen atom.<sup>8</sup> Thus, the anti-inflammatory activity of 9 $\alpha$ -halo-17 $\alpha$ -



hydroxycorticosterone acetates was found to be in the following order:  $I < Br \ll Cl$ . This trend obviously prompted the authors to study the last remaining member of this group, the  $9\alpha$ -fluoro derivative, which was prepared by reaction of the corresponding alcohol with anhydrous hydrofluoric acid.<sup>9</sup> This compound, later known as Fludrocortisone (**1**), was found to possess a remarkable glucocorticoid activity, which exceeded by a factor of 10 that of the parent hormones (Figure 2).

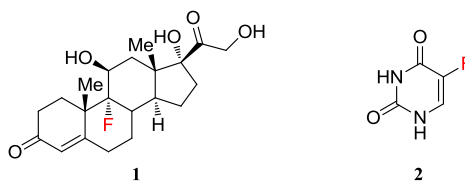


**Figure 2.** Structures of Fludrocortisone (**1**) and 5-fluorouracil (**2**).

A few years later, Heidelberger *et al.* demonstrated that 5-fluorouracil (5-FU) (**2**) can act as an antimetabolite of natural uracil.<sup>10</sup> Further studies have shown that 5-FU (**2**) and many of its derivatives serve as potent mechanism-based inhibitors of thymidylate synthase, the enzyme responsible for the transformation of 2-deoxyuridine-5-monophosphate into thymidine-5-monophosphate.<sup>7</sup> Due to the remarkable antitumor-inhibiting activity of 5-FU (**2**), the search for its more potent and tumor-selective analogs is still a very active area of research.<sup>7</sup>

These two drugs, Fludrocortisone (**1**) and 5-FU (**2**), constituted the fundamental paradigm change in the view of fluorine's place in biology-related research, assuring that the role of fluorine in life sciences would increase. In fact, the research carried out in the 1950s demonstrated three general principles of fluorine application in the design and development of biologically active compounds: (i) the substitution of fluorine for hydrogen and (ii) hydroxyl group, as well as (iii) the use of fluorinated derivatives of natural compounds as antimetabolites. These breakthroughs in medicinal chemistry of fluorine represent the major strategies currently used in drug design to rationally impart unique properties, such as the enhancement of therapeutic efficacy and the improvement of pharmacokinetics.<sup>11</sup>

## 1.2 Fundamental Atomic Properties of Fluorine

To better comprehend the reasons why the incorporation of fluorine into organic molecules can impart such outstanding properties, it is necessary to study the intrinsic nature of this peculiar element. Most of the effects induced by the presence of fluorine in a molecule come from both its structure and fundamental atomic properties.

In fact, fluorine has very specific attributes arising from its electronic structure  $1s^2 2s^2 2p^5$ , as indicated by the extreme values of the atomic parameters given in Table 1. The very high ionization potential and low polarizability of the fluorine atom imply that fluorinated compounds participate only in weak intermolecular interactions. Thus, perfluoroalkylated compounds have very weak surface energies, dielectric constants, and refracting indexes.<sup>12</sup>

**Table 1.** Atomic parameters of selected atoms.

Atom	Ionization Potential (kcal/mol)	Electron Affinity (kcal/mol)	Atom Polarizability ( $\text{\AA}^3$ )	van der Waals Radii ( $\text{\AA}$ )	Pauling's Electronegativity $\chi_p$
H	313.6	17.7	0.667	1.20	2.20
F	401.8	79.5	0.557	1.47	3.98
Cl	299.0	83.3	2.18	1.75	3.16
Br	272.4	72.6	3.05	1.85	2.96
I	241.2	70.6	4.7	1.98	2.66
C	240.5	29.0	1.76	1.70	2.55
N	335.1	-6.2	1.10	1.55	3.04
O	314.0	33.8	0.82	1.52	3.44

The important electronegativity of fluorine, its small size, and the excellent overlap of the  $2s$  or  $2p$  orbitals with the corresponding orbitals of carbon, along with the presence of three lone pairs of electrons, mean that a fluorine atom borne by a carbon atom is always an electron-withdrawing substituent. Also, it results that C–F bonds are always strongly polarized from the  $sp^3$  carbon ( $\delta^+$ ) to the fluorine ( $\delta^-$ ).

These features, associated with the low polarizability of the fluorine atom, imply that the C–F bond has a relatively important ionic character and a stronger energy than the bond between carbon and any other halogen. Furthermore, the dipolar nature of the C–F bond in lightly fluorinated molecules provides the latter with a polar character.<sup>13</sup> Consequently, their physicochemical properties can be quite different from those of hydrocarbon compounds and from those of the corresponding perfluorinated compounds.<sup>14</sup>

### 1.3 Effects of Fluorine Substitution on Biological Properties

The introduction of fluorine atoms into a molecule has an impact on its resulting physical and chemical properties, with severe consequences on biological activity. The absorption, distribution, recognition, and interaction processes with the biological targets, as well as the metabolism and the elimination of this molecule, can be dramatically affected.<sup>11</sup>

The possibility to modify or modulate the pharmacological profile of a molecule by simply inserting fluorine atoms clearly explains why the bioorganic and medicinal chemistry of fluorine has become so important over the last decades, and why many drugs and pesticides nowadays are fluorinated compounds.<sup>15</sup> Despite the progress achieved recently, it should be underlined that the effects of fluorine are only understood to a limited extent, and that predicting the overall behavior of a fluorinated compound often remains a challenge.

#### 1.3.1 Drug-Target Binding Affinity

The affinity of a substrate with its biological target is first connected to their complementarity. The molecular recognition and affinity depend on all the favorable interactions that exist in the supramolecular assembly formed by the substrate and the macromolecule. If the presence of fluorine atoms enhances the strength or number of these favorable interactions, the affinity of the fluorinated substrate will be higher than that of the parent non-fluorinated compound. The main parameters involved in the recognition are the steric and conformational effects, the dipolar/hydrophobic interactions, and the hydrogen bonds.

##### 1.3.1.1 Steric Effects

The van der Waals radius of a fluorine atom (1.47 Å) is between that of hydrogen (1.20 Å) and oxygen (1.52 Å). Many experimental data have shown that, despite their difference in size, substitution of a hydrogen atom by fluorine induces only weak steric disturbances.<sup>11</sup> By contrast, the steric volumes of  $CF_2$  and  $CF_3$  groups are much larger than that of the respective methylene or methyl groups.<sup>16</sup>

In the vast majority of cases, fluoroalkyl groups turn out to be much bulkier than alkyl groups, and it is therefore commonly accepted that the size of a  $CF_3$  group is equivalent to that of an isotropic ethyl group.<sup>17-19</sup> Consequently, the steric hindrance induced by the presence of fluorine atoms may destabilize the supramolecular structure formed by a macromolecule and a fluorinated analog of the substrate, or even prevent its formation.

Comparison of the olfactory properties of the trifluoro analog of (R)-citronellol is a noteworthy example (Figure 3).<sup>20,21</sup> While the non-fluorinated analogs, **3** and **4**, exhibit only minor differences in olfactory properties, this is quite different for (R)-trifluorocitronellol **5**.<sup>21</sup> In the absence of other factors, the great differences observed between (R)-citronellol (**4**) and (R)-trifluorocitronellol (**5**) are very likely due to a different recognition by the olfactory receptors, related to the bigger size of the  $CF_3$  group with respect to  $CH_3$ .<sup>20</sup>

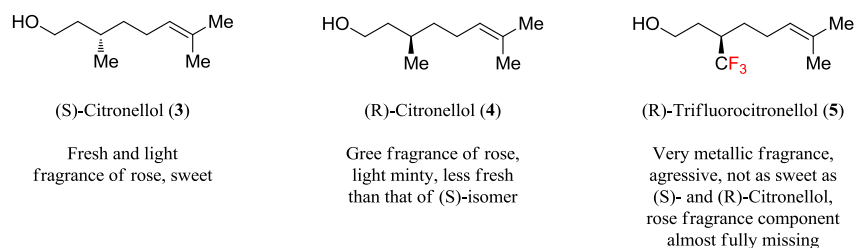


**Figure 3.** Olfactory properties of citronellols (**3**, **4**) and (R)-trifluorocitronellol (**5**).<sup>21</sup>

The rather considerable size of the  $CF_3$  group allows it to efficiently mimic the side chain of several amino acids involved in ligands or in enzyme inhibitors (e.g. valine, leucine, phenyl alanine, phenyl glycine).<sup>11</sup> Moreover, the hydrophobic character of the  $CF_3$  group favors complementarity with the lipophilic pockets of proteins receiving the side chains of lipophilic amino acids.<sup>13</sup> Interestingly, the ability of a trifluoromethyl group to mimic a big lipophilic substituent (e.g. isobutyl, benzyl) can be accompanied by a change of the agonist/antagonist character of the ligand, when the binding activity remains unchanged.<sup>22</sup>

These isolated instances reveal that although fluorine is sterically close to hydrogen, the former can lead to drastically different physical and chemical properties induced by steric effects.

### 1.3.1.2 Conformational Changes

It is well known that 1,2-difluoroethane prefers a *gauche* rather than *trans* conformation (Figure 4, left). Various gas phase calculations and experimental observations support a *gauche* preference of about 0.5–0.9 kcal/mol. For 1,2-dichloro- and 1,2-dibromoethanes the *trans* conformers are lower in energy, as expected. This observation is perhaps counterintuitive as one might predict that the fluorine atoms would repel each other, favoring a *trans* conformation. Although this must happen to some extent, it is overridden by other stabilizing effects.

The most convincing explanation for the fluorine *gauche* effect in 1,2-difluoroethane is hyperconjugation. In the hyperconjugation model, the *gauche* conformer supports two

stabilizing  $\sigma_{CH} \rightarrow \sigma_{CF}^*$  interactions. Then, in the case of the *trans* conformer, an electron deficient C–F bond ends up *trans* to the  $\sigma_{CF}^*$  orbital and hyperconjugation does not occur.<sup>23</sup> It is therefore not surprising to observe experimental manifestations of such effect through the conformational preference of more complex fluorinated molecules, although isolated instances may prove this rule wrong.

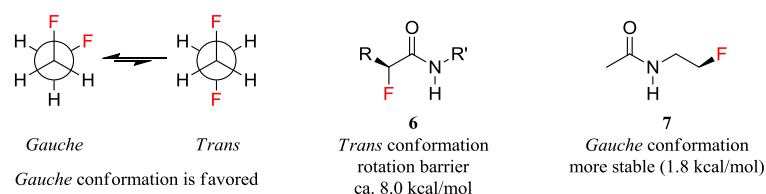


**Figure 4.** Conformational changes in fluorinated compounds.

Interestingly, *ab initio* calculations and crystallographic data have shown that  $\alpha$ -fluoroamides (**6**) prefer adopting the *trans*-periplanar conformation, with the C–F bond *trans* with respect to the carbonyl (Figure 4, center). In that case, electrostatic repulsion between fluorine and oxygen atoms accounts for the observed conformational preference.<sup>23</sup> On the contrary, the crystal structure of *N*-fluoroethyl acetamide **7** has revealed that the conformation stabilized by the *gauche* effect is the most stable (Figure 4, right).<sup>24–26</sup>

Furthermore, this intrinsic property of fluorinated derivatives has already been applied to fine-tuning molecular structures, thus acting as conformational lock. In this regard, the use of the fluorine *gauche* effect to favor the active conformation of the ribofuranose cycle of sangivamycine analog, a nucleoside that inhibits protein kinase C, is a prominent example.<sup>27</sup>

### 1.3.1.3 Dipolar Interactions

The dipolar interactions between a bioactive compound and its target are an important factor determining their affinity, especially because biological macromolecule targets exhibit many polar units in their binding sites.<sup>28</sup>

Also, since it results from basic electrostatic rules that the energy involved in the interaction between dipoles is even more stabilizing when the product of the electric charges is high, the strong electronegativity of the fluorine atom, and thus the strong dipole moment of the C–F bond, favors dipolar interactions.

For this reason, a fluorine atom can conveniently serve as a replacement of another halogen, and even an oxygen atom, or a hydroxyl group, in order to provide more stabilizing interactions between dipoles in the binding site.<sup>6</sup>

### 1.3.1.4 Hydrogen Bonds

In the body, proteins are the most common biological targets. Due to their intrinsic structural complexity, they exhibit numerous functional groups susceptible to engage with substrates into specific interactions. Amongst the latter, hydrogen bonding has been shown to be a major mode of interaction, which can be greatly influenced by the selective introduction of fluorine atoms in relevant positions of a substrate.

#### a) Fluorine as Hydrogen Bond Acceptor

Unlike a hydroxyl group, fluorine cannot be a hydrogen bond donor (Figure 5). On the other hand, it is a poor acceptor of hydrogen bonds despite its strong electronegativity and its lone pairs of electrons. This specificity mainly originates from the low polarizability of the electron pairs of the fluorine atom.<sup>13,29,30</sup>



**Figure 5.** Hydroxyl group and fluorine atom as potential hydrogen bond donors or acceptors.

Theoretical calculations estimate the strength of a  $F\cdots H$  bond to be between 2.0 and 3.2 kcal/mol, while that of an  $O\cdots H$  bond varies between 5.0 and 10 kcal/mol.<sup>6</sup> Examination of a range of crystalline structures measured for protein–ligand complexes showed a multitude of examples where fluorine is involved in close contacts with hydrogen atoms (search performed in the CSD, December 2013).<sup>13,29,31–33</sup> However, these close contacts can often be interpreted as the result of a geometry imposed by other types of interactions, and do not necessarily stem from the active participation of the fluorine atom.<sup>34,35</sup>

#### b) Influence of Fluorine on Neighboring Hydrogen Bond Donors/Acceptors

Fluorination has an important indirect impact on hydrogen bonds through neighboring functional groups (hydroxyl, amine, carbonyl, hydrogen). The electron-withdrawing nature of fluorine and other fluoroalkyl groups ( $CF_2$ ,  $CF_3$ , etc.) modifies the  $pK_a$  of neighboring functional groups, and hence their hydrogen bond donor or acceptor character.

In drug design, it is of particular interest to medicinal chemists to evaluate the propensity of a given compound to act as a proton donor or acceptor. Since having access to such information is instrumental in gauging the potential drug-receptor interactions, Abraham *et al.* have developed a scale of hydrogen bond acidity that is based on equilibrium constants measured in  $CCl_3CH_3$ .<sup>36,37</sup> Thanks to this work,  $\alpha_2^H$  and  $\beta_2^H$  have become two particularly relevant

parameters often used by medicinal chemists, which represent respectively the hydrogen bond donor and acceptor ability of a substituent.

On the one hand, values of the  $\alpha_2^H$  parameter reported for various series of compounds (entries 1–5) with varying degrees of fluorination (a–d) show that the presence of fluorine atoms notably enhances the hydrogen bond donor ability of a neighboring functional group (Table 2). On the other hand, values of  $\beta_2^H$  reveal a reverse influence of fluorination on the ability to accept hydrogen bonds.<sup>6</sup>

**Table 2.**  $pK_a$ ,  $\alpha_2^H$ , and  $\beta_2^H$  values of fluorinated compounds in  $CCl_4$ .<sup>6</sup>

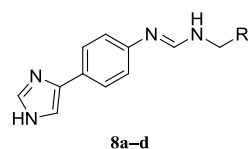
Entry	Compound	$pK_a$	$\alpha_2^H$	$\beta_2^H$	Entry	Compound	$pK_a$	$\alpha_2^H$	$\beta_2^H$
1a	$CH_3CH_2NH_2$	10.7	0	0.70	3c	$CF_3CH_2OH$	12.4	0.57	0.18
1b	$CF_3CH_2NH_2$	5.9	n.a.	0.36	3d	$CF_3CH(OH)CF_3$	9.3	0.77	0.03
2a	$MeCONEt_2$	n.a.	n.a.	0.71	4a	$C_6H_5OH$	10.0	0.60	0.22
2b	$CF_3CONEt_2$	n.a.	n.a.	0.47	4b	$C_6F_5OH$	5.5	0.76	0.02
3a	$CH_3CH_2OH$	15.9	0.33	0.44	5a	$CH_3COCH_3$	n.a.	n.a.	0.48
3b	$FCH_2CH_2OH$	n.a.	0.40	0.36	5b	$CF_3COCF_3$	n.a.	n.a.	0.20

These data point out the great interest of fluorine in the modulation of a molecule's hydrogen-bonding properties, and underline the potential of such concept when applied to medicinal chemistry.

### 1.3.1.5 $pK_a$ Modulation of Amines

As suggested above, the  $pK_a$ -lowering induced by the presence of fluorine atoms can make the protonation of an amine function more difficult. This decreased basicity may thus alter the affinity for a receptor, depending on whether the active species operates through its neutral or protonated form.

For instance, Figure 6 shows the impact of fluorination on the  $H_2$ -receptor affinity with a series of partially fluorinated analogs of Mifentidine (**8a–d**).<sup>38</sup> The results obtained in that case confirm that the degree of protonation of the amidine plays a role in receptor affinity. In fact, since the selective introduction of fluorine atoms favors the active neutral form of the  $H_2$ -antagonist, it results that the affinity increases with the degree of fluorination, from **8a** to **8d**.



Compound	R	pK <sub>a</sub>		Protonated at pH 7.4 (mol%)		Activity of H <sub>2</sub> -antagonist (pM)
		Imidazole	Amidine	Monocation	Neutral	
<b>8a</b>	CH <sub>3</sub>	5.57	8.65	93.2	5.3	177
<b>8b</b>	CH <sub>2</sub> F	5.55	8.12	82.6	16	61
<b>8c</b>	CF <sub>2</sub> H	4.54	6.60	13.5	86.3	21
<b>8d</b>	CF <sub>3</sub>	4.45	6.14	5.1	94.8	7.6

**Figure 6.** Activities of fluorinated analogs of Mifentidine (**8a-d**).<sup>38</sup>

In a similar way, this lowering may facilitate an enzymatic reaction when the non-protonated species is a better substrate for an enzyme than the protonated one. For instance, the rate of methylation of  $\beta,\beta$ -difluoroethylamine by *N*-methyltransferase of rabbit lung is increased by a factor of 4 when compared to the non-fluorinated parent.<sup>39</sup>

### 1.3.1.6 Fluorous Interactions

The introduction of a single fluorine atom into a molecular fragment already induces significant effects, but as the number of fluorine atoms increases the material starts to behave as a completely different species. Striking is the comparison between the physicochemical properties of perfluorocarbons and hydrocarbons. Fluorous compounds, consisting in highly fluorinated molecules, are usually colorless liquids of high density, inert, non-polar, and amphiphobic, i.e. at the same time hydrophobic and lipophobic.

For these reasons, they are usually immiscible with organic solvents and water, as well as with ionic liquids. This behavior is sometimes referred to as fluorous effect, and can simply be described as the tendency of perfluoroalkyl chains to segregate in order to favour fluorine-fluorine interactions, or, more appropriately, to avoid unfavoured interactions of fluorine atoms with other elements.<sup>14</sup> In this regard, it has been shown that perfluoroaromatic rings are of special interest, because of C<sub>6</sub>F<sub>6</sub>-C<sub>6</sub>H<sub>5</sub>X stacking interactions<sup>40,41</sup> and of their binding properties,<sup>42</sup> thus suggesting potentially useful applications in medicinal chemistry.



For instance, fluorine effects in the active site of DNA polymerase have been observed when highly fluorinated nucleotides are present in the DNA template or are supplied as nucleoside triphosphates. When supplied opposite the non-natural bases in the template strand, the hydrophobic fluorinated nucleoside triphosphates have been incorporated by up to two orders of magnitude more efficiently than the natural deoxynucleoside triphosphates.<sup>43</sup> These results suggested the importance of hydrophobicity, stacking, and steric interaction in the polymerase-mediated replication of DNA base pairs that lack hydrogen bonds.

### 1.3.2 Absorption

The presence of fluorine atoms may have an influence on parameters involved in the transport and absorption steps of drug administration.<sup>44</sup> Biological membranes, which are constituted of lipid bilayers, are major obstacles for the distribution of a drug to its target. In the case of a drug administered orally, it must overcome several hurdles in the body, like crossing the intestinal barrier, the blood-brain barrier, or simply cells barriers. Each of these steps of transportation and absorption are dependent on various factors, such as lipophilicity,  $pK_a$ , solubility, and molecular weight of the drug.<sup>28</sup> The effects of fluorine on these parameters have been documented but not clarified until now.<sup>6,45-47</sup>

#### 1.3.2.1 Lipophilicity

Due to the experimental difficulties encountered when measuring the lipophilicity of a compound, calculated values of  $\log P$  ( $c \log P$ ) are often used and reported by medicinal chemists. Notwithstanding, since relatively important gaps are commonly observed between calculated and measured values, even inside homogeneous series,<sup>48</sup> caution is required when using  $c \log P$  values, and experimental  $\log P$  values are preferred whenever possible.

Although experimentally determined  $\log P$  values are comparatively scarce, several methods to measure lipophilicity exist depending on the molecule of interest.<sup>49</sup> The most common way to proceed to date still remains by determining the partition coefficient of a given compound between 1-octanol and water. This value is particularly useful in medicinal chemistry, as it is fairly representative of a molecule's ability to permeate through lipid bilayer membranes.<sup>49</sup>

In the context of fluorinated molecules, it appears that introducing fluorine atoms can lead to diametrically opposed effects on lipophilicity. Interesting examples illustrating the influence of fluorination on lipophilicity are reported in Table 3.<sup>6,12</sup>

**Table 3.** Experimental  $\log P$  values of selected fluorinated and non-fluorinated compounds.

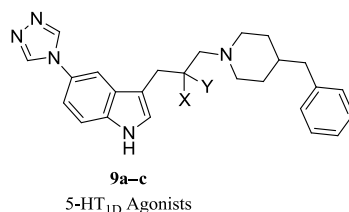
Entry	Compound	$\log P$	Entry	Compound	$\log P$
1a	C <sub>6</sub> H <sub>6</sub>	2.1	3a	CH <sub>3</sub> CH <sub>3</sub>	1.81
1b	C <sub>6</sub> H <sub>5</sub> F	2.3	3b	CH <sub>3</sub> CHF <sub>2</sub>	0.75
2a	C <sub>6</sub> H <sub>5</sub> CH <sub>3</sub>	2.7	4a	CH <sub>3</sub> (CH <sub>2</sub> ) <sub>3</sub> CH <sub>3</sub>	3.11
2b	C <sub>6</sub> H <sub>5</sub> CF <sub>3</sub>	3.0	4b	CH <sub>3</sub> (CH <sub>2</sub> ) <sub>3</sub> CH <sub>2</sub> F	2.33

Thus, upon substitution of hydrogen atoms by fluorine in benzene derivatives (entries 1a–2b), Smart noticed that lipophilicity increases with the degree of aromatic fluorination (Table 3, left).<sup>12</sup> Conversely, an opposite behavior was revealed in saturated alkyl derivatives (entries 3a–4b), where the partially fluorinated analogs typically exhibit a marked lipophilicity decrease (Table 3, right).<sup>12</sup> Although only sparse lipophilicity values are available for partially fluorinated compounds, these isolated instances highlight the ambivalent impact of fluorination on lipophilicity.

### 1.3.2.2 Bioavailability

The effect of fluorine atoms on the  $pK_a$  of neighboring ionizable functions alters the absorption properties of a molecule. Indeed, the absorption process of an ionizable drug relies on the respective proportions and lipophilicity of charged and neutral species. Also, the introduction of fluorine atoms in a molecule may enable the modulation of its ionization potential at physiological pH. Hence, lowering the  $pK_a$  of amines and nitrogen-containing heterocycles by means of fluorinated substituents can be a very important factor to facilitate absorption, particularly for oral administration of drugs.<sup>50</sup>

In a report by van Niel *et al.*, the authors studied the effect of fluorination on the  $pK_a$ , bioavailability, and receptor binding of a set of 5HT<sub>1D</sub> agonists **9a–c** depicted in Figure 7. Their results revealed that the non-fluorinated parent, compound **9a**, is a very potent receptor ligand, but also has a very low bioavailability. The monofluorinated analog **9b** has a lower  $pK_a$  that is still compatible with the requirements for receptor binding, but that also results in a substantially increased bioavailability. As for the difluoro derivative **9c**, it exhibits a drastically reduced  $pK_a$  that makes it no longer basic enough to achieve high binding affinity for the 5HT<sub>1D</sub> receptor. These results pinpoint the strong potential of selective fluorination in view of tuning bioavailability of active compounds.



Compound	X	Y	log <i>P</i>	log <i>D</i> (pH 7)	p <i>K</i> <sub>a</sub>	IC <sub>50</sub>	EC <sub>50</sub>
<b>9a</b>	H	H	4.97	2.34	9.7	0.3 nM	0.6 nM <i>very low bioavailability</i>
<b>9b</b>	F	H	4.63	3.25	8.7	0.9 nM	0.9 nM <i>moderate bioavailability</i>
<b>9c</b>	F	F	4.89	4.80	6.7	78 nM	<i>affinity decreased due to lowering of p<i>K</i><sub>a</sub></i>

**Figure 7.** Influence of fluorine atoms on the p*K*<sub>a</sub>, bioavailability, and receptor binding of selected 5-HT<sub>1D</sub> agonists **9a-c**.<sup>51</sup>

### 1.3.3 Metabolism

Introduction of fluorine atoms in a molecule can be used to modify the processes and the rates of drugs metabolism, in order to extend the plasma half-life or avoid the formation of toxic metabolites. Due to the properties of the fluorine atom, in particular its electronic effects, it may interact differently during the biotransformation steps, depending on the metabolic process involved (oxidation, reduction, hydrolysis, etc.) in the clearance of the exogenous molecule.<sup>52</sup>

#### 1.3.3.1 Oxidative Metabolism

Slowing down the oxidative metabolism process is one of the most frequent reasons for introducing one or several fluorine atoms into a lead compound. This approach is usually employed to impede the oxidation of aromatic rings, as their hydroxylation is often the first step in the detoxification of an exogenous compound in the liver (Figure 8).<sup>28,52</sup>

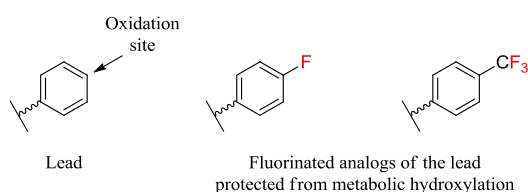


**Figure 8.** Fluorination as a means to impede the biological oxidation of aromatic rings.

The stability of fluorinated compounds towards oxidative processes is generally attributed to the strength of the C–F bond, which is more important than that of the C–H bond. However, since biological oxidations do not involve the homolysis of C–F bonds, their metabolic stability cannot be directly associated with the bond strength. Therefore, it seems more judicious to invoke the difficult formation of the O–F bond to explain the protection against the hydroxylation of the *ipso*-carbon.<sup>52</sup>

Fluoroalkyl groups such as  $CF_2$ ,  $CF_3$ , and  $C_2F_5$  exhibit an almost complete inertia towards oxidation. Consequently, they can advantageously replace an alkyl group to prevent any oxidative metabolism to happen in a given position. Also, as illustrated in Figure 9, no metabolism occurs in the neighbourhood of the fluorinated site, and goes through alternative mechanisms in other positions.<sup>53–55</sup>

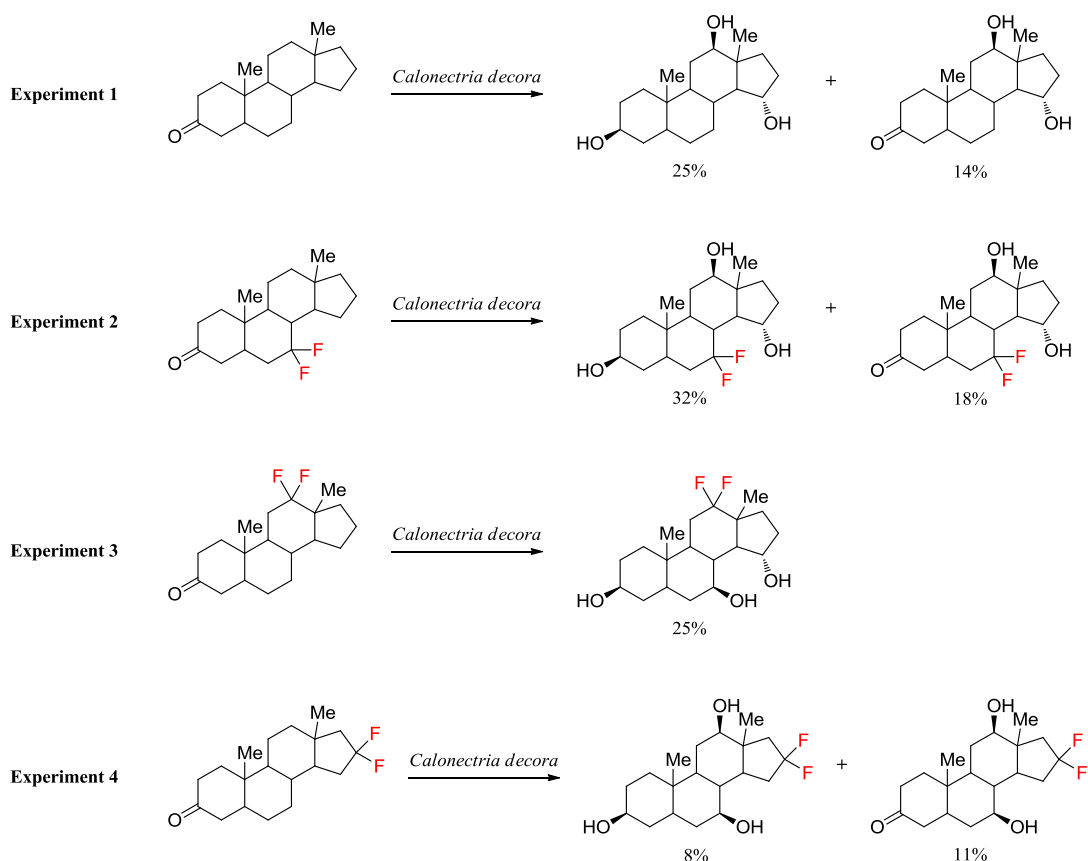


**Figure 9.** Influence of fluorine atoms on microbiological hydroxylation of 5 $\alpha$ -androstane derivatives.<sup>54</sup>

The influence of fluorination on the microbiological hydroxylation of 5 $\alpha$ -androstane derivatives by the fungus called *Calonectria decora* was reported in a study by Bird *et al.* (Figure 9).<sup>54</sup> The main products isolated from the first experiment pointed out two main oxidation sites. The second experiment the authors carried out showed that introducing a

difluoromethyl group in a position remote from any of the previously identified oxidation sites has no influence on the hydroxylation process. Nonetheless, when a difluoromethyl unit was inserted in one of the favored oxidation sites, experiments 3 and 4 not only revealed that the hydroxylation was completely inhibited in the fluorinated positions, but also showed that an alternative oxidation site appeared. These results thus confirmed the possibility to block specific metabolic positions by means of fluorination.

### 1.3.3.2 Hydrolytic Metabolism

As previously underlined, the presence of fluorine atoms in a molecule impedes oxidative metabolism, but it can also prevent proteolysis by disfavoring the formation of cationic intermediates involved in the process. This is particularly important for oral administration of drugs that are sensitive to acidic media because of the very acidic pH in the stomach.<sup>56,57</sup>

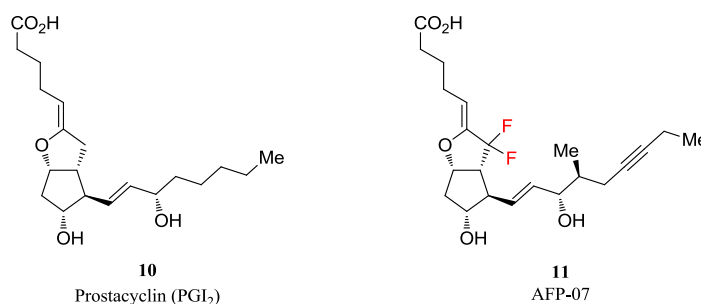


**Figure 10.** Structures of prostaglandin derivatives **10** and **11**.<sup>58</sup>

In this regard, a study reported on the metabolic stability of Prostacyclin (**10**) is quite revealing (Figure 10). Due to the presence of an enol ether function, Prostacyclin (**10**) is unstable at physiological pH with a half-life ranging from 5 to 10 min at 37 °C. The rapid hydrolysis that takes place in the biological medium in fact precludes its use as vasodilator or inhibitor of platelet adhesion. To remedy this weakness, fluorine atoms were introduced in  $\beta$ -position of the enol double bond, as exemplified in compound **11**. This structural modification led to an improved metabolic stability, while retaining a strong activity as inhibitor of platelet adhesion.<sup>58</sup> In fact, hydrolysis is slowed down as the oxonium resulting from the protonation of the enol ether is destabilized by the  $CF_2$  group.

### 1.3.3.3 Metabolic Defluorination

Although the presence of fluorine atoms in a molecule globally enhances its capacity to resist metabolism, it never precludes completely all metabolic processes. In fact, it has been shown that fluorinated derivatives are readily metabolized in the body through various mechanisms that involve defluorination reactions.<sup>52</sup> Indeed, despite the strength of the C–F bond,

defluorination can occur spontaneously during the various biotransformations of a molecule. This process favors in the end the excretion of fluorine atoms in the form of stable fluoride ions. For instance, the release of fluoride from aliphatic compounds is readily achieved by simple hydroxylation at centers adjacent to the C–F bond. Thus  $\alpha$ -hydroxylation, and subsequent elimination of hydrofluoric acid, will yield a ketone or an acyl halide. On the contrary, fluorinated aromatic compounds are generally more resistant to metabolism.<sup>52</sup> Despite the interest in developing metabolically stable molecules, too high persistence in the body is neither sought nor desired by medicinal chemists.<sup>28</sup> This is why it is actually crucial for a fluorinated bioactive compound that CYP-catalyzed metabolic defluorination still occurs.

## 1.4 Impact of Fluorine in Pharmaceuticals

As seen in the previous paragraphs, introducing fluorine atoms into bioactive molecules can impart various beneficial effects, which are often highly desired characteristics in drug design. Thus, it is no surprise to realize that in 1970 only about 2% of marketed drugs were fluorinated, while the current number has grown to about 25% in 2013.<sup>7</sup> It should be emphasized that fluorine is making an impact in pharmaceuticals not only in a fast-growing number of fluorinated drugs, but also in development of best health care products. Also, it is quite remarkable that three out of five top-selling pharmaceuticals contain fluorine. In fact, in 2008, atorvastatin (Lipitor<sup>®</sup>) (**12**) was registered as the best-selling drug globally with a revenue of \$US 5.9 billion (Figure 11).<sup>7</sup>

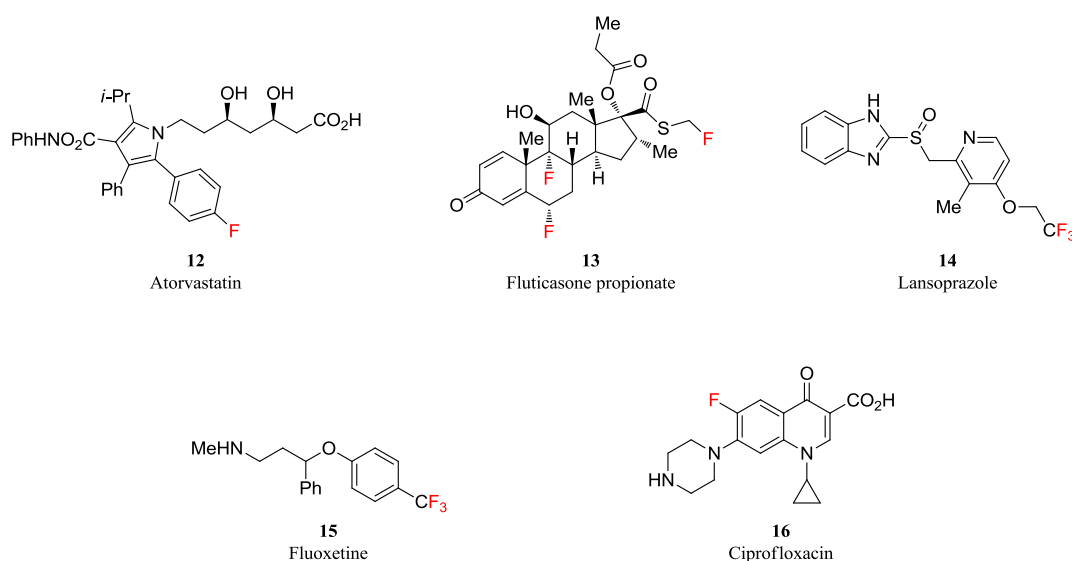


**Figure 11.** Structures of Atorvastatin (**12**), Fluticasone propionate (**13**), Lansoprazole (**14**), Fluoxetine (**15**), and Ciprofloxacin (**16**).

Atorvastatin is used in the treatment of high cholesterol and triglyceride levels and prevention of heart attacks and strokes. Steroidal anti-inflammatory drug Fluticasone propionate (**13**) and Lansoprazole (Prevacid<sup>®</sup>) (**14**) regulating gastric acid secretion make the list of top-selling fluorinated drugs. Furthermore, antidepressant Fluoxetine (Prozac<sup>®</sup>) (**15**) and the antibacterial Ciprofloxacin (Ciprobay<sup>®</sup>) (**16**) should also be mentioned among the most successful fluorine-containing drugs.<sup>46</sup>

In general, about one-third of the top-performing drugs currently on the market contain fluorine atoms in their structure. These statistical data clearly suggest that the paramount role of fluorine in medicinal chemistry and drug design has been firmly established, and more fluorinated drugs can be expected in the near future.

### **1.5 Aim of the Present Work**

This project aimed at exploring the potential application of partially fluorinated building blocks in medicinal chemistry as new tools to fine-tune lipophilicity of lead compounds. To this end, the present work focused on the basic understanding and the rationalization of the lipophilicity-lowering effect imparted by some partially fluorinated alkyl groups. Based on literature precedents and molecular modelling, relevant sets of model compounds were designed and synthesized, which were then subjected to experimental measurements. The results and conclusions of this study are reported in the following chapters of this thesis.





## 2 Partially Fluorinated Methyl Groups

### 2.1 Introduction

In modern drug discovery, the optimization of physicochemical and pharmacokinetic properties is a process that runs in parallel to the interest in increasing activity. Integration of property optimization at an early stage of the discovery process has led pharmaceutical research to an exceptional reduction of development attrition due to inadequate pharmacokinetics and bioavailability. Property-based design is more than ever a priority for medicinal chemists who, thanks to the constant development of high-throughput assays, can now rapidly access the full ADMET (absorption, distribution, metabolism, excretion, toxicity) profile of drug candidates.<sup>28</sup>

Accordingly, while HTS (high throughput screening) and combinatorial chemistry often afford promisingly active hits with poor drug-like properties,<sup>59</sup> medicinal chemists are permanently looking for new tools that would enable the selective fine-tuning of specific parameters such as basicity ( $pK_a$ ),<sup>47</sup> lipophilicity ( $\log P$ ),<sup>49</sup> solubility ( $Sol.$ ), and clearance rate ( $Cl_{int}$ ).<sup>60</sup>

In this context, the unique characteristics of fluorine have already afforded numerous applications in lead optimization, ranging from the  $pK_a$  modulation of amines<sup>39</sup> to the selective blocking of oxidative metabolic sites.<sup>61</sup> Although lipophilicity plays a decisive role in the pharmacokinetic behavior of drug molecules,<sup>49</sup> solely fragmentary data documenting the influence of fluorine on lipophilicity are currently available.<sup>12,50</sup>

In an effort to fill this gap and investigate further the potential of fluorinated building blocks as modulators of lipophilicity with applications in medicinal chemistry, a research project was initiated aiming at studying systematically the specific influence of fluorine substitution on the lipophilicity of relevant series of partially fluorinated model compounds and, more broadly, on their pharmacokinetics. Herein are documented and discussed the first results of this work.

## 2.2 Study on the Polarity of Partially Fluorinated Methyl Groups

### 2.2.1 Preliminary Observations

At the outset of this project, a statistical search revealed that most of the fluorine-containing drugs on the market, or at various stages of clinical development, carry the *p*-fluorophenyl unit (40%) or the trifluoromethyl group (25%). By contrast, monofluoro- and difluoromethyl groups, as well as higher corresponding alkyl groups, are encountered with considerably lower frequency.<sup>6</sup> Mono- or difluoromethyl groups directly attached to aromatic or heteroaromatic moieties are rarely reported, whereas the difluoromethyl unit is occasionally found in corresponding methoxy or methylsulfanyl groups. On the contrary, the monofluoromethyl unit is typically embedded in fluoroethyl, fluoropropyl, or larger fluoroalkyl groups that can be easily grafted to a heterofunction of active molecules. This is particularly effective in the context of <sup>18</sup>F-labeling of drug candidates for exploratory PET studies.<sup>11</sup>

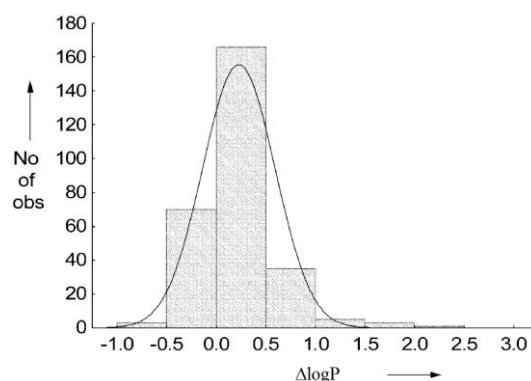


**Figure 12.** Histogram of change in  $\log P$  observed upon substitution of a hydrogen by a fluorine atom.

An early investigation aimed at examining the change in polarity upon replacement of a hydrogen by fluorine ( $H \rightarrow F$ ) by matched molecular pair analysis (MMPA)<sup>62</sup> resulted in a histogram with an approximate Gaussian distribution around a maximum at  $\Delta \log P \sim 0.2$  (Figure 12). Similarly, a histogram with a maximum at  $\Delta \log P \sim 0.5$  was obtained for the exchange of a methyl group by a trifluoromethyl unit ( $CH_3 \rightarrow CF_3$ ).<sup>50</sup> These values are in line with the general observation that introduction of fluorine in place of hydrogen leads to increased lipophilicity.<sup>11,12</sup>

Interestingly, however, both histograms reveal tails extending not only into much more positive  $\log P$  changes but equally into ranges of  $\Delta \log P < 0$ . As already noted by Böhm *et al.*,<sup>50</sup> the latter cases are of particular interest, as the introduction of a single fluorine or a  $CF_3$

group would result in both potential blocking of metabolism and lowering of lipophilicity. In this regard, noteworthy examples are fluorooxetane **17**, which is more polar than its non-fluorinated parent **18** by 0.4  $\log P$  units,<sup>63</sup> or trifluoropropylbenzene **19**, which has a lower  $\log P$  than the parent *n*-propylbenzene **20** (Figure 13) (MedChem Database, version 2010). The case of *n*-propylbenzene represents an example of lipophilicity decrease by terminal fluorination of a saturated alkyl group that has been recognized early by Smart.<sup>12</sup>

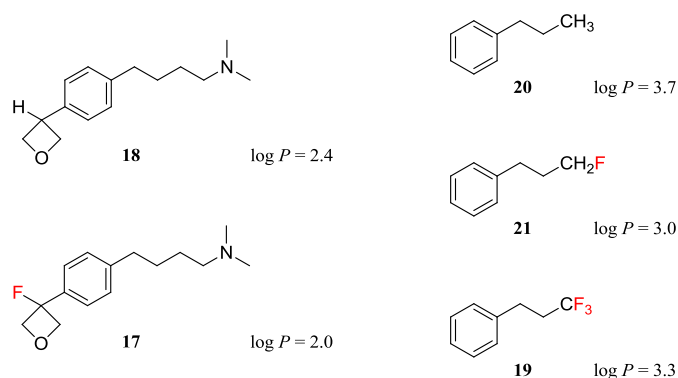


**Figure 13.** Two prominent cases of molecular lipophilicity decrease upon  $H \rightarrow F$  replacement.

In view of understanding why these peculiar occurrences display a manifestly marked lipophilicity-lowering effect upon fluorine substitution, one must consider the impact resulting from such structural modification. As a matter of fact, based on the intrinsic properties of the fluorine atom discussed earlier, the substitution of hydrogen atoms by fluorine results in two main consequences: (i) a volume increase, and (ii) a polarity increase.

As the volume of a  $CF_3$  group corresponds approximately to that of an isotropic ethyl group,<sup>19</sup> the increase in lipophilicity upon exchange of  $CH_3$  by  $CF_3$  can be rationalized in terms of an increase in bulk, which can be approximated by the volume of a methyl group. This is borne out by the observed  $\Delta \log P \sim 0.5$  when comparing *p*-toluylamide and its trifluoromethyl analog.

Additionally, MMPA of a series of simple *p*- and *m*-substituted toluene derivatives and their corresponding  $CF_3$  counterparts reveals, however, that the lipophilicity increase upon  $CH_3 \rightarrow CF_3$  exchange decreases more or less linearly with increasing lipophilicity of the parent toluene derivative (Figure 14).<sup>45</sup> This may be interpreted in terms of the polarity effect of the  $CF_3$  group gaining increased prominence as substrates become more lipophilic.

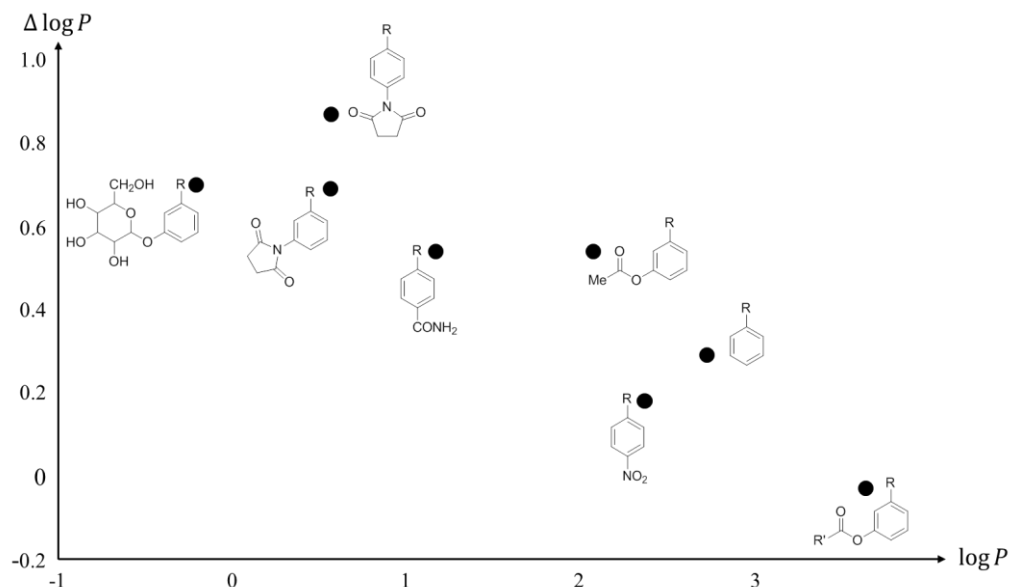


**Figure 14.** MMPA for the lipophilicity of simple *p*- and *m*-substituted toluene derivatives ( $R = CH_3$ ) and their trifluoromethyl counterparts ( $R = CF_3$ ) (MedChem Database, version 2010).

Consequently, the introduction of terminal fluorine atoms onto saturated alkyl groups may then be regarded as a peculiar situation in which polarity effects on lipophilicity generally dominate compensating effects due to the net increase in volume, thus resulting in a global decrease of lipophilicity. As a matter of fact, polarity enhancement has been observed in several scattered examples involving the introduction of a terminal  $CF_3$  group or by single ( $H \rightarrow F$ ) or double ( $CH_2 \rightarrow CF_2$ ) exchange at the terminal position of a saturated alkyl unit.<sup>11,12</sup>

### 2.2.2 The *n*-Propylbenzene Case

Based on these initial statistical observations, it was decided to investigate further the lipophilicity-lowering effect of partially fluorinated methyl groups borne by saturated alkyl chains, in view of rationalizing this singular phenomenon by means of basic concepts. To this end, the case of *n*-propylbenzene was identified as particularly interesting for several reasons that shall be reviewed herein.

First of all, the corresponding monofluoro derivative **21** is known to display a significantly reduced  $\log P$  value compared to the non-fluorinated parent **20**.<sup>11,64</sup> This effect is actually even more pronounced than for the trifluoro derivative **19**, which results in the remarkable lipophilicity pattern shown in Figure 15.<sup>45</sup> Unfortunately, the corresponding difluoro derivative **22** has thus far not been reported, which suggested to evaluate where it would stand in the series.

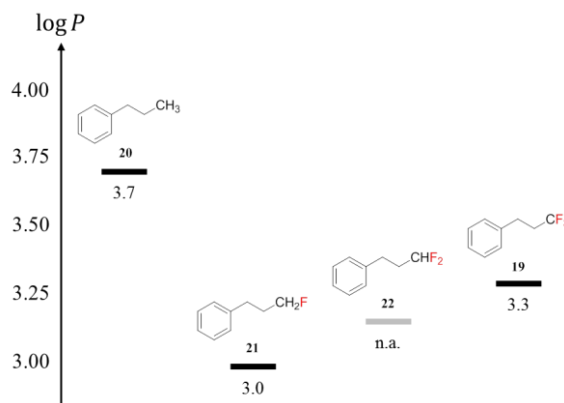


**Figure 15.** Lipophilicity values for a series of *n*-propylbenzene derivatives (**19–22**) with varying degrees of terminal fluorination (n.a. – not available).

Thus, an analysis of the given system was initiated relying on a number of key assumptions:

- 1) Molecular dipole moments can be ascribed to the individual bond dipole moments,  $\mu_{CF}$ , of the highly polarized C–F bonds;
- 2) C–F dipole moments are essentially invariant of their structural context;
- 3) Geometries around tetravalent carbon centers are ideally tetrahedral.

Under these conditions, the three C–F bond dipole moments in the  $CF_3$  group combine to furnish a net dipole moment of  $1 \mu_{CF}$ , which is equal to that found for the  $CH_2F$  moiety. For the  $CHF_2$  unit, however, the two C–F bond vectors sum to afford a dipole moment vector of approximately  $1.16 \mu_{CF}$ . Examination of the gas phase dipole moments of monofluoro-, difluoro-, and trifluoromethane illustrates that these simple assumptions do not strictly hold (Figure 16).<sup>45</sup>

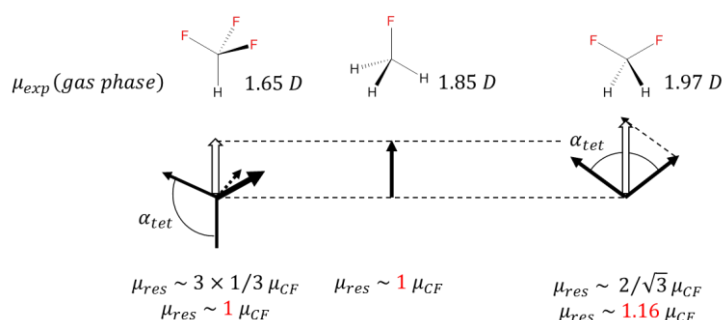


**Figure 16.** Comparison of the simple C–F polarity vector analysis of monofluoro-, difluoro-, and trifluoromethane to their respective gas phase dipole moments.

Indeed, although  $CH_2F_2$  possesses a higher dipole moment than its other two congeners, as expected, the dipole moment of  $CHF_3$  is surprisingly smaller than that of  $CH_3F$ . This may reflect the electronic stabilization effects involving geminal C–F bonds, which result in

significant deviations from tetrahedral geometries.<sup>65</sup> Despite this discrepancy, which pointed out the weaknesses of the initial assumptions, a valuable qualitative estimate of the lipophilicity of difluoride **22** could still be determined. Therefore, applying the simple concepts outlined above to the *n*-propylbenzene case, one might expect comparable polarity effects for both **19** and **21** which are compensated by  $1 \Delta \log P (\Delta V_{H/F})$ , i.e. the lipophilicity effect due to the volume increase  $\Delta V_{H/F}$  upon one *H/F* exchange, in **21**, but three times as much as in **19**.

With the experimental  $\log P$  values for **19–21**, the volume effect for  $\log P$  upon  $CH_3/CF_3$  exchange would be calculated as  $3 \Delta \log P (\Delta V_{H/F}) \sim 0.45$ . This is in good agreement with expectation since  $3 \Delta V_{H/F} \sim \Delta V_{H/CH_3}$  and  $\Delta \log P (\Delta V_{H/CH_3}) \sim 0.5$ .<sup>45</sup> Furthermore, this simple analysis would indicate a 16% polarity increase for the corresponding difluoropropyl case (**22**). Based on these basic calculations, the lipophilicity change from **20** to **22** would therefore be anticipated to be similar to that from **20** to **21**, as the larger polarity effect on  $\log P$  is back-compensated by  $2 \Delta \log P (\Delta V_{H/F})$  (Figure 17).

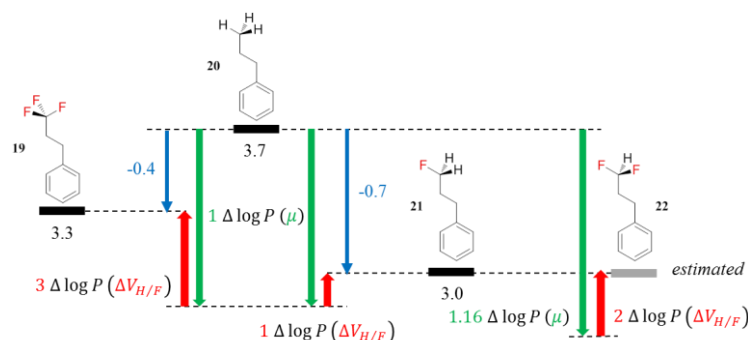


**Figure 17.** Simple model based on molecular polarity and volume effects to rationalize experimental  $\log P$  values of **19–21**, and estimate the  $\log P$  value of difluoro derivative **22**.

In order to render the analysis more realistic, one could employ the dipole moments of partially fluorinated propane. However, since not all of the dipole moments were experimentally available at the time of this work, reliably computed dipole moments were used (Table 4; for computational details, see Experimental Section).

Several aspects are worth noting based on the results displayed in Table 4. Molecular dipole moments in the ethane and higher alkane series are systematically larger than in the methane series, since polarization by the C–F unit can involve interactions with the antiperiplanar C–H bonds, or can operate inductively through the aliphatic framework. The increase in dipole moment from 1-fluoroethane to 1,1-difluoroethane nicely reflects the expected increase in the

dipole moment for a *gem*-difluoro group as already noted in the methane series. However, 1,1,1-trifluoroethane exhibits a larger dipole moment than the counterparts incorporating fewer fluorines.

**Table 4.** Calculated and experimental gas phase dipole moments of partially fluorinated methane, ethane, and propane derivatives.

Compound	Scaled computed dipole moment <sup>45</sup> (Debye)	Exp. dipole moment in the gas phase (Debye)
FCH <sub>3</sub>	1.81	1.85 <sup>66</sup>
F <sub>2</sub> CH <sub>2</sub>	1.91	1.97 <sup>66</sup>
F <sub>3</sub> CH	1.58	1.65 <sup>66</sup>
FCH <sub>2</sub> CH <sub>3</sub>	1.93	1.94 <sup>66</sup>
F <sub>2</sub> CHCH <sub>3</sub>	2.26	2.27 <sup>67</sup>
F <sub>3</sub> CCH <sub>3</sub>	2.32	2.32 <sup>67</sup>
FCH <sub>2</sub> CH <sub>2</sub> CH <sub>3</sub> <i>gauche</i> <sup>a</sup>	1.87	1.90 <sup>68</sup>
FCH <sub>2</sub> CH <sub>2</sub> CH <sub>3</sub> <i>trans</i> <sup>a</sup>	2.00	2.05 <sup>68</sup>
F <sub>2</sub> CHCH <sub>2</sub> CH <sub>3</sub> <i>gauche-gauche</i> <sup>b</sup>	2.20	n.a.
F <sub>2</sub> CHCH <sub>2</sub> CH <sub>3</sub> <i>trans-gauche</i> <sup>b</sup>	2.34	n.a.
F <sub>3</sub> CCH <sub>2</sub> CH <sub>3</sub>	2.43	n.a.
CH <sub>3</sub> CHFCH <sub>3</sub>	1.98	1.96 <sup>69</sup>
CH <sub>3</sub> CF <sub>2</sub> CH <sub>3</sub>	2.39	2.40 <sup>70</sup>

<sup>a</sup> The *gauche* conformation is predicted to be preferred over the *trans* conformation by 0.3 kcal/mol (experimentally  $0.47 \pm 0.3$  kcal/mol).<sup>68</sup>

<sup>b</sup> The *trans-gauche* conformation is predicted to be preferred over the *gauche-gauche* conformation by 0.3 kcal/mol.

It was hypothesized that for the case of F<sub>3</sub>CCH<sub>3</sub>, all C–F bonds effectively interact with the three respective vicinal C–H units. This is in contrast with the trifluoromethane case, where the three fluorine atoms compete for one single C–H unit. Similar patterns could be seen in the propane series.

For 1-fluoropropane, two conformations have been observed in the gas phase<sup>68</sup> and the preferred *gauche* conformation has a slightly smaller dipole moment than the *trans* conformation in which the C–F bond can polarize more effectively through the aliphatic backbone. These experimental results as well as the small *trans-gauche* energy difference are well reproduced by the computational results.

No experimental data are available for 1,1-difluoropropane, which is predicted to prefer the *gauche-trans* arrangement of the two terminal fluorine atoms. As expected, the molecular dipole moment for this conformation is anticipated to be slightly larger than that for the *gauche-gauche* arrangement, in which both C–F bonds polarize essentially through interactions with their respective antiperiplanar C–H units, but not so much through the alkane backbone.<sup>45</sup>

For comparison purposes, the cases of 2-fluoropropane and 2,2-difluoropropane are included here, where polarization effects are increased by the presence of two antiperiplanar C–H units for each C–F bond. Thus, 2-fluoropropane exhibits a conspicuously larger dipole moment than *gauche* 1-fluoropropane, and 2,2-difluoropropane shows a further increase of the dipole moment, which is characteristic of the *gem*-difluoro unit.

Under the assumption that the relative lipophilicities of the compounds in the fluorinated *n*-propylbenzene series are mimicked and dictated by the relative polarities of the corresponding fluorinated propane derivatives, it was decided to take the relative dipole moments of difluoropropane, in the preferred *trans-gauche* conformation, and trifluoropropane as 1.25 and 1.30 times, respectively, the dipole moment of fluoropropane in its preferred *gauche* conformation.

These data, along with the experimental  $\Delta \log P$  values for **19** and **21** relative to **20**, then led to a predicted lipophilicity for difluoropropylbenzene **22** of  $\log P \sim 3.1$ , whereas a value of  $\log P \sim 3.0$  resulted from the simple dipole vector considerations (Figure 18). Therefore, implementation of the basic and more realistic approaches to the calculation of  $\log P$  afford essentially the same prediction: both terminal mono- and difluorination of a propyl group result in a marked lowering of  $\log P$ , contrasting with the modest  $\log P$  decrease upon replacement of all three terminal hydrogen atoms by fluorine.



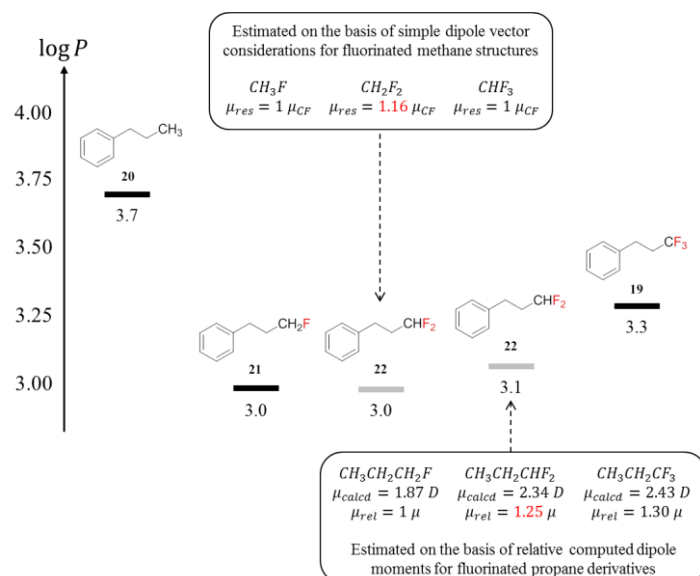


**Figure 18.** Comparison of the predicted  $\log P$  values for difluoropropylbenzene **22** depending on the method used to approximate the resulting dipole moment of the difluoromethyl group.

Due to the low solubility of difluoropropylbenzene **22**, it was unfortunately impossible to directly access its  $\log P$  value by standard method (for details, see Experimental Section). Hence, it was decided to design a suitable prototypical series of model compounds that would enable a thorough and reliable study on the influence of partially fluorinated methyl groups on lipophilicity, and verify experimentally the theoretical predictions made earlier.

## 2.3 Design and Synthesis of a Prototypical Set of Model Compounds

### 2.3.1 A Suitable Model

In view of conceiving an appropriate set of model compounds, the characteristics required for the desired measurements were defined accurately. Firstly, it was of interest to measure lipophilicity ( $\log P$ ) following a standard method (for details, see Experimental Section). Secondly, it was envisioned the possibility to determine other key pharmacokinetic properties like solubility ( $Sol.$ ) and metabolic stability ( $Cl_{int}$ ). Thirdly, it was believed that probing the conformational properties of the model compounds via X-ray structure analysis would be particularly valuable, as it could provide some insights on the relationship between conformation and lipophilicity.

Following the conclusion drawn from the MMPA reported in Figure 14, the model compounds were designed so that other functional groups or scaffolds, especially those with low intrinsic lipophilicity, would not interfere while evaluating the influence of the

fluorinated moieties. However, although *n*-propylbenzene derivatives could have been chosen as model compounds, it turned out that while trying to measure the lipophilicity of difluoropropylbenzene **22** such compounds were insufficiently soluble in water, thus precluding any  $\log P$  measurement. Therefore, this initial setback suggested to graft the fluorinated scaffolds of interest to a core unit that would provide adequate aqueous solubility and UV-activity, which are two crucial characteristics for the measurement of lipophilicity (for details, see Experimental Section). Furthermore, the core unit bearing the partially fluorinated moiety should ideally be a pharmacophore whose characteristics are well-established in medicinal chemistry. Finally, in order to investigate several series of analogs and their respective properties, a molecular core that could be easily derivatized was desired.

Once the characteristics of the desired model compounds were clearly defined, it appeared that the indole nucleus would be a relevant substrate. Nowadays, indoles are widely found amongst pharmacophores in medicinal chemistry, mainly because their versatility imparts a wide spectrum of biological activities.<sup>71</sup> In fact, countless bioactive indole-based natural or synthetic molecules have already been isolated, synthesized, and used as pharmaceuticals, thus suggesting that indole would be the perfect platform for our study. Looking at the possible sites to introduce the partially fluorinated alkyl scaffolds, C(3) seemed the most natural as several indole-based bioactive compounds like tryptophan only bear a substituent in that position.

In order to probe the effects of partially fluorinated alkyl chains on the parameters of interest, four series of model compounds were designed (Figure 19). The first 3-substituted indole-based series of compounds (**23x**) was designed to verify the predictions made in the *n*-propylbenzene case (Figure 18), and thus only featured the partially fluorinated propyl moieties.

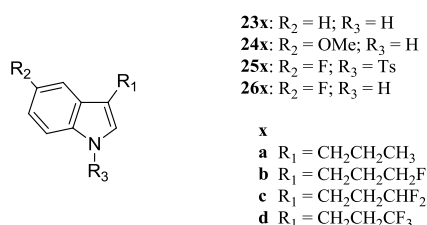


**Figure 19.** The four series of indole-based model compounds **23x–26x** used in this study (**x = a–d**).

On the contrary, it was chosen to include an additional methoxy group at C(5) to the second series of derivatives (**24x**) since it has been reported to reduce the metabolism of aromatic rings.<sup>60</sup> This series of compounds was therefore expected to exhibit a higher metabolic

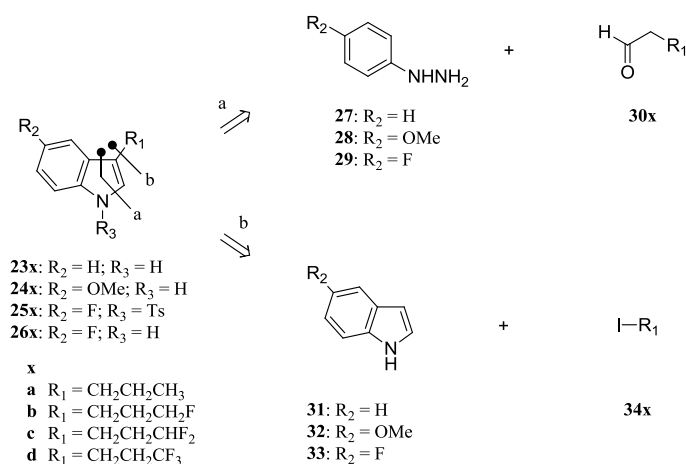
stability than series **23x**. Furthermore, since the data collected by Smart showed that the introduction of a methoxy group on an aromatic ring has generally no influence on lipophilicity,<sup>12</sup> series **24x** should thus have log *P* values similar or equal to series **23x**.

In the third and fourth series of model compounds (**25x**, **26x**), the methoxy group was replaced by a fluorine atom, because reported experimental data suggested that the aromatic fluorine atom should lead to increased lipophilicity and metabolic stability.<sup>12,52</sup> Also, as it was assumed that X-ray crystal structure analyses would provide relevant data about the conformation of the propyl chains, it was envisioned that the protection of the indole nitrogen with a tosyl group would not only enable easier crystallization, but also provide some insights about the influence of the tosyl group on metabolism. However, it was anticipated that the solubility of these compounds during lipophilicity measurements could be an issue.

## 2.3.2 Access to 3-Substituted Indole Derivatives

### 2.3.2.1 Retrosynthetic Analysis

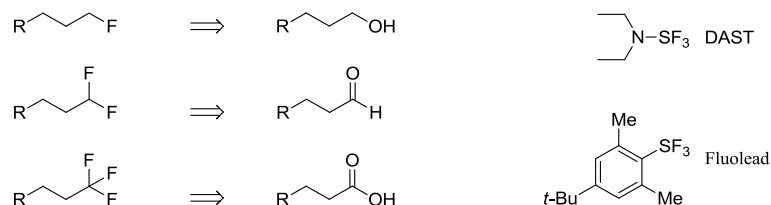
In the retrosynthetic analysis of 3-substituted indole derivatives **23x–26x**, displayed in Scheme 1, two approaches were envisioned. The first one (a) consisted in building the indole nucleus via Fischer indole synthesis, starting from phenyl hydrazines **27–29** and aldehydes **30x**. The second one (b) would afford the expected derivatives by cross-coupling reaction of indoles **31–33** with iodides **34x**.



**Scheme 1.** Retrosynthetic analysis of 3-substituted indole derivatives **23x–26x** (**x = a–d**).

Although it was assumed here that fluorinated building blocks (**30b–d**, **34b–d**) could be used, it is worth noting that fluorine atoms could as well be introduced at a later stage in case such compounds were not commercially available. In fact, the selective introduction of fluorine atoms into saturated alkyl chains can be conveniently achieved using deoxofluorinating

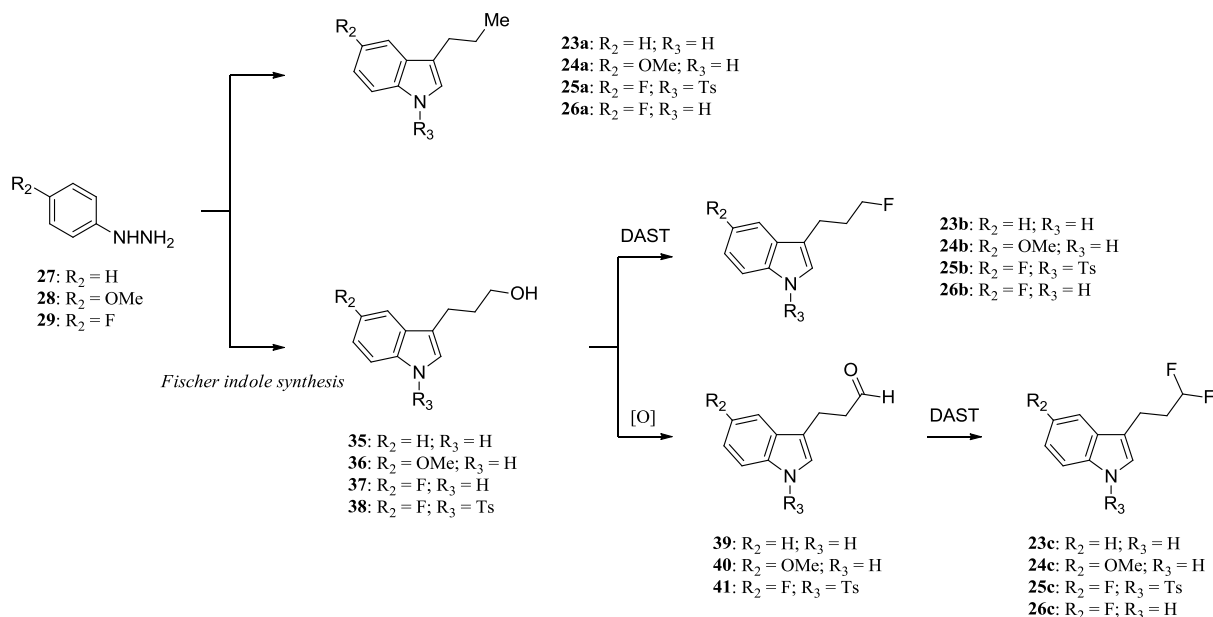
agents, amongst which DAST and Fluolead are prominent examples.<sup>72–74</sup> These powerful reagents enable the synthesis of mono-, di-, and trifluoromethyl groups by reaction with alcohols, aldehydes, or carboxylic acids, respectively (Scheme 2).



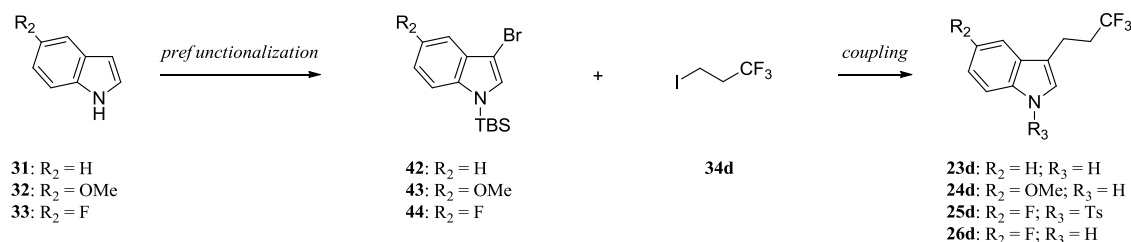
**Scheme 2.** Late stage fluorination strategy using deoxofluorinating agents.

Despite the few instances reported by Umemoto *et al.* where Fluolead converted carboxylic acids into trifluoromethyl-containing products,<sup>74</sup> this reagent suffers from poor functional group tolerance. Additionally, the paucity of Fluolead motivated the use of a widely available trifluoromethyl-containing building block (**34d**). Hence, the two strategies implemented in order to access the mono-, di-, and trifluorinated derivatives are displayed in Scheme 3.

### 1) Late stage fluorination strategy



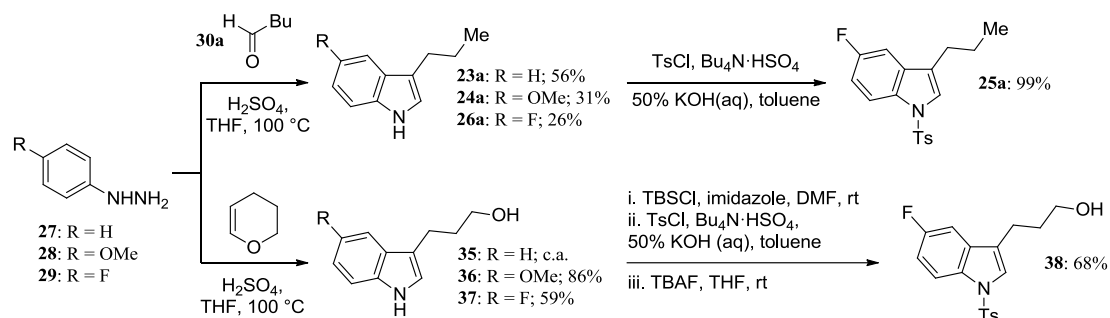
### 2) Building block strategy



**Scheme 3.** Two complementary strategies to access model compounds **23x–26x** ( $x = a-d$ ).

### 2.3.2.2 Late Stage Fluorination Strategy

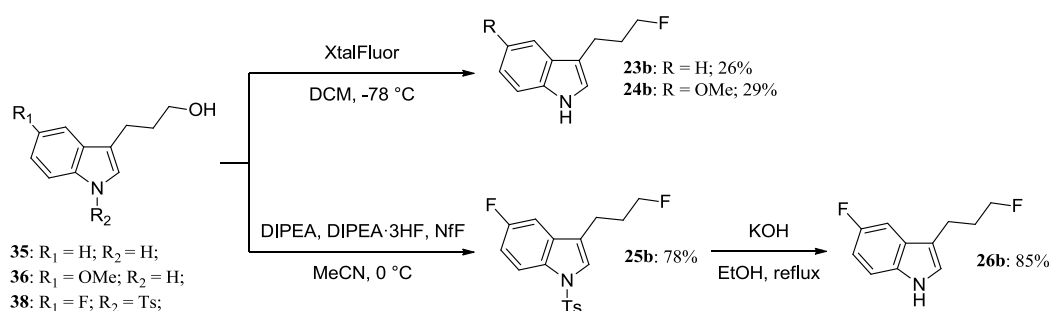
The late stage fluorination strategy started with Fischer indole synthesis (Scheme 4).<sup>75</sup> Following standard conditions,<sup>76</sup> reacting hydrazines **27–29** with pentanal (**30a**) in acidic conditions at high temperature afforded 3-propylindole derivatives **23a**, **24a**, and **26a** in acceptable yields. Further tosyl-protection of 5-fluoroindole derivative **26a** under phase transfer catalysis conditions<sup>77</sup> yielded quantitatively the protected analog **25a**.



**Scheme 4.** Fischer indole synthesis for the elaboration of 3-substituted indole derivatives.

Reacting hydrazines **28** and **29** with dihydropyran<sup>76</sup> afforded respectively alcohols **36** and **37** in satisfactory yields, whereas analog **35** was commercially available (c.a.). Selective protection of alcohol **37** as a silyl ether, followed by tosyl-protection of the indole nitrogen, and concluded by TBAF deprotection of the alcohol gave indole **38** in good yield over three steps.<sup>77,78</sup>

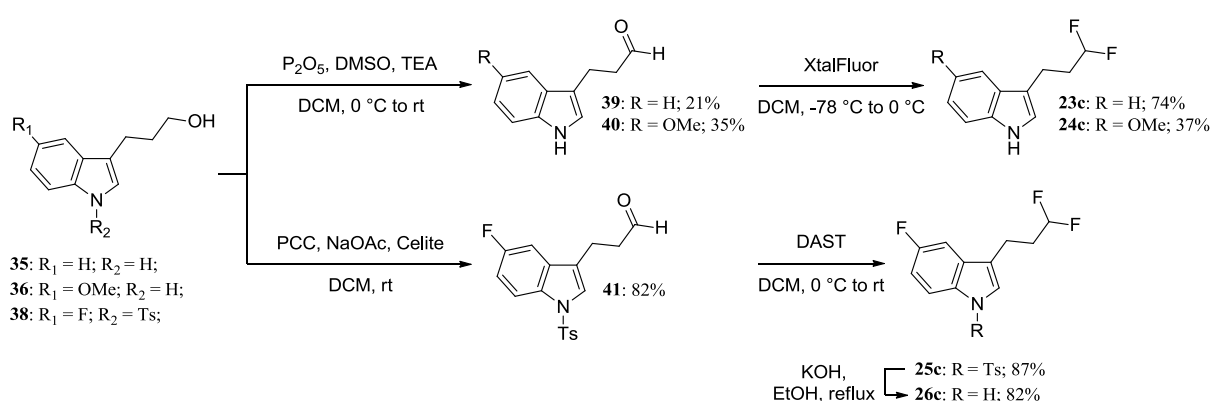
The deoxofluorination reaction of primary alcohols was then attempted on the tosyl-protected (**38**) and unprotected indole derivatives (**35**, **36**). The direct reaction of unprotected indoles **35** and **36** with DAST only afforded minute amounts of fluorinated products. Therefore, to circumvent this issue, a DAST-derived deoxofluorinating agent (XtalFluor) was employed.<sup>79</sup> More stable and less reactive than DAST, XtalFluor afforded the unprotected monofluorinated targets **23b** and **24b** in acceptable yields (Scheme 5, top).



**Scheme 5.** Access to monofluorinated targets **23b–26b**.

By contrast, fluorination of protected indole **38** proceeded smoothly following a procedure developed by Yin *et al.* (Scheme 5, bottom).<sup>80</sup> In this isolated work, the authors reported the conversion of primary alcohols into their corresponding monofluorides using a combination of perfluorobutanesulfonyl fluoride (NfF), triethylamine trihydrofluoride (Et<sub>3</sub>N·3HF), and triethylamine in acetonitrile. Although this procedure requires several reagents, it presents the main advantage to rely on widely available and inexpensive chemicals, whose reactivity is much less hazardous than DAST.

Furthermore, in the case of alcohols prone to elimination, *N,N*-diisopropylethylamine trihydrofluoride (DIPEA·3HF) and *N,N*-diisopropylethylamine (DIPEA) were used with NfF at 0 °C as an alternative to obtain the corresponding fluorinated derivatives. Under these more selective reaction conditions, monofluorinated compound **25b** was isolated in high yield. Further cleavage of the tosyl group with potassium hydroxide in boiling ethanol afforded deprotected target **26b** in high yield.<sup>81</sup>



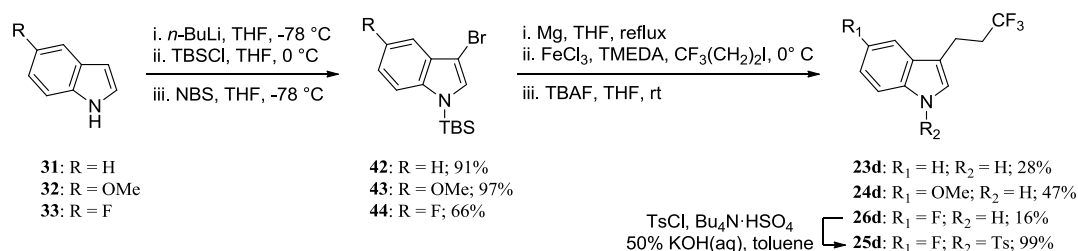
**Scheme 6.** Acces to difluoro derivatives **23c**–**26c**.

On the one hand, *en route* to difluorinated targets **23c** and **24c**, alcohols **35** and **36** were converted into the corresponding aldehydes, **39** and **40** respectively, using a combination of phosphorus pentoxide, dimethylsulfoxide, and triethylamine.<sup>82</sup> On the other hand, PCC oxidation of tosyl-protected analog **38** afforded aldehyde **41** in high yield.<sup>83</sup>

Fluorination of aldehydes **39** and **40** proceeded with XtalFluor and yielded difluorinated targets **23c** and **24c** in moderate to good yields.<sup>79</sup> Treatment of aldehyde **41** with DAST cleanly yielded tosyl-protected difluoride **25c**,<sup>84</sup> which was readily deprotected with potassium hydroxide in boiling ethanol to afford **26c**.<sup>81</sup>

### 2.3.2.3 Building Block Strategy

The synthetic strategy towards trifluoromethyl-containing targets **23d–26d** relied on the iron-catalyzed cross-coupling reaction of an indole Grignard reagent and iodopropane **34**. Also, as depicted in Scheme 7, following a reported three-step one-pot procedure,<sup>85</sup> it was possible to access bromides **42–44** from commercially available indoles **31–33**.



**Scheme 7.** Access to trifluorinated targets **23d–26d**.

The indole Grignard reagents were generated *in situ* and reacted with **34** in presence of iron trichloride and TMEDA at 0 °C.<sup>86</sup> Further TBAF deprotection of the coupled products thus afforded unprotected trifluorides **23d**, **24d** and **26d**. Finally, tosyl-protection of **26d** proceeded quantitatively to yield protected target **25d**.<sup>77</sup>

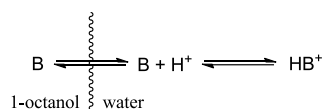
## 2.4 Physicochemical and Pharmacological Properties

The required set of model compounds was then subjected to standard physicochemical and pharmacological tests, whereby the influence of fluorination on their respective lipophilicity, metabolic stability, and structure conformation could be investigated.

### 2.4.1 Lipophilicity

#### 2.4.1.1 Introduction

Lipophilicity is a fundamental property of modern drug design that is commonly defined as the affinity of a molecule for a lipophilic environment. It is routinely measured by determining the partitioning of the given compound between 1-octanol and an aqueous buffer. The resulting partition coefficient is then used to define the numeric representations of lipophilicity, namely  $\log D$  and  $\log P$  (Equation 1).



$$\log D = \log \left( \frac{[\text{HB}^+]_{\text{oct}} + [\text{B}]_{\text{oct}}}{[\text{B}]_{\text{aq}} + [\text{HB}^+]_{\text{aq}}} \right) \text{ and } \log P = \log \left( \frac{[\text{B}]_{\text{oct}}}{[\text{B}]_{\text{aq}}} \right)$$

**Equation 1.** Definition of  $\log D$  and  $\log P$  for a basic compound B.

As a direct consequence of their definition,  $\log D$  and  $\log P$  are usually not identical, unless the compound of interest is not ionized at the pH of measurement. Furthermore,  $\log D$  values depend on the  $\text{p}K_{\text{a}}$  of the compound as well as the pH of the medium (Equation 2).

$$\log P = \log D + \log(1 + 10^{(\text{pH} - \text{p}K_{\text{a}})})$$

**Equation 2.** Correlation between  $\log P$  and  $\log D$  for acidic compounds.

In the context of our study,  $\log P$  values were measured at physiological  $\text{pH} = 7.4$ , thus implying that  $\log D = \log P$ . Indeed, because the  $\text{p}K_{\text{a}}$  of indole is higher than 7.4 (ca. 16.2 in water), none of the measured compounds were ionized at physiological pH (for details about the standard procedure used, see Experimental Section).

#### 2.4.1.2 Results and Discussion

Unfortunately, although all compounds were UV-active, since tosyl-protected indole derivatives **25x** were not soluble enough to yield any significant results, the measurements could only be performed on unprotected compounds **23x**, **24x**, and **26x**. Furthermore, solubility issues were also encountered for compounds **26a** and **26d**, which precluded  $\log P$  measurements. All experimental results are combined in Figure 20, where compounds **26a** and **26d** are positioned arbitrarily, based on the values recorded for the series of compounds **23x** and **24x**.

The  $\log P$  values measured for indole and 5-methoxyindole series **23x** and **24x**, respectively, reproduce the characteristic lipophilicity pattern displayed by *n*-propylbenzene (**20**) and its mono- and trifluoro derivatives **21** and **19**. These results also confirm the theoretical expectation that difluoro derivatives should be less lipophilic than trifluoro derivatives, and slightly more lipophilic than monofluoro derivatives.



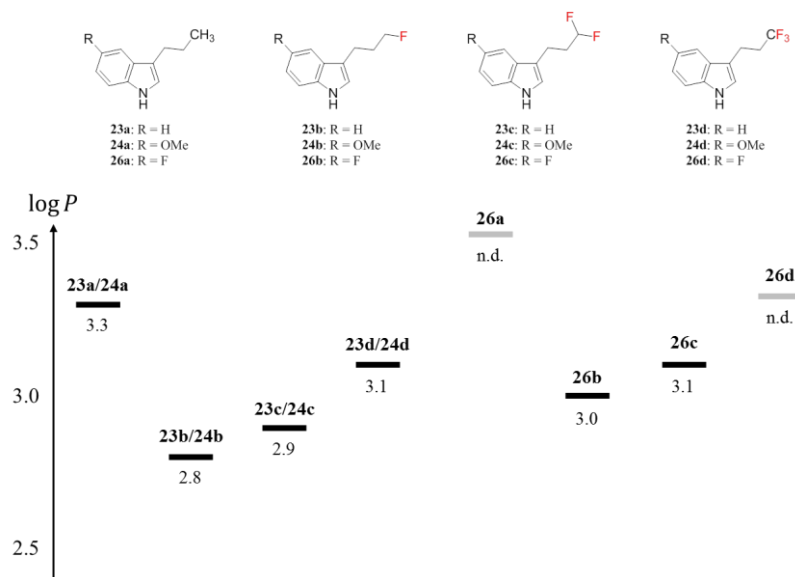


**Figure 20.** Lipophilicity measurements for the series of 3-propylindole model compounds **23x**, **24x** and **26x** ( $x = \mathbf{a-d}$ ; n.d. – not determined).

As anticipated, no  $\log P$  difference was noticed between the indole and 5-methoxyindole series **23x** and **24x**, thus confirming that a methoxy group grafted to an aromatic ring does not influence the resulting lipophilicity of a given compound.<sup>12</sup> By contrast, 5-fluoroindole derivatives **26b** and **26c** revealed the typical lipophilicity increase of +0.2  $\log P$  units compared to their respective analogs from series **23x** and **24x**. This observation is actually in line with literature data reported by Smart where it is shown that the introduction of fluorine atoms onto aromatic rings increases lipophilicity.<sup>12</sup>

Overall, these results are in nice agreement with the predictions made earlier and corroborate the previously documented lipophilicity trend of  $CH_3 > CF_3 \gg CH_2F \sim CHF_2$ . The next goal of this work was to study the relationship between lipophilicity and other pharmacological properties, with a particular emphasis on metabolic stability.

## 2.4.2 Metabolic Stability

### 2.4.2.1 Introduction

A frequently encountered issue in drug development is that many promising lead scaffolds do not reach the clinical phase because of their metabolic instability. Optimizing this key parameter has therefore become one of the main goals of modern drug design.<sup>87</sup> To provide metabolically robust molecules, medicinal chemists, together with pharmacologists, have extensively studied the biological processes at play in the body that account for the metabolic degradation of exogenous molecules, and the various ways to counter them.

The metabolic degradation of a molecule usually proceeds in three distinct phases. In phase I metabolism, a variety of enzymes acts to introduce reactive and polar groups into their substrates, i.e. the exogenous molecules. In subsequent phase II metabolism, these activated xenobiotics are conjugated with charged species such as glutathione in order to produce more polar metabolites that can no longer diffuse across membranes. After that, the conjugates and their metabolites can be excreted from the cells in phase III metabolism. To increase the metabolic stability of a molecule, medicinal chemists look for molecular structures able to resist phase I metabolism. However, to design relevant structural modifications able to play this role, it is crucial to understand the transformations that can occur at this initial stage of the metabolic pathway. Phase I metabolism comprises three main types of reactions that often occur in the liver, i.e. oxidation, reduction, and hydrolysis. Amongst those, one of the most common modifications is the hydroxylation catalyzed by the cytochrome P-450 (CYP) family of enzymes. In general, these enzymes act to incorporate an atom of oxygen into non-activated hydrocarbons, which implies that they have an evolutionary preference for lipophilic molecules.<sup>28</sup>

As seen earlier, the selective introduction of fluorine atoms has already been used to afford metabolically robust derivatives.<sup>6</sup> Although literature precedents have underlined the fact that fluorination induces electronic effects that impede oxidative metabolic pathways, no one has ever studied the correlation between the lipophilicity of fluorinated derivatives and their metabolic stability.<sup>52</sup> Indeed, despite the higher affinity of metabolizing enzymes for lipophilic molecules, there is still no clear rationale behind the fact that aromatic fluorination leads to more lipophilic derivatives that are also more metabolically robust.<sup>12</sup> It was therefore interesting to determine whether partially fluorinated saturated alkyl groups would behave differently, and thus follow a stability trend proportional to their measured lipophilicity values, i.e.  $CHF_2 \sim CH_2F \gg CF_3 > CH_3$ .

In order to mimic phase I metabolism, the model compounds were subjected to preparations of human liver microsomes. By measuring how much substrate remained in solution after incubation, the proportion that had been metabolized by the enzymes was deduced. This test yielded overall pseudo-1<sup>st</sup>-order decay constants ( $hCl_{int}$ ) that indicate at which rate the substrate is cleared from the solution depending on the amount of metabolizing enzymes present (for details about the procedure, see Experimental Section).

### 2.4.2.2 Results and Discussion

Unfortunately, as mentioned earlier, solubility issues were encountered for the 5-fluoroindole series of model compounds **25x** and **26x**, which precluded reliable measurements of metabolic stability. Nonetheless, in order to take this issue into account, it was decided to report the results recorded for these series separately from the others. Therefore, metabolic stability measurements in the human model ( $hCl_{int}$ ) restricted to series **23x** and **24x** are reported in Figure 21, where the missing value for compound **23b** is positioned arbitrarily to match the trend exhibited by series **24x**.

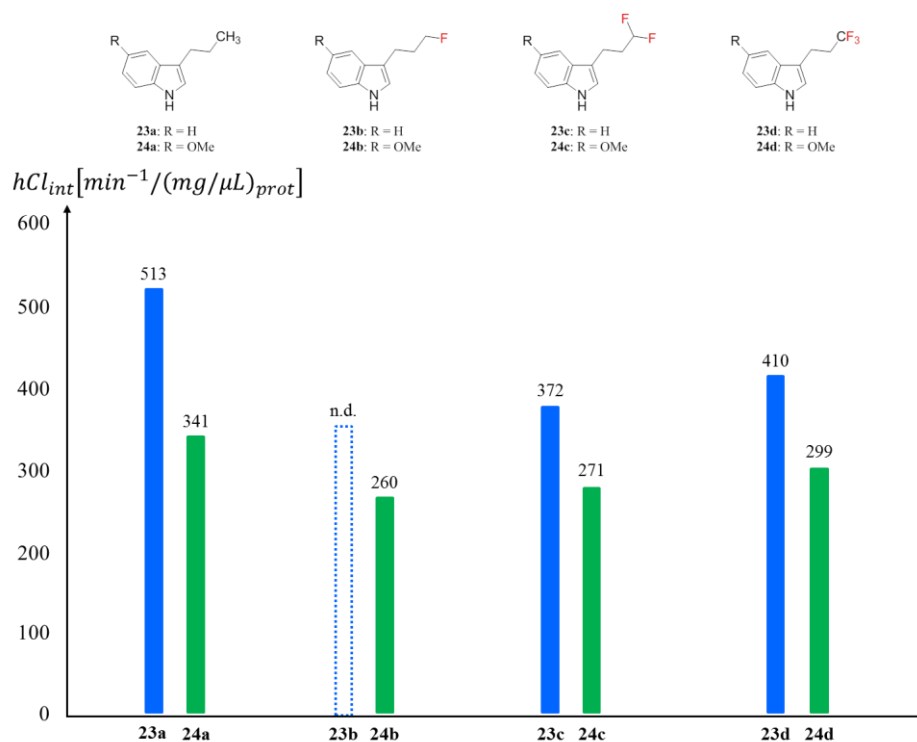


**Figure 21.** Metabolic stability profile obtained for the indole and 5-methoxyindole series of model compounds **23x** and **24x** ( $x = \mathbf{a-d}$ ; n.d. – not determined).

These experimental data suggested that, within each series of compounds (**23x**, **24x**), the clearance rate follows the same trend as the one shown in Figure 20 for lipophilicity. It was therefore tried to determine the correlation existing between these two parameters, which led to the results presented in Figure 22. It appears that both series of model compounds exhibit clearance rates that vary proportionally to lipophilicity, with good linear correlation coefficients. These results thus confirm the predicted stability trend based on lipophilicity, and underline that the metabolism of the partially fluorinated alkyl moieties tested in this study is mainly governed by their respective lipophilicity.

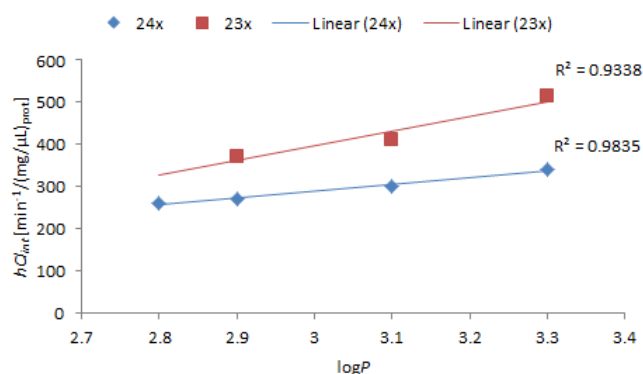


**Figure 22.** Correlation between  $\log P$  and  $hCl_{int}$  for the indole and 5-methoxyindole series of model compounds **23x** and **24x** ( $x = \mathbf{a-d}$ ).

Furthermore, it is worth noting that the introduction of a methoxy group on the indole nucleus results in a significant improvement of metabolic stability, regardless of the degree of terminal fluorination of the propyl moiety. Although this effect was expected, these results support the idea that a methoxyaryl group can enhance the metabolic stability of aromatic compounds without significantly increasing their lipophilicity.<sup>12</sup>

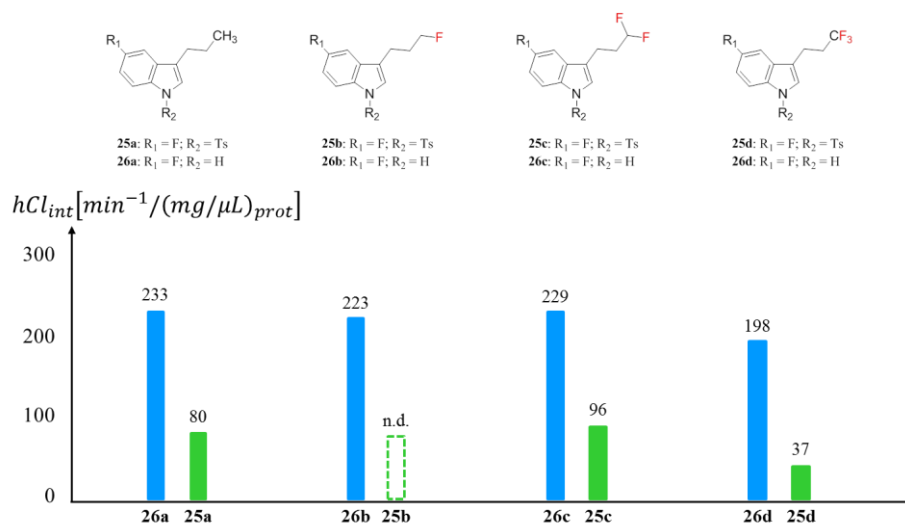


**Figure 23.** Metabolic stability profile obtained for the 5-fluoroindole series of model compounds **25x** and **26x** ( $x = \mathbf{a-d}$ ; n.d. – not determined).

Contrary to the previous series, experimental data on the metabolic stability of the 5-fluoroindole derivatives **25x** and **26x** did not exhibit any obvious trend, neither for the protected nor for the unprotected series of model compounds (Figure 23). Taking into account the problems encountered when these compounds were subjected to lipophilicity measurements, it was assumed that these results were most likely the reflection of a poor aqueous solubility. Unfortunately, this led us to disregard this set of inconclusive data.

## 2.5 Influence of Conformation on Polarity

### 2.5.1 Introduction

The model used to formulate the qualitative predictions for the lipophilicity trend of partially fluorinated 3-propylindole model compounds relied on key assumptions which fitted particularly well the *n*-propylbenzene case. Indeed, since benzene itself has no dipole moment by symmetry, it was surmised that the resulting dipole moment of a partially fluorinated *n*-propylbenzene could be approximated by the dipole moment of the sole propyl unit.

Although this approximation was reasonable for *n*-propylbenzene derivatives, its application to 3-propylindole derivatives appears arguable, even more so because the indole nucleus has an intrinsic dipole moment of 2.1 D,<sup>88</sup> pointing approximately from the nitrogen atom through the mid-point of C(4) and C(5). Also, since the total molecular dipole moment is a composite of the local dipole moments of the fluoropropyl unit and the indole nucleus, it may not reflect the characteristic variations of the fluoropropyl unit due to the different conformationally dependent vector superpositions.

It is therefore remarkable to realize *a posteriori* that, despite neglecting the conformational dependence of the total molecular dipole moment, the experimental observations on the lipophilicity and metabolic stability of 3-propylindole derivatives matched the predictions. In order to rationalize this phenomenon, a study was initiated aiming at probing the influence of conformation on the resulting polarity of partially fluorinated 3-propylindole derivatives.

### 2.5.2 Conformational Preference of 3-Substituted Indole Derivatives

The investigation started with a search in the Cambridge Structural Database (Version 5.34, November 2012) for 3-substituted indole derivatives lacking substituents at C(2) and C(4). Unfortunately, as one could have expected, it revealed little conformational preference in crystal structures for side chains at C(3), with representation by essentially in-plane to orthogonal orientations of a non-branched  $CH_2-CH_2-X$  substituent, *X* being any group (Figure 24).

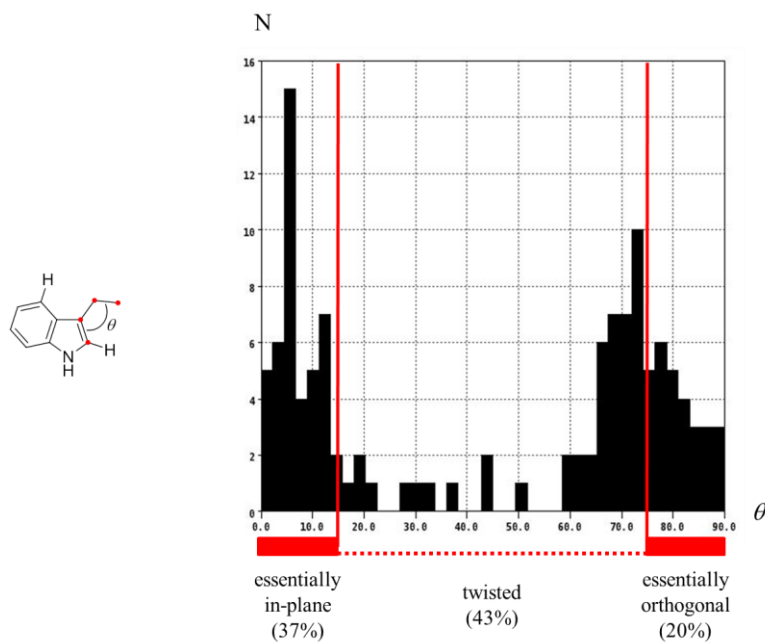


**Figure 24.** Conformational preference for side chains at C(3) for 3-substituted indole derivatives lacking substituents at C(2) and C(4) (CSD, Version 5.34, November 2012).  $\theta$  – dihedral angle formed by the side chains at C(3) and the indole plane. N – number of occurrences.

This statistical observation was in fact not supported by the molecular structures determined by X-ray crystal diffraction for tosyl-protected 5-fluoroindole derivatives **25x**. Indeed, as depicted in Figure 25, each compound presents a propyl chain adopting an essentially in-plane orientation with respect to the indole nucleus, and a remarkably staggered CCC backbone.

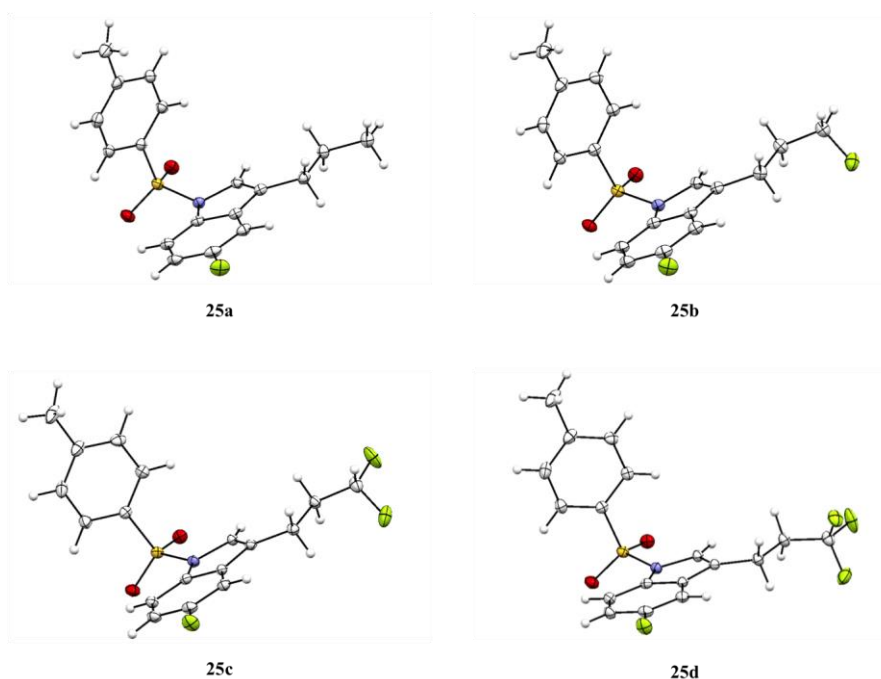


**Figure 25.** Molecular structures of tosyl-protected 5-fluoroindole derivatives **25x**, as determined by X-ray crystal diffraction ( $x = \mathbf{a-d}$ ).

Furthermore, the structure of compound **25b** reveals that the terminal  $CH_2F$  unit adopts a *gauche* conformation, which was measured to be preferred over the *trans* conformation in the gas phase (for 1-fluoropropane, Table 4). Also, in accordance with the calculations reported for 1,1-difluoropropane, compound **25c** confirms that the terminal  $CHF_2$  unit prefers to adopt the *trans-gauche* conformation over the *gauche-gauche* conformation. Taking into account the fact that the apparent conformational preference of compounds **25x** may result from interactions inherent to the solid state, such as  $\pi$ -stacking, short contacts, or even dipolar interactions, one could also expect different conformations to prevail in the solvated form.

In the end, these results suggested that any orientation of the side chain at C(3) would be a reasonable choice in view of *in silico* determination of molecular dipole moments in the gas phase. However, since properties relying on the aqueous solubility of our model compounds were measured, it was surmised that it would also be relevant to calculate their respective solvation energies in water. Thus, comparing these two key parameters could lead to valuable conclusions.

### 2.5.3 Calculation of Conformationally Dependent Dipole Moments

Calculations of the molecular dipole moments for compounds **23x**, assuming an orthogonal arrangement of the *n*-propyl side chain in an antiplanar conformation, but allowing for different staggered conformations of the terminal fluoromethyl or difluoromethyl groups in **23b** and **23c**, resulted in conformationally dependent molecular dipole moments (Figure 26).

The effect is very pronounced in the monofluorinated case **23b** where the local C–F bond moment can either positively or negatively superimpose with the inherent local dipole of the indole nucleus. For the difluoromethyl case **23c**, the effects are slightly attenuated. However, when estimating solvation energies based on the Poisson-Boltzman approximation<sup>89</sup> for a polar continuum of  $\epsilon = 80$  (water), the variations in dipole moments are largely mitigated.

### 2.5.4 Solvation Energy: Qualitative Approximation of Polarity

One would anticipate that for small compact molecules the solvation energies would correlate essentially with the magnitude of the total molecular dipole moment. For larger molecules, however, solvation energies result from the sum of many local interactions between surface charges and the polar environment.

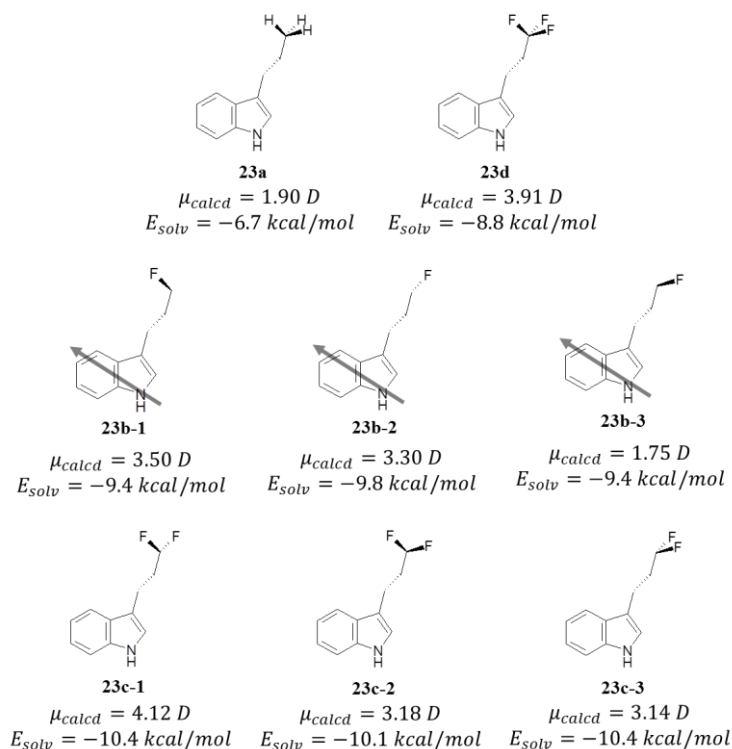


**Figure 26.** Calculated molecular dipole moments and solvation energies for model compounds **23x** ( $x = \mathbf{a-d}$ ). The dipole moment of the indole unit is inscribed as a gray vector to emphasize its superposition with the local dipole moments of the fluorinated methyl groups.

Therefore, even when the local dipole moment in the fluoropropyl side chain largely compensates the dipole moment of the indole unit (as in conformation **23b-3**), the partial solvation energies for the fluoropropyl group and the indole unit are essentially the same as in the conformation where their local dipole moments add up (as in conformation **23b-1**) or are essentially orthogonal to each other (as in **23b-2**). Indeed, the calculated solvation energies appear more properly to reflect the surface accessibility of the molecule to the polar environment. Thus, the two conformations **23b-1** and **23b-3** of the fluoropropyl group with the terminal fluorine substituent in the *endo* conformation (*gauche* to the CCC backbone), exhibit slightly less pronounced solvation interactions than the conformation **23b-2** in which the terminal fluorine group is *exo*-oriented (*trans* to the CCC backbone) and thus more exposed to solvent. A similar result is seen for difluoropropylindole **23c**. For this structure, two conformations **23c-1** and **23c-3**, each possessing one fluorine *exo* to the propane chain, exhibit similar and more pronounced solvation interactions than conformation **23c-2** with both fluorine atoms positioned *endo* to the propane chain. Overall, the estimated solvation energies then clearly enable some predictions to be made: 1) trifluoropropylindole derivative **23d** should be more polar than the parent 3-propylindole **23a**; 2) both monofluoro and difluoro derivatives, **23b** and **23c**, should be substantially more polar than **23a**.



### 2.5.5 Conclusion

To summarize, these theoretical predictions were in qualitative agreement with the  $\log P$  values measured for each of the three series we prepared, and implicitly suggested that the initial predictive model (Figure 17), based on molecular dipole moments, could not reliably account for the lipophilicity trend of more complex fluorinated molecules. On the contrary, calculations indicated that solvation energy is a key parameter that should be taken into account when approximating the influence of conformationally flexible, partially fluorinated alkyl scaffolds.

## 2.6 Study on the Polarity of Conformationally Restricted Model Compounds

### 2.6.1 The Cyclohexyl Ring: Conformational Lock and Molecular Spacer

Further to these initial experimental and theoretical observations, it became obvious that understanding the lipophilicity of partially fluorinated methyl groups borne by a conformationally flexible alkyl unit is a rather complex endeavour. Consequently, the possibility to design a set of model compounds that would allow us to gauge the effect of conformational flexibility on lipophilicity was investigated.

It was assumed that introducing a rigid linker separating the partially fluorinated methyl group further from the intrinsically polar indole moiety would both serve as conformational lock and molecular spacer. Therefore, a polarity-neutral spacer was needed, with a rigid conformation, and whose size would not generate too much steric hindrance. Under these conditions, the cyclohexyl ring was selected as it meets the previously mentioned requirements.

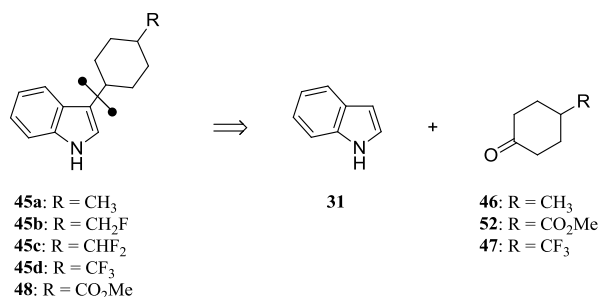
By introducing such a linker, it could be possible to verify if the observed lipophilicity trend for the series of 3-propylindole derivatives **23x**, **24x**, and **26x** would still hold if the partially fluorinated methyl unit were borne by a conformationally rigid moiety. It was also interesting to separate further the partially fluorinated methyl groups from the intrinsically polar indole nucleus, because it was surmised that a too close proximity between each polar moieties could result in an amplified compensation effect.

Despite these desired properties, it was also foreseen that using a cyclohexyl group would imply a major drawback that is a lipophilicity increase. Thus, solubility issues similar to the ones encountered earlier with model compounds **25x** and **26x** were expected, which might preclude direct lipophilicity measurements.

## 2.6.2 Synthesis of Cyclohexyl-Containing Indole Derivatives

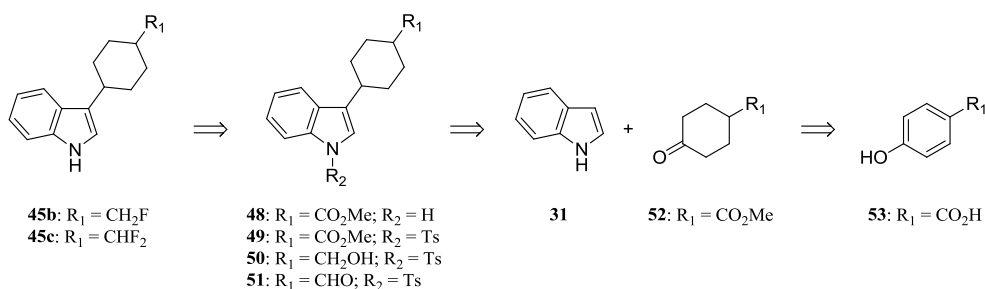
### 2.6.2.1 Retrosynthetic Analysis

The retrosynthetic analysis to access indole derivatives **45x** relied on the method developed by Rizzo *et al.* that describes the reductive coupling of indole with ketones.<sup>90</sup> Therefore, as depicted in Scheme 8, it was envisioned that compounds **45x** could be prepared from indole (**31**) and the appropriate 4-methylcyclohexanones.



**Scheme 8.** Key disconnection for the synthesis of model compounds **45x** (x = a–d).

However, since ketones **46** and **47** were commercially available whereas the monofluoro and difluoro analogs were not, a modified strategy was planned to synthesize mono- and difluorinated targets **45b** and **45c** (Scheme 9), which was based on the previously described late stage fluorination approach.



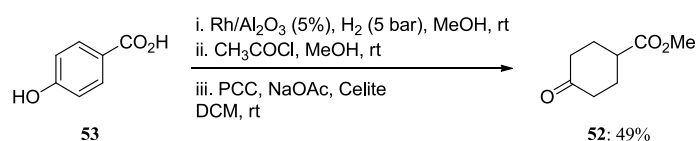
**Scheme 9.** Retrosynthesis of mono- and difluorinated targets **45b** and **45c**.

Therefore, compounds **45b** and **45c** could be accessed from ester **48**, which could be obtained by coupling indole (**31**) and keto ester **52**. The latter could then be synthesized from commercially available 4-hydroxybenzoic acid (**53**).

### 2.6.2.2 Synthetic Access

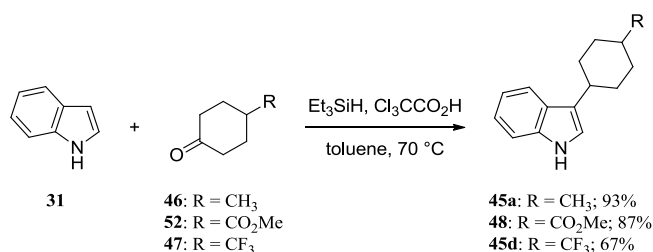
Since cyclohexanones **46** and **47** were commercially available, the synthesis of ketone **52** was required, which was achieved in three steps (Scheme 10). Thus, 4-hydroxybenzoic acid (**53**) was subjected to rhodium-catalyzed hydrogenation conditions, thereby affording the fully reduced acid, which was then selectively esterified with acetyl chloride in methanol. The

resulting methyl ester was eventually oxidized to cyclohexanone **52** with pyridinium chlorochromate.



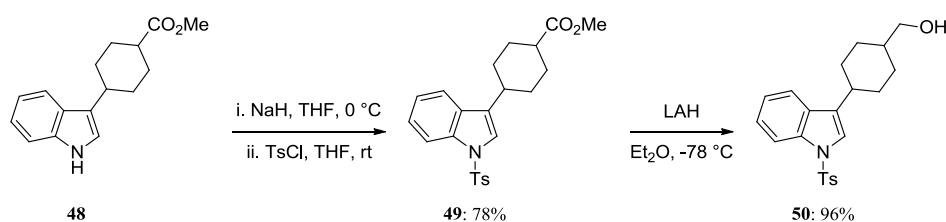
**Scheme 10.** Three-step synthesis of ketone **52**.

Cyclohexanones **46**, **47**, and **52** were then separately reacted with indole (**31**) in presence of triethylsilane and trichloroacetic acid in toluene at 70 °C,<sup>90</sup> thus affording respectively coupled products **45a**, **45d**, and **48** in good to excellent yields (Scheme 11).



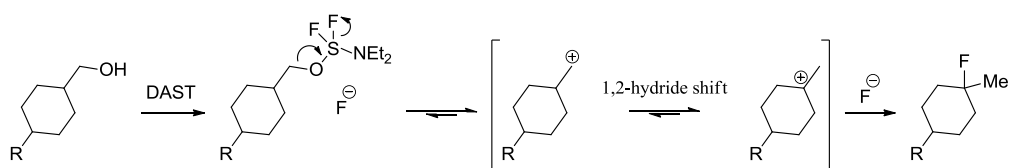
**Scheme 11.** Reductive alkylation reaction leading to coupled products **45a**, **45d**, and **48**.

In order to avoid any undesired side-reactions related to the unprotected indole moiety in a future step, indole **48** was protected with a tosyl group (Scheme 12).<sup>91</sup> Further reduction of ester **49** with LAH at low temperature then afforded alcohol **50** quantitatively.<sup>92</sup>



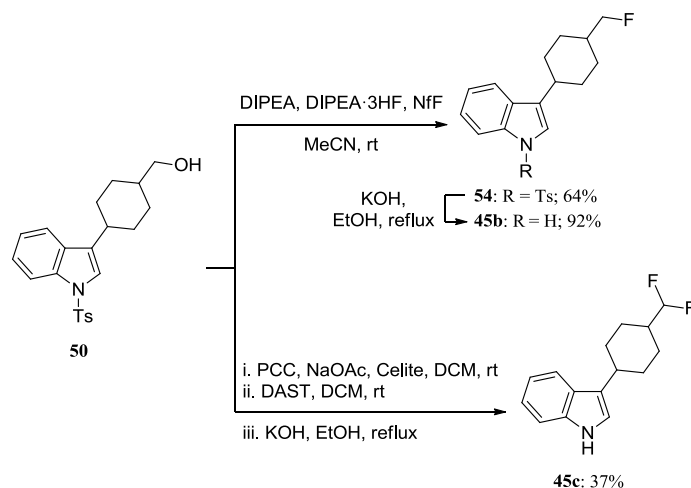
**Scheme 12.** Synthesis of alcohol **50**.

It was initially planned to access compounds **45b** and **45c** from alcohol **50**. However, reaction of the latter with DAST under standard conditions did not afford the expected product. Instead, a rearranged product featuring a tertiary fluorine atom was isolated. Since it has been previously reported that fluorination with DAST could proceed via S<sub>N</sub>1 mechanism,<sup>72</sup> it was assumed that the formation of such a rearranged product could result from a 1,2-hydride shift, followed by fluorination of the more stable tertiary carbocation (Scheme 13).



**Scheme 13.** Plausible fluorination mechanism.

To circumvent this issue, the milder deoxofluorination conditions reported by Yin *et al.*<sup>80</sup> were employed. Then, treatment of alcohol **50** with DIPEA, DIPEA·3HF, and NfF in acetonitrile cleanly yielded primary fluoride **54**. The latter was further deprotected with potassium hydroxide in boiling ethanol to afford monofluorinated target **45b** in excellent yield.



**Scheme 14.** Divergent synthesis to mono- and difluorinated targets **45b** and **45c**.

On the other hand, alcohol **50** was converted into difluorinated target **45c** after a three-step sequence consisting in PCC oxidation,<sup>83</sup> followed by DAST deoxofluorination,<sup>84</sup> and concluded with potassium hydroxide deprotection.<sup>81</sup>

Compounds **45x** were synthesized as *cis/trans* mixtures that were further separated by chiral preparative chromatography (for details, see Experimental Section), thus allowing the isolation of all stereoisomers as pure crystalline compounds. The assignment of *cis*- and *trans*-stereochemistry for compounds **45x** was then based on X-ray crystal structure analysis.

### 2.6.3 Lipophilicity Measurements

With the set of model compounds **45x** in hand, the measurement of their log *P* values was attempted following a standard procedure (for details, see Experimental Section). Unfortunately, as expected, these cyclohexyl derivatives proved to be insufficiently soluble for direct log *P* measurements. However, their relative polarities could be measured

chromatographically<sup>49</sup> in various acetonitrile/water mixtures (for details, see Experimental Section). Thus, the results obtained for capacity factors  $\log k_{60}$ ,  $\log k_{50}$ , and  $\log k_{40}$  for, respectively, 60%/vol, 50%/vol, and 40%/vol of acetonitrile are presented in Figure 27.

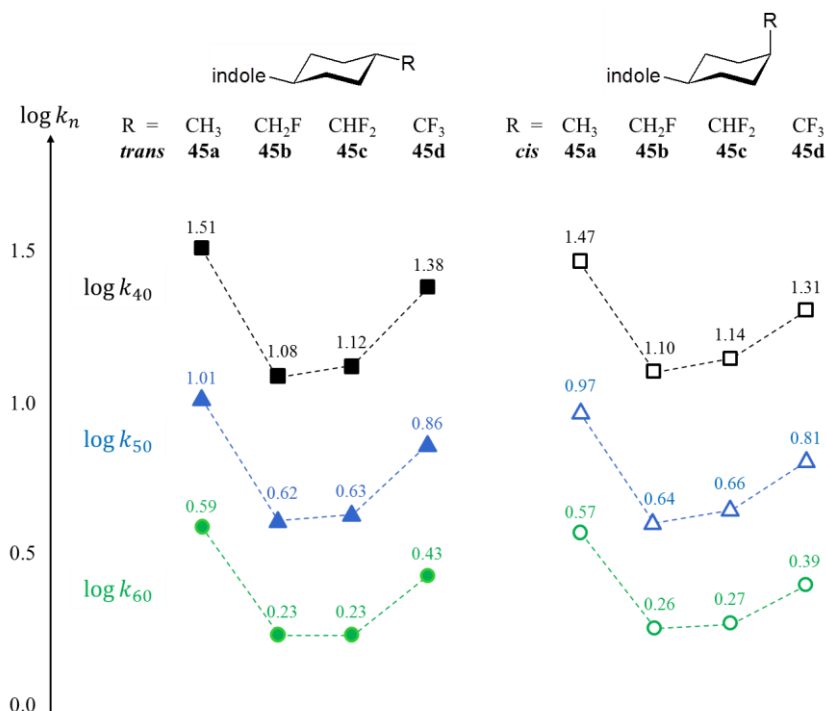


**Figure 27.** Experimental chromatographic capacity factors ( $\log k_n$ ) for *cis*- and *trans*-3-(4-methylcyclohexyl)indole derivatives **45x** at three different isocratic acetonitrile/water mixtures (**x = a–d**).

In principle,  $\log k_w$  for 0%/vol of acetonitrile could then be obtained by extrapolation. Although the experimental data points have been determined relatively accurately, they are distant from the 0% extrapolation limit, resulting in relatively large standard deviations for  $\log k_w$ , thus rendering the latter statistically less meaningful.

Gratifyingly, at all concentrations of acetonitrile the relative polarities displayed the same pattern as already noted for the partially fluorinated 3-propylindole derivatives **23x** and **24x**. Thus, trifluoromethyl derivative **45d** is slightly more lipophilic than the non-fluorinated parent **45a**; monofluoro- and difluoromethyl derivatives **45b** and **45c** are significantly more lipophilic than trifluoro derivative **45d**. Remarkably, this was verified for both the *trans*-series, with the methyl group in equatorial position, and the *cis*-series, where the methyl group is axial.

These results were in accordance with our initial findings for 3-propylindole derivatives **23x** and **24x**, thus confirming that the observed lipophilicity trend persists regardless of the

conformational flexibility of the saturated alkyl chain bearing the partially fluorinated methyl group. Also, it appeared that the direct vicinity of a polar moiety, like the indole nucleus, does not seem to influence dramatically the resulting lipophilicity pattern imparted by the partially fluorinated scaffold.

In view of providing a rational explanation to the trend displayed by the cyclohexyl-containing series of compounds **45x**, it was decided to study their basic physicochemical properties, starting with structural considerations.

### 2.6.4 X-ray Crystal Structures

The X-ray crystal structure analyses obtained for the crystalline series of 3-(4-methylcyclohexyl)indole derivatives **45x** not only confirmed the stereochemical assignments, but also revealed remarkable structural information. Thus, due to the paucity of experimental data about the size of a  $CF_3$  group, it is of particular interest to first examine the structure of *cis*-**45d**, relative to its non-fluorinated parent **45a**, as well as their corresponding *trans*-counterparts (Figure 28).

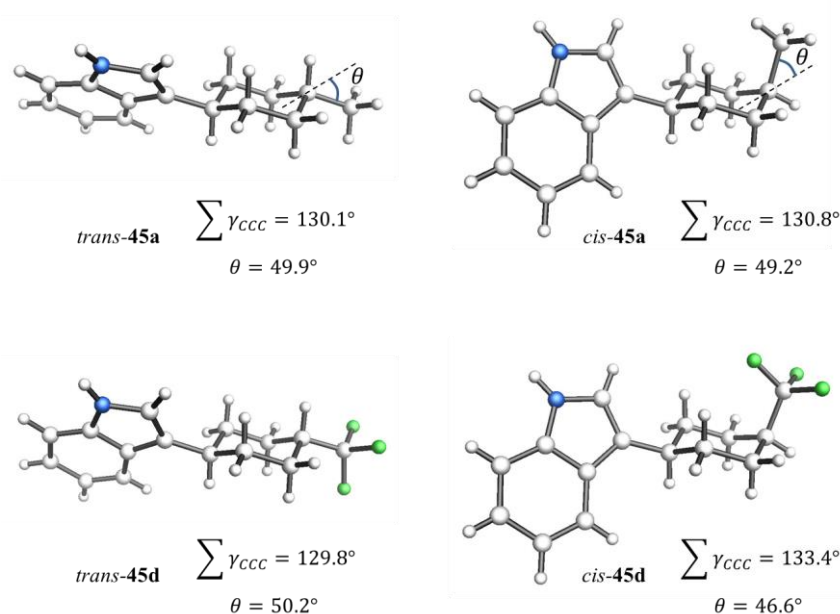


**Figure 28.** Molecular structures of *cis*- and *trans*-derivatives **45a** and **45d**, as determined by X-ray crystal diffraction. For each structure, the calculated sum of the three CCC valence angles,  $\gamma_{CCC}$ , at C(4) and the out-of-plane angle  $\theta$  are given as measures of deviations from exact tetrahedral geometry.

As a measure of steric congestion, the local deformations from ideal tetrahedral geometries may be taken, as measured by the sum of *endo*- and *exo*-cyclic CCC valence angles at C(4) as well as the out-of-plane angle  $\theta$ , measured between the *exo*-cyclic C–C bond and the bisector

of the *endo*-cyclic CCC angle. For idealized tetrahedral geometries, these two parameters take values of  $328.4^\circ$  and  $54.7^\circ$ , respectively.

In the case of compound **45a**, X-ray crystal structures indicated that an axial  $CH_3$  group results in some flattening of the local tetrahedral geometry at C(4). Interestingly a very similar flattening effect was also observed for the equatorial  $CH_3$  group, although this was less obvious from visual inspection. The same effect is more evident in the axial position by the conspicuous outward splaying of the  $CH_3$  group, or by its non-parallel arrangement with respect to the axial C–H bonds at C(2) and C(6).

Turning to the corresponding  $CF_3$  derivatives **45d**, X-ray crystal structures showed that the geometrical deformations for the equatorial  $CF_3$  group are essentially the same as those for the  $CH_3$  group. The axial  $CF_3$  group, on the other hand, enforces a significantly larger deformation. However, the effect was found to be less than what might have been anticipated, as the out-of-plane angle for the  $CF_3$  group is diminished by only  $2.6^\circ$  further from that of the axial  $CH_3$  group. In fact, the intramolecular non-bonded H $\cdots$ H distances between  $CH_3$  and the axial H-atoms at C(2) and C(6) in *cis*-**45a** are  $2.4 \text{ \AA}$ , thus corresponding to twice the van der Waals radius of covalent H-atoms. Therefore, the tetrahedral geometry at C(4) is deformed to the extent so as to place the axial  $CH_3$  group at van der Waals contact distances to the axial C–H's, just avoiding non-bonded repulsions.

For the axial  $CF_3$  group in *cis*-**45d**, the non-bonded H $\cdots$ F contact distances are  $2.6 \text{ \AA}$ , i.e. slightly less than the van der Waals contact distance of  $2.67 \text{ \AA}$ , using the Bondi radius of  $1.47 \text{ \AA}$  for covalent fluorine. This result either indicates that the deformation at C(4) and the non-bonded contact distances are at compromise values, thus minimizing overall molecular strain, or that some attractive forces between oppositely charged H and F atoms operate, thus enabling closer contacts than given by the sum of the van der Waals radii.

This is further illustrated by monofluorinated compounds *cis*-**45b** and *trans*-**45b** (Figure 29). In the case of equatorial *trans*-**45b**, the fluorine atom takes a position corresponding to the favored *endo*-1-fluoropropane conformation. In this arrangement, the polar C–F bond could benefit twice from 1,3-antiparallel dipolar interactions with the axial C–H bonds at C(3) and C(5).

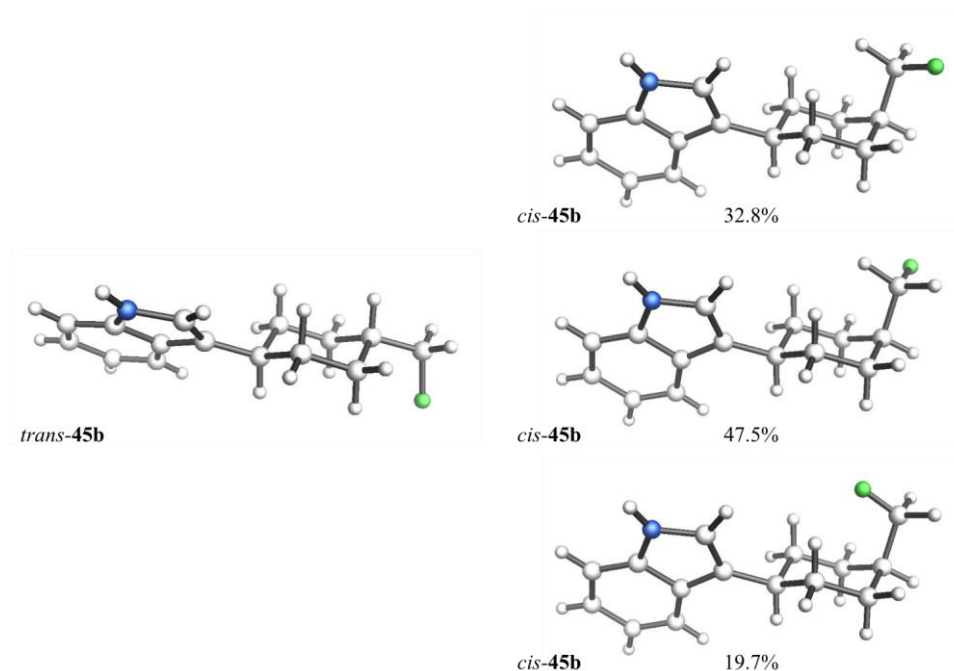


**Figure 29.** Molecular structures of *cis*- and *trans*-45b, as determined by X-ray crystal diffraction.

By contrast, the crystal structure of the *cis*-isomer showed conformational disorder, with the single fluorine atom occupying all three possible staggered conformations. Surprisingly, the *endo*-position with the fluorine atom pointing towards the axial H atoms at C(2) and C(6) is substantially populated (ca. 20%). The non-bonded H $\cdots$ F contact distances are ca. 2.5 Å, below van der Waals contact distances.

It should be pointed out that the positions of the hydrogen atoms are modeled, rather than rigorously determined experimentally. Therefore, some small displacement of the H atoms may be present, alleviating too close contacts to the fluorine. Nevertheless, the substantial population of the *endo*-conformation appeared to support the notion of weak stabilizing H $\cdots$ F interactions with the axial H atoms.

A similar confirmation for potentially favorable 1,5-non-bonded H $\cdots$ F interactions was obtained from the X-ray structures of difluorinated derivatives *cis*-45c and *trans*-45c (Figure 30). While equatorial isomer *trans*-45c crystallized in one single conformation with the fluorine atoms in the *endo*- and *exo*-positions, thus maximizing the number of 1,3-antiparallel dipolar interactions with C–H bonds, axial isomer *cis*-45c exhibited structural disorder in the crystal.



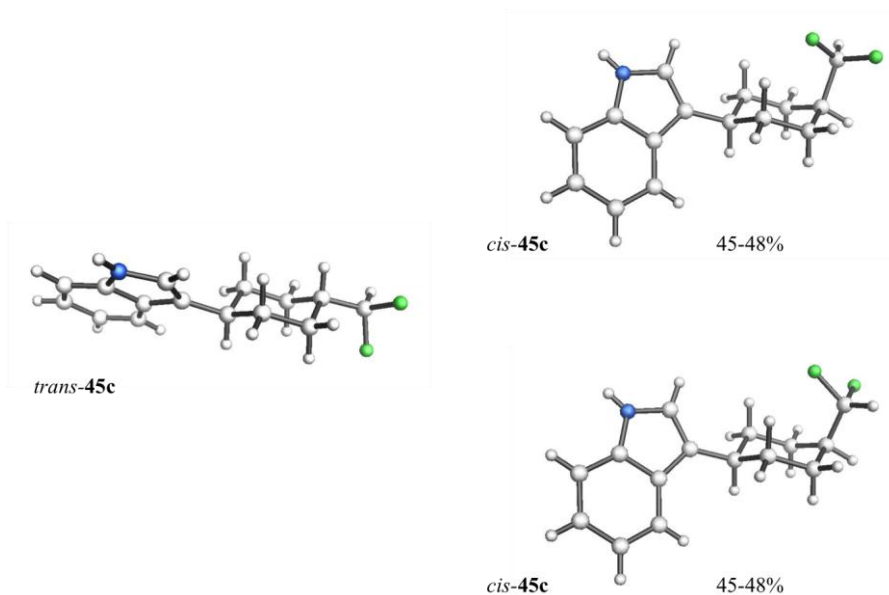


**Figure 30.** Molecular structures of *cis*- and *trans*-**45c**, as determined by X-ray crystal diffraction.

It is however remarkable to observe that each of the two dominant conformations, representing a total occupancy of about 90–95%, contains one fluorine atom in the *exo*-position, whereas the other fluorine atom takes the *endo*-position in close contact to the axial H-atoms at C(2) and C(6). The alternative conformation with both fluorine atoms in the unencumbered *exo*-positions is only marginally populated. Interestingly, the exocyclic C–C bond axis in *cis*-**45c** for the two dominant conformations is nicely superimposable to the one for the axial  $CF_3$  group in *cis*-**45d**.

### 2.6.5 Theoretical Examination: 1,4-Dimethylcyclohexane

In view of the conformational aspects revealed by the X-ray crystal structures of indole derivatives **45x**, a theoretical examination of valence geometries, energy differences, dipole moments, and solvation energies for such cyclohexyl derivatives would provide valuable information that could help rationalizing the polarity trend observed experimentally.

In order to facilitate the calculations, *cis*- and *trans*-1,4-dimethylcyclohexyl derivatives **55–58** (Figure 31) were chosen as simplified models of the corresponding indole derivatives **45x**. All calculations were performed with the B3LYP density functional method available in Jaguar using a standard polarized double-zeta basis set with coupled-cluster correlation (for details about calculations, see Experimental Section). Relevant results are summarized in Table 5.

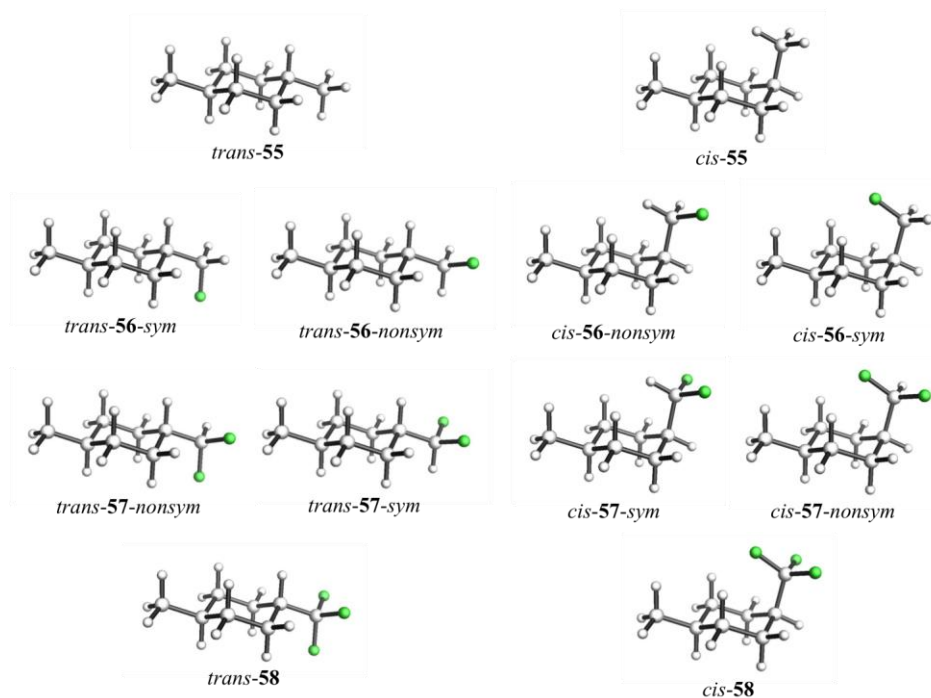


**Figure 31.** Molecular structures of 1,4-dimethylcyclohexanes **55–58** as prototypical models of the corresponding 1-(3-indolyl)-4-methylcyclohexanes **45x** with different degrees of fluorination and staggered conformations of the 4-methyl group.

While B3LYP overestimates slightly the axial-equatorial energy difference for a  $CH_3$  group attached to cyclohexane (2.2 kcal/mol compared to 1.74 kcal/mol in  $CDCl_3$  solution<sup>93</sup>), it correctly predicts that a  $CF_3$  group does not exhibit a dramatically larger axial-equatorial energy difference (2.5 kcal/mol compared to 2.3–2.4 kcal/mol experimentally<sup>94</sup>), and that both the  $CH_2F$  and  $CHF_2$  groups are comparable to the  $CH_3$  group (experimental  $A$ -values for  $CH_2F$  and  $CHF_2$ : 1.6 and 1.8 kcal/mol, respectively<sup>95</sup>).

The characteristic valence deformations at C(4), identified in the X-ray structures of *cis*- and *trans*-**45a** as well as *cis*- and *trans*-**45d** (Figure 28), were found to be identical to the calculated ones. In particular, it was noted that the slight flattening of the tetrahedral arrangement is similar for the equatorial and axial  $CH_3$  group, as well as the equatorial  $CF_3$  group, and in agreement with those seen in the crystal structures. Only the axial  $CF_3$  group is predicted to induce a more pronounced, albeit moderate, deformation with a further splaying out of the  $CF_3$  group by ca.  $2^\circ$  compared to the  $CH_3$  group, in excellent agreement with experiment.

The amount of valence deformations calculated for the  $CH_2F$  and  $CHF_2$  groups is similar to those of the  $CH_3$  group, both in equatorial and axial positions, as long as the fluorine atoms are placed in *exo*-positions. However, for the alternative conformations of the  $CH_2F$  and

$CHF_2$  groups, in which one fluorine atom occupies the *endo*-position, the corresponding valence deformations are consistently similar to those calculated and observed for the  $CF_3$  group, in which always one fluorine must be *endo*.

**Table 5.** B3LYP/cc-pVDZ++ calculations on *cis*- and *trans*-1,4-dimethylcyclohexanes **55–58** with varying degrees of fluorination at the C(4) methyl group.

Compound	Arrangement of 4-methyl group	Conformation of C(4) methyl group	$\sum \gamma_{CCC}$ at C(4)	Out-of-plane angle at C(4)	$\Delta E$ (kcal/mol) (g-phase)	$\Delta E_{solv}$ (kcal/mol)	$\mu$ (D) scaled B3LYP
<i>trans</i> - <b>55</b>	4- $CH_3$ eq	staggered	333.8°	49.5°	0	2.2	0
<i>cis</i> - <b>55</b>	4- $CH_3$ ax	staggered	334.8°	48.2°	2.2	2.3	0.19
<i>trans</i> - <b>56</b>	4- $CH_2F$ eq	symmetrical (C-F <i>endo</i> )	335.8°	47.7°	0.1	-0.4	1.68
<i>trans</i> - <b>56</b>	4- $CH_2F$ eq	nonsymmetrical (C-F <i>exo</i> )	333.1°	50.5°	0	-0.6	1.95
<i>cis</i> - <b>56</b>	4- $CH_2F$ ax	symmetrical (C-F <i>endo</i> )	338.8°	44.3°	2.9	0.1	1.76
<i>cis</i> - <b>56</b>	4- $CH_2F$ ax	nonsymmetrical (C-F <i>exo</i> )	334.4°	49.1°	2.1	-0.6	1.95
<i>trans</i> - <b>57</b>	4- $CHF_2$ eq	symmetrical ( $CF_2$ <i>exo-exo</i> )	332.6°	51.1°	0	-1.4	2.52
<i>trans</i> - <b>57</b>	4- $CHF_2$ eq	nonsymmetrical ( $CF_2$ <i>endo-exo</i> )	335.0°	48.6°	0.2	-1.3	2.28
<i>cis</i> - <b>57</b>	4- $CHF_2$ ax	symmetrical ( $CF_2$ <i>exo-exo</i> )	334.2°	49.2°	2.1	-1.3	2.54
<i>cis</i> - <b>57</b>	4- $CHF_2$ ax	nonsymmetrical ( $CF_2$ <i>endo-exo</i> )	337.9°	45.6°	2.9	-1.0	2.18
<i>trans</i> - <b>58</b>	4- $CF_3$ eq	staggered	334.4°	49.3°	0	-0.1	2.68
<i>cis</i> - <b>58</b>	4- $CF_3$ ax	staggered	337.1°	46.3°	2.5	0.1	2.49

The computed dipole moments reflect qualitatively the trends already established by the prototypical calculations for 1-fluoro-, 1,1-difluoro-, and 1,1,1-trifluoropropane (see Table 4).

Thus, in all cases the conformations with a fluorine atom in *endo*-position (*gauche* to the CCC backbone) exhibit a reduced dipole moment (ca. 10%) compared to that of the conformation with an *exo*-fluorine atom.

Interestingly, the patterns of computed dipole moments are generally the same for either equatorial or axial arrangements of the  $CH_2F$  or  $CHF_2$  groups, and only for the  $CF_3$  group a smaller dipole moment (ca. 7%) is obtained for the axial compared to the equatorial position. It is then not surprising that the Poisson-Boltzmann-estimated solvation energies in water are similar for corresponding axial/equatorial molecular pairs and that, within a given pair, the solvation energies display a distinctive conformational dependence, reflecting more on the degree of shielding or exposure of the polar fluorine atoms than on the variation of molecular dipole moments.

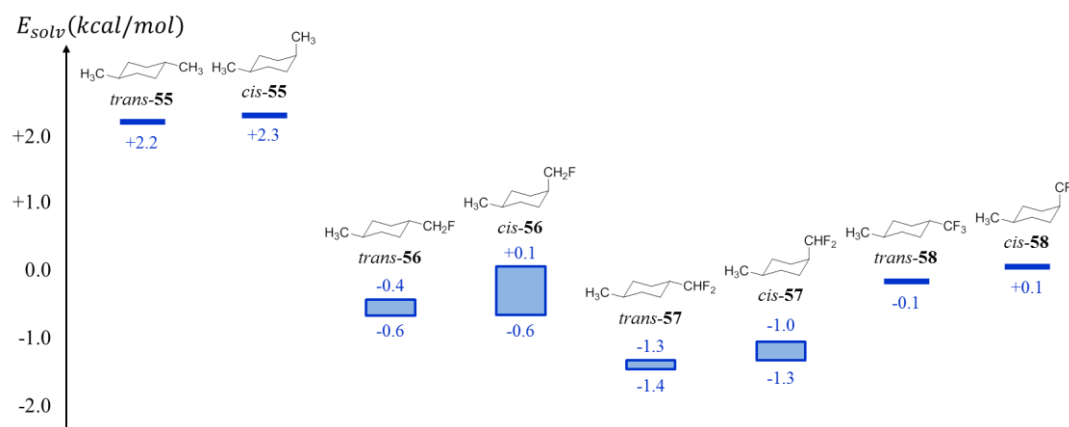


**Figure 32.** Polarity trend deduced from the computed solvation energy values for the model series of compounds **55–58**.

The polarity pattern deduced from computed solvation energies for the model series of compounds **55–58** is remarkably similar to the one obtained for the indole series **45x**, where the indole unit in place of a  $CH_3$  group contributes to a constant solvation energy of ca. -5.5 kcal/mol (Figure 32). Also, and quite consistently, a distinct conformational dependence of the solvation energy was noted in both cases of  $CH_2F$  and  $CHF_2$  groups (Figure 33).

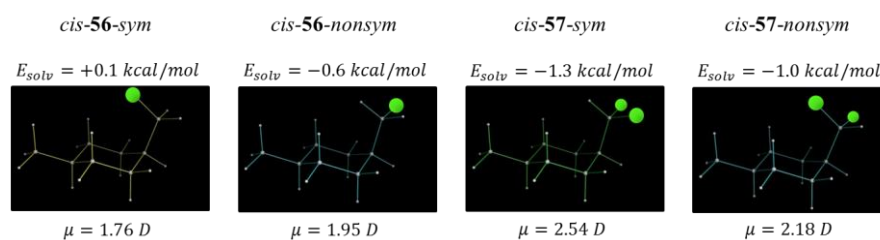


**Figure 33.** Conformational dependence of solvation energy and dipole moment for *cis*-**56** and *cis*-**57** model compounds.

The effect is most pronounced for the  $CH_2F$  group in the axial position, where the fluorine in the *endo*-position is significantly shielded by the axial H atoms at C(2) and C(6). Hence, both the mono- and difluoromethyl groups may not only impart higher polarity to a given molecule, but also, as a consequence of their axially non-isotropic nature, may be able to modulate molecular polarity by conformational adjustment, thus allowing a molecule to adapt to changing local environments.

## 2.7 Conclusion

In conclusion, 3-substituted indole derivatives have been synthesized, carrying either a propyl or the larger 4-methylcyclohexyl group as model systems, to study the effects of different degrees of fluorination of the terminal methyl group. The lipophilicity trend of  $CH_3 > CF_3 \gg CH_2F \sim CHF_2$ , already seen in part for *n*-propylbenzene, was generally confirmed, but it was also revealed that this trend cannot only rely on molecular dipole moments.

It has been shown in this regard that computed solvation energies represent a valuable predictive tool that conveniently complements the basic polarity analysis based on vector analysis, especially for conformationally flexible partially fluorinated moieties. Furthermore, the impact of fluorinated *n*-propyl building blocks on metabolic stability has been documented, thus bringing to light a remarkable, albeit expected, correlation with the measured lipophilicity values.

The crystal structure analyses of all equatorial and axial isomers of 1-indolyl-4-methylcyclohexanes with varying degrees of fluorination of the 4-methyl group revealed remarkably consistent patterns of relatively modest valence angle deformations at the tertiary C(4) atom. Furthermore, both axial isomers of the monofluoro and difluoro derivatives exhibited disorder in their respective crystals, providing valuable information about conformational flexibility of these groups, with surprisingly high populations of conformations with a fluorine atom in a shielded *endo*-position.

Finally, computational analyses suggested the possibility of substantial modulation of polarity by conformational adaptation of the axially non-isotropic  $CH_2F$  or  $CHF_2$  groups, which distinguishes these two groups from their axially isotropic  $CH_3$  or  $CF_3$  counterparts, and makes them particularly interesting modules for molecular design.



## 3 Vicinal and Multi-Vicinal Fluoroalkyl Groups

### 3.1 Introduction

The previous investigation on the polarity of partially fluorinated methyl groups extensively confirmed that the resulting lipophilicity of such saturated alkyl units essentially stems from the combination of two antagonistic parameters, namely polarity and volume. Based on this principle, it was surmised that the lipophilicity-lowering effect imparted by a partially fluorinated alkyl moiety could be maximized if one was able to enhance the polarity of a given unit without engendering a volume increase.

In this regard, the *gem*-difluoromethyl case was of particular interest for two main reasons that shall be recalled. First, the volume increase induced by the  $H \rightarrow F$  atom exchange ( $2 \Delta V_{H/F}$ ) is at the midpoint between the mono- and trifluoro units. Second, the vector addition of the dipole moments ascribed to each C–F bond results in a substantially bigger dipole moment than in the mono- or trifluoro cases. The combination of these effects resulted in the lipophilicity trend highlighted in the previous chapter ( $CH_3 > CF_3 \gg CH_2F \sim CHF_2$ ). Based on these facts, it was tried to imagine how two fluorine atoms could be combined along an alkyl chain to afford a higher polarity than in the *gem*-difluoromethyl case. The solution to this problem resided in the way fluorine atoms would be distributed on the alkyl chain.

Due to the fluorine *gauche* effect, it has been shown that the dihedral angle resulting from the preferred *gauche* arrangement of two vicinal fluorine atoms<sup>96</sup> is significantly smaller than for geminal ones.<sup>65</sup> Therefore, a simple vector addition applied to these respective cases suggested *a priori* that the dipole moment resulting from the vicinal arrangement of two fluorine atoms should be larger than for geminal ones. Then, assuming that the volume effect resulting from a *vic*-difluoroethyl unit is similar, if not identical, to a *gem*-difluoro analog, the former were expected to impart a marked lipophilicity decrease compared to the latter.

From this assumption, a follow-up study was initiated aiming at gaining insight into the effect on polarity of the vicinal arrangement of fluorine atoms in small saturated alkyl units.

## 3.2 Study on the Polarity of Vicinal and Multi-Vicinal Fluoroalkyl Groups

### 3.2.1 Molecular Dipole Moment

#### 3.2.1.1 Introduction

Following an approach similar to the one employed in the previous chapter, the properties that might arise from a vicinal arrangement of fluorine atoms were initially studied through vector analysis. Although it has already been shown that these simple considerations might not accurately reproduce *ab initio* calculations, their usefulness in qualitative predictions was acknowledged. Thus, in view of comparing the *vic*-difluoro to the *gem*-difluoro motif, the simplest alkyl moiety was first considered, i.e. ethane.

#### 3.2.1.2 Vector Analysis

Under the same key assumptions as stated in the previous chapter, it was noted that the two bond dipole moments ( $\mu_{CF}$ ) ascribed to the geminal C–F bonds sum to afford a dipole moment of approximately  $1.16 \mu_{CF}$  (Figure 34, top). Likewise, when the two vicinal fluorine atoms adopt a *gauche* conformation, the corresponding bond dipole moments combine to furnish a net dipole moment of ca.  $1.63 \mu_{CF}$  (Figure 34, bottom). As a result, calculations predicted a ca. 40% polarity increase from *gem*- to *vic*-difluoroethane.

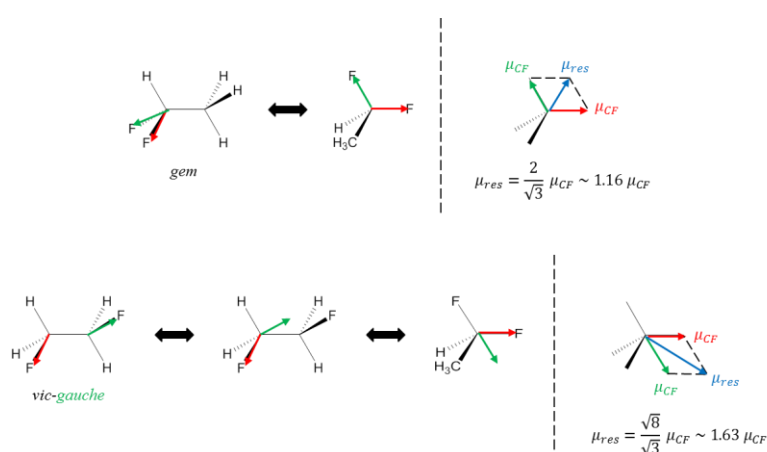


**Figure 34.** Vector analysis comparing the resulting dipole moments ( $\mu_{res}$ ) of *gem*- and *vic*-difluoroethane.

Because the initial assumptions neglected the fact that fluorinated molecules do not strictly adopt the geometry of simple hydrocarbons, the polarity increase determined by this simple means was likely to differ from more realistic models based on DFT calculations. This suggested to pursue the investigation by examining calculated gas phase dipole moments.



### 3.2.1.3 Calculated Gas Phase Dipole Moments

Unfortunately, at the time of this study, no experimental data were reported for the fluorinated alkyl groups of interest. Therefore, reliably computed dipole moments in the gas phase were considered (for details about calculations, see Experimental Section). The results obtained underline the fact that the *gauche* conformation of *vic*-difluoroethane largely prevails in the gas phase over the *trans* conformation by 1.3 kcal/mol (Figure 35, top). More importantly, the *gauche* conformation is anticipated to display a marked polarity increase (ca. 20%) compared to *gem*-difluoroethane. This result taking into account the conformational specificities of fluorinated molecules is in fair agreement with the initial estimate based on vector analysis.

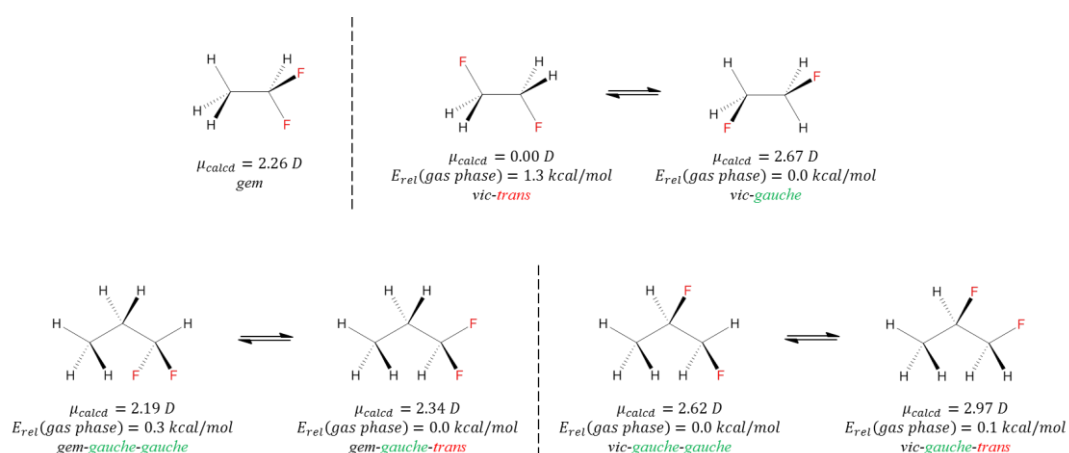


**Figure 35.** Computed gas phase dipole moments ( $\mu_{calcd}$ ) for *gem*- and *vic*-difluoroalkyl groups (ethane or propane). Relative energies calculated in the gas phase ( $E_{rel}$ ) are also provided for each conformation of the same compound.

Moving on to the propane case (Figure 35, bottom), it was noticed that both *gem*- and *vic*-difluoropropane exhibit more than one possible conformation, each of them having significantly different dipole moments (the *trans* conformation of *vic*-difluoropropane has been omitted for clarity). Also, it appears that the energy difference between *gauche-gauche* (*gg*) and *gauche-trans* (*gt*) conformations in the gas phase is small, which suggests that both conformations may coexist in equilibrium by significant amounts. This observation implies that the polarity increase from *gem*- to *vic*-difluoropropane could vary between 12 and 35%, depending on the adopted conformation. Therefore, such variability makes it difficult to anticipate with certainty the real effect that the *vic*-difluoro pattern may have on the resulting polarity.

### 3.2.1.4 Extrapolated Lipophilicity Trend

With these computed values in hand, it was attempted to predict the impact on lipophilicity of the *vic*-difluoropropyl moiety. Hence, based on the *n*-propylbenzene model (Figure 17), and considering the two *gauche* conformations of *vic*-difluoropropane as isoenergetic, it was calculated that the log *P* value of compound **59** could vary between 2.9 and 2.7 (Figure 36). The latter prediction supports the idea that a *vic*-difluoropropyl moiety might impart a substantial polarity increase, which could further translate into lower lipophilicity.

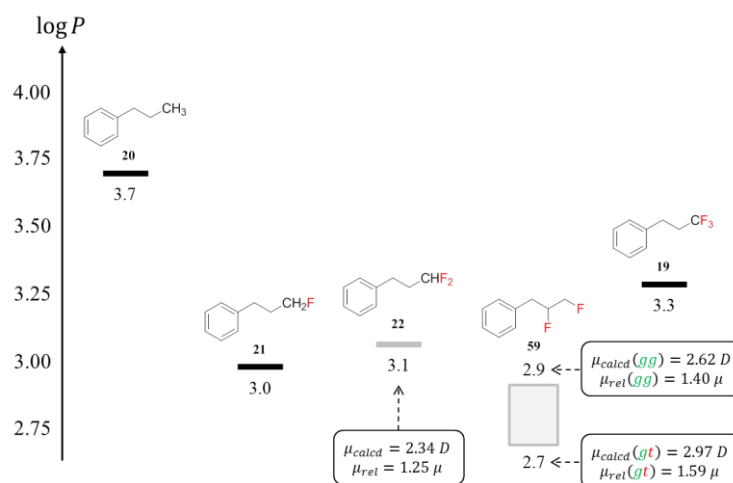


**Figure 36.** Predicted log *P* values for *vic*-difluoropropylbenzene **59** based on gas phase calculations.

## 3.2.2 Solvation Energy

### 3.2.2.1 Introduction

Although these initial considerations comforted the theory put forward at the beginning of this chapter, another support was sought by examining the calculated solvation energies of some relevant fluorinated alkyl groups (for details about calculations, see Experimental Section). Indeed, as already shown for a series of 3-substituted indole derivatives (**23x**, Figure 26), the calculated solvation energies were generally in good qualitative agreement with the experimentally determined polarity trend, and can serve as reliable predictive tools.

### 3.2.2.2 Calculated Solvation Energies

Solvation energies determined for the *trans* and *gauche* conformations of *vic*-difluoroethane (Figure 37, top) corroborate the conclusion drawn from computed dipole moments in the gas phase. On the one hand, the energy difference between these two conformations in water is much more pronounced than in the gas phase. This observation follows the logic consisting in assuming that a polar environment stabilizes more polar conformations. On the other hand, the marked solvation energy difference ( $\Delta E_{solv}(t/g) = -1.4 \text{ kcal/mol}$ ) between *trans* and

*gauche* conformations suggests once more that such fluorinated scaffolds could exhibit a variable polarity through conformational flexibility.

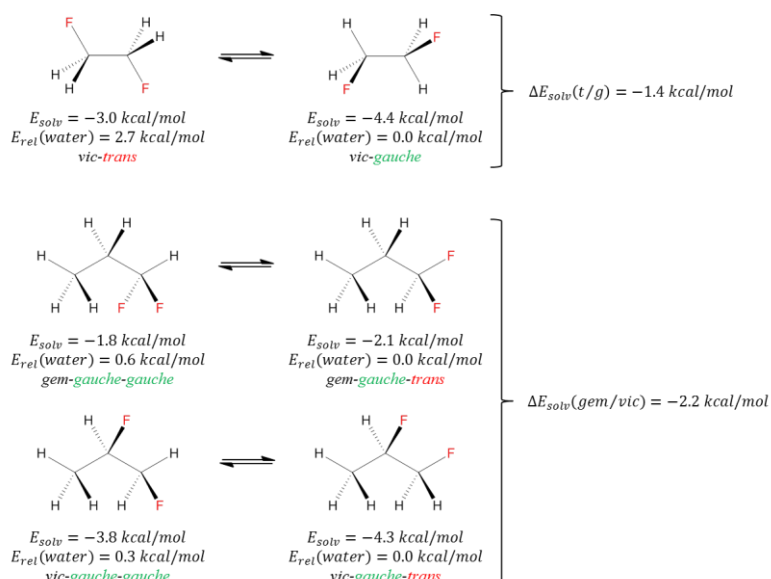


**Figure 37.** Computed solvation energies ( $E_{solv}$ ) for a relevant set of difluoroethyl and difluoropropyl analogs. Relative energies calculated in water ( $E_{rel}$ ;  $\epsilon = 80$ ) are also provided for each conformation of the same compound.

Comparing the solvation energies of *gem*- and *vic*-difluoropropane revealed that the solvation energy difference between these two fluorinated alkyl groups, taken in their respective favored conformations (*gem-gauche-trans* and *vic-gauche-trans*), is  $\Delta E_{solv}(\text{gem}/\text{vic}) = -2.2 \text{ kcal/mol}$  (Figure 37, bottom). Such difference is particularly striking, especially when considering the minor structural variation from which it stems.

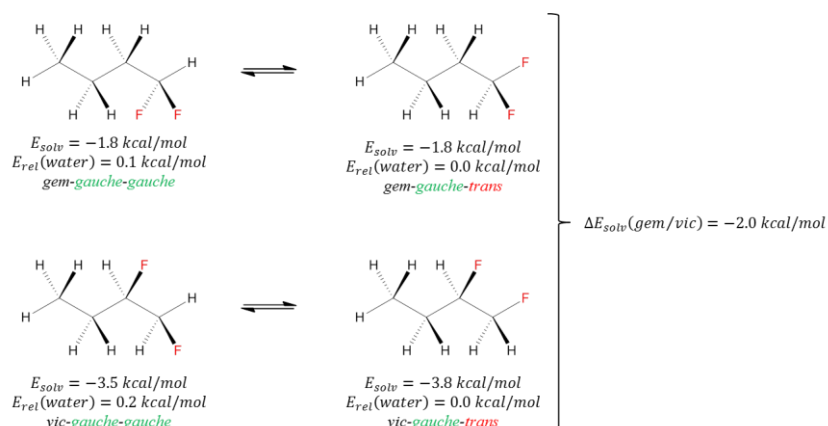


**Figure 38.** Computed solvation energies ( $E_{solv}$ ) for a relevant set of difluorobutyl analogs. Relative energies calculated in water ( $E_{rel}$ ;  $\epsilon = 80$ ) are also provided for each conformation of the same compound.

Very similar results were obtained for difluorobutane analogs, for which a solvation energy difference  $\Delta E_{solv}(gem/vic) = -2.0 \text{ kcal/mol}$  was calculated, which is slightly smaller than that of difluoropropane analogs (Figure 38). Hence, it seems that the effect on solvation energy imparted by the *vic*-difluoro motif is smaller when it is borne by a longer alkyl chain.

In summary, all cases confirmed that a substantial solvation energy decrease is expected upon replacement of a *gem*- by a *vic*-difluoro motif. Furthermore, these results highlighted that the influence of a partially fluorinated alkyl group on polarity should be more pronounced for shorter alkyl chains. For instance, it is expected that a *vic*-difluoropropyl moiety should have a stronger impact on polarity than the corresponding *vic*-difluorobutyl unit.

### 3.2.2.3 Extrapolated Polarity Trend

Based on these calculations, the polarity trend expected for a series of 3-substituted indole derivatives could be determined qualitatively by approximating the solvation energy of *vic*-difluoropropylindole **60** (Figure 39).

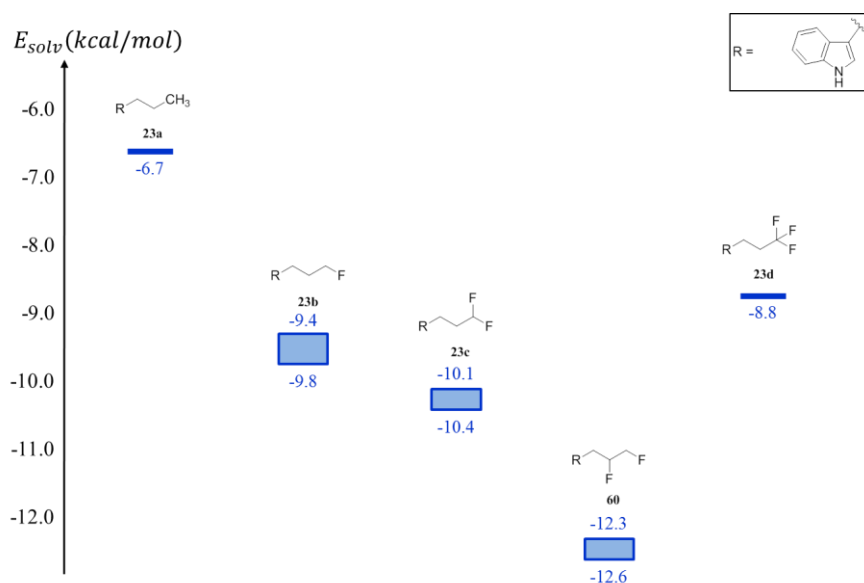


**Figure 39.** Polarity trend extrapolated from the solvation energies ( $E_{solv}$ ) computed for 3-substituted indole derivatives **23x** ( $x = \mathbf{a-d}$ ).

As previously, the contribution of the indole ring was assumed to be constant regardless of the alkyl moiety at C(3). Thus, with  $\Delta E_{solv}(gem/vic) = -2.2 \text{ kcal/mol}$  in the propyl case, it was deduced from the solvation energy of *gem*-difluoro derivative **23c** calculated earlier (Figure 26) that *vic*-difluoro analog **60** should have a solvation energy comprised between -12.3 and -12.6 kcal/mol (Figure 39). The polarity trend resulting from this simple hypothesis is in qualitative agreement with the one shown in Figure 36.

### 3.2.3 Impact of the Fluorine *Gauche* Effect on Physicochemical Properties

#### 3.2.3.1 Introduction

Many theoretical studies on the fluorine *gauche* effect have attempted to rationalize the underlying forces governing this singular phenomenon.<sup>96–100</sup> Because understanding this effect is instrumental in anticipating its physical manifestations on molecules, the two general cases of possible *vic*-difluoroalkyl derivatives were analyzed, i.e. the *threo* and *erythro* configurations (Figure 40).



**Figure 40.** Two general cases of possible *vic*-difluoroalkyl derivatives: the *threo* and *erythro* configurations.

#### 3.2.3.2 Theoretical Considerations

The main physical interaction that accounts for the fluorine *gauche* effect is a conjugative stabilization between two antiperiplanar C–H and C–F bonds. Indeed, in such a conformation, *in silico* calculations revealed the possibility for a C–H bonding orbital ( $\sigma_{CH}$ ) to interact with the empty C–F antibonding orbital ( $\sigma_{CF}^*$ ).<sup>98</sup>

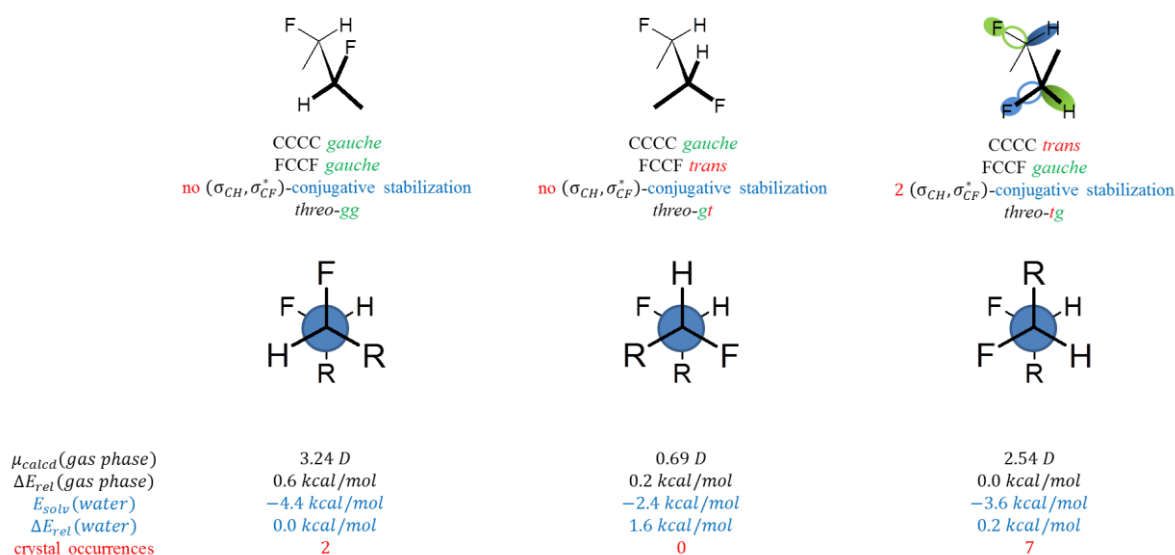


**Figure 41.** Possible staggered conformations for *threo* acyclic R–CHFCHF–R compounds, their respective computed properties, and their occurrence in X-ray crystal structures.

Applying this principle to the *threo* case shows that only one conformation can benefit from conjugative stabilization (Figure 41). For each conformation, the dipole moment, relative

energy difference in the gas phase, solvation energy, and relative energy difference in water were calculated (for details about calculations, see Experimental Section). Additionally, the number of occurrences of each conformation in X-ray crystal structures found for acyclic R–CHFCHF–R compounds was counted (CSD, version 5.33, November 2011).

The *threo-gg* conformation exhibits the largest dipole moment, as well as the strongest solvation energy of the series, and two occurrences were found in crystal structures. By contrast, the *threo-tg* conformation possesses a weaker solvation energy and appears in seven occurrences. The latter also benefits from two conjugative stabilizations, and has a moderate dipole moment. As for the *threo-gt* conformation, it benefits from no conjugative stabilization, has the weakest solvation energy, and presents the smallest dipole moment of the series. The combination of these parameters may account for the fact that no occurrences were found for this particular conformation.

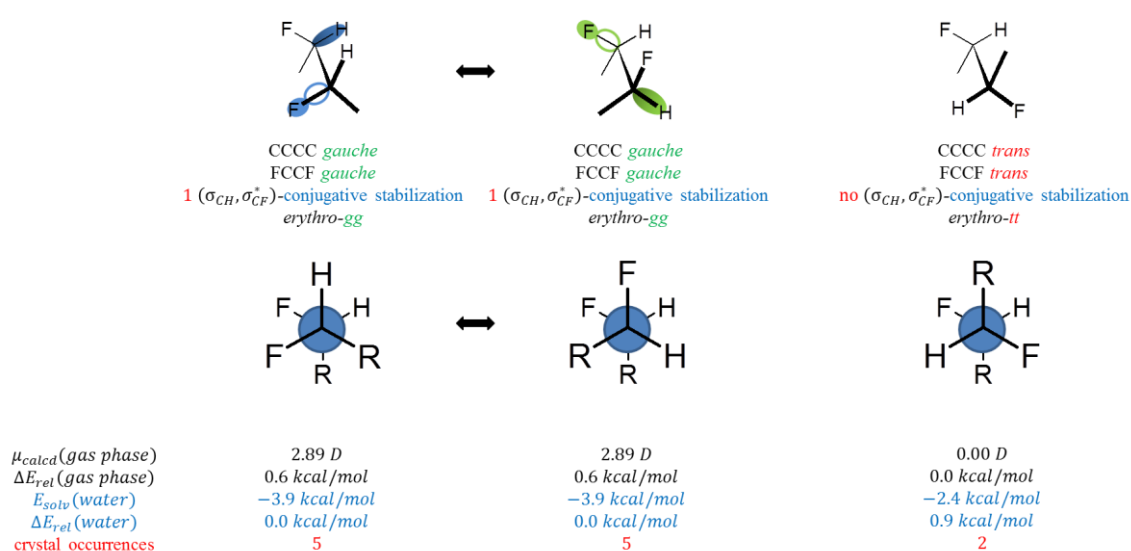


**Figure 42.** Possible staggered conformations for *erythro* acyclic R–CHFCHF–R compounds, their respective computed properties, and their occurrence in X-ray crystal structures.

Examining the *erythro* case reveals that only two distinct conformations exist (Figure 42). The *erythro-tt* conformation does not benefit from any stabilizing effect, has no dipole moment by symmetry, and the weakest solvation energy of the series. On the contrary, the *erythro-gg* conformation benefits from one conjugative stabilization, has a moderately high dipole moment, and an intermediate solvation energy.

### 3.2.3.3 Experimental Manifestations

Based on these considerations, it was attempted to understand how the influence of each conformation's properties might account for their respective occurrence in X-ray crystal

structures. To this end, the population repartition of all conformations was plotted based on their relative energy difference calculated in the gas phase and in water (Figure 43).

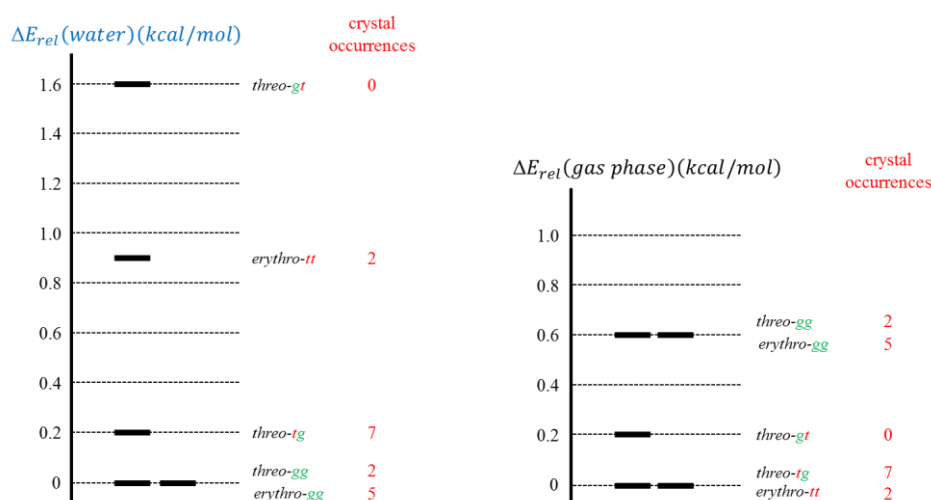


**Figure 43.** Population repartition of *threo* and *erythro* conformers found in X-ray crystal structures based on their relative energy difference ( $\Delta E_{rel}$ ) calculated in the gas phase and in water.

Although these results can only be taken as an initial indication, it appears that the *threo-tg* conformation is favored over the *threo-gg* conformation (7:2 occurrences), whereas the *erythro-gg* conformation is favored over the *erythro-tt* conformation (5:2 occurrences).

Additionally, it was noted that the distribution order corresponding to the various conformations seems to be directly dependent on the reference medium. This key observation highlights the fact that the environment of an acyclic *vic*-difluoro derivative apparently determines which conformation is favored to obtain the best polarity match. It therefore suggests that since the more polar conformation is favored in aqueous medium, the less polar might be preferred when subjected to an apolar environment. Such a unique characteristic may greatly facilitate key biological mechanisms in the body where a molecule has to face media of opposite polarities, especially for membrane permeation, prior to reaching the targeted receptors.

As shown earlier for the series of 3-substituted indole derivatives depicted in Figure 26, dipole moments and solvation energies are not linearly correlated parameters. In the general case of acyclic *vic*-difluoro derivatives, interesting characteristics could be observed, which are nicely illustrated in Figure 44.

The solvation energy calculated in the Poisson-Boltzmann approximation reflects the interaction energy of the medium with partial charges on the molecular surface, partly compensated by the cavitation energy due to the immersion of the molecule into the medium.

For a series of acyclic *erythro* and *threo vic*-difluoro isomers with different conformations, the molecular volumes remain essentially constant; hence, the cavitation energy needs not be considered explicitly.

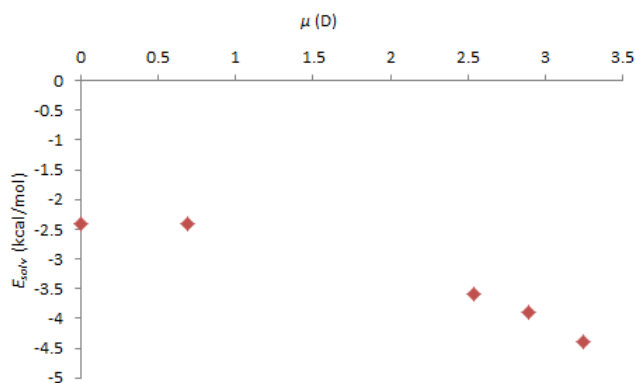


**Figure 44.** Solvation energy ( $E_{solv}$ ) against dipole moment ( $\mu$ ) for acyclic *vic*-difluoro derivatives.

Figure 44 then confirms that since non-polar conformations by symmetry ( $\mu \sim 0.0 D$ ) also have surface charges, the solvation energy does not vanish. However, it can be anticipated that with increasing molecular polarity ( $\mu > 1.0 D$ ), the solvation energy gets stronger. Or, in reverse, with decreasing polarity, we expect a reduction of solvation energy; however, not to zero, but to a final limiting value for non-polar conformers (threshold value:  $E_{solv} = -2.4 kcal/mol$ ).

Another characteristic of acyclic *vic*-difluoro derivatives is that the range of polarity covered by the different conformations is quite significant. Compared to the model series of compounds **55–58**, where *cis*-**56** (Figure 32) had the largest solvation energy variation ( $\Delta E_{solv} = 0.7 kcal/mol$ ), any *threo vic*-difluoro derivative could benefit from a range of variation nearly three times as large ( $\Delta E_{solv} = 2.0 kcal/mol$ ). As for the *erythro vic*-difluoro derivative, it benefits from a smaller sizable variation of solvation energy  $\Delta E_{solv} = 1.5 kcal/mol$ .

### 3.2.3.4 Conclusion

In summary, the analysis of the basic characteristics of the *vic*-difluoro motif enabled the prediction of its influence on a molecule's polarity. Based on these initial conclusions, *vic*-difluoroalkyl scaffolds appear potentially interesting in view of their use as modulators of lipophilicity.



### 3.2.4 The *bis*-Vicinal Trifluoro Motif

#### 3.2.4.1 Introduction

Most of the theoretical aspects connected to the *vic*-difluoro motif as a replacement of the *gem*-difluoro unit have been explored, but the possibility of arranging three consecutive fluorine atoms along an alkyl chain has not been considered until now. This option has been neglected because it was assumed that the volume increase resulting from the exchange of three  $H \rightarrow F$  may override any polarity increase obtained by structural modification, thus precluding any lipophilicity-lowering effect. However, in light of the potential effects predicted for the *vic*-difluoro motif, studying the *bis-vic*-trifluoro case could lead to unexpected observations.

#### 3.2.4.2 Vector Analysis

It was therefore attempted to determine the estimate of the dipole moment resulting from such an arrangement of fluorine atoms. In that case, the smallest alkyl chain to consider was propane. The simple vector analysis of a 1,1,1-trifluoropropyl group leads to a resulting dipole moment equal to  $\mu_{res} = 1 \mu_{CF} = \mu_{gem}$  (Figure 45, top).

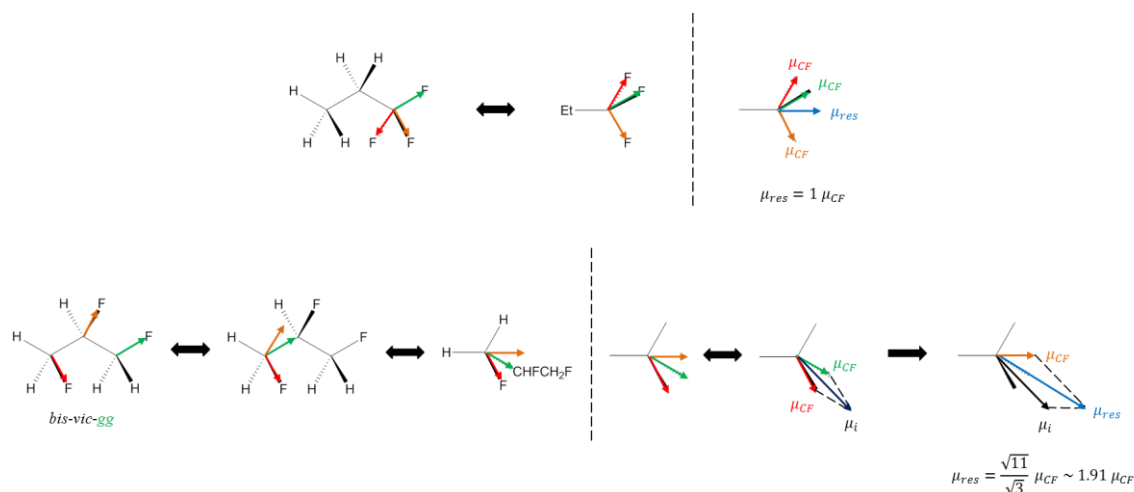


**Figure 45.** Vector analysis comparing the resulting dipole moments ( $\mu_{res}$ ) of 1,1,1-trifluoropropyl and the *bis*-vicinal *gauche-gauche* 1,2,3-trifluoropropyl group.

Applying the same concept to the most favored *bis*-vicinal *gauche-gauche* 1,2,3-trifluoropropyl unit afforded a resulting dipole moment of  $\mu_{res} = 1.91 \mu_{gem} = \mu_{bis-vic}$  (Figure 45, bottom). Hence, compared to the *vic*-difluoro case with  $\mu_{res} \sim 1.6 \mu_{CF}$ , the *bis-vic*-trifluoro case benefits from a higher polarity ( $\mu_{res} \sim 1.9 \mu_{CF}$ ), but also suffers from a higher volume (1  $H/F$ -volume increment). In a comparable alkyl series, the polarity increase of  $0.3 \mu_{CF}$  from a *vic*-difluoro derivative to a *bis-vic*-trifluoro analog would then be just about

compensated by the  $H/F$  volume effect. Hence, *bis-vic*-trifluorobutyl units are expected to have similar effects on lipophilicity as *vic*-difluorobutyl groups. However, both should have significantly lower lipophilicities than *gem*-difluoro- or *gem*-trifluorobutyl groups.

### 3.2.4.3 Calculated Gas Phase Dipole Moments

The computed dipole moments in the gas phase for trifluoropropyl and trifluorobutyl derivatives revealed a much more modest impact of the *bis-vic*-trifluoro motif than predicted by vector analysis (Figure 46). Only looking at the favored *gauche-gauche* conformations of the *bis*-vicinal 1,2,3-trifluoroalkyl derivatives, it turns out that the resulting dipole moment determined *in silico* is  $\mu_{bis-vic} \sim 1.13 \mu_{gem}$ .

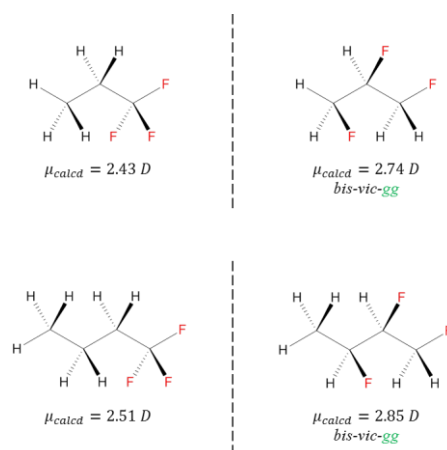


**Figure 46.** Calculated dipole moments in the gas phase ( $\mu_{calcd}$ ) for 1,1,1-trifluoroalkyl and *bis*-vicinal *gauche-gauche* 1,2,3-trifluoroalkyl groups (*n*-propyl or *n*-butyl).

Hence, based on computed dipole moments, the polarity decrease resulting from such structural modification would actually not be significant enough to have a noticeable impact on lipophilicity. However, since previous calculations revealed the dramatic impact of the *vic*-difluoro motif on solvation energy compared to its *gem*-difluoro counterpart, a similar effect might be expected when converting a 1,1,1-trifluoropropyl group into a 1,2,3-trifluoropropyl analog.

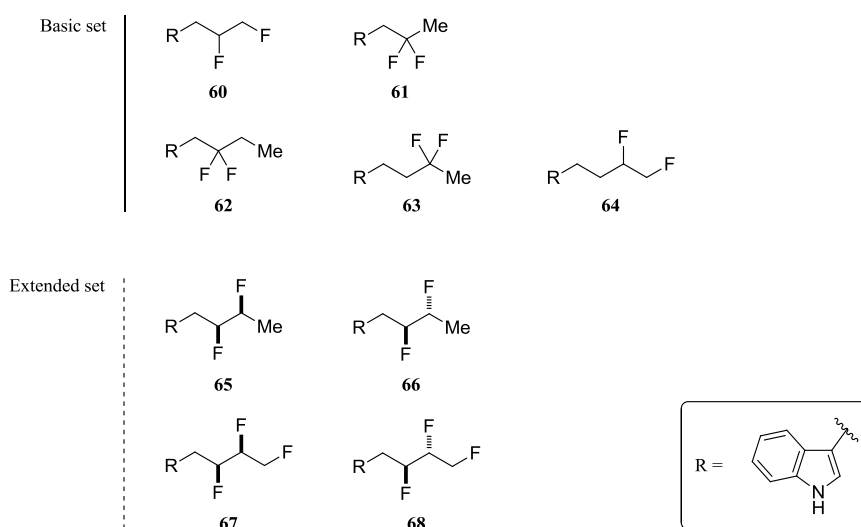
### 3.2.4.4 Conclusion

At this point, vector analysis and calculations did not afford a clear indication suggesting the strong interest of the *bis*-vicinal trifluoro motif as effective means to lower lipophilicity. Although more calculations could have been run on solvation energy to support these initial results, it was decided that conclusions on the influence of this fluorination pattern would rather be compared, discussed, and rationalized on the basis of experimental measurements.

### 3.3 Design and Synthesis of a Prototypical Set of Model Compounds

#### 3.3.1 The Appropriate Candidates

Further to this preliminary investigation on the polarity of vicinal and multi-vicinal fluoroalkyl groups, two sets of 3-substituted indole model compounds were chosen, bearing a propyl or butyl chain decorated with the respective fluorination patterns shown in Scheme 15.



**Scheme 15.** Two sets of relevant model compounds (**60–68**).

Having the *gem*-difluoropropylindole derivative **23c** as reference, the basic set of model compounds **60–64** was designed so that the influence of the *vic*-difluoro pattern in both propyl and butyl alkyl chains could be studied. With the extended set of model compounds, it was envisioned to study the more complex fluorination motifs comprising the *threo* and *erythro* configurations of the respective internal *vic*-difluoro and *bis-vic*-trifluoro moieties **65–68**.

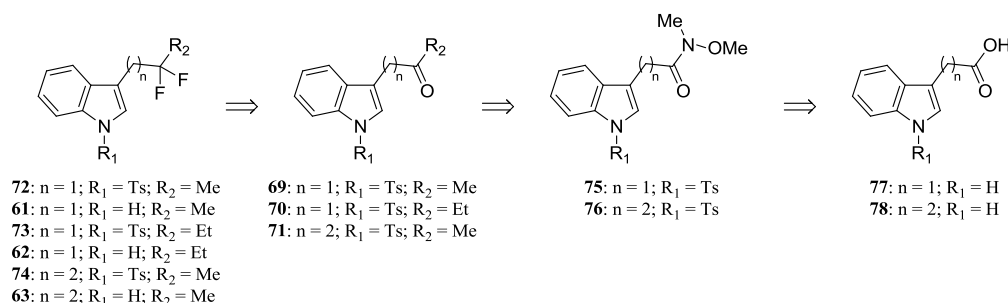
With this collection of structures in hand, it was assumed that it would be possible to draw the first conclusions on the influence of vicinal and multi-vicinal fluoroalkyl units on the physicochemical properties of the series of model molecules.

#### 3.3.2 Retrosynthetic Analysis

##### 3.3.2.1 Geminal Difluoroalkyl Groups

The synthesis of *gem*-difluoroalkyl derivatives is commonly achieved by deoxofluorination of aldehydes or ketones with DAST.<sup>72</sup> Therefore, as shown in retrosynthetic Scheme 16, ketone precursors **69–71** of *gem*-difluoro derivatives **61–63** and **72–74** could easily be accessed from

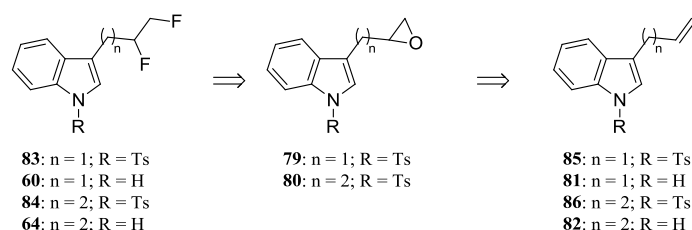
the selective substitution of Weinreb amides **75** and **76**. The latter could then originate from commercially available carboxylic acids **77** and **78**.



**Scheme 16.** Retrosynthetic analysis of *gem*-difluoroalkyl derivatives **61–63** and their tosyl-protected analogs **72–74**.

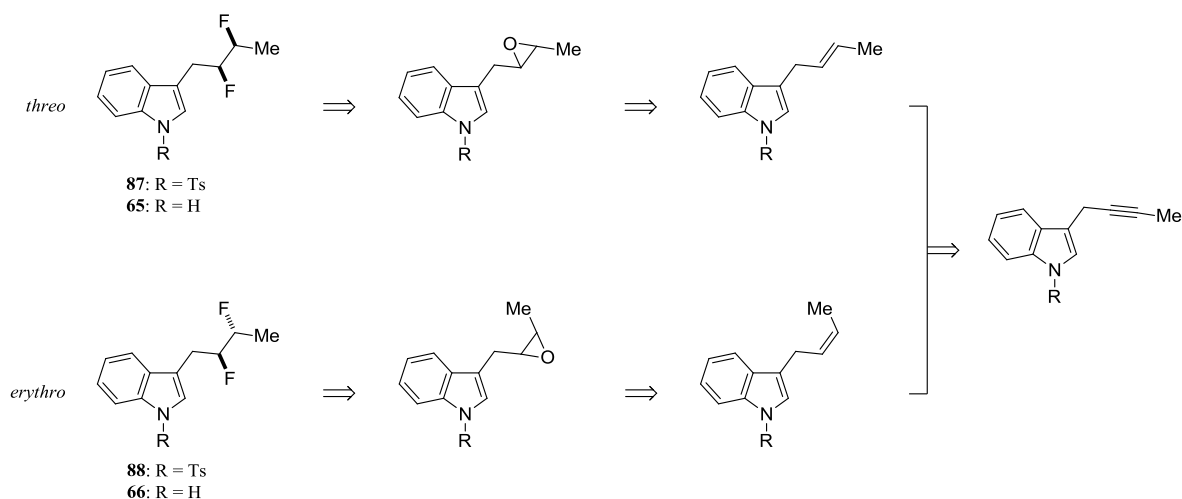
### 3.3.2.2 Vicinal and Multi-Vicinal Fluoroalkyl Groups

Terminal vicinal difluoroalkanes have already been source of work in the past and several literature precedents have reported their synthesis from the parent terminal epoxides.<sup>101</sup> Therefore, the synthesis of vicinal difluorides **60** and **64** was envisioned from epoxides **79** and **80** (Scheme 17). This transformation usually proceeds in two steps: (i) opening of the terminal oxirane with a nucleophilic source of fluoride, and (ii) deoxofluorination reaction of the resulting fluorohydrin. As for terminal epoxides **79** and **80**, it was anticipated that they could be directly obtained from olefins **81** and **82**, respectively.



**Scheme 17.** Retrosynthetic analysis of *vic*-difluoroalkyl derivatives **60** and **64**, and their respective tosyl-protected analogs **83** and **84**.

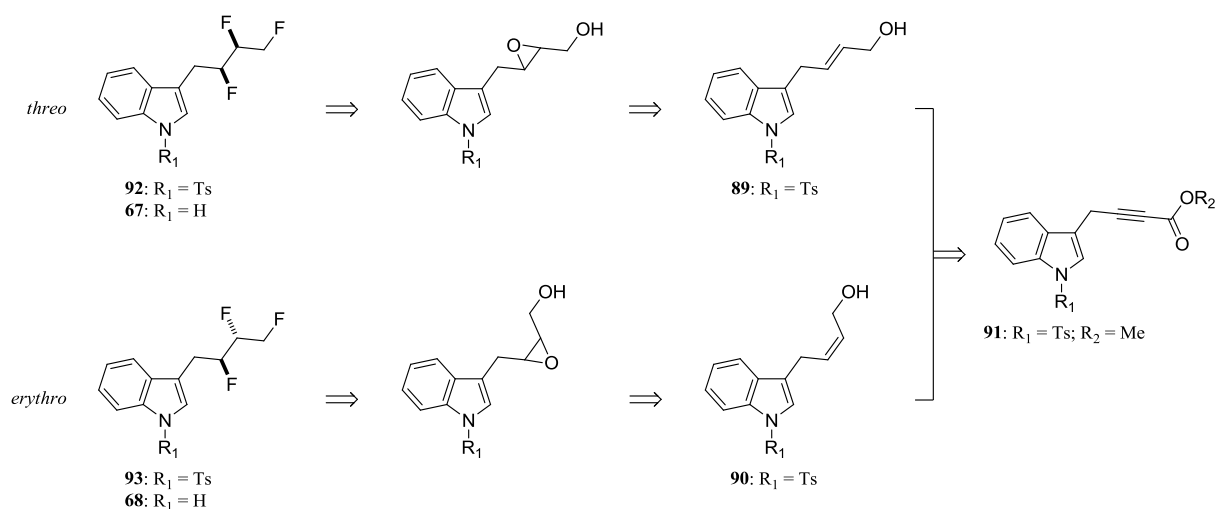
Although *threo* and *erythro* *vic*-difluoroalkyl groups are structurally similar to the terminal *vic*-difluoroalkyl unit, literature precedents reporting the synthesis of the former are relatively scarce.<sup>101–105</sup> Several reasons may account for this state of facts, and examining the synthetic strategies used to access such fluorination patterns is quite revealing. In fact, it turns out that the opening of a disubstituted epoxide with fluoride on either end is much more tedious than that of a terminal one.<sup>102,105</sup> This reactivity difference can be attributed to the generally poor nucleophilic character of fluoride, which makes it even more sensitive to steric hindrance when involved in nucleophilic reactions.



**Scheme 18.** Initial retrosynthetic analysis of *threo* and *erythro* vic-difluoro derivatives **65** and **66**.

Despite this reactivity difference, it was assumed that each racemic mixture of *threo* and *erythro* vic-difluorobutyl derivatives **65** and **66** could be obtained from the *trans*- and *cis*-epoxides respectively (Scheme 18). These could then result from the epoxidation of the corresponding *trans*- or *cis*-alkenes, each of them being accessible from the corresponding alkyne via selective hydrogenation.

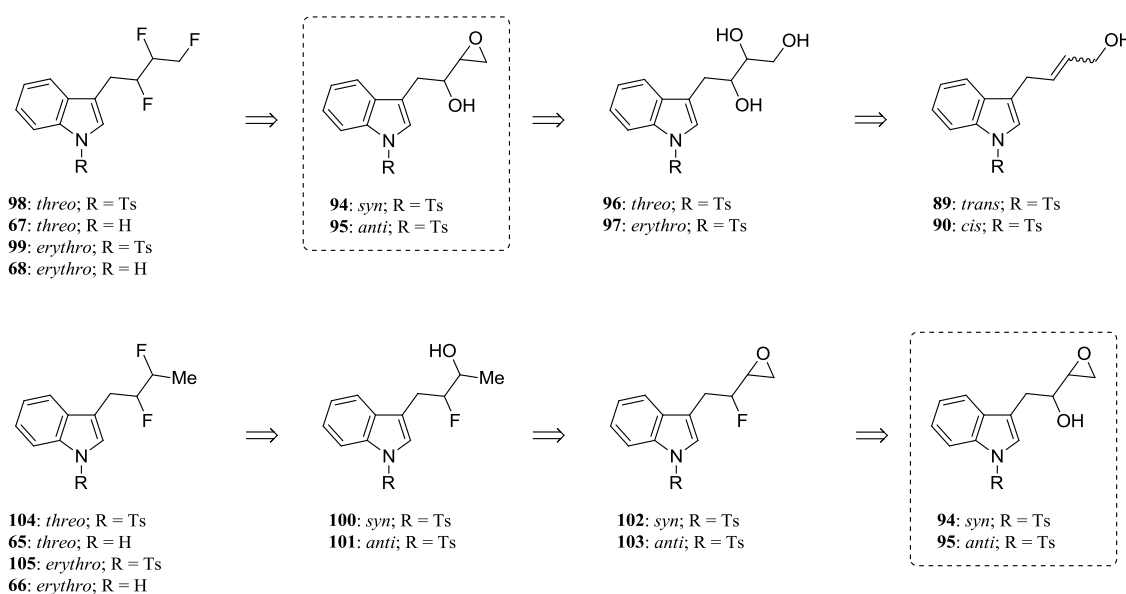
Hunter *et al.* were the first to report the synthesis and evaluation of multi-vicinal fluoroalkanes and their strategy towards *bis*-vic-trifluoroalkanes required an epoxyalcohol precursor.<sup>105</sup> Hence, following this precedent, it was assumed that each racemic mixture of *threo* and *erythro* bis-vic-trifluorobutyl derivatives **67** and **68** could be accessed from the corresponding *cis*- or *trans*-epoxyalcohol (Scheme 19). Finally, each epoxyalcohol could derive from allylic alcohols **89** and **90**, which could be synthesized from alkyne **91**.



**Scheme 19.** Initial retrosynthetic analysis of *threo* and *erythro* bis-vic-trifluoro derivatives **67** and **68**.

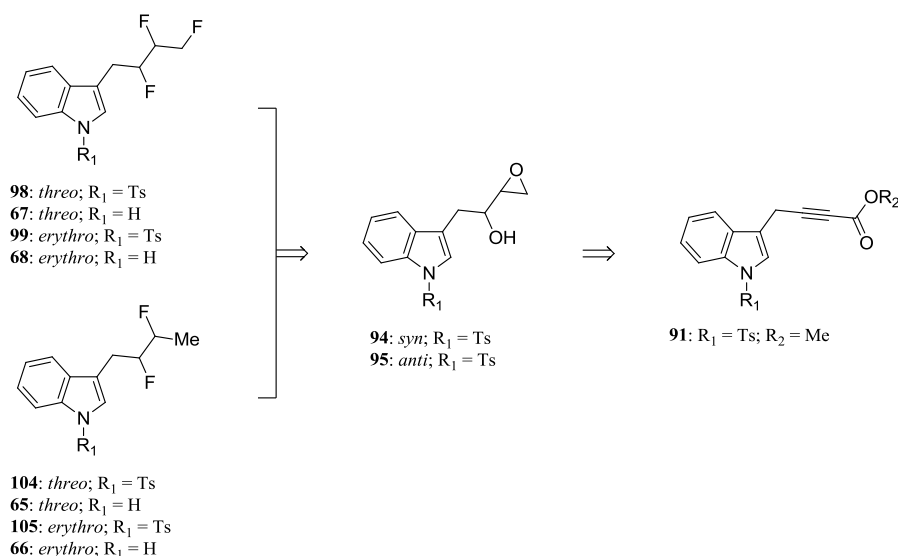
In view of developing a more efficient synthetic route, the possibility to use a common precursor leading to both series of *threo* and *erythro* vic-difluoro and *bis-vic*-trifluoro derivatives **65–68** was envisioned. Since the precursors resulting from the previous retrosynthetic analyses led to structurally related alkynes, it was assumed that a minor modification of this initial strategy could enable a fully divergent synthetic approach.

The key to finding a common intermediate to both series resided in reconsidering the way *bis-vic*-trifluorobutyl derivatives **67** and **68** would be accessed (Scheme 20, top). Accordingly, it was assumed that it would be more efficient to use a monosubstituted epoxyalcohol precursor (**94**, **95**) rather than the one initially proposed in Scheme 19. However, to synthesize such epoxyalcohol from a linear allylic alcohol (**89**, **90**), it was identified that the missing intermediate would be a triol (**96**, **97**), provided that the terminal epoxide could be formed selectively from such a system.



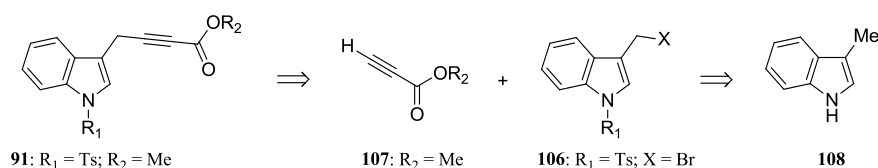
**Scheme 20.** Revisited retrosynthesis with a new common intermediate epoxyalcohol (**94**, **95**).

With this new epoxyalcohol precursor (**94**, **95**), it thus became possible to plan a different synthesis for *threo* and *erythro* vic-difluoroalkyl derivatives **65** and **66** (Scheme 20, bottom). Hence, the *vic*-difluoro motif could originate from a fluorohydrin (**100**, **101**), which could be conveniently obtained from the selective terminal opening of a fluoroepoxide (**102**, **103**) with a hydride source. The latter could then result from the selective deoxofluorination reaction of the common intermediate epoxyalcohol (**94**, **95**).



**Scheme 21.** Divergent synthetic approach to *threo* and *erythro* derivatives **65–68**.

In the end, all *threo* and *erythro* derivatives (**65–68**) could be derived from a single common intermediate: alkyne **91** (Scheme 21). The latter's synthesis was planned via a coupling reaction between prefunctionalized 3-methylindole **106** and propiolate **107** (Scheme 22). 3-Methylindole **108** would thus be the key starting material of the whole synthetic pathway.

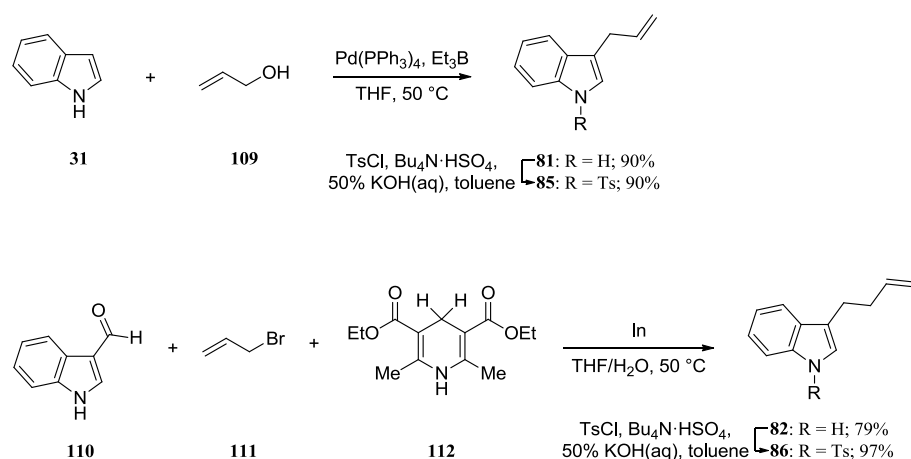


**Scheme 22.** Retrosynthetic analysis of alkyne **91**.

### 3.3.3 Synthetic Access

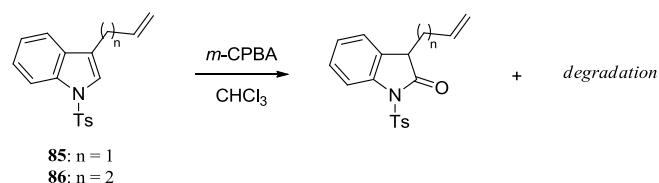
#### 3.3.3.1 Terminal *vic*-Difluoro Derivatives

The synthesis of terminal *vic*-difluoro derivatives **60** and **64** initially required an access to the corresponding olefins, **81** and **82** respectively. As depicted in Scheme 23, olefin **81** could be isolated in high yield via palladium-catalyzed allylation reaction between indole **31** and allyl alcohol **109**, promoted by triethylborane.<sup>106</sup> As for butyl analog **82**, it was obtained in high yield through a three-component indium-mediated domino allylation of indole-3-carbaldehyde **110** with allyl bromide **111** in presence of Hantzsch's ester **112**.<sup>107</sup> Each olefin, **81** and **82**, was then further tosyl-protected under standard phase transfer catalysis conditions, thus affording protected compounds **85** and **86** in high yields.<sup>77</sup>



**Scheme 23.** Synthetic access to terminal olefins **85** and **86**.

With protected olefins **85** and **86** in hand, they were subjected to standard epoxidation conditions using *m*-CPBA (Scheme 24). Unfortunately, even at lower temperature (-78 °C), no epoxidized product could be isolated. Instead, the oxindole derivative was formed along with other unidentified side-products. This result highlights the relative electron-deficiency of the terminal olefins compared to the indole nucleus.



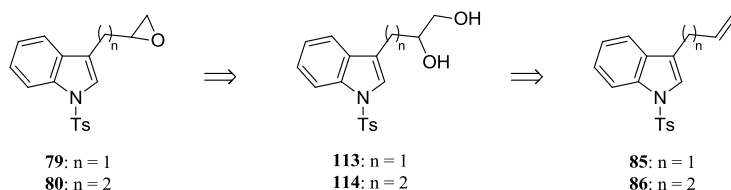
**Scheme 24.** First attempts to epoxidize terminal olefins **85** and **86**.

This setback suggested to envision an indirect epoxidation strategy, which consisted in a two-step procedure involving the selective dihydroxylation of terminal olefins **85** and **86**, followed by the conversion of vicinal diols **113** and **114** into epoxides **79** and **80**, respectively (Scheme 25, top).

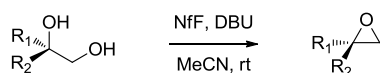
This possibility has already been reported for several systems but, unlike other procedures, Klar *et al.* published the one-pot conversion of vicinal diols into the corresponding epoxides.<sup>108</sup> Their simple conditions, combining perfluorobutanesulfonyl fluoride and DBU, allowed them to cleanly afford the desired epoxide in high yield (74%), and on multigram scale (Scheme 25, center).



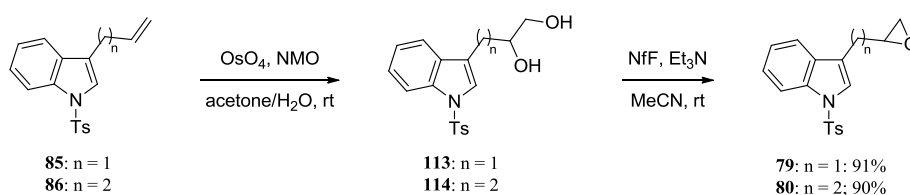
Idea:



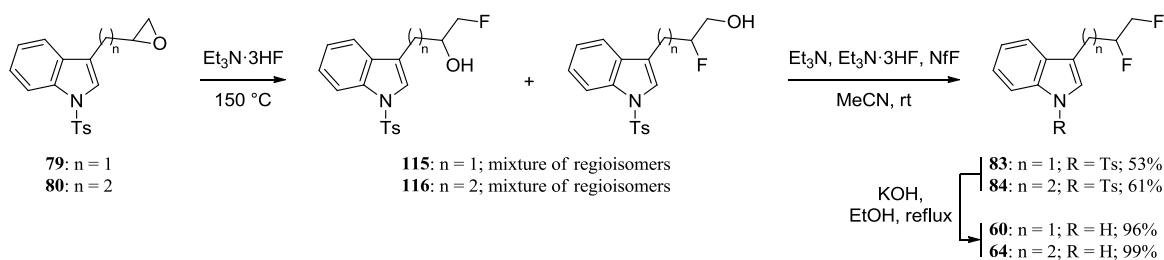
Precedent:



Synthesis:

**Scheme 25.** Two-step procedure towards terminal epoxides **79** and **80**.

It was actually discovered that, after standard dihydroxylation,<sup>109</sup> vicinal diols **113** and **114** could be directly treated with a combination of perfluorobutanesulfonyl fluoride and triethylamine in acetonitrile at room temperature (Scheme 25, bottom). The combined yields obtained over two steps were satisfactory, and the mildness of the conditions allowed us to work conveniently on multigram scale.

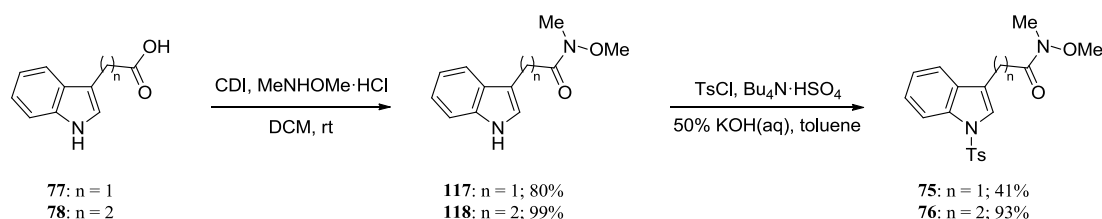
**Scheme 26.** Late stage fluorination towards *vic*-difluoro derivatives **60** and **64**.

With the epoxide in place, and the indole nucleus protected, the synthesis proceeded with the late stage fluorination strategy, which consisted in a two-step procedure. As reported by Hamatani *et al.*, one of the most common ways to synthesize terminal vicinal difluoroalkanes commences with the nucleophilic opening of a terminal epoxide with triethylamine trihydrofluoride (Scheme 26).<sup>102</sup> This fluoride source, although much less reactive than Olah's reagent, allows for a better chemoselectivity, but requires harsher conditions. The resulting fluorohydrin is then subjected to standard deoxofluorination conditions, thereby affording the terminal vicinal difluoride.

Accordingly, substrate epoxides **79** and **80** were heated in neat triethylamine trihydrofluoride at 150 °C. Fluorohydrins **115** and **116** were isolated as mixtures of regioisomers, which were then subjected to standard deoxofluorination conditions.<sup>80</sup> Overall, each *vic*-difluoro derivative, **83** and **84**, could be synthesized in good yield following this procedure. Further tosyl-deprotection finally afforded compounds **60** and **64** quantitatively.<sup>81</sup>

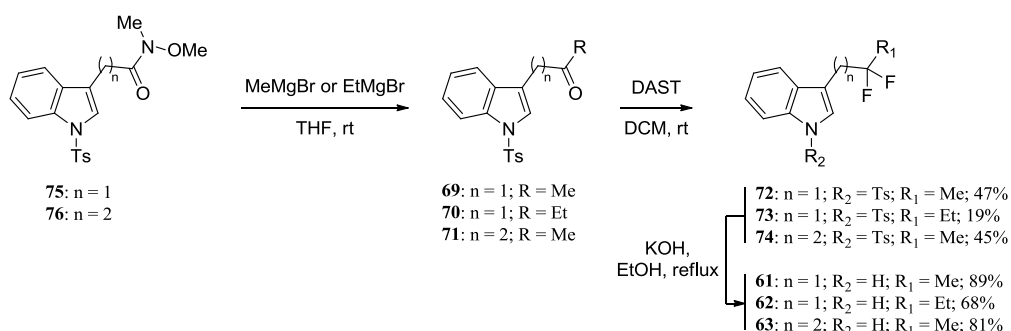
### 3.3.3.2 Internal *gem*-Difluoro Derivatives

Based on the initial retrosynthetic plan (Scheme 16), the synthesis of *gem*-difluoro derivatives **61–63** required the corresponding Weinreb amides (**117**, **118**) that would serve as common intermediates to access all desired analogs. Thus, starting from commercially available carboxylic acids **77** and **78**, standard reaction conditions smoothly afforded Weinreb amides **117** and **118** in high yield (Scheme 27).<sup>110</sup> When subjected to phase transfer catalysis conditions, both protected indole derivatives **75** and **76** could be isolated.<sup>77</sup>



**Scheme 27.** Synthesis of Weinreb amides **75** and **76**.

Tosyl-protected amides **75** and **76** were selectively substituted using either methylmagnesium bromide or ethylmagnesium bromide (Scheme 28), thus yielding the required range of ketone precursors **69–71**.<sup>110</sup> Conversion of these ketones into the corresponding *gem*-difluoro products **72–74** with DAST turned out to be sluggish and low-yielding.<sup>84</sup>



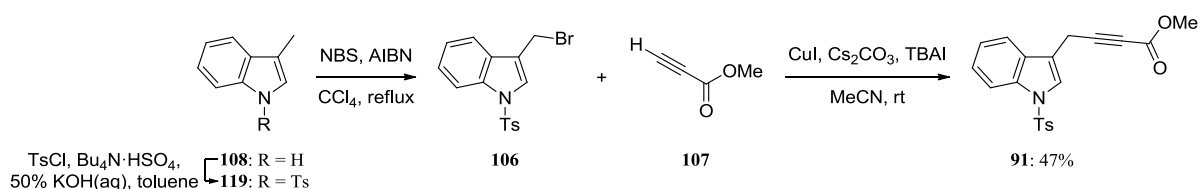
**Scheme 28.** Derivatization and late stage fluorination towards *gem*-difluoro derivatives **61–63**.

Although steric hindrance might be a reason for this observation (see ethyl ketone **73**), no significant degradation of the substrates could be noticed over time (based on recovered material). Also, using more equivalents of DAST (from 2.00 to 10.0 equiv) did not influence

the outcome of the reaction. Eventually, *gem*-difluoro derivatives **61–63** were isolated after treatment with potassium hydroxide in boiling ethanol.<sup>81</sup>

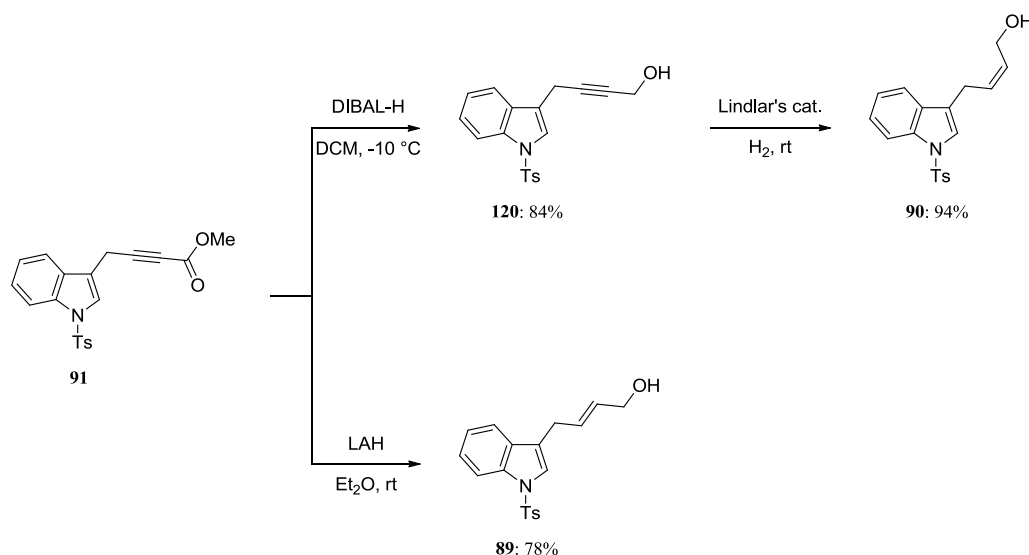
### 3.3.3.3 *Threo* and *Erythro vic*-Difluoro and *bis-vic*-Trifluoro Derivatives

*En route* to *threo* and *erythro vic*-difluoro and *bis-vic*-trifluoro derivatives **65–68**, the multigram scale three-step synthesis of alkyne **91** was developed and optimized (Scheme 29). Thus, indole **119** was isolated after tosyl-protection of 3-methylindole (**108**),<sup>77</sup> and its subsequent Wohl-Ziegler bromination afforded bromide **106**.<sup>111</sup> The brominated product was further subjected to copper-promoted coupling conditions with methyl propiolate (**107**),<sup>112</sup> which afforded alkyne **91** in 47% yield over three steps after recrystallization.



**Scheme 29.** Three-step procedure towards the key intermediate alkyne **91**.

The key intermediate alkyne **91** could then be selectively converted into the *cis*- or *trans*-allylic alcohols, **90** and **89** respectively (Scheme 30). On the one hand, when alkyne **91** was treated with lithium aluminium hydride at room temperature, the fully reduced *trans*-allylic alcohol **89** was isolated in high yield.<sup>113</sup>

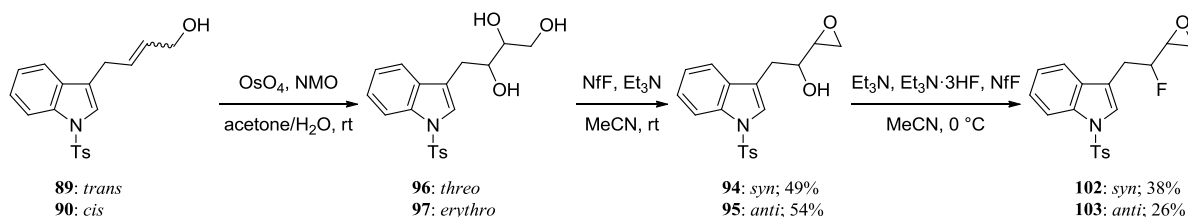


**Scheme 30.** Selective synthesis of *cis*- and *trans*-allylic alcohols **89** and **90**.

On the other hand, the stereoselective hydrogenation leading to *cis*-allylic alcohol **90** required the preliminary isolation of propargylic alcohol **120**. Hence, selective reduction of the ester

with diisobutylaluminium hydride at low temperature afforded effortlessly alcohol **120**.<sup>114</sup> The latter was then selectively reduced with hydrogen in presence of Lindlar's catalyst, thus affording *cis*-allylic alcohol **90** in excellent yield.<sup>114</sup>

With both *cis*- and *trans*-allylic alcohols in hand, the synthesis of fluoroepoxides **102** and **103** followed (Scheme 31). To this end, an unprecedented two-step procedure was developed relying on the selective epoxidation of an aliphatic 1,2,3-triol. In fact, after standard dihydroxylation of allylic alcohols **89** and **90**,<sup>109</sup> the corresponding *threo* and *erythro* triols, **96** and **97**, were subjected to the epoxidation conditions described earlier for the synthesis of epoxides **79** and **80** (Scheme 25). Gratifyingly, it was possible to isolate *syn*- and *anti*-epoxyalcohols **94** and **95** in good yields over two steps. Under these conditions, it was assumed that the primary alcohol is first converted into a leaving group, and the formation of the three-membered ring is then favored over the four-membered ring, thus leading to the selective formation of the epoxide in terminal position of the aliphatic chain (Scheme 31).



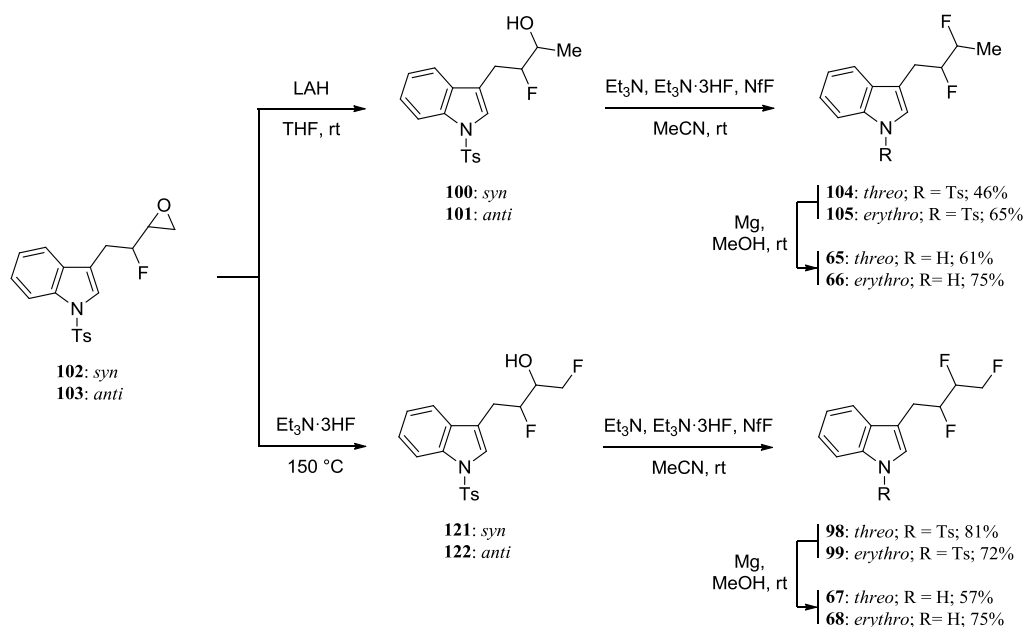
**Scheme 31.** Stereospecific access to *syn*- and *anti*-fluoroepoxides **102** and **103**.

Having overcome this first synthetic hurdle, the selective deoxofluorination of the resulting secondary alcohol was then tried. Unfortunately, upon treatment with DAST, none of the previously prepared alcohols, **94** and **95**, afforded the fluorinated product. Instead, complete decomposition of the starting material was observed within minutes at  $-78$  °C. By contrast, when subjecting the same alcohols to the milder fluorination conditions reported by Yin *et al.*,<sup>80</sup> fluoroepoxides **102** and **103** were isolated in acceptable yields.

The reactivity of such substrates can be explained by the fact that, due to its position with respect to the indole nucleus, once the secondary alcohol is converted into a leaving group, any benzylic proton in its vicinity can easily eliminate to generate a stable conjugated olefin. As a matter of fact, because of its intrinsic basicity, the fluoride anion can act as a base rather than a nucleophile. This side reaction was reported by Yin *et al.* to yield around 10% of elimination product on a model substrate.<sup>80</sup> Epoxyalcohols **94** and **95** then represent peculiar instances where these milder conditions proved their superiority over DAST.

Having obtained *syn*- and *anti*-fluoroepoxides **102** and **103**, the epoxide was selectively opened in terminal position either with a hydride or a fluoride source. In fact, opening with lithium aluminium hydride afforded fluorohydrins **100** and **101** (Scheme 32, top),<sup>115</sup> which were further converted into *threo* and *erythro* *vic*-difluoro derivatives **104** and **105** in good yield over two steps.<sup>80</sup>

As for the deprotection reaction, standard conditions employing potassium hydroxide did not furnish the desired product. In fact, elimination of one or more fluorine atoms turned out to be the main side-reaction. Therefore, milder conditions were employed, which consisted in vigorous stirring of activated magnesium in methanol.<sup>116</sup> Under these conditions, deprotected products **65** and **66** were isolated in good yield.



**Scheme 32.** Late stage fluorination strategy towards *threo* and *erythro* *vic*-difluoro and *bis*-*vic*-trifluoro derivatives **65–68**.

Following a similar strategy, terminal opening of epoxides **102** and **103** with triethylamine trihydrofluoride at 150 °C afforded a clean terminal-selective nucleophilic epoxide opening.<sup>102</sup> The resulting fluorohydrins, **121** and **122**, were then subjected to the mild deoxofluorination conditions,<sup>80</sup> which smoothly led to *threo* and *erythro* *bis*-*vic*-trifluoro derivatives **98** and **99** in good yield over two steps. Finally, tosyl-deprotection of **98** and **99** with magnesium in methanol<sup>116</sup> cleanly afforded *bis*-*vic*-trifluoro derivatives **67** and **68**.

### 3.4 Physicochemical and Pharmacological Properties

To investigate the influence of the *vic*-difluoro and *bis-vic*-trifluoro motifs on the physicochemical and pharmacological properties of saturated alkyl scaffolds, the model compounds were subjected to a series of tests aiming at measuring lipophilicity, metabolic stability, as well as aqueous solubility.

#### 3.4.1 Lipophilicity

Based on preliminary calculations of molecular dipole moments and solvation energies, it has been determined that the vicinal arrangement of two fluorine atoms should impart a clear polarity increase compared to the parent *gem*-difluoro derivative. Furthermore, it was surmised that the multi-vicinal arrangement of three fluorine atoms along an alkyl chain could provide a strong polarity increase. To relate these theoretical considerations to experimental results, the physicochemical and pharmacological properties of the basic (**60–64**) and extended (**65–68**) sets of model compounds were evaluated and compared. The results and conclusions of this study on lipophilicity are reported and discussed in the following paragraphs.

##### 3.4.1.1 Basic Set of Model Compounds

To assess the impact on lipophilicity of the *vic*-difluoro motif compared to the *gem*-difluoro analog, the results obtained for the basic set of model compounds **60–64** were combined in Figure 47, where *gem*-difluoro derivative **23c** was taken as reference.

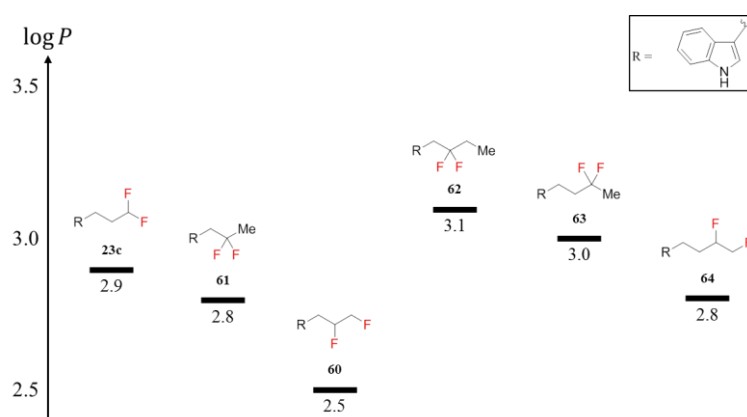


**Figure 47.** Experimental  $\log P$  values measured for the basic set of model compounds **60–64**.

In the propyl series, it was observed that the internal *gem*-difluoropropyl derivative **61** shows a slightly reduced  $\log P$  value compared to the terminal analog **23c**, whereas the terminal *vic*-

difluoro derivative **60** exhibits a dramatic lipophilicity drop ( $\Delta \log P \sim 0.4$ ). Reassuringly, these results are in agreement with our predictions.

Moving on to butyl derivatives **62–64**, it was noted that the lipophilicity trend is identical, although all  $\log P$  values are shifted by  $\Delta \log P (Bu/Pr) \sim + 0.3$ . This relative deviation is most likely due to the longer alkyl chain (butyl/propyl), which matches data found in the literature.<sup>12</sup> Nevertheless, the strong influence of the *vic*-difluoro motif is confirmed with butyl derivatives **62–64**, albeit slightly mitigated. In fact, as computed solvation energies suggested, the lipophilicity drop between *gem*- and *vic*-difluoro derivatives of the same alkyl series varies with the chain length. Indeed,  $\Delta E_{solv}(gem/vic) = -2.2 \text{ kcal/mol}$  was calculated in the propyl series (Figure 37), and  $\Delta E_{solv}(gem/vic) = -2.0 \text{ kcal/mol}$  in the butyl series (Figure 38). The experimental manifestation of this phenomenon is highlighted by  $\Delta \log P (\mathbf{61}/\mathbf{60}) \sim -0.3$  in the propyl series compared to  $\Delta \log P (\mathbf{63}/\mathbf{64}) \sim -0.2$  in the butyl series.

In summary, this first set of results is in agreement with our theoretical expectations, and underlines that the *vic*-difluoro motif can impart a marked lipophilicity drop compared to the parent *gem*-difluoro unit. Furthermore, experimental data confirm that the effect of such a structural modification on lipophilicity is even more pronounced when the saturated alkyl chain is shorter. In this regard, the *vic*-difluoropropyl scaffold appears to be the most potent lipophilicity-lowering partially fluorinated building block.

#### 3.4.1.2 Extended Set of Model Compounds

To investigate the impact on lipophilicity of *threo* and *erythro* *vic*-difluoro and *bis-vic*-trifluoroalkyl moieties, the  $\log P$  values of the extended set of model compounds **65–68** were measured. The results that were obtained are reported in Figure 48, where terminal *vic*-difluorobutyl derivative **64** is taken as reference.

*Erythro* *vic*-difluoro derivative **65** exhibits a lipophilicity value similar to that of the terminal *vic*-difluoro isomer **64**. More importantly, although compounds **67** and **68** are trifluorinated analogs, it turns out that the volume effect expected upon  $H \rightarrow F$  exchange is indeed overridden by the polarity increase imparted by the *bis*-vicinal arrangement of three fluorine atoms. *Threo* and *erythro* derivatives, **67** and **68** respectively, exhibit identical  $\log P$  values, thus making them the least lipophilic derivatives of the butyl series.

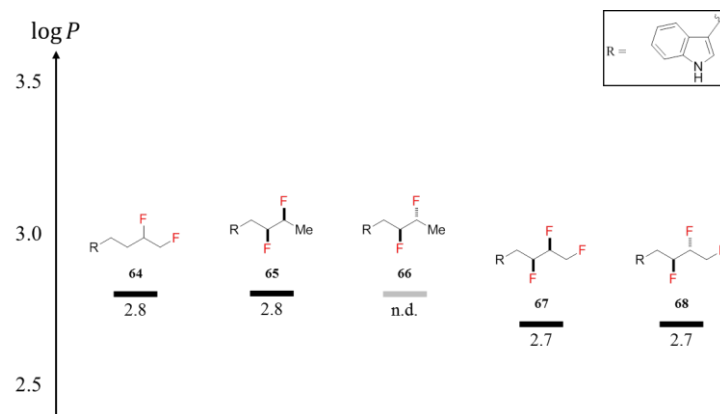


**Figure 48.** Experimental  $\log P$  values measured for the extended set of model compounds **65–68** (n.d. – not determined).

In the end, the lipophilicity change between trifluoromethyl derivatives **23d** and **24d** (propyl series) and *bis-vic*-trifluoro derivatives **67** and **68** (butyl series) is  $\Delta \log P \sim -0.4$ . Therefore, since the lipophilicity increase from propyl to butyl series was determined to be  $\Delta \log P (Bu/Pr) \sim +0.3$ , it results that the estimated influence of the multi-vicinal arrangement of three fluorine atoms in the butyl series is  $\Delta \log P \sim -0.7$  compared to its non-fluorinated analog. Additionally, it should be underlined that lipophilicity does not seem to depend on configuration, since diastereoisomers **67** and **68** display the same  $\log P$  value. Therefore, although the lipophilicity of compound **66** was not determined, one can assume that it should be similar, if not identical, to that of diastereoisomer **65**.

In summary, although the multi-vicinal arrangement of three fluorine atoms proved to be very influential on the measured  $\log P$  values, the lipophilicity-lowering potential of such scaffolds is limited by the length of their alkyl chain.

## 3.4.2 Aqueous Solubility

### 3.4.2.1 Introduction

In the early development of a new drug, the importance of aqueous solubility cannot be emphasized enough. Because this crucial parameter can turn the most active drug *in vitro* into an inactive substance *in vivo*, medicinal chemists have developed strategies to optimize the aqueous solubility of a lead compound in parallel of its activity. Amongst the various means to tune aqueous solubility, structure modification is the favored approach.<sup>117</sup> However, since literature precedents reporting the use of fluorine atoms to tune aqueous solubility are scarce, it motivated the solubility measurement of the partially fluorinated model molecules that were prepared. Also, in light of the experimental hurdles encountered when measuring the



lipophilicity and metabolic stability of the 5-fluoroindole series of model compounds **26x**, it appeared very important to gauge the impact of fluorination on solubility.

### 3.4.2.2 Results

For this study, the thermodynamic solubility of the model compounds was measured in an aqueous buffer at pH 10. The solubility values measured for the basic set of model compounds **60–64** are combined in Figure 49.

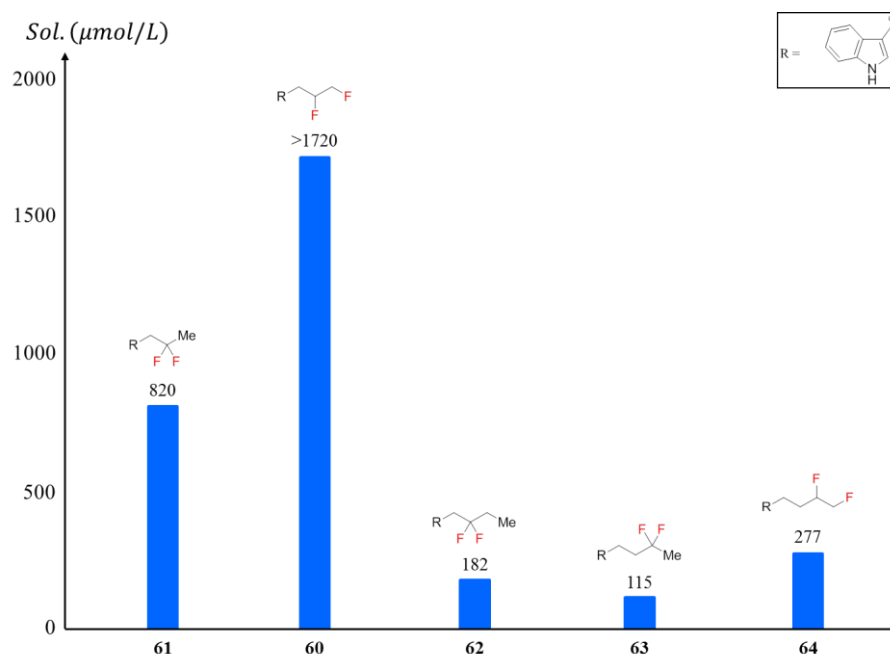


**Figure 49.** Thermodynamic solubility values (*Sol.*) measured for the basic set of model compounds **60–64**.

Figure 49 shows the conspicuous influence on solubility of the basic set of partially fluorinated derivatives **60–64**. In the propyl series, *vic*-difluoro derivative **60** outperforms its *gem*-difluoro analog **61** by a factor of two. As for the butyl series, it was noted that the solubility trend is not that marked, but *vic*-difluoro derivative **64** ends up being the most soluble.

The direct comparison between propyl and butyl series emphasizes even more the crucial role of the alkyl chain length. The fact that compound **60** is more than 6 times more soluble than its butyl analog **64** strongly suggests that this dramatic difference is not only the result of polarity change, but rather the combination of distinct factors. As a matter of fact, comparing the two molecular pairs (**61;60**) and (**63;64**), taken from the same respective alkyl series, reveals that in both cases the *vic*-difluoro derivative is ca. twice as soluble as its *gem*-difluoro counterpart. Thus, converting a *gem*-difluoro motif into a *vic*-difluoro results in a solubility

that is at least increased by a factor of two. By contrast, comparing the two molecular pairs **(61;63)** and **(60;64)** that share the same respective fluorination pattern, shows that the solubility decreases by a factor of 6 when switching from the propyl series to the butyl series.

The direct conclusion from this observation is that, when it comes to solubility, the length of the partially fluorinated alkyl chain is even more determining than the fluorination pattern itself. Also, it should be underlined that the ideal combination of factors increasing solubility is obtained when the *vic*-difluoro motif is borne by a propyl chain.

### 3.4.2.3 Discussion

The introduction of building blocks capable of increasing solubility is highly desirable, but only to a certain extent. Such approach indeed suffers from intrinsic limitations due to the fact that the structural properties determining solubility are also closely correlated with those influencing permeability.<sup>118</sup> Therefore, medicinal chemists have to face the challenge of finding the balance between all relevant parameters involved in order to obtain suitable pharmacokinetics.

In view of simplifying this optimization process, structural modifications with improved specificity and fewer side effects are of high interest. The most commonly used structure modification to date able to improve solubility still remains the addition of ionizable groups.<sup>119</sup> This strategy, although effective, suffers from its pH dependence, which turns out to be problematic in a biological environment where the pH can vary dramatically.<sup>120</sup> Additionally, charged molecules are known to permeate through the lipid bilayer membrane at much slower rates than uncharged ones.

In this context, partially fluorinated building blocks, which are able to induce enhanced solubility without resorting to ionizable groups, are thereby superior. Furthermore, it is worth noting that these short fluoroalkyl chains should have a minimal influence on the size and molecular weight of the modified drug if they are used in replacement of non-fluorinated alkyl chains already in place. Likewise, while adding hydrogen bonding groups usually enhances solubility, a reverse effect is expected on permeability. Hence, fluorine being a poor hydrogen bond acceptor,<sup>12</sup> such building blocks should then have a negligible negative impact on permeability due to hydrogen bonding.

### 3.4.3 Metabolic Stability

#### 3.4.3.1 Results

Based on the results obtained for the series of 3-substituted indole derivatives **23x** and **24x**, it was established that a direct correlation exists between lipophilicity and metabolic stability of partially fluorinated alkyl scaffolds. It was therefore interesting to check if such correlation also applies to the basic set of model compounds **60–64**. To this end, the compounds were subjected to standard microsomal degradation assays (for details, see Experimental Section). Both human and rat microsomes were employed, and the corresponding clearance rates are reported in Figure 50.

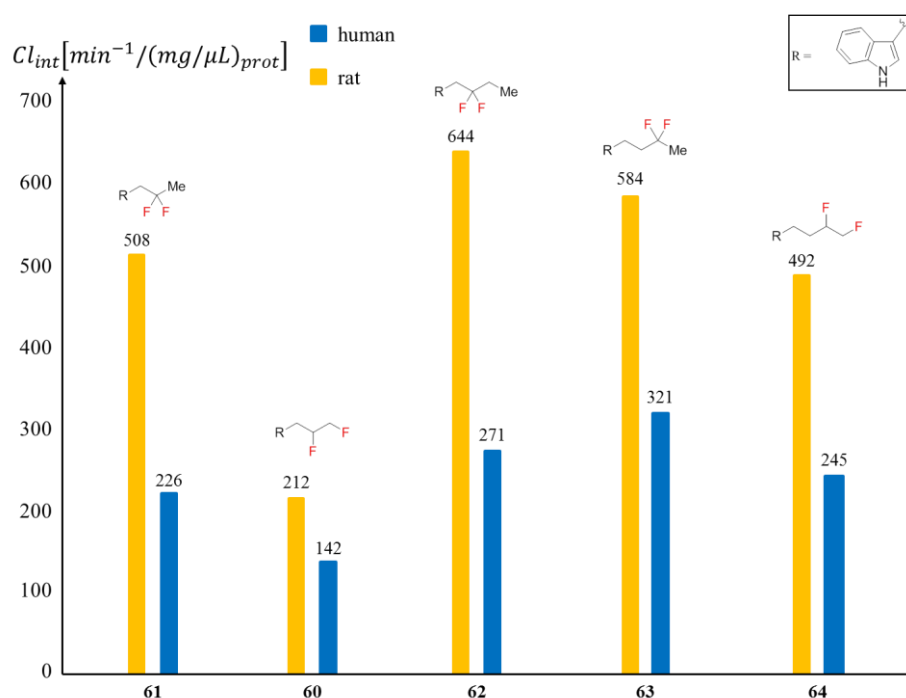


**Figure 50.** Clearance rates ( $Cl_{int}$ ) measured in human and rat for the basic set of model compounds **60–64**.

For propyl derivatives **60** and **61**, both rat and human models report that *vic*-difluoro derivative **60** has a much lower clearance rate than its *gem*-difluoro counterpart **61**. This trend is further exemplified with butyl derivatives **62–64**, thus confirming that the *vic*-difluoro derivative is the most metabolically stable.

With this set of experimental data, the correlation between metabolic stability and lipophilicity could then be determined (Figure 51). In agreement with what has been seen in the previous chapter, clearance rates obtained for the rat model show an excellent correlation with lipophilicity, whereas a slight discrepancy appears in the human model.

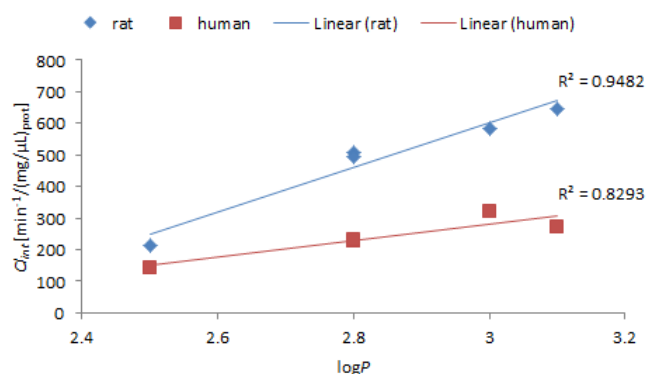


**Figure 51.** Correlation between clearance rate ( $Cl_{int}$ ) and lipophilicity ( $\log P$ ) for rat and human models.

Overall, these results consistently corroborate initial observations and reaffirm the superiority of the *vic*-difluoropropyl scaffold. However, taking into account the fact that the *gem*-difluoro unit is considered by medicinal chemists as one of the most metabolically stable functionalities,<sup>6,52</sup> the low clearance rate recorded for the *vic*-difluoropropyl derivative appears remarkable. Therefore, an investigation was carried out about other possible stabilizing effects that could account for such a pronounced metabolic stability.

### 3.4.3.2 Discussion

Metabolic defluorination pathways have already been the subject of studies, but only fragmentary data addressing the case of aliphatic fluorine atoms have been published to date.<sup>52</sup> As for the *vic*-difluoro motif, there are no literature precedents reporting its systematic study. Nonetheless, the investigation of fluorine-18 labeled radiopharmaceuticals as *in vivo* diagnostic imaging agents has led French *et al.* to an interesting observation on the stability of the fluoroethyl group compared to that of the fluoroethoxy unit (Figure 52).<sup>121,122</sup>

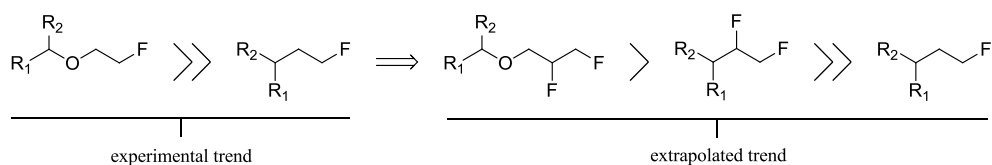


**Figure 52.** Relative stability of some  $\beta$ -stabilized fluoroalkyl group towards metabolic defluorination.

While the metabolic defluorination of monofluoroalkanes is now a well-understood mechanism,<sup>52</sup> they noticed that compounds bearing an electron-withdrawing atom (oxygen in their case) in  $\beta$  position to the fluorine atom are dramatically more stable. The authors claimed that the  $\beta$ -heteroatom disfavors the metabolic hydroxylation process through inductive effect.

Considering the strong electronegativity of fluorine, it can reasonably be assumed that if this  $\beta$ -heteroatom was replaced by a fluorine atom, the effect French *et al.* reported should then be more pronounced in such a case. Coincidentally, as a result of their vicinity, such  $\beta$ -fluorine atoms should afford a mutual stabilizing effect, thereby supporting the surprising metabolic stability of these building blocks.

Further extrapolation of this stabilizing effect suggests that a *vic*-difluoropropoxy group could be an interesting scaffold, provided that it retains all the properties of a *vic*-difluoropropyl group.

### 3.5 Conclusion

In this second chapter, a set of 3-substituted indole derivatives has been designed aiming at gaining insight into the influence of vicinal and multi-vicinal fluoroalkyl groups on polarity. Additionally, efficient syntheses have been developed leading to a structurally diverse range of model compounds following reliable strategies. Physicochemical and pharmacological properties like lipophilicity, aqueous solubility, and metabolic stability were then measured on the relevant set of model compounds.

The results that were obtained not only underscored the strong influence of the *vic*-difluoro motif on polarity, but also brought to light the crucial impact of the alkyl chain length on resulting properties. In this regard, it was shown that, unlike any other partially fluorinated alkyl moiety tested in this work, the *vic*-difluoropropyl group affords the largest lipophilicity decrease, the highest solubility, and the lowest clearance rates.

In summary, this study showed that, due to its unique characteristics, fluorine can impart outstanding properties through simple, but rationally planned structural modifications of known fluorinated moieties.



## 4 Partially Fluorinated Alkyl Ethers

### 4.1 Introduction

Tuning metabolic stability has become one of the most prominent applications of fluorine in modern drug design.<sup>87</sup> Due to its specific properties, it has been shown that fluorine substitution can have a profound effect on drug disposition, in terms of distribution, drug clearance, route(s), and extent of drug metabolism.<sup>52</sup> In this regard, the *p*-fluorophenyl group is the most widely used unit, as it is found in about 40% of the fluorine-containing drugs on the market, or at various stages of clinical development.<sup>45</sup>

It has been established that the *p*-fluorophenyl group is especially optimal for the activity of butyrophenones like Haloperidol (**123**), a major class of neuroleptics that acts by blocking dopamine receptors in the central nervous system (Figure 53).<sup>52</sup> In that particular case, the drug's increased activity not only stems from its enhanced metabolic stability, but also from its higher lipophilicity. Since passive diffusion of a drug across lipid bilayer membranes is mainly governed by its resulting lipophilicity, such a fluorine-containing functional group facilitates the permeation of centrally acting drugs through the very selective blood-brain barrier. Interestingly, in the search for more potent neuroleptics, it was even found that the diarylbutylamine, Pimozide (**124**), which contains two *p*-fluorophenyl groups, was longer acting than Haloperidol (**123**).

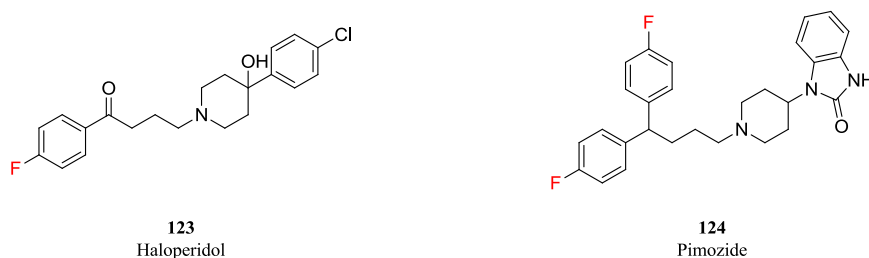


**Figure 53.** Examples of *p*-fluorophenyl-containing neuroleptics: Haloperidol (**123**) and Pimozide (**124**).

Depending on the drug's application, an enhanced lipophilicity can sometimes be desirable. However, experience has shown that increasing lipophilicity considerably usually occurs to the detriment of other pharmacological parameters. Accordingly, medicinal chemists recommend to keep lipophilicity within a reasonable range,  $1 < \log P < 3$ , which usually ensures balanced properties to the drug molecule.<sup>28</sup> Such concept is exemplified by the metabolic optimization of lead compound **125** (Figure 54).<sup>52</sup>

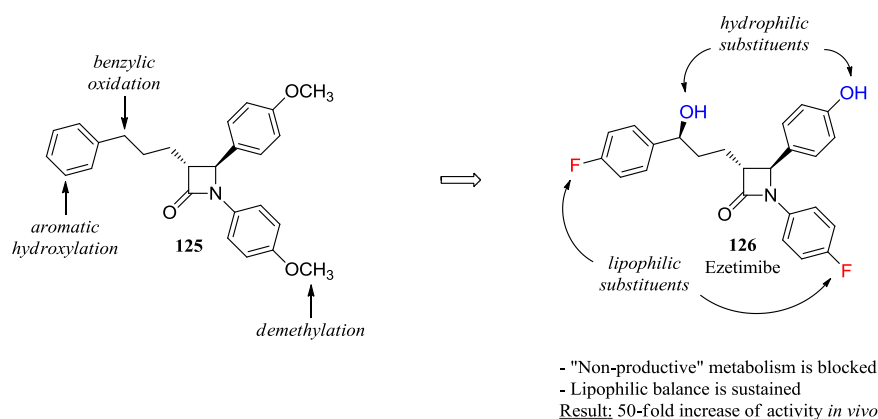


**Figure 54.** Metabolic optimization of lead compound **125** afforded Ezetimibe (**126**).

In this case, the initial lead structure suffered from poor metabolic stability due to its propensity for aromatic hydroxylation, benzylic oxidation, and demethylation reaction. To circumvent this “non-productive” metabolism, two *p*-fluorophenyl groups were introduced. However, due to the higher lipophilicity of these substituents, two hydroxyl groups were simultaneously installed in key positions, thus balancing the resulting lipophilicity. This rational optimization led to a dramatic 50-fold activity increase *in vivo* for compound **126**, better known as Ezetimibe.

This example is representative of the current dilemma faced by medicinal chemists when introducing fluorine atoms onto aromatic rings: it is impossible to block metabolism without increasing lipophilicity.<sup>12</sup> Nonetheless, it has been shown earlier with the series of 5-methoxyindole derivatives (**24x**) that the methoxy group is a good example of liponeutral aromatic substituent able to impart enhanced metabolic stability (Figure 21). Unfortunately, this substituent proved to be relatively prone to metabolic dealkylation reactions (Figure 54).

In this context, it was surmised that it would be possible to use partially fluorinated alkoxy groups to simultaneously block metabolism directed towards aromatic rings, and lower lipophilicity. Such building blocks would thus offer unprecedented opportunities to medicinal chemists seeking for new means of tuning pharmacokinetics. Intrigued by the potential of such a concept, a study was initiated aiming at probing the influence of aromatic fluoroalkyl ethers on fundamental physicochemical properties.



## 4.2 Study on the Polarity of Partially Fluorinated Alkyl Ethers

### 4.2.1 Preliminary Observations

At the outset of this study, it was noticed that marketed molecules featuring fluorinated alkyl ethers were mostly pesticides and herbicides, whereas rare examples of pharmaceuticals could be found.<sup>6</sup> Furthermore, as depicted in Figure 55, it appeared that the structural diversity of such fluorinated alkyl ethers is strictly limited to trifluoromethyl, difluoromethyl, and trifluoroethyl ethers.

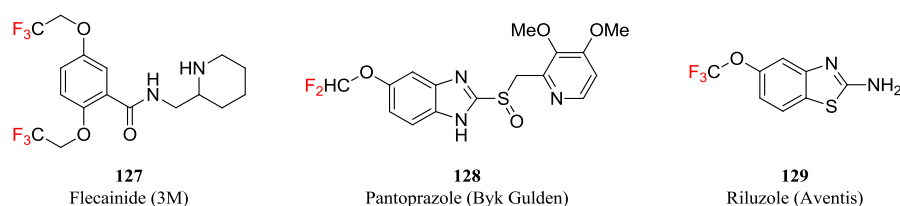
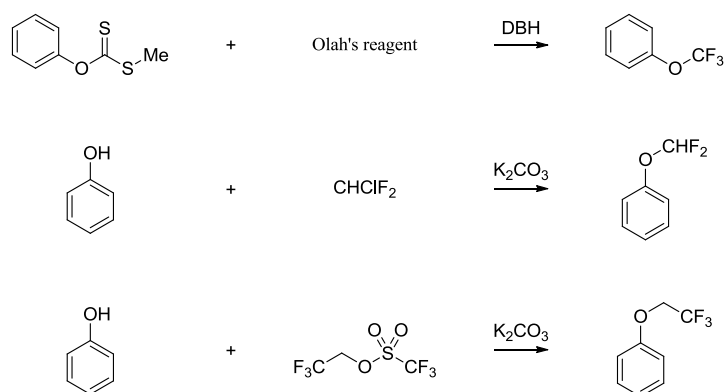


**Figure 55.** Examples of marketed pharmaceuticals bearing one or more fluoroalkyl ether groups: Flecainide (**127**), Pantoprazole (**128**), and Riluzole (**129**).

It seems that the limited use of these fluorinated alkyl ethers in medicinal chemistry mainly stems from the late development of practical synthetic pathways, which rely on a limited set of reactions (Scheme 33): (i) HF-pyridine complex (Olah's reagent), in combination with DBH, is used to convert methyl xanthates into trifluoromethyl ethers;<sup>123</sup> (ii) chlorodifluoromethane can be reacted with a phenol moiety under mildly basic conditions to afford difluoromethyl ethers;<sup>124</sup> (iii) trifluoroethyl triflate can be substituted by a phenol scaffold under mildly basic conditions to access trifluoroethyl ethers.<sup>6</sup>



**Scheme 33.** Common synthetic pathways to fluoroalkyl ethers.

Due to the paucity of molecules bearing fluoroalkyl ethers, only sparse literature precedents have reported that such functionalities proved to be very robust towards oxidative metabolism, and impart higher lipophilicity than their non-fluorinated parents.<sup>6,125</sup> In this

regard, matched molecular pair analysis for the lipophilicity change imparted by partially fluorinated methyl ethers tethered to aromatic rings is revealing (Figure 56).

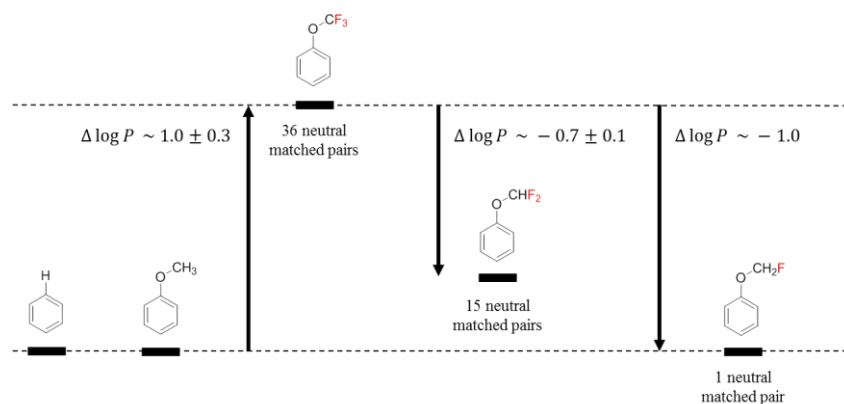


**Figure 56.** Matched molecular pair analysis for the lipophilicity of partially fluorinated methoxyphenyl derivatives and their non-fluorinated parents (MedChem Database, version 2010).

Converting a methoxy group into its trifluorinated analog results in a marked lipophilicity increase ( $\Delta \log P_{CH_3/CF_3} \sim 1.0$ ). Such behaviour is diametrically opposed to what was observed for the series of 3-substituted indole derivatives **23x** and **24x** (Figure 20). Conversely, comparing the trifluoromethoxy group to its difluorinated analog reveals a reverse trend ( $\Delta \log P_{CF_3/CHF_2} \sim -0.7$ ), which is even reinforced in the monofluoromethoxy case ( $\Delta \log P_{CF_3/CH_2F} \sim -1.0$ ). Interestingly, the trend observed within the  $OCH_{3-n}F_n$  series ( $n = 1, 2, 3$ ) is however analogous to the alkyl- $CH_{3-n}F_n$  series.

In light of these preliminary observations, it was attempted to explain why partially fluorinated methyl ethers tethered to aromatic rings induce a lipophilicity increase. Therefore, basic parameters that could account for such a trend were examined.

## 4.2.2 Deciphering the Trend

### 4.2.2.1 Statistical Analysis

In order to identify the origin of the properties that partially fluorinated methyl ethers exhibit, investigating the structural characteristics of aromatic derivatives bearing such scaffolds was expected to provide valuable data. Accordingly, this study started with a search in the Cambridge Structural Database (version 5.33, November 2011) for methoxyphenyl and trifluoromethoxyphenyl derivatives without substituents in *ortho*-positions.

The results obtained allowed to plot the statistical distribution of occurrences observed in crystal structures (N) depending on the dihedral angle ( $\theta$ ) between the phenyl ring and the alkyl ether substituent (Figure 57).

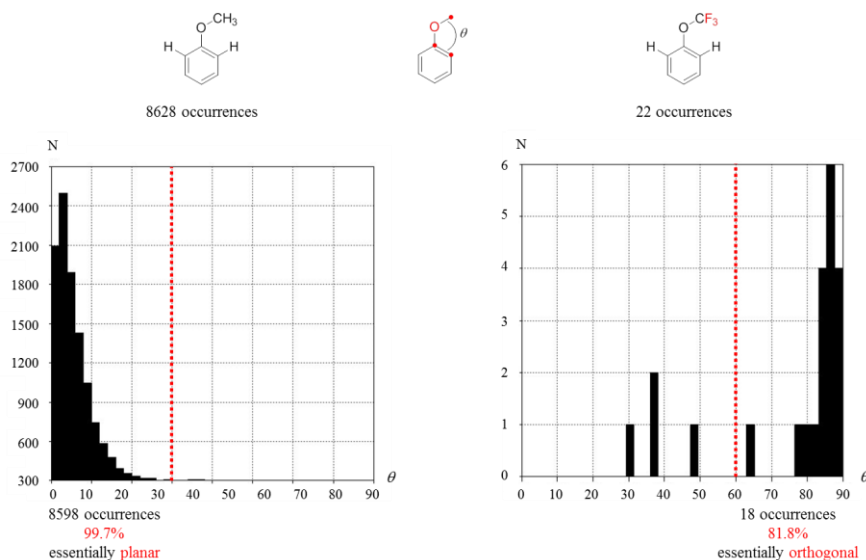


**Figure 57.** Population distribution for methoxyphenyl and trifluoromethoxyphenyl derivatives in crystal structures (CSD version 5.33, November 2011). N – number of occurrences in crystal structures;  $\theta$  – dihedral angle between the phenyl ring and the fluoroalkyl ether substituent.

Among the 8628 occurrences found for derivatives bearing a methoxy group, it resulted that the vast majority adopts an essentially planar conformation ( $\theta < 35^\circ$ ). On the contrary, with only 22 occurrences, the trifluoromethoxy group exhibits a conspicuous preference for the orthogonal conformation ( $\theta > 60^\circ$ ). Therefore, this first observation suggested that an underlying stabilizing effect may govern the out-of-plane orientation of the trifluoromethoxy group.

A similar investigation performed for difluoromethoxyphenyl derivatives revealed a scattered population distribution of the 19 occurrences found in crystal structures (Figure 58). In fact, it appears that the difluoromethoxy group benefits from a relative conformational flexibility which allows for such a pattern. This behaviour thus suggested that the effect responsible for the preferred orthogonal orientation of the trifluoromethoxy group is less pronounced for the difluoromethoxy analog.

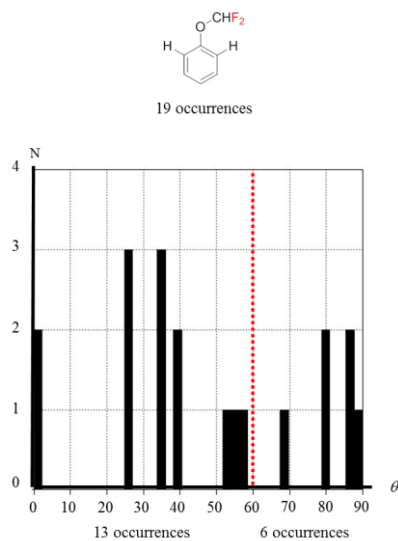


**Figure 58.** Population distribution for difluoromethoxyphenyl derivatives in crystal structures (CSD version 5.33, November 2011). N – number of occurrences in crystal structures;  $\theta$  – dihedral angle between the phenyl ring and the fluoroalkyl ether substituent.

As for the monofluoromethoxyphenyl case, there were no X-ray structures available at the time of the search, thus precluding any direct conclusion based on experimental measurements. The dearth of data in this particular field motivated the use of computational methods as predictive tools to deepen the theoretical understanding of the lipophilicity trend observed in Figure 56.

#### 4.2.2.2 Molecular Modelling of Structural Properties

In order to rationalize the putative stabilizing effect that accounts for the conformational preference of the trifluoromethoxy group in crystal structures, a model structure of trifluoromethoxybenzene was designed (Figure 59, top), from which key characteristics were identified: (i) the hyperconjugative stabilization between the lone pairs of the oxygen and the antibonding orbitals of the anomeric C–F bonds is maximized; (ii) the conjugation existing between the lone pairs of the oxygen and the neighboring  $\pi$ -orbitals of the aromatic ring is weakened; (iii) the bulky trifluoromethyl group induces a partial shielding of one face of the aromatic ring, thus increasing steric hindrance.

The conformational minimum determined *in silico* for trifluoromethoxybenzene resulted in a structure (Figure 59, bottom) that is in agreement with the previous observations made on the simplified model. Additionally, the bond lengths calculated for the trifluoromethyl group confirm the hyperconjugative stabilization suggested earlier, which manifests itself in the lengthening of the anomeric C–F bonds.

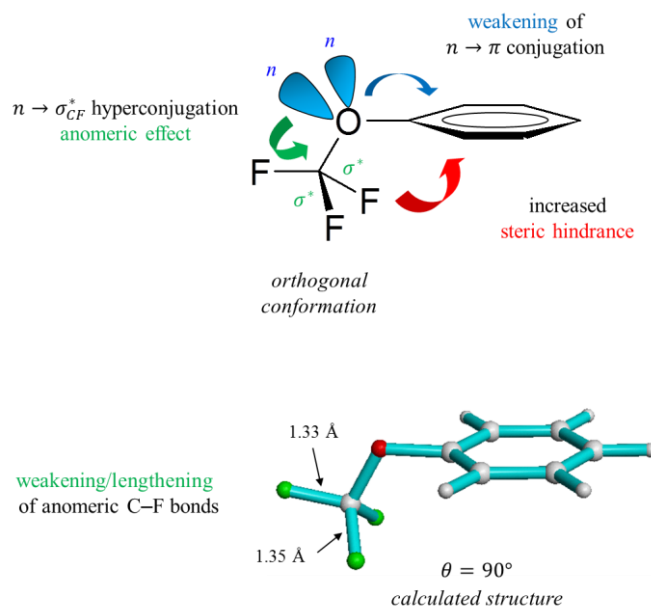


**Figure 59.** Structure-derived properties determined for the conformational minimum of trifluoromethoxybenzene.  $\theta$  – dihedral angle between the benzene ring and the trifluoromethyl group.

Calculations applied to difluoromethoxybenzene revealed that two conformational minima are in close equilibrium (Figure 60). The first one (Figure 60, left) presents the difluoromethyl group orthogonal to the benzene ring ( $\theta = 90.0^\circ$ ), with both C–F bonds pointing *endo*. Despite the partial shielding of the benzene ring that it generates, this conformation is predicted to be more stable as it apparently benefits from the previously underlined hyperconjugative stabilizations. On the contrary, the second conformation (Figure 60, right) shows an essentially in-plane difluoromethyl group ( $\theta < 35^\circ$ ) with one fluorine atom pointing *exo*. Despite losing one hyperconjugative stabilization, this conformation minimizes steric interactions between the fluoroalkyl substituent and the aromatic ring, which explains why the energy difference between these two conformers is only  $\Delta E_{rel} = 0.2 \text{ kcal/mol}$ . In the end, our calculations support the experimental observation suggesting that difluoromethoxyaryl derivatives benefit from a higher conformational flexibility.

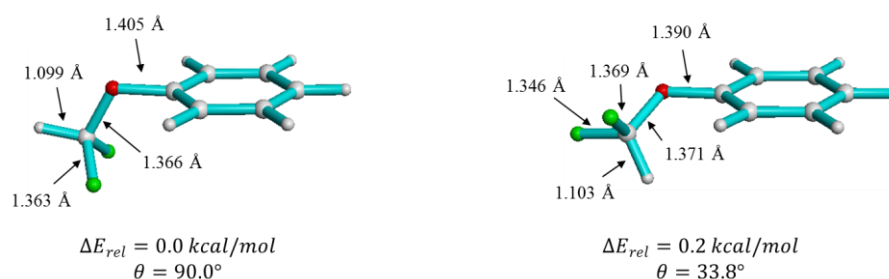


**Figure 60.** Computed conformational minima determined for difluoromethoxybenzene.  $\theta$  – dihedral angle between the benzene ring and the difluoromethyl group.

The conformational minimum calculated for monofluoromethoxybenzene shows an essentially planar orientation of the fluoromethyl group ( $\theta < 35^\circ$ ) where the *endo* fluorine atom holds a position stabilized by hyperconjugation (Figure 61).

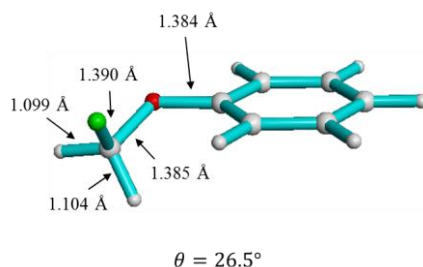


**Figure 61.** Computed conformational minimum determined for monofluoromethoxybenzene.  $\theta$  – dihedral angle between the benzene ring and the monofluoromethyl group.

In summary, the structure-derived properties of this series of model compounds underline that the trifluoromethoxy group is forced to adopt a conformation which leads to higher steric hindrance. This conformational bias provides a reasonable explanation to the observed lipophilicity trend, which is quite reminiscent of the corresponding Alkyl- $CH_{3-n}F_n$  ( $n = 1, 2, 3$ ) cases. However, the Ar- $OCH_2F$  case should be considered with caution since only one neutral matched pair was available at the time of this work. Therefore, investigating the resulting dipole moment of such fluoroalkyl ethers might help to furnish a more definite rationale to this phenomenon.

#### 4.2.2.3 Local Dipole Moments

In order to rationalize the lipophilicity trend revealed in Figure 56, it was attempted to determine the crude estimate of the total resulting local polarity imparted by each partially fluorinated methyl ether (Figure 62).

When trying to correlate bond-vector-predicted polarities with B3LYP-calculated dipole moments, it was determined that  $\mu_{CO} \sim 0.65 \mu_{CF}$  gave the best correlation. Interestingly, it is quite comforting to realize that this corresponds approximately to what one would calculate based on electronegativity differences for C, F, and O (from electronegativity values in Table 1:  $\mu_{CO} \sim 0.62 \mu_{CF}$ ). Therefore, considering that the dipole moment ascribed to a C–O bond is  $\mu_{CO} \sim 0.65 \mu_{CF}$ , the resulting local dipole moment of a trifluoromethyl ether is predicted to be 17% smaller than that of the parent alkyl- $CF_3$ . As expected, the conformationally flexible difluoromethyl ether exhibits different dipole moments depending on whether it adopts an *endo-endo* or *endo-exo* conformation. Also, based on previous calculations (Figure 60), the *endo-endo* conformation should be slightly favored in the gas phase over the *endo-exo*,

whereas the latter should be favored in a polar medium due to its higher polarity. As for the monofluoromethyl ether, it appears that the *gauche* conformation is the only one observed in crystal structures (Personal communication K. Müller), which exhibits a resulting dipole moment equivalent to that of the trifluoromethyl analog.

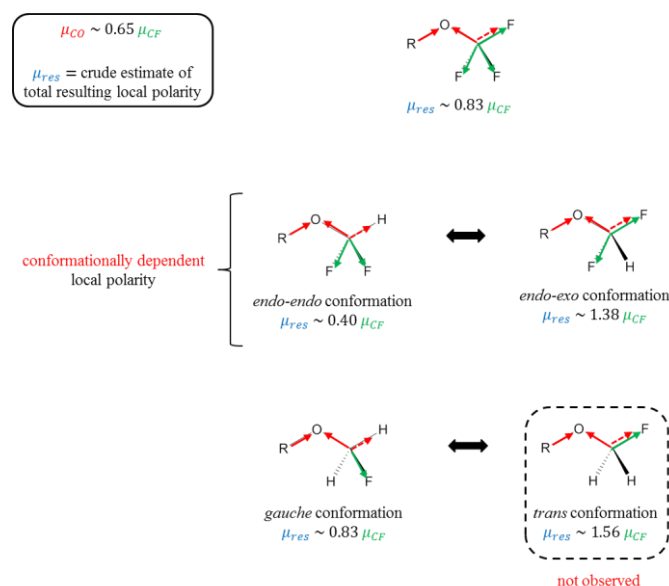


**Figure 62.** Vector analysis of the resulting dipole moments ( $\mu_{res}$ ) of fluoromethyl ethers.

Overall, it appears that the direct vicinity of the polar oxygen atom near the partially fluorinated methyl group in  $OCH_{3-n}F_n$  derivatives results in a local polarity lower than for simple alkyl- $CH_{3-n}F_n$  analogs.

#### 4.2.2.4 Conclusion

Based on the careful investigation of the various features exhibited by partially fluorinated alkyl ethers, it was possible to better apprehend and rationalize the reasons that account for the observed lipophilicity trend (Figure 56). As a result, this analysis leads to the conclusion that the oxygen atom, through short range stabilizing interactions with the C–F bonds, is directly involved in this rather unexpected phenomenon. Therefore, in view of designing partially fluorinated alkyl ethers presenting a lipophilicity-lowering effect similar to the one unveiled in the series of 3-substituted indole derivatives **23x** and **24x**, it was surmised that separating further the fluoromethyl moiety from the oxygen atom would disrupt the stabilizing interactions that led to a marked lipophilicity increase.

### 4.2.3 Towards Lipophilicity-Lowering Alkyl Ethers

An investigation by Smart on the lipophilicity of partially fluorinated alcohols is particularly instructive.<sup>12</sup> In this work, the author reported the influence of the alkyl chain length on the lipophilicity of terminal trifluoromethylated alcohols. The set of data combined in Table 6 underlines the fact that  $\Delta \log P_{CH_3/CF_3}$  between trifluoro derivatives and their non-fluorinated parents depends on the position of the trifluoromethyl group with respect to the oxygen atom.

**Table 6.** Lipophilicity values ( $\log P$ ) of selected trifluoromethylated alcohols<sup>12</sup>

Compound	$\log P$	$\Delta \log P_{CH_3/CF_3}$
CH <sub>3</sub> CH <sub>2</sub> OH	-0.32	
CF <sub>3</sub> CH <sub>2</sub> OH	0.36	0.68
CH <sub>3</sub> (CH <sub>2</sub> ) <sub>2</sub> OH	0.34	
CF <sub>3</sub> (CH <sub>2</sub> ) <sub>2</sub> OH	0.39	0.05
CH <sub>3</sub> (CH <sub>2</sub> ) <sub>3</sub> OH	0.88	
CF <sub>3</sub> (CH <sub>2</sub> ) <sub>3</sub> OH	0.90	0.02
CH <sub>3</sub> (CH <sub>2</sub> ) <sub>4</sub> OH	1.19	
CF <sub>3</sub> (CH <sub>2</sub> ) <sub>4</sub> OH	1.15	-0.04

Smart also noticed that if the trifluoromethyl unit was sufficiently removed from the heteroatom, it not only led to cancellation of lipophilicity increase, but also lowered lipophilicity. This data set, in addition to being in agreement with the hypothesis formulated earlier, underlines a key feature of such systems: the local polarity effects of a trifluoromethyl group manifest themselves independently of the presence of the oxygen atom when they are separated by at least two methylene units.

Assuming that such effect could also be applied to alkoxy groups attached to aromatic rings, it was anticipated that partially fluorinated propyl ethers or higher alkyl analogs should follow the lipophilicity trend of 3-substituted indole derivatives **23x** and **24x**. Encouraged by this eventuality and the lack of experimental data in the field, a suitable set of model compounds was designed that would enable the direct evaluation of this concept.



## 4.3 Design and Synthesis of a Prototypical Set of Model Compounds

### 4.3.1 The Appropriate Candidates

Further to the preliminary investigation on the polarity of partially fluorinated alkyl ethers, it was hypothesized that a minimum of two methylene units would be required for a fluoromethyl group to express the lipophilicity-lowering effect that we revealed earlier for a series of 3-substituted indole derivatives (**23x**, **24x**). Therefore, in order to verify experimentally this theory, a set of indole-based model compounds was designed for the measurement of basic physicochemical properties like lipophilicity and metabolic stability. To this end, a series of 5-substituted indole derivatives (**130x**) equipped with propoxy scaffolds of varying degrees of terminal fluorination was chosen as model system (Figure 63).

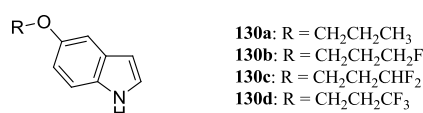


**Figure 63.** Basic set of model compounds **130x** (x = a–d).

The results gathered in the second chapter of this thesis brought to light the marked lipophilicity-lowering properties of more complex fluorination patterns, and especially the vicinal arrangement of two or more fluorine atoms. Encouraged by these precedents, it was envisioned the possibility to synthesize an extended set of model compounds, which would include structurally complex partially fluorinated alkyl ethers **131–137** (Figure 64).

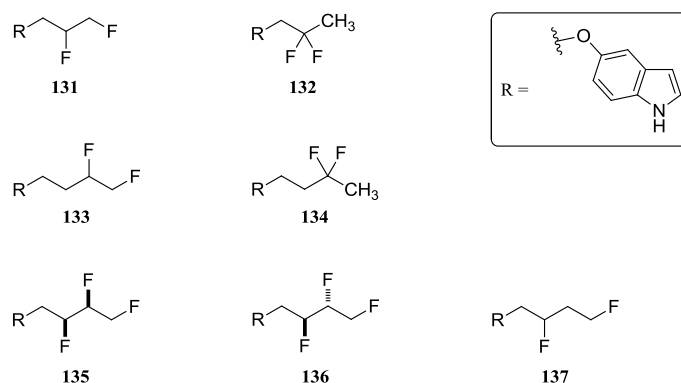
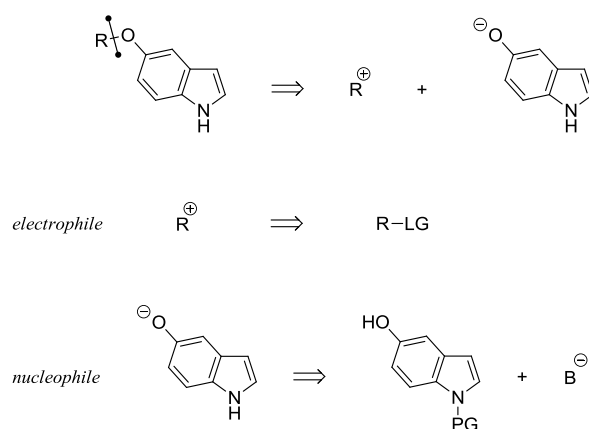


**Figure 64.** Extended set of model compounds **131–137**.

With this structurally diverse range of model compounds, the first conclusions on the polarity of partially fluorinated propyl- and butyloxy derivatives could be drawn, and their effects on prime physicochemical properties could be measured.

### 4.3.2 Retrosynthetic Analysis

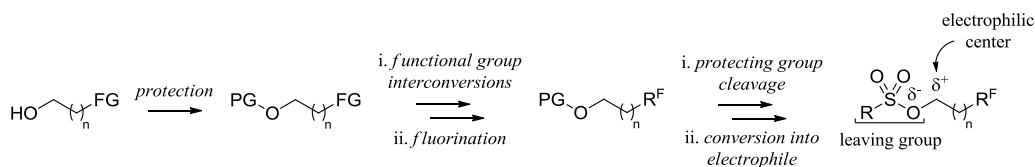
Variably complex strategies to access 5-(alkoxy)indole derivatives have been proposed and developed, but a particularly simple disconnection based on nucleophilic substitution was preferred (Scheme 34). Accordingly, the formation of 5-(alkoxy)indole derivatives could result from the reaction of an electrophilic alkyl source and a nucleophilic indole alkoxide. In that case, it was surmised that the electrophile could originate from the corresponding alkyl bearing an appropriate leaving group, whereas the indole nucleophile could result from the deprotonation in basic conditions of the corresponding protected 5-hydroxyindole.



**Scheme 34.** Key disconnection towards 5-(alkoxy)indole derivatives. LG – leaving group; PG – protecting group; B – base.

This key disconnection would then open the way to a building block strategy involving the reaction of a prefunctionalized partially fluorinated alkyl electrophile and the protected 5-hydroxyindole. The main advantage of such a strategy is that it allows complex building blocks to be introduced at late stages. Nonetheless, the synthesis of reactive, stable, and easy-to-handle partially fluorinated electrophiles was required. Based on previous experience, a general synthetic strategy was then designed to access the desired electrophiles.

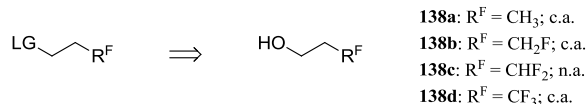
A commercially available alcohol bearing a functional group that could be further converted into the required fluorination pattern would initially be protected with a moiety able to stand the various functional group interconversions and fluorination steps (Scheme 35). After the introduction of all fluorine atoms, the selective protecting group cleavage would release the partially fluorinated alcohol, which could then be converted into a reactive electrophile (e.g. a sulfonate).



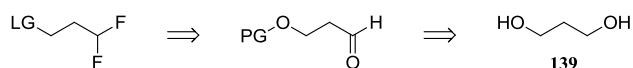
**Scheme 35.** Synthetic strategy towards partially fluorinated alkyl electrophiles. FG – functional group; PG – protecting group;  $n = 1, 2$ ;  $R^F$  – partially fluorinated scaffold.

Of course, in case of commercial availability of partially fluorinated alkyl alcohols, their conversion into sulfonates would directly afford the required electrophiles (Scheme 36, top). However, since only structurally simple building blocks were widely available at the time of this work, most of the required electrophiles had to be prepared (Scheme 36, bottom). In this regard, although a quick access to model compounds **130a**, **130b**, and **130d** could be anticipated from the respective commercially available alcohols **138a**, **138b**, and **138d**, the unavailability of 3,3-difluoropropan-1-ol (**138c**) led to the design of an alternative pathway to access *gem*-difluoro analog **130c**. Based on a simple synthetic plan (Scheme 36, bottom) it was assumed that the *gem*-difluoromethyl moiety could result from the deoxofluorination reaction of an appropriate aldehyde, whereas the latter could be obtained from commercially available propan-1,3-diol (**139**).

General strategy

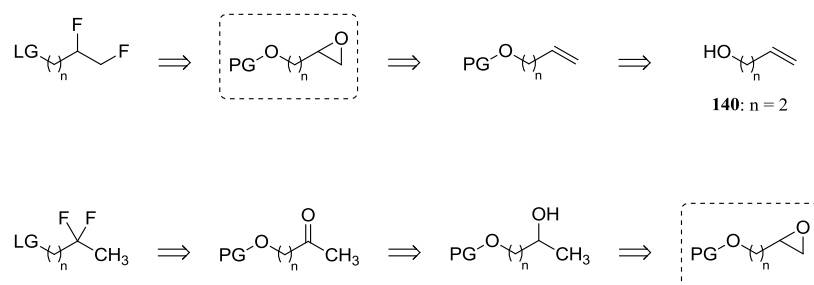


Alternative



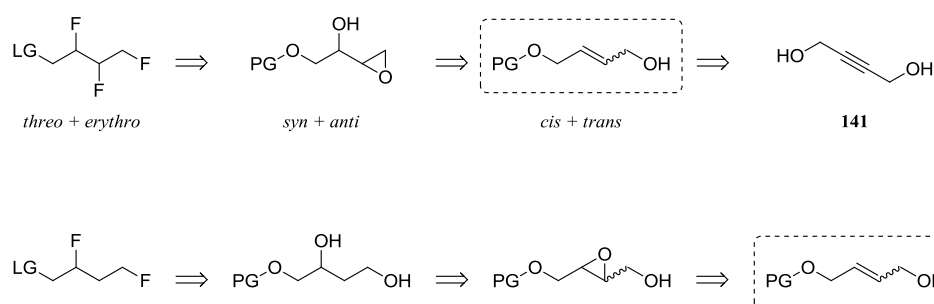
**Scheme 36.** Retrosynthetic analysis of the basic set of partially fluorinated alkyl electrophiles (c.a. – commercially available; n.a. – not available).

Likewise, the synthesis of *vic*-difluoroalkyl electrophiles was envisioned from terminal epoxides, which could be synthesized from the corresponding allylic or homoallylic (**140**) alcohols (Scheme 37, top). The internal *gem*-difluoro derivatives could then be obtained from the deoxofluorination of the corresponding ketones, which could be derived from the oxidation of the appropriate branched alcohols (Scheme 37, bottom).



**Scheme 37.** Retrosynthetic analysis of *vic*- and *gem*-difluoroalkyl electrophiles.

Ultimately, reusing a transformation reminiscent of the one employed for the synthesis of *threo* and *erythro vic*-difluorobutyl derivatives **65** and **66**, it was anticipated that the branched alcohols could stem from the corresponding terminal epoxides, as suggested earlier (Scheme 32). Overall, both series of *vic*- and *gem*-difluoroalkyl electrophiles could be accessed from the same precursor in a divergent fashion.



**Scheme 38.** Restrosynthetic analysis of *bis-vic*-trifluoro- and 1,3-difluorobutyl building blocks.

Building on the experience accumulated in the synthesis of *bis-vic*-trifluorobutyl derivatives **67** and **68**, it was assumed that an identical strategy could be followed for the synthesis of the required *threo* and *erythro bis-vic*-trifluoroalkyl electrophiles (Scheme 38, top). Accordingly, both building blocks could be obtained from the widely available butyne-1,4-diol (**141**). Furthermore, it was surmised that the 1,3-difluorobutyl electrophile could result from the deoxofluorination of the corresponding 1,3-diol (Scheme 38, bottom). Thereby, assuming that this diol could originate from the selective opening of an appropriate epoxyalcohol, it was planned to access the latter from an intermediate allylic alcohol also used in the synthesis of the *bis-vic*-trifluoro analogs.

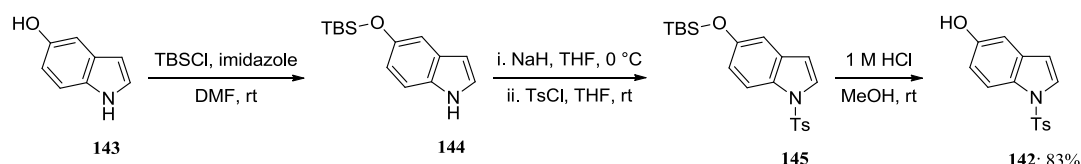
Having set the basis of the required synthetic plans, the protecting group and the sulfonate that would be employed in the synthesis of partially fluorinated alkyl electrophiles were decided. On the one hand, the trityl protecting group was chosen because (i) it is easily installed on terminal alcohols, (ii) it is generally robust towards any kind of basic conditions that can be faced when a fluoride source is used, (iii) it converts any aliphatic alcohol into a

UV-active species, (iv) it usually affords crystalline compounds that would enable X-ray crystal structure analysis, and (v) it can be readily cleaved in acidic conditions. On the other hand, the *p*-nitrobenzenesulfonate leaving group was chosen because (i) it is a well-tried strategy to convert alcohols into versatile leaving groups, and it usually affords (ii) UV-active and (iii) crystalline products.

### 4.3.3 Synthetic Access

#### 4.3.3.1 Basic Set of Model Compounds

*En route* to the synthesis of the basic set of model compounds **130x**, it was a prerequisite to develop a reliable access to the *N*-protected 5-hydroxyindole **142**. Hence, combining the results of previous reports,<sup>126,127</sup> a three-step procedure was optimized starting from commercially available 5-hydroxyindole (**143**) (Scheme 39).



**Scheme 39.** Three-step synthesis of protected indole **142**.

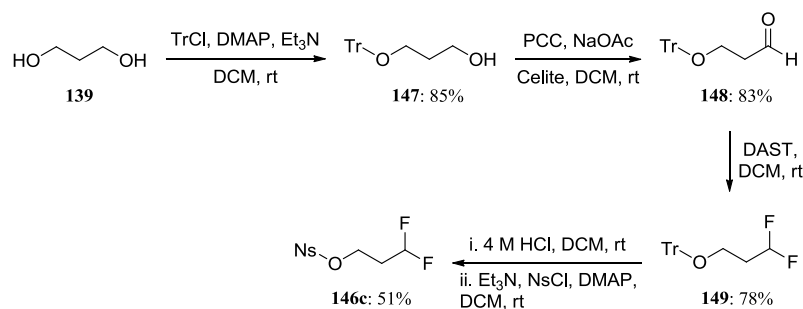
After selective TBS-protection of the free alcohol **143**, tosyl-protection of the indole nitrogen proceeded from **144**.<sup>126</sup> Finally, selective cleavage of the silyl protecting group took place upon treatment of **145** with HCl in methanol.<sup>127</sup> Overall, the desired 5-hydroxyindole **142** was isolated in excellent yield over three steps after crashing out from the reaction mixture. This high-yielding and operationally simple three-step synthesis allowed compound **142** to be conveniently prepared on a multi-gram scale.

With the indole precursor in hand, the synthesis of the basic set of nosylates **146x** could be carried out. All commercially available alcohols, **138a**, **138b**, and **138d**, were readily converted into the corresponding nosylates in good to acceptable yields (Scheme 40, top).<sup>128</sup> Nosylate **146c** was synthesized in four steps starting with the trityl-protection of diol **139** (Scheme 40, bottom).<sup>129</sup> The monoprotected alcohol **147** was then further oxidized to aldehyde **148** with PCC,<sup>83</sup> and the following deoxofluorination with DAST afforded difluoride **149** in high yield.<sup>84</sup>

Direct synthesis



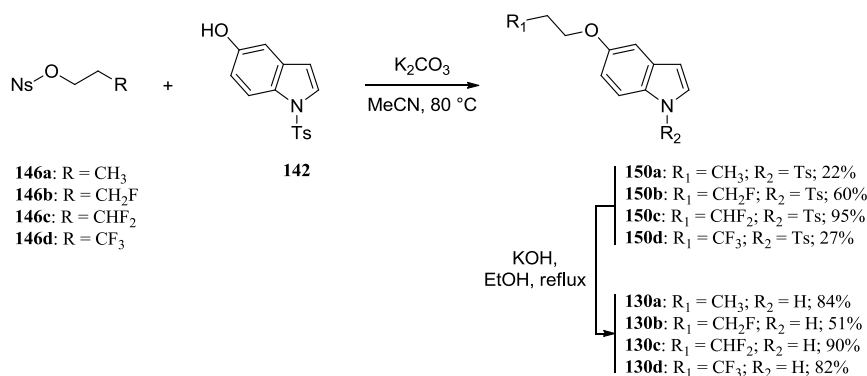
Indirect synthesis



**Scheme 40.** Synthetic access to partially fluorinated alkyl nosylates **146x** (x = a–d).

The conversion of **149** into nosylate **146c** turned out to be more problematic than anticipated. Despite the effective cleavage of the trityl protecting group, it was impossible to isolate more than minute amounts of unprotected alcohol after careful distillation. To circumvent this issue, a two-step one-pot procedure was developed in which the transient alcohol was converted *in situ* into the corresponding nosylate. Thus, after trityl cleavage with HCl, the reaction could be *in situ* basified with triethylamine, and further addition of nosyl chloride afforded **146c** in good yield.<sup>128,130</sup>

After having successfully overcome this first synthetic hurdle, it was finally possible to test the initial approach to model compounds **130x**. Although a range of bases susceptible to generate the indole alkoxide was tried, the higher yielding conditions required the use of potassium carbonate (Scheme 41). When reacting a mixture of a nosylate (**146x**) with 5-hydroxyindole **142** and potassium carbonate in acetonitrile at 80 °C, the corresponding alkyl ether (**150x**) could be isolated in moderate to excellent yields.<sup>131</sup> Further deprotection of ethers **150x** proceeded smoothly with potassium hydroxide in boiling ethanol, thus affording model compounds **130x**.<sup>81</sup>



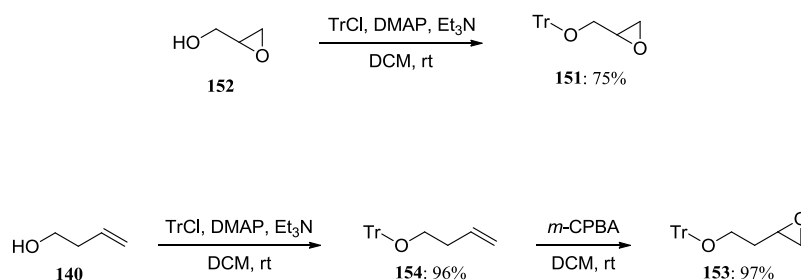
**Scheme 41.** Late stage synthesis of model compounds **130x** (x = a–d).

In an attempt to rationalize the extreme yield variations observed for the formation of compounds **130x**, the key factors influencing this reaction that most likely proceeds via S<sub>N</sub>2 mechanism were examined: i.e. steric hindrance and electronic effects. Due to the strong electron-withdrawing character of the fluorine atom, it results that a fluoromethyl group inductively reinforces the electron-deficiency in β-position. Additionally, due to the larger radius of the fluorine atom compared to hydrogen, the substitution of hydrogen atoms by fluorine generates a substantial volume increase, which translates into more steric hindrance in the direct vicinity of the fluorinated position. Consequently, it is not surprising to observe that high yields are obtained for mono- and difluoro nosylates **146b** and **146c**, since they both enhance the electrophilicity without engendering too much steric hindrance, unlike the trifluorinated analog **146d**.

These results showed that this strategy can yield the desired partially fluorinated alkyl ethers, and was expected to enable the synthesis of the more complex model compounds **131–137**. Nevertheless, as pointed out in the previous paragraph, the nucleophilic substitution proved to be sensitive to steric hindrance and electronic effects induced by the replacement of hydrogen atoms by fluorine, which suggested unexpected issues with particularly destabilizing fluorination patterns.

#### 4.3.3.2 Extended Set of Model Compounds

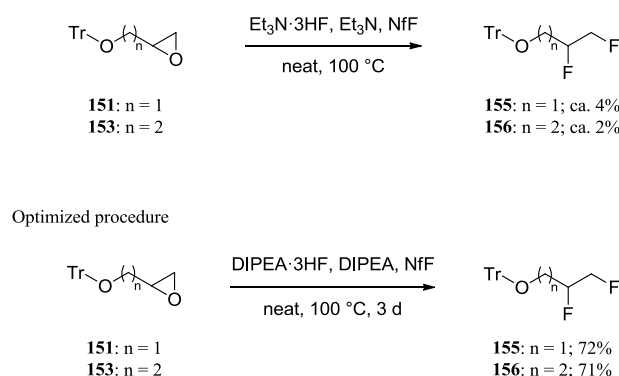
The synthesis of the extended set of model compounds commenced with the *vic*-difluoro derivatives, which first required the synthesis of terminal epoxides (Scheme 42). Propyl analog **151** was synthesized by direct trityl-protection of commercially available glycidol **152**, whereas butyl analog **153** was obtained after trityl-protection of homoallylic alcohol **140** and further *m*-CPBA epoxidation of olefin **154**.<sup>129,132</sup>



**Scheme 42.** Synthesis of terminal epoxides **151** and **153**.

With the terminal epoxides in hand, it was initially planned to access *vic*-difluorides **155** and **156** with the previously employed two-step fluorination procedure. However, as both the opening of the epoxide and the deoxofluorination of the resulting fluorohydrin relied on the same source of nucleophilic fluoride, i.e. triethylamine trihydrofluoride, it was attempted to develop a one-pot procedure that could directly convert each epoxide into the corresponding *vic*-difluoride.

The first attempts consisted in reacting the epoxides in a neat mixture of  $\text{Et}_3\text{N}\cdot 3\text{HF}$ ,  $\text{NfF}$ , and  $\text{Et}_3\text{N}$  at  $100\text{ }^\circ\text{C}$  (Scheme 43, top). Under these conditions, only trace amounts of the desired *vic*-difluorides were isolated, along with several side-products resulting from concomitant elimination reactions. According to Yin *et al.*, the use of  $\text{DIPEA}\cdot 3\text{HF}$ , in combination with  $\text{DIPEA}$ , could mitigate competitive pathways during the fluorination.<sup>80</sup> Hence, treatment of terminal epoxides **151** and **153** with  $\text{DIPEA}\cdot 3\text{HF}$ ,  $\text{DIPEA}$ , and  $\text{NfF}$  afforded, after three days at  $100\text{ }^\circ\text{C}$  in a sealed flask, the corresponding *vic*-difluoro ethers **155** and **156** in high yields (Scheme 43, bottom).

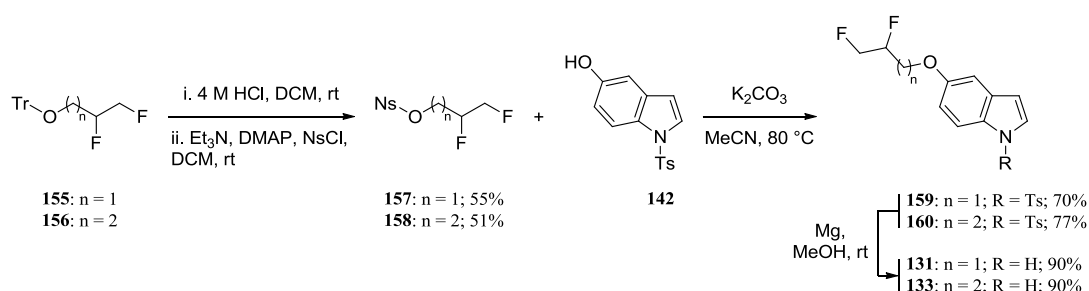


**Scheme 43.** One-pot difluorination reaction of terminal epoxides **151** and **153**.

The newly prepared *vic*-difluoro ethers **155** and **156** were converted in good yields into the nosylates following our previously developed procedure (Scheme 44).<sup>128,130</sup> Further substitution reaction of nosylates **157** and **158** with 5-hydroxyindole **142** proceeded smoothly in both cases.<sup>131</sup> Finally, tosyl-deprotection of ethers **159** and **160** with magnesium in



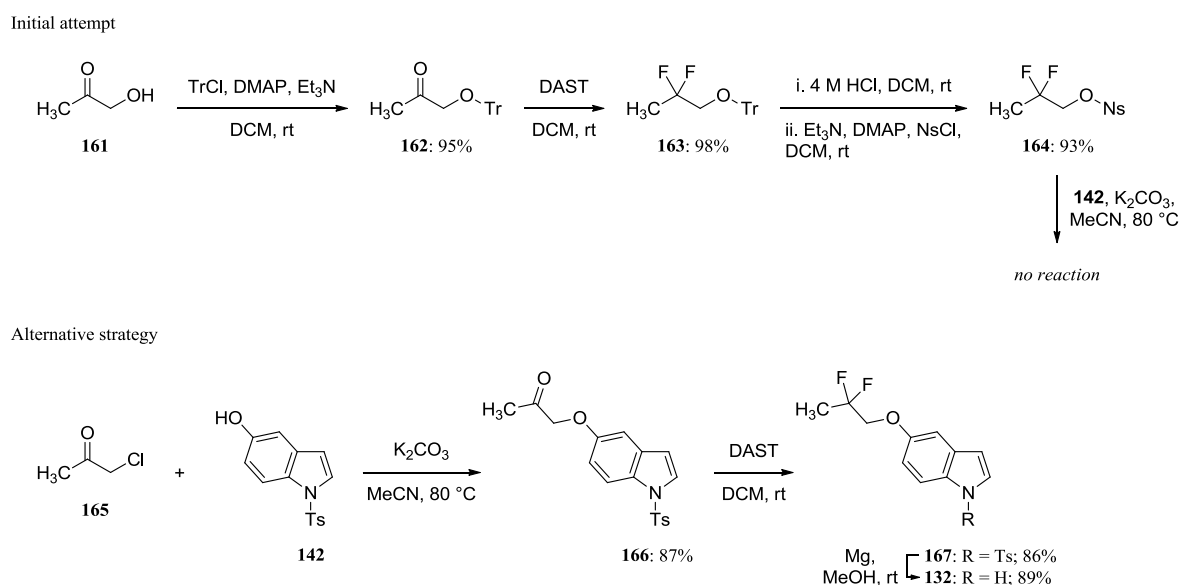
methanol was preferred over potassium hydroxide as it avoided side-reactions and afforded model compounds **131** and **133** in high yields.<sup>116</sup>



**Scheme 44.** Access to *vic*-difluoroalkyl ethers **131** and **133**.

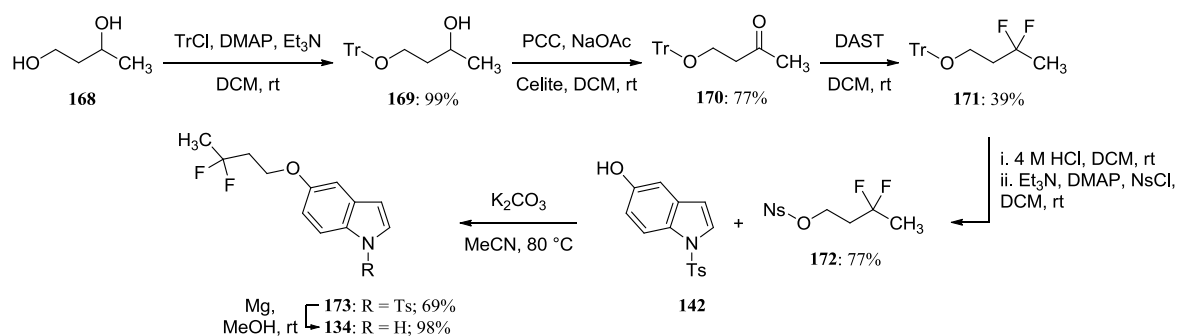
In the synthesis of *gem*-difluoropropyl ether **132** (Scheme 45, top), the required nosylate was prepared in three steps from hydroxyacetone **161** instead of using the terminal epoxide, as initially suggested in the retrosynthetic plan (Scheme 37). After trityl-protection, ketone **162** was treated with DAST, thus affording *gem*-difluoride **163** in quantitative yield.<sup>84,129</sup>

Although the conversion of the trityl-protected scaffold into the corresponding nosylate proceeded in excellent yield,<sup>128,130</sup> it was impossible to isolate any ether product after subjecting nosylate **164** to standard reaction conditions.<sup>131</sup> This result is in agreement with the previous observations on the impact of fluorination on the substitution reaction (Scheme 41). In that particular case, the *gem*-difluoromethyl unit inductively increases the electrophilicity of the neighboring carbon, but brings some additional steric and electronic shielding. The combination of these negative factors presumably precludes any nucleophilic attack.



**Scheme 45.** Synthesis of *gem*-difluoropropyl ether **132**.

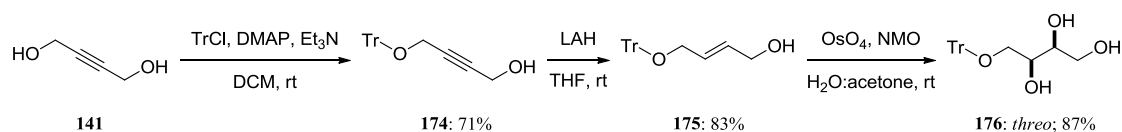
To circumvent this problem, a late stage fluorination strategy was carried out (Scheme 45, bottom), starting with the reaction of chloroacetone (**165**) with 5-hydroxyindole **142**, which afforded ketone **166**.<sup>133</sup> The latter was then treated with DAST, which led to the corresponding *gem*-difluoride **167**.<sup>84</sup> Deprotection with magnesium in methanol finally gave *gem*-difluoropropyl ether **132** in high yield.<sup>116</sup>



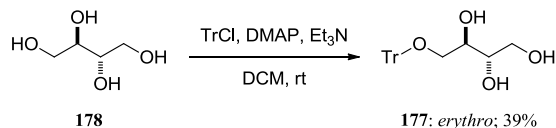
**Scheme 46.** Synthesis of *gem*-difluorobutyl ether **134**.

The synthesis of the butyl analog worked according to the initial plan, although it was possible to commence directly with diol **168** (Scheme 46). After quantitative trityl-protection of the primary alcohol, the remaining hydroxyl group of **169** was oxidized to ketone **170** in high yield.<sup>83,129</sup> The latter was then treated with DAST, which afforded *gem*-difluoride **171** in acceptable yield.<sup>84</sup> Its conversion into nosylate **172** worked effectively under standard conditions, as well as the subsequent substitution reaction.<sup>128,130,131</sup> Finally, *gem*-difluorobutyl ether **134** was isolated after tosyl-deprotection of ether **173** with magnesium in methanol.<sup>116</sup>

*Threo* multi-vicinal triol



*Erythro* multi-vicinal triol

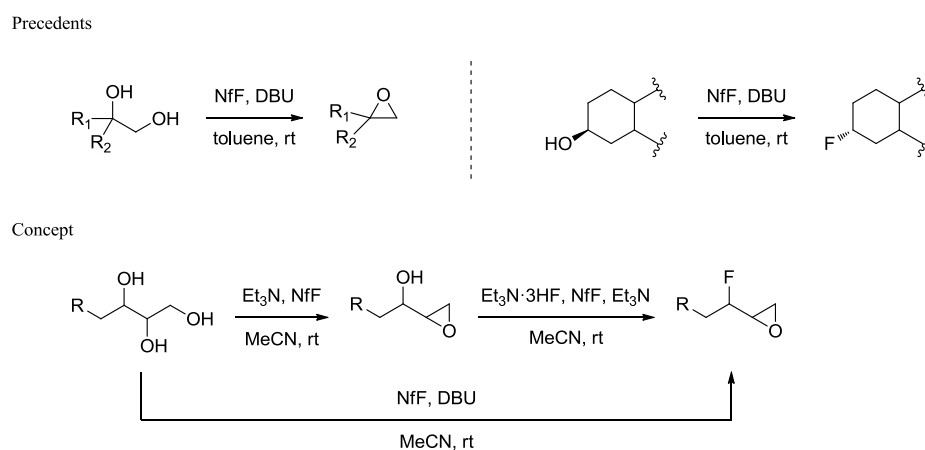


**Scheme 47.** Synthesis of multi-vicinal triols **176** and **177**.

The synthesis of the final set of model compounds commenced with the *threo* and *erythro* multi-vicinal triols. As planned, butyne-1,4-diol **141** was monoprotected to alcohol **174**, which was then reduced with lithium aluminium hydride to afford *trans*-allylic alcohol **175** in good yield (Scheme 47, top).<sup>113,129</sup> Under standard dihydroxylation conditions, **175** was

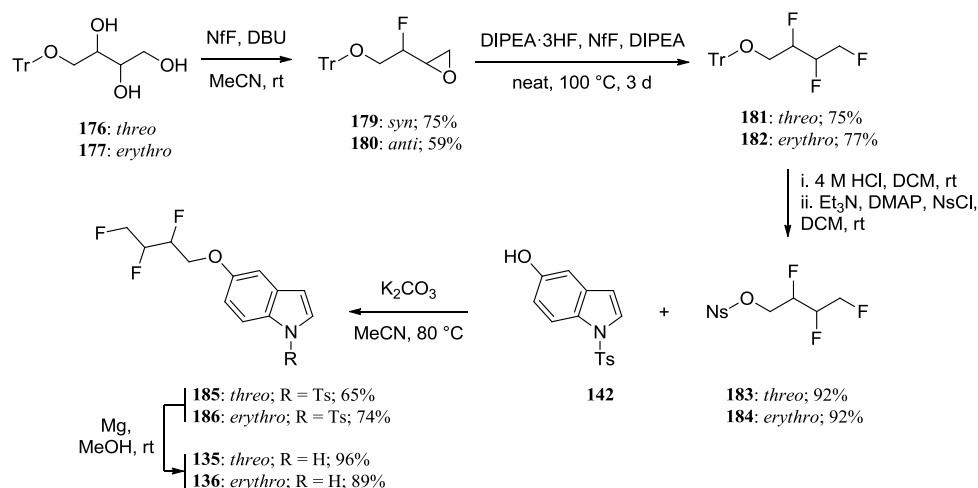
converted into *threo bis-vic-triol* **176** in excellent yield.<sup>109</sup> The *erythro* isomer **177** was synthesized in one step after trityl-protection of commercially available *meso*-erythritol (**178**).<sup>129</sup>

Having already applied the combination of NfF and Et<sub>3</sub>N to the selective epoxide formation from 1,2-diols, it was interesting to investigate the fluorination potential of these reagents (Scheme 48, top). As reported by Vorbrüggen *et al.*, the treatment of a secondary alcohol with NfF in presence of DBU in toluene at room temperature afforded the corresponding fluorinated analog in good yield.<sup>134</sup> The authors underlined the importance of the base in the formation of the active DBU·(HF)<sub>n</sub> complex, as any other base was unable to afford an effective nucleophilic source of fluoride. The conditions reported by Yin *et al.* require the use of an external source of Et<sub>3</sub>N·3HF or DIPEA·3HF for the same reason: the *in situ* generated HF-complex is not sufficiently nucleophilic for the displacement of perfluorobutanesulfonates.<sup>80</sup>



**Scheme 48.** Unprecedented two-step one-pot fluoroepoxidation reaction.

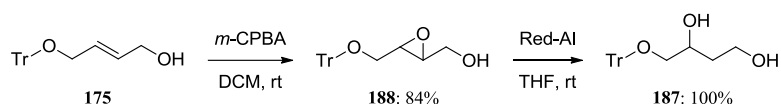
Considering that the combination of NfF and DBU can convert 1,2-diols into epoxides,<sup>108</sup> and deoxofluorinate secondary alcohols,<sup>134</sup> it was anticipated that it would be possible to use these reagents for the one-pot fluoroepoxidation of a *bis-vic-triol* (Scheme 48, bottom). In fact, good isolated yields of fluoroepoxides **179** and **180** were recorded after subjecting *threo* and *erythro* triols **176** and **177** to the NfF/DBU system of reagents (Scheme 49). This unprecedented transformation proved to be consistently reproducible on multi-gram scale, which makes it an efficient strategy to access complex fluorinated scaffolds from inexpensive reagents.



**Scheme 49.** Synthesis of *bis-vic*-trifluorobutyl ethers **135** and **136**.

When the resulting fluoroepoxides **179** and **180** were subjected to the difluorination conditions,<sup>80,102</sup> the corresponding *bis-vic*-trifluoro ethers **181** and **182** were isolated in excellent yields. The latter were then converted into nosylates **183** and **184** in quantitative yield,<sup>128,130</sup> and their further reaction with 5-hydroxyindole **142** proceeded under standard conditions.<sup>131</sup> Unprotected model compounds **135** and **136** were finally isolated upon treatment of ethers **185** and **186** with magnesium in methanol.<sup>116</sup> Overall, *threo* and *erythro* *bis-vic*-trifluorobutyl ethers **135** and **136** were synthesized in five steps from *threo* and *erythro* *bis-vic*-triols **176** and **177** in respectively 25 and 35% yield.

It was then surmised that it would be possible to directly fluorinate 1,3-diol **187** in order to obtain 1,3-difluorobutyl ether **137**. Following the initially designed strategy, allylic alcohol **175** was epoxidized with *m*-CPBA,<sup>132</sup> and the resulting epoxyalcohol **188** afforded 1,3-diol **187** upon treatment with Red-Al in quantitative yield (Scheme 50).<sup>135</sup>



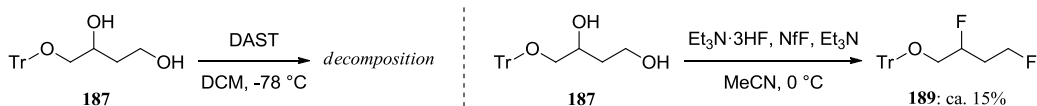
**Scheme 50.** Synthesis of 1,3-diol **187**.

With 1,3-diol **187** in hand, the possibility to convert it directly into the 1,3-difluorobutyl ether was examined. According to predominant literature precedents, such substrates fail to afford any difluoride upon direct treatment with DAST,<sup>72</sup> and usually yield the cyclic sulfate instead (Scheme 51, top). Interestingly, similar sulfates were conveniently used by Nicoletti *et al.* to convert vicinal diols into the corresponding vicinal difluorides.<sup>136</sup> However, the initial attempt to treat 1,3-diol **187** with DAST at low temperature led to complete decomposition of the starting material (Scheme 51, center left).

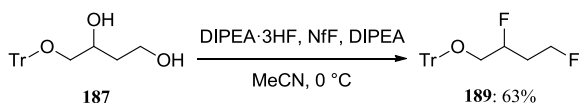
Precedents



Initial attempts

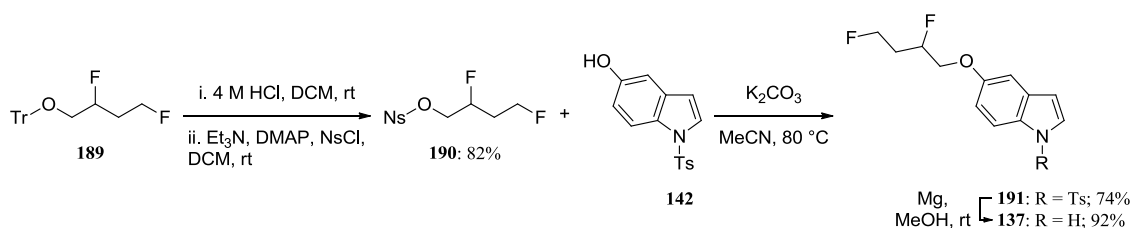


Optimized conditions

**Scheme 51.** Deoxofluorination reaction of 1,3-diol **187**.

On the contrary, when treating 1,3-diol **187** with a combination of  $\text{Et}_3\text{N}\cdot 3\text{HF}$ ,  $\text{Et}_3\text{N}$ , and  $\text{NfF}$ ,<sup>80</sup> ca. 15% of 1,3-difluoride **189** could be isolated (Scheme 51, center right). This promising result suggested to try with a combination of  $\text{DIPEA}\cdot 3\text{HF}$  and  $\text{DIPEA}$ , which resulted in a dramatic yield improvement. It was thus possible to isolate 1,3-difluorobutyl ether **189** in 63% yield upon direct deoxofluorination of 1,3-diol **187** (Scheme 51, bottom).

The multi-gram scale synthesis of 1,3-difluorobutyl ether **189** enabled the isolation of nosylate **190** in high yield after standard functional group interconversion.<sup>128,130</sup> Reaction between nosylate **190** and 5-hydroxyindole **142** finally afforded ether **191**,<sup>131</sup> which was then deprotected to model compound **137**.<sup>116</sup>

**Scheme 52.** Access to 1,3-difluorobutyl ether **137**.

In summary, unprecedented expedient syntheses of structurally complex partially fluorinated alkyl electrophiles have been developed, and their practical usefulness as reactive building blocks to access a range of partially fluorinated 5-(alkyloxy)indole derivatives has been demonstrated. This strategy offers new perspectives to medicinal chemists interested in grafting partially fluorinated alkyl moieties onto aromatic hydroxyl groups. All compounds were isolated in amounts and purities suitable for further experimental measurements.

## 4.4 Physicochemical and Pharmacological Properties

### 4.4.1 Basic Set of Model Compounds

#### 4.4.1.1 Lipophilicity

The basic set of model compounds was initially designed to evaluate whether a series of propyl ethers fluorinated in terminal position could impart lipophilicity-lowering properties. Therefore, the series of partially fluorinated propyl ethers **130x** was subjected to standard  $\log P$  measurements (for details, see Experimental Section), whose results are combined in Figure 65.

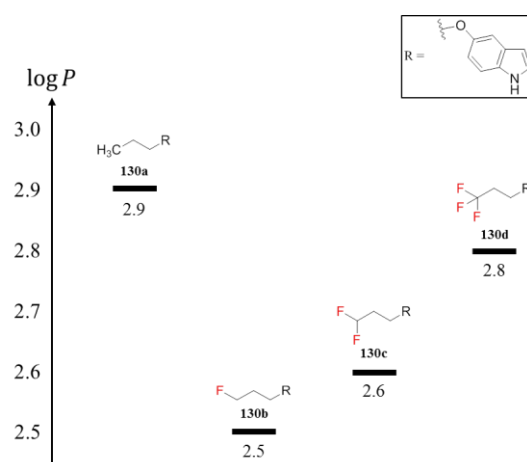


**Figure 65.** Lipophilicity values ( $\log P$ ) determined for the basic set of partially fluorinated propyl ether derivatives **130x** (**x = a–d**).

The lipophilicity trend recorded for the basic series of model compounds is identical to the one reported earlier for the series of 3-substituted indole derivatives **23x** and **24x**. The relative  $\Delta \log P$  values are consistently reproduced in that case, and the relative polarity order is confirmed, i.e.  $\text{CH}_2\text{F} \geq \text{CHF}_2 \gg \text{CF}_3 \geq \text{CH}_3$ . These results corroborate the fundamental hypothesis formulated on the influence of the chain length on the resulting lipophilicity of partially fluorinated alkyl ethers. Therefore, it appears that two methylene units separating the fluoromethyl group from the oxygen atom are sufficient to impart the expected lipophilicity-lowering effect.

In summary, the experimental data on the lipophilicity of 5-(propyloxy)indole derivatives **130x** revealed how a minor structural modification, like the introduction of a methylene unit, can lead to drastically modified properties. This highlights the potential of partially fluorinated alkyl ethers as lipophilicity-tuning building blocks, and suggested to pursue the evaluation of their impact on metabolic stability.

#### 4.4.1.2 Metabolic Stability

Previous results obtained for 3-substituted indole derivatives **23x** and **24x** revealed the direct correlation existing between lipophilicity and metabolic stability (Figure 22). However, the fact that  $Ar-OCH_{3-n}F_n$  and  $Ar-OCH_2CH_{3-n}F_n$  ( $n = 2, 3$ ) ethers are not only more lipophilic, but also more metabolically stable than their non-fluorinated counterparts<sup>6,125</sup> suggested that such derivatives influence metabolic stability differently from alkyl- $CH_{3-n}F_n$  analogs.

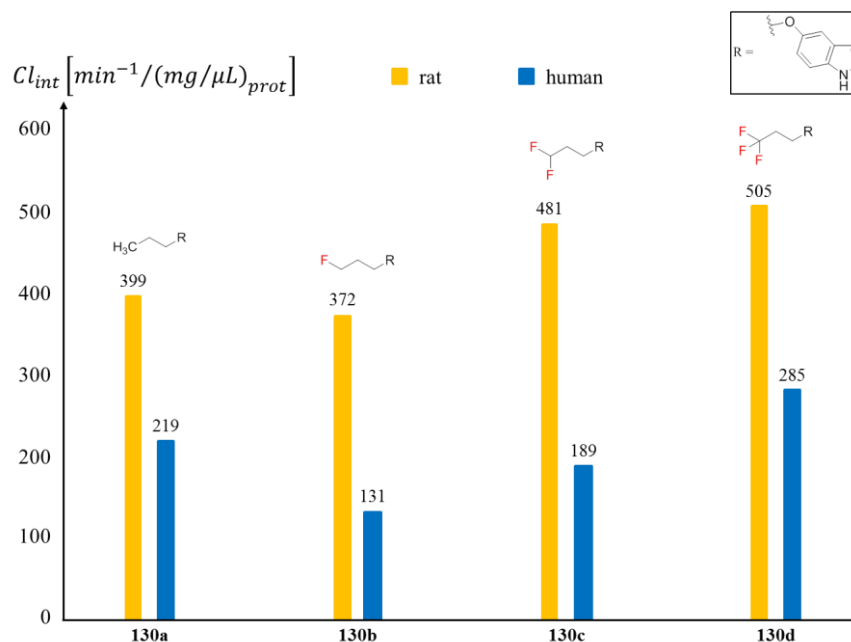


**Figure 66.** Clearance rates ( $Cl_{int}$ ) determined in rat and human models for the series of partially fluorinated propyl ethers **130x** ( $x = a-d$ ).

To study their metabolic stability, partially fluorinated alkyl ethers **130x** were subjected to rat and human liver microsomes under standard conditions (for details, see Experimental Section), which afforded the set of  $Cl_{int}$  values presented in Figure 66 (these values should be considered with caution as standard deviations have not yet been determined). Considering the series of partially fluorinated alkyl ethers **130b-d**, it is striking to realize that the relative stability trend revealed in both models correlates well with the lipophilicity, albeit higher discrepancy could be noted in the rat model (Figure 67).

This observation is in agreement with our prior results and emphasizes the net influence of the partially fluorinated propyl ether moieties on metabolic stability. It should however be noted that the values recorded for the non-fluorinated analog **130a** do not match the previously established correlation shown in Figure 67.

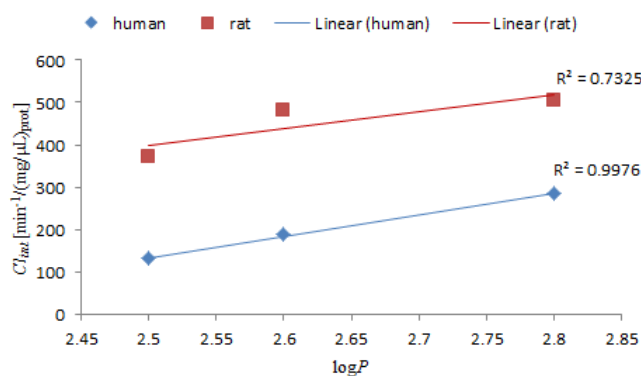


**Figure 67.** Correlation between lipophilicity ( $\log P$ ) and metabolic stability ( $Cl_{int}$ ) in rat and human models for partially fluorinated propyl ethers **130b–d**.

Hence, since fluorinated compounds **130b–d** display clearance rates that are higher than expected based on their respective lipophilicity values, it suggests that the introduction of fluorine atoms not only induces lower lipophilicity, but also translates into lower relative metabolic stability. As a result, the favorable effect of lower polarity on metabolic stability seems to be counterbalanced by the negative influence of terminal fluorination of the propyl chain. In the end, only the monofluoro analog **130b** exhibits a pronounced positive effect on metabolic stability compared to the non-fluorinated parent **130a**.

In summary, these experimental results indicated that, although introducing two methylene units between the fluoromethyl group and the oxygen atom proved to influence lipophilicity in the expected way, this structural modification induced a relatively lower metabolic stability.

In order to rationalize the effect of partially fluorinated propyl ethers on metabolic stability, one must consider the metabolic pathways that could lead to the degradation of such units. On the one hand, alkyl ethers are functionalities which are known to be prone to CYP-mediated *O*-dealkylation reactions.<sup>137</sup> On the other hand, literature precedents reported that fluorinated compounds are mostly excreted after metabolic defluorination.<sup>52</sup> The *O*-dealkylation reaction involves the oxidation of the methylene unit adjacent to the oxygen of the ether bond, whereas the defluorination of aliphatic compounds is readily achieved by  $\alpha$ -hydroxylation, followed by subsequent elimination of hydrofluoric acid.<sup>52</sup>

Interestingly, although French *et al.* reported that fluoroethyl ethers are less prone to metabolic defluorination than simple fluoroethyl scaffolds,<sup>121</sup> which is the result of the inductive effect of the oxygen atom at C(1) (Figure 68, left), they did not comment on the influence of the fluorine atom on the *O*-dealkylation reaction. Due to the strong electron-



withdrawing character of the fluorine atom, it should also inductively disfavor any metabolic oxidation at C(2), thus impeding the *O*-dealkylation reaction. The combination of these  $\beta$ -inductive effects implies that the fluoroethyl ether scaffold is not only less prone to metabolic defluorination, but also less prone to metabolic *O*-dealkylation.

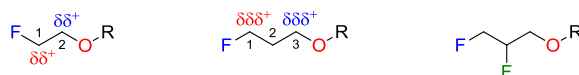


**Figure 68.** Structures of 1-fluoroethyl, 1-fluoropropyl, and 1,2-difluoropropyl ethers.

Inserting an additional methylene unit between the fluoromethyl group and the oxygen atom leads to the fluoropropyl ether case where the sites of metabolic oxidation, C(1) and C(3), are further removed from the neighboring electron-withdrawing atom, O and F, respectively (Figure 68, center). This implies that the oxygen atom has a much weaker inductive effect at C(1), and that the fluorine atom has a much weaker inductive effect at C(3). The combination of these effects should then make the fluoropropyl ether moiety consequently more susceptible to metabolic degradation than the fluoroethyl analog.

In order to rationalize the relative metabolic stability difference between fluorinated derivatives **130b–d** and their non-fluorinated counterpart **130a**, it could then be suggested that the former are relatively more metabolized than the latter because the presence of fluorine atoms introduces another possible metabolic pathway (metabolic defluorination) that is not strongly disfavored by the oxygen atom in  $\gamma$ -position of the fluorine atoms.

Finally, further to what has already been suggested in Figure 52, the *vic*-difluoropropyl ether scaffold would therefore be particularly interesting, as the combination of inductive effects in such a setting would impede metabolic oxidation at all carbons (Figure 68, right). Provided that the effect of the *vic*-difluoropropyl ether unit on lipophilicity is similar to that of the *vic*-difluoropropyl moiety in compound **60** (Figure 47), it was expected that the former would display high lipophilicity-lowering potency and significantly enhanced metabolic stability.

#### 4.4.1.3 X-ray Structures

Structural analysis of trifluoromethoxyphenyl derivatives revealed a marked preference for the orthogonal conformation (Figure 57, right), which was identified as the main reason why the trifluoromethoxy moiety induces a lipophilicity increase. Therefore, since the results obtained for the series of partially fluorinated propyl ethers **130x** revealed a lipophilicity trend similar to that of 3-substituted indole derivatives **23x** and **24x**, it was reasonable to assume that the former should present an essentially planar conformation.

In order to verify this hypothesis, the X-ray crystal structures of the tosyl-protected compounds **150x** could be recorded (Figure 69). For each structure, the ether substituent at C(5) adopts a clear planar orientation, thus confirming that the preference for the orthogonal conformation disappears when the fluoromethyl unit is further removed from the oxygen atom. Furthermore, as previously noted in Figure 25 for compounds **25b** and **25c**, the terminal  $CH_2F$  and  $CHF_2$  units in compounds **150b** and **150c** adopt respectively the preferred *gauche* and *trans-gauche* conformations.

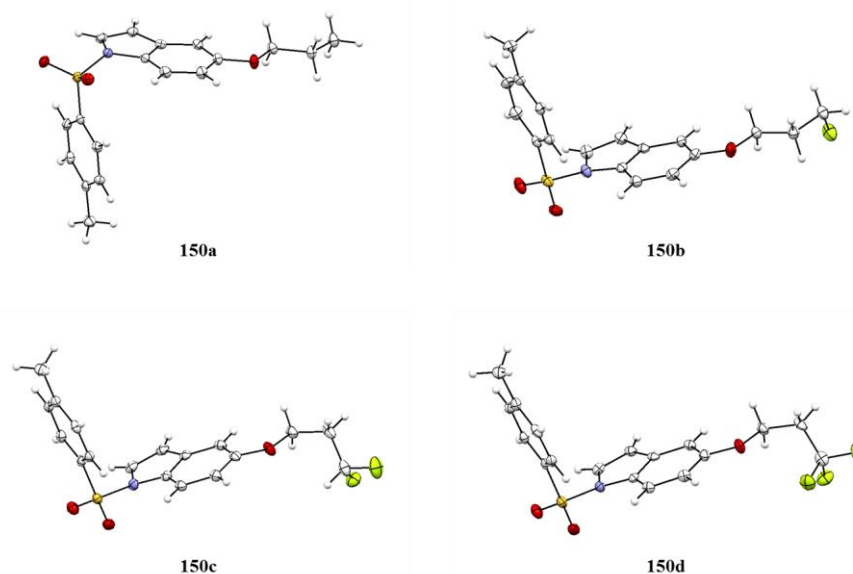


**Figure 69.** X-ray crystal structures determined for partially fluorinated propyl ethers **150x** ( $x = \mathbf{a-d}$ ).

Interestingly, compounds **150c** and **150d** also exhibit an unusual *gauche*-OCCC backbone. In the case of the difluoro derivative (**150c**), this structural feature can be rationalized by an intramolecular  $O \cdots H-C$  interaction because the C–H bond of the terminal  $CHF_2$  unit is highly polarized. However, since such a stabilizing interaction does not exist for the trifluoro derivative (**150d**), the observed conformation is difficult to rationalize.

#### 4.4.2 Extended Set of Model Compounds

At the time of writing this thesis, the lipophilicity and metabolic stability data for the extended set of model compounds **131–137** were not yet available, which left many questions unanswered and our scientific curiosity unsatisfied. Nevertheless, it was possible to obtain some particularly interesting results on the structural properties of *bis-vic*-trifluorobutyl ethers **181** and **182**.

Due to the paucity of crystallographic data related to such complex fluorinated scaffolds, it was a unique opportunity to learn more about their conformational characteristics. Also, based on these experimentally determined structures, an *in silico* investigation of their physicochemical properties was pursued, which could provide qualitative indications on the potential effects of such moieties.

#### 4.4.2.1 X-ray Structures

Conformational analysis of multi-vicinal fluoroalkanes has already attracted the attention of the scientific community, since these complex fluorinated molecules usually exhibit unique properties that could find potential applications in the field of performance materials.<sup>103,105,136</sup>

It has already been shown in this work that the resulting molecular dipole moment of partially fluorinated scaffolds can influence physicochemical properties such as lipophilicity. Also, since conformational features are key factors that influence the way local dipole moments combine, gaining insights into the conformational preference of partially fluorinated alkyl ethers in crystal structures could be instrumental in formulating qualitative predictions about their influence on lipophilicity.

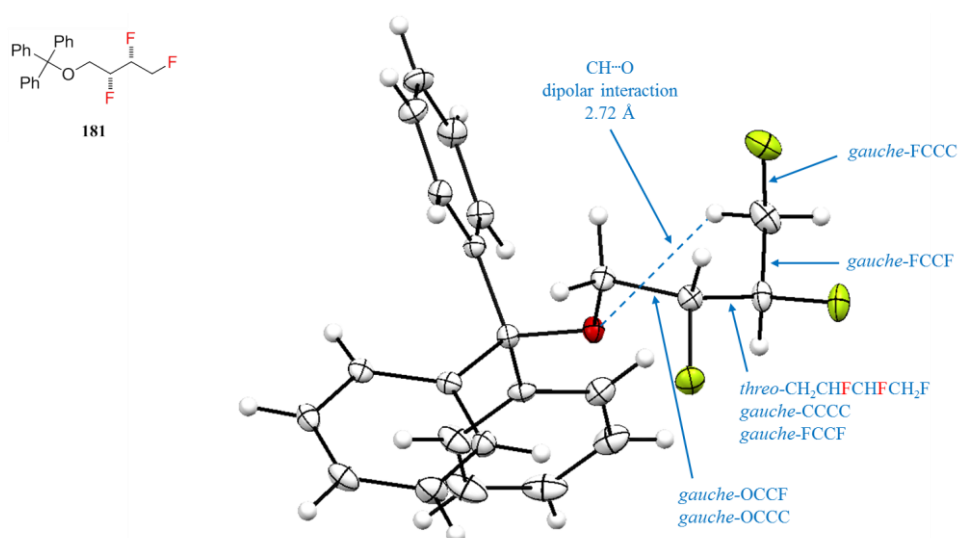


**Figure 70.** X-ray crystal structure determined for *threo* bis-vicinal trifluorobutyl ether derivative **181**.

*En route* to the synthesis of *bis-vic*-trifluorobutyl ethers **135** and **136**, the trityl-protected scaffolds **181** and **182** were isolated as crystalline compounds. The X-ray crystal structure of *threo* isomer **181** displays typical features of multi-vicinal fluoroalkanes, including the alternate backbone conformation for a *threo* vic-difluorobutyl unit with the *gauche*-CCCC and *gauche*-FCCF arrangements (Figure 70). This all-*gauche* conformation then brings the

polarized C–H bond of the terminal  $CH_2F$  unit into close intramolecular interaction with the ether-oxygen (2.72 Å), thus providing an additional source of stabilization.

Similar observations were made for the *erythro* isomer **182**, which displays a conformation where all vicinal fluorine atoms also adopt *gauche* arrangements (Figure 71). In that case, the conformational restriction brings one terminal C–H bond to engage in an even closer dipolar interaction with the oxygen atom (2.58 Å). More importantly, a peculiar structural characteristic exhibited by the terminal fluorine atom could be noticed, which ends up in a *trans*-FCCC conformation because of both *gauche*-FCCC conformations being precluded by unfavorable intramolecular interactions. Considering these possible *gauche*-FCCC conformations, it results that they are not observed because:

- 1) 1,3-Diaxial interactions between two C–F bonds are disfavored;
- 2) The *trans*-FCCF conformation is usually not favored;
- 3) Dipolar interactions between fluorine and oxygen atoms are unfavorable.

The combination of these factors leads to the only conformation where the fluorine atom avoids any unfavorable intramolecular interaction.

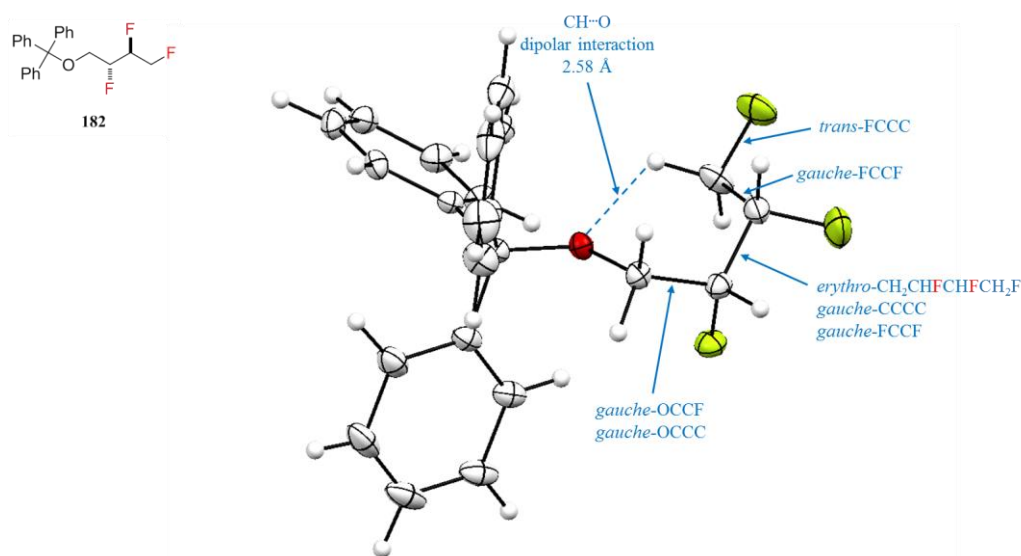


**Figure 71.** X-ray structure determined for *erythro* bis-vicinal trifluorobutyl ether derivative **182**.

In summary, both *threo* and *erythro* isomers of *bis-vic*-trifluorobutyl ethers **181** and **182** follow the previously established conformational preferences for multi-vicinal fluoroalkanes.<sup>105</sup> Furthermore, the structural features shown by each compound support the potential of such fluorination patterns as conformational locks, which might be of interest in drug design.<sup>6</sup>

#### 4.4.2.2 Computed Properties

In order to formulate qualitative predictions about the physicochemical properties of model compounds **135** and **136**, the crystal structure coordinates of *bis-vic*-trifluorobutyl ethers **181** and **182** were used to compute their respective molecular dipole moments and solvation energies. Also, to simplify the calculations (for details, see Experimental Section), it was decided to work on a model system where a methyl unit replaced the trityl protecting group.

At the outset of this *in silico* study, we were interested in determining reference values to which we could compare the ones we would obtain for *bis-vic*-trifluorobutyl ethers, as well as investigating the influence of the alkyl chain length on the resulting polarity of terminally trifluoromethylated alkyl ethers. Therefore, the molecular dipole moments in the gas phase and the solvation energies in water were computed for the lower energy conformers of 1,1,1-trifluoroethoxy-, 1,1,1-trifluoropropoxy-, and 1,1,1-trifluorobutoxymethyl ethers. The results obtained revealed unexpected characteristics depending on the alkyl chain length (Figure 72).

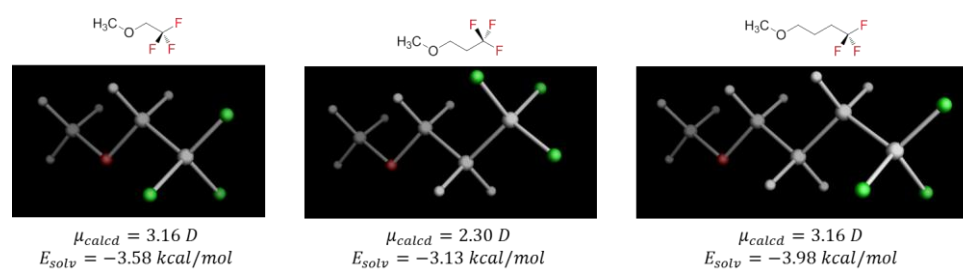


**Figure 72.** Computed molecular dipole moments ( $\mu_{calcd}$ , gas phase) and solvation energies ( $E_{solv}$ , water) for the lower energy conformers of 1,1,1-trifluoroethoxy-, 1,1,1-trifluoropropoxy-, and 1,1,1-trifluorobutoxymethyl ethers.

The comparison of trifluoroethoxy and trifluoropropoxy ethers revealed that the latter has a substantially lower molecular dipole moment and a weaker solvation energy than the former. The weaker solvation energy of the trifluoropropoxy unit can be rationalized by the bulk increase resulting from the additional methylene unit compared to the trifluoroethoxy analog. Also, similarly to the vector analysis shown in Figure 62, the smaller molecular dipole moment of the trifluoropropoxy ether can be rationalized by the way the respective dipole moments ascribed to C–O and C–F bonds combine depending on their relative positions. Thus, when the oxygen atom is separated from the trifluoromethyl group by either one or three methylene units, its contribution to the resulting molecular dipole moment is positive, whereas a reverse influence is expected with two methylene units. It is however surprising to realize that the computed solvation energy in water for the trifluorobutoxy unit is substantially stronger than that observed for the shorter analogs. Since the trifluorobutoxy unit contains

four additional slightly positively charged H atoms ( $CH_2CH_2$  unit) compared to its trifluoroethoxy analog, their interactions with the medium could provide a rationale to these respective computed solvation energies.

Based on the X-ray structures obtained for trityl ethers **181** and **182**, it was possible to compute the respective dipole moments and solvation energies of each model isomer. The results presented in Figure 73 revealed that the multi-vicinal arrangement of three fluorine atoms along a butyl chain enhances substantially the resulting dipole moment when compared to the 1,1,1-trifluorobutoxy analog. More importantly, these calculations highlighted the dramatic influence this complex fluorination pattern has on solvation energy. Indeed, although both isomers present nearly identical solvation energies, the difference between each *bis-vic*-trifluorobutoxy model compound and its trifluoromethylated counterpart is remarkable ( $\Delta E_{solv} \sim -3.0$  kcal/mol).

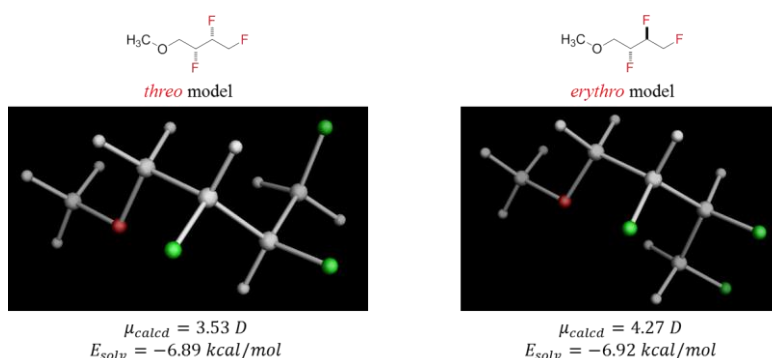


**Figure 73.** Computed molecular dipole moments ( $\mu_{calcd}$ , gas phase) and solvation energies ( $E_{solv}$ , water) for the conformations of *threo* and *erythro* *bis-vic*-trifluorobutoxy-methyl ethers based on the crystal structure coordinates of model compounds **181** and **182**.

These computed properties strongly suggest that *bis-vic*-trifluorobutyl ethers **135** and **136** should benefit from a much stronger polarity than the trifluoropropoxy analog **130d**, thus implying that a stronger lipophilicity-lowering effect can be expected for the former. It will therefore be particularly interesting to verify this theoretical prediction with experimentally determined results.

In the end, these preliminary calculations not only pointed out the importance of the alkyl chain length on the physicochemical properties of trifluorinated alkyl ethers, but also underlined the relative complexity of such systems. This unique behaviour makes partially fluorinated alkyl ethers even more interesting to study as they bring to light new features that challenge the current perception of the problems at stake.

## 4.5 Conclusion

In this third chapter, a set of partially fluorinated propyl and butyl ethers of varying complexity has been designed, assuming that such scaffolds would exhibit a lipophilicity trend similar to the one shown in a series of 3-substituted indole derivatives. Unprecedented synthetic pathways were therefore developed towards partially fluorinated alkyl electrophiles, which were successfully reacted with 5-hydroxyindole.

The results obtained for the basic set of model compounds **130x** confirmed the theory that was initially formulated and unveiled the lipophilicity-lowering effect that these partially fluorinated alkyl ethers impart. The experimental results underlined the relative metabolic instability of model compounds **130x**, which led to surmise that the *vic*-difluoropropyl ether analog **131** would be an even better candidate. Finally, computed properties based on the experimental X-ray structures of *threo* and *erythro bis*-vicinal trifluorobutyl ethers **181** and **182** confirmed the influence of the multi-vicinal arrangement of fluorine atoms on polarity, which is expected to be reflected in experimentally determined physicochemical properties.

In summary, preliminary results gathered on the effects of partially fluorinated alkyl ethers suggest their great potential as metabolically robust building blocks to fine-tune lipophilicity. Further results on the more complex set of model compounds will help verify the initial predictions, and support the usefulness of such scaffolds in medicinal chemistry.





## 5 Conclusion and Outlook

In the course of this work, synthetic strategies to access partially fluorinated building blocks have been developed, and the influence of different fluorination patterns has been studied on key properties, such as lipophilicity and metabolic stability.

In particular, a series of partially fluorinated *n*-propylbenzene derivatives with varying degrees of terminal fluorination has been initially investigated, which led to devise a predictive model for lipophilicity based on the relative effects of fluorination on molecular dipole moment and volume. Thanks to basic calculations, it was possible to estimate the general lipophilicity trend that such derivatives should exhibit, i.e.  $CH_3 > CF_3 \gg CHF_2 \geq CH_2F$ . A set of partially fluorinated 3-propylindole model compounds has then been designed, synthesized, and evaluated, which consistently confirmed the predicted lipophilicity trend. The results obtained for this series of compounds also highlighted that their metabolic stability paralleled their measured lipophilicity. In order to exclude cumulative polarity effects resulting from the intrinsic polarity of the indole nucleus and the conformational flexibility of the partially fluorinated propyl chain, a series of conformationally restricted 3-(4-methylcyclohexyl)indole derivatives with varying degrees of fluorination at the methyl group has been designed, synthesized, and evaluated, which confirmed the initially determined lipophilicity trend.

In a second part of this work, a set of 3-substituted indole derivatives bearing vicinal and multi-vicinal fluoroalkyl scaffolds has been designed, synthesized, and evaluated, as such fluorination patterns were expected to increase polarity without a substantial volume change. The experimental measurements carried out on this series of model compounds matched the theoretical predictions and confirmed the expected lipophilicity drop imparted by the vicinal difluoroalkyl moieties, which translated into enhanced solubility and metabolic stability. Additionally, the measurements carried out on *bis-vic*-trifluorobutyl analogs showed that such fluorination motifs feature a marked lipophilicity decrease, and that their influence is mitigated by the higher chain length. Overall, calculated properties and experimental data converged to point out the superiority of the *vic*-difluoropropyl moiety, which benefits from unrivalled effects on prime pharmacokinetics.

Finally, aiming at broadening their scope of applications, it was surmised that short partially fluorinated alkyl groups could be grafted to aromatic nuclei via an ether linkage to

simultaneously impede oxidative metabolism and lower lipophilicity. The study of partially fluorinated methoxyaryl derivatives indicated that at least two methylene units were required between the oxygen atom and the fluoromethyl group for the latter to exhibit the characteristic lipophilicity-lowering pattern as observed for the 3-propyl- and 3-(4-methylcyclohexyl)-indole series. To access the relevant set of 5-(alkyloxy)indole model compounds, unprecedented synthetic pathways have been developed allowing for the multi-gram scale production of complex partially fluorinated alkyl electrophiles, which were utilized in the functionalization of the 5-(hydroxy)indole nucleus. Besides confirming the possibility to lower lipophilicity by means of propyl ethers fluorinated in terminal position, their relative metabolic instability was also revealed. Rationalization of this unforeseen effect suggested that a *vic*-difluoropropyl ether could afford a more metabolically robust scaffold. Furthermore, X-ray crystal structure analyses complemented by computational modelling revealed that the multi-vicinal arrangement of fluorine atoms could provide ether moieties of drastically reduced polarity.

In summary, the potential of partially fluorinated alkyl groups as modulators of lipophilicity has been unveiled, and their multifaceted influence on prime pharmacokinetic parameters has been brought to light. This research has opened additional questions, whose answers could deepen the understanding of complex fluorinated scaffolds. In this regard, it is expected that *in silico* molecular modelling, in conjunction with experimental data, will be instrumental in rationalizing the unique properties of these moieties. Application of the novel concepts reported herein to *N*-alkyl derivatives seemed a promising perspective to pursue, and results in this field will soon follow. The results of this work may motivate medicinal chemists to employ partially fluorinated alkyl building blocks in their research programs as versatile tools to fine-tune lipophilicity. Finally, the present work has laid the basis for a rational use of partially fluorinated alkyl or alkoxy groups, which should lead to the design of further particularly promising subunits in both the life and material sciences.

# Experimental Section

## • Materials and Methods

**Reaction Conditions:** All non-aqueous reactions were carried out using oven-dried or flame-dried glassware under inert atmosphere (dry nitrogen) unless otherwise stated. All temperatures are given in degrees Celsius. Stainless steel syringes were used to transfer air- and moisture-sensitive liquids. Reactions were magnetically stirred if not indicated otherwise and monitored by thin layer chromatography using *Merck Silica Gel 60 F254* TLC aluminium plates and visualized by fluorescence quenching under UV light. In addition, TLC plates were stained with ceric ammonium molybdate, potassium permanganate, or *p*-anisaldehyde stain.

**Purifications:** Column chromatographic purification was performed as flash chromatography with 0.3–0.5 bar of air pressure on silica gel (60 Å, 230–400 mesh, *Fluka Analytical*). Technical grade solvents were employed, which were distilled prior to use. Concentration under reduced pressure was performed by rotary evaporation at 40 °C at the appropriate pressure. Purified compounds were further dried under high vacuum. Yields refer to chromatographically purified and spectroscopically pure compounds, unless otherwise stated.

**Reaction Solvents:** Tetrahydrofuran, acetonitrile, toluene, diethylether and dichloromethane were dried by passage over two 4 x 36 inch columns of anhydrous neutral A-2 alumina (8 x 14 mesh; *Macherey und Nagel*; activated under a flow of nitrogen at 300 °C overnight; solvent drying system) under an argon atmosphere (H<sub>2</sub>O content < 30 ppm as determined by Karl-Fischer titration). Analytical grade methanol, ethanol, and *N,N*-dimethylformamide from *Aldrich* or *Acros* were used without further purification unless otherwise stated.

**Reagents:** Triethylamine and pyridine were distilled from potassium hydroxide under an atmosphere of dry nitrogen. *N,N*-Diisopropylethylamine was distilled from sodium hydride under an atmosphere of dry nitrogen. All other chemicals were purchased from *Acros*, *Aldrich*, *Fluka*, *Merck*, *Lancaster*, *ABCR*, *Fluorochem*, *Combi-Blocks*, *SynQuest Labs* or *TCI* and used without further purification unless otherwise stated.

**Melting Points:** Melting points were measured using a *Büchi B-540* melting-point apparatus in open capillaries and are uncorrected.

**NMR Spectra:** Proton nuclear magnetic resonance (<sup>1</sup>H NMR) spectra, carbon nuclear magnetic resonance (<sup>13</sup>C NMR) spectra, and fluorine nuclear magnetic resonance (<sup>19</sup>F NMR)

spectra were recorded on a *Bruker AV400* spectrometer operating at 400 MHz. All measurements were carried out at room temperature (ca. 22 °C) unless otherwise specified. Chemical shifts ( $\delta$ ) are reported in parts per million (ppm), and are referenced to the residual solvent signal as internal standard (deuterated chloroform at 7.26 ppm for  $^1\text{H}$  NMR, and 77.16 ppm for  $^{13}\text{C}$  NMR).  $^{19}\text{F}$  NMR spectra are referenced relative to  $\text{CFCl}_3$  ( $\delta = 0.00$  ppm) in deuterated chloroform. Coupling constants ( $J$ ) are reported in units of hertz (Hz). Multiplicities are abbreviated as follows: s (singlet), bs (broad singlet), d (doublet), t (triplet), q (quartet), p (quintet), h (sextet), and m (multiplet). All  $^{13}\text{C}$  NMR spectra were recorded with proton decoupling. All  $^{19}\text{F}$  NMR spectra were respectively recorded either with (decoupled) or without (not decoupled) proton decoupling.

**IR Spectra:** Infrared spectra were recorded on a *Perkin Elmer Spectrum RX-I FT-IR* spectrometer as thin film. Absorptions are given in wavenumbers ( $\text{cm}^{-1}$ ).

**Mass Spectra:** Mass spectrometric analyses were recorded by the mass spectrometry service at *ETH Zurich* under the direction of Dr. Zhang. EI-MS ( $m/z$ ): *Waters Micromass AutoSpec Ultima* spectrometer. ESI-MS ( $m/z$ ): *Bruker Daltonics maXis* spectrometer.

**X-ray Crystallography:** X-ray crystallography analyses were performed by Dr. Bernd Schweizer, Dr. Nils Trapp, and Michael Solar at *ETH Zurich*. Structures were solved by direct methods and refined by full-matrix least-squares analysis using the *OLEX2*<sup>138</sup> and *Bruker SHELXTL*<sup>139</sup> Software Package.

**Chemical Names and Structures:** Chemical names and structures of the reported molecules were generated with *ChemBioDraw Ultra 12.0 (Cambridgesoft)* and modified where appropriate.

**Computational Details** (F. Hoffmann-La Roche, Basel): Initial geometries of all model compounds were built with the modeling software *MOLOC* and their structures subsequently optimized with the B3LYP hybrid density functional and Dunning's correlation-consistent polarized split-valence double-zeta basis set with diffuse functions (cc-pVDZ++), as implemented in the software package *Jaguar*. Default convergence criteria were applied. Estimates of solvation energies in water were computed with the Poisson-Boltzmann solver in *Jaguar*. Dipole moments were calculated in the gas-phase and empirically scaled by 0.946 to match the experimental dipole moments.

**Determination of Lipophilicity** (F. Hoffmann-La Roche, Basel): In the high-throughput assay method, which is derived from the conventional "shake flask" method, the compound of

interest is distributed between a 50 mM aqueous TAPSO buffer at pH 7.4 and 1-octanol. The distribution coefficient is then calculated from the difference in concentration in the aqueous phase before and after partitioning and the volume ratio of the two phases. To measure  $\log D$  values within the range of -1 to 3.5, it is necessary to carry out the procedure at four different 1-octanol/water ratios. The “one-phase analysis” experiment starts with 2 or 9  $\mu\text{L}$  of a pure DMSO solution of the compound, which is dispensed into, respectively, 38 or 171  $\mu\text{L}$  of the aqueous buffer solution, bringing the compound concentration to approximately  $c = 0.5$  mM. A small part of this solution is then analyzed by UV. The observed optical density corresponds to the concentration of the substance before partitioning. To a measured aliquot of the aqueous solution, a matching aliquot of 1-octanol is added, and the mixture is incubated by quiet shaking for 2 h at  $23 \pm 1$  °C. The emulsion is allowed to stand overnight at the same temperature to ensure that partition equilibrium is reached. Then, thorough centrifugation at 3000 rpm for 10 min is applied to separate the layers, and the concentration of the compound in the aqueous phase is determined again by measuring the UV absorption under the same conditions as the reference. For neutral compounds,  $\log D = \log P$ . Each  $\log P$  determination was carried out at least three times within absolute standard deviations  $< 0.1$  in all cases.

**Determination of Capacity Factors  $k_n$  by HPLC** (F. Hoffmann-La Roche, Basel): For the determination of  $k_{50}$  values, the compounds of interest were introduced as 10 mM DMSO stock solutions into a mixture of water and acetonitrile (50 %/vol), both containing 0.1 %/vol formic acid, resulting in 100  $\mu\text{M}$  sample solutions. Prior to analysis, the solutions were filtrated (filter plate: *Millipore*, Cat.No. MSGVN2250) into a 96-well receiver plate. Compound retention times were quantified using an *Agilent 1200* HPLC-MS system (*Agilent Technologies*, CA, USA) equipped with a degasser, auto-sampler, column oven, binary pump, DAD detector and API single-quadrupole mass spectrometer (*Agilent 6140*). A 5  $\mu\text{L}$  aliquot of each sample was injected onto a Kinetex 2.6  $\mu\text{m}$ , 2.1 x 50 mm analytical column (*Phenomenex*, Germany) operated at 60 °C. The mobile phase consisted of water and acetonitrile (50 %/vol), both containing 0.1 %/vol formic acid. The isocratic elution on the *Agilent 1200* system was performed with a flow rate of 1 mL/min. After passing the DAD detector, the eluent was introduced into the electrospray interface maintaining the following source settings: capillary voltage +3.5 kV, auxiliary gas flow 13 L/min, drying gas temperature 350 °C, dwell time 50 ms. Electrospray was initiated with a time delay of 0.4 min to prevent extensive entry of DMSO into the API source. The integral of the pseudo-molecular ion intensity,  $[\text{M}+\text{H}]^+$ , was acquired in single-reaction monitoring mode (SRM) in

order to identify the compound peak in the DAD response. For each compound the capacity factors  $k_{50}$  (retention factors) were then calculated according to the equation below:

$$\log k_n = \log((t_R - t_M)/t_M)$$

- where  $t_R$  = retention time (time between injection and elution),
- and  $t_M$  = retention time of the non-retained component (i.e. DMSO).

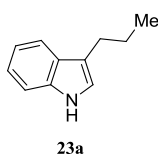
By analogy, capacity factors  $k_{60}$  and  $k_{40}$  were obtained for all compounds using solvent ratios of, respectively, 60 %/vol and 40 %/vol acetonitrile in aqueous 0.1 %/vol formic acid. In principle,  $\log k_w$ , for 0%/vol acetonitrile could be obtained by extrapolation; although, the experimental data points have been determined relatively accurately, they are quite distant from the 0% extrapolation limit, thus resulting in relatively large standard deviations of  $\pm 0.13$  for  $\log k_w$ .

**Determination of Metabolic Stability in Liver Microsomes** (F. Hoffmann-La Roche, Basel): Microsomal incubations were carried out in 96-well plates in 200  $\mu$ L of liver microsome incubation medium containing potassium phosphate buffer (50 mM, pH 7.4),  $MgCl_2$  (10 mM), EDTA (1 mM),  $NADP^+$  (2 mM), glucose-6-phosphate $\cdot 2H_2O$  (20 mM), glucose-6-phosphate dehydrogenase (4 units/mL) with 0.1 mg of liver microsomal protein per mL. Test compounds were incubated at 2  $\mu$ L for up to 30 min at 37  $^{\circ}C$  under vortexing at 800 rpm. The reaction was stopped by transferring 30  $\mu$ L incubation aliquots to 90  $\mu$ L of ice-cold methanol. Levels of non-metabolized drug were determined by high-performance liquid chromatography (HPLC) coupled with tandem-mass spectrometry (LC/MS/MS). The system consisted of a *Shimadzu* binary gradient HPLC system, a *Waters XTerra*<sup>®</sup> MS C18 column (1 mm x 50 mm) and a *Sciex* API 2000 mass spectrometer. A two-component mobile phase, pumped at 0.15 mL/min, contained the following solvents: solvent A (1% aqueous formic acid and MeOH 80:20) and solvent B (MeOH). An initial isocratic step of 0.5 min solvent A was followed by a gradient of 0 to 80% solvent B within 1 min. Detection was performed in positive mode. The intrinsic clearance ( $Cl_{int}$ ) was determined in semi-logarithmic plots of compound concentrations *versus* time.

**Determination of Solubility at Thermodynamic Equilibrium** (F. Hoffmann-La Roche, Basel): For each compound, a sample of approximately 2 mg was added to ca. 150  $\mu$ L of a 50 mM aqueous phosphate buffer and transferred to a standard 96-well plate at room temperature ( $22.5 \pm 1$   $^{\circ}C$ ). The pH of each compound suspension was adjusted to pH 10 by using a concentrated aqueous NaOH solution and the 96-well plate was placed on a plate

shaker which agitated the suspensions overnight. On the next day, the samples were filtered with a micronic filter plate (MSGVN2250) to separate the solid material from the solution. After confirming unchanged pH of the solutions by means of micro-pH-meter measurements, the solution concentrations were determined by calibrated HPLC. The calibrations were obtained by HPLC analysis of different concentrations of each compound in DMSO.

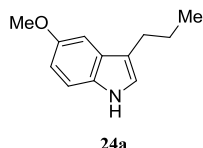
- **Synthetic Procedures**



**3-Propyl-1H-indole (23a):**<sup>76</sup>

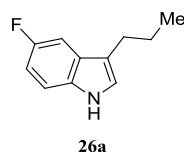
To a solution of phenylhydrazine (**27**) (1.84 mL, 18.3 mmol, 1.00 equiv) in a 1:1 mixture (48.0 mL) of 4% aqueous H<sub>2</sub>SO<sub>4</sub> and THF at rt was added valeraldehyde (**30a**) (2.41 mL, 22.0 mmol, 1.20 equiv) dropwise upon stirring. The resulting solution was heated to 100 °C for 5 h, cooled down to rt, and quenched with saturated aqueous NaHCO<sub>3</sub>. The aqueous layer was extracted with EtOAc, and the combined organic extracts were washed with brine, dried over Na<sub>2</sub>SO<sub>4</sub>, filtered, and concentrated *in vacuo*. The resulting crude material was purified by silica gel flash column chromatography (20:1 hexanes/EtOAc) to afford indole **23a** (1.64 g, 10.3 mmol, 56%) as a brown oil.

**TLC:**  $R_f$  = 0.17 (10:1 hexanes/EtOAc; UV, CAM). **<sup>1</sup>H NMR** (400 MHz, CDCl<sub>3</sub>): δ 7.88 (bs, 1H), 7.62 (d,  $J$  = 7.9 Hz, 1H), 7.36 (d,  $J$  = 8.1 Hz, 1H), 7.22–7.17 (m, 1H), 7.14–7.09 (m, 1H), 6.99–6.96 (m, 1H), 2.75 (t,  $J$  = 7.3 Hz, 2H), 1.75 (h,  $J$  = 7.3 Hz, 2H), 1.01 (t,  $J$  = 7.3 Hz, 3H) ppm. **<sup>13</sup>C NMR** (100 MHz, CDCl<sub>3</sub>): δ 136.5, 127.8, 122.0, 121.2, 119.2, 117.2, 111.1, 27.4, 23.5, 14.3 ppm. **IR** (thin film): ν 3427, 2929, 1581, 1483, 1451, 1172, 936, 849, 793, 593 cm<sup>-1</sup>. **HRMS** (ESI<sup>+</sup>): exact mass calculated for C<sub>11</sub>H<sub>14</sub>N ([M+H]<sup>+</sup>), 160.1121; found 160.1122.

**5-Methoxy-3-propyl-1H-indole (24a):**<sup>76</sup>

To a solution of 4-methoxyphenylhydrazine hydrochloride (**28**) (2.50 g, 14.2 mmol, 1.00 equiv) in a 1:1 mixture (48.0 mL) of 4% aqueous H<sub>2</sub>SO<sub>4</sub> and THF at rt was added valeraldehyde (**30a**) (1.51 g, 1.86 mL, 17.0 mmol, 1.20 equiv) dropwise upon stirring. The resulting solution was heated to 100 °C for 5 h, cooled down to rt, and quenched with saturated aqueous NaHCO<sub>3</sub>. The aqueous layer was extracted with EtOAc, and the combined organic extracts were washed with brine, dried over Na<sub>2</sub>SO<sub>4</sub>, filtered, and concentrated *in vacuo*. The resulting crude material was purified by silica gel flash column chromatography (20:1 hexanes/EtOAc) to afford indole **24a** (0.820 g, 4.33 mmol, 31%) as a brown oil.

**TLC:**  $R_f$  = 0.17 (10:1 hexanes/EtOAc; UV, CAM). **<sup>1</sup>H NMR** (400 MHz, CDCl<sub>3</sub>): δ 7.79 (bs, 1H), 7.24 (d,  $J$  = 8.8 Hz, 1H), 7.05 (d,  $J$  = 2.4 Hz, 1H), 6.96 (bs, 1H), 6.86 (dd,  $J$  = 8.8 Hz,  $J$  = 2.4 Hz, 1H), 3.88 (s, 3H), 2.71 (t,  $J$  = 7.4 Hz, 2H), 1.74 (h,  $J$  = 7.4 Hz, 2H), 1.01 (t,  $J$  = 7.4 Hz, 3H) ppm. **<sup>13</sup>C NMR** (100 MHz, CDCl<sub>3</sub>): δ 153.9, 131.7, 128.2, 122.1, 116.9, 112.1, 111.8, 101.2, 56.1, 27.5, 23.3, 14.3 ppm. **IR** (thin film): ν 3429, 2931, 1580, 1481, 1449, 1170, 938, 849, 793, 593 cm<sup>-1</sup>. **HRMS** (ESI<sup>+</sup>): exact mass calculated for C<sub>12</sub>H<sub>16</sub>NO ([M+H]<sup>+</sup>), 190.1226; found 190.1225.

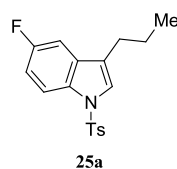
**5-Fluoro-3-propyl-1H-indole (26a):**<sup>76</sup>

(4-Fluorophenyl)hydrazine hydrochloride (**29**) (1.00 g, 5.97 mmol, 1.00 equiv) was added in one portion to a solution of 4% aqueous H<sub>2</sub>SO<sub>4</sub> (60.0 mL) heated at 50 °C. After complete dissolution of the starting material, valeraldehyde (**30a**) (719 μL, 6.56 mmol, 1.10 equiv) was added dropwise. The reaction was then heated to reflux for 1 h, cooled down to rt, and quenched with saturated aqueous NaHCO<sub>3</sub>. The aqueous phase was extracted with EtOAc and the combined organic extracts were washed with brine, dried over Na<sub>2</sub>SO<sub>4</sub>, filtered, and concentrated *in vacuo*. The resulting crude material was purified by silica gel flash column



chromatography (20:1 hexanes/EtOAc) to afford indole **26a** (0.280 g, 1.58 mmol, 26%) as a brown oil.

**TLC:**  $R_f$  = 0.24 (10:1 hexanes/EtOAc; UV, CAM).  **$^1\text{H}$  NMR** (400 MHz,  $\text{CDCl}_3$ ):  $\delta$  8.02–7.75 (bs, 1H), 7.29–7.21 (m, 2H), 7.04–7.00 (m, 1H), 6.93 (td,  $J$  = 9.1 Hz,  $J$  = 2.5 Hz, 1H), 2.73–2.65 (m, 2H), 1.72 (h,  $J$  = 7.4 Hz, 2H), 1.00 (t,  $J$  = 7.4 Hz, 3H) ppm.  **$^{13}\text{C}$  NMR** (100 MHz,  $\text{CDCl}_3$ ):  $\delta$  157.8 (d,  $J$  = 233.9 Hz), 133.0, 128.2 (d,  $J$  = 9.5 Hz), 123.1, 117.3 (d,  $J$  = 4.8 Hz), 111.7 (d,  $J$  = 9.7 Hz), 110.3 (d,  $J$  = 26.4 Hz), 104.1 (d,  $J$  = 23.2 Hz), 27.4, 23.4, 14.3 ppm.  **$^{19}\text{F}$  NMR** (376 MHz,  $\text{CDCl}_3$ , decoupled):  $\delta$  -125.28 (s) ppm.  **$^{19}\text{F}$  NMR** (376 MHz,  $\text{CDCl}_3$ , not decoupled):  $\delta$  -125.28 (td,  $J$  = 9.3 Hz,  $J$  = 4.3 Hz) ppm. **IR** (thin film):  $\nu$  3427, 2929, 1581, 1483, 1451, 1172, 936, 849, 793, 593  $\text{cm}^{-1}$ . **HRMS** (EI+): exact mass calculated for  $\text{C}_{11}\text{H}_{12}\text{FN}$  ( $[\text{M}]^+$ ), 177.0949; found 177.0949.

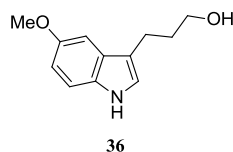


### 5-Fluoro-3-propyl-1-tosyl-1H-indole (**25a**):<sup>77</sup>

To a solution of 5-fluoro-3-propyl-1H-indole (**26a**) (218 mg, 1.23 mmol, 1.00 equiv), *p*-toluenesulfonyl chloride (284 mg, 1.48 mmol, 1.20 equiv), and tetrabutylammonium hydrogen sulfate (30.0 mg,  $9.00 \times 10^{-5}$  mol,  $7.00 \times 10^{-2}$  equiv) in toluene (12.3 mL) at 0 °C was added a 50% aqueous KOH solution (12.3 mL) dropwise upon vigorous stirring. The reaction was stirred for 1 h at rt before it was diluted with a 1:1  $\text{Et}_2\text{O}$ /water mixture. The aqueous phase was extracted with  $\text{Et}_2\text{O}$  and the combined organic extracts were washed with brine, dried over  $\text{Na}_2\text{SO}_4$ , filtered, and concentrated *in vacuo*. The resulting crude material was purified by silica gel flash column chromatography (10:1 hexanes/EtOAc) to afford indole **25a** (403 mg, 1.22 mmol, 99%) as a yellow crystalline solid (mp = 80 °C).

**TLC:**  $R_f$  = 0.34 (5:1 hexanes/EtOAc; UV, CAM).  **$^1\text{H}$  NMR** (400 MHz,  $\text{CDCl}_3$ ):  $\delta$  7.91 (dd,  $J$  = 9.0 Hz,  $J$  = 4.4 Hz, 1H), 7.71 (d,  $J$  = 8.4 Hz, 2H), 7.34 (s, 1H), 7.20 (d,  $J$  = 8.2 Hz, 2H), 7.10 (dd,  $J$  = 8.9 Hz,  $J$  = 2.6 Hz, 1H), 7.01 (td,  $J$  = 9.0 Hz,  $J$  = 2.6 Hz, 1H), 2.61–2.53 (m, 2H), 2.33 (s, 3H), 1.68 (h,  $J$  = 7.4 Hz, 2H), 0.95 (t,  $J$  = 7.3 Hz, 3H) ppm.  **$^{13}\text{C}$  NMR** (100 MHz,  $\text{CDCl}_3$ ):  $\delta$  159.7 (d,  $J$  = 240 Hz), 145.0, 135.3, 132.5 (d,  $J$  = 9.5 Hz), 131.9 (d,  $J$  = 0.8 Hz), 129.9, 126.8, 124.6, 123.5 (d,  $J$  = 4.0 Hz), 115.0 (d,  $J$  = 9.4 Hz), 112.6 (d,  $J$  = 25.5 Hz),

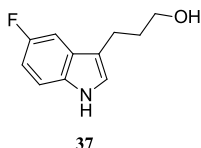
105.4 (d,  $J = 23.8$  Hz), 27.0, 22.1, 21.7, 14.0 ppm.  $^{19}\text{F}$  NMR (376 MHz,  $\text{CDCl}_3$ , decoupled):  $\delta$  -119.95 (s) ppm.  $^{19}\text{F}$  NMR (376 MHz,  $\text{CDCl}_3$ , not decoupled):  $\delta$  -119.95 (td,  $J = 9.0$  Hz,  $J = 4.4$  Hz) ppm. IR (thin film):  $\nu$  2960, 1466, 1444, 1369, 1186, 1169, 1138, 1113, 1087, 880, 809, 666, 589, 537  $\text{cm}^{-1}$ . HRMS (ESI+): exact mass calculated for  $\text{C}_{18}\text{H}_{19}\text{FNO}_2\text{S}$  ( $[\text{M}+\text{H}]^+$ ), 332.1115; found 332.1121.



### 3-(5-Methoxy-1H-indol-3-yl)propan-1-ol (**36**):<sup>76</sup>

To a solution of (4-methoxyphenyl)hydrazine hydrochloride (**28**) (0.500 g, 2.86 mmol, 1.00 equiv) in a 1:1 mixture (12.0 mL) of 4% aqueous  $\text{H}_2\text{SO}_4$  and THF at rt was added 3,4-dihydropyran (0.320 mL, 1.86 mL, 3.44 mmol, 1.20 equiv) dropwise upon stirring. The resulting solution was heated to 100  $^\circ\text{C}$  for 5 h, cooled down to rt, and quenched with saturated aqueous  $\text{NaHCO}_3$ . The aqueous layer was extracted with EtOAc, and the combined organic extracts were washed with brine, dried over  $\text{Na}_2\text{SO}_4$ , filtered, and concentrated *in vacuo*. The resulting crude material was purified by silica gel flash column chromatography (1:1 hexanes/EtOAc) to afford alcohol **36** (503 mg, 2.45 mmol, 86%) as a brown oil.

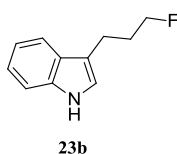
**TLC:**  $R_f = 0.19$  (1:1 hexanes/EtOAc; UV, CAM).  $^1\text{H}$  NMR (400 MHz,  $\text{CDCl}_3$ ):  $\delta$  7.98 (bs, 1H), 7.23 (dd,  $J = 8.7$  Hz,  $J = 0.4$  Hz, 1H), 7.06 (d,  $J = 2.5$  Hz, 1H), 6.97–6.94 (m, 1H), 6.87 (dd,  $J = 2.5$  Hz,  $J = 8.7$  Hz, 1H), 3.88 (s, 3H), 3.74 (t,  $J = 6.4$  Hz, 2H), 2.83 (t,  $J = 7.5$  Hz, 2H), 2.05–1.94 (m, 2H), 1.67 (bs, 1H) ppm.  $^{13}\text{C}$  NMR (100 MHz,  $\text{CDCl}_3$ ):  $\delta$  153.9, 131.8, 128.0, 122.4, 115.7, 112.2, 112.0, 101.0, 62.7, 56.2, 32.9, 21.5 ppm. IR (thin film):  $\nu$  3420, 3306, 2932, 1483, 1454, 1023, 932, 784, 735, 593  $\text{cm}^{-1}$ . HRMS (ESI+): exact mass calculated for  $\text{C}_{12}\text{H}_{16}\text{NO}_2$  ( $[\text{M}+\text{H}]^+$ ), 206.1176; found 206.1173.



### 3-(5-Fluoro-1H-indol-3-yl)propan-1-ol (**37**):<sup>76</sup>

(4-Fluorophenyl)hydrazine hydrochloride (**33**) (5.00 g, 29.8 mmol, 1.00 equiv) was added in one portion to a solution of 4% aqueous H<sub>2</sub>SO<sub>4</sub> (298 mL) heated at 50 °C. After complete dissolution of the starting material, 3,4-dihydro-2H-pyran (3.27 mL, 35.8 mmol, 1.20 equiv) was added dropwise. The reaction was then heated to reflux for 1 h, cooled down to rt, and quenched with saturated aqueous NaHCO<sub>3</sub>. The aqueous phase was extracted with EtOAc and the combined organic extracts were washed with brine, dried over Na<sub>2</sub>SO<sub>4</sub>, filtered, and concentrated *in vacuo*. The resulting crude material was purified by silica gel flash column chromatography (1:1 hexanes/EtOAc) to afford alcohol **37** (3.43 g, 17.8 mmol, 59%) as an orange syrup.

**TLC:**  $R_f$  = 0.13 (1:1 hexanes/EtOAc; UV, CAM). **<sup>1</sup>H NMR** (400 MHz, CDCl<sub>3</sub>): δ 8.11–7.85 (bs, 1H), 7.30–7.21 (m, 2H), 7.06–7.01 (m, 1H), 6.94 (td,  $J$  = 9.1 Hz,  $J$  = 2.5 Hz, 1H), 3.73 (t,  $J$  = 6.4 Hz, 2H), 2.81 (td,  $J$  = 7.4 Hz,  $J$  = 0.9 Hz, 2H), 2.02–1.92 (m, 2H), 1.66–1.30 (bs, 1H) ppm. **<sup>13</sup>C NMR** (100 MHz, CDCl<sub>3</sub>): δ 157.8 (d,  $J$  = 234.4 Hz), 133.0, 128.0 (d,  $J$  = 9.5 Hz), 123.2, 116.3 (d,  $J$  = 4.7 Hz), 111.8 (d,  $J$  = 9.7 Hz), 110.5 (d,  $J$  = 26.4 Hz), 103.9 (d,  $J$  = 23.2 Hz), 62.7, 32.9, 21.4 ppm. **<sup>19</sup>F NMR** (376 MHz, CDCl<sub>3</sub>, decoupled): δ -124.97 (s) ppm. **<sup>19</sup>F NMR** (376 MHz, CDCl<sub>3</sub>, not decoupled): δ -124.97 (td,  $J$  = 9.6 Hz,  $J$  = 4.4 Hz) ppm. **IR** (thin film): ν 3420, 3306, 2937, 1484, 1452, 1024, 935, 794, 736, 594 cm<sup>-1</sup>. **HRMS** (ESI<sup>+</sup>): exact mass calculated for C<sub>11</sub>H<sub>12</sub>FNNaO ([M+Na]<sup>+</sup>), 216.0795; found 216.0796.

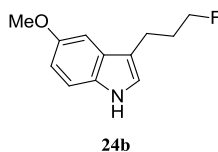


### 3-(3-Fluoropropyl)-1H-indole (**23b**):<sup>79</sup>

To a suspension of XtalFluor-E<sup>®</sup> (404 mg, 1.71 mmol, 1.50 equiv) in CH<sub>2</sub>Cl<sub>2</sub> (11.0 mL) under inert atmosphere at -78 °C were successively added triethylamine trihydrofluoride (285 μL, 1.71 mmol, 1.50 equiv) and 3-(1H-indol-3-yl)propan-1-ol (**35**) (174 μL, 1.14 mmol, 1.00 equiv) dropwise. The resulting mixture was stirred at -78 °C for 1 h, and quenched with saturated aqueous NaHCO<sub>3</sub>. The aqueous layer was extracted with EtOAc, and the combined

organic extracts were washed with brine, dried over Na<sub>2</sub>SO<sub>4</sub>, filtered, and concentrated *in vacuo*. The resulting crude material was purified by silica gel flash column chromatography (20:1 hexanes/EtOAc) to afford indole **23b** (53.0 mg, 3.00 10<sup>-4</sup> mol, 26%) as a colorless oil.

**TLC:**  $R_f = 0.29$  (5:1 hexanes/EtOAc; UV, CAM). **<sup>1</sup>H NMR** (400 MHz, CDCl<sub>3</sub>):  $\delta$  7.94 (bs, 1H), 7.62 (d,  $J = 7.8$  Hz, 1H), 7.37 (d,  $J = 8.1$  Hz, 1H), 7.24–7.18 (m, 1H), 7.17–7.11 (m, 1H), 7.03–7.00 (m, 1H), 4.52 (dt,  $J = 47.6$  Hz,  $J = 5.9$  Hz, 2H), 2.92 (t,  $J = 7.5$  Hz, 2H), 2.19–2.04 (m, 2H) ppm. **<sup>13</sup>C NMR** (100 MHz, CDCl<sub>3</sub>):  $\delta$  136.5, 127.5, 122.2, 121.6, 119.4, 119.0, 115.5, 111.3, 83.6 (d,  $J = 164.2$  Hz), 31.0 (d,  $J = 19.7$  Hz), 20.8 (d,  $J = 5.9$  Hz) ppm. **<sup>19</sup>F NMR** (376 MHz, CDCl<sub>3</sub>, decoupled):  $\delta$  -220.09 (s) ppm. **<sup>19</sup>F NMR** (376 MHz, CDCl<sub>3</sub>, not decoupled):  $\delta$  -220.09 (tt,  $J = 47.6$  Hz,  $J = 26.0$  Hz) ppm. **IR** (thin film):  $\nu$  3451, 2903, 1488, 1450, 1165, 1018, 936, 851, 799, 597 cm<sup>-1</sup>. **HRMS** (ESI<sup>+</sup>): exact mass calculated for C<sub>11</sub>H<sub>13</sub>FN ([M+H]<sup>+</sup>), 178.1027; found 178.1025.

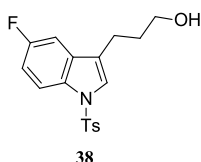


### 3-(3-Fluoropropyl)-5-methoxy-1H-indole (**24b**):<sup>79</sup>

To a suspension of XtalFluor-E<sup>®</sup> (305 mg, 1.29 mmol, 1.50 equiv) in CH<sub>2</sub>Cl<sub>2</sub> (10.0 mL) under inert atmosphere at rt was added triethylamine trihydrofluoride (287  $\mu$ L, 1.73 mmol, 1.50 equiv) dropwise upon stirring. The resulting mixture was stirred at rt for 15 min, cooled down to -78 °C, and a solution of 3-(5-methoxy-1H-indol-3-yl)propan-1-ol (**36**) (177 mg, 8.60 10<sup>-4</sup> mol, 1.00 equiv) in CH<sub>2</sub>Cl<sub>2</sub> (4mL) was added dropwise. The reaction was stirred at -78 °C for 1 h, and quenched with saturated aqueous NaHCO<sub>3</sub>. The aqueous layer was extracted with EtOAc, and the combined organic extracts were washed with brine, dried over Na<sub>2</sub>SO<sub>4</sub>, filtered, and concentrated *in vacuo*. The resulting crude material was purified by silica gel flash column chromatography (1:1 hexanes/CH<sub>2</sub>Cl<sub>2</sub>) to afford indole **24b** (52.0 mg, 2.50 10<sup>-4</sup> mol, 29%) as a pale yellow oil.

**TLC:**  $R_f = 0.35$  (1:1 hexanes/CH<sub>2</sub>Cl<sub>2</sub>; UV, CAM). **<sup>1</sup>H NMR** (400 MHz, CDCl<sub>3</sub>):  $\delta$  7.85 (bs, 1H), 7.26 (d,  $J = 8.9$  Hz, 1H), 7.04 (d,  $J = 2.4$  Hz, 1H), 7.01–6.98 (m, 1H), 6.87 (dd,  $J = 8.9$  Hz,  $J = 2.4$  Hz, 1H), 4.52 (dt,  $J = 47.3$  Hz,  $J = 5.9$  Hz, 2H), 3.87 (s, 3H), 2.87 (td,  $J = 7.5$  Hz,  $J = 0.9$  Hz, 2H), 2.17–2.02 (m, 2H) ppm. **<sup>13</sup>C NMR** (100 MHz, CDCl<sub>3</sub>):  $\delta$  154.1, 131.7, 128.0, 122.5, 115.2, 112.3, 112.0, 100.9, 83.6 (d,  $J = 164.2$  Hz), 56.1, 30.9 (d,  $J = 19.7$  Hz),

20.8 (d,  $J = 5.8$  Hz) ppm.  $^{19}\text{F}$  NMR (376 MHz,  $\text{CDCl}_3$ , decoupled):  $\delta$  -220.11 (s) ppm.  $^{19}\text{F}$  NMR (376 MHz,  $\text{CDCl}_3$ , not decoupled):  $\delta$  -220.11 (tt,  $J = 47.3$  Hz,  $J = 25.8$  Hz) ppm. IR (thin film):  $\nu$  3451, 2905, 1488, 1452, 1166, 1015, 931, 845, 781, 595  $\text{cm}^{-1}$ . HRMS (ESI+): exact mass calculated for  $\text{C}_{12}\text{H}_{15}\text{FNO}$  ( $[\text{M}+\text{H}]^+$ ), 208.1132; found 208.1130.



### 3-(5-Fluoro-1-tosyl-1H-indol-3-yl)propan-1-ol (38):

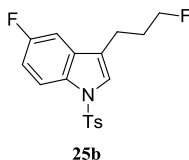
**Step 1:**<sup>78</sup> To a solution of 3-(5-fluoro-1H-indol-3-yl)propan-1-ol (**37**) (628 mg, 3.25 mmol, 1.00 equiv) in DMF (16.3 mL) under inert atmosphere at rt was added imidazole (497 mg, 7.15 mmol, 2.20 equiv) in one portion. The reaction mixture was cooled down to 0 °C and *tert*-butyldimethylsilyl chloride (0.550 g, 3.58 mmol, 1.10 equiv) was added portionwise. The reaction was then stirred at rt for 16 h before it was diluted with EtOAc. The organic solution was successively washed with water and brine, dried over  $\text{Na}_2\text{SO}_4$ , filtered, and concentrated *in vacuo*. The resulting crude material was purified by silica gel flash column chromatography (20:1 hexanes/EtOAc) to afford the silyl ether (792 mg) as an orange oil that was used as such in the next step.

**Step 2:**<sup>77</sup> To a vigorously stirred solution of the previously isolated silyl ether (792 mg), *p*-toluenesulfonyl chloride (595 mg, 3.09 mmol, 1.20 equiv), and tetrabutylammonium hydrogen sulfate (63.0 mg,  $1.80 \cdot 10^{-4}$  mol,  $7.00 \cdot 10^{-2}$  equiv) in toluene (12.9 mL) at 0 °C was added a 50% aqueous KOH solution (12.9 mL) dropwise. The reaction was then stirred at 0 °C for 1 h before it was diluted with a 1:1 water/ $\text{Et}_2\text{O}$  mixture and stirred for 5 min at rt. The aqueous phase was extracted with  $\text{Et}_2\text{O}$  and the combined organic extracts were washed with brine, dried over  $\text{Na}_2\text{SO}_4$ , filtered, and concentrated *in vacuo*. The resulting crude material was purified by silica gel flash column chromatography (20:1 hexanes:EtOAc) to afford the tosyl-protected indole (1.16 g) as a yellow oil that was used as such in the next step.

**Step 3:**<sup>78</sup> To a solution of the previously isolated tosyl-protected indole (1.16 g) in THF (12.6 mL) at 0 °C was added tetrabutylammonium fluoride (1 M, 2.76 mL, 2.76 mmol, 1.10 equiv) dropwise. After stirring for 1 h at rt, the reaction was diluted with EtOAc. The organic mixture was then successively washed with water and brine, dried over  $\text{Na}_2\text{SO}_4$ , filtered, and

concentrated *in vacuo*. The resulting crude material was purified by silica gel flash column chromatography (1:1 hexanes/EtOAc) to afford alcohol **38** (775 mg, 2.23 mmol, 68% over three steps) as a colorless syrup.

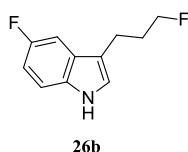
**TLC:**  $R_f = 0.21$  (1:1 hexanes/EtOAc; UV, CAM).  **$^1\text{H NMR}$**  (400 MHz,  $\text{CDCl}_3$ ):  $\delta$  7.91 (dd,  $J = 9.0$  Hz,  $J = 4.4$  Hz, 1H), 7.74–7.68 (m, 2H), 7.36 (s, 1H), 7.21 (d,  $J = 8.3$  Hz, 2H), 7.13 (dd,  $J = 8.9$  Hz,  $J = 2.6$  Hz, 1H), 7.02 (td,  $J = 9.0$  Hz,  $J = 2.6$  Hz, 1H), 3.69 (td,  $J = 6.2$  Hz,  $J = 4.7$  Hz, 2H), 2.71 (ddd,  $J = 7.9$  Hz,  $J = 7.0$  Hz,  $J = 1.1$  Hz, 2H), 2.34 (s, 3H), 1.97–1.87 (m, 2H), 1.41–1.34 (m, 1H) ppm.  **$^{13}\text{C NMR}$**  (100 MHz,  $\text{CDCl}_3$ ):  $\delta$  159.7 (d,  $J = 240.4$  Hz), 145.1, 135.2, 132.3 (d,  $J = 9.4$  Hz), 131.8 (d,  $J = 0.8$  Hz), 130.0, 126.8, 124.6, 122.8 (d,  $J = 4.2$  Hz), 115.0 (d,  $J = 9.4$  Hz), 112.7 (d,  $J = 25.5$  Hz), 105.3 (d,  $J = 23.8$  Hz), 62.1, 31.7, 21.7, 21.2 ppm.  **$^{19}\text{F NMR}$**  (376 MHz,  $\text{CDCl}_3$ , decoupled):  $\delta$  -119.72 (s) ppm.  **$^{19}\text{F NMR}$**  (376 MHz,  $\text{CDCl}_3$ , not decoupled):  $\delta$  -119.72 (td,  $J = 8.7$  Hz,  $J = 4.4$  Hz) ppm. **IR** (thin film):  $\nu$  3370, 2934, 1467, 1445, 1367, 1188, 1168, 1137, 1114, 895, 810, 736, 702, 667, 589, 537  $\text{cm}^{-1}$ . **HRMS** (ESI+): exact mass calculated for  $\text{C}_{18}\text{H}_{19}\text{FNO}_3\text{S}$  ( $[\text{M}+\text{H}]^+$ ), 348.1064; found 348.1063.



### 5-Fluoro-3-(3-fluoropropyl)-1-tosyl-1H-indole (**25b**):<sup>80</sup>

To a solution of 3-(5-fluoro-1-tosyl-1H-indol-3-yl)propan-1-ol (**38**) (765 mg, 2.20 mmol, 1.00 equiv) in MeCN (11.0 mL) under inert atmosphere at 0 °C were successively added *N,N*-diisopropylethylamine (1.52 mL, 8.81 mmol, 4.00 equiv), *N,N*-diisopropylethylamine trihydrofluoride (682  $\mu\text{L}$ , 3.30 mmol, 1.50 equiv), and perfluorobutanesulfonyl fluoride (824  $\mu\text{L}$ , 4.40 mmol, 2.00 equiv) dropwise. After stirring at 0 °C for 30 min, the reaction was quenched with saturated aqueous  $\text{NaHCO}_3$ . The aqueous phase was extracted with EtOAc and the combined organic extracts were washed with brine, dried over  $\text{Na}_2\text{SO}_4$ , filtered, and concentrated *in vacuo*. The resulting crude material was purified by silica gel flash column chromatography (20:1 hexanes/EtOAc) to afford indole **25b** (603 mg, 1.73 mmol, 78%) as a white crystalline solid (mp = 100 °C).

**TLC:**  $R_f = 0.21$  (10:1 hexanes/EtOAc; UV, CAM).  **$^1\text{H NMR}$**  (400 MHz,  $\text{CDCl}_3$ ):  $\delta$  7.92 (dd,  $J = 9.0$  Hz,  $J = 4.4$  Hz, 1H), 7.75–7.68 (m, 2H), 7.38 (s, 1H), 7.22 (d,  $J = 8.3$  Hz, 2H), 7.12 (dd,  $J = 8.8$  Hz,  $J = 2.5$  Hz, 1H), 7.04 (td,  $J = 9.0$  Hz,  $J = 2.5$  Hz, 1H), 4.46 (dt,  $J = 47.2$  Hz,  $J = 5.8$  Hz, 2H), 2.76 (td,  $J = 7.5$  Hz,  $J = 1.1$  Hz, 2H), 2.34 (s, 3H), 2.11–1.95 (m, 2H) ppm.  **$^{13}\text{C NMR}$**  (100 MHz,  $\text{CDCl}_3$ ):  $\delta$  159.7 (d,  $J = 240.6$  Hz), 145.1, 135.2, 132.1 (d,  $J = 9.5$  Hz), 131.8, 130.0, 126.8, 124.8, 122.1 (d,  $J = 4.2$  Hz), 115.1 (d,  $J = 9.4$  Hz), 112.8 (d,  $J = 25.6$  Hz), 105.2 (d,  $J = 24.0$  Hz), 83.0 (d,  $J = 165.4$  Hz), 29.8 (d,  $J = 20.1$  Hz), 21.7, 20.7 (d,  $J = 5.3$  Hz) ppm.  **$^{19}\text{F NMR}$**  (376 MHz,  $\text{CDCl}_3$ , decoupled):  $\delta$  -119.59 (s), -220.52 (s) ppm.  **$^{19}\text{F NMR}$**  (376 MHz,  $\text{CDCl}_3$ , not decoupled):  $\delta$  -119.59 (td,  $J = 9.6$  Hz,  $J = 5.0$  Hz), -220.52 (tt,  $J = 47.4$  Hz,  $J = 26.3$  Hz) ppm. **IR** (thin film):  $\nu$  2961, 1467, 1445, 1367, 1169, 1140, 1115, 1092, 896, 810, 797, 666, 588, 536, 508  $\text{cm}^{-1}$ . **HRMS** (ESI+): exact mass calculated for  $\text{C}_{18}\text{H}_{18}\text{F}_2\text{NO}_2\text{S}$  ( $[\text{M}+\text{H}]^+$ ), 350.1021; found 350.1024.

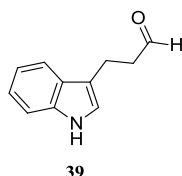


### 5-Fluoro-3-(3-fluoropropyl)-1H-indole (**26b**).<sup>81</sup>

To a degassed solution of 5-fluoro-3-(3-fluoropropyl)-1-tosyl-1H-indole (**25b**) (369 mg, 1.06 mmol, 1.00 equiv) in EtOH (10.6 mL) under inert atmosphere at rt was added potassium hydroxide (1.19 g, 21.1 mmol, 20.0 equiv). The reaction was heated to reflux overnight before it was then cooled down to rt and quenched with saturated aqueous  $\text{NH}_4\text{Cl}$ . The aqueous phase was extracted with EtOAc and the combined organic extracts were washed with brine, dried over  $\text{Na}_2\text{SO}_4$ , filtered, and concentrated *in vacuo*. The crude material was purified by silica gel flash column chromatography (5:1 hexanes/EtOAc) to afford indole **26b** (176 mg,  $9.00 \times 10^{-4}$  mol, 85%) as a yellow oil.

**TLC:**  $R_f = 0.15$  (5:1 hexanes/EtOAc; UV, CAM, *p*-anisaldehyde).  **$^1\text{H NMR}$**  (400 MHz,  $\text{CDCl}_3$ ):  $\delta$  8.11–7.77 (bs, 1H), 7.31–7.20 (m, 2H), 7.09–7.03 (m, 1H), 6.95 (td,  $J = 9.0$  Hz,  $J = 2.5$  Hz, 1H), 4.50 (td,  $J = 47.2$  Hz,  $J = 5.8$  Hz, 2H), 2.86 (td,  $J = 7.5$  Hz,  $J = 0.8$  Hz, 2H), 2.16–2.00 (m, 2H) ppm.  **$^{13}\text{C NMR}$**  (100 MHz,  $\text{CDCl}_3$ ):  $\delta$  157.9 (d,  $J = 234.5$  Hz), 133.0, 128.0 (d,  $J = 9.5$  Hz), 123.4, 115.7 (d,  $J = 4.8$  Hz), 111.8 (d,  $J = 9.7$  Hz), 110.6 (d,  $J = 26.4$  Hz), 103.9 (d,  $J = 23.2$  Hz), 83.5 (d,  $J = 164.3$  Hz), 30.9 (d,  $J = 19.8$  Hz), 20.8 (d,  $J = 5.6$  Hz) ppm.  **$^{19}\text{F NMR}$**  (376 MHz,  $\text{CDCl}_3$ , decoupled):  $\delta$  -124.83 (s), -220.27 (s) ppm.  **$^{19}\text{F NMR}$**  (376

MHz, CDCl<sub>3</sub>, not decoupled):  $\delta$  -124.83 (td,  $J = 10.1$  Hz,  $J = 4.5$  Hz), -220.27 (tt,  $J = 47.5$  Hz,  $J = 26.1$  Hz) ppm. **IR** (thin film):  $\nu$  3453, 2905, 1484, 1452, 1167, 1017, 936, 852, 795, 595 cm<sup>-1</sup>. **HRMS** (ESI<sup>+</sup>): exact mass calculated for C<sub>11</sub>H<sub>12</sub>F<sub>2</sub>N ([M+H]<sup>+</sup>), 196.0932; found 196.0936.

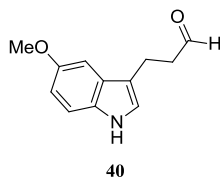


### 3-(1H-Indol-3-yl)propanal (**39**):<sup>82</sup>

To a solution of 3-(1H-indol-3-yl)propan-1-ol (**35**) (366  $\mu$ L, 2.40 mmol, 1.00 equiv) in CH<sub>2</sub>Cl<sub>2</sub> (15.0 mL) under inert atmosphere at 0 °C were successively added dimethylsulfoxide (0.340 mL, 4.79 mmol, 2.00 equiv) and phosphorus pentoxide (680 mg, 4.79 mmol, 2.00 equiv) upon stirring. The resulting mixture was stirred at rt for 1 h, cooled down to 0 °C, and triethylamine (1.18 mL, 8.39 mmol, 3.50 equiv) was added dropwise. After stirring for 1 h at rt, the reaction was neutralized with 0.1 M aqueous HCl and the aqueous layer was extracted with EtOAc. The combined organic extracts were washed with brine, dried over Na<sub>2</sub>SO<sub>4</sub>, filtered, and concentrated *in vacuo*. The resulting crude material was purified by silica gel flash column chromatography (10:1 hexanes/EtOAc) to afford aldehyde **39** (86.0 mg, 5.00  $\cdot 10^{-4}$  mol, 21%) as a colorless oil.

**TLC**:  $R_f = 0.24$  (5:1 hexanes/EtOAc; UV, CAM). **<sup>1</sup>H NMR** (400 MHz, CDCl<sub>3</sub>):  $\delta$  9.85 (t,  $J = 1.6$  Hz, 1H), 7.97 (bs, 1H), 7.60 (d,  $J = 8.0$  Hz, 1H), 7.37 (d,  $J = 8.1$  Hz, 1H), 7.24–7.18 (m, 1H), 7.16–7.11 (m, 1H), 7.01–6.98 (m, 1H), 3.13 (t,  $J = 7.3$  Hz, 2H), 2.86 (td,  $J = 7.3$  Hz,  $J = 1.6$  Hz, 2H) ppm. **<sup>13</sup>C NMR** (100 MHz, CDCl<sub>3</sub>):  $\delta$  202.6, 136.5, 127.2, 122.4, 121.6, 119.6, 118.8, 114.9, 111.3, 44.2, 18.0 ppm. **IR** (thin film):  $\nu$  3451, 2905, 1726, 1619, 1467, 1444, 1361, 1188, 1166, 1137, 1112, 1090, 979, 899, 851, 820, 734, 701, 668, 595, 567, 536 cm<sup>-1</sup>. **HRMS** (ESI<sup>+</sup>): exact mass calculated for C<sub>11</sub>H<sub>12</sub>NO ([M+H]<sup>+</sup>), 174.0913; found 174.0910.

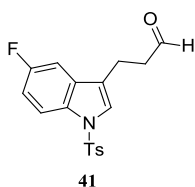




### 3-(5-Methoxy-1*H*-indol-3-yl)propanal (40):<sup>82</sup>

To a solution of 3-(5-methoxy-1*H*-indol-3-yl)propan-1-ol (**36**) (2.04 g, 9.94 mmol, 1.00 equiv) in CH<sub>2</sub>Cl<sub>2</sub> (0.100 L) under inert atmosphere at 0 °C were successively added dimethylsulfoxide (2.82 mL, 39.8 mmol, 4.00 equiv) and phosphorus pentoxide (5.64 g, 39.8 mmol, 4.00 equiv) upon stirring. The resulting mixture was stirred at rt for 1 h, cooled down to 0 °C, and triethylamine (9.78 mL, 69.6 mmol, 7.00 equiv) was added dropwise. After stirring for 1 h at rt, the reaction was neutralized with 0.1 M aqueous HCl and the aqueous layer was extracted with EtOAc. The combined organic extracts were washed with brine, dried over Na<sub>2</sub>SO<sub>4</sub>, filtered, and concentrated *in vacuo*. The resulting crude material was purified by silica gel flash column chromatography (3:1 pentane/EtOAc) to afford aldehyde **40** (715 mg, 3.52 mmol, 35%) as a yellow oil.

**TLC:**  $R_f = 0.20$  (3:1 pentane/EtOAc; UV, CAM). **<sup>1</sup>H NMR** (400 MHz, CDCl<sub>3</sub>):  $\delta$  9.86 (t,  $J = 1.5$  Hz, 1H), 7.89 (bs, 1H), 7.25 (d,  $J = 8.8$  Hz, 1H), 7.02 (d,  $J = 2.4$  Hz, 1H), 6.98–6.96 (m, 1H), 6.87 (dd,  $J = 8.8$  Hz,  $J = 2.4$  Hz, 1H), 3.87 (s, 3H), 3.08 (t,  $J = 7.2$  Hz, 2H), 2.85 (td,  $J = 7.2$  Hz,  $J = 1.5$  Hz, 2H) ppm. **<sup>13</sup>C NMR** (100 MHz, CDCl<sub>3</sub>):  $\delta$  202.7, 154.2, 131.6, 127.6, 122.4, 114.6, 112.5, 112.1, 100.7, 56.1, 44.0, 18.0 ppm. **IR** (thin film):  $\nu$  3450, 2908, 1721, 1615, 1467, 1443, 1361, 1189, 1165, 1134, 1111, 1090, 977, 899, 855, 810, 735, 703, 666, 597, 568, 537 cm<sup>-1</sup>. **HRMS** (ESI<sup>+</sup>): exact mass calculated for C<sub>12</sub>H<sub>14</sub>NO<sub>2</sub> ([M+H]<sup>+</sup>), 204.1019; found 204.1020.

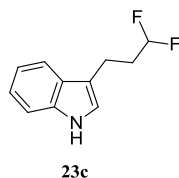


### 3-(5-Fluoro-1-tosyl-1*H*-indol-3-yl)propanal (41):<sup>83</sup>

To a suspension of pyridinium chlorochromate (2.91 g, 13.2 mmol, 1.50 equiv), sodium acetate (221 mg, 2.64 mmol, 3.00 10<sup>-1</sup> equiv), and oven-dried Celite<sup>®</sup> (ca. 3 g) in CH<sub>2</sub>Cl<sub>2</sub> (44.0 mL) under inert atmosphere at rt was added a solution of 3-(5-fluoro-1-tosyl-1*H*-indol-3-yl)propan-1-ol (**38**) (3.06 g, 8.81 mmol, 1.00 equiv) in CH<sub>2</sub>Cl<sub>2</sub> (44.0 mL) dropwise. After

stirring for 1.5 h at rt, the reaction was diluted with Et<sub>2</sub>O (ca. 100 mL) and stirred for 10 min at rt. The resulting suspension was filtered over a pad of Celite<sup>®</sup>, and the filtrate was concentrated *in vacuo*. The crude material was then purified by silica gel flash column chromatography (5:2 hexanes/EtOAc) to afford aldehyde **41** (2.49 g, 7.20 mmol, 82%) as a yellow crystalline solid (mp = 130 °C).

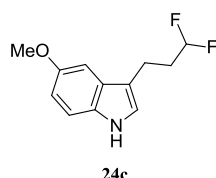
**TLC:**  $R_f$  = 0.10 (10:3 hexanes/EtOAc; UV, CAM). **<sup>1</sup>H NMR** (400 MHz, CDCl<sub>3</sub>): δ 9.82 (s, 1H), 7.91 (dd,  $J$  = 9.0 Hz,  $J$  = 4.4 Hz, 1H), 7.71 (d,  $J$  = 8.3 Hz, 2H), 7.36 (s, 1H), 7.22 (d,  $J$  = 8.1 Hz, 2H), 7.11 (dd,  $J$  = 8.6 Hz,  $J$  = 2.6 Hz, 1H), 7.04 (td,  $J$  = 9.0 Hz,  $J$  = 2.6 Hz, 1H), 2.94 (t,  $J$  = 7.2 Hz, 2H), 2.83 (t,  $J$  = 7.2 Hz, 2H), 2.34 (s, 3H) ppm. **<sup>13</sup>C NMR** (100 MHz, CDCl<sub>3</sub>): δ 200.8, 159.7 (d,  $J$  = 240.9 Hz), 145.2, 135.1, 131.8–131.6 (m), 130.0, 126.9, 124.9, 121.4 (d,  $J$  = 4.2 Hz), 115.1 (d,  $J$  = 9.3 Hz), 113.0 (d,  $J$  = 25.5 Hz), 105.1 (d,  $J$  = 23.9 Hz), 42.8, 21.7, 17.4 ppm. **<sup>19</sup>F NMR** (376 MHz, CDCl<sub>3</sub>, decoupled): δ -119.41 (s) ppm. **<sup>19</sup>F NMR** (376 MHz, CDCl<sub>3</sub>, not decoupled): δ -119.41 (td,  $J$  = 8.9 Hz,  $J$  = 4.5 Hz) ppm. **IR** (thin film): ν 3111, 2926, 1724, 1616, 1468, 1445, 1367, 1187, 1168, 1138, 1114, 1091, 983, 893, 856, 811, 735, 703, 667, 590, 569, 537 cm<sup>-1</sup>. **HRMS** (ESI<sup>+</sup>): exact mass calculated for C<sub>18</sub>H<sub>16</sub>FNNaO<sub>3</sub>S ([M+Na]<sup>+</sup>), 368.0727; found 368.0735.



### 3-(3,3-Difluoropropyl)-1H-indole (**23c**):<sup>79</sup>

To a suspension of XtalFluor-E<sup>®</sup> (176 mg, 7.50 10<sup>-4</sup> mol, 1.50 equiv) in CH<sub>2</sub>Cl<sub>2</sub> (5.00 mL) under inert atmosphere at rt was added triethylamine trihydrofluoride (165 μL, 9.90 10<sup>-4</sup> mol, 2.00 equiv) dropwise upon stirring. After 5 min stirring at rt, the resulting solution was cooled down to -78 °C, and a solution of 3-(1H-indol-3-yl)propanal (**39**) (86.0 mg, 5.00 10<sup>-4</sup> mol, 1.00 equiv) in CH<sub>2</sub>Cl<sub>2</sub> (2.00 mL) was added dropwise. The solution was stirred at -78 °C for 15 min, warmed up to 0 °C, and stirred for 30 min. The reaction was quenched with saturated aqueous NaHCO<sub>3</sub>, and the aqueous layer was extracted with EtOAc. The combined organic extracts were washed with brine, dried over Na<sub>2</sub>SO<sub>4</sub>, filtered, and concentrated *in vacuo*. The resulting crude material was purified by silica gel flash column chromatography (20:1 hexanes/EtOAc) to afford indole **23c** (72.0 mg, 3.70 10<sup>-4</sup> mol, 74%) as a yellow oil.

**TLC:**  $R_f = 0.30$  (5:1 hexanes/EtOAc; UV, CAM).  **$^1\text{H NMR}$**  (400 MHz,  $\text{CDCl}_3$ ):  $\delta$  7.95 (bs, 1H), 7.64–7.59 (m, 1H), 7.38 (dt,  $J = 8.1$  Hz,  $J = 1.0$  Hz, 1H), 7.26–7.21 (m, 1H), 7.19–7.14 (m, 1H), 7.03–7.00 (m, 1H), 5.87 (tt,  $J = 56.6$  Hz,  $J = 4.6$  Hz, 1H), 2.96 (t,  $J = 7.8$  Hz, 2H), 2.33–2.19 (m, 2H) ppm.  **$^{13}\text{C NMR}$**  (100 MHz,  $\text{CDCl}_3$ ):  $\delta$  136.5, 127.2, 122.4, 121.5, 119.6, 118.8, 117.3 (t,  $J = 238.6$  Hz), 114.4, 111.4, 34.7 (t,  $J = 20.9$  Hz), 18.2 (t,  $J = 6.4$  Hz) ppm.  **$^{19}\text{F NMR}$**  (376 MHz,  $\text{CDCl}_3$ , decoupled):  $\delta$  -117.22 (s) ppm.  **$^{19}\text{F NMR}$**  (376 MHz,  $\text{CDCl}_3$ , not decoupled):  $\delta$  -117.22 (dt,  $J = 56.6$  Hz,  $J = 17.2$  Hz) ppm. **IR** (thin film):  $\nu$  3474, 2933, 1486, 1453, 1160, 1116, 1038, 939, 851, 793, 599  $\text{cm}^{-1}$ . **HRMS** (ESI+): exact mass calculated for  $\text{C}_{11}\text{H}_{12}\text{F}_2\text{N}$  ( $[\text{M}+\text{H}]^+$ ), 196.0932; found 196.0933.

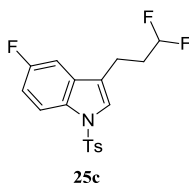


### 3-(3,3-Difluoropropyl)-5-methoxy-1H-indole (**24c**):<sup>79</sup>

To a suspension of XtalFluor-E<sup>®</sup> (1.25 g, 5.28 mmol, 1.50 equiv) in  $\text{CH}_2\text{Cl}_2$  (20.0 mL) under inert atmosphere at rt was added triethylamine trihydrofluoride (1.17 mL, 7.04 mmol, 2.00 equiv) upon stirring. After 5 min stirring at rt, the resulting solution was cooled down to -78 °C, and a solution of 3-(5-methoxy-1H-indol-3-yl)propanal (**40**) (715 mg, 3.52 mmol, 1.00 equiv) in  $\text{CH}_2\text{Cl}_2$  (10.0 mL) was added dropwise. The solution was stirred at -78 °C for 15 min, warmed up to 0 °C, and stirred for 30 min. The reaction was quenched with saturated aqueous  $\text{NaHCO}_3$ , and the aqueous layer was extracted with EtOAc. The combined organic extracts were washed with brine, dried over  $\text{Na}_2\text{SO}_4$ , filtered, and concentrated *in vacuo*. The resulting crude material was purified by silica gel flash column chromatography (2:1  $\text{CH}_2\text{Cl}_2$ /cyclohexane) to afford indole **24c** (293 mg, 1.30 mmol, 37%) as a clear yellow oil.

**TLC:**  $R_f = 0.15$  (2:1  $\text{CH}_2\text{Cl}_2$ /cyclohexane; UV, CAM).  **$^1\text{H NMR}$**  (400 MHz,  $\text{CDCl}_3$ ):  $\delta$  7.87 (bs, 1H), 7.26 (dd,  $J = 8.8$  Hz,  $J = 0.5$  Hz, 1H), 7.02 (d,  $J = 2.5$  Hz, 1H), 7.01–6.98 (m, 1H), 6.88 (dd,  $J = 8.8$  Hz,  $J = 2.5$  Hz, 1H), 5.86 (tt,  $J = 56.7$  Hz,  $J = 4.6$  Hz, 1H), 3.88 (s, 3H), 2.91 (t,  $J = 7.8$  Hz, 2H), 2.32–2.15 (m, 2H) ppm.  **$^{13}\text{C NMR}$**  (100 MHz,  $\text{CDCl}_3$ ):  $\delta$  154.2, 131.7, 127.7, 122.3, 117.3 (t,  $J = 238.8$  Hz), 114.2, 112.6, 112.1, 100.7, 56.1, 34.7 (t,  $J = 20.9$  Hz), 18.2 (t,  $J = 6.3$  Hz) ppm.  **$^{19}\text{F NMR}$**  (376 MHz,  $\text{CDCl}_3$ , decoupled):  $\delta$  -117.24 (s) ppm.  **$^{19}\text{F NMR}$**  (376 MHz,  $\text{CDCl}_3$ , not decoupled):  $\delta$  -117.24 (dt,  $J = 56.7$  Hz,  $J = 17.2$  Hz) ppm. **IR**

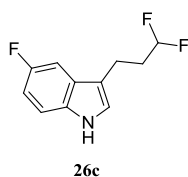
(thin film):  $\nu$  3475, 2935, 1487, 1453, 1165, 1115, 1031, 934, 852, 798, 594  $\text{cm}^{-1}$ . **HRMS** (ESI+): exact mass calculated for  $\text{C}_{12}\text{H}_{14}\text{F}_2\text{NO}$  ( $[\text{M}+\text{H}]^+$ ), 226.1038; found 226.1039.



**3-(3,3-Difluoropropyl)-5-fluoro-1-tosyl-1H-indole (25c):**<sup>84</sup>

To a solution of 3-(5-fluoro-1-tosyl-1H-indol-3-yl)propanal (**41**) (1.00 g, 2.90 mmol, 1.00 equiv) in  $\text{CH}_2\text{Cl}_2$  (29.0 mL) under inert atmosphere at 0 °C was added diethylaminosulfur trifluoride (604  $\mu\text{L}$ , 4.34 mmol, 1.50 equiv) dropwise. After stirring for 2 h at rt, the reaction was carefully quenched with saturated aqueous  $\text{NaHCO}_3$ . The aqueous phase was extracted with  $\text{CH}_2\text{Cl}_2$  and the combined organic extracts were dried over  $\text{Na}_2\text{SO}_4$ , filtered, and concentrated *in vacuo*. The resulting crude material was purified by silica gel flash column chromatography (10:1 hexanes/EtOAc) to afford indole **25c** (922 mg, 2.51 mmol, 87%) as a white crystalline solid (mp = 130 °C).

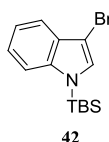
**TLC:**  $R_f$  = 0.33 (10:3 hexanes/EtOAc; UV, CAM).  **$^1\text{H}$  NMR** (400 MHz,  $\text{CDCl}_3$ ):  $\delta$  7.93 (dd,  $J$  = 9.0 Hz,  $J$  = 4.4 Hz, 1H), 7.72 (d,  $J$  = 8.4 Hz, 2H), 7.39 (s, 1H), 7.23 (d,  $J$  = 8.1 Hz, 2H), 7.10 (dd,  $J$  = 8.8 Hz,  $J$  = 2.5 Hz, 1H), 7.05 (td,  $J$  = 9.0 Hz,  $J$  = 2.5 Hz, 1H), 5.83 (tt,  $J$  = 56.5 Hz,  $J$  = 4.3 Hz, 1H), 2.83–2.75 (m, 2H), 2.35 (s, 3H), 2.27–2.11 (m, 2H) ppm.  **$^{13}\text{C}$  NMR** (100 MHz,  $\text{CDCl}_3$ ):  $\delta$  159.8 (d,  $J$  = 241.1 Hz), 145.3, 135.1, 131.8 (d,  $J$  = 0.7 Hz), 131.7 (d,  $J$  = 9.5 Hz), 130.1, 126.9, 124.8, 121.0 (d,  $J$  = 4.2 Hz), 116.5 (t,  $J$  = 239.4 Hz), 115.1 (d,  $J$  = 9.4 Hz), 113.1 (d,  $J$  = 25.5 Hz), 105.1 (d,  $J$  = 23.9 Hz), 33.5 (t,  $J$  = 21.5 Hz), 21.7, 17.7 (t,  $J$  = 6.3 Hz) ppm.  **$^{19}\text{F}$  NMR** (376 MHz,  $\text{CDCl}_3$ , decoupled):  $\delta$  -117.31 (s), -119.31 (s) ppm.  **$^{19}\text{F}$  NMR** (376 MHz,  $\text{CDCl}_3$ , not decoupled):  $\delta$  -117.31 (dt,  $J$  = 56.8 Hz,  $J$  = 17.1 Hz), -119.31 (td,  $J$  = 8.9 Hz,  $J$  = 4.4 Hz) ppm. **IR** (thin film):  $\nu$  3113, 2932, 1596, 1469, 1446, 1369, 1187, 1169, 1140, 1114, 1092, 1050, 894, 810, 666, 589, 537  $\text{cm}^{-1}$ . **HRMS** (ESI+): exact mass calculated for  $\text{C}_{18}\text{H}_{17}\text{F}_3\text{NO}_2\text{S}$  ( $[\text{M}+\text{H}]^+$ ), 368.0927; found 368.0925.



### 3-(3,3-Difluoropropyl)-5-fluoro-1*H*-indole (**26c**):<sup>81</sup>

To a degassed solution of 3-(3,3-difluoropropyl)-5-fluoro-1-tosyl-1*H*-indole (**25c**) (728 mg, 1.98 mmol, 1.00 equiv) in EtOH (19.8 mL) under inert atmosphere at rt was added potassium hydroxide (2.22 g, 39.6 mmol, 20.0 equiv). The reaction was heated to reflux overnight before it was then cooled down to rt and quenched with saturated aqueous NH<sub>4</sub>Cl. The aqueous phase was extracted with EtOAc and the combined organic extracts were washed with brine, dried over Na<sub>2</sub>SO<sub>4</sub>, filtered, and concentrated *in vacuo*. The crude material was purified by silica gel flash column chromatography (5:1 hexanes/EtOAc) to afford indole **26c** (348 mg, 1.63 mmol, 82%) as a yellow oil.

**TLC:**  $R_f$  = 0.11 (5:1 hexanes/EtOAc; UV, CAM, *p*-anisaldehyde). **<sup>1</sup>H NMR** (400 MHz, CDCl<sub>3</sub>): δ 8.14–7.80 (bs, 1H), 7.33–7.21 (m, 2H), 7.09–7.04 (m, 1H), 6.98 (td,  $J$  = 9.0 Hz,  $J$  = 2.5 Hz, 1H), 5.86 (tt,  $J$  = 56.8 Hz,  $J$  = 4.6 Hz, 1H), 2.96–2.85 (m, 2H), 2.32–2.14 (m, 2H) ppm. **<sup>13</sup>C NMR** (100 MHz, CDCl<sub>3</sub>): δ 157.9 (d,  $J$  = 234.7 Hz), 133.0, 127.6 (d,  $J$  = 9.6 Hz), 123.4, 117.2 (t,  $J$  = 238.8 Hz), 114.6 (d,  $J$  = 4.7 Hz), 112.0 (d,  $J$  = 9.6 Hz), 110.7 (d,  $J$  = 26.4 Hz), 103.7 (d,  $J$  = 23.4 Hz), 34.6 (t,  $J$  = 21.0 Hz), 18.1 (t,  $J$  = 6.4 Hz) ppm. **<sup>19</sup>F NMR** (376 MHz, CDCl<sub>3</sub>, decoupled): δ -117.18 (s), -124.48 (s) ppm. **<sup>19</sup>F NMR** (376 MHz, CDCl<sub>3</sub>, not decoupled): δ -117.18 (dt,  $J$  = 56.5 Hz,  $J$  = 17.2 Hz), -124.48 (td,  $J$  = 9.6 Hz,  $J$  = 4.4 Hz) ppm. **IR** (thin film): ν 3475, 2934, 1484, 1453, 1165, 1116, 1033, 934, 852, 795, 594 cm<sup>-1</sup>. **HRMS** (ESI+): exact mass calculated for C<sub>11</sub>H<sub>11</sub>F<sub>3</sub>N ([M+H]<sup>+</sup>), 214.0838; found 214.0843.

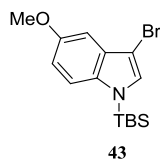


### 3-Bromo-1-(*tert*-butyldimethylsilyl)-1*H*-indole (**42**):<sup>85</sup>

To a solution of 1*H*-indole (**31**) (1.60 g, 13.5 mmol, 1.00 equiv) in THF (40.0 mL) under inert atmosphere at -78 °C was added *n*-butyllithium (1.6 M in hexanes, 9.30 mL, 14.9 mmol, 1.10 equiv) dropwise upon stirring. The reaction mixture was stirred at -10 °C for 15 min and cooled down to -78 °C before a solution of *tert*-butyldimethylsilyl chloride (2.34 g, 15.6

mmol, 1.15 equiv) in THF (20.0 mL) was added dropwise. The resulting solution was warmed up to 0 °C, stirred for 3 h, and cooled down to -78 °C before *N*-bromosuccinimide (2.55 g, 14.2 mmol, 1.05 equiv) was added portionwise. The reaction was stirred at rt for 1 h, and a mixture of *n*-hexane (25.0 mL) and pyridine (0.250 mL) was added. The resulting mixture was stirred for 15 min at rt, filtered over a pad of Celite<sup>®</sup>, and the filtrate was concentrated *in vacuo*. The crude material was purified by silica gel flash column chromatography (100% hexanes) to afford indole **42** (3.82 g, 12.3 mmol, 91%) as a colorless syrup.

**TLC:**  $R_f$  = 0.27 (100% hexanes; UV, CAM). **<sup>1</sup>H NMR** (400 MHz, CDCl<sub>3</sub>): δ 7.60–7.54 (m, 1H), 7.51–7.45 (m, 1H), 7.24–7.17 (m, 2H), 7.17 (s, 1H), 0.94 (s, 9H), 0.60 (s, 6H) ppm. **<sup>13</sup>C NMR** (100 MHz, CDCl<sub>3</sub>): δ 140.4, 130.1, 129.8, 122.6, 120.7, 119.3, 114.3, 93.8, 26.4, 19.6, -3.8 ppm. **IR** (thin film): ν 2930, 2862, 1476, 1445, 1257, 1154, 1143, 1019, 900, 834, 817, 802, 792, 732 cm<sup>-1</sup>. **HRMS** (ESI<sup>+</sup>): exact mass calculated for C<sub>14</sub>H<sub>21</sub>BrNSi ([M+H]<sup>+</sup>), 310.0621; found 310.0623.

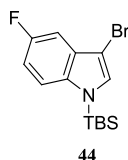


### 3-Bromo-1-(*tert*-butyldimethylsilyl)-5-methoxy-1*H*-indole (**43**):<sup>85</sup>

To a solution of 5-methoxy-1*H*-indole (**32**) (2.56 g, 17.2 mmol, 1.00 equiv) in THF (50.0 mL) under inert atmosphere at -78 °C was added *n*-butyllithium (1.6 M in hexanes, 11.8 mL, 18.9 mmol, 1.10 equiv) dropwise upon stirring. The reaction mixture was stirred at -10 °C for 15 min and cooled down to -78 °C before a solution of *tert*-butyldimethylsilyl chloride (2.98 g, 19.8 mmol, 1.15 equiv) in THF (15.0 mL) was added dropwise. The resulting solution was warmed up to 0 °C, stirred for 3 h, and cooled down to -78 °C before *N*-bromosuccinimide (3.83 g, 21.5 mmol, 1.25 equiv) was added portionwise. The reaction was stirred at rt for 1 h, and a mixture of *n*-hexane (25.0 mL) and pyridine (0.250 mL) was added. The resulting mixture was stirred for 15 min at rt, filtered over a pad of Celite<sup>®</sup>, and the filtrate was concentrated *in vacuo*. The crude material was purified by silica gel flash column chromatography (40:1 hexanes/EtOAc) to afford indole **43** (5.71 g, 16.8 mmol, 97%) as a colorless syrup.

**TLC:**  $R_f$  = 0.40 (10:1 hexanes/EtOAc; UV, CAM). **<sup>1</sup>H NMR** (400 MHz, CDCl<sub>3</sub>): δ 7.36 (d,  $J$  = 9.0 Hz, 1H), 7.14 (s, 1H), 6.98 (d,  $J$  = 2.6 Hz, 1H), 6.85 (dd,  $J$  = 9.0 Hz,  $J$  = 2.6 Hz, 1H),

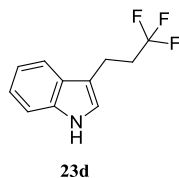
3.88 (s, 3H), 0.92 (s, 9H), 0.58 (s, 6H) ppm.  $^{13}\text{C}$  NMR (100 MHz,  $\text{CDCl}_3$ ):  $\delta$  155.0, 135.3, 130.6, 130.4, 115.1, 113.1, 100.5, 93.4, 55.9, 26.4, 19.5, -3.9 ppm. IR (thin film):  $\nu$  2931, 2865, 1474, 1441, 1255, 1161, 1150, 1020, 909, 835, 820, 806, 787, 733  $\text{cm}^{-1}$ . HRMS (ESI+): exact mass calculated for  $\text{C}_{15}\text{H}_{23}\text{BrNOSi}$  ( $[\text{M}+\text{H}]^+$ ), 340.0727; found 340.0727.



### 3-Bromo-1-(*tert*-butyldimethylsilyl)-5-fluoro-1*H*-indole (**44**).<sup>85</sup>

To a solution of 5-fluoro-1*H*-indole (**33**) (2.00 g, 14.7 mmol, 1.00 equiv) in THF (50.0 mL) under inert atmosphere at  $-78$  °C was added *n*-butyllithium (1.6 M in hexanes, 10.1 mL, 16.1 mmol, 1.10 equiv) dropwise upon stirring. The reaction mixture was stirred at  $-10$  °C for 15 min and cooled down to  $-78$  °C before a solution of *tert*-butyldimethylsilyl chloride (2.55 g, 16.6 mmol, 1.13 equiv) in THF (15.0 mL) was added dropwise. The resulting solution was warmed up to  $0$  °C, stirred for 1 h, and cooled down to  $-78$  °C before *N*-bromosuccinimide (2.63 g, 14.8 mmol, 1.01 equiv) was added portionwise. The reaction was stirred at  $-78$  °C for 2 h, and a mixture of *n*-hexane (25.0 mL) and pyridine (0.250 mL) was added. The resulting solution was warmed up to rt and stirred for 15 min, filtered over a pad of Celite<sup>®</sup>, and the filtrate was concentrated *in vacuo*. The crude material was purified by silica gel flash column chromatography (100% hexanes) to afford indole **44** (3.20 g, 9.74 mmol, 66%) as a colorless oil.

TLC:  $R_f$  = 0.41 (hexanes; UV, CAM, *p*-anisaldehyde).  $^1\text{H}$  NMR (400 MHz,  $\text{CDCl}_3$ ):  $\delta$  7.41 (dd,  $J$  = 9.0 Hz,  $J$  = 4.1 Hz, 1H), 7.25–7.20 (m, 2H), 6.90 (td,  $J$  = 9.0 Hz,  $J$  = 2.6 Hz, 1H), 0.94 (s, 9H), 0.60 (s, 6H) ppm.  $^{13}\text{C}$  NMR (100 MHz,  $\text{CDCl}_3$ ):  $\delta$  158.5 (d,  $J$  = 237.0 Hz), 136.9, 131.6, 130.8 (d,  $J$  = 10.4 Hz), 115.0 (d,  $J$  = 9.4 Hz), 111.1 (d,  $J$  = 26.0 Hz), 104.3 (d,  $J$  = 24.3 Hz), 93.4 (d,  $J$  = 4.7 Hz), 26.3, 19.5, -3.9 ppm.  $^{19}\text{F}$  NMR (376 MHz,  $\text{CDCl}_3$ , decoupled):  $\delta$  -123.14 (s) ppm.  $^{19}\text{F}$  NMR (376 MHz,  $\text{CDCl}_3$ , not decoupled):  $\delta$  -123.14 (td,  $J$  = 9.2 Hz,  $J$  = 4.1 Hz) ppm. IR (thin film):  $\nu$  2931, 2860, 1475, 1441, 1256, 1159, 1145, 1018, 907, 835, 820, 806, 789, 730  $\text{cm}^{-1}$ . HRMS (EI+): exact mass calculated for  $\text{C}_{14}\text{H}_{19}\text{BrFNSi}$  ( $[\text{M}]^+$ ), 327.0449; found 327.0445.

**3-(3,3,3-Trifluoropropyl)-1H-indole (23d):**<sup>86</sup>

**Step 1:** To a solution of 3-bromo-1-(*tert*-butyldimethylsilyl)-1H-indole (**42**) (4.50 g, 14.5 mmol, 1.00 equiv) in THF (15.0 mL) under inert atmosphere at rt were added magnesium turnings (531 mg, 21.8 mmol, 1.50 equiv) upon vigorous stirring. The resulting mixture was heated to reflux for 3 h, cooled down to rt, and titrated,<sup>140</sup> thus providing a 0.54 M solution of Grignard adduct in THF (solution **S1**), which was used in **Step 2**.

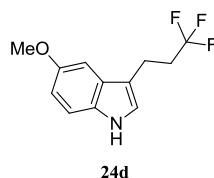
**Step 2:** A solution **S2** made of 1,1,1-trifluoro-3-iodopropane (**34d**) (164  $\mu$ L, 1.37 mmol, 1.50 equiv) and iron trichloride (0.1 M in THF, 458  $\mu$ L,  $5.00 \cdot 10^{-5}$  mol,  $5.00 \cdot 10^{-2}$  equiv) was prepared under inert atmosphere at 0 °C. A solution **S3** made of TMEDA (165  $\mu$ L, 1.10 mmol, 1.20 equiv) diluted in **S1** (0.54 M in THF, 1.70 mL,  $9.20 \cdot 10^{-4}$  mol, 1.00 equiv) was prepared at rt under inert atmosphere. Solution **S3** was then added dropwise upon stirring to **S2**, and the resulting reaction mixture was stirred at 0 °C for 15 min. The reaction was carefully quenched with aqueous.  $\text{NH}_4\text{Cl}$ , and the aqueous layer was extracted with  $\text{Et}_2\text{O}$ . The combined organic extracts were washed with brine, dried over  $\text{Na}_2\text{SO}_4$ , filtered, and concentrated *in vacuo*. The resulting crude material was purified by silica gel flash column chromatography (100% hexanes) to afford a colorless oil (0.100 g) that was then used in **Step 3**.

**TLC:**  $R_f = 0.25$  (100% hexanes; UV, CAM).  **$^1\text{H NMR}$**  (400 MHz,  $\text{CDCl}_3$ ):  $\delta$  7.57–7.47 (m, 2H), 7.21–7.10 (m, 2H), 6.97 (s, 1H), 3.06–2.97 (m, 2H), 2.58–2.39 (m, 2H), 0.93 (s, 9H), 0.59 (s, 6H). **HRMS** (ESI<sup>+</sup>): exact mass calculated for  $\text{C}_{17}\text{H}_{25}\text{F}_3\text{NSi}$  ( $[\text{M}+\text{H}]^+$ ), 328.1703; found 328.1709.

**Step 3:** To a solution of the previously isolated product (0.100 g,  $3.00 \cdot 10^{-4}$  mol, 1.00 equiv) in THF (2.00 mL) under inert atmosphere at rt was added TBAF (1 M in THF,  $1.80 \cdot 10^{-4}$  L,  $6.10 \cdot 10^{-4}$  mol, 2.00 equiv) dropwise upon stirring. The reaction was stirred at rt for 15 min, quenched with saturated aqueous  $\text{NaHCO}_3$ , and the aqueous layer was extracted with  $\text{Et}_2\text{O}$ . The combined organic extracts were washed with brine, dried over  $\text{Na}_2\text{SO}_4$ , filtered, and concentrated *in vacuo*. The resulting crude material was purified by silica gel flash column chromatography (2:1 hexanes/ $\text{CH}_2\text{Cl}_2$ ) to afford indole **23d** (55.0 mg,  $2.60 \cdot 10^{-4}$  mol, 28% over 3 steps) as a colorless syrup.



**TLC:**  $R_f$  = 0.16 (2:1 hexanes/ $\text{CH}_2\text{Cl}_2$ ; UV, CAM).  **$^1\text{H NMR}$**  (400 MHz,  $\text{CDCl}_3$ ):  $\delta$  7.98 (bs, 1H), 7.59 (d,  $J$  = 8.0 Hz, 1H), 7.38 (d,  $J$  = 8.1 Hz, 1H), 7.25–7.20 (m, 1H), 7.18–7.12 (m, 1H), 7.05–7.01 (m, 1H), 3.07–3.01 (m, 2H), 2.56–2.42 (m, 2H) ppm.  **$^{13}\text{C NMR}$**  (100 MHz,  $\text{CDCl}_3$ ):  $\delta$  136.5, 127.8 (q,  $J$  = 142.1 Hz), 122.5, 121.5, 119.7, 118.6, 113.8, 111.4, 34.8 (q,  $J$  = 28.1 Hz), 18.1 (q,  $J$  = 3.2 Hz) ppm.  **$^{19}\text{F NMR}$**  (376 MHz,  $\text{CDCl}_3$ , decoupled):  $\delta$  -66.75 (s) ppm.  **$^{19}\text{F NMR}$**  (376 MHz,  $\text{CDCl}_3$ , not decoupled):  $\delta$  -66.75 (t,  $J$  = 10.8 Hz) ppm. **IR** (thin film):  $\nu$  3475, 3432, 2924, 1482, 1449, 1258, 1175, 1133, 1115, 1087, 848, 799, 756, 592  $\text{cm}^{-1}$ . **HRMS** (ESI+): exact mass calculated for  $\text{C}_{11}\text{H}_{11}\text{F}_3\text{N}$  ( $[\text{M}+\text{H}]^+$ ), 214.0838; found 214.837.



**5-Methoxy-3-(3,3,3-trifluoropropyl)-1H-indole (24d).**<sup>86</sup>

**Step 1:** To a solution of 3-bromo-1-(*tert*-butyldimethylsilyl)-5-methoxy-1H-indole (**43**) (5.70 g, 16.8 mmol, 1.00 equiv) in THF (17.0 mL) under inert atmosphere at rt were added magnesium turnings (614 mg, 25.1 mmol, 1.50 equiv) upon vigorous stirring. The resulting mixture was heated to reflux for 3 h, cooled down to rt, and titrated,<sup>140</sup> thus providing a 0.52 M solution of Grignard adduct in THF (solution **S1**), which was used in **Step 2**.

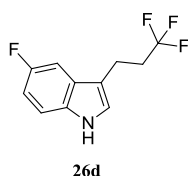
**Step 2:** A solution **S2** made of 1,1,1-trifluoro-3-iodopropane (**34d**) (251  $\mu\text{L}$ , 2.20 mmol, 1.50 equiv) and iron trichloride (0.1 M in THF, 699  $\mu\text{L}$ ,  $7.00 \times 10^{-5}$  mol,  $5.00 \times 10^{-2}$  equiv) was prepared under inert atmosphere at 0 °C. A solution **S3** made of TMEDA (252  $\mu\text{L}$ , 1.68 mmol, 1.20 equiv) diluted in **S1** (0.52 M in THF, 2.29 mL, 1.40 mmol, 1.00 equiv) was prepared at rt under inert atmosphere. Solution **S3** was then added dropwise upon stirring to **S2**, and the resulting reaction mixture was stirred at 0 °C for 15 min. The reaction was carefully quenched with saturated aqueous  $\text{NH}_4\text{Cl}$ , and the aqueous layer was extracted with  $\text{Et}_2\text{O}$ . The combined organic extracts were washed with brine, dried over  $\text{Na}_2\text{SO}_4$ , filtered, and concentrated *in vacuo*. The resulting crude material was purified by silica gel flash column chromatography (40:1 hexanes/ $\text{EtOAc}$ ) to afford a colorless oil (0.270 g) that was then used in **Step 3**.

**TLC:**  $R_f$  = 0.27 (2:1 hexanes/ $\text{CH}_2\text{Cl}_2$ ; UV, CAM).  **$^1\text{H NMR}$**  (400 MHz,  $\text{CDCl}_3$ ):  $\delta$  7.37 (d,  $J$  = 8.9 Hz, 1H), 6.96 (d,  $J$  = 2.6 Hz, 1H), 6.94 (s, 1H), 6.83 (dd,  $J$  = 8.9 Hz,  $J$  = 2.6 Hz, 1H),

3.87 (s, 3H), 3.01–2.94 (m, 2H), 2.54–2.40 (m, 2H), 0.91 (s, 9H), 0.57 (s, 6H) ppm. **HRMS** (ESI+): exact mass calculated for  $C_{18}H_{27}F_3NOSi$  ( $[M+H]^+$ ), 358.1809; found 358.1808.

**Step 3:** To a solution of the previously isolated product (0.270 g,  $7.60 \times 10^{-4}$  mol, 1.00 equiv) in THF (10.0 mL) under inert atmosphere at rt was added TBAF (1 M in THF, 1.51 mL, 1.51 mmol, 2.00 equiv) dropwise upon stirring. The reaction was stirred at rt for 15 min, quenched with saturated aqueous  $NaHCO_3$ , and the aqueous layer was extracted with  $Et_2O$ . The combined organic extracts were washed with brine, dried over  $Na_2SO_4$ , filtered, and concentrated *in vacuo*. The resulting crude material was purified by silica gel flash column chromatography (10:1 hexanes/ $EtOAc$ ) to afford indole **24d** (172 mg,  $6.60 \times 10^{-4}$  mol, 47% over 3 steps) as a colorless oil.

**TLC:**  $R_f = 0.18$  (2:1 hexanes/ $CH_2Cl_2$ ; UV, CAM).  **$^1H$  NMR** (400 MHz,  $CDCl_3$ ):  $\delta$  7.91 (bs, 1H), 7.27 (d,  $J = 8.7$  Hz, 1H), 7.02 (d,  $J = 2.4$  Hz, 1H), 7.01–6.98 (m, 1H), 6.90 (dd,  $J = 8.7$  Hz,  $J = 2.4$  Hz, 1H), 3.90 (s, 3H), 3.05–2.97 (m, 2H), 2.56–2.42 (m, 2H) ppm.  **$^{13}C$  NMR** (100 MHz,  $CDCl_3$ ):  $\delta$  154.3, 131.6, 127.5, 127.1 (q,  $J = 276.7$  Hz), 122.3, 113.5, 112.6, 112.6, 100.5, 56.1, 34.6 (q,  $J = 28.0$  Hz), 18.1 (q,  $J = 3.6$  Hz) ppm.  **$^{19}F$  NMR** (376 MHz,  $CDCl_3$ , decoupled):  $\delta$  -66.67 (s) ppm.  **$^{19}F$  NMR** (376 MHz,  $CDCl_3$ , not decoupled):  $\delta$  -66.67 (t,  $J = 10.8$  Hz) ppm. **IR** (thin film):  $\nu$  3476, 3429, 2926, 1483, 1450, 1258, 1175, 1133, 1119, 1091, 851, 801, 755, 592  $cm^{-1}$ . **HRMS** (ESI+): exact mass calculated for  $C_{12}H_{13}F_3NO$  ( $[M+H]^+$ ), 244.0944; found 244.0943.



**5-Fluoro-3-(3,3,3-trifluoropropyl)-1H-indole (26d):**<sup>86</sup>

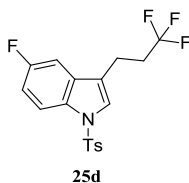
**Step 1:** To a solution of 3-bromo-1-(*tert*-butyldimethylsilyl)-5-fluoro-1H-indole (**44**) (2.40 g, 7.31 mmol, 1.00 equiv) in THF (15.0 mL) under inert atmosphere at rt were added magnesium turnings (3.55 g, 146 mmol, 20.0 equiv) upon vigorous stirring. The resulting mixture was heated to reflux for 3 h, cooled down to rt, thus providing a solution of Grignard adduct in THF (solution **S1**) which was used as such in **Step 2**.

**Step 2:** A solution **S2** made of 1,1,1-trifluoro-3-iodopropane (**34d**) (1.31 mL, 11.0 mmol, 1.50 equiv) and iron trichloride (61.0 mg,  $3.70 \times 10^{-4}$  mol,  $5.00 \times 10^{-2}$  equiv) was prepared under inert

atmosphere at 0 °C. A solution **S3** made of TMEDA (1.34 mL, 8.77 mmol, 1.20 equiv) diluted in **S1** was prepared at rt under inert atmosphere. Solution **S3** was then added dropwise upon stirring to **S2**, and the resulting reaction mixture was stirred at 0 °C for 15 min. The reaction was carefully quenched with saturated aqueous NH<sub>4</sub>Cl, and the aqueous layer was extracted with Et<sub>2</sub>O. The combined organic extracts were washed with brine, dried over Na<sub>2</sub>SO<sub>4</sub>, filtered, and concentrated *in vacuo*. The resulting crude material was purified by silica gel flash column chromatography (hexanes) to afford a colorless oil that was then used in **Step 3**.

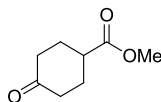
**Step 3:** To a solution of the previously isolated product in THF (13.1 mL) under inert atmosphere at rt was added tetrabutylammonium fluoride (1 M in THF, 5.25 mL, 5.25 mmol, 2.00 equiv) dropwise upon stirring. The reaction was stirred at rt for 15 min, quenched with saturated aqueous NaHCO<sub>3</sub>, and the aqueous layer was extracted with Et<sub>2</sub>O. The combined organic extracts were washed with brine, dried over Na<sub>2</sub>SO<sub>4</sub>, filtered, and concentrated *in vacuo*. The resulting crude material was purified by silica gel flash column chromatography (2:1 hexanes/CH<sub>2</sub>Cl<sub>2</sub>) to afford indole **26d** (467 mg, 2.02 mmol, 16% over 3 steps) as a white crystalline solid (mp = 45 °C).

**TLC:**  $R_f$  = 0.18 (2:1 hexanes/CH<sub>2</sub>Cl<sub>2</sub>; UV, CAM, *p*-anisaldehyde). **<sup>1</sup>H NMR** (400 MHz, CDCl<sub>3</sub>): δ 8.12–7.83 (bs, 1H), 7.28 (dt,  $J$  = 9.6 Hz,  $J$  = 4.9 Hz, 1H), 7.22 (dd,  $J$  = 9.5 Hz,  $J$  = 2.4 Hz, 1H), 7.07 (s, 1H), 6.97 (td,  $J$  = 9.0 Hz,  $J$  = 2.5 Hz, 1H), 3.04–2.94 (m, 2H), 2.54–2.39 (m, 2H) ppm. **<sup>13</sup>C NMR** (100 MHz, CDCl<sub>3</sub>): δ 158.0 (d,  $J$  = 235.1 Hz), 132.9, 127.4 (d,  $J$  = 9.5 Hz), 127.0 (q,  $J$  = 276.8 Hz), 123.3, 113.9 (d,  $J$  = 4.7 Hz), 112.1 (d,  $J$  = 9.6 Hz), 110.9 (d,  $J$  = 26.4 Hz), 103.6 (d,  $J$  = 23.4 Hz), 34.6 (q,  $J$  = 28.1 Hz), 18.0 (q,  $J$  = 3.5 Hz) ppm. **<sup>19</sup>F NMR** (376 MHz, CDCl<sub>3</sub>, decoupled): δ -66.69 (s), -124.34 (s) ppm. **<sup>19</sup>F NMR** (376 MHz, CDCl<sub>3</sub>, not decoupled): δ -66.69 (t,  $J$  = 11.6 Hz), 124.34 (td,  $J$  = 10.2 Hz,  $J$  = 4.7 Hz) ppm. **IR** (thin film): ν 3474, 3430, 2925, 1483, 1453, 1255, 1177, 1133, 1116, 1090, 850, 796, 755, 592 cm<sup>-1</sup>. **HRMS** (EI+): exact mass calculated for C<sub>11</sub>H<sub>9</sub>F<sub>4</sub>N ([M]<sup>+</sup>), 231.0666; found 231.0667.

**5-Fluoro-1-tosyl-3-(3,3,3-trifluoropropyl)-1H-indole (25d):**<sup>77</sup>

To a vigorously stirred solution of 5-fluoro-3-(3,3,3-trifluoropropyl)-1H-indole (**26d**) (217 mg,  $9.40 \cdot 10^{-4}$  mol, 1.00 equiv), *p*-toluenesulfonyl chloride (217 mg, 1.13 mmol, 1.20 equiv), and tetrabutylammonium hydrogen sulfate (23.0 mg,  $7.00 \cdot 10^{-5}$  mol,  $7.00 \cdot 10^{-2}$  equiv) in toluene (9.40 mL) at 0 °C was added a 50% aqueous KOH solution (9.40 mL) dropwise. The reaction was then stirred at 0 °C for 1 h before it was diluted with a 1:1 water/Et<sub>2</sub>O mixture and stirred for 5 min at rt. The aqueous phase was extracted with Et<sub>2</sub>O and the combined organic extracts were washed with brine, dried over Na<sub>2</sub>SO<sub>4</sub>, filtered, and concentrated *in vacuo*. The resulting crude material was purified by silica gel flash column chromatography (20:1 hexanes/EtOAc) to afford indole **25d** (357 mg,  $9.30 \cdot 10^{-4}$  mol, 99%) as a white powder (mp = 141 °C).

**TLC:**  $R_f$  = 0.29 (20:1 hexanes/EtOAc; UV, CAM, *p*-anisaldehyde). **<sup>1</sup>H NMR** (400 MHz, CDCl<sub>3</sub>): δ 7.93 (dd,  $J$  = 8.9 Hz,  $J$  = 4.3 Hz, 1H), 7.72 (d,  $J$  = 7.9 Hz, 2H), 7.41 (s, 1H), 7.23 (d,  $J$  = 8.1 Hz, 2H), 7.13–7.02 (m, 2H), 2.93–2.84 (m, 2H), 2.52–2.38 (m, 2H), 2.35 (s, 3H) ppm. **<sup>13</sup>C NMR** (100 MHz, CDCl<sub>3</sub>): δ 159.8 (d,  $J$  = 241.1 Hz), 145.3, 135.1, 131.7 (d,  $J$  = 0.6 Hz), 131.4 (d,  $J$  = 9.5 Hz), 130.1, 126.9, 126.7 (q,  $J$  = 276.7 Hz), 124.8, 120.0 (d,  $J$  = 4.2 Hz), 115.2 (d,  $J$  = 9.4 Hz), 113.2 (d,  $J$  = 25.5 Hz), 104.9 (d,  $J$  = 24.0 Hz), 33.5 (q,  $J$  = 28.9 Hz), 21.7, 17.9 (q,  $J$  = 3.6 Hz) ppm. **<sup>19</sup>F NMR** (376 MHz, CDCl<sub>3</sub>, decoupled): δ -66.58 (s), -119.20 (s) ppm. **<sup>19</sup>F NMR** (376 MHz, CDCl<sub>3</sub>, not decoupled): δ -66.58 (t,  $J$  = 11.4 Hz), -119.20 (td,  $J$  = 9.4 Hz,  $J$  = 4.9 Hz) ppm. **IR** (thin film): ν 3115, 2926, 1469, 1447, 1372, 1255, 1187, 1170, 1139, 1113, 1101, 1091, 986, 898, 802, 671, 656, 585 cm<sup>-1</sup>. **HRMS** (ESI+): exact mass calculated for C<sub>18</sub>H<sub>15</sub>F<sub>4</sub>NNaO<sub>2</sub>S ([M+Na]<sup>+</sup>), 408.0652; found 408.0653.



52

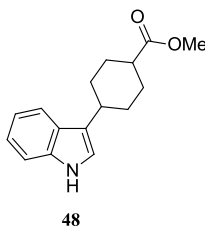
**Methyl 4-oxocyclohexanecarboxylate (52):**

**Step 1:**<sup>141</sup> 4-Hydroxybenzoic acid (**53**) (25.0 g, 181 mmol, 1.00 equiv) was hydrogenated in degassed MeOH (0.250 L) under 5 bar of hydrogen pressure with rhodium (5% on alumina, 3.53 g, 1.72 mmol, 1.00  $10^{-2}$  equiv) at rt for 24 h. The reaction mixture was filtered through a pad of Celite<sup>®</sup>, and the filtrate was concentrated *in vacuo*. The resulting crude material was recrystallized from Et<sub>2</sub>O, thus yielding 4-hydroxycyclohexanecarboxylic acid (mixture of isomers, 16.0 g, 111 mmol, 61%) as a white crystalline solid, whose analytical data matched the previously reported ones.

**Step 2:** To a solution of 4-hydroxycyclohexanecarboxylic acid (mixture of isomers, 2.42 g, 16.8 mmol, 1.00 equiv) in MeOH (50.0 mL) at rt was added acetyl chloride (0.600 mL, 8.39 mmol, 5.00  $10^{-1}$  equiv) dropwise upon stirring. The reaction was stirred at rt for 3 h, concentrated *in vacuo*, and the resulting crude material was purified by silica gel flash column chromatography (1:1 hexanes/EtOAc) to afford methyl 4-hydroxycyclohexanecarboxylate (mixture of isomers, 2.40 g, 15.2 mmol, 90%) as a colorless oil, whose analytical data matched the previously reported ones.<sup>141</sup>

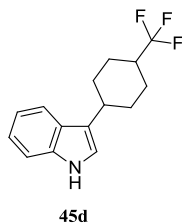
**Step 3:** To a suspension of oven-dried Celite<sup>®</sup> (1.40 g), and sodium acetate (373 mg, 4.55 mmol, 3.00  $10^{-1}$  equiv) in CH<sub>2</sub>Cl<sub>2</sub> (40.0 mL) under inert atmosphere at rt was added pyridinium chlorochromate (5.01 g, 22.8 mmol, 1.50 equiv) portionwise upon stirring, followed by a solution of methyl 4-hydroxycyclohexanecarboxylate (mixture of isomers, 2.40 g, 15.2 mmol, 1.00 equiv) in CH<sub>2</sub>Cl<sub>2</sub> (3.00 mL). The reaction was stirred at rt for 2 h, Et<sub>2</sub>O (40.0 mL) was added, and stirring was continued for 10 min. The slurry was filtered through a pad of Celite<sup>®</sup>, and the filtrate was concentrated *in vacuo*. The resulting crude material was purified by silica gel flash column chromatography (2:1 hexanes/EtOAc) to afford ketone **52** (2.11 g, 13.5 mmol, 89%) as a colorless oil.

**TLC:**  $R_f$  = 0.22 (2:1 hexanes/EtOAc; CAM). **<sup>1</sup>H NMR** (400 MHz, CDCl<sub>3</sub>):  $\delta$  3.73 (s, 3H), 2.77 (tt,  $J$  = 9.7 Hz,  $J$  = 3.9 Hz, 1H), 2.55–2.43 (m, 2H), 2.43–2.29 (m, 2H), 2.29–2.15 (m, 2H), 2.11–1.95 (m, 2H) ppm. **<sup>13</sup>C NMR** (100 MHz, CDCl<sub>3</sub>):  $\delta$  210.0, 174.6, 51.5, 40.6, 39.7, 28.5 ppm. **IR** (thin film):  $\nu$  1731, 1711 cm<sup>-1</sup>. **HRMS** (ESI+): exact mass calculated for C<sub>8</sub>H<sub>13</sub>O<sub>3</sub> ([M+H]<sup>+</sup>), 157.0859; found 157.0862.

**Methyl 4-(1H-indol-3-yl)cyclohexanecarboxylate (48):**<sup>90</sup>

To a solution of triethylsilane (4.94 mL, 30.9 mmol, 3.00 equiv) and trichloroacetic acid (1.56 mL, 15.5 mmol, 1.50 equiv) in toluene (5.00 mL) at 70 °C was added a solution of indole (**31**) (1.45 g, 12.4 mmol, 1.20 equiv) and methyl 4-oxocyclohexanecarboxylate (**52**) (1.61 g, 10.3 mmol, 1.00 equiv) in toluene (5.00 mL) dropwise upon stirring. The resulting mixture was stirred at 70 °C for 1.5 h, cooled down to rt, quenched with saturated aqueous NaHCO<sub>3</sub>, and the aqueous layer was extracted with Et<sub>2</sub>O. The combined organic extracts were washed with brine, dried over Na<sub>2</sub>SO<sub>4</sub>, filtered, and concentrated *in vacuo*. The resulting crude material was purified by silica gel flash column chromatography (10:1 hexanes /EtOAc) to afford indole **48** (*trans/cis* = 7:3 by NMR, 2.32 g, 9.02 mmol, 87%) as a colorless oil.

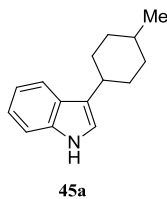
**TLC:**  $R_f$  = 0.36 (2:1 hexanes/EtOAc; UV, CAM). **<sup>1</sup>H NMR** (400 MHz, CDCl<sub>3</sub>, mixture of isomers):  $\delta$  7.94 (bs, 1H), 7.67 (d,  $J$  = 7.8 Hz, 0.7H, major), 7.65 (d,  $J$  = 7.8 Hz, 0.3 H, minor) 7.39–7.32 (m, 1H, both isomers), 7.22–7.15 (m, 1H, both isomers), 7.14–7.07 (m, 1H, both isomers), 6.98 (d,  $J$  = 1.6 Hz, 0.3H, minor), 6.95 (d,  $J$  = 1.6 Hz, 0.7H, major), 3.71 (d,  $J$  = 2.0 Hz, 3H, both isomers), 3.01–2.92 (m, 0.3H, minor), 2.86 (tt,  $J$  = 12.1 Hz,  $J$  = 3.4 Hz, 0.7H, major), 2.75–2.68 (m, 0.3H, minor), 2.41 (tt,  $J$  = 12.1 Hz,  $J$  = 3.6 Hz, 0.7H, major), 2.27–1.95 (m, 4H), 1.84–1.46 (m, 4H) ppm. **<sup>13</sup>C NMR** (100 MHz, CDCl<sub>3</sub>, mixture of isomers):  $\delta$  176.8 (major), 176.0 (minor), 136.5 (both isomers), 126.9 (minor), 126.8 (major), 122.2, 122.1, 122.0, 120.1, 119.5, 119.3, 119.2 (both isomers), 111.3(both isomers), 51.7 (both isomers), 43.4, 40.0, 34.8, 34.1, 33.0, 30.2, 29.5, 27.4, 14.4 ppm. **IR** (thin film):  $\nu$  3470, 3431, 2926, 1731, 1480, 1449, 1258, 1178, 1133, 1114, 1087, 848, 800, 756, 595 cm<sup>-1</sup>. **HRMS** (ESI+): exact mass calculated for C<sub>16</sub>H<sub>20</sub>NO<sub>2</sub> ([M+H]<sup>+</sup>), 258.1489; found 258.1490.



### 3-(4-(Trifluoromethyl)cyclohexyl)-1H-indole (**45d**):<sup>90</sup>

To a solution of triethylsilane (721  $\mu\text{L}$ , 3.51 mmol, 3.00 equiv) and trichloroacetic acid (228  $\mu\text{L}$ , 2.26 mmol, 1.50 equiv) in toluene (2.50 mL) at 70  $^{\circ}\text{C}$  was added a solution of indole (**31**) (212 mg, 1.81 mmol, 1.20 equiv) and 4-(trifluoromethyl)cyclohexanone (**47**) (0.250 g, 1.51 mmol, 1.00 equiv) in toluene (2.50 mL) dropwise upon stirring. The resulting mixture was stirred at 70  $^{\circ}\text{C}$  for 1.5 h, cooled down to rt, quenched with saturated aqueous  $\text{NaHCO}_3$ , and the aqueous layer was extracted with  $\text{Et}_2\text{O}$ . The combined organic extracts were washed with brine, dried over  $\text{Na}_2\text{SO}_4$ , filtered, and concentrated *in vacuo*. The resulting crude material was purified by silica gel flash column chromatography (20:1 hexanes /EtOAc) to afford indole **45d** (*trans/cis* = 7:3 by NMR, 0.270 g, 1.01 mmol, 67%) as a colorless syrup. The two isomers were further separated by preparative HPLC (**Column**: Reprosil Chiral-NR, 8 mm, 250\*30 mm; **Elution Conditions**: 10% ethanol/*n*-heptane, isocratic, 35 mL/min; **Detection**: UV, 220 nm; Runtime = 60 min).

**TLC**:  $R_f$  = 0.33 (4:1 hexanes/EtOAc; UV, CAM).  **$^1\text{H}$  NMR** (400 MHz,  $\text{CDCl}_3$ , *trans* isomer):  $\delta$  7.92 (bs, 1H), 7.64 (d,  $J$  = 7.9 Hz, 1H), 7.37 (d,  $J$  = 8.1 Hz, 1H), 7.23–7.17 (m, 1H), 7.16–7.09 (m, 1H), 6.96 (s,  $J$  = 1.8 Hz, 1H), 2.92–2.79 (m, 1H), 2.33–2.02 (m, 5H), 1.64–1.46 (m, 4H) ppm.  **$^{13}\text{C}$  NMR** (100 MHz,  $\text{CDCl}_3$ , *trans* isomer):  $\delta$  136.4, 128.1 (q,  $J$  = 278.3 Hz), 126.7, 122.2, 121.8, 119.5, 119.3, 119.2, 111.4, 42.1 (q,  $J$  = 26.4 Hz), 34.7, 32.3, 25.5 (q,  $J$  = 2.6 Hz) ppm.  **$^{19}\text{F}$  NMR** (376 MHz,  $\text{CDCl}_3$ , decoupled, *trans* isomer):  $\delta$  -73.72 (s) ppm.  **$^{19}\text{F}$  NMR** (376 MHz,  $\text{CDCl}_3$ , not decoupled, *trans* isomer):  $\delta$  -73.72 (d,  $J$  = 7.9 Hz) ppm.  **$^1\text{H}$  NMR** (400 MHz,  $\text{CDCl}_3$ , *cis* isomer):  $\delta$  7.95 (bs, 1H), 7.63 (d,  $J$  = 7.8 Hz, 1H), 7.37 (d,  $J$  = 8.1 Hz, 1H), 7.23–7.17 (m, 1H), 7.14–7.09 (m, 1H), 7.07–7.04 (m, 1H), 3.28–3.19 (m, 1H), 2.32–2.19 (m, 1H), 2.17–2.06 (m, 2H), 1.95–1.74 (m, 6H) ppm.  **$^{13}\text{C}$  NMR** (100 MHz,  $\text{CDCl}_3$ , *cis* isomer):  $\delta$  136.4, 128.4 (q,  $J$  = 279.6 Hz), 127.1, 122.1, 120.8, 120.2, 119.3, 111.3, 40.0 (q,  $J$  = 25.6 Hz), 31.5, 29.0, 22.4 (q,  $J$  = 2.2 Hz) ppm.  **$^{19}\text{F}$  NMR** (376 MHz,  $\text{CDCl}_3$ , decoupled, *cis* isomer):  $\delta$  -70.96 (s) ppm.  **$^{19}\text{F}$  NMR** (376 MHz,  $\text{CDCl}_3$ , not decoupled, *cis* isomer):  $\delta$  -70.96 (bs) ppm. **IR** (thin film):  $\nu$  3471, 3434, 2925, 1481, 1448, 1254, 1170, 1131, 1114, 1086, 849, 795, 753, 593  $\text{cm}^{-1}$ . **HRMS** (ESI<sup>+</sup>): exact mass calculated for  $\text{C}_{15}\text{H}_{17}\text{F}_3\text{N}$  ( $[\text{M}+\text{H}]^+$ ), 268.1308; found 268.1309.

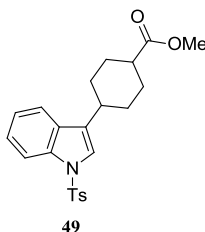


### 3-(4-Methylcyclohexyl)-1H-indole (**45a**):<sup>90</sup>

To a solution of triethylsilane (2.14 mL, 13.4 mmol, 3.00 equiv) and trichloroacetic acid (670  $\mu$ L, 6.69 mmol, 1.50 equiv) in toluene (5.00 mL) at 70 °C was added a solution of indole (**31**) (627 mg, 5.35 mmol, 1.20 equiv) and 4-methylcyclohexanone (**46**) (547  $\mu$ L, 4.46 mmol, 1.00 equiv) in toluene (5.00 mL) dropwise upon stirring. The resulting mixture was stirred at 70 °C for 1.5 h, cooled down to rt, quenched with saturated aqueous NaHCO<sub>3</sub>, and the aqueous layer was extracted with Et<sub>2</sub>O. The combined organic extracts were washed with brine, dried over Na<sub>2</sub>SO<sub>4</sub>, filtered, and concentrated *in vacuo*. The resulting crude material was purified by silica gel flash column chromatography (15:1 hexanes /EtOAc) to afford indole **45a** (*trans/cis* = 7:3 by NMR, 885 mg, 4.15 mmol, 93%) as a colorless syrup. The two isomers were further separated by preparative HPLC (**Column**: Reprosil Chiral-NR, 8 mm, 250\*30 mm; **Elution Conditions**: 10% ethanol/*n*-heptane, isocratic, 35 mL/min; **Detection**: UV, 220 nm; Runtime = 60 min).

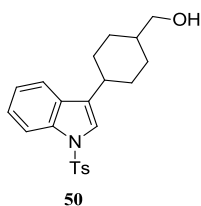
**TLC**:  $R_f$  = 0.31 (4:1 hexanes/EtOAc; UV, CAM). **<sup>1</sup>H NMR** (400 MHz, CDCl<sub>3</sub>, *trans* isomer):  $\delta$  7.86 (bs, 1H), 7.67 (d,  $J$  = 7.9 Hz, 1H), 7.35 (d,  $J$  = 8.1 Hz, 1H), 7.21–7.16 (m, 1H), 7.14–7.08 (m, 1H), 6.95 (d,  $J$  = 1.7 Hz, 1H), 2.79 (tt,  $J$  = 12.0 Hz,  $J$  = 3.4 Hz, 1H), 2.18–2.09 (m, 2H), 1.88–1.79 (m, 2H), 1.52 (qd,  $J$  = 12.1 Hz,  $J$  = 3.2 Hz, 2H), 1.50–1.41 (m, 1H), 1.17 (qd,  $J$  = 12.9 Hz,  $J$  = 3.2 Hz, 2H), 0.97 (d,  $J$  = 6.5 Hz, 3H) ppm. **<sup>13</sup>C NMR** (100 MHz, CDCl<sub>3</sub>, *trans* isomer):  $\delta$  136.6, 127.0, 123.1, 121.9, 119.5, 119.4, 119.1, 111.2, 35.8, 35.2, 34.0, 32.9, 23.0 ppm. **<sup>1</sup>H NMR** (400 MHz, CDCl<sub>3</sub>, *cis* isomer):  $\delta$  7.88 (bs, 1H), 7.67 (d,  $J$  = 7.9 Hz, 1H), 7.36 (d,  $J$  = 8.1 Hz, 1H), 7.22–7.16 (m, 1H), 7.14–7.08 (m, 1H), 7.02 (d,  $J$  = 1.5 Hz, 1H), 3.01 (p,  $J$  = 6.5 Hz, 1H), 1.93–1.82 (m, 5H), 1.74–1.65 (m, 2H), 1.57–1.46 (m, 2H), 1.08 (d,  $J$  = 7.0 Hz, 3H) ppm. **<sup>13</sup>C NMR** (100 MHz, CDCl<sub>3</sub>, *cis* isomer):  $\delta$  136.5, 127.1, 122.4, 121.9, 120.2, 119.5, 119.1, 111.2, 30.0, 32.0, 29.1, 28.9, 19.5 ppm. **IR** (thin film):  $\nu$  3426, 2928, 1583, 1481, 1455, 1172, 935, 847, 793, 593 cm<sup>-1</sup>. **HRMS** (ESI<sup>+</sup>): exact mass calculated for C<sub>15</sub>H<sub>20</sub>N ([M+H]<sup>+</sup>), 214.1590; found 214.1590.



**Methyl 4-(1-tosyl-1H-indol-3-yl)cyclohexanecarboxylate (49):**<sup>91</sup>

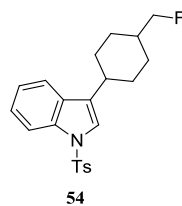
To a solution of methyl 4-(1H-indol-3-yl)cyclohexanecarboxylate (**48**) (*trans/cis* = 7:3 by NMR, 2.32 g, 9.02 mmol, 1.00 equiv) in THF (20.0 ml) at 0 °C under inert atmosphere was added sodium hydride (60% in mineral oil, 0.400 g, 9.92 mmol, 1.10 equiv) portionwise upon stirring. The resulting suspension was allowed to warm up to rt, and stirred for 1 h. A solution of *p*-toluenesulfonyl chloride (2.08 g, 10.8 mmol, 1.20 equiv) in THF (20.0 mL) was then added dropwise to the reaction mixture which was stirred at rt for 1 h. The reaction was carefully quenched with water, and the aqueous layer was extracted with Et<sub>2</sub>O. The combined organic extracts were washed with brine, dried over Na<sub>2</sub>SO<sub>4</sub>, filtered, and concentrated *in vacuo*. The resulting crude material was purified by silica gel flash column chromatography (10:1 hexanes/EtOAc) to afford indole **49** (*trans/cis* = 15:1 by NMR, 2.91 g, 7.07 mmol, 78%) as a colorless syrup.

**TLC:**  $R_f$  = 0.34 (2:1 hexanes/EtOAc; UV, CAM). **<sup>1</sup>H NMR** (400 MHz, CDCl<sub>3</sub>, major isomer): δ 7.96 (d,  $J$  = 8.1 Hz, 1H), 7.73 (d,  $J$  = 8.3 Hz, 2H), 7.50 (d,  $J$  = 7.8 Hz, 1H), 7.32–7.27 (m, 2H), 7.24–7.18 (m, 3H), 3.70 (s, 3H), 2.72 (tt,  $J$  = 12.0 Hz,  $J$  = 2.8 Hz, 1H), 2.39 (tt,  $J$  = 12.1 Hz,  $J$  = 3.5 Hz, 1H), 2.33 (s, 3H), 2.20–2.08 (m, 4H), 1.70–1.57 (m, 2H), 1.52–1.40 (m, 2H) ppm. **<sup>13</sup>C NMR** (100 MHz, CDCl<sub>3</sub>, major isomer): δ 176.4, 144.8, 135.5, 130.4, 129.9, 128.3, 126.9, 124.7, 123.0, 121.3, 119.8, 114.0, 51.8, 43.2, 34.5, 32.2, 29.2, 21.7 ppm. **IR** (thin film): ν 2961, 1729, 1465, 1443, 1368, 1185, 1168, 1139, 1111, 1086, 879, 808, 667, 588, 535 cm<sup>-1</sup>. **HRMS** (ESI<sup>+</sup>): exact mass calculated for C<sub>23</sub>H<sub>26</sub>NO<sub>4</sub>S ([M+H]<sup>+</sup>), 412.1577; found 412.1578.

**4-(1-Tosyl-1H-indol-3-yl)cyclohexylmethanol (50):**<sup>92</sup>

To a solution of methyl 4-(1-tosyl-1H-indol-3-yl)cyclohexanecarboxylate (**49**) (*trans/cis* = 15:1 by NMR, 1.37 g, 3.33 mmol, 1.00 equiv) in Et<sub>2</sub>O (30.0 mL) at -78 °C under inert atmosphere was added lithium aluminium hydride (0.920 mL, 3.66 mmol, 1.10 equiv) dropwise upon stirring. The resulting white suspension was then allowed to warm up to 0 °C, and stirred for 15 min. The reaction was quenched with saturated aqueous NaHCO<sub>3</sub>, warmed up to rt, and the aqueous layer was extracted with Et<sub>2</sub>O. The combined organic extracts were washed with brine, dried over Na<sub>2</sub>SO<sub>4</sub>, filtered, and concentrated *in vacuo*. The resulting crude material was purified by silica gel flash column chromatography (2:1 hexanes/EtOAc) to afford alcohol **50** (*trans/cis* = 15:1 by NMR, 1.22 g, 3.18 mmol, 96%) as a colorless syrup.

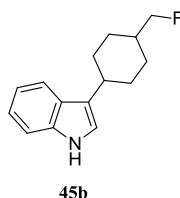
**TLC:** *R<sub>f</sub>* = 0.10 (2:1 hexanes/EtOAc; UV, CAM). **<sup>1</sup>H NMR** (400 MHz, CDCl<sub>3</sub>, major isomer): δ 7.96 (d, *J* = 8.3 Hz, 1H), 7.73 (d, *J* = 8.4 Hz, 2H), 7.51 (d, *J* = 7.4 Hz, 1H), 7.32 (dd, *J* = 9.7 Hz, *J* = 1.2 Hz, 1H), 7.29 (d, *J* = 1.0 Hz, 1H), 7.24–7.18 (m, 3H), 3.53 (d, *J* = 6.3 Hz, 2H), 2.69 (tt, *J* = 12.1 Hz, *J* = 3.1 Hz, 1H), 2.33 (s, 3H), 2.16–2.09 (m, 2H), 1.98–1.90 (m, 2H), 1.72–1.53 (m, 2H), 1.46 (qd, *J* = 13.1 Hz, *J* = 3.1 Hz, 2H), 1.17 (qd, *J* = 13.0 Hz, *J* = 3.3 Hz, 2H) ppm. **<sup>13</sup>C NMR** (100 MHz, CDCl<sub>3</sub>, major isomer): δ 144.8, 135.6, 130.6, 129.9, 128.9, 126.9, 124.6, 123.0, 121.3, 119.8, 114.0, 68.7, 40.4, 35.3, 32.6, 29.7, 21.7 ppm. **IR** (thin film): ν 3372, 2933, 1465, 1442, 1365, 1189, 1166, 1132, 1117, 897, 811, 735, 700, 668, 589, 536 cm<sup>-1</sup>. **HRMS** (ESI<sup>+</sup>): exact mass calculated for C<sub>22</sub>H<sub>26</sub>NO<sub>3</sub>S ([M+H]<sup>+</sup>), 384.1628; found 384.1627.

**3-(4-(Fluoromethyl)cyclohexyl)-1-tosyl-1H-indole (54):**<sup>80</sup>

To a solution of (4-(1-tosyl-1H-indol-3-yl)cyclohexyl)methanol (**50**) (*dr* = 15:1 by NMR, 144 mg, 3.80 10<sup>-4</sup> mol, 1.00 equiv) in MeCN (0.380 mL) at rt under inert atmosphere were

successively added *N,N*-diisopropylethylamine (294  $\mu\text{L}$ , 1.69 mmol, 4.5 equiv), perfluorobutanesulfonyl fluoride (135  $\mu\text{L}$ ,  $7.50 \cdot 10^{-4}$  mol, 2.00 equiv), and *N,N*-diisopropylethylamine trihydrofluoride (114  $\mu\text{L}$ ,  $5.60 \cdot 10^{-4}$  mol, 1.50 equiv) dropwise upon stirring. The resulting mixture was stirred at 50  $^{\circ}\text{C}$  for 30 min, cooled down to rt, and quenched with saturated aqueous  $\text{NaHCO}_3$ . Stirring was continued until no evolution of gas could be noted, and the aqueous layer was extracted with  $\text{Et}_2\text{O}$ . The combined organic extracts were washed with brine, dried over  $\text{Na}_2\text{SO}_4$ , filtered, and concentrated *in vacuo*. The resulting crude material was purified by silica gel flash column chromatography (10:1 hexanes/ $\text{EtOAc}$ ) to afford indole **54** (*trans/cis* = 15:1 by NMR, 93.0 mg,  $2.40 \cdot 10^{-4}$  mol, 64%) as a colorless syrup.

**TLC:**  $R_f$  = 0.49 (2:1 hexanes/ $\text{EtOAc}$ ; UV, CAM).  **$^1\text{H}$  NMR** (400 MHz,  $\text{CDCl}_3$ , major isomer):  $\delta$  7.97 (d,  $J$  = 8.3 Hz, 1H), 7.73 (d,  $J$  = 8.4 Hz, 2H), 7.51 (d,  $J$  = 7.5 Hz, 1H), 7.34–7.27 (m, 2H), 7.24–7.18 (m, 3H), 4.31 (dd,  $J$  = 47.6 Hz,  $J$  = 5.9 Hz, 2H), 2.69 (tt,  $J$  = 11.9 Hz,  $J$  = 3.0 Hz, 1H), 2.33 (s, 3H), 2.18–2.09 (m, 2H), 1.97–1.88 (m, 2H), 1.89–1.72 (m, 1H), 1.47 (qd,  $J$  = 13.1 Hz,  $J$  = 3.3 Hz, 2H), 1.25 (qd,  $J$  = 12.9 Hz,  $J$  = 3.2 Hz, 2H) ppm.  **$^{13}\text{C}$  NMR** (100 MHz,  $\text{CDCl}_3$ , major isomer):  $\delta$  144.8, 135.6, 130.5, 129.9, 128.7, 126.9, 124.7, 123.0, 121.3, 119.8, 114.0, 88.6 (d,  $J$  = 168.3 Hz), 38.6 (d,  $J$  = 18.1 Hz), 35.0, 32.3, 28.7, 28.6, 21.7 ppm.  **$^{19}\text{F}$  NMR** (376 MHz,  $\text{CDCl}_3$ , decoupled, major isomer):  $\delta$  -222.96 (s) ppm.  **$^{19}\text{F}$  NMR** (376 MHz,  $\text{CDCl}_3$ , not decoupled, major isomer):  $\delta$  -222.96 (td,  $J$  = 47.6 Hz,  $J$  = 17.7 Hz) ppm. **IR** (thin film):  $\nu$  2960, 1467, 1444, 1367, 1168, 1140, 1112, 1092, 895, 810, 796, 665, 588, 533  $\text{cm}^{-1}$ . **HRMS** (ESI+): exact mass calculated for  $\text{C}_{22}\text{H}_{25}\text{FNO}_2\text{S}$  ( $[\text{M}+\text{H}]^+$ ), 386.1585; found 386.1586.

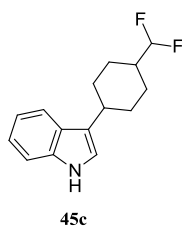


### 3-(4-(Fluoromethyl)cyclohexyl)-1*H*-indole (**45b**):<sup>81</sup>

To a degassed solution of 3-(4-(fluoromethyl)cyclohexyl)-1-tosyl-1*H*-indole (**54**) (825 mg, 2.14 mmol, 1.00 equiv) in  $\text{EtOH}$  (70.0 mL) at rt under inert atmosphere was added  $\text{KOH}$  (2.40 g, 42.8 mmol, 20.0 equiv) in one portion upon stirring. The resulting mixture was heated to reflux and stirred for 12 h. The reaction was cooled down to rt, quenched with saturated

aqueous  $\text{NH}_4\text{Cl}$ , and the aqueous layer was extracted with  $\text{Et}_2\text{O}$ . The combined organic extracts were washed with brine, dried over  $\text{Na}_2\text{SO}_4$ , filtered, and concentrated *in vacuo*. The resulting crude material was purified by silica gel flash column chromatography (20:1 hexanes/ $\text{EtOAc}$ ) to afford indole **45b** (*trans/cis* = 15:1 by NMR, 455 mg, 1.97 mmol, 92%) as a colorless syrup. The two isomers were further separated by preparative HPLC (**Column**: Reprisil Chiral-NR, 8 mm, 250\*30 mm; **Elution Conditions**: 10% ethanol/*n*-heptane, isocratic, 35 mL/min; **Detection**: UV, 220 nm; Runtime = 60 min).

**TLC**:  $R_f$  = 0.44 (2:1 hexanes/ $\text{EtOAc}$ ; UV, CAM).  **$^1\text{H}$  NMR** (400 MHz,  $\text{CDCl}_3$ , *trans* isomer):  $\delta$  7.90 (bs, 1H), 7.65 (d,  $J$  = 7.9 Hz, 1H), 7.36 (d,  $J$  = 8.1 Hz, 1H), 7.21–7.16 (m, 1H), 7.14–7.08 (m, 1H), 6.96 (d,  $J$  = 1.7 Hz, 1H), 4.32 (dd,  $J$  = 47.7 Hz,  $J$  = 3.0 Hz, 2H), 2.83 (tt,  $J$  = 12.0 Hz,  $J$  = 3.4 Hz, 1H), 2.25–2.16 (m, 2H), 1.98–1.90 (m, 2H), 1.89–1.73 (m, 1H), 1.54 (qd,  $J$  = 13.2 Hz,  $J$  = 3.3 Hz, 2H), 1.28 (qd,  $J$  = 12.8 Hz,  $J$  = 3.4 Hz, 2H) ppm.  **$^{13}\text{C}$  NMR** (100 MHz,  $\text{CDCl}_3$ , *trans* isomer):  $\delta$  136.5, 126.9, 122.6, 122.0, 119.5, 119.4, 119.2, 111.3, 88.8 (d,  $J$  = 167.9 Hz), 38.7 (d,  $J$  = 17.9 Hz), 35.3, 33.1, 29.0, 28.9 ppm.  **$^{19}\text{F}$  NMR** (376 MHz,  $\text{CDCl}_3$ , decoupled, *trans* isomer):  $\delta$  -222.43 (s) ppm.  **$^{19}\text{F}$  NMR** (376 MHz,  $\text{CDCl}_3$ , not decoupled, *trans* isomer):  $\delta$  -222.43 (td,  $J$  = 47.7 Hz,  $J$  = 17.2 Hz) ppm.  **$^1\text{H}$  NMR** (400 MHz,  $\text{CDCl}_3$ , *cis* isomer):  $\delta$  7.92 (bs, 1H), 7.64 (d,  $J$  = 7.9 Hz, 1H), 7.36 (d,  $J$  = 8.1 Hz, 1H), 7.22–7.16 (m, 1H), 7.14–7.08 (m, 1H), 7.01 (d,  $J$  = 1.5 Hz, 1H), 4.46 (dd,  $J$  = 47.6 Hz,  $J$  = 7.1 Hz, 2H), 3.09 (tt,  $J$  = 8.2 Hz,  $J$  = 4.2 Hz, 1H), 2.16–2.02 (m, 1H), 1.99–1.78 (m, 4H), 1.71 (q,  $J$  = 5.7 Hz, 4H) ppm.  **$^{13}\text{C}$  NMR** (100 MHz,  $\text{CDCl}_3$ , *cis* isomer):  $\delta$  136.5, 127.0, 122.0, 121.6, 120.3, 119.4, 119.2, 111.3, 86.6 (d,  $J$  = 167 Hz), 35.4 (d,  $J$  = 17.7 Hz), 33.5, 29.2, 25.9, 25.8 ppm.  **$^{19}\text{F}$  NMR** (376 MHz,  $\text{CDCl}_3$ , decoupled, *cis* isomer):  $\delta$  -221.92 (s) ppm.  **$^{19}\text{F}$  NMR** (376 MHz,  $\text{CDCl}_3$ , not decoupled, *cis* isomer):  $\delta$  -221.92 (td,  $J$  = 47.6 Hz,  $J$  = 16.2 Hz) ppm. **IR** (thin film):  $\nu$  3451, 2905, 1483, 1452, 1165, 1017, 935, 852, 797, 595  $\text{cm}^{-1}$ . **HRMS** (ESI<sup>+</sup>): exact mass calculated for  $\text{C}_{15}\text{H}_{19}\text{FN}$  ( $[\text{M}+\text{H}]^+$ ), 232.1496; found 232.1496.



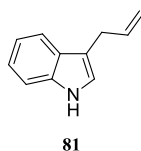
### 3-(4-(Difluoromethyl)cyclohexyl)-1H-indole (**45c**):

**Step 1:** To a stirred suspension of oven-dried Celite<sup>®</sup> (2.40 g), sodium acetate (308 mg, 3.75 mmol, 3.00  $10^{-1}$  equiv), and pyridinium chlorochromate (4.13 g, 18.8 mmol, 1.50 equiv) in  $\text{CH}_2\text{Cl}_2$  (50.0 mL) at rt under inert atmosphere was added a solution of (4-(1-tosyl-1H-indol-3-yl)cyclohexyl)methanol (**50**) (4.80 g, 12.5 mmol, 1.00 equiv) in  $\text{CH}_2\text{Cl}_2$  (50.0 mL) dropwise. The resulting slurry was stirred at rt for 1h, diluted with  $\text{Et}_2\text{O}$ , stirred for 15 min, and filtered through a pad of Celite<sup>®</sup>. The filtrate was concentrated *in vacuo*, and the resulting crude material was purified by silica gel flash column chromatography (10:1 hexanes/ $\text{EtOAc}$ ) to afford a colorless oil (2.05 g) that was used in **Step 2**.

**Step 2:**<sup>84</sup> To a stirred solution of the previously prepared product (2.05 g, 5.36 mmol, 1.00 equiv) in  $\text{CH}_2\text{Cl}_2$  (54.0 mL) at rt under inert atmosphere was added diethylaminosulfur trifluoride (1.06 mL, 8.04 mmol, 1.50 equiv) dropwise. The resulting solution was stirred at rt for 2 h, carefully quenched with saturated aqueous  $\text{NaHCO}_3$ , and the aqueous layer was then extracted with  $\text{CH}_2\text{Cl}_2$ . The combined organic extracts were washed with brine, dried over  $\text{Na}_2\text{SO}_4$ , filtered, and concentrated *in vacuo*. The resulting crude material was purified by silica gel flash column chromatography (20:1 hexanes/ $\text{EtOAc}$ ) to afford a colorless oil (1.99 g) that was used in **Step 3**.

**Step 3:**<sup>81</sup> To a degassed solution of the previously prepared product (1.99 g, 4.93 mmol, 1.00 equiv) in  $\text{EtOH}$  (0.160 L) at rt under inert atmosphere was added KOH (5.53 g, 99.0 mmol, 20.0 equiv) in one portion upon stirring. The resulting mixture was heated to reflux and stirred for 12 h. The reaction was cooled down to rt, quenched with saturated aqueous  $\text{NH}_4\text{Cl}$ , and the aqueous layer was extracted with  $\text{Et}_2\text{O}$ . The combined extracts were washed with brine, dried over  $\text{Na}_2\text{SO}_4$ , filtered, and concentrated *in vacuo*. The resulting crude material was purified by silica gel flash column chromatography (20:1 hexanes/ $\text{EtOAc}$ ) to afford indole **45c** (*trans/cis* = 15:1 by NMR, 1.14 g, 4.59 mmol, 37% over 3 steps) as a colorless syrup. The two isomers were further separated by preparative HPLC (**Column:** Reprosil Chiral-NR, 8 mm, 250\*30 mm; **Elution Conditions:** 10% ethanol/*n*-heptane, isocratic, 35 mL/min; **Detection:** UV, 220 nm; Runtime = 60 min).

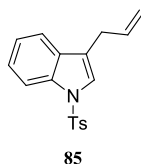
**TLC:**  $R_f = 0.27$  (5:1 hexanes/EtOAc; UV, CAM).  **$^1\text{H}$  NMR** (400 MHz,  $\text{CDCl}_3$ , *trans* isomer):  $\delta$  7.88 (bs, 1H), 7.67 (d,  $J = 8.5$  Hz, 1H), 7.37 (d,  $J = 8.1$  Hz, 1H), 7.25–7.19 (m, 1H), 7.18–7.12 (m, 1H), 6.95 (d,  $J = 2.4$  Hz, 1H), 5.65 (td,  $J = 56.9$  Hz,  $J = 4.4$  Hz, 1H), 2.85 (tt,  $J = 11.8$  Hz,  $J = 3.4$  Hz, 1H), 2.31–2.21 (m, 2H), 2.05–1.97 (m, 2H), 1.97–1.81 (m, 1H), 1.53 (qd,  $J = 13.1$  Hz,  $J = 3.1$  Hz, 2H), 1.43 (qd,  $J = 12.9$  Hz,  $J = 2.8$  Hz, 2H) ppm.  **$^{13}\text{C}$  NMR** (100 MHz,  $\text{CDCl}_3$ , *trans* isomer):  $\delta$  136.5, 126.8, 122.1, 119.5, 119.4 (t,  $J = 241.5$  Hz), 119.3, 117.0, 111.3, 41.7 (t,  $J = 19.3$  Hz), 25.1, 32.5, 25.8 (t,  $J = 4.5$  Hz) ppm.  **$^{19}\text{F}$  NMR** (376 MHz,  $\text{CDCl}_3$ , decoupled, *trans* isomer):  $\delta$  -122.76 (s) ppm.  **$^{19}\text{F}$  NMR** (376 MHz,  $\text{CDCl}_3$ , not decoupled, *trans* isomer):  $\delta$  -122.76 (dd,  $J = 56.9$  Hz,  $J = 13.3$  Hz) ppm.  **$^1\text{H}$  NMR** (400 MHz,  $\text{CDCl}_3$ , *cis* isomer):  $\delta$  7.90 (bs, 1H), 7.66 (d,  $J = 8.2$  Hz, 1H), 7.37 (d,  $J = 8.1$  Hz, 1H), 7.25–7.19 (m, 1H), 7.17–7.11 (m, 1H), 7.04–7.00 (m, 1H), 5.82 (td,  $J = 57.2$  Hz,  $J = 5.6$  Hz, 1H), 3.18 (p,  $J = 6.0$  Hz, 1H), 2.13–2.00 (m, 1H), 1.97 (q,  $J = 6.0$  Hz, 4H), 1.88–1.69 (m, 4H) ppm.  **$^{13}\text{C}$  NMR** (100 MHz,  $\text{CDCl}_3$ , *cis* isomer):  $\delta$  136.4, 127.0, 122.1, 120.8, 120.5, 119.4, 119.2, 119.0 (t,  $J = 241.2$  Hz), 111.3, 39.2 (t,  $J = 19.3$  Hz), 32.6, 29.2, 23.4 (t,  $J = 4.8$  Hz) ppm.  **$^{19}\text{F}$  NMR** (376 MHz,  $\text{CDCl}_3$ , decoupled, *cis* isomer):  $\delta$  -121.88 (s) ppm.  **$^{19}\text{F}$  NMR** (376 MHz,  $\text{CDCl}_3$ , not decoupled, *cis* isomer):  $\delta$  -121.88 (dd,  $J = 57.2$  Hz,  $J = 14.3$  Hz) ppm. **IR** (thin film):  $\nu$  3471, 2934, 1480, 1453, 1166, 1116, 1038, 934, 851, 795, 595  $\text{cm}^{-1}$ . **HRMS** (ESI<sup>+</sup>): exact mass calculated for  $\text{C}_{15}\text{H}_{18}\text{F}_2\text{N}$  ( $[\text{M}+\text{H}]^+$ ), 250.1402; found 250.1403.



### 3-Allyl-1H-indole (**81**):<sup>106</sup>

To a  $\text{N}_2$ -purged flask loaded with 1H-indole (**31**) (117 mg, 1.00 mmol, 1.00 equiv) and tetrakis(triphenylphosphine)palladium(0) (58.0 mg,  $5.00 \times 10^{-5}$  mol,  $5.00 \times 10^{-2}$  equiv) were successively added THF (2.50 mL), prop-2-en-1-ol (**109**) (75.0  $\mu\text{L}$ , 1.10 mmol, 1.10 equiv), and triethylborane (0.300 mL,  $3.00 \times 10^{-4}$  mol,  $3.00 \times 10^{-1}$  equiv). The reaction solution was heated at 50  $^\circ\text{C}$  for 24 h, then cooled down to rt, and diluted with EtOAc. The resulting mixture was successively washed with saturated aqueous  $\text{NaHCO}_3$  and brine. The organic layer was dried over  $\text{Na}_2\text{SO}_4$ , filtered, and concentrated *in vacuo*. The resulting crude material was purified by silica gel flash column chromatography (10:1 hexanes/EtOAc) to afford olefin **81** (142 mg,  $9.00 \times 10^{-4}$  mol, 90%) as a pale yellow oil.

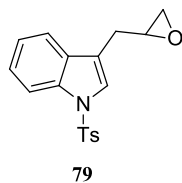
**TLC:**  $R_f = 0.15$  (10:1 hexanes/EtOAc; UV, *p*-anisaldehyde, CAM).  **$^1\text{H NMR}$**  (400 MHz,  $\text{CDCl}_3$ ):  $\delta$  7.96 (bs, 1H), 7.64 (dd,  $J = 7.9$  Hz,  $J = 1$  Hz, 1H), 7.39 (dt,  $J = 8.1$  Hz,  $J = 0.8$  Hz, 1H), 7.25–7.20 (m, 1H), 7.17–7.12 (m, 1H), 7.04–7.00 (m, 1H), 6.10 (ddt,  $J = 16.6$  Hz,  $J = 10.0$  Hz,  $J = 6.5$  Hz, 1H), 5.20 (ddd,  $J = 17.0$  Hz,  $J = 3.5$  Hz,  $J = 1.6$  Hz, 1H), 5.11 (ddd,  $J = 10.0$  Hz,  $J = 3.4$  Hz,  $J = 1.3$  Hz, 1H), 3.56 (ddd,  $J = 6.4$  Hz,  $J = 2.5$  Hz,  $J = 1.4$  Hz, 2H) ppm.  **$^{13}\text{C NMR}$**  (100 MHz,  $\text{CDCl}_3$ ):  $\delta$  137.3, 136.4, 127.4, 122.0, 121.6, 119.3, 119.1, 115.2, 114.6, 111.0, 29.8 ppm. **IR** (thin film):  $\nu$  3411, 3058, 2972, 2895, 2358, 1637, 1613, 1458, 1422, 1350, 1337, 1223, 1088, 1007, 992, 911, 808, 740  $\text{cm}^{-1}$ . **HRMS** (ESI+): exact mass calculated for  $\text{C}_{11}\text{H}_{12}\text{N}$  ( $[\text{M}+\text{H}]^+$ ), 158.0964; found 158.0966.



### 3-Allyl-1-tosyl-1H-indole (**85**):<sup>77</sup>

To a solution of 3-allyl-1H-indole (**81**) (3.32 g, 21.1 mmol, 1.00 equiv), *p*-toluenesulfonyl chloride (4.88 g, 25.3 mmol, 1.20 equiv), and tetrabutylammonium hydrogen sulfate (517 mg, 1.48 mmol, 7.00  $10^{-2}$  equiv) in toluene (84.0 mL) at 0 °C was added a 50% aqueous KOH solution (30.0 mL) dropwise. After stirring for 1 h at 0 °C, the reaction was diluted with water and the organic phase was successively washed with water and brine. The organic layer was then dried over  $\text{Na}_2\text{SO}_4$ , filtered, and concentrated *in vacuo*. The resulting crude material was purified by silica gel flash column chromatography (20:1 hexanes/EtOAc) to afford indole **85** (5.89 g, 18.9 mmol, 90%) as a colorless syrup.

**TLC:**  $R_f = 0.37$  (5:1 hexanes/EtOAc; UV, CAM).  **$^1\text{H NMR}$**  (400 MHz,  $\text{CDCl}_3$ ):  $\delta$  8.00 (dt,  $J = 8.3$  Hz,  $J = 0.8$  Hz, 1H), 7.77 (d,  $J = 8.4$  Hz, 2H), 7.49 (dt,  $J = 7.8$  Hz,  $J = 1.0$  Hz, 1H), 7.36 (t,  $J = 1.0$  Hz, 1H), 7.35–7.30 (m, 1H), 7.27–7.20 (m, 3H), 6.01 (ddt,  $J = 16.8$  Hz,  $J = 10.3$  Hz,  $J = 6.4$  Hz, 1H), 5.16 (ddd,  $J = 8.7$  Hz,  $J = 3.4$  Hz,  $J = 1.7$  Hz, 1H), 5.13 (t,  $J = 1.4$  Hz, 1H), 3.44 (ddd,  $J = 6.4$  Hz,  $J = 2.7$  Hz,  $J = 1.3$  Hz, 2H), 2.36 (s, 3H) ppm.  **$^{13}\text{C NMR}$**  (100 MHz,  $\text{CDCl}_3$ ):  $\delta$  144.7, 135.4, 135.2, 130.8, 129.8, 126.8, 124.6, 123.3, 123.0, 121.1, 119.6, 116.6, 113.7, 29.4, 21.6 ppm. **IR** (thin film):  $\nu$  3071, 2921, 2826, 2358, 1640, 1597, 1445, 1371, 1273, 1184, 1173, 1020, 1094, 1018, 977, 918, 812, 751  $\text{cm}^{-1}$ . **HRMS** (ESI+): exact mass calculated for  $\text{C}_{18}\text{H}_{18}\text{NO}_2\text{S}$  ( $[\text{M}+\text{H}]^+$ ), 312.1053; found 312.1056.

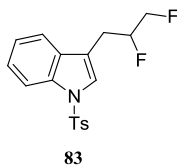
**3-(Oxiran-2-ylmethyl)-1-tosyl-1H-indole (79):**

**Step 1:**<sup>109</sup> To a solution of 3-allyl-1-tosyl-1H-indole (**85**) (5.70 g, 18.3 mmol, 1.00 equiv) in a 4:1 acetone/water mixture (0.260 L) at rt were successively added *N*-methylmorpholine *N*-oxide (3.32 g, 27.5 mmol, 1.50 equiv) and osmium tetroxide (2.5% in *t*-BuOH, 7.57 mL, 6.00  $10^{-4}$  mol, 3.00  $10^{-2}$  equiv). After stirring for 24 h at rt, the reaction was quenched with saturated aqueous  $\text{Na}_2\text{S}_2\text{O}_3$  and stirred for 45 min at rt. The resulting mixture was then extracted with EtOAc, and the combined organic extracts were washed with brine, dried over  $\text{Na}_2\text{SO}_4$ , filtered, and concentrated *in vacuo*. The resulting crude diol (**113**) was isolated as a colorless syrup that was used as such in the next step.

**Step 2:**<sup>108</sup> To a solution of the previously isolated diol (**113**) in MeCN (45.7 mL) at rt was added triethylamine (7.65 mL, 54.9 mmol, 3.00 equiv). The reaction solution was cooled down to 0 °C before perfluorobutanesulfonyl fluoride (5.14 mL, 27.4 mmol, 1.50 equiv) was added dropwise. The reaction was allowed to stir at rt for 1 h and then quenched with water. The aqueous phase was extracted with EtOAc, and the combined organic extracts were washed with brine, dried over  $\text{Na}_2\text{SO}_4$ , filtered, and concentrated *in vacuo*. The resulting crude material was purified by silica gel flash column chromatography (2:1 hexanes/EtOAc) to afford epoxide **79** (5.45 g, 16.6 mmol, 91% over two steps) as a colorless syrup.

**TLC:**  $R_f$  = 0.27 (2:1 hexanes/EtOAc; UV, CAM).  **$^1\text{H}$  NMR** (400 MHz,  $\text{CDCl}_3$ ):  $\delta$  8.01 (dt,  $J$  = 8.3 Hz,  $J$  = 0.8 Hz, 1H), 7.79 (d,  $J$  = 8.4 Hz, 2H), 7.55 (dt,  $J$  = 7.8 Hz,  $J$  = 0.9 Hz, 1H), 7.49 (s, 1H), 7.38–7.32 (m, 1H), 7.30–7.21 (m, 3H), 3.24–3.19 (m, 1H), 3.00–2.90 (m, 2H), 2.83 (dd,  $J$  = 4.9 Hz,  $J$  = 3.9 Hz, 1H), 2.57 (dd,  $J$  = 4.9 Hz,  $J$  = 2.6 Hz, 1H), 2.36 (s, 3H) ppm.  **$^{13}\text{C}$  NMR** (100 MHz,  $\text{CDCl}_3$ ):  $\delta$  144.8, 135.3, 135.2, 130.9, 129.8, 126.8, 124.8, 123.8, 123.2, 119.6, 118.3, 113.7, 51.2, 45.9, 28.3, 21.6 ppm. **IR** (thin film):  $\nu$  3109, 3054, 2991, 2920, 2359, 1597, 1445, 1368, 1277, 1188, 1174, 1120, 1090, 1020, 975, 814, 745, 702, 670  $\text{cm}^{-1}$ . **HRMS** (ESI<sup>+</sup>): exact mass calculated for  $\text{C}_{18}\text{H}_{18}\text{NO}_3\text{S}$  ( $[\text{M}+\text{H}]^+$ ), 328.1002; found 328.1002.





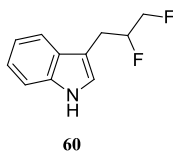
### 3-(2,3-Difluoropropyl)-1-tosyl-1H-indole (**83**):

**Step 1:**<sup>102</sup> A mixture of 3-(oxiran-2-ylmethyl)-1-tosyl-1H-indole (**79**) (4.50 g, 13.7 mmol, 1.00 equiv) and triethylamine trihydrofluoride (4.55 mL, 27.4 mmol, 2.00 equiv) was heated to 150 °C in a sealed flask and vigorously stirred for 3 h. The reaction was then cooled down to rt, diluted in a 1:1 EtOAc/water mixture and stirred for 10 min. The aqueous phase was then extracted with EtOAc and the combined organic extracts were washed with brine, dried over Na<sub>2</sub>SO<sub>4</sub>, filtered, and concentrated *in vacuo*. The resulting crude material was purified by silica gel flash column chromatography (1:1 hexanes/EtOAc) to afford fluorohydrin **115** as a brown oil that was used as such in the next step.

**Step 2:**<sup>80</sup> To a solution of the previously isolated fluorohydrin (**115**) and triethylamine (8.12 mL, 58.3 mmol, 4.50 equiv) in MeCN (0.130 L) under inert atmosphere at 0 °C were successively added triethylamine trihydrofluoride (3.23 mL, 19.4 mmol, 1.50 equiv) and perfluorobutanesulfonyl fluoride (4.85 mL, 25.9 mmol, 2.00 equiv) dropwise. The reaction was then stirred at 0 °C for 1 h, followed by 1 h at rt, before it was quenched with saturated aqueous NaHCO<sub>3</sub> and extracted with EtOAc. The combined organic extracts were washed with brine, dried over Na<sub>2</sub>SO<sub>4</sub>, filtered, and concentrated *in vacuo*. The resulting crude material was purified by silica gel flash column chromatography (10:1 hexanes/EtOAc) to afford indole **83** (2.40 g, 6.87 mmol, 53%) as a white crystalline solid (mp = 98 °C).

**TLC:**  $R_f$  = 0.25 (10:3 hexanes/EtOAc; UV, CAM). **<sup>1</sup>H NMR** (400 MHz, CDCl<sub>3</sub>): δ 8.02 (d,  $J$  = 8.3 Hz, 1H), 7.78 (d,  $J$  = 8.4 Hz, 2H), 7.52 (d,  $J$  = 7.9 Hz, 1H), 7.50 (s, 1H), 7.39–7.34 (m, 1H), 7.31–7.26 (m, 1H), 7.24 (d,  $J$  = 8.1 Hz, 2H), 4.93 (ddtdd,  $J$  = 47.7 Hz,  $J$  = 20.8 Hz,  $J$  = 6.8 Hz,  $J$  = 4.7 Hz,  $J$  = 2.8 Hz, 1H), 4.66–4.33 (m, 2H), 3.21–3.04 (m, 2H), 2.37 (s, 3H) ppm. **<sup>13</sup>C NMR** (100 MHz, CDCl<sub>3</sub>): δ 145.0, 135.2, 135.1, 130.5, 129.9, 126.8, 125.0, 124.6 (d,  $J$  = 1.4 Hz), 123.3, 119.3, 116.6 (d,  $J$  = 6.5 Hz), 113.8, 91.4 (d,  $J$  = 19.9 Hz), 89.6 (d,  $J$  = 19.9 Hz), 26.0 (d,  $J$  = 23.4 Hz,  $J$  = 7.2 Hz), 21.6 ppm. **<sup>19</sup>F NMR** (376 MHz, CDCl<sub>3</sub>, decoupled): δ -185.9 (d,  $J$  = 14.1 Hz), -232.6 (d,  $J$  = 14.0 Hz) ppm. **<sup>19</sup>F NMR** (376 MHz, CDCl<sub>3</sub>, not decoupled): δ -185.7 – -186.1 (m), -232.6 (tdd,  $J$  = 47.3 Hz,  $J$  = 21.0 Hz,  $J$  = 13.7 Hz) ppm. **IR** (thin film): ν 3100, 3081, 2955, 2923, 2355, 2334, 1595, 1448, 1366, 1279, 1189, 1172,

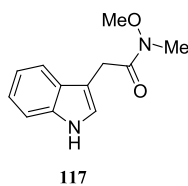
1122, 1086, 1019, 976, 814, 747, 699, 671  $\text{cm}^{-1}$ . **HRMS** (ESI+): exact mass calculated for  $\text{C}_{18}\text{H}_{18}\text{F}_2\text{NO}_2\text{S}$  ( $[\text{M}+\text{H}]^+$ ), 350.1021; found 350.1016.



### 3-(2,3-Difluoropropyl)-1H-indole (**60**):<sup>81</sup>

To a degassed solution of 3-(2,3-difluoropropyl)-1-tosyl-1H-indole (**83**) (2.40 g, 6.87 mmol, 1.00 equiv) in EtOH (0.230 L) under inert atmosphere at rt was added potassium hydroxide (7.71 g, 137 mmol, 20.0 equiv) in one portion. The reaction mixture was then heated to reflux overnight, cooled down to rt and quenched with saturated aqueous  $\text{NH}_4\text{Cl}$ . The aqueous phase was extracted with EtOAc and the combined organic extracts were washed with brine, dried over  $\text{Na}_2\text{SO}_4$ , filtered, and concentrated *in vacuo*. The resulting crude material was purified by silica gel flash column chromatography (10:1 hexanes/EtOAc) to afford indole **60** (1.29 g, 6.59 mmol, 96%) as a colorless oil.

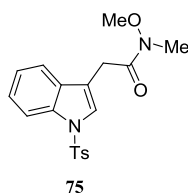
**TLC**:  $R_f$  = 0.18 (5:1 hexanes/EtOAc; UV, CAM).  **$^1\text{H}$  NMR** (400 MHz,  $\text{CDCl}_3$ ):  $\delta$  8.08 (bs, 1H), 7.64 (d,  $J$  = 7.9 Hz, 1H), 7.41 (dt,  $J$  = 8.1 Hz,  $J$  = 0.9 Hz, 1H), 7.28–7.23 (m, 1H), 7.21–7.16 (m, 1H), 7.14 (d,  $J$  = 2.4 Hz, 1H), 5.11–4.88 (m, 1H), 4.70–4.38 (m, 2H), 3.31–3.15 (m, 2H) ppm.  **$^{13}\text{C}$  NMR** (100 MHz,  $\text{CDCl}_3$ ):  $\delta$  136.2, 127.3, 123.0, 122.3, 119.8, 118.6, 111.3, 109.8 (d,  $J$  = 8.3 Hz), 91.6 (dd,  $J$  = 175.7 Hz,  $J$  = 19.3 Hz), 83.4 (dd,  $J$  = 173.4 Hz,  $J$  = 22.6 Hz), 26.2 (dd,  $J$  = 23.3 Hz,  $J$  = 7.3 Hz) ppm.  **$^{19}\text{F}$  NMR** (376 MHz,  $\text{CDCl}_3$ , decoupled):  $\delta$  -184.8 (d,  $J$  = 14.1 Hz), -232.5 (d,  $J$  = 13.0 Hz) ppm.  **$^{19}\text{F}$  NMR** (376 MHz,  $\text{CDCl}_3$ , not decoupled):  $\delta$  -184.6 – -185.0 (m), -232.5 (tdd,  $J$  = 47.4 Hz,  $J$  = 21.5 Hz,  $J$  = 13.6 Hz) ppm. **IR** (thin film):  $\nu$  3455, 3412, 3060, 2955, 2365, 1622, 1459, 1425, 1340, 1252, 1230, 1080, 1015, 915, 892, 840, 815, 744  $\text{cm}^{-1}$ . **HRMS** (ESI+): exact mass calculated for  $\text{C}_{11}\text{H}_{12}\text{F}_2\text{N}$  ( $[\text{M}+\text{H}]^+$ ), 196.0932; found 196.0934.



**2-(1*H*-Indol-3-yl)-*N*-methoxy-*N*-methylacetamide (117):**<sup>142</sup>

To a solution of 2-(1*H*-indol-3-yl)acetic acid (**77**) (2.00 g, 11.2 mmol, 1.00 equiv) in CH<sub>2</sub>Cl<sub>2</sub> (28.0 mL) under inert atmosphere at rt was added carbonyldiimidazole (2.15 g, 12.9 mmol, 1.15 equiv) portionwise. The reaction was stirred for 2 h at rt before *N,O*-dimethylhydroxylamine hydrochloride (1.28 g, 12.9 mmol, 1.15 equiv) was added. The resulting suspension was stirred overnight before its pH was adjusted to 10 with a 3 M aqueous NaOH solution. The aqueous phase was extracted with CH<sub>2</sub>Cl<sub>2</sub> and the combined organic extracts were dried over Na<sub>2</sub>SO<sub>4</sub>, filtered, and concentrated *in vacuo*. The resulting crude material was purified by silica gel flash column chromatography (2:3 hexanes/EtOAc) to afford amide **117** (1.95 g, 8.91 mmol, 80%) as a yellowish solid (mp = 124 °C).

**TLC:**  $R_f$  = 0.13 (1:1 hexanes/EtOAc; UV, CAM). **<sup>1</sup>H NMR** (400 MHz, CDCl<sub>3</sub>): δ 8.18 (bs, 1H), 7.69 (d,  $J$  = 7.9 Hz, 1H), 7.37 (dt,  $J$  = 8.1 Hz,  $J$  = 0.9 Hz, 1H), 7.24–7.12 (m, 3H), 3.94 (s, 2H), 3.69 (s, 3H), 3.24 (s, 3H) ppm. **<sup>13</sup>C NMR** (100 MHz, CDCl<sub>3</sub>): δ 172.9, 136.1, 127.5, 123.1, 122.1, 119.6, 118.9, 111.1, 109.1, 61.4, 32.3, 29.0 ppm. **IR** (thin film): ν 3400, 3293, 3055, 2969, 2931, 1641, 1456, 1422, 1384, 1340, 1232, 1175, 1099, 1005, 923, 799, 737, 599 cm<sup>-1</sup>. **HRMS** (ESI<sup>+</sup>): exact mass calculated for C<sub>12</sub>H<sub>15</sub>N<sub>2</sub>O<sub>2</sub> ([M+H]<sup>+</sup>), 219.1128; found 219.1125.

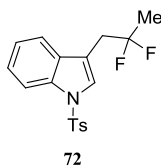


***N*-Methoxy-*N*-methyl-2-(1-tosyl-1*H*-indol-3-yl)acetamide (75):**<sup>77</sup>

To a solution of 2-(1*H*-indol-3-yl)-*N*-methoxy-*N*-methylacetamide (**117**) (0.100 g, 4.60 10<sup>-4</sup> mol, 1.00 equiv), tetrabutylammonium hydrogen sulfate (11.0 mg, 3.00 10<sup>-5</sup> mol, 7.00 10<sup>-2</sup> equiv), and *p*-toluenesulfonyl chloride (106 mg, 5.50 10<sup>-4</sup> mol, 1.20 equiv) in toluene (1.90 mL) at 0 °C was added a 50% aqueous KOH solution (1.00 mL) dropwise. The reaction mixture was then vigorously stirred at 0 °C for 1 h before it was diluted with water and

extracted with Et<sub>2</sub>O. The combined organic extracts were washed with brine, dried over Na<sub>2</sub>SO<sub>4</sub>, filtered, and concentrated *in vacuo*. The resulting crude material was purified by silica gel flash column chromatography (1:1 hexanes/EtOAc) to afford amide **75** (70.0 mg, 1.90 10<sup>-4</sup> mol, 41%) as an orange oil.

**TLC:**  $R_f$  = 0.18 (1:1 hexanes/EtOAc; UV, CAM). **<sup>1</sup>H NMR** (400 MHz, CDCl<sub>3</sub>): δ 8.02–7.97 (m, 1H), 7.80–7.75 (m, 2H), 7.60–7.56 (m, 2H), 7.35–7.30 (m, 1H), 7.28–7.23 (m, 1H), 7.23–7.18 (d,  $J$  = 8.0 Hz, 2H), 3.84 (s, 2H), 3.65 (s, 3H), 3.22 (s, 3H), 2.33 (s, 3H) ppm. **<sup>13</sup>C NMR** (100 MHz, CDCl<sub>3</sub>): δ 171.1, 144.9, 135.3, 135.0, 130.8, 129.8, 126.8, 124.8, 123.2, 119.8, 116.0, 113.6, 61.4, 32.3, 29.0, 21.5 ppm. **IR** (thin film): ν 3112, 3058, 2968, 2940, 1663, 1595, 1446, 1369, 1305, 1274, 1170, 1120, 1093, 1002, 975, 911, 812, 744, 703, 671, 612, 576, 536 cm<sup>-1</sup>. **HRMS** (ESI<sup>+</sup>): exact mass calculated for C<sub>19</sub>H<sub>21</sub>N<sub>2</sub>O<sub>4</sub>S ([M+H]<sup>+</sup>), 373.1217; found 373.1220.



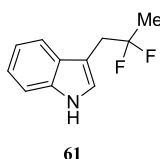
### 3-(2,2-Difluoropropyl)-1-tosyl-1H-indole (**72**):

**Step 1:**<sup>110</sup> To a solution of *N*-methoxy-*N*-methyl-2-(1-tosyl-1*H*-indol-3-yl)acetamide (**75**) (2.64 g, 7.08 mmol, 1.00 equiv) in THF (142 mL) under inert atmosphere at 0 °C was added methylmagnesium bromide (3 M, 5.19 mL, 15.6 mmol, 2.20 equiv) dropwise. The reaction was then stirred at rt for 30 min before it was quenched with saturated aqueous NH<sub>4</sub>Cl. The aqueous phase was extracted with Et<sub>2</sub>O and the combined organic extracts were washed with brine, dried over Na<sub>2</sub>SO<sub>4</sub>, filtered, and concentrated *in vacuo*. The crude ketone (**69**) was isolated as a yellow crystalline solid that was used as such in the next step.

**Step 2:**<sup>84</sup> To a solution of the previously isolated ketone (**69**) in CH<sub>2</sub>Cl<sub>2</sub> (142 mL) under inert atmosphere at 0 °C was added diethylaminosulfur trifluoride (4.92 mL, 35.4 mmol, 5.00 equiv) dropwise. The reaction was then stirred at rt for 24 h before it was carefully quenched with saturated aqueous NaHCO<sub>3</sub>. The aqueous phase was extracted with CH<sub>2</sub>Cl<sub>2</sub> and the combined organic extracts were dried over Na<sub>2</sub>SO<sub>4</sub>, filtered, and concentrated *in vacuo*. The resulting crude material was purified by silica gel flash column chromatography (10:1

hexanes/EtOAc) to afford indole **72** (1.16 g, 3.32 mmol, 47% over two steps) as a yellow crystalline solid (mp = 98 °C).

**TLC:**  $R_f$  = 0.31 (4:1 hexanes/EtOAc; UV, CAM).  **$^1\text{H NMR}$**  (400 MHz,  $\text{CDCl}_3$ ):  $\delta$  8.03–7.98 (m, 1H), 7.80–7.75 (m, 2H), 7.56–7.52 (m, 2H), 7.38–7.32 (m, 1H), 7.31–7.26 (m, 1H), 7.26–7.21 (m, 2H), 3.24 (t,  $J$  = 15.2 Hz, 2H), 2.36 (s, 3H), 1.54 (t,  $J$  = 18.3 Hz, 3H) ppm.  **$^{13}\text{C NMR}$**  (100 MHz,  $\text{CDCl}_3$ ):  $\delta$  145.0, 135.2, 135.0, 130.8, 129.9, 126.8, 125.6, 124.9, 123.3, 123.3 (t,  $J$  = 239.4 Hz), 119.7, 114.9 (t,  $J$  = 5.6 Hz), 113.7, 34.0 (t,  $J$  = 28.6 Hz), 22.9 (t,  $J$  = 27.5 Hz), 21.6 ppm.  **$^{19}\text{F NMR}$**  (376 MHz,  $\text{CDCl}_3$ , decoupled):  $\delta$  -88.32 (s) ppm.  **$^{19}\text{F NMR}$**  (376 MHz,  $\text{CDCl}_3$ , not decoupled):  $\delta$  -88.19 – -88.46 (m) ppm. **IR** (thin film):  $\nu$  3041, 3007, 2977, 2931, 1593, 1447, 1391, 1364, 1272, 1236, 1172, 1122, 1091, 975, 884, 811, 747, 674, 601, 573, 536  $\text{cm}^{-1}$ . **HRMS** (ESI+): exact mass calculated for  $\text{C}_{18}\text{H}_{18}\text{F}_2\text{NO}_2\text{S}$  ( $[\text{M}+\text{H}]^+$ ), 350.1021; found 350.1019.

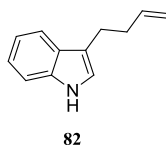


### 3-(2,2-Difluoropropyl)-1H-indole (**61**):<sup>81</sup>

To a suspension of 3-(2,2-difluoropropyl)-1-tosyl-1H-indole (**72**) (1.10 g, 3.15 mmol, 1.00 equiv) in EtOH (105 mL) under inert atmosphere at rt was added potassium hydroxyde (3.53 g, 63.0 mmol, 20.0 equiv). The reaction was then heated to reflux overnight before it was quenched with saturated aqueous  $\text{NH}_4\text{Cl}$ . The aqueous phase was extracted with EtOAc and the combined organic extracts were washed with brine, dried over  $\text{Na}_2\text{SO}_4$ , filtered, and concentrated *in vacuo*. The resulting crude material was purified by silica gel flash column chromatography (10:1 hexanes/EtOAc) to afford indole **61** (544 mg, 2.79 mmol, 89%) as a red crystalline solid (mp = 50 °C).

**TLC:**  $R_f$  = 0.18 (10:1 hexanes/EtOAc; UV, CAM).  **$^1\text{H NMR}$**  (400 MHz,  $\text{CDCl}_3$ ):  $\delta$  8.10 (s, 1H), 7.67 (d,  $J$  = 7.8 Hz, 1H), 7.41 (d,  $J$  = 8.0 Hz, 1H), 7.28–7.23 (m, 1H), 7.22–7.17 (m, 1H), 7.17–7.14 (m, 1H), 3.35 (t,  $J$  = 15.4 Hz, 2H), 1.61 (t,  $J$  = 18.3 Hz, 3H) ppm.  **$^{13}\text{C NMR}$**  (100 MHz,  $\text{CDCl}_3$ ):  $\delta$  136.0, 127.7, 124.2 (t,  $J$  = 239.0 Hz), 123.9, 122.2, 119.8, 119.0, 111.2, 108.4 (t,  $J$  = 5.9 Hz), 34.2 (t,  $J$  = 28.2 Hz), 22.8 (t,  $J$  = 27.6 Hz) ppm.  **$^{19}\text{F NMR}$**  (376 MHz,  $\text{CDCl}_3$ , decoupled):  $\delta$  -88.47 (s) ppm.  **$^{19}\text{F NMR}$**  (376 MHz,  $\text{CDCl}_3$ , not decoupled):  $\delta$  -88.33 – -88.60 (m) ppm. **IR** (thin film):  $\nu$  3145 (bs), 3051, 2998, 2915, 2360, 1456, 1421, 1390, 1358,

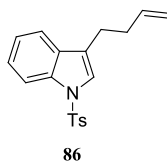
1339, 1240, 1171, 1135, 1099, 1008, 962, 926, 876, 785, 744  $\text{cm}^{-1}$ . **HRMS** (ESI+): exact mass calculated for  $\text{C}_{11}\text{H}_{12}\text{F}_2\text{N}$  ( $[\text{M}+\text{H}]^+$ ), 196.0932; found 196.0933.



### 3-(But-3-en-1-yl)-1H-indole (**82**):<sup>107</sup>

To a solution of 1H-indole-3-carbaldehyde (**110**) (2.50 g, 17.1 mmol, 1.00 equiv) and allyl bromide (**111**) (2.98 mL, 34.1 mmol, 2.00 equiv) in a 1:1 THF/water mixture (0.200 L) at rt were added indium (2.74 g, 23.9 mmol, 1.40 equiv) and Hantzsch ester (**112**) (4.36 g, 17.1 mmol, 1.00 equiv). The reaction was then stirred at 50 °C for 10 h, cooled down to rt, and diluted with water. The aqueous phase was extracted with EtOAc and the combined organic extracts were successively washed with water and brine, dried over  $\text{Na}_2\text{SO}_4$ , filtered, and concentrated *in vacuo*. The resulting crude material was purified by silica gel flash column chromatography (20:1 hexanes/EtOAc) to afford olefin **82** (2.31 g, 13.5 mmol, 79%) as a yellow oil.

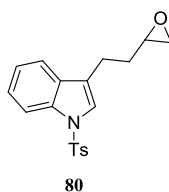
**TLC**:  $R_f$  = 0.16 (10:1 hexanes/EtOAc; UV, *p*-anisaldehyde, CAM).  **$^1\text{H}$  NMR** (400 MHz,  $\text{CDCl}_3$ ):  $\delta$  7.93 (bs, 1H), 7.65 (dd,  $J$  = 7.9 Hz,  $J$  = 1.0 Hz, 1H), 7.39 (dt,  $J$  = 8.1 Hz,  $J$  = 0.8 Hz, 1H) 7.25–7.19 (m, 1H), 7.17–7.12 (m, 1H), 7.04–7.01 (m, 1H), 5.97 (ddt,  $J$  = 16.9 Hz,  $J$  = 10.2 Hz,  $J$  = 6.6 Hz, 1H), 5.12 (ddd,  $J$  = 17.1 Hz,  $J$  = 3.5 Hz,  $J$  = 1.7 Hz, 1H), 5.03 (ddt,  $J$  = 10.2 Hz,  $J$  = 2.2 Hz,  $J$  = 1.2 Hz, 1H), 2.90 (t,  $J$  = 7.5 Hz, 2H), 2.55–2.48 (m, 2H) ppm.  **$^{13}\text{C}$  NMR** (100 MHz,  $\text{CDCl}_3$ ):  $\delta$  138.8, 136.3, 127.5, 121.9, 121.1, 119.1, 118.9, 116.3, 114.7, 111.0, 34.3, 24.7 ppm. **IR** (thin film):  $\nu$  3411, 3062, 2976, 2915, 2846, 2360, 1635, 1618, 1458, 1417, 1353, 1337, 1223, 1089, 1010, 910, 800, 739  $\text{cm}^{-1}$ . **HRMS** (ESI+): exact mass calculated for  $\text{C}_{12}\text{H}_{14}\text{N}$  ( $[\text{M}+\text{H}]^+$ ), 172.1121; found 172.1123.



### 3-(But-3-en-1-yl)-1-tosyl-1H-indole (**86**):<sup>77</sup>

To a solution of 3-(but-3-en-1-yl)-1H-indole (**82**) (2.31 g, 13.5 mmol, 1.00 equiv), tetrabutylammonium hydrogen sulfate (331 mg, 0.95 mmol, 7.00  $10^{-2}$  equiv), and *p*-toluenesulfonyl chloride (3.12 g, 16.2 mmol, 1.20 equiv) in toluene (54.0 mL) at 0 °C was added a 50% aqueous KOH solution (20.0 mL) dropwise. The reaction was stirred at 0 °C for 1 h before it was diluted with water. The organic phase was then separated, successively washed with water and brine, dried over Na<sub>2</sub>SO<sub>4</sub>, filtered, and concentrated *in vacuo*. The resulting crude material was purified by silica gel flash column chromatography (10:1 hexanes/EtOAc) to afford indole **86** (4.28 g, 13.2 mmol, 97%) as a colorless syrup.

**TLC:**  $R_f$  = 0.36 (5:1 hexanes/EtOAc; UV, CAM). **<sup>1</sup>H NMR** (400 MHz, CDCl<sub>3</sub>): δ 8.00 (dt,  $J$  = 8.2 Hz,  $J$  = 1.0 Hz, 1H), 7.75 (d,  $J$  = 8.4 Hz, 2H), 7.50 (dt,  $J$  = 7.9 Hz,  $J$  = 1.0 Hz, 1H), 7.36–7.30 (m, 2H), 7.28–7.20 (m, 3H), 5.87 (ddt,  $J$  = 16.9 Hz,  $J$  = 10.2 Hz,  $J$  = 6.6 Hz, 1H), 5.09–4.99 (m, 2H), 2.81–2.74 (m, 2H), 2.50–2.41 (m, 2H), 2.35 (s, 3H) ppm. **<sup>13</sup>C NMR** (100 MHz, CDCl<sub>3</sub>): δ 144.6, 137.7, 135.4, 131.1, 129.7, 126.7, 124.6, 123.0, 122.9, 122.7, 119.4, 115.4, 113.8, 32.9, 24.3, 21.5 ppm. **IR** (thin film): ν 3071, 2925, 2852, 2358, 1640, 1595, 1445, 1364, 1275, 1105, 1171, 1117, 1093, 1019, 972, 915, 814, 744 cm<sup>-1</sup>. **HRMS** (ESI<sup>+</sup>): exact mass calculated for C<sub>19</sub>H<sub>20</sub>NO<sub>2</sub>S ([M+H]<sup>+</sup>), 326.1209; found 326.1210.



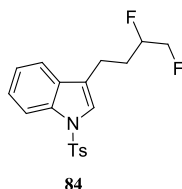
### 3-(2-(Oxiran-2-yl)ethyl)-1-tosyl-1H-indole (**80**):

**Step 1:**<sup>109</sup> To a solution of 3-(but-3-en-1-yl)-1-tosyl-1H-indole (**86**) (4.18 g, 12.8 mmol, 1.00 equiv) in a 4:1 acetone/water mixture (184 mL) at rt were successively added *N*-methylmorpholine *N*-oxide (2.33 g, 19.3 mmol, 1.50 equiv) and osmium tetroxide (2.5% in *t*-BuOH, 3.54 mL, 2.80  $10^{-4}$  mol, 3.00  $10^{-2}$  equiv). After stirring for 9 h at rt, the reaction was quenched with saturated aqueous Na<sub>2</sub>S<sub>2</sub>O<sub>3</sub> and stirred for 45 min at rt. The resulting mixture was then extracted with EtOAc, and the combined organic extracts were washed with brine,

dried over  $\text{Na}_2\text{SO}_4$ , filtered, and concentrated *in vacuo*. The resulting crude material was purified by silica gel flash column chromatography (1:3 hexanes/EtOAc) to afford diol **114** as a white foam (4.17 g) that was used as such in the next step.

**Step 2:**<sup>108</sup> To a solution of the previously isolated diol (**114**, 4.17 g) in MeCN (29.0 mL) under inert atmosphere at rt was added triethylamine (4.86 mL, 34.8 mmol, 3.00 equiv). The resulting solution was cooled down to 0 °C before perfluorobutanesulfonyl fluoride (3.26 mL, 17.4 mmol, 1.50 equiv) was added dropwise. The reaction was stirred for 1 h at rt before it was quenched with water. The aqueous phase was extracted with EtOAc and the combined organic extracts were washed with brine, dried over  $\text{Na}_2\text{SO}_4$ , filtered, and concentrated *in vacuo*. The resulting crude material was purified by silica gel flash column chromatography (2:1 hexanes/EtOAc) to afford epoxide **80** (3.96 g, 11.6 mmol, 90% over two steps) as a yellowish syrup.

**TLC:**  $R_f$  = 0.28 (2:1 hexanes/EtOAc; UV, CAM).  **$^1\text{H}$  NMR** (400 MHz,  $\text{CDCl}_3$ ):  $\delta$  8.01 (d,  $J$  = 8.3 Hz, 1H), 7.76 (d,  $J$  = 8.4 Hz, 2H), 7.51 (d,  $J$  = 7.8 Hz, 1H), 7.38 (s, 1H), 7.36–7.31 (m, 1H), 7.28–7.20 (m, 3H), 3.01–2.96 (m, 1H), 2.93–2.79 (m, 2H), 2.78–2.75 (m, 1H), 2.50 (dd,  $J$  = 5.0 Hz,  $J$  = 2.7 Hz, 1H), 2.35 (s, 3H), 2.06–1.96 (m, 1H), 1.93–1.82 (m, 1H) ppm.  **$^{13}\text{C}$  NMR** (100 MHz,  $\text{CDCl}_3$ ):  $\delta$  144.8, 135.4, 130.8, 129.8, 126.7, 124.7, 123.1, 122.8, 122.2, 119.4, 113.8, 51.7, 47.2, 31.9, 21.6, 21.4 ppm. **IR** (thin film):  $\nu$  3112, 3055, 2990, 2925, 2854, 2359, 1597, 1451, 1365, 1276, 1189, 1173, 1118, 1093, 1020, 973, 814, 746, 702, 671  $\text{cm}^{-1}$ . **HRMS** (ESI<sup>+</sup>): exact mass calculated for  $\text{C}_{19}\text{H}_{19}\text{NNaO}_3\text{S}$  ( $[\text{M}+\text{H}]^+$ ), 364.0978; found 364.0977.



### 3-(3,4-Difluorobutyl)-1-tosyl-1H-indole (**84**):

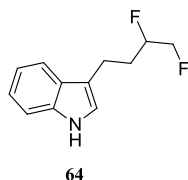
**Step 1:**<sup>102</sup> A mixture of 3-(2-(oxiran-2-yl)ethyl)-1-tosyl-1H-indole (**80**) (3.96 g, 11.6 mmol, 1.00 equiv) and triethylamine trihydrofluoride (4.00 mL, 24.1 mmol, 2.10 equiv) in a sealed flask was heated at 150 °C for 3 h upon vigorous stirring. The reaction was then cooled down to rt, dissolved in a 1:1 EtOAc/water mixture and stirred for 10 min. The aqueous phase was extracted with EtOAc and the combined organic extracts were washed with brine, dried over



Na<sub>2</sub>SO<sub>4</sub>, filtered and concentrated *in vacuo*. The resulting crude material was purified by silica gel flash column chromatography (1:1 hexanes/EtOAc) to afford fluorohydrin **116** as a colorless oil (3.92 g) that was used as such in the next step.

**Step 2:**<sup>80</sup> To a solution of the previously isolated fluorohydrin (**116**, 3.92 g) and triethylamine (6.80 mL, 48.8 mmol, 4.50 equiv) in MeCN (108 mL) under inert atmosphere at 0 °C were successively added triethylamine trihydrofluoride (2.70 mL, 16.3 mmol, 1.50 equiv) and prefluorobutanesulfonyl fluoride (4.06 mL, 21.7 mmol, 2.00 equiv) dropwise. The reaction was stirred at 0 °C for 1 h before it was quenched with water. The aqueous phase was extracted with EtOAc and the combined organic extracts were washed with brine, dried over Na<sub>2</sub>SO<sub>4</sub>, filtered, and concentrated *in vacuo*. The resulting crude material was purified by silica gel flash column chromatography (5:1 hexanes/EtOAc) to afford indole **84** (2.40 g, 6.60 mmol, 61% over two steps) as a white crystalline solid (mp = 113 °C).

**TLC:**  $R_f$  = 0.28 (10:3 hexanes/EtOAc; UV, CAM). **<sup>1</sup>H NMR** (400 MHz, CDCl<sub>3</sub>): δ 8.02 (dt,  $J$  = 8.3 Hz,  $J$  = 0.8 Hz, 1H), 7.77 (d,  $J$  = 8.4 Hz, 2H), 7.50 (dt,  $J$  = 7.6 Hz,  $J$  = 1.0 Hz, 1H), 7.39 (s, 1H), 7.38–7.32 (m, 1H), 7.30–7.21 (m, 3H), 4.79–4.36 (m, 3H), 2.98–2.78 (m, 2H), 2.36 (s, 3H), 2.22–2.06 (m, 1H), 2.03–1.85 (m, 1H) ppm. **<sup>13</sup>C NMR** (100 MHz, CDCl<sub>3</sub>): δ 144.8, 135.4, 135.3, 130.6, 129.8, 126.7, 124.8, 123.2, 123.1, 121.5, 119.3, 113.9, 90.7 (dd,  $J$  = 173.5 Hz,  $J$  = 19.5 Hz), 83.9 (dd,  $J$  = 174.4 Hz,  $J$  = 23.0 Hz), 29.5 (dd,  $J$  = 21.2 Hz,  $J$  = 6.2 Hz), 21.6, 20.1 (d,  $J$  = 4.7 Hz) ppm. **<sup>19</sup>F NMR** (376 MHz, CDCl<sub>3</sub>, decoupled): δ -191.3 (d,  $J$  = 13.3 Hz), -230.2 (d,  $J$  = 13.4 Hz) ppm. **<sup>19</sup>F NMR** (376 MHz, CDCl<sub>3</sub>, not decoupled): δ -191.1 – -191.5 (m), -230.2 (tdd,  $J$  = 47.4 Hz,  $J$  = 21.3 Hz,  $J$  = 13.8 Hz) ppm. **IR** (thin film): ν 3100, 3081, 2952, 2925, 2358, 2936, 1597, 1449, 1365, 1276, 1189, 1173, 1121, 1095, 1020, 972, 814, 748, 699, 671 cm<sup>-1</sup>. **HRMS** (ESI<sup>+</sup>): exact mass calculated for C<sub>19</sub>H<sub>20</sub>F<sub>2</sub>NO<sub>2</sub>S ([M+H]<sup>+</sup>), 364.1177; found 364.1170.

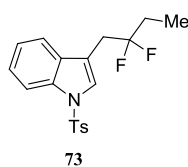


### 3-(3,4-Difluorobutyl)-1H-indole (**64**):<sup>81</sup>

To a degassed solution of 3-(3,4-difluorobutyl)-1-tosyl-1H-indole (**84**) (2.40 g, 6.60 mmol, 1.00 equiv) in EtOH (0.220 L) under inert atmosphere at rt was added potassium hydroxide

(7.41 g, 132 mmol, 20.0 equiv). The reaction was heated to reflux overnight before it was then cooled down to rt and quenched with saturated aqueous  $\text{NH}_4\text{Cl}$ . The aqueous phase was extracted with EtOAc and the combined organic extracts were washed with brine, dried over  $\text{Na}_2\text{SO}_4$ , filtered, and concentrated *in vacuo*. The crude material was purified by silica gel flash column chromatography (25:2 hexanes/EtOAc) to afford indole **64** (1.38 g, 6.60 mmol, 99%) as a brownish oil that crystallized over time at rt (mp = 42 °C).

**TLC:**  $R_f$  = 0.22 (10:3 hexanes/EtOAc; UV, CAM).  **$^1\text{H}$  NMR** (400 MHz,  $\text{CDCl}_3$ ):  $\delta$  7.99 (bs, 1H), 7.64 (d,  $J$  = 8.2 Hz, 1H), 7.40 (dt,  $J$  = 8.1 Hz,  $J$  = 0.8 Hz, 1H), 7.27–2.21 (m, 1H), 7.19–7.13 (m, 1H), 7.08–7.03 (m, 1H), 4.88–4.37 (m, 3H), 3.09–2.88 (m, 2H), 2.26–2.11 (m, 1H), 2.09–1.89 (m, 1H) ppm.  **$^{13}\text{C}$  NMR** (100 MHz,  $\text{CDCl}_3$ ):  $\delta$  136.4, 127.2, 122.2, 121.6, 119.4, 118.7, 114.9, 111.2, 91.1 (dd,  $J$  = 172.6 Hz,  $J$  = 19.2 Hz), 84.2 (dd,  $J$  = 173.8 Hz,  $J$  = 22.7 Hz), 30.5 (dd,  $J$  = 21.0 Hz,  $J$  = 6.0 Hz), 20.3 (d,  $J$  = 4.8 Hz) ppm.  **$^{19}\text{F}$  NMR** (376 MHz,  $\text{CDCl}_3$ , decoupled):  $\delta$  -191.0 (d,  $J$  = 13.2 Hz), -229.8 (d,  $J$  = 13.1 Hz) ppm.  **$^{19}\text{F}$  NMR** (376 MHz,  $\text{CDCl}_3$ , not decoupled):  $\delta$  -190.8 – -191.2 (m), -229.8 (tdd,  $J$  = 47.5 Hz,  $J$  = 21.2 Hz,  $J$  = 13.2 Hz) ppm. **IR** (thin film):  $\nu$  3455, 3413, 3052, 2952, 2852, 1618, 1459, 1421, 1357, 1341, 1251, 1230, 1089, 1028, 983, 920, 882, 855, 744  $\text{cm}^{-1}$ . **HRMS** (ESI+): exact mass calculated for  $\text{C}_{12}\text{H}_{14}\text{F}_2\text{N}$  ( $[\text{M}+\text{H}]^+$ ), 210.1089; found 210.1095.



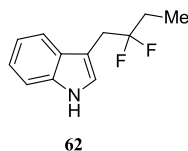
### 3-(2,2-Difluorobutyl)-1-tosyl-1H-indole (**73**):

**Step 1:**<sup>110</sup> To a solution of *N*-methoxy-*N*-methyl-2-(1-tosyl-1*H*-indol-3-yl)acetamide (**75**) (2.34 g, 6.27 mmol, 1.00 equiv) in THF (125 mL) under inert atmosphere at 0 °C was added ethylmagnesium bromide (1 M, 13.8 mL, 13.8 mmol, 2.20 equiv) dropwise. The reaction was then stirred at rt for 30 min before it was quenched with saturated aqueous  $\text{NH}_4\text{Cl}$ . The aqueous phase was extracted with  $\text{Et}_2\text{O}$  and the combined organic extracts were washed with brine, dried over  $\text{Na}_2\text{SO}_4$ , filtered, and concentrated *in vacuo*. The crude ketone (**70**) was isolated as a yellow crystalline solid that was used as such in the next step.

**Step 2:**<sup>84</sup> To a solution of the previously isolated ketone (**70**) in  $\text{CH}_2\text{Cl}_2$  (125 mL) under inert atmosphere at 0 °C was added diethylaminosulfur trifluoride (5.24 mL, 37.6 mmol, 6.00

equiv) dropwise. The reaction was then stirred at rt for 24 h before it was carefully quenched with saturated aqueous NaHCO<sub>3</sub>. The aqueous phase was extracted with CH<sub>2</sub>Cl<sub>2</sub> and the combined organic extracts were dried over Na<sub>2</sub>SO<sub>4</sub>, filtered, and concentrated *in vacuo*. The resulting crude material was purified by silica gel flash column chromatography (10:1 hexanes/EtOAc) to afford indole **73** (416 mg, 1.15 mmol, 19%) as a white crystalline solid (mp = 83 °C).

**TLC:**  $R_f$  = 0.25 (4:1 hexanes/EtOAc; UV, CAM). **<sup>1</sup>H NMR** (400 MHz, CDCl<sub>3</sub>): δ 8.00 (d,  $J$  = 8.2 Hz, 1H), 7.77 (d,  $J$  = 8.4 Hz, 2H), 7.58–7.50 (m, 2H), 7.38–7.31 (m, 1H), 7.30–7.20 (m, 3H), 3.23 (t,  $J$  = 15.7 Hz, 2H), 2.36 (s, 3H), 1.82 (ddt,  $J$  = 24.1 Hz,  $J$  = 16.5 Hz,  $J$  = 7.5 Hz, 2H), 1.04 (t,  $J$  = 7.5 Hz, 3H) ppm. **<sup>13</sup>C NMR** (100 MHz, CDCl<sub>3</sub>): δ 144.9, 135.2, 135.0, 130.9, 129.9, 126.8, 125.6, 124.8, 123.3, 119.8 (t,  $J$  = 1.5 Hz), 114.8 (t,  $J$  = 5.3 Hz), 113.7, 100.0, 32.3 (t,  $J$  = 28.6 Hz), 29.0 (t,  $J$  = 25.7 Hz), 21.6, 6.5 (t,  $J$  = 5.5 Hz) ppm. **<sup>19</sup>F NMR** (376 MHz, CDCl<sub>3</sub>, decoupled): δ -97.98 (s) ppm. **<sup>19</sup>F NMR** (376 MHz, CDCl<sub>3</sub>, not decoupled): δ -97.98 (p,  $J$  = 16.4 Hz) ppm. **IR** (thin film): ν 2931, 1597, 1446, 1368, 1172, 1122, 1090, 971, 742, 674, 573 cm<sup>-1</sup>. **HRMS** (ESI<sup>+</sup>): exact mass calculated for C<sub>19</sub>H<sub>20</sub>F<sub>2</sub>NO<sub>2</sub>S ([M+H]<sup>+</sup>), 364.1177; found 364.1178.

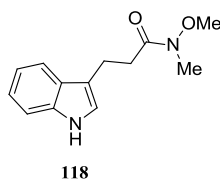


### 3-(2,2-Difluorobutyl)-1H-indole (**62**):<sup>81</sup>

To a suspension of 3-(2,2-difluorobutyl)-1-tosyl-1H-indole (**73**) (0.400 g, 1.10 mmol, 1.00 equiv) in EtOH (37.0 mL) under inert atmosphere at rt was added potassium hydroxide (1.24 g, 22.0 mmol, 20.0 equiv). The reaction was heated to reflux overnight before it was cooled down to rt and quenched with saturated aqueous NH<sub>4</sub>Cl. The aqueous phase was extracted with EtOAc and the combined organic extracts were washed with brine, dried over Na<sub>2</sub>SO<sub>4</sub>, filtered, and concentrated *in vacuo*. The resulting crude material was purified by silica gel flash column chromatography (10:1 hexanes/EtOAc) to afford indole **62** (156 mg, 7.50 10<sup>-4</sup> mol, 68%) as an orange oil that solidified (mp = 38 °C) upon standing at rt.

**TLC:**  $R_f$  = 0.11 (10:1 hexanes/EtOAc; UV, CAM). **<sup>1</sup>H NMR** (400 MHz, CDCl<sub>3</sub>): δ 8.10 (s, 1H), 7.67 (d,  $J$  = 7.8 Hz, 1H), 7.40 (d,  $J$  = 8.0 Hz, 1H), 7.27–7.22 (m, 1H), 7.21–7.14 (m, 2H), 3.34 (t,  $J$  = 15.9 Hz, 2H), 1.95–1.79 (m, 2H), 1.06 (t,  $J$  = 7.5 Hz, 3H) ppm. **<sup>13</sup>C NMR** (100

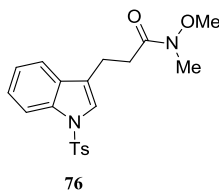
MHz, CDCl<sub>3</sub>):  $\delta$  136.0, 127.8, 125.2 (t,  $J = 241.5$  Hz), 123.8, 122.2, 119.8, 119.0, 111.1, 108.2 (t,  $J = 5.8$  Hz), 32.5 (t,  $J = 28.2$  Hz), 28.8 (t,  $J = 25.9$  Hz), 6.5 (t,  $J = 5.5$  Hz) ppm. <sup>19</sup>F NMR (376 MHz, CDCl<sub>3</sub>, decoupled):  $\delta$  -98.25 (s) ppm. <sup>19</sup>F NMR (376 MHz, CDCl<sub>3</sub>, not decoupled):  $\delta$  -98.25 (p,  $J = 16.1$  Hz) ppm. IR (thin film):  $\nu$  3414 (bs), 3060, 2978, 2941, 2887, 2360, 1456, 1422, 1336, 1140, 1095, 972, 881, 744 cm<sup>-1</sup>. HRMS (ESI+): exact mass calculated for C<sub>12</sub>H<sub>14</sub>F<sub>2</sub>N ([M+H]<sup>+</sup>), 210.1089; found 210.1088.



### 3-(1H-Indol-3-yl)-N-methoxy-N-methylpropanamide (**118**):<sup>142</sup>

To a solution of 3-(1H-indol-3-yl)propanoic acid (**78**) (2.01 g, 10.5 mmol, 1.00 equiv) in CH<sub>2</sub>Cl<sub>2</sub> (27.0 mL) under inert atmosphere at rt was added carbonyldiimidazole (2.02 g, 12.1 mmol, 1.15 equiv) portionwise. The reaction was stirred for 2 h at rt before *N,O*-dimethylhydroxylamine hydrochloride (1.20 g, 12.1 mmol, 1.15 equiv) was added. The resulting suspension was stirred overnight before its pH was adjusted to 10 with a 3 M aqueous NaOH solution. The aqueous phase was extracted with CH<sub>2</sub>Cl<sub>2</sub> and the combined organic extracts were dried over Na<sub>2</sub>SO<sub>4</sub>, filtered, and concentrated *in vacuo*. The resulting crude material was purified by silica gel flash column chromatography (1:1 hexanes/EtOAc) to afford amide **118** (2.44 g, 10.5 mmol, 99%) as a pinky oil.

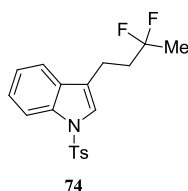
**TLC:**  $R_f = 0.31$  (1:2 hexanes/EtOAc; UV, CAM). <sup>1</sup>H NMR (400 MHz, CDCl<sub>3</sub>):  $\delta$  8.04 (bs, 1H), 7.66 (d,  $J = 7.9$  Hz, 1H), 7.41–7.36 (m, 1H), 7.25–7.19 (m, 1H), 7.18–7.12 (m, 1H), 7.09–7.05 (m, 1H), 3.62 (s, 3H), 3.22 (s, 3H), 3.18–3.11 (m, 2H), 2.86 (t,  $J = 7.7$  Hz, 2H) ppm. <sup>13</sup>C NMR (100 MHz, CDCl<sub>3</sub>):  $\delta$  174.2, 136.3, 127.3, 122.0, 121.6, 119.3, 118.8, 115.6, 111.1, 61.2, 32.7, 32.2, 20.3 ppm. IR (thin film):  $\nu$  3410, 3295, 3050, 2918, 2851, 2352, 1640, 1455, 1432, 1385, 1337, 1229, 1177, 1097, 1070, 1012, 984, 932, 808, 743 cm<sup>-1</sup>. HRMS (ESI+): exact mass calculated for C<sub>13</sub>H<sub>17</sub>N<sub>2</sub>O<sub>2</sub> ([M+H]<sup>+</sup>), 233.1285; found 233.1276.



### ***N*-Methoxy-*N*-methyl-3-(1-tosyl-1*H*-indol-3-yl)propanamide (76):**<sup>77</sup>

To a solution of 3-(1*H*-indol-3-yl)-*N*-methoxy-*N*-methylpropanamide (**118**) (2.44 g, 10.5 mmol, 1.00 equiv), tetrabutylammonium hydrogen sulfate (258 mg, 7.40  $\times 10^{-4}$  mol, 0.07 equiv), and *p*-toluenesulfonyl chloride (2.43 g, 12.6 mmol, 1.20 equiv) in toluene (42.0 mL) at 0 °C was added a 50% aqueous KOH solution (40.0 mL) dropwise. The reaction mixture was then vigorously stirred at 0 °C for 1 h before it was quenched with saturated aqueous NH<sub>4</sub>Cl. The aqueous phase was extracted with EtOAc and the combined organic extracts were washed with brine, dried over Na<sub>2</sub>SO<sub>4</sub>, filtered, and concentrated *in vacuo*. The resulting crude material was purified by silica gel flash column chromatography (1:1 hexanes/EtOAc) to afford indole **76** (3.78 g, 9.78 mmol, 93%) as a white crystalline solid (mp = 140 °C).

**TLC:**  $R_f$  = 0.24 (1:1 hexanes/EtOAc; UV, CAM). **<sup>1</sup>H NMR** (400 MHz, CDCl<sub>3</sub>):  $\delta$  8.02–7.97 (m, 1H), 7.79–7.74 (m, 2H), 7.56–7.51 (m, 1H), 7.41–7.38 (m, 1H), 7.36–7.30 (m, 1H), 7.28–7.20 (m, 3H), 3.63 (s, 3H), 3.21 (s, 3H), 3.07–3.00 (m, 2H), 2.87–2.77 (m, 2H), 2.35 (s, 3H) ppm. **<sup>13</sup>C NMR** (100 MHz, CDCl<sub>3</sub>):  $\delta$  173.3, 144.7, 135.4, 135.3, 130.8, 129.8, 126.8, 124.7, 123.1, 122.8, 122.2, 119.4, 113.7, 61.3, 32.3, 31.4, 21.6, 19.9 ppm. **IR** (thin film):  $\nu$  3455, 2930, 2352, 1658, 1445, 1365, 1171, 1120, 983, 747, 665, 597, 573, 536 cm<sup>-1</sup>. **HRMS** (ESI<sup>+</sup>): exact mass calculated for C<sub>20</sub>H<sub>23</sub>N<sub>2</sub>O<sub>4</sub>S ([M+H]<sup>+</sup>), 387.1373; found 387.1362.



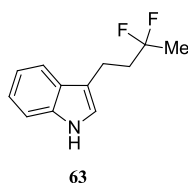
### **3-(3,3-Difluorobutyl)-1-tosyl-1*H*-indole (74):**

**Step 1:**<sup>110</sup> To a solution of *N*-methoxy-*N*-methyl-3-(1-tosyl-1*H*-indol-3-yl)propanamide (**76**) (1.00 g, 2.59 mmol, 1.00 equiv) in THF (26.0 mL) under inert atmosphere at 0 °C was added methylmagnesium bromide (3 M, 1.90 mL, 5.69 mmol, 2.20 equiv) dropwise. The reaction was then stirred at rt for 30 min before it was quenched with saturated aqueous NH<sub>4</sub>Cl. The aqueous phase was extracted with Et<sub>2</sub>O and the combined organic extracts were washed with

brine, dried over  $\text{Na}_2\text{SO}_4$ , filtered, and concentrated *in vacuo*. The crude material was purified by silica gel flash column chromatography (10:3 hexanes/EtOAc) to afford ketone **71** as a white crystalline solid that was used as such in the next step.

**Step 2:**<sup>84</sup> To a solution of the previously isolated ketone (**71**) in  $\text{CH}_2\text{Cl}_2$  (24.0 mL) under inert atmosphere at 0 °C was added diethylaminosulfur trifluoride (3.38 mL, 24.3 mmol, 10.0 equiv) dropwise. The reaction was then stirred at rt for 48 h before it was carefully quenched with saturated aqueous  $\text{NaHCO}_3$ . The aqueous phase was extracted with  $\text{CH}_2\text{Cl}_2$  and the combined organic extracts were dried over  $\text{Na}_2\text{SO}_4$ , filtered, and concentrated *in vacuo*. The resulting crude material was purified by silica gel flash column chromatography (10:1 hexanes/EtOAc) to afford indole **74** (414 mg, 1.14 mmol, 45% over two steps) as a white crystalline solid (mp = 73 °C).

**TLC:**  $R_f$  = 0.44 (10:3 hexanes/EtOAc; UV, CAM).  **$^1\text{H}$  NMR** (400 MHz,  $\text{CDCl}_3$ ):  $\delta$  8.04–8.00 (m, 1H), 7.80–7.74 (m, 2H), 7.52–7.48 (m, 1H), 7.39–7.32 (m, 2H), 7.30–7.21 (m, 3H), 2.93–2.85 (m, 2H), 2.36 (s, 3H), 2.32–2.17 (m, 2H), 1.78 (t,  $J$  = 18.4 Hz, 3H) ppm.  **$^{13}\text{C}$  NMR** (100 MHz,  $\text{CDCl}_3$ ):  $\delta$  144.8, 135.3, 130.6, 129.8, 126.8, 124.8, 123.6 (t,  $J$  = 238.3 Hz), 123.1, 122.6, 121.6, 119.2, 113.8, 37.4 (t,  $J$  = 25.7 Hz), 23.5 (t,  $J$  = 27.8 Hz), 21.6, 18.1 (t,  $J$  = 5.5 Hz) ppm.  **$^{19}\text{F}$  NMR** (376 MHz,  $\text{CDCl}_3$ , decoupled):  $\delta$  -91.86 (s) ppm.  **$^{19}\text{F}$  NMR** (376 MHz,  $\text{CDCl}_3$ , not decoupled):  $\delta$  -91.86 (h,  $J$  = 17.5 Hz) ppm. **IR** (thin film):  $\nu$  2927, 1723, 1596, 1445, 1365, 1172, 1120, 969, 903, 747, 672  $\text{cm}^{-1}$ . **HRMS** (ESI+): exact mass calculated for  $\text{C}_{19}\text{H}_{20}\text{F}_2\text{NO}_2\text{S}$  ( $[\text{M}+\text{H}]^+$ ), 364.1177; found 364.1172.

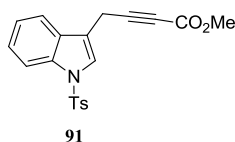


### 3-(3,3-Difluorobutyl)-1H-indole (**63**):<sup>81</sup>

To a suspension of 3-(3,3-difluorobutyl)-1-tosyl-1H-indole (**74**) (414 mg, 1.14 mmol, 1.00 equiv) in EtOH (38.0 mL) under inert atmosphere at rt was added potassium hydroxide (1.28 g, 22.8 mmol, 20.0 equiv). The reaction was heated to reflux overnight before it was cooled down to rt and quenched with saturated aqueous  $\text{NH}_4\text{Cl}$ . The aqueous phase was extracted with EtOAc and the combined organic extracts were washed with brine, dried over  $\text{Na}_2\text{SO}_4$ , filtered, and concentrated *in vacuo*. The resulting crude material was purified by silica gel

flash column chromatography (10:1 hexanes/EtOAc) to afford indole **63** (193 mg,  $9.20 \times 10^{-4}$  mol, 81%) as a brown oil that solidified (mp = 41 °C) upon standing at rt.

**TLC:**  $R_f$  = 0.11 (10:1 hexanes/EtOAc; UV, CAM).  **$^1\text{H}$  NMR** (400 MHz,  $\text{CDCl}_3$ ):  $\delta$  7.95 (s, 1H), 7.62–7.67 (m, 1H), 7.42–7.38 (m, 1H), 7.28–7.22 (m, 1H), 7.20–7.15 (m, 1H), 7.04–7.01 (m, 1H), 3.04–2.97 (m, 2H), 2.38–2.24 (m, 2H), 1.71 (t,  $J$  = 18.5 Hz, 3H) ppm.  **$^{13}\text{C}$  NMR** (100 MHz,  $\text{CDCl}_3$ ):  $\delta$  136.4, 127.2, 124.1 (t,  $J$  = 238.0 Hz), 122.2, 121.1, 119.4, 118.7, 115.1, 111.2, 38.6 (t,  $J$  = 25.3 Hz), 23.4 (t,  $J$  = 27.9 Hz), 18.5 (t,  $J$  = 5.5 Hz) ppm.  **$^{19}\text{F}$  NMR** (376 MHz,  $\text{CDCl}_3$ , decoupled):  $\delta$  -91.21 (s) ppm.  **$^{19}\text{F}$  NMR** (376 MHz,  $\text{CDCl}_3$ , not decoupled):  $\delta$  -91.09 – -91.35 (m) ppm. **IR** (thin film):  $\nu$  3468, 3414 (bs), 3051, 3005, 2932, 2860, 2360, 1456, 1394, 1335, 1239, 1221, 1171, 1135, 1062, 899, 745  $\text{cm}^{-1}$ . **HRMS** (ESI+): exact mass calculated for  $\text{C}_{12}\text{H}_{14}\text{F}_2\text{N}$  ( $[\text{M}+\text{H}]^+$ ), 210.1089; found 210.1090.



#### Methyl 4-(1-tosyl-1H-indol-3-yl)but-2-ynoate (**91**):

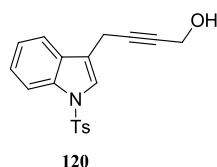
**Step 1:**<sup>77</sup> To a solution of 3-methyl-1H-indole (**108**) (10.9 g, 82.0 mmol, 1.00 equiv), *p*-toluenesulfonyl chloride (16.7 g, 87.0 mmol, 1.05 equiv), and tetrabutylammonium hydrogen sulfate (2.02 g, 5.77 mmol,  $7.00 \times 10^{-2}$  equiv) in toluene (0.330 L) at 0 °C was added a 50% aqueous KOH solution (0.330 L) dropwise upon vigorous stirring. The reaction was stirred for 1 h at rt before it was diluted with a 1:1  $\text{Et}_2\text{O}$ /water mixture. The aqueous phase was extracted with  $\text{Et}_2\text{O}$  and the combined organic extracts were washed with brine, dried over  $\text{Na}_2\text{SO}_4$ , filtered, and concentrated *in vacuo*. The resulting crude tosyl-protected indole (**119**) was isolated as a yellowish crystalline solid that was used as such in the next step.

**Step 2:**<sup>111</sup> To a suspension of the previously isolated indole (**119**) in  $\text{CCl}_4$  (412 mL) under inert atmosphere at rt were successively added *N*-bromosuccinimide (15.6 g, 87.0 mmol, 1.05 equiv) and azobisisobutyronitrile (2.07 g, 12.4 mmol,  $1.50 \times 10^{-1}$  equiv). The reaction mixture was then heated to reflux for 2 h before it was cooled down to rt and filtered over Celite<sup>®</sup>. The filtrate was concentrated *in vacuo* to afford bromide **106** as a yellow crystalline solid that was used as such in the next step.

**Step 3:**<sup>112</sup> To a stirred suspension of the previously isolated bromide (**106**), copper iodide (16.6 g, 86.0 mmol, 1.05 equiv), cesium carbonate (28.2 g, 86.0 mmol, 1.05 equiv), and

tetrabutylammonium iodide (32.3 g, 86.0 mmol, 1.05 equiv) in MeCN (824 mL) under inert atmosphere at rt was added methyl propiolate (**107**) (15.5 mL, 173 mmol, 2.10 equiv) dropwise. The reaction mixture was stirred at rt for 4.5 h before it was quenched with saturated aqueous NH<sub>4</sub>Cl. The aqueous phase was extracted with Et<sub>2</sub>O and the combined organic extracts were washed with brine, dried over Na<sub>2</sub>SO<sub>4</sub>, filtered, and concentrated *in vacuo*. The resulting crude material was purified by silica gel flash column chromatography (5:1 hexanes/EtOAc) to afford alkyne **91** that was recrystallized from hexane/CH<sub>2</sub>Cl<sub>2</sub>. Alkyne **91** was then isolated (14.3 g, 38.8 mmol, 47% over three steps) as a yellow crystalline solid (mp = 105 °C).

**TLC:**  $R_f$  = 0.11 (5:1 hexanes/EtOAc; UV, CAM). **<sup>1</sup>H NMR** (400 MHz, CDCl<sub>3</sub>): δ 8.01–7.96 (m, 1H), 7.80–7.75 (m, 2H), 7.54–7.52 (m, 1H), 7.52–7.48 (m, 1H), 7.37–7.32 (m, 1H), 7.29–7.20 (m, 3H), 3.79 (s, 3H), 3.74 (d,  $J$  = 1.3 Hz, 2H), 2.35 (s, 3H) ppm. **<sup>13</sup>C NMR** (100 MHz, CDCl<sub>3</sub>): δ 154.1, 145.2, 135.4, 135.3, 130.1, 129.6, 127.0, 125.3, 124.0, 123.4, 119.3, 115.6, 114.0, 85.0, 74.3, 52.9, 21.7, 15.8 ppm. **IR** (thin film): ν 2954, 2353, 2229, 1712, 1594, 1442, 1367, 1260, 1174, 1127, 1090, 974, 812, 754, 664, 577, 537 cm<sup>-1</sup>. **HRMS** (ESI<sup>+</sup>): exact mass calculated for C<sub>20</sub>H<sub>17</sub>NNaO<sub>4</sub>S ([M+Na]<sup>+</sup>), 390.0770; found 390.0778.



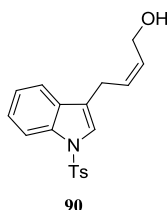
#### **4-(1-Tosyl-1H-indol-3-yl)but-2-yn-1-ol (120):**<sup>114</sup>

To a solution of methyl 4-(1-tosyl-1H-indol-3-yl)but-2-ynoate (**91**) (974 mg, 2.65 mmol, 1.00 equiv) in CH<sub>2</sub>Cl<sub>2</sub> (26.5 mL) under inert atmosphere at -10 °C was added diisobutylaluminium hydride (1 M, 5.83 mL, 5.83 mmol, 2.20 equiv) dropwise. The reaction was stirred at -10 °C for 1.5 h before it was quenched with MeOH and vigorously stirred overnight with saturated Rochelle's salt solution. The organic phase was successively washed with water, saturated aqueous NaHCO<sub>3</sub>, and brine, dried over Na<sub>2</sub>SO<sub>4</sub>, filtered, and concentrated *in vacuo*. The resulting crude material was purified by silica gel flash column chromatography (2:1 hexanes/EtOAc) to afford alcohol **120** (753 mg, 2.22 mmol, 84%) as a yellow oil.

**TLC:**  $R_f$  = 0.25 (1:1 hexanes/EtOAc; UV, CAM). **<sup>1</sup>H NMR** (400 MHz, CDCl<sub>3</sub>): δ 8.03–7.98 (m, 1H), 7.81–7.76 (m, 2H), 7.56–7.50 (m, 2H), 7.38–7.32 (m, 1H), 7.29–7.19 (m, 3H), 4.34



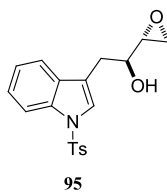
(bs, 2H), 3.66–3.61 (m, 2H), 2.34 (s, 3H), 1.84 (bs, 1H) ppm.  $^{13}\text{C}$  NMR (100 MHz,  $\text{CDCl}_3$ ):  $\delta$  144.9, 135.3, 129.9, 126.8, 124.9, 123.6, 123.2, 119.3, 118.0, 113.8, 82.2, 80.2, 51.3, 21.6, 15.6 ppm. IR (thin film):  $\nu$  3374, 3106, 3049, 2918, 2861, 1595, 1446, 1365, 1270, 1170, 1127, 1003, 970, 812, 745, 669, 573, 535  $\text{cm}^{-1}$ . HRMS (ESI+): exact mass calculated for  $\text{C}_{19}\text{H}_{18}\text{NO}_3\text{S}$  ( $[\text{M}+\text{H}]^+$ ), 340.1002; found 340.1003.



**(Z)-4-(1-Tosyl-1H-indol-3-yl)but-2-en-1-ol (90):**<sup>114</sup>

To a degassed solution of 4-(1-tosyl-1H-indol-3-yl)but-2-en-1-ol (**120**) (3.48 g, 10.3 mmol, 1.00 equiv) in EtOAc (103 mL), under inert atmosphere at rt was added Lindlar's catalyst (273 mg, 2.56 mmol, 2.50  $10^{-1}$  equiv). The reaction was then flushed with  $\text{H}_2$  and vigorously stirred at rt for 4 h before it was filtered over Celite<sup>®</sup> and the filtrate concentrated *in vacuo*. The crude material was purified by silica gel flash column chromatography (4:3 hexanes/EtOAc) to afford allylic alcohol **90** (3.30 g, 9.67 mmol, 94%) as a yellow oil.

**TLC:**  $R_f$  = 0.24 (1:1 hexanes/EtOAc; UV, CAM).  $^1\text{H}$  NMR (400 MHz,  $\text{CDCl}_3$ ):  $\delta$  8.03–7.98 (m, 1H), 7.79–7.74 (m, 2H), 7.51–7.46 (m, 1H), 7.37–7.31 (m, 2H), 7.28–7.19 (m, 3H), 5.87–5.75 (m, 2H), 4.34 (d,  $J$  = 5.5 Hz, 2H), 3.47 (d,  $J$  = 6.5 Hz, 2H), 2.35 (s, 3H), 1.50 (bs, 1H) ppm.  $^{13}\text{C}$  NMR (100 MHz,  $\text{CDCl}_3$ ):  $\delta$  144.8, 135.4, 135.3, 130.6, 130.4, 129.8, 128.8, 126.8, 124.8, 123.1, 123.0, 121.4, 119.4, 113.8, 58.6, 23.3, 21.6 ppm. IR (thin film):  $\nu$  3370, 3016, 3021, 2918, 2870, 2361, 2248, 1596, 1445, 1365, 1275, 1172, 1120, 1096, 1021, 974, 912, 813, 743, 667, 578, 533  $\text{cm}^{-1}$ . HRMS (ESI+): exact mass calculated for  $\text{C}_{19}\text{H}_{19}\text{NNaO}_3\text{S}$  ( $[\text{M}+\text{Na}]^+$ ), 364.0978; found 364.0975.

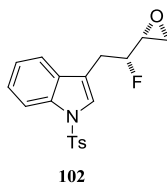


**(±)-Anti-1-(Oxiran-2-yl)-2-(1-tosyl-1H-indol-3-yl)ethanol (95):**

**Step 1:**<sup>109</sup> To a solution of (*Z*)-4-(1-tosyl-1*H*-indol-3-yl)but-2-en-1-ol (**90**) (3.20 g, 9.37 mmol, 1.00 equiv) in a 4:1 acetone/water mixture (134 mL) at rt were successively added *N*-methylmorpholine *N*-oxide (1.70 g, 14.1 mmol, 1.50 equiv) and osmium tetroxide (2.5% in *t*-BuOH, 3.88 mL, 3.10 10<sup>-4</sup> mol, 3.00 10<sup>-2</sup> equiv). After stirring for 24 h at rt, the reaction was quenched with saturated aqueous Na<sub>2</sub>S<sub>2</sub>O<sub>3</sub> and stirred for 45 min at rt. The resulting mixture was then extracted with EtOAc, and the combined organic extracts were washed with brine, dried over Na<sub>2</sub>SO<sub>4</sub>, filtered, and concentrated *in vacuo*. The resulting crude material was purified by silica gel flash column chromatography (100% EtOAc) to afford triol **97** as a colorless syrup (3.08 g) that was used as such in the next step.

**Step 2:**<sup>108</sup> To a solution of the previously isolated triol (**97**, 3.08 g) in MeCN (82.0 mL) under inert atmosphere at rt was added triethylamine (3.43 mL, 24.6 mmol, 3.00 equiv). The resulting solution was cooled down to 0 °C before perfluorobutanesulfonyl fluoride (2.31 mL, 12.3 mmol, 1.50 equiv) was added dropwise. The reaction was stirred for 10 min at rt before it was quenched with saturated aqueous NaHCO<sub>3</sub>. The aqueous phase was extracted with EtOAc and the combined organic extracts were washed with brine, dried over Na<sub>2</sub>SO<sub>4</sub>, filtered, and concentrated *in vacuo*. The resulting crude material was purified by silica gel flash column chromatography (5:3 hexanes/EtOAc) to afford epoxyalcohol **95** (1.83 g, 5.12 mmol, 54% over two steps) as a colorless syrup.

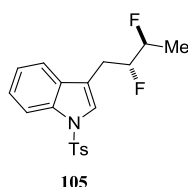
**TLC:** *R<sub>f</sub>* = 0.22 (5:3 hexanes/EtOAc; UV, CAM). **<sup>1</sup>H NMR** (400 MHz, CDCl<sub>3</sub>): δ 8.04–8.00 (m, 1H), 7.80–7.76 (m, 2H), 7.57–7.53 (m, 1H), 7.51 (s, 1H), 7.38–7.32 (m, 1H), 7.29–7.21 (m, 3H), 4.11–4.05 (m, 1H), 3.06–2.91 (m, 3H), 2.70–2.80 (m, 2H), 2.36 (s, 3H), 1.88 (d, *J* = 2.7 Hz, 1H) ppm. **<sup>13</sup>C NMR** (100 MHz, CDCl<sub>3</sub>): δ 144.9, 135.3, 135.2, 131.0, 129.8, 126.8, 124.8, 124.4, 123.2, 119.6, 118.1, 113.8, 68.4, 53.9, 43.9, 29.3, 21.6 ppm. **IR** (thin film): ν 3450, 3104, 3047, 2990, 2923, 2352, 1595, 1443, 1358, 1276, 1172, 1119, 1090, 971, 809, 743, 671, 571, 603 cm<sup>-1</sup>. **HRMS** (ESI<sup>+</sup>): exact mass calculated for C<sub>19</sub>H<sub>19</sub>NNaO<sub>4</sub>S ([M+Na]<sup>+</sup>), 380.0927; found 380.0937.



**(±)-Syn-3-(2-Fluoro-2-(oxiran-2-yl)ethyl)-1-tosyl-1H-indole (102):**<sup>80</sup>

To a solution of 1-(oxiran-2-yl)-2-(1-tosyl-1H-indol-3-yl)ethanol (**95**) (1.81 g, 5.06 mmol, 1.00 equiv) and triethylamine (3.17 mL, 22.8 mmol, 4.50 equiv) in MeCN (51.0 mL) under inert atmosphere at rt were successively added triethylamine trihydrofluoride (2.10 mL, 12.7 mmol, 2.50 equiv) and perfluorobutanesulfonyl fluoride (2.87 mL, 15.2 mmol, 3.00 equiv) dropwise. The reaction was stirred at 0 °C for 1 h before it was quenched with saturated aqueous NaHCO<sub>3</sub>. The aqueous phase was extracted with EtOAc and the combined organic extracts were washed with brine, dried over Na<sub>2</sub>SO<sub>4</sub>, filtered, and concentrated *in vacuo*. The resulting crude material was purified by silica gel flash column chromatography (5:1 hexanes/EtOAc) to afford fluoroepoxide **102** (686 mg, 1.91 mmol, 38%) as a yellow oil.

**TLC:**  $R_f$  = 0.35 (5:3 hexanes/EtOAc; UV, CAM). **<sup>1</sup>H NMR** (400 MHz, CDCl<sub>3</sub>): δ 8.05–8.00 (m, 1H), 7.80–7.74 (m, 2H), 7.54–7.49 (m, 2H), 7.39–7.33 (m, 1H), 7.31–7.21 (m, 3H), 7.67–7.47 (m, 1H), 3.26–3.05 (m, 3H), 2.80–2.74 (m, 1H), 2.63–2.58 (m, 1H), 2.36 (s, 3H) ppm. **<sup>13</sup>C NMR** (100 MHz, CDCl<sub>3</sub>): δ 145.0, 135.2, 135.1, 130.6, 129.9, 126.8, 125.0, 124.6 (d,  $J$  = 1.7 Hz), 123.3, 119.3 (d,  $J$  = 1.1 Hz), 116.8 (d,  $J$  = 6.3 Hz), 113.8, 92.0 (d,  $J$  = 178.1 Hz), 52.5 (d,  $J$  = 23.7 Hz), 43.9 (d,  $J$  = 9.0 Hz), 27.9 (d,  $J$  = 24.5 Hz), 21.6 ppm. **<sup>19</sup>F NMR** (376 MHz, CDCl<sub>3</sub>, decoupled): δ -185.46 (s) ppm. **<sup>19</sup>F NMR** (376 MHz, CDCl<sub>3</sub>, not decoupled): δ -185.29 – -185.63 (m) ppm. **IR** (thin film): ν 3104, 3056, 2999, 2915, 2857, 1595, 1445, 1366, 1172, 1119, 1095, 1014, 971, 809, 747, 669, 571, 538 cm<sup>-1</sup>. **HRMS** (ESI<sup>+</sup>): exact mass calculated for C<sub>19</sub>H<sub>19</sub>FNO<sub>3</sub>S ([M+H]<sup>+</sup>), 360.1064; found 360.1065.



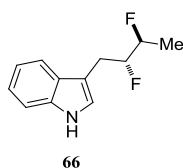
**(±)-Erythro-3-(2,3-Difluorobutyl)-1-tosyl-1H-indole (105):**

**Step 1:**<sup>115</sup> To a suspension of lithium aluminium hydride (99.0 mg, 6.62 mmol, 5.00 equiv) in THF (5.23 mL) under inert atmosphere at 0 °C was added a solution of 3-(2-fluoro-2-(oxiran-

2-yl)ethyl)-1-tosyl-1*H*-indole (**102**) (188 mg,  $5.20 \cdot 10^{-4}$  mol, 1.00 equiv) in THF (5.23 mL) dropwise. The reaction was stirred at rt for 3 h before Na<sub>2</sub>SO<sub>4</sub> (ca. 1 g) was added. Water was then added dropwise until the suspension turned white. After filtration of the suspension, the filtrate was concentrated *in vacuo* and the resulting crude material was purified by silica gel flash column chromatography (5:2 hexanes/EtOAc) to afford alcohol **100** as a colorless oil (172 mg) that was used as such in the next step.

**Step 2:**<sup>80</sup> To a solution of the previously isolated alcohol (**100**, 172 mg) and triethylamine (298  $\mu$ L, 2.14 mmol, 4.50 equiv) in MeCN (4.76 mL) under inert atmosphere at 0 °C were successively added triethylamine trihydrofluoride (119  $\mu$ L,  $7.10 \cdot 10^{-4}$  mol, 1.50 equiv) and perfluorobutanesulfonyl fluoride (178  $\mu$ L,  $9.50 \cdot 10^{-4}$  mol, 2.00 equiv) dropwise. The reaction was stirred at rt for 1 h before it was quenched with saturated aqueous NaHCO<sub>3</sub>. The aqueous phase was extracted with EtOAc and the combined organic extracts were washed with brine, dried over Na<sub>2</sub>SO<sub>4</sub>, filtered, and concentrated *in vacuo*. The resulting crude material was purified by silica gel flash column chromatography (10:1 hexanes/EtOAc) to afford difluoride **105** (123 mg,  $3.40 \cdot 10^{-4}$  mol, 65% over two steps) as a colorless oil.

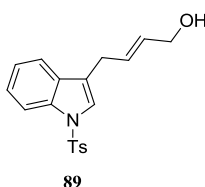
**TLC:**  $R_f$  = 0.44 (2:1 hexanes/EtOAc; UV, CAM). **<sup>1</sup>H NMR** (400 MHz, CDCl<sub>3</sub>):  $\delta$  8.01–7.97 (m, 1H), 7.77–7.73 (m, 2H), 7.51–7.47 (m, 2H), 7.35–7.30 (m, 1H), 7.27–7.19 (m, 3H), 4.78–4.52 (m, 2H), 3.12–3.00 (m, 2H), 2.34 (s, 3H), 1.42 (ddd,  $J$  = 24.5 Hz,  $J$  = 6.2 Hz,  $J$  = 1.7 Hz, 3H) ppm. **<sup>13</sup>C NMR** (100 MHz, CDCl<sub>3</sub>):  $\delta$  144.9, 135.3, 135.1, 130.8, 129.8, 126.8, 124.8, 124.6 (d,  $J$  = 1.3 Hz), 123.2, 119.4 (d,  $J$  = 1.7 Hz), 117.2 (d,  $J$  = 2.5 Hz), 113.8, 93.1 (dd,  $J$  = 176.8 Hz,  $J$  = 25.7 Hz), 89.3 (dd,  $J$  = 170.6 Hz,  $J$  = 25.9 Hz), 26.2 (dd,  $J$  = 22.2 Hz,  $J$  = 5.0 Hz), 21.6, 16.3 (dd,  $J$  = 22.4 Hz,  $J$  = 4.7 Hz) ppm. **<sup>19</sup>F NMR** (376 MHz, CDCl<sub>3</sub>, decoupled):  $\delta$  -185.00 (d,  $J$  = 14.4 Hz), -189.73 (d,  $J$  = 14.4 Hz) ppm. **<sup>19</sup>F NMR** (376 MHz, CDCl<sub>3</sub>, not decoupled):  $\delta$  -184.80 – -185.22 (m), -189.54 – -189.92 (m) ppm. **IR** (thin film):  $\nu$  3114, 3055, 2954, 2921, 2352, 1645, 1445, 1364, 1172, 1115, 1096, 972, 810, 743, 671, 571, 532 cm<sup>-1</sup>. **HRMS** (ESI+): exact mass calculated for C<sub>19</sub>H<sub>20</sub>F<sub>2</sub>NO<sub>2</sub>S ([M+H]<sup>+</sup>), 364.1177; found 364.1177.



**(±)-Erythro-3-(2,3-Difluorobutyl)-1H-indole (66):**<sup>116</sup>

A suspension of *erythro*-3-(2,3-difluorobutyl)-1-tosyl-1H-indole (**105**) (123 mg, 3.40  $10^{-4}$  mol, 1.00 equiv) and magnesium turnings (82.0 mg, 3.38 mmol, 10.0 equiv) in MeOH (3.40 mL) at rt was stirred vigorously overnight. The reaction was then quenched with saturated aqueous  $\text{NH}_4\text{Cl}$  and further diluted with water. The aqueous phase was extracted with EtOAc and the combined organic extracts were washed with brine, dried over  $\text{Na}_2\text{SO}_4$ , filtered, and concentrated *in vacuo*. The resulting crude material was purified by silica gel flash column chromatography (10:1 hexanes/EtOAc) to afford indole **66** (53.0 mg, 2.50  $10^{-4}$  mol, 75%) as a colorless oil.

**TLC:**  $R_f$  = 0.44 (2:1 hexanes/EtOAc; UV, CAM, *p*-anisaldehyde).  **$^1\text{H}$  NMR** (400 MHz,  $\text{CDCl}_3$ ):  $\delta$  8.04 (bs, 1H), 7.61 (d,  $J$  = 7.7 Hz, 1H), 7.40–7.36 (m, 1H), 7.25–7.19 (m, 1H), 7.18–7.10 (m, 2H), 4.89–4.59 (m, 2H), 3.21–3.10 (m, 2H), 1.49–1.39 (m, 3H) ppm.  **$^{13}\text{C}$  NMR** (100 MHz,  $\text{CDCl}_3$ ):  $\delta$  136.1, 127.5, 122.9, 122.2, 119.6, 118.7 (d,  $J$  = 1.3 Hz), 111.2, 110.5 (d,  $J$  = 3.9 Hz), 94.0 (dd,  $J$  = 176.1 Hz,  $J$  = 24.8 Hz), 89.6 (dd,  $J$  = 169.9 Hz,  $J$  = 25.2 Hz), 26.5 (dd,  $J$  = 22.1 Hz,  $J$  = 5.4 Hz), 15.8 (dd,  $J$  = 22.6 Hz,  $J$  = 5.2 Hz) ppm.  **$^{19}\text{F}$  NMR** (376 MHz,  $\text{CDCl}_3$ , decoupled):  $\delta$  -184.13 (d,  $J$  = 14.3 Hz), -190.44 (d,  $J$  = 14.3 Hz) ppm.  **$^{19}\text{F}$  NMR** (376 MHz,  $\text{CDCl}_3$ , not decoupled):  $\delta$  -183.92 – -184.35 (m), -190.25 – -190.63 (m) ppm. **IR** (thin film):  $\nu$  3451, 3412, 2992, 2915, 2351, 1650, 1454, 1421, 1330, 1225, 1144, 1092, 1053, 972, 919, 738, 580  $\text{cm}^{-1}$ . **HRMS** (ESI+): exact mass calculated for  $\text{C}_{12}\text{H}_{14}\text{F}_2\text{N}$  ( $[\text{M}+\text{H}]^+$ ), 210.1089; found 210.1089.

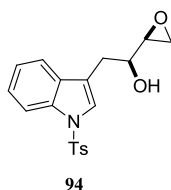


**(E)-4-(1-Tosyl-1H-indol-3-yl)but-2-en-1-ol (89):**<sup>113</sup>

To a suspension of lithium aluminium hydride (2.98 g, 79.0 mmol, 4.00 equiv) in THF (98.0 mL) under inert atmosphere at 0 °C was added a solution of methyl 4-(1-tosyl-1H-indol-3-yl)but-2-ynoate (**91**) in THF (98.0 mL) dropwise. The reaction was stirred at rt for 6 h before

Na<sub>2</sub>SO<sub>4</sub> (ca. 10 g) was added portionwise. Water was then added dropwise until the suspension turned white. After filtration of the suspension, the filtrate was concentrated *in vacuo* and the resulting crude material was purified by silica gel flash column chromatography (2:1 hexanes/EtOAc) to afford allylic alcohol **89** (5.24 g, 15.4 mmol, 78%) as a yellowish syrup.

**TLC:**  $R_f = 0.29$  (1:1 hexanes/EtOAc; UV, CAM). **<sup>1</sup>H NMR** (400 MHz, CDCl<sub>3</sub>):  $\delta$  8.00–7.95 (m, 1H), 7.77–7.72 (m, 2H), 7.48–7.44 (m, 1H), 7.34–7.28 (m, 2H), 7.25–7.18 (m, 3H), 5.92–5.83 (m 1H), 5.78–5.70 (m, 1H), 4.17–4.09 (m, 2H), 3.45–3.39 (m, 2H), 2.34 (s, 3H), 1.32 (s, 1H) ppm. **<sup>13</sup>C NMR** (100 MHz, CDCl<sub>3</sub>):  $\delta$  144.8, 135.4, 131.1, 130.7, 129.8, 129.1, 126.8, 124.7, 123.2, 123.0, 121.1, 119.6, 113.7, 63.4, 27.9, 21.6 ppm. **IR** (thin film):  $\nu$  3364, 2925, 2867, 1445, 1363, 1172, 1115, 1091, 967, 743, 668, 572, 534 cm<sup>-1</sup>. **HRMS** (ESI<sup>+</sup>): exact mass calculated for C<sub>19</sub>H<sub>20</sub>NO<sub>3</sub>S ([M+H]<sup>+</sup>), 342.1158; found 342.1156.



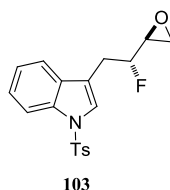
**(±)-Syn-1-(Oxiran-2-yl)-2-(1-tosyl-1H-indol-3-yl)ethanol (94):**

**Step 1:**<sup>109</sup> To a solution of (*E*)-4-(1-tosyl-1H-indol-3-yl)but-2-en-1-ol (**89**) (5.24 g, 15.4 mmol, 1.00 equiv) in a 4:1 acetone/water mixture (219 mL) at rt were successively added *N*-methylmorpholine *N*-oxide (2.84 g, 23.0 mmol, 1.50 equiv) and osmium tetroxide (2.5% in *t*-BuOH, 3.97 mL, 5.10 10<sup>-4</sup> mol, 3.00 10<sup>-2</sup> equiv). After stirring for 24 h at rt, the reaction was quenched with saturated aqueous Na<sub>2</sub>S<sub>2</sub>O<sub>3</sub> and stirred for 45 min at rt. The resulting mixture was then extracted with EtOAc, and the combined organic extracts were washed with brine, dried over Na<sub>2</sub>SO<sub>4</sub>, filtered, and concentrated *in vacuo*. The resulting crude material was purified by silica gel flash column chromatography (100% EtOAc) to afford triol **96** as a white foam that was used as such in the next step.

**Step 2:**<sup>108</sup> To a solution of the previously isolated triol (**97**) in MeCN (153 mL) under inert atmosphere at rt was added triethylamine (6.55 mL, 46.0 mmol, 3.00 equiv). The resulting solution was cooled down to 0 °C before perfluorobutanesulfonyl fluoride (4.31 mL, 23.0 mmol, 1.50 equiv) was added dropwise. The reaction was stirred for 10 min at rt before it was quenched with saturated aqueous NaHCO<sub>3</sub>. The aqueous phase was extracted with EtOAc and

the combined organic extracts were washed with brine, dried over Na<sub>2</sub>SO<sub>4</sub>, filtered, and concentrated *in vacuo*. The resulting crude material was purified by silica gel flash column chromatography (5:3 hexanes/EtOAc) to afford epoxyalcohol **94** (2.67 g, 7.47 mmol, 49% over two steps) as a white foam.

**TLC:**  $R_f$  = 0.22 (5:3 hexanes/EtOAc; UV, CAM). **<sup>1</sup>H NMR** (400 MHz, CDCl<sub>3</sub>): δ 8.02–7.97 (m, 1H), 7.77–7.72 (m, 2H), 7.53–7.49 (m, 1H), 7.48 (s, 1H), 7.35–7.30 (m, 1H), 7.27–7.18 (m, 3H), 3.84–3.76 (m, 1H), 3.05–2.93 (m, 3H), 2.72–2.68 (m, 1H), 2.62–2.58 (m, 1H), 2.33 (s, 3H), 1.98 (d,  $J$  = 6.1 Hz, 1H) ppm. **<sup>13</sup>C NMR** (100 MHz, CDCl<sub>3</sub>): δ 144.9, 135.3, 135.2, 130.9, 129.8, 126.8, 124.9, 124.4, 123.2, 119.4, 118.1, 113.8, 70.5, 54.5, 45.0, 30.3, 21.6 ppm. **IR** (thin film): ν 3420, 3101, 3055, 2992, 2919, 1594, 1444, 1362, 1171, 1116, 1089, 975, 742, 672, 570 cm<sup>-1</sup>. **HRMS** (ESI<sup>+</sup>): exact mass calculated for C<sub>19</sub>H<sub>19</sub>NNaO<sub>4</sub>S ([M+Na]<sup>+</sup>), 380.0927; found 380.0919.

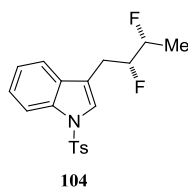


**(±)-Anti-3-(2-Fluoro-2-(oxiran-2-yl)ethyl)-1-tosyl-1H-indole (103):**<sup>80</sup>

To a solution of 1-(oxiran-2-yl)-2-(1-tosyl-1H-indol-3-yl)ethanol (**94**) (2.67 g, 7.47 mmol, 1.00 equiv) and triethylamine (4.69 mL, 33.6 mmol, 4.50 equiv) in MeCN (75.0 mL) under inert atmosphere at rt were successively added triethylamine trihydrofluoride (3.10 mL, 18.7 mmol, 2.50 equiv) and perfluorobutanesulfonyl fluoride (4.24 mL, 22.4 mmol, 3.00 equiv) dropwise. The reaction was stirred at 0 °C for 1 h before it was quenched with saturated aqueous NaHCO<sub>3</sub>. The aqueous phase was extracted with EtOAc and the combined organic extracts were washed with brine, dried over Na<sub>2</sub>SO<sub>4</sub>, filtered, and concentrated *in vacuo*. The resulting crude material was purified by silica gel flash column chromatography (10:3 hexanes/EtOAc) to afford fluoroepoxide **103** (0.710 g, 1.98 mmol, 26%) as a yellow oil.

**TLC:**  $R_f$  = 0.35 (5:3 hexanes/EtOAc; UV, CAM). **<sup>1</sup>H NMR** (400 MHz, CDCl<sub>3</sub>): δ 8.01–7.97 (m, 1H), 7.78–7.72 (m, 2H), 7.53–7.48 (m, 2H), 7.35–7.30 (m, 1H), 7.28–7.18 (m, 3H), 4.64–4.46 (m, 1H), 3.18–3.02 (m, 3H), 2.83–2.71 (m, 2H), 2.33 (s, 3H) ppm. **<sup>13</sup>C NMR** (100 MHz, CDCl<sub>3</sub>): δ 145.0, 135.4, 135.2, 131.0, 130.0, 126.9, 125.0, 124.8 (d,  $J$  = 1.1 Hz), 123.4, 119.6 (d,  $J$  = 1.8 Hz), 117.0 (d,  $J$  = 2.8 Hz), 113.9, 91.7 (d,  $J$  = 176.2 Hz), 51.8 (d,  $J$  = 30.5 Hz),

45.6 (d,  $J = 4.4$  Hz), 28.2 (d,  $J = 22.7$  Hz), 21.7 ppm.  $^{19}\text{F}$  NMR (376 MHz,  $\text{CDCl}_3$ , decoupled):  $\delta$  -188.12 (s) ppm.  $^{19}\text{F}$  NMR (376 MHz,  $\text{CDCl}_3$ , not decoupled):  $\delta$  -188.12 (dtd,  $J = 49.8$  Hz,  $J = 25.6$  Hz,  $J = 9.1$  Hz) ppm. IR (thin film):  $\nu$  3109, 3050, 2991, 2924, 1445, 1363, 1170, 1119, 1098, 968, 744, 669, 572  $\text{cm}^{-1}$ . HRMS (ESI+): exact mass calculated for  $\text{C}_{19}\text{H}_{19}\text{FNO}_3\text{S}$  ( $[\text{M}+\text{H}]^+$ ), 360.1064; found 360.1069.



**(±)-Threo-3-(2,3-Difluorobutyl)-1-tosyl-1H-indole (104):**

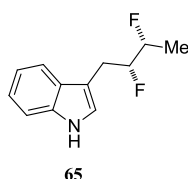
**Step 1:**<sup>115</sup> To a suspension of lithium aluminium hydride (375 mg, 9.88 mmol, 5.00 equiv) in THF (9.88 mL) under inert atmosphere at 0 °C was added a solution of 3-(2-fluoro-2-(oxiran-2-yl)ethyl)-1-tosyl-1H-indole (**103**) (0.710 g, 1.98 mmol, 1.00 equiv) in THF (9.88 mL) dropwise. The reaction was stirred at rt for 3 h before  $\text{Na}_2\text{SO}_4$  (ca. 3 g) was added. Water was then added dropwise until the suspension turned white. After filtration of the suspension, the filtrate was concentrated *in vacuo* and the resulting crude material was purified by silica gel flash column chromatography (5:2 hexanes/EtOAc) to afford alcohol **101** as a white crystalline solid (0.600 g) that was used as such in the next step.

**Step 2:**<sup>80</sup> To a solution of the previously isolated alcohol (**101**, 0.600 g) and triethylamine (1.04 mL, 7.47 mmol, 4.50 equiv) in MeCN (16.6 mL) under inert atmosphere at 0 °C were successively added triethylamine trihydrofluoride (414  $\mu\text{L}$ , 2.49 mmol, 1.50 equiv) and perfluorobutanesulfonyl fluoride (622  $\mu\text{L}$ , 3.32 mmol, 2.00 equiv) dropwise. The reaction was stirred at rt for 1 h before it was quenched with saturated aqueous  $\text{NaHCO}_3$ . The aqueous phase was extracted with EtOAc and the combined organic extracts were washed with brine, dried over  $\text{Na}_2\text{SO}_4$ , filtered, and concentrated *in vacuo*. The resulting crude material was purified by silica gel flash column chromatography (10:1 hexanes/EtOAc) to afford difluoride **104** (334 mg,  $9.20 \cdot 10^{-4}$  mol, 46% over two steps) as a colorless oil.

**TLC:**  $R_f = 0.44$  (2:1 hexanes/EtOAc; UV, CAM).  $^1\text{H}$  NMR (400 MHz,  $\text{CDCl}_3$ ):  $\delta$  8.02–7.97 (m, 1H), 7.79–7.72 (m, 2H), 7.54–7.47 (m, 2H), 7.36–7.30 (m, 1H), 7.29–7.18 (m, 3H), 7.74–7.47 (m, 2H), 3.21–3.01 (m, 2H), 2.34 (s, 3H), 1.47–1.36 (m, 3H) ppm.  $^{13}\text{C}$  NMR (100 MHz,  $\text{CDCl}_3$ ):  $\delta$  145.1, 135.3, 130.8, 130.0, 126.9, 125.0, 124.7, 123.4, 119.5, 117.3 (d,  $J = 6.5$  Hz),



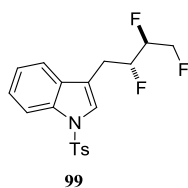
113.9, 93.1 (dd,  $J = 180.9$  Hz,  $J = 20.4$  Hz), 88.9 (dd,  $J = 174.6$  Hz,  $J = 20.7$  Hz), 26.4 (dd,  $J = 24.0$  Hz,  $J = 6.0$  Hz), 21.7, 16.4 (dd,  $J = 23.2$  Hz, 5.9 Hz) ppm.  $^{19}\text{F}$  NMR (376 MHz,  $\text{CDCl}_3$ , decoupled):  $\delta$  -191.49 (d,  $J = 10.5$  Hz), -194.05 (d,  $J = 10.5$  Hz) ppm.  $^{19}\text{F}$  NMR (376 MHz,  $\text{CDCl}_3$ , not decoupled):  $\delta$  -191.27 – -191.71 (m), -193.86 – -194.25 (m) ppm. **IR** (thin film):  $\nu$  2937, 1596, 1447, 1369, 1173, 1121, 974, 746, 668, 571  $\text{cm}^{-1}$ . **HRMS** (ESI+): exact mass calculated for  $\text{C}_{19}\text{H}_{20}\text{F}_2\text{NO}_2\text{S}$  ( $[\text{M}+\text{H}]^+$ ), 364.1177; found 364.1177.



(±)-**Threo-3-(2,3-Difluorobutyl)-1H-indole (65)**:<sup>116</sup>

A suspension of *threo*-3-(2,3-difluorobutyl)-1-tosyl-1H-indole (**104**) (334 mg,  $9.20 \times 10^{-4}$  mol, 1.00 equiv) and magnesium turnings (223 mg, 9.19 mmol, 10.0 equiv) in MeOH (9.20 mL) at rt was stirred vigorously overnight. The reaction was then quenched with saturated aqueous  $\text{NH}_4\text{Cl}$  and further diluted with water. The aqueous phase was extracted with EtOAc and the combined organic extracts were washed with brine, dried over  $\text{Na}_2\text{SO}_4$ , filtered, and concentrated *in vacuo*. The resulting crude material was purified by silica gel flash column chromatography (10:1 hexanes/EtOAc) to afford indole **65** (117 mg,  $5.60 \times 10^{-4}$  mol, 61%) as a colorless oil.

**TLC**:  $R_f = 0.45$  (2:1 hexanes/EtOAc; UV, CAM, *p*-anisaldehyde).  $^1\text{H}$  NMR (400 MHz,  $\text{CDCl}_3$ ):  $\delta$  8.13–7.89 (bs, 1H), 7.67 (d,  $J = 7.8$  Hz, 1H), 7.38 (d,  $J = 8.1$  Hz, 1H), 7.29–7.23 (m, 1H), 7.22–7.16 (m, 1H), 7.13–7.08 (m, 1H), 4.82–4.56 (m, 2H), 3.26 (dd,  $J = 19.2$  Hz,  $J = 6.7$  Hz, 2H), 1.44 (dd,  $J = 23.4$  Hz,  $J = 6.5$  Hz, 3H) ppm.  $^{13}\text{C}$  NMR (100 MHz,  $\text{CDCl}_3$ ):  $\delta$  136.3, 127.5, 123.3, 122.3, 119.8, 118.7, 111.4, 110.2 (d,  $J = 8.2$  Hz), 94.1 (dd,  $J = 179.7$  Hz,  $J = 19.6$  Hz), 89.0 (dd,  $J = 173.6$  Hz,  $J = 20.2$  Hz), 26.6 (dd,  $J = 23.8$  Hz,  $J = 5.9$  Hz), 16.5 (dd,  $J = 23.2$  Hz,  $J = 6.0$  Hz) ppm.  $^{19}\text{F}$  NMR (376 MHz,  $\text{CDCl}_3$ , decoupled):  $\delta$  -191.74 (d,  $J = 11.4$  Hz), -193.16 (d,  $J = 11.4$  Hz) ppm.  $^{19}\text{F}$  NMR (376 MHz,  $\text{CDCl}_3$ , not decoupled):  $\delta$  -191.49 – -191.98 (m), -193.36 – 192.95 (m) ppm. **IR** (thin film):  $\nu$  3453, 3415, 2990, 2918, 2358, 1651, 1456, 1420, 1327, 1223, 1141, 1090, 1058, 972, 918, 737, 582  $\text{cm}^{-1}$ . **HRMS** (ESI+): exact mass calculated for  $\text{C}_{12}\text{H}_{14}\text{F}_2\text{N}$  ( $[\text{M}+\text{H}]^+$ ), 210.1089; found 210.1089.



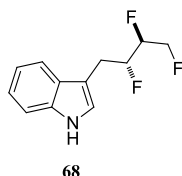
**(±)-Erythro-1-Tosyl-3-(2,3,4-trifluorobutyl)-1H-indole (99):**

**Step 1:**<sup>102</sup> A vigorously stirred mixture of 3-(2-fluoro-2-(oxiran-2-yl)ethyl)-1-tosyl-1H-indole (**102**) (686 mg, 1.91 mmol, 1.00 equiv) and triethylamine trihydrofluoride (693  $\mu$ L, 4.17 mmol, 2.20 equiv) was heated at 150 °C for 3 h. After cooling down to rt, the reaction was diluted with a 1:1 water/EtOAc mixture and the aqueous phase was further extracted with EtOAc. The combined organic extracts were washed with brine, dried over Na<sub>2</sub>SO<sub>4</sub>, filtered, and concentrated *in vacuo*. The resulting crude material was purified by silica gel flash column chromatography (5:2 hexanes/EtOAc) to afford fluorohydrin **121** as an orange syrup (651 mg) that was used as such in the next step.

**Step 2:**<sup>80</sup> To a solution of the previously isolated fluorohydrin (**121**, 651 mg) and triethylamine (1.08 mL, 7.72 mmol, 4.50 equiv) in MeCN (17.2 mL) under inert atmosphere at 0 °C were successively added triethylamine trihydrofluoride (428  $\mu$ L, 2.57 mmol, 1.50 equiv) and perfluorobutanesulfonyl fluoride (0.650 mL, 3.43 mmol, 2.00 equiv) dropwise. The reaction was stirred at rt for 1 h before it was quenched with saturated aqueous NaHCO<sub>3</sub>. The aqueous phase was extracted with EtOAc and the combined organic extracts were washed with brine, dried over Na<sub>2</sub>SO<sub>4</sub>, filtered, and concentrated *in vacuo*. The resulting crude material was purified by silica gel flash column chromatography (10:1 hexanes/EtOAc) to afford trifluoride **99** (526 mg, 1.38 mmol, 72% over two steps) as a colorless oil.

**TLC:**  $R_f$  = 0.20 (5:1 hexanes/EtOAc; UV, CAM). **<sup>1</sup>H NMR** (400 MHz, CDCl<sub>3</sub>):  $\delta$  8.04–8.01 (m, 1H), 7.80–7.76 (m, 2H), 7.55–7.51 (m, 2H), 7.39–7.33 (m, 1H), 7.31–7.26 (m, 1H), 7.26–7.22 (m, 2H), 5.06–4.86 (m, 1H), 4.83–4.43 (m, 3H), 3.34–3.05 (m, 2H), 2.36 (s, 3H) ppm. **<sup>13</sup>C NMR** (100 MHz, CDCl<sub>3</sub>):  $\delta$  145.0, 135.2, 135.1, 130.8, 129.9, 126.8, 125.0, 124.9, 123.3, 119.5 (d,  $J$  = 2.2 Hz), 116.3 (d,  $J$  = 1.9 Hz), 113.8, 89.7 (ddd,  $J$  = 178.1 Hz,  $J$  = 28.7 Hz,  $J$  = 19.0 Hz), 88.0 (ddd,  $J$  = 175.2 Hz,  $J$  = 28.2 Hz,  $J$  = 6.6 Hz), 80.9 (ddd,  $J$  = 174.6 Hz,  $J$  = 21.5 Hz,  $J$  = 4.1 Hz), 26.6 (dd,  $J$  = 21.4 Hz,  $J$  = 2.9 Hz), 21.6 ppm. **<sup>19</sup>F NMR** (376 MHz, CDCl<sub>3</sub>, decoupled):  $\delta$  -191.5 (d,  $J$  = 15.0 Hz), -200.25 (dd,  $J$  = 15.0 Hz,  $J$  = 11.6 Hz), -236.04 (d,  $J$  = 11.6 Hz) ppm. **<sup>19</sup>F NMR** (376 MHz, CDCl<sub>3</sub>, not decoupled):  $\delta$  -191.16 – -191.55 (m), -200.05 – -200.45 (m), -236.04 (tdd,  $J$  = 47.2 Hz,  $J$  = 24.2 Hz,  $J$  = 11.6 Hz) ppm. **IR** (thin film):  $\nu$  3114, 3055, 2954, 2921, 1592, 1445, 1365, 1281, 1172, 1118, 1097, 1017, 971, 811, 744, 664,

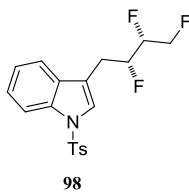
573, 534  $\text{cm}^{-1}$ . **HRMS** (ESI+): exact mass calculated for  $\text{C}_{19}\text{H}_{19}\text{F}_3\text{NO}_2\text{S}$  ( $[\text{M}+\text{H}]^+$ ), 382.1083; found 382.1087.



**(±)-Erythro-3-(2,3,4-Trifluorobutyl)-1H-indole (68):**<sup>116</sup>

A suspension of *erythro*-1-tosyl-3-(2,3,4-trifluorobutyl)-1*H*-indole (**99**) (208 mg, 5.50  $10^{-4}$  mol, 1.00 equiv) and magnesium turnings (133 mg, 5.45 mmol, 10.0 equiv) in MeOH (5.45 mL) at rt was stirred vigorously overnight. The reaction was then quenched with saturated aqueous  $\text{NH}_4\text{Cl}$  and further diluted with water. The aqueous phase was extracted with EtOAc and the combined organic extracts were washed with brine, dried over  $\text{Na}_2\text{SO}_4$ , filtered, and concentrated *in vacuo*. The resulting crude material was purified by silica gel flash column chromatography (10:1 hexanes/EtOAc) to afford indole **68** (93.0 mg, 4.10  $10^{-4}$  mol, 75%) as a colorless oil.

**TLC:**  $R_f = 0.38$  (2:1 hexanes/EtOAc; UV, CAM, *p*-anisaldehyde).  **$^1\text{H}$  NMR** (400 MHz,  $\text{CDCl}_3$ ):  $\delta$  8.07 (bs, 1H), 7.63 (d,  $J = 7.9$  Hz, 1H), 7.41–7.37 (m, 1H), 7.25–7.20 (m, 1H), 7.19–7.12 (m, 2H), 5.08–4.89 (m, 1H), 4.81–4.51 (m, 3H), 3.40–3.13 (m, 2H) ppm.  **$^{13}\text{C}$  NMR** (100 MHz,  $\text{CDCl}_3$ ):  $\delta$  136.1, 127.6, 123.4, 122.3, 119.8, 118.8 (d,  $J = 1.6$  Hz), 111.2, 109.4 (d,  $J = 3.0$  Hz), 90.0 (ddd,  $J = 176.8$  Hz,  $J = 28.1$  Hz,  $J = 19.0$  Hz), 89.2 (ddd,  $J = 173.9$  Hz,  $J = 27.6$  Hz,  $J = 6.6$  Hz), 81.2 (ddd,  $J = 173.5$  Hz,  $J = 21.7$  Hz,  $J = 4.5$  Hz), 26.8 (dd,  $J = 21.4$  Hz,  $J = 3.3$  Hz) ppm.  **$^{19}\text{F}$  NMR** (376 MHz,  $\text{CDCl}_3$ , decoupled):  $\delta$  -191.47 (d,  $J = 14.5$  Hz), -199.64 – -199.74 (m), -235.54 (d,  $J = 12.3$  Hz) ppm.  **$^{19}\text{F}$  NMR** (376 MHz,  $\text{CDCl}_3$ , not decoupled):  $\delta$  -191.28 – -191.67 (m), -199.49 – -199.88 (m), -235.35 – -235.73 (m) ppm. **IR** (thin film):  $\nu$  3460, 3402, 3059, 2954, 1617, 1452, 1421, 1335, 1230, 1092, 1072, 1058, 1005, 862, 743, 580  $\text{cm}^{-1}$ . **HRMS** (ESI+): exact mass calculated for  $\text{C}_{12}\text{H}_{13}\text{F}_3\text{N}$  ( $[\text{M}+\text{H}]^+$ ), 228.0995; found 228.0994.



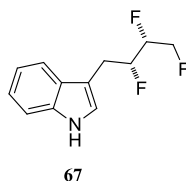
**(±)-Threo-1-Tosyl-3-(2,3,4-trifluorobutyl)-1H-indole (98):**

**Step 1:**<sup>102</sup> A vigorously stirred mixture of 3-(2-fluoro-2-(oxiran-2-yl)ethyl)-1-tosyl-1H-indole (**111**) (643 mg, 1.79 mmol, 1.00 equiv) and triethylamine trihydrofluoride (1.21 mL, 7.29 mmol, 4.10 equiv) was heated at 150 °C for 3 h. After cooling down to rt, the reaction was diluted with a 1:1 water/EtOAc mixture and the aqueous phase was further extracted with EtOAc. The combined organic extracts were washed with brine, dried over Na<sub>2</sub>SO<sub>4</sub>, filtered, and concentrated *in vacuo*. The resulting crude material was purified by silica gel flash column chromatography (5:2 hexanes/EtOAc) to afford fluorohydrin **122** as an orange crystalline solid (573 mg) that was used as such in the next step.

**Step 2:**<sup>80</sup> To a solution of the previously isolated fluorohydrin (**122**, 573 mg) and triethylamine (947 μL, 6.80 mmol, 4.50 equiv) in MeCN (15.1 mL) under inert atmosphere at 0 °C were successively added triethylamine trihydrofluoride (376 μL, 2.27 mmol, 1.50 equiv) and perfluorobutanesulfonyl fluoride (566 μL, 3.02 mmol, 2.00 equiv) dropwise. The reaction was stirred at rt for 1 h before it was quenched with saturated aqueous NaHCO<sub>3</sub>. The aqueous phase was extracted with EtOAc and the combined organic extracts were washed with brine, dried over Na<sub>2</sub>SO<sub>4</sub>, filtered, and concentrated *in vacuo*. The resulting crude material was purified by silica gel flash column chromatography (10:1 hexanes/EtOAc) to afford trifluoride **98** (554 mg, 1.45 mmol, 81% over two steps) as a colorless oil.

**TLC:**  $R_f$  = 0.52 (5:2 hexanes/EtOAc; UV, CAM). **<sup>1</sup>H NMR** (400 MHz, CDCl<sub>3</sub>): δ 8.02–7.98 (m, 1H), 7.77–7.73 (m, 2H), 7.53–7.50 (d,  $J$  = 5.3 Hz, 1H), 7.50 (s, 1H), 7.38–7.32 (m, 1H), 7.29–7.24 (m, 1H), 7.24–7.19 (m, 2H), 4.96–4.49 (m, 4H), 3.24–3.10 (m, 2H), 2.34 (s, 3H) ppm. **<sup>13</sup>C NMR** (100 MHz, CDCl<sub>3</sub>): δ 145.2, 135.3, 130.5, 130.1, 126.9, 125.3, 125.2, 123.5, 119.3, 116.5 (d,  $J$  = 7.5 Hz), 114.1, 90.0 (ddd,  $J$  = 181.7 Hz,  $J$  = 21.4 Hz,  $J$  = 19.7 Hz), 90.0 (ddd,  $J$  = 180.2 Hz,  $J$  = 20.1 Hz,  $J$  = 6.9 Hz), 81.3 (ddd,  $J$  = 172.1 Hz,  $J$  = 26.0 Hz,  $J$  = 8.1 Hz), 26.1 (dd,  $J$  = 23.7 Hz,  $J$  = 6.2 Hz), 21.7 ppm. **<sup>19</sup>F NMR** (376 MHz, CDCl<sub>3</sub>, decoupled): δ -195.34 (d,  $J$  = 10.0 Hz), -208.13 (dd,  $J$  = 15.3 Hz,  $J$  = 10.0 Hz) -232.85 (d,  $J$  = 15.3 Hz) ppm. **<sup>19</sup>F NMR** (376 MHz, CDCl<sub>3</sub>, not decoupled): δ -195.17 – -195.52 (m), -207.94 – -208.33 (m), -232.68 – -233.03 (m) ppm. **IR** (thin film): ν 3114, 3055, 2954, 2921, 1592, 1445, 1365,

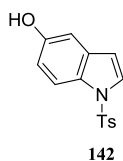
1281, 1172, 1118, 1097, 1017, 971, 811, 744, 664, 573, 534  $\text{cm}^{-1}$ . **HRMS** (ESI+): exact mass calculated for  $\text{C}_{19}\text{H}_{19}\text{F}_3\text{NO}_2\text{S}$  ( $[\text{M}+\text{H}]^+$ ), 382.1083; found 382.1084.



**(±)-Threo-3-(2,3,4-Trifluorobutyl)-1H-indole (67):**<sup>116</sup>

A suspension of *threo*-1-tosyl-3-(2,3,4-trifluorobutyl)-1H-indole (**98**) (554 mg, 1.45 mmol, 1.00 equiv) and magnesium turnings (353 mg, 14.5 mmol, 10.0 equiv) in MeOH (14.5 mL) at rt was stirred vigorously overnight. The reaction was then quenched with saturated aqueous  $\text{NH}_4\text{Cl}$  and further diluted with water. The aqueous phase was extracted with EtOAc and the combined organic extracts were washed with brine, dried over  $\text{Na}_2\text{SO}_4$ , filtered, and concentrated *in vacuo*. The resulting crude material was purified by silica gel flash column chromatography (10:1 hexanes/EtOAc) to afford indole **67** (187 mg,  $8.20 \times 10^{-4}$  mol, 57%) as a colorless oil.

**TLC:**  $R_f = 0.38$  (2:1 hexanes/EtOAc; UV, CAM, *p*-anisaldehyde).  **$^1\text{H}$  NMR** (400 MHz,  $\text{CDCl}_3$ ):  $\delta$  8.08 (bs, 1H), 7.63 (d,  $J = 7.8$  Hz, 1H), 7.42–7.37 (m, 1H), 7.26–7.21 (m, 1H), 7.19–7.15 (m, 1H), 7.14 (d,  $J = 2.2$  Hz, 1H), 5.00–4.49 (m, 4H), 3.36–3.27 (m, 2H) ppm.  **$^{13}\text{C}$  NMR** (100 MHz,  $\text{CDCl}_3$ ):  $\delta$  136.3, 127.3, 123.4, 122.6, 120.0, 118.6, 111.5, 109.5 (d,  $J = 9.6$  Hz), 90.9 (ddd,  $J = 179.3$  Hz,  $J = 19.8$  Hz,  $J = 6.9$  Hz), 90.0 (ddd,  $J = 180.1$  Hz,  $J = 21.0$  Hz,  $J = 19.2$  Hz), 81.8 (ddd,  $J = 171.6$  Hz,  $J = 26.1$  Hz,  $J = 7.7$  Hz), 26.2 (dd,  $J = 23.6$  Hz,  $J = 6.0$  Hz) ppm.  **$^{19}\text{F}$  NMR** (376 MHz,  $\text{CDCl}_3$ , decoupled):  $\delta$  -194.54 (d,  $J = 10.1$  Hz), -208.88 (dd,  $J = 15.4$  Hz,  $J = 10.1$  Hz), -232.57 (d,  $J = 15.4$  Hz) ppm.  **$^{19}\text{F}$  NMR** (376 MHz,  $\text{CDCl}_3$ , not decoupled):  $\delta$  -194.37 – -194.71 (m), -208.67 – -209.08 (m), -232.38 – -232.76 (m) ppm. **IR** (thin film):  $\nu$  3458, 3416, 3058, 2958, 1620, 1456, 1422, 1353, 1337, 1251, 1230, 1096, 1046, 999, 840, 745, 582  $\text{cm}^{-1}$ . **HRMS** (ESI+): exact mass calculated for  $\text{C}_{12}\text{H}_{13}\text{F}_3\text{N}$  ( $[\text{M}+\text{H}]^+$ ), 228.0995; found 228.0998.

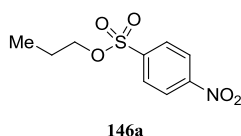
**1-Tosyl-1H-indol-5-ol (142):**

**Step 1:**<sup>126</sup> 1H-Indol-5-ol (**143**) (9.16 g, 67.4 mmol, 1.00 equiv) and imidazole (9.46 g, 136 mmol, 2.02 equiv) were loaded in a flask under inert atmosphere and dissolved in DMF (337 mL) upon stirring. The resulting reaction mixture was cooled down to 0 °C and a solution of *tert*-butyldimethylsilyl chloride (15.6 g, 101 mmol, 1.50 equiv) in DMF (337 mL) was added dropwise via cannula. Once the addition was complete, the reaction was kept stirring at rt for 3 h, quenched with water, and extracted with Et<sub>2</sub>O. The combined organic extracts were washed with brine, dried over Na<sub>2</sub>SO<sub>4</sub>, filtered, and concentrated *in vacuo*. The resulting crude material was purified by silica gel flash column chromatography (5:1 hexanes/EtOAc) to afford silyl ether **144** as a colorless oil that was used as such in the next step.

**Step 2:**<sup>126</sup> Sodium hydride (9.17 g, 229 mmol, 3.40 equiv) was loaded in a flask under inert atmosphere with THF (112 mL) upon stirring at rt. A solution of the previously isolated silyl ether (**144**) in THF (112 mL) was then added to the just prepared suspension via cannula at 0 °C. The reaction mixture was kept stirring at 0 °C for 1 h, and then a solution of *p*-toluenesulfonyl chloride (26.0 g, 135 mmol, 2.00 equiv) in THF (112 mL) was added via cannula. After the addition was complete, the reaction was kept stirring at rt for 3 h. The reaction was carefully diluted with EtOAc, then quenched with water. The organic phase was washed with water and brine, dried over Na<sub>2</sub>SO<sub>4</sub>, and concentrated *in vacuo*. The resulting crude material was purified by silica gel flash column chromatography (20:1 hexanes/EtOAc) to afford tosyl-protected indole **145** as a colorless oil that was used as such in the next step.

**Steps 3:**<sup>127</sup> The previously isolated tosyl-protected indole (**145**) was reacted in 1 M HCl in MeOH (674 mL) at rt upon vigorous stirring. The reaction was kept stirring at rt for 1.5 h and was then carefully quenched with saturated aqueous NaHCO<sub>3</sub>. Upon addition of saturated aqueous NaHCO<sub>3</sub>, a solid precipitated and formed a suspension which was then poured into a vigorously stirred solution of saturated aqueous NaHCO<sub>3</sub>. The suspension was kept stirring for 15 min and filtered off. The remaining solid was washed with water, then dried *in vacuo* to afford indole **142** (16.2 g, 56.2 mmol, 83% over three steps) as a white powder (mp = 163 °C).

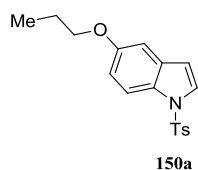
**TLC:**  $R_f = 0.10$  (10:1 hexanes/EtOAc; UV, CAM, *p*-anisaldehyde).  **$^1\text{H}$  NMR** (400 MHz,  $\text{CDCl}_3$ ):  $\delta$  7.84 (d,  $J = 8.9$  Hz, 1H), 7.75–7.69 (m, 2H), 7.51 (d,  $J = 3.6$  Hz, 1H), 7.20 (d,  $J = 8.3$  Hz, 2H), 6.92 (d,  $J = 2.5$  Hz, 1H), 6.83 (dd,  $J = 8.8$  Hz,  $J = 2.5$  Hz, 1H), 6.53 (dd,  $J = 3.6$  Hz,  $J = 0.8$  Hz, 1H), 4.72 (s, 1H), 2.33 (s, 3H) ppm.  **$^{13}\text{C}$  NMR** (100 MHz,  $\text{CDCl}_3$ ):  $\delta$  152.2, 145.0, 135.3, 132.2, 130.0, 129.9, 127.6, 126.9, 114.6, 113.7, 109.0, 106.4, 21.7 ppm. **IR** (thin film):  $\nu$  3400, 1448, 1364, 1222, 1188, 1170, 1142, 1122, 1090, 810, 720, 674, 591, 543  $\text{cm}^{-1}$ . **HRMS** (ESI<sup>+</sup>): exact mass calculated for  $\text{C}_{15}\text{H}_{14}\text{NO}_3\text{S}$  ( $[\text{M}+\text{H}]^+$ ), 288.0689; found 288.0692.



**Propyl 4-nitrobenzenesulfonate (146a):**<sup>128</sup>

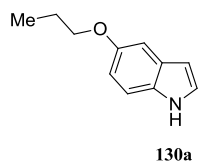
To a solution of propan-1-ol (**138a**) (1.25 mL, 16.5 mmol, 1.00 equiv), 4-(*N,N*-dimethylamino)pyridine (205 mg, 1.65 mmol, 1.00  $10^{-1}$  equiv), and 4-nitrobenzenesulfonyl chloride (4.47 g, 19.8 mmol, 1.20 equiv) in  $\text{CH}_2\text{Cl}_2$  (41.2 mL) at rt under inert atmosphere, was added triethylamine (4.69 mL, 32.9 mmol, 2.00 equiv) dropwise. The resulting solution was then stirred at rt overnight. After aqueous workup, the aqueous phase was extracted with  $\text{CH}_2\text{Cl}_2$ , the combined organic extracts were then dried over  $\text{Na}_2\text{SO}_4$ , filtered, and concentrated *in vacuo*. The resulting crude oil was purified by silica gel flash column chromatography (10:3 hexanes/EtOAc) to afford nosylate **146a** (2.34 g, 9.55 mmol, 58%) as a white crystalline solid (mp = 77 °C).

**TLC:**  $R_f = 0.45$  (4:1 hexanes/EtOAc; UV,  $\text{KMnO}_4$ ).  **$^1\text{H}$  NMR** (400 MHz,  $\text{CDCl}_3$ ):  $\delta$  8.44–8.37(m, 2H), 8.15–8.08 (m, 2H), 4.11 (td,  $J = 6.6$  Hz,  $J = 1.3$  Hz, 2H), 1.77–1.67 (m, 2H), 0.92 (td,  $J = 7.4$  Hz,  $J = 1.6$  Hz, 3H) ppm.  **$^{13}\text{C}$  NMR** (100 MHz,  $\text{CDCl}_3$ ):  $\delta$  150.9, 142.2, 129.3, 124.6, 73.5, 22.5, 10.0 ppm. **IR** (thin film):  $\nu$  3093, 2977, 2871, 1604, 1522, 1349, 1180, 1009, 935, 839, 743, 613  $\text{cm}^{-1}$ . **HRMS** (EI<sup>+</sup>): exact mass calculated for  $\text{C}_9\text{H}_{11}\text{NO}_5\text{S}$  ( $[\text{M}]^+$ ), 245.0358; found 245.0355.

**5-Propoxy-1-tosyl-1H-indole (150a):**<sup>131</sup>

A suspension of 1-tosyl-1H-indol-5-ol (**142**) (0.500 g, 1.74 mmol, 1.20 equiv) and potassium carbonate (601 mg, 4.35 mmol, 3.00 equiv) in DMF (7.25 mL) at rt under inert atmosphere was stirred for 1 h. A solution of propyl 4-nitrobenzenesulfonate (**146a**) (356 mg, 1.45 mmol) in DMF (7.25 mL) was then added via cannula, and the resulting suspension was stirred for 2 h at 80 °C. The reaction was quenched by addition of saturated aqueous NH<sub>4</sub>Cl and extracted with Et<sub>2</sub>O. The combined organic extracts were washed with brine, dried over Na<sub>2</sub>SO<sub>4</sub>, filtered, and concentrated *in vacuo*. The resulting crude material was purified by silica gel flash column chromatography (10:1 hexanes/EtOAc) to afford ether **150a** (106 mg, 3.20 10<sup>-4</sup> mol, 22%) as a white solid (mp = 136 °C).

**TLC:**  $R_f$  = 0.20 (10:1 hexanes/EtOAc; UV, CAM). **<sup>1</sup>H NMR** (400 MHz, CDCl<sub>3</sub>): δ 7.87 (d,  $J$  = 8.9 Hz, 1H), 7.73 (d,  $J$  = 8.3 Hz, 2H), 7.50 (d,  $J$  = 3.7 Hz, 1H), 7.19 (d,  $J$  = 8.2 Hz, 2H), 6.96 (d,  $J$  = 2.5 Hz, 1H), 6.92 (dd,  $J$  = 8.9 Hz,  $J$  = 2.5 Hz, 1H), 6.56 (d,  $J$  = 3.6 Hz, 1H), 3.91 (t,  $J$  = 6.6 Hz, 2H), 2.32 (s, 3H), 1.80 (h,  $J$  = 7.2 Hz, 2H), 1.03 (t,  $J$  = 7.4 Hz, 3H) ppm. **<sup>13</sup>C NMR** (100 MHz, CDCl<sub>3</sub>): δ 156.1, 144.9, 135.4, 131.9, 129.9, 129.6, 127.2, 126.9, 114.5, 114.31, 109.3, 104.6, 70.1, 22.8, 21.7, 10.7 ppm. **IR** (thin film): ν 2965, 1456, 1369, 1224, 1188, 1174, 1156, 1143, 1091, 994, 813, 720, 675, 594, 572, 538 cm<sup>-1</sup>. **HRMS** (ESI<sup>+</sup>): exact mass calculated for C<sub>18</sub>H<sub>20</sub>NO<sub>3</sub>S ([M+H]<sup>+</sup>), 330.1158; found 330.1163.

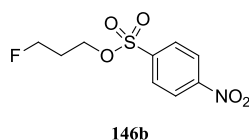
**5-Propoxy-1H-indole (130a):**<sup>81</sup>

To a solution of 5-propoxy-1-tosyl-1H-indole (**150a**) (0.200 g, 6.10 10<sup>-4</sup> mol, 1.00 equiv) in EtOH (6.07 mL) at rt was added potassium hydroxide (681 mg, 12.1 mmol, 20.0 equiv) in one portion. The resulting mixture was then heated to reflux under inert atmosphere overnight. The reaction was quenched by an addition of saturated aqueous NH<sub>4</sub>Cl and extracted with Et<sub>2</sub>O. The combined organic extracts were dried over Na<sub>2</sub>SO<sub>4</sub>, filtered and concentrated *in*



*vacuo*. The crude product was purified by silica gel flash column chromatography (10:1 hexanes/EtOAc) to afford indole **130a** (89.0 mg,  $5.10 \cdot 10^{-4}$  mol, 84 %) as a yellow oil that crystallized (mp = 43 °C) upon standing at rt.

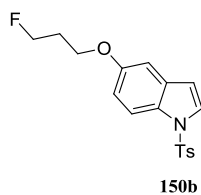
**TLC:**  $R_f$  = 0.53 (2:1 hexanes/EtOAc; UV, CAM, *p*-anisaldehyde).  **$^1\text{H NMR}$**  (400 MHz,  $\text{CDCl}_3$ ):  $\delta$  8.03 (bs, 1H), 7.31–7.24 (m, 1H), 7.17 (t,  $J$  = 2.8 Hz, 1H), 7.13 (d,  $J$  = 2.4 Hz, 1H), 6.89 (dd,  $J$  = 8.8 Hz,  $J$  = 2.4 Hz, 1H), 6.51–6.46 (m, 1H), 3.99 (t,  $J$  = 6.6 Hz, 2H), 1.91–1.80 (m, 2H), 1.07 (t,  $J$  = 7.4 Hz, 3H) ppm.  **$^{13}\text{C NMR}$**  (100 MHz,  $\text{CDCl}_3$ ):  $\delta$  153.8, 131.1, 128.4, 124.9, 113.1, 111.7, 103.7, 102.48, 70.6, 22.9, 10.8 ppm. **IR** (thin film):  $\nu$  3428, 3107, 2971, 1530, 1348, 1183, 936, 855, 834, 753, 744, 735, 613  $\text{cm}^{-1}$ . **HRMS** (EI+): exact mass calculated for  $\text{C}_{11}\text{H}_{13}\text{NO}$  ( $[\text{M}]^+$ ), 175.0992; found 175.0994.



### 3-Fluoropropyl 4-nitrobenzenesulfonate (**146b**):<sup>128</sup>

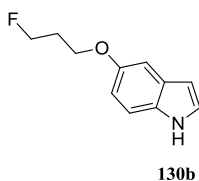
To a solution of 3-fluoropropan-1-ol (**138b**) (3.00 mL, 38.7 mmol, 1.00 equiv), 4-(*N,N*-dimethylamino)pyridine (483 mg, 3.87 mmol,  $1.00 \cdot 10^{-1}$  equiv), and 4-nitrobenzenesulfonyl chloride (10.5 g, 46.5 mmol, 1.20 equiv) in  $\text{CH}_2\text{Cl}_2$  (97.0 mL) at rt under inert atmosphere, was added triethylamine (11.0 mL, 77.0 mmol, 2.00 equiv) dropwise. The resulting solution was then stirred at rt for 2.5 h. After aqueous workup, the aqueous phase was extracted with  $\text{CH}_2\text{Cl}_2$ , the combined organic extracts were then dried over  $\text{Na}_2\text{SO}_4$ , filtered, and concentrated *in vacuo*. The resulting crude oil was purified by silica gel flash column chromatography (10:3 hexanes/EtOAc) to afford nosylate **146b** (3.35 g, 12.7 mmol, 33%) as a yellow oil.

**TLC:**  $R_f$  = 0.68 (3:2 hexanes/EtOAc; UV,  $\text{KMnO}_4$ ).  **$^1\text{H NMR}$**  (400 MHz,  $\text{CDCl}_3$ ):  $\delta$  8.45–8.38 (m, 2H), 8.15–8.09 (m, 2H), 4.50 (dt,  $J$  = 46.8 Hz,  $J$  = 5.6 Hz, 2H), 4.28 (t,  $J$  = 6.1 Hz, 2H), 2.16–2.02 (m, 2H) ppm.  **$^{13}\text{C NMR}$**  (100 MHz,  $\text{CDCl}_3$ ):  $\delta$  151.0, 141.7, 129.4, 124.7, 79.3 (d,  $J$  = 166.6 Hz), 67.5 (d,  $J$  = 4.6 Hz), 30.1 (d,  $J$  = 20.2 Hz) ppm.  **$^{19}\text{F NMR}$**  (376 MHz,  $\text{CDCl}_3$ , decoupled):  $\delta$  -223.86 (s) ppm.  **$^{19}\text{F NMR}$**  (376 MHz,  $\text{CDCl}_3$ , not decoupled):  $\delta$  -223.64 – -224.08 (m) ppm. **IR** (thin film):  $\nu$  2919, 2852, 1527, 1350, 1183, 910, 743  $\text{cm}^{-1}$ . **HRMS** (EI+): exact mass calculated for  $\text{C}_9\text{H}_{10}\text{FNO}_5\text{S}$  ( $[\text{M}]^+$ ), 263.0264; found 263.0259.

**5-(3-Fluoropropoxy)-1-tosyl-1H-indole (150b):**<sup>131</sup>

A suspension of 1-tosyl-1H-indol-5-ol (**142**) (819 mg, 2.85 mmol, 1.20 equiv) and potassium carbonate (985 mg, 7.13 mmol, 3.00 equiv) in DMF (11.9 mL) at rt under inert atmosphere was stirred for 1 h. A solution of 3-fluoropropyl 4-nitrobenzenesulfonate (**146b**) (625 mg, 2.38 mmol) in DMF (11.9 mL) was then added via cannula, and the resulting suspension was stirred for 2 h at 80 °C. The reaction was quenched by addition of saturated aqueous NH<sub>4</sub>Cl and extracted with Et<sub>2</sub>O. The combined organic extracts were washed with brine, dried over Na<sub>2</sub>SO<sub>4</sub>, filtered, and concentrated *in vacuo*. The resulting crude material was purified by silica gel flash column chromatography (10:1 hexanes/EtOAc) to afford ether **150b** (501 mg, 1.44 mmol, 60%) as a white solid (mp = 93 °C).

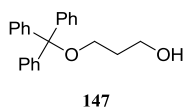
**TLC:**  $R_f$  = 0.25 (2:1 hexanes/EtOAc; UV, CAM). **<sup>1</sup>H NMR** (400 MHz, CDCl<sub>3</sub>): δ 7.88 (d,  $J$  = 9.0 Hz, 1H), 7.76–7.67 (m, 2H), 7.51 (d,  $J$  = 3.6 Hz, 1H), 7.20 (d,  $J$  = 8.2 Hz, 2H), 6.97 (d,  $J$  = 2.5 Hz, 1H), 6.92 (dd,  $J$  = 8.9 Hz,  $J$  = 2.5 Hz, 1H), 6.57 (dd,  $J$  = 3.7 Hz,  $J$  = 0.7 Hz, 1H), 4.64 (dt,  $J$  = 47.1 Hz,  $J$  = 5.8 Hz, 2H), 4.09 (t,  $J$  = 6.1 Hz, 2H), 2.33 (s, 3H), 2.16 (dp,  $J$  = 26.1 Hz,  $J$  = 5.9 Hz, 2H) ppm. **<sup>13</sup>C NMR** (100 MHz, CDCl<sub>3</sub>): δ 155.7, 145.0, 135.4, 131.9, 129.9, 129.8, 127.3, 126.9, 114.6, 114.2, 109.3, 104.7, 80.9 (d,  $J$  = 164.4 Hz), 64.1 (d,  $J$  = 5.2 Hz), 30.6 (d,  $J$  = 20.0 Hz), 21.7 ppm. **<sup>19</sup>F NMR** (376 MHz, CDCl<sub>3</sub>, decoupled): δ -222.28 (s) ppm. **<sup>19</sup>F NMR** (376 MHz, CDCl<sub>3</sub>, not decoupled): δ -222.28 (tt,  $J$  = 47.0 Hz,  $J$  = 26.1 Hz) ppm. **IR** (thin film): ν 2965, 1457, 1368, 1224, 1174, 1154, 1091, 1050, 994, 812, 758, 720, 703, 675, 593, 538 cm<sup>-1</sup>. **HRMS** (ESI<sup>+</sup>): exact mass calculated for C<sub>18</sub>H<sub>19</sub>FNO<sub>3</sub>S ([M+H]<sup>+</sup>), 348.1064; found 348.1065.



### 5-(3-Fluoropropoxy)-1H-indole (**130b**):<sup>81</sup>

To a solution of 5-(3-fluoropropoxy)-1-tosyl-1H-indole (**150b**) (501 mg, 1.44 mmol, 1.00 equiv) in EtOH (14.4 mL) at rt was added potassium hydroxide (1.62 g, 20.8 mmol, 20.0 equiv) in one portion. The resulting mixture was then heated to reflux under inert atmosphere overnight. The reaction was quenched by an addition of saturated aqueous NH<sub>4</sub>Cl and extracted with Et<sub>2</sub>O. The combined organic extracts were dried over Na<sub>2</sub>SO<sub>4</sub>, filtered and concentrated *in vacuo*. The resulting crude material was purified by silica gel flash column chromatography (10:1 hexanes/EtOAc) to afford indole **130b** (143 mg, 7.40 × 10<sup>-4</sup> mol, 51%) as a yellow oil.

**TLC:**  $R_f$  = 0.15 (5:1 hexanes/EtOAc; UV, CAM, *p*-anisaldehyde). **<sup>1</sup>H NMR** (400 MHz, CDCl<sub>3</sub>): δ 8.04 (bs, 1H), 7.28 (d,  $J$  = 8.7 Hz, 1H), 7.18 (t,  $J$  = 2.8 Hz, 1H), 7.14 (d,  $J$  = 2.4 Hz, 1H), 6.88 (dd,  $J$  = 8.8 Hz,  $J$  = 2.4 Hz, 1H), 6.49 (ddd,  $J$  = 3.1 Hz,  $J$  = 2.0 Hz,  $J$  = 0.9 Hz, 1H), 4.70 (dt,  $J$  = 47.0 Hz,  $J$  = 5.9 Hz, 2H), 4.16 (t,  $J$  = 6.1 Hz, 2H), 2.21 (dp,  $J$  = 25.8 Hz,  $J$  = 6.0 Hz, 2H) ppm. **<sup>13</sup>C NMR** (100 MHz, CDCl<sub>3</sub>): δ 153.4, 131.3, 128.4, 125.1, 112.9, 111.8, 103.8, 102.5, 81.2 (d,  $J$  = 164.1 Hz), 64.5 (d,  $J$  = 5.5 Hz), 30.8 (d,  $J$  = 19.9 Hz) ppm. **<sup>19</sup>F NMR** (376 MHz, CDCl<sub>3</sub>, decoupled): δ -221.80 (s) ppm. **<sup>19</sup>F NMR** (376 MHz, CDCl<sub>3</sub>, not decoupled): δ -221.80 (tt,  $J$  = 47.0 Hz,  $J$  = 25.8 Hz) ppm. **IR** (thin film): ν 3412, 2967, 1471, 1454, 1282, 1223, 1155, 1124, 1047, 986, 950, 895, 838, 801, 756, 723, 605, 790 cm<sup>-1</sup>. **HRMS** (ESI<sup>+</sup>): exact mass calculated for C<sub>11</sub>H<sub>13</sub>FNO ([M+H]<sup>+</sup>), 194.0976; found 194.0972.

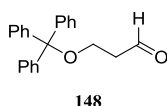


### 3-(Trityloxy)propan-1-ol (**147**):<sup>129</sup>

To a stirred solution of propane-1,3-diol (**139**) (15.8 mL, 209 mmol, 10.0 equiv) in CH<sub>2</sub>Cl<sub>2</sub> (70.0 mL) under inert atmosphere at 0 °C were successively added triethylamine (3.23 mL, 23.0 mmol, 1.10 equiv), 4-(*N,N*-dimethylamino)pyridine (103 mg, 8.40 × 10<sup>-4</sup> mol, 4.00 × 10<sup>-2</sup> equiv) and trityl chloride (6.00 g, 20.9 mmol, 1.00 equiv). The reaction was stirred at rt for 19 h before it was quenched with saturated aqueous NH<sub>4</sub>Cl. The aqueous phase was then

extracted with  $\text{CH}_2\text{Cl}_2$  and the combined organic extracts were dried over  $\text{Na}_2\text{SO}_4$ , filtered and concentrated *in vacuo*. The resulting crude material was purified by silica gel flash column chromatography (2:1 hexanes/EtOAc) to afford alcohol **147** (5.63 g, 17.7 mmol, 85%) as a white solid (mp = 121 °C).

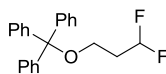
**TLC:**  $R_f$  = 0.45 (7:3 hexanes/EtOAc; UV, CAM).  **$^1\text{H}$  NMR** (400 MHz,  $\text{CDCl}_3$ ):  $\delta$  7.49–7.43 (m, 6H), 7.37–7.22 (m, 9H), 3.79 (q,  $J$  = 5.8 Hz, 2H), 3.30 (t,  $J$  = 5.8 Hz, 2H), 2.13 (bs, 1H), 1.88 (p,  $J$  = 5.8 Hz, 2H) ppm.  **$^{13}\text{C}$  NMR** (100 MHz,  $\text{CDCl}_3$ ):  $\delta$  144.2, 128.7, 128.0, 127.2, 87.2, 62.6, 62.0, 32.6 ppm. **IR** (thin film):  $\nu$  3232, 2948, 2869, 1591, 1488, 1443, 1208, 1066, 757, 698  $\text{cm}^{-1}$ . **HRMS** (EI+): exact mass calculated for  $\text{C}_{22}\text{H}_{22}\text{O}_2$  ( $[\text{M}]^+$ ), 318.1620; found 318.1617.



### 3-(Trityloxy)propanal (**148**):<sup>83</sup>

A solution of 3-(trityloxy)propan-1-ol (**147**) (5.63 g, 17.7 mmol, 1.00 equiv) in  $\text{CH}_2\text{Cl}_2$  (28.0 mL) under inert atmosphere at rt was added to a stirred suspension of pyridinium chlorochromate (5.83 g, 26.5 mmol, 1.50 equiv) and Celite<sup>®</sup> (ca. 6.0 g) in  $\text{CH}_2\text{Cl}_2$  (44.0 mL) under inert atmosphere at rt. The resulting mixture was kept stirring at rt for 3 h before it was diluted with  $\text{Et}_2\text{O}$  and stirred for 10 min. The suspension was then filtered over a pad of Celite<sup>®</sup> and the filtrate was concentrated *in vacuo*. The resulting crude material was purified by silica gel flash column chromatography (4:1 hexanes/EtOAc) to afford aldehyde **148** (4.64 g, 14.7 mmol, 83%) as a white solid (mp = 84 °C).

**TLC:**  $R_f$  = 0.51 (4:1 hexanes/EtOAc; UV, CAM).  **$^1\text{H}$  NMR** (400 MHz,  $\text{CDCl}_3$ ):  $\delta$  9.75 (s, 1H), 7.49–7.38 (m, 6H), 7.36–7.17 (m, 9H), 3.48 (q,  $J$  = 6.0 Hz, 2H), 2.63 (t,  $J$  = 6.0 Hz, 2H) ppm.  **$^{13}\text{C}$  NMR** (100 MHz,  $\text{CDCl}_3$ ):  $\delta$  201.7, 143.9, 128.7, 128.0, 127.3, 87.1, 58.0, 44.2 ppm. **IR** (thin film):  $\nu$  3040, 2881, 2724, 1719, 1489, 1449, 1214, 1150, 1077, 905, 748, 699, 638  $\text{cm}^{-1}$ . **HRMS** (EI+): exact mass calculated for  $\text{C}_{22}\text{H}_{22}\text{NO}_2$  ( $[\text{M}]^+$ ), 316.1458; found 316.1461.

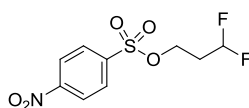


149

**((3,3-Difluoropropoxy)methanetriyl)tribenzene (149):**<sup>84</sup>

To a solution of 3-(trityloxy)propanal (**148**) (4.64 g, 14.7 mmol, 1.00 equiv) in CH<sub>2</sub>Cl<sub>2</sub> (49.0 mL) under inert atmosphere at 0 °C was added diethylaminosulfur trifluoride (4.08 mL, 29.3 mmol, 2.00 equiv) dropwise. The reaction was then stirred at rt for 10 min before it was quenched with saturated aqueous NaHCO<sub>3</sub>. The aqueous phase was extracted with CH<sub>2</sub>Cl<sub>2</sub> and the combined organic extracts were dried over Na<sub>2</sub>SO<sub>4</sub>, filtered, and concentrated *in vacuo*. The resulting crude material was purified by silica gel flash column chromatography (20:1 hexanes/EtOAc) to afford difluoride **149** (3.89 g, 11.5 mmol, 78%) as a white solid (mp = 87 °C).

**TLC:**  $R_f$  = 0.44 (10:1 hexanes/EtOAc; UV, CAM). **<sup>1</sup>H NMR** (400 MHz, CDCl<sub>3</sub>): δ 7.49–7.41 (m, 6H), 7.37–7.23 (m, 9H), 6.11 (tq,  $J$  = 56.9 Hz,  $J$  = 4.5 Hz, 1H), 3.34–3.25 (m, 2H), 2.21–2.03 (m, 2H) ppm. **<sup>13</sup>C NMR** (100 MHz, CDCl<sub>3</sub>): δ 143.9, 128.7, 128.0, 127.3, 116.3 (t,  $J$  = 238.4 Hz), 87.0, 57.8 (t,  $J$  = 6.8 Hz), 35.1 (t,  $J$  = 21.4 Hz) ppm. **<sup>19</sup>F NMR** (376 MHz, CDCl<sub>3</sub>, decoupled): δ -116.96 – -117.01 (m) ppm. **<sup>19</sup>F NMR** (376 MHz, CDCl<sub>3</sub>, not decoupled): δ -116.83 – -117.13 (m) ppm. **IR** (thin film): ν 3077, 2909, 2930, 2881, 1597, 1489, 1440, 1381, 1090, 1031, 1002, 977, 894, 761, 703, 623 cm<sup>-1</sup>. **HRMS** (EI+): exact mass calculated for C<sub>22</sub>H<sub>20</sub>F<sub>2</sub>O ([M]<sup>+</sup>), 338.1477; found 338.1477.



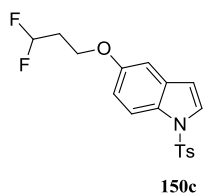
146c

**3,3-Difluoropropyl 4-nitrobenzenesulfonate (146c):**<sup>128,130</sup>

To a solution of ((3,3-difluoropropoxy)methanetriyl)tribenzene (**149**) (3.04 g, 8.97 mmol, 1.00 equiv) in CH<sub>2</sub>Cl<sub>2</sub> (44.9 mL) at rt under inert atmosphere was added hydrochloric acid (4.0 M in dioxane) (4.49 mL, 18.0 mmol, 2.00 equiv) dropwise. The resulting solution was then stirred for 1 h at rt. The reaction was cooled down to 0 °C and triethylamine (5.05 mL, 35.9 mmol, 4.00 equiv) was added dropwise. The white solution was then stirred for 15 min at rt, and 4-(*N,N*-dimethylamino)pyridine (111 mg, 9.00 10<sup>-4</sup> mol, 1.00 10<sup>-1</sup> equiv), followed by 4-nitrobenzene-1-sulfonyl chloride (4.46 g, 19.7 mmol, 2.20 equiv), were successively added. The resulting suspension was stirred at rt for 1 h. The reaction was quenched with water,

extracted with CH<sub>2</sub>Cl<sub>2</sub>, and the combined organic extracts were dried over Na<sub>2</sub>SO<sub>4</sub>, filtered and concentrated *in vacuo*. The resulting crude material was purified by silica gel flash column chromatography (5:1 hexanes/EtOAc) to afford nosylate **146c** (1.29 g, 4.58 mmol, 51%) as a yellow crystalline solid (mp = 79 °C).

**TLC:**  $R_f$  = 0.52 (7:3 hexanes/EtOAc; UV, KMnO<sub>4</sub>). **<sup>1</sup>H NMR** (400 MHz, CDCl<sub>3</sub>): δ 8.47–8.38 (m, 2H), 8.16–8.09 (m, 2H), 5.92 (tt,  $J$  = 55.8 Hz,  $J$  = 4.3 Hz, 1H), 4.31 (t,  $J$  = 6.1 Hz, 2H), 2.28 (ttt,  $J$  = 16.3 Hz,  $J$  = 6.1 Hz,  $J$  = 4.3 Hz, 2H) ppm. **<sup>13</sup>C NMR** (100 MHz, CDCl<sub>3</sub>): δ 151.1, 141.4, 129.4, 124.8, 114.3 (t,  $J$  = 239.9 Hz), 65.0 (t,  $J$  = 7.0 Hz), 33.9 (t,  $J$  = 22.7 Hz) ppm. **<sup>19</sup>F NMR** (376 MHz, CDCl<sub>3</sub>, decoupled): δ -118.44 (s) ppm. **<sup>19</sup>F NMR** (376 MHz, CDCl<sub>3</sub>, not decoupled): δ -118.44 (dt,  $J$  = 55.8 Hz,  $J$  = 16.3 Hz) ppm. **IR** (thin film): ν 3111, 1531, 1350, 1311, 1190, 1095, 1014, 969, 923, 856, 836, 777, 745, 733, 684, 612 cm<sup>-1</sup>. **HRMS** (EI<sup>+</sup>): exact mass calculated for C<sub>9</sub>H<sub>9</sub>F<sub>2</sub>NO<sub>5</sub>S ([M]<sup>+</sup>), 281.0169; found 281.0172.

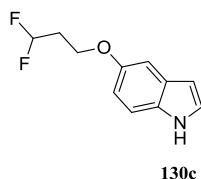


### 5-(3,3-Difluoropropoxy)-1-tosyl-1H-indole (**150c**):<sup>131</sup>

A suspension of 1-tosyl-1H-indol-5-ol (**142**) (1.28 g, 4.45 mmol, 1.20 equiv), 3,3-difluoropropyl 4-nitrobenzenesulfonate (**146c**) (1.04 g, 3.71 mmol, 1.00 equiv), and potassium carbonate (641 mg, 4.64 mmol) in MeCN (37.1 mL) was heated at 80 °C for 4 h. The reaction mixture was then allowed to cool down to rt, quenched with water, and extracted with EtOAc. The combined organic extracts were washed with brine, dried over Na<sub>2</sub>SO<sub>4</sub>, filtered, and concentrated *in vacuo*. The resulting crude material was purified by silica gel flash column chromatography (10:1 hexanes/EtOAc) to afford ether **150c** (1.28 g, 3.51 mmol, 95%) as a yellow crystalline solid (mp = 133 °C).

**TLC:**  $R_f$  = 0.40 (2:1 hexanes/EtOAc; UV, CAM, *p*-anisaldehyde). **<sup>1</sup>H NMR** (400 MHz, CDCl<sub>3</sub>): δ 7.88 (d,  $J$  = 9.0 Hz, 1H), 7.78–7.68 (m, 2H), 7.52 (d,  $J$  = 3.6 Hz, 1H), 7.21 (d,  $J$  = 8.0 Hz, 2H), 6.96 (d,  $J$  = 2.5 Hz, 1H), 6.91 (dd,  $J$  = 9.0 Hz,  $J$  = 2.5 Hz, 1H), 6.57 (d,  $J$  = 3.6 Hz, 1H), 6.08 (tt,  $J$  = 56.6 Hz,  $J$  = 4.7 Hz, 1H), 4.11 (t,  $J$  = 6.0 Hz, 2H), 2.39–2.24 (m, 5H) ppm. **<sup>13</sup>C NMR** (100 MHz, CDCl<sub>3</sub>): δ 155.2, 145.0, 135.4, 131.9, 130.1–129.9 (m), 127.4, 126.9, 115.7 (t,  $J$  = 238.6 Hz), 114.7, 114.1, 109.2, 104.8, 62.4 (t,  $J$  = 7.0 Hz), 34.5 (t,  $J$  =

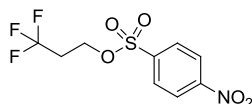
21.9 Hz), 21.7 ppm.  $^{19}\text{F}$  NMR (376 MHz,  $\text{CDCl}_3$ , decoupled):  $\delta$  -118.06 (s) ppm.  $^{19}\text{F}$  NMR (376 MHz,  $\text{CDCl}_3$ , not decoupled):  $\delta$  -118.06 (dt,  $J = 57.1$  Hz,  $J = 17.0$  Hz) ppm. IR (thin film):  $\nu$  2931, 1457, 1367, 1224, 1174, 1155, 1142, 1121, 1087, 1048, 982, 813, 760, 674, 587, 563, 538  $\text{cm}^{-1}$ . HRMS (ESI+): exact mass calculated for  $\text{C}_{18}\text{H}_{18}\text{F}_2\text{NO}_3\text{S}$  ( $[\text{M}+\text{H}]^+$ ), 366.0970; found 366.0971.



### 5-(3,3-Difluoropropoxy)-1H-indole (**130c**):<sup>116</sup>

To a solution of 5-(3,3-difluoropropoxy)-1-tosyl-1H-indole (**150c**) (842 mg, 2.30 mmol, 1.00 equiv) in MeOH (15.4 mL) at rt were added magnesium turnings (0.560 g, 23.0 mmol, 10.0 equiv). The resulting suspension was vigorously stirred at rt for 3 h. The reaction was then quenched with saturated aqueous  $\text{NH}_4\text{Cl}$ , and the aqueous phase was extracted with EtOAc. The combined organic extracts were washed with brine, dried over  $\text{Na}_2\text{SO}_4$ , filtered, and concentrated *in vacuo*. The resulting crude material was purified by silica gel flash column chromatography (10:1 hexanes/EtOAc) to afford indole **130c** (439 mg, 2.08 mmol, 90%) as a brownish oil.

**TLC:**  $R_f = 0.24$  (10:3 hexanes/EtOAc; UV, CAM, *p*-anisaldehyde).  $^1\text{H}$  NMR (400 MHz,  $\text{CDCl}_3$ ):  $\delta$  8.05 (bs, 1H), 7.29 (d,  $J = 8.8$  Hz, 1H), 7.19 (t,  $J = 2.8$  Hz, 1H), 7.13 (d,  $J = 2.5$  Hz, 1H), 6.87 (dd,  $J = 8.8$  Hz,  $J = 2.5$  Hz, 1H), 6.50 (ddd,  $J = 3.1$  Hz,  $J = 2.0$  Hz,  $J = 0.9$  Hz, 1H), 6.14 (tt,  $J = 56.8$  Hz,  $J = 4.8$  Hz, 1H), 4.18 (t,  $J = 6.0$  Hz, 2H), 2.35 (tt,  $J = 16.5$  Hz,  $J = 6.0$  Hz,  $J = 4.8$  Hz, 2H) ppm.  $^{13}\text{C}$  NMR (100 MHz,  $\text{CDCl}_3$ ):  $\delta$  153.0, 131.4, 128.4, 125.2, 115.9 (t,  $J = 238.4$  Hz), 112.8, 111.9, 103.9, 102.6, 62.8 (t,  $J = 6.9$  Hz), 34.7 (t,  $J = 27.1$  Hz) ppm.  $^{19}\text{F}$  NMR (376 MHz,  $\text{CDCl}_3$ , decoupled):  $\delta$  -117.83 (s) ppm.  $^{19}\text{F}$  NMR (376 MHz,  $\text{CDCl}_3$ , not decoupled):  $\delta$  -117.83 (dt,  $J = 57.1$  Hz,  $J = 16.9$  Hz) ppm. IR (thin film):  $\nu$  3412, 2940, 1473, 1455, 1223, 1157, 1119, 1081, 978, 802, 756, 724  $\text{cm}^{-1}$ . HRMS (ESI+): exact mass calculated for  $\text{C}_{11}\text{H}_{11}\text{F}_2\text{NNaO}$  ( $[\text{M}+\text{Na}]^+$ ), 234.0701; found 234.0705.

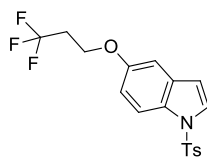


146d

### 3,3,3-Trifluoropropyl 4-nitrobenzenesulfonate (**146d**):<sup>128</sup>

To a solution of 4-nitrobenzenesulfonyl chloride (3.00 g, 13.3 mmol, 1.20 equiv) and 4-(*N,N*-dimethylamino)pyridine (136 mg, 1.11 mmol, 1.00  $10^{-1}$  equiv) in  $\text{CH}_2\text{Cl}_2$  (55.3 mL) under inert atmosphere at 0 °C were successively added 3,3,3-trifluoropropan-1-ol (**138d**) (1.01 mL, 11.1 mmol, 1.00 equiv) and *N,N*-diisopropylethylamine (2.93 mL, 16.6 mmol, 1.50 equiv) dropwise. The reaction was stirred at rt for 2 h before it was quenched with saturated aqueous  $\text{NH}_4\text{Cl}$ . The aqueous phase was extracted with  $\text{CH}_2\text{Cl}_2$  and the combined organic extracts were dried over  $\text{Na}_2\text{SO}_4$ , filtered, and concentrated *in vacuo*. The resulting crude material was purified by silica gel flash column chromatography (10:3 hexanes/EtOAc) to afford nosylate **146d** (2.31 g, 7.73 mmol, 70%) as a pale yellow crystalline solid (mp = 70 °C).

**TLC**:  $R_f$  = 0.52 (3:1 hexanes/EtOAc; UV,  $\text{KMnO}_4$ ).  **$^1\text{H NMR}$**  (400 MHz,  $\text{CDCl}_3$ ):  $\delta$  8.46–8.40 (m, 2H), 8.15–8.10 (m, 2H), 4.35 (t,  $J$  = 6.3 Hz, 2H), 2.57 (qt,  $J$  = 10.0 Hz,  $J$  = 6.3 Hz, 2H) ppm.  **$^{13}\text{C NMR}$**  (100 MHz,  $\text{CDCl}_3$ ):  $\delta$  151.1, 141.3, 129.5, 125.0 (q,  $J$  = 276.9 Hz), 124.7, 63.5 (q,  $J$  = 3.8 Hz), 33.9 (q,  $J$  = 30.1 Hz) ppm.  **$^{19}\text{F NMR}$**  (376 MHz,  $\text{CDCl}_3$ , decoupled):  $\delta$  -64.96 (s) ppm.  **$^{19}\text{F NMR}$**  (376 MHz,  $\text{CDCl}_3$ , not decoupled):  $\delta$  -64.96 (t,  $J$  = 10.1 Hz) ppm. **IR** (thin film):  $\nu$  3110, 1612, 1545, 1368, 1349, 1306, 1249, 1182, 1153, 1134, 901, 918, 856, 784, 732, 679, 636, 579  $\text{cm}^{-1}$ . **HRMS** (EI+): exact mass calculated for  $\text{C}_9\text{H}_8\text{F}_3\text{NO}_5\text{S}$  ( $[\text{M}]^+$ ), 299.0070; found 299.0075.



150d

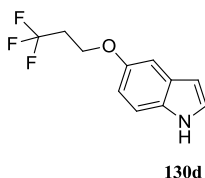
### 1-Tosyl-5-(3,3,3-trifluoropropoxy)-1H-indole (**150d**):<sup>131</sup>

To a solution of 1-tosyl-1H-indol-5-ol (**142**) (1.44 g, 5.01 mmol, 1.00 equiv) and 3,3,3-trifluoropropyl 4-nitrobenzenesulfonate (**146d**) (3.00 g, 10.0 mmol, 2.00 equiv) in MeCN (25.1 mL) at rt under inert atmosphere was added potassium carbonate (2.10 g, 15.0 mmol, 3.00 equiv). The resulting suspension was then stirred at 80 °C for 2 h before it was quenched with water. The aqueous phase was then extracted with  $\text{Et}_2\text{O}$ , and the combined organic



extracts were washed with brine, dried over Na<sub>2</sub>SO<sub>4</sub>, filtered, and concentrated *in vacuo*. The resulting crude material was purified by silica gel flash column chromatography (10:1 hexanes/EtOAc) to afford ether **150d** (0.510 g, 1.33 mmol, 27%) as a white crystalline solid (mp = 107 °C).

**TLC:**  $R_f$  = 0.25 (10:3 hexanes/EtOAc; UV, CAM, *p*-anisaldehyde). **<sup>1</sup>H NMR** (400 MHz, CDCl<sub>3</sub>): δ 7.89 (d,  $J$  = 9.0 Hz, 1H), 7.76–7.70 (m, 2H), 7.53 (d,  $J$  = 3.6 Hz, 1H), 7.21 (d,  $J$  = 8.3 Hz, 2H), 6.97 (d,  $J$  = 2.5 Hz, 1H), 6.92 (dd,  $J$  = 8.9 Hz,  $J$  = 2.5 Hz, 1H), 6.58 (dd,  $J$  = 3.6 Hz,  $J$  = 0.7 Hz, 1H), 4.19 (t,  $J$  = 6.6 Hz, 2H), 2.62 (qt,  $J$  = 10.5 Hz,  $J$  = 6.6 Hz, 2H), 2.33 (s, 3H) ppm. **<sup>13</sup>C NMR** (100 MHz, CDCl<sub>3</sub>): δ 155.0, 145.0, 135.4, 131.9, 130.1, 130.0, 127.5, 126.9, 126.1 (q,  $J$  = 276.6 Hz), 114.7, 114.2, 109.2, 105.0, 61.6 (q,  $J$  = 3.7 Hz), 34.2 (q,  $J$  = 28.8 Hz) 21.7 ppm. **<sup>19</sup>F NMR** (376 MHz, CDCl<sub>3</sub>, decoupled): δ -64.75 (s) ppm. **<sup>19</sup>F NMR** (376 MHz, CDCl<sub>3</sub>, not decoupled): δ -64.75 (t,  $J$  = 10.8 Hz) ppm. **IR** (thin film): ν 2927, 1458, 1368, 1253, 1221, 1173, 1134, 1091, 1011, 995, 811, 759, 720, 675, 590, 577, 547, 536 cm<sup>-1</sup>. **HRMS** (ESI+): exact mass calculated for C<sub>18</sub>H<sub>17</sub>F<sub>3</sub>NO<sub>3</sub>S ([M+H]<sup>+</sup>), 384.0876; found 384.0877.

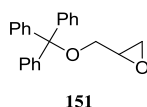


### 5-(3,3,3-Trifluoropropoxy)-1H-indole (**130d**):<sup>116</sup>

To a solution of 1-tosyl-5-(3,3,3-trifluoropropoxy)-1H-indole (**150d**) (675 mg, 1.76 mmol, 1.00 equiv) in MeOH (17.6 mL) at rt were added magnesium turnings (428 mg, 17.6 mmol, 10.0 equiv). The resulting suspension was vigorously stirred at rt for 5 h. The reaction was then quenched with saturated aqueous NH<sub>4</sub>Cl, and the aqueous phase was extracted with EtOAc. The combined organic extracts were washed with brine, dried over Na<sub>2</sub>SO<sub>4</sub>, filtered, and concentrated *in vacuo*. The resulting crude material was purified by silica gel flash column chromatography (10:1 hexanes/EtOAc) to afford indole **130d** (0.330 g, 1.44 mmol, 82%) as a brownish oil that crystallized (mp = 55 °C) upon standing at rt.

**TLC:**  $R_f$  = 0.29 (5:1 hexanes/EtOAc; UV, CAM, *p*-anisaldehyde). **<sup>1</sup>H NMR** (400 MHz, CDCl<sub>3</sub>): δ 8.06 (s, 1H), 7.29 (d,  $J$  = 8.8 Hz, 1H), 7.20 (t,  $J$  = 2.8 Hz, 1H), 7.14 (d,  $J$  = 2.5 Hz, 1H), 6.88 (dd,  $J$  = 8.8 Hz,  $J$  = 2.4 Hz, 1H), 6.50 (ddd,  $J$  = 3.1 Hz,  $J$  = 2.0 Hz,  $J$  = 0.9 Hz, 1H),

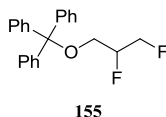
4.26 (t,  $J = 6.7$  Hz, 2H), 2.65 (qt,  $J = 10.6$  Hz,  $J = 6.7$  Hz, 2H) ppm.  $^{13}\text{C}$  NMR (100 MHz,  $\text{CDCl}_3$ ):  $\delta$  152.8, 131.5, 128.4, 126.2 (q,  $J = 276.6$  Hz), 125.2, 113.0, 112.0, 104.2, 102.6, 62.1 (q,  $J = 3.7$  Hz), 34.3 (q,  $J = 28.5$  Hz) ppm.  $^{19}\text{F}$  NMR (376 MHz,  $\text{CDCl}_3$ , decoupled):  $\delta$  -64.66 (s) ppm.  $^{19}\text{F}$  NMR (376 MHz,  $\text{CDCl}_3$ , not decoupled):  $\delta$  -64.66 (t,  $J = 10.8$  Hz) ppm. IR (thin film):  $\nu$  3414, 2928, 1474, 1455, 1285, 1251, 1220, 1134, 1069, 1008, 956, 895, 875, 839, 803, 756, 724, 603  $\text{cm}^{-1}$ . HRMS (ESI+): exact mass calculated for  $\text{C}_{11}\text{H}_{11}\text{F}_3\text{NO}$  ( $[\text{M}+\text{H}]^+$ ), 230.0787; found 230.0793.



### 2-((Trityloxy)methyl)oxirane (**151**):<sup>129</sup>

Trityl chloride (15.6 g, 54.3 mmol, 1.00 equiv) and 4-(*N,N*-dimethylamino)pyridine (268 mg, 2.17 mmol, 4.00  $10^{-2}$  equiv) were dissolved in  $\text{CH}_2\text{Cl}_2$  (271 mL) at rt under inert atmosphere. The resulting solution was cooled down to 0  $^\circ\text{C}$  prior to successively adding glycidol (**152**) (7.50 mL, 109 mmol, 2.00 equiv) and triethylamine (9.17 mL, 65.2 mmol, 1.20 equiv) dropwise. The reaction mixture was then stirred at rt for 2 h before it was quenched with water. The aqueous phase was extracted with  $\text{CH}_2\text{Cl}_2$  and the combined organic extracts were dried over  $\text{Na}_2\text{SO}_4$ , filtered, and concentrated *in vacuo*. The resulting crude material was purified by silica gel flash column chromatography (20:1 hexanes/EtOAc) to afford epoxide **151** (12.9 g, 40.8 mmol, 75%) as a white crystalline solid (mp = 80  $^\circ\text{C}$ ).

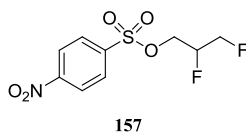
**TLC**:  $R_f = 0.27$  (5:1 hexanes/EtOAc; UV, CAM).  $^1\text{H}$  NMR (400 MHz,  $\text{CDCl}_3$ ):  $\delta$  7.50–7.44 (m, 6H), 7.35–7.21 (m, 9H), 3.37–3.29 (m, 1H), 3.19–3.10 (m, 2H), 2.82–2.76 (m, 1H), 2.64–2.61 (m, 1H) ppm.  $^{13}\text{C}$  NMR (100 MHz,  $\text{CDCl}_3$ ):  $\delta$  144.0, 128.8, 128.0, 127.2, 86.9, 64.9, 51.2, 44.8 ppm. IR (thin film):  $\nu$  3461, 3057, 2923, 2872, 1490, 1448, 1069, 1032, 916, 900, 776, 764, 747, 698, 646, 632  $\text{cm}^{-1}$ . HRMS (EI+): exact mass calculated for  $\text{C}_{22}\text{H}_{20}\text{O}_2$  ( $[\text{M}]^+$ ), 316.1458; found 316.1465.



**((2,3-Difluoropropoxy)methanetriyl)tribenzene (155):**<sup>80,102</sup>

2-((Trityloxy)methyl)oxirane (**151**) (1.00 g, 3.16 mmol, 1.00 equiv), *N,N*-diisopropylethylamine (5.02 mL, 28.4 mmol, 9.00 equiv), *N,N*-diisopropylethylamine trihydrofluoride (1.96 mL, 9.48 mmol, 3.00 equiv), and perfluorobutanesulfonyl fluoride (1.24 mL, 6.32 mmol, 2.00 equiv) were loaded in a flask at rt. The reaction flask was sealed, and the resulting mixture was vigorously stirred at 100 °C for 48 h. The reaction mixture was cooled down to rt, diluted with CH<sub>2</sub>Cl<sub>2</sub>, and carefully quenched with saturated aqueous NaHCO<sub>3</sub> dropwise. The biphasic mixture was stirred vigorously until no evolution of gas could be noticed, after what the aqueous phase was extracted with CH<sub>2</sub>Cl<sub>2</sub>. The combined organic extracts were dried over Na<sub>2</sub>SO<sub>4</sub>, filtered, and concentrated *in vacuo*. The resulting crude material was purified by silica gel flash column chromatography (20:1 hexanes/EtOAc) to afford difluoride **155** (766 mg, 2.26 mmol, 72%) as a white crystalline solid (mp = 103 °C).

**TLC:**  $R_f$  = 0.16 (20:1 hexanes/EtOAc; UV, CAM). **<sup>1</sup>H NMR** (400 MHz, CDCl<sub>3</sub>): δ 7.50–7.44 (m, 6H), 7.38–7.25 (m, 9H), 4.94–4.49 (m, 3H), 3.49–3.32 (m, 2H) ppm. **<sup>13</sup>C NMR** (100 MHz, CDCl<sub>3</sub>): δ 143.5, 128.7, 128.1, 127.4, 90.7 (dd,  $J$  = 176.1 Hz,  $J$  = 19.7 Hz), 87.1, 82.7 (dd,  $J$  = 172.3 Hz,  $J$  = 23.0 Hz), 62.1 (dd,  $J$  = 24.4 Hz,  $J$  = 8.1 Hz) ppm. **<sup>19</sup>F NMR** (376 MHz, CDCl<sub>3</sub>, decoupled): δ -195.70 (d,  $J$  = 13.6 Hz), -232.57 (d,  $J$  = 13.6 Hz) ppm. **<sup>19</sup>F NMR** (376 MHz, CDCl<sub>3</sub>, not decoupled): δ -195.48 – -195.92 (m), -232.38 – -232.76 (m) ppm. **IR** (thin film): ν 3059, 3033, 2953, 2878, 1491, 1449, 1090, 1033, 1002, 776, 765, 747, 703, 632 cm<sup>-1</sup>. **HRMS** (EI<sup>+</sup>): exact mass calculated for C<sub>22</sub>H<sub>20</sub>F<sub>2</sub>O ([M]<sup>+</sup>), 338.1477; found 338.1470.

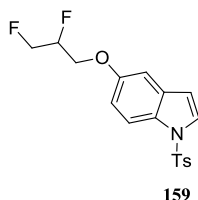


**2,3-Difluoropropyl 4-nitrobenzenesulfonate (157):**<sup>128,130</sup>

((2,3-Difluoropropoxy)methanetriyl)tribenzene (**155**) (737 mg, 2.18 mmol, 1.00 equiv) was dissolved in CH<sub>2</sub>Cl<sub>2</sub> (10.9 mL) at rt under inert atmosphere. The resulting solution was cooled down to 0 °C prior to adding hydrochloric acid (4.0 M in dioxane) (653 μL, 2.61 mmol, 1.20 equiv) dropwise. The reaction was then stirred at 0 °C for 30 min before *N,N*-diisopropylethylamine (922 μL, 5.23 mmol, 2.40 equiv) was added dropwise. 4-(*N,N*-

Dimethylamino)pyridine (11.0 mg,  $9.00 \cdot 10^{-5}$  mol,  $4.00 \cdot 10^{-2}$  equiv) and 4-nitrobenzene-1-sulfonyl chloride (591 mg, 2.61 mmol, 1.20 equiv) were successively added, and the resulting solution was stirred at 0 °C for 1 h. The reaction was then quenched with water, and the aqueous phase was extracted with  $\text{CH}_2\text{Cl}_2$ . The combined organic extracts were dried over  $\text{Na}_2\text{SO}_4$ , filtered, and concentrated *in vacuo*. The resulting crude material was purified by silica gel flash column chromatography (5:1 hexanes/EtOAc) to afford nosylate **157** (338 mg, 1.20 mmol, 55%) as a yellow crystalline solid (mp = 72 °C).

**TLC:**  $R_f$  = 0.18 (10:3 hexanes/EtOAc; UV).  **$^1\text{H}$  NMR** (400 MHz,  $\text{CDCl}_3$ ):  $\delta$  8.45–8.39 (m, 2H), 8.15–8.10 (m, 2H), 4.99–4.76 (m, 1H), 4.73–4.32 (m, 4H) ppm.  **$^{13}\text{C}$  NMR** (100 MHz,  $\text{CDCl}_3$ ):  $\delta$  151.1, 141.2, 129.5, 124.7, 88.0 (dd,  $J$  = 180.2 Hz,  $J$  = 20.9 Hz), 80.7 (dd,  $J$  = 174.6 Hz,  $J$  = 24.2 Hz), 68.0 (dd,  $J$  = 25.2 Hz,  $J$  = 8.0 Hz) ppm.  **$^{19}\text{F}$  NMR** (376 MHz,  $\text{CDCl}_3$ , decoupled):  $\delta$  -197.05 (d,  $J$  = 13.9 Hz), -235.40 (d,  $J$  = 14.3 Hz) ppm.  **$^{19}\text{F}$  NMR** (376 MHz,  $\text{CDCl}_3$ , not decoupled):  $\delta$  -196.84 – -197.25 (m), -235.40 (tdd,  $J$  = 46.8 Hz,  $J$  = 21.1 Hz,  $J$  = 13.4 Hz) ppm. **IR** (thin film):  $\nu$  3111, 2966, 1530, 1369, 1350, 1184, 996, 977, 855, 814, 745, 737, 609, 464  $\text{cm}^{-1}$ . **HRMS** (EI+): exact mass calculated for  $\text{C}_9\text{H}_9\text{F}_2\text{NO}_5\text{S}$  ( $[\text{M}]^+$ ), 281.0164; found 281.0161.

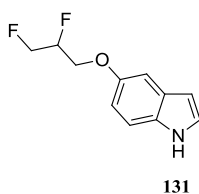


### 5-(2,3-Difluoropropoxy)-1-tosyl-1H-indole (**159**):<sup>131</sup>

To a solution of 1-tosyl-1H-indol-5-ol (**142**) (141 mg,  $4.90 \cdot 10^{-4}$  mol, 1.20 equiv) and 2,3-difluoropropyl 4-nitrobenzenesulfonate (**157**) (115 mg,  $4.10 \cdot 10^{-4}$  mol, 1.00 equiv) in MeCN (4.09 mL) at rt under inert atmosphere was added potassium carbonate (71.0 mg,  $5.10 \cdot 10^{-4}$  mol, 1.25 equiv). The resulting suspension was then stirred at 80 °C for 48 h, then cooled down to rt, filtered over a pad of Celite<sup>®</sup>, and the filtrate was concentrated *in vacuo*. The resulting crude material was purified by silica gel flash column chromatography (5:1 hexanes/EtOAc) to afford ether **159** (105 mg,  $2.90 \cdot 10^{-4}$  mol, 70%) as a yellow syrup.

**TLC:**  $R_f$  = 0.27 (5:2 hexanes/EtOAc; UV, CAM, *p*-anisaldehyde).  **$^1\text{H}$  NMR** (400 MHz,  $\text{CDCl}_3$ ):  $\delta$  7.89 (d,  $J$  = 8.9 Hz, 1H), 7.75–7.69 (m, 2H), 7.53 (d,  $J$  = 3.6 Hz, 1H), 7.21 (d,  $J$  = 8.2 Hz, 2H), 6.99 (d,  $J$  = 2.5 Hz, 1H), 6.94 (dd,  $J$  = 9.0 Hz,  $J$  = 2.5 Hz, 1H), 6.58 (dd,  $J$  = 3.5

Hz,  $J = 0.7$  Hz, 1H), 5.12–4.88 (m, 1H), 4.85–4.59 (m, 2H), 4.22 (ddd,  $J = 18.5$  Hz,  $J = 5.1$  Hz,  $J = 1.2$  Hz, 2H), 2.34 (s, 3H) ppm.  $^{13}\text{C}$  NMR (100 MHz,  $\text{CDCl}_3$ ):  $\delta$  155.0, 145.1, 135.3, 131.9, 130.2, 130.0, 127.6, 126.9, 114.7, 114.2, 109.2, 105.0, 89.5 (dd,  $J = 176.6$  Hz,  $J = 20.0$  Hz), 81.9 (dd,  $J = 173.1$  Hz,  $J = 23.4$  Hz), 66.4 (dd,  $J = 26.0$  Hz,  $J = 7.9$  Hz), 21.7 ppm.  $^{19}\text{F}$  NMR (376 MHz,  $\text{CDCl}_3$ , decoupled):  $\delta$  -196.94 (d,  $J = 13.3$  Hz), -234.34 (d,  $J = 13.3$  Hz) ppm.  $^{19}\text{F}$  NMR (376 MHz,  $\text{CDCl}_3$ , not decoupled):  $\delta$  -196.73 – -197.16 (m), -234.34 (tdd,  $J = 47.6$  Hz,  $J = 21.7$  Hz,  $J = 13.4$  Hz) ppm. IR (thin film):  $\nu$  3144, 2958, 1447, 1367, 1224, 1188, 1174, 1157, 1142, 1124, 1091, 1038, 996, 812, 721, 703, 671, 591, 538  $\text{cm}^{-1}$ . HRMS (ESI+): exact mass calculated for  $\text{C}_{18}\text{H}_{18}\text{F}_2\text{NO}_3\text{S}$  ( $[\text{M}+\text{H}]^+$ ), 366.0970; found 366.0971.

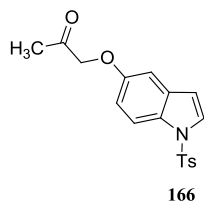


### 5-(2,3-Difluoropropoxy)-1H-indole (**131**):<sup>116</sup>

To a solution of 5-(2,3-difluoropropoxy)-1-tosyl-1H-indole (**159**) (224 mg,  $6.10 \cdot 10^{-4}$  mol, 1.00 equiv) in MeOH (4.09 mL) at rt were added magnesium turnings (149 mg, 6.13 mmol, 10.0 equiv). The resulting suspension was vigorously stirred at rt for 3 h. The reaction was then quenched with saturated aqueous  $\text{NH}_4\text{Cl}$ , and the aqueous phase was extracted with EtOAc. The combined organic extracts were washed with brine, dried over  $\text{Na}_2\text{SO}_4$ , filtered, and concentrated *in vacuo*. The resulting crude material was purified by silica gel flash column chromatography (5:1 hexanes/EtOAc) to afford indole **131** (117 mg,  $5.50 \cdot 10^{-4}$  mol, 90%) as a colorless oil.

TLC:  $R_f = 0.27$  (5:2 hexanes/EtOAc; UV, CAM, *p*-anisaldehyde).  $^1\text{H}$  NMR (400 MHz,  $\text{CDCl}_3$ ):  $\delta$  8.08 (bs, 1H), 7.32–7.28 (m, 1H), 7.20 (t,  $J = 2.8$  Hz, 1H), 7.14 (d,  $J = 2.5$  Hz, 1H), 6.89 (dd,  $J = 8.8$  Hz,  $J = 2.5$  Hz, 1H), 6.49 (ddd,  $J = 3.0$  Hz,  $J = 2.0$  Hz,  $J = 0.9$  Hz, 1H), 5.17–4.92 (m, 1H), 4.88–4.65 (m, 2H), 4.34–4.20 (m, 2H) ppm.  $^{13}\text{C}$  NMR (100 MHz,  $\text{CDCl}_3$ ):  $\delta$  152.8, 131.6, 128.4, 125.3, 112.8, 112.0, 104.2, 102.6, 89.8 (dd,  $J = 176.2$  Hz,  $J = 19.8$  Hz), 82.2 (dd,  $J = 172.7$  Hz,  $J = 23.1$  Hz), 66.9 (dd,  $J = 25.8$  Hz,  $J = 8.0$  Hz) ppm.  $^{19}\text{F}$  NMR (376 MHz,  $\text{CDCl}_3$ , decoupled):  $\delta$  -196.75 (d,  $J = 13.0$  Hz), -233.91 (d,  $J = 13.0$  Hz) ppm.  $^{19}\text{F}$  NMR (376 MHz,  $\text{CDCl}_3$ , not decoupled):  $\delta$  -196.51 – -196.99 (m), -233.91 (tdd,  $J = 47.8$  Hz,  $J = 21.9$  Hz,  $J = 13.2$  Hz) ppm. IR (thin film):  $\nu$  3415, 2957, 1478, 1452, 1285,

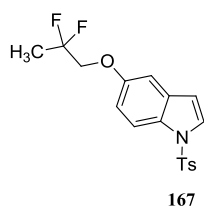
1225, 1162, 1124, 1105, 1032, 860, 807, 758, 727  $\text{cm}^{-1}$ . **HRMS** (EI+): exact mass calculated for  $\text{C}_{11}\text{H}_{11}\text{F}_2\text{NO}$  ( $[\text{M}]^+$ ), 211.0804; found 211.0804.



**1-((1-Tosyl-1H-indol-5-yl)oxy)propan-2-one (166):**<sup>133</sup>

To a suspension of 1-tosyl-1H-indol-5-ol (**142**) (2.50 g, 8.27 mmol, 1.00 equiv) and potassium carbonate (1.75 g, 12.4 mmol, 1.50 equiv) in MeCN (41.3 mL) under inert atmosphere at rt was added 1-chloropropan-2-one (**165**) (1.01 mL, 12.4 mmol, 1.50 equiv) dropwise. The reaction was stirred at 80 °C for 3 h, cooled down to rt, and filtered over a pad of Celite<sup>®</sup>. The filtrate was concentrated *in vacuo*, and the resulting crude material was purified by silica gel flash column chromatography (5:1 hexanes/EtOAc) to afford ketone **166** (2.46 g, 7.17 mmol, 87%) as a yellow crystalline solid (mp = 119 °C).

**TLC:**  $R_f$  = 0.18 (5:1 hexanes/EtOAc; UV, CAM, *p*-anisaldehyde). **<sup>1</sup>H NMR** (400 MHz,  $\text{CDCl}_3$ ):  $\delta$  7.90 (d,  $J$  = 9.0 Hz, 1H), 7.75–7.71 (m, 2H), 7.53 (d,  $J$  = 3.6 Hz, 1H), 7.21 (d,  $J$  = 8.3 Hz, 2H), 6.95 (dd,  $J$  = 9.0 Hz,  $J$  = 2.6 Hz, 1H), 6.90 (d,  $J$  = 2.5 Hz, 1H), 6.56 (dd,  $J$  = 3.6 Hz,  $J$  = 0.8 Hz, 1H), 4.53 (s, 2H), 2.34 (s, 3H), 2.27 (s, 3H) ppm. **<sup>13</sup>C NMR** (100 MHz,  $\text{CDCl}_3$ ):  $\delta$  206.0, 154.7, 145.1, 135.3, 131.8, 130.3, 130.0, 127.6, 126.9, 114.8, 114.1, 109.1, 104.9, 73.8, 26.8, 21.7 ppm. **IR** (thin film):  $\nu$  3142, 2922, 1735, 1459, 1433, 1366, 1220, 1188, 1171, 1144, 1125, 1092, 996, 812, 759, 721, 703, 674, 590, 537  $\text{cm}^{-1}$ . **HRMS** (ESI+): exact mass calculated for  $\text{C}_{18}\text{H}_{18}\text{NO}_4\text{S}$  ( $[\text{M}+\text{H}]^+$ ), 344.0951; found 344.0958.

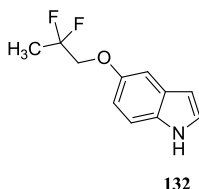


**5-(2,2-Difluoropropoxy)-1-tosyl-1H-indole (167):**<sup>84</sup>

To a solution of 1-((1-tosyl-1H-indol-5-yl)oxy)propan-2-one (**166**) (664 mg, 1.93 mmol, 1.00 equiv) in  $\text{CH}_2\text{Cl}_2$  (9.67 mL) under inert atmosphere at 0 °C was added diethylaminosulfur

trifluoride (511  $\mu\text{L}$ , 3.87 mmol, 2.00 equiv) dropwise. The reaction was stirred at rt for 2 h before it was carefully quenched with saturated aqueous  $\text{NaHCO}_3$ . The aqueous phase was then extracted with  $\text{CH}_2\text{Cl}_2$ , and the combined organic extracts were dried over  $\text{Na}_2\text{SO}_4$ , filtered, and concentrated *in vacuo*. The resulting crude material was purified by silica gel flash column chromatography (5:1 hexanes/EtOAc) to afford difluoride **167** (0.610 g, 1.67 mmol, 86%) as a colorless syrup that crystallized (mp = 94  $^\circ\text{C}$ ) upon standing at rt.

**TLC:**  $R_f$  = 0.33 (5:2 hexanes/EtOAc; UV, CAM, *p*-anisaldehyde).  **$^1\text{H}$  NMR** (400 MHz,  $\text{CDCl}_3$ ):  $\delta$  7.90 (d,  $J$  = 8.9 Hz, 1H), 7.75–7.70 (m, 2H), 7.54 (d,  $J$  = 3.7 Hz, 1H), 7.21 (d,  $J$  = 8.4 Hz, 2H), 6.99 (d,  $J$  = 2.3 Hz, 1H), 6.96 (dd,  $J$  = 8.9 Hz,  $J$  = 2.6 Hz, 1H), 6.58 (dd,  $J$  = 3.6 Hz,  $J$  = 0.8 Hz, 1H), 4.10 (t,  $J$  = 11.4 Hz, 2H), 2.33 (s, 3H), 1.77 (t,  $J$  = 18.8 Hz, 3H) ppm.  **$^{13}\text{C}$  NMR** (100 MHz,  $\text{CDCl}_3$ ):  $\delta$  154.9, 145.1, 135.3, 131.8, 130.3, 130.0, 127.6, 126.9, 121.7 (t,  $J$  = 239.3 Hz), 114.7, 114.2, 109.2, 105.2, 70.4 (t,  $J$  = 34.6 Hz), 21.7, 21.1 (t,  $J$  = 25.9 Hz) ppm.  **$^{19}\text{F}$  NMR** (376 MHz,  $\text{CDCl}_3$ , decoupled):  $\delta$  -98.07 (s) ppm.  **$^{19}\text{F}$  NMR** (376 MHz,  $\text{CDCl}_3$ , not decoupled):  $\delta$  -97.94 – -98.19 (m) ppm. **IR** (thin film):  $\nu$  3144, 1449, 1369, 1221, 1188, 1174, 1156, 1145, 1125, 1092, 1059, 993, 908, 813, 676, 586, 541  $\text{cm}^{-1}$ . **HRMS** (ESI+): exact mass calculated for  $\text{C}_{18}\text{H}_{18}\text{F}_2\text{NO}_3\text{S}$  ( $[\text{M}+\text{H}]^+$ ), 366.0970; found 366.0970.

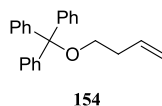


### 5-(2,2-Difluoropropoxy)-1H-indole (**132**):<sup>116</sup>

To a solution of 5-(2,2-difluoropropoxy)-1-tosyl-1H-indole (**167**) (0.580 g, 1.59 mmol, 1.00 equiv) in MeOH (10.6 mL) at rt were added magnesium turnings (386 mg, 15.9 mmol, 10.0 equiv). The resulting suspension was vigorously stirred at rt for 3 h. The reaction was then quenched with saturated aqueous  $\text{NH}_4\text{Cl}$ , and the aqueous phase was extracted with EtOAc. The combined organic extracts were washed with brine, dried over  $\text{Na}_2\text{SO}_4$ , filtered, and concentrated *in vacuo*. The resulting crude material was purified by silica gel flash column chromatography (5:1 hexanes/EtOAc) to afford indole **132** (0.300 g, 1.42 mmol, 89%) as a colorless oil that crystallized (mp = 40  $^\circ\text{C}$ ) upon standing at rt.

**TLC:**  $R_f$  = 0.45 (5:2 hexanes/EtOAc; UV, CAM, *p*-anisaldehyde).  **$^1\text{H}$  NMR** (400 MHz,  $\text{CDCl}_3$ ):  $\delta$  8.08 (bs, 1H), 7.30 (d,  $J$  = 8.8 Hz, 1H), 7.21 (t,  $J$  = 2.8 Hz, 1H), 7.13 (d,  $J$  = 2.5 Hz,

1H), 6.91 (dd,  $J = 8.8$  Hz,  $J = 2.5$  Hz, 1H), 6.50 (ddd,  $J = 3.1$  Hz,  $J = 2.1$  Hz,  $J = 0.9$  Hz, 1H), 4.16 (t,  $J = 11.5$  Hz, 2H), 1.81 (t,  $J = 18.8$  Hz, 3H) ppm.  $^{13}\text{C}$  NMR (100 MHz,  $\text{CDCl}_3$ ):  $\delta$  152.9, 131.7, 128.4, 125.3, 122.0 (t,  $J = 239.1$  Hz), 112.9, 111.9, 104.3, 102.7, 71.0 (t,  $J = 34.2$  Hz), 21.1 (t,  $J = 26.0$  Hz) ppm.  $^{19}\text{F}$  NMR (376 MHz,  $\text{CDCl}_3$ , decoupled):  $\delta$  -98.02 (s) ppm.  $^{19}\text{F}$  NMR (376 MHz,  $\text{CDCl}_3$ , not decoupled):  $\delta$  -98.02 (qt,  $J = 19.3$  Hz,  $J = 11.5$  Hz) ppm. IR (thin film):  $\nu$  3417, 2938, 1478, 1454, 1391, 1220, 1183, 1158, 1147, 1125, 1058, 904, 757, 725  $\text{cm}^{-1}$ . HRMS (EI+): exact mass calculated for  $\text{C}_{11}\text{H}_{11}\text{F}_2\text{NO}$  ( $[\text{M}]^+$ ), 211.0804; found 211.0802.

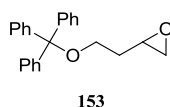


**((But-3-en-1-yloxy)methanetriyl)tribenzene (154):**<sup>129</sup>

Trityl chloride (19.6 g, 66.9 mmol, 1.00 equiv) and 4-(*N,N*-dimethylamino)pyridine (0.330 g, 2.68 mmol,  $4.00 \times 10^{-2}$  equiv) were dissolved in  $\text{CH}_2\text{Cl}_2$  (335 mL) at rt under inert atmosphere. The resulting solution was cooled down to 0 °C prior to successively adding but-3-en-1-ol (**140**) (12.0 mL, 134 mmol, 2.00 equiv) and triethylamine (11.3 mL, 80.0 mmol, 1.20 equiv) dropwise. The reaction mixture was then stirred at rt for 2 h before it was quenched with water. The aqueous phase was extracted with  $\text{CH}_2\text{Cl}_2$  and the combined organic extracts were dried over  $\text{Na}_2\text{SO}_4$ , filtered, and concentrated *in vacuo*. The resulting crude material was purified by silica gel flash column chromatography (20:1 hexanes/EtOAc) to afford olefin **154** (20.2 g, 64.6 mmol, 96%) as a light yellow syrup.

**TLC:**  $R_f = 0.45$  (10:1 hexanes/EtOAc; UV, CAM).  $^1\text{H}$  NMR (400 MHz,  $\text{CDCl}_3$ ):  $\delta$  7.50–7.45 (m, 6H), 7.35–7.22 (m, 9H), 5.88 (ddt,  $J = 17.1$  Hz,  $J = 10.2$  Hz,  $J = 6.9$  Hz, 1H), 5.13–5.01 (m, 2H), 3.15 (t,  $J = 6.7$  Hz, 2H), 2.40 (qt,  $J = 6.8$  Hz,  $J = 1.3$  Hz, 2H) ppm.  $^{13}\text{C}$  NMR (100 MHz,  $\text{CDCl}_3$ ):  $\delta$  144.5, 135.8, 128.8, 127.9, 127.0, 116.4, 86.6, 63.3, 34.8 ppm. IR (thin film):  $\nu$  3058, 3022, 2924, 2870, 1490, 1448, 1216, 1068, 1032, 1001, 990, 913, 899, 772, 760, 744, 703, 695, 650, 631  $\text{cm}^{-1}$ . HRMS (EI+): exact mass calculated for  $\text{C}_{23}\text{H}_{22}\text{O}$  ( $[\text{M}]^+$ ), 314.1666; found 314.1666.

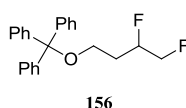




### 2-(2-(Trityloxy)ethyl)oxirane (**153**):<sup>132</sup>

To a solution of ((but-3-en-1-yloxy)methanetriyl)tribenzene (**154**) (20.2 g, 64.4 mmol, 1.00 equiv) in CH<sub>2</sub>Cl<sub>2</sub> (129 mL) at 0 °C was added *m*-chloroperoxybenzoic acid (19.0 g, 77.0 mmol, 1.20 equiv). The reaction was stirred overnight at rt, then quenched with 3 M NaOH (aq), and poured into stirring water. The aqueous phase was extracted with CH<sub>2</sub>Cl<sub>2</sub>, and the combined organic extracts were dried over Na<sub>2</sub>SO<sub>4</sub>, filtered, and concentrated *in vacuo*. The resulting crude material was purified by silica gel flash column chromatography (10:1 hexanes/EtOAc) to afford epoxide **153** (20.6 g, 62.4 mmol, 97%) as a white crystalline solid (mp = 88 °C).

**TLC:**  $R_f$  = 0.13 (20:1 hexanes/EtOAc; UV, CAM). **<sup>1</sup>H NMR** (400 MHz, CDCl<sub>3</sub>): δ 7.51–7.45 (m, 6H), 7.38–7.23 (m, 9H), 3.28 (qt,  $J$  = 9.2 Hz,  $J$  = 6.2 Hz, 2H), 3.17–3.09 (m, 1H), 2.82 (dd,  $J$  = 5.1 Hz,  $J$  = 4.0 Hz, 1H), 2.54 (dd,  $J$  = 5.1 Hz,  $J$  = 2.7 Hz, 1H), 1.85 (q,  $J$  = 6.1 Hz, 2H) ppm. **<sup>13</sup>C NMR** (100 MHz, CDCl<sub>3</sub>): δ 144.3, 128.8, 127.9, 127.1, 86.8, 60.8, 50.5, 47.4, 33.5 ppm. **IR** (thin film): ν 3056, 3033, 2923, 2875, 1490, 1448, 1071, 1031, 774, 762, 746, 705, 698, 632 cm<sup>-1</sup>. **HRMS** (EI<sup>+</sup>): exact mass calculated for C<sub>23</sub>H<sub>22</sub>O<sub>2</sub> ([M]<sup>+</sup>), 330.1615; found 330.1619.

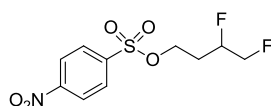


### ((3,4-Difluorobutoxy)methanetriyl)tribenzene (**156**):<sup>80,102</sup>

2-(2-(Trityloxy)ethyl)oxirane (**153**) (2.00 g, 6.05 mmol, 1.00 equiv), *N,N*-diisopropylethylamine (9.61 mL, 54.5 mmol, 9.00 equiv), *N,N*-diisopropylethylamine trihydrofluoride (3.75 mL, 18.2 mmol, 3.00 equiv), and perfluorobutanesulfonyl fluoride (2.37 mL, 12.1 mmol, 2.00 equiv) were loaded in a flask at rt. The reaction flask was sealed, and the resulting mixture was vigorously stirred at 100 °C for 96 h. The reaction mixture was cooled down to rt, diluted with CH<sub>2</sub>Cl<sub>2</sub>, and carefully quenched with saturated aqueous NaHCO<sub>3</sub> dropwise. The biphasic mixture was stirred vigorously until no evolution of gas could be noticed, after what the aqueous phase was extracted with CH<sub>2</sub>Cl<sub>2</sub>. The combined organic extracts were dried over Na<sub>2</sub>SO<sub>4</sub>, filtered, and concentrated *in vacuo*. The resulting

crude material was purified by silica gel flash column chromatography (20:1 hexanes/EtOAc) to afford difluoride **156** (1.51 g, 4.29 mmol, 71%) as a white crystalline solid (mp = 75 °C).

**TLC:**  $R_f$  = 0.33 (5:1 hexanes/EtOAc; UV, CAM).  **$^1\text{H NMR}$**  (400 MHz,  $\text{CDCl}_3$ ):  $\delta$  7.47–7.41 (m, 6H), 7.35–7.22 (m, 9H), 5.10–4.82 (m, 1H), 4.69–4.31 (m, 2H), 3.37–3.17 (m, 2H), 2.07–1.78 (m, 2H) ppm.  **$^{13}\text{C NMR}$**  (100 MHz,  $\text{CDCl}_3$ ):  $\delta$  144.1, 128.7, 128.0, 127.2, 89.7 (dd,  $J$  = 172.6 Hz,  $J$  = 19.2 Hz), 87.0, 84.4 (dd,  $J$  = 173.7 Hz,  $J$  = 22.1 Hz), 59.0 (d,  $J$  = 5.8 Hz), 30.8 (dd,  $J$  = 21.1 Hz,  $J$  = 6.7 Hz) ppm.  **$^{19}\text{F NMR}$**  (376 MHz,  $\text{CDCl}_3$ , decoupled):  $\delta$  -190.18 (d,  $J$  = 13.1 Hz), -229.88 (d,  $J$  = 13.1 Hz) ppm.  **$^{19}\text{F NMR}$**  (376 MHz,  $\text{CDCl}_3$ , not decoupled):  $\delta$  -189.96 – -190.40 (m), -229.88 (tdd,  $J$  = 47.7 Hz,  $J$  = 22.4 Hz,  $J$  = 13.3 Hz) ppm. **IR** (thin film):  $\nu$  3058, 3024, 2954, 2884, 1490, 1448, 1072, 1031, 1001, 898, 772, 760, 745, 704, 696, 647, 632  $\text{cm}^{-1}$ . **HRMS** (EI+): exact mass calculated for  $\text{C}_{23}\text{H}_{22}\text{F}_2\text{O}$  ( $[\text{M}]^+$ ), 352.1634; found 352.1633.



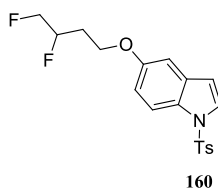
158

**3,4-Difluorobutyl 4-nitrobenzenesulfonate (158):**<sup>128,130</sup>

((3,4-Difluorobutoxy)methanetriyl)tribenzene (**156**) (2.17 g, 6.17 mmol, 1.00 equiv) was dissolved in  $\text{CH}_2\text{Cl}_2$  (30.8 mL) at rt under inert atmosphere. The resulting solution was cooled down to 0 °C prior to adding hydrochloric acid (4.0 M in dioxane) (3.08 mL, 12.3 mmol, 2.00 equiv) dropwise. The reaction was then stirred at 0 °C for 30 min before triethylamine (3.47 mL, 24.7 mmol, 4.00 equiv) was added dropwise. 4-(*N,N*-Dimethylamino)pyridine (76.0 mg, 6.20  $\cdot 10^{-4}$  mol, 1.00  $\cdot 10^{-1}$  equiv) and 4-nitrobenzene-1-sulfonyl chloride (3.07 g, 13.6 mmol, 2.20 equiv) were successively added, and the resulting solution was stirred at rt for 2 h. The reaction was then quenched with saturated aqueous  $\text{NH}_4\text{Cl}$ , and the aqueous phase was extracted with  $\text{CH}_2\text{Cl}_2$ . The combined organic extracts were dried over  $\text{Na}_2\text{SO}_4$ , filtered, and concentrated *in vacuo*. The resulting crude material was purified by silica gel flash column chromatography (10:1 hexanes/EtOAc) to afford nosylate **158** (0.930 g, 3.15 mmol, 51%) as a yellow oil that crystallized (mp = 77 °C) upon standing at rt.

**TLC:**  $R_f$  = 0.16 (10:3 hexanes/EtOAc; UV, CAM, *p*-anisaldehyde).  **$^1\text{H NMR}$**  (400 MHz,  $\text{CDCl}_3$ ):  $\delta$  8.45–8.39 (m, 2H), 8.15–8.10 (m, 2H), 4.90–4.25 (m, 5H), 2.22–1.97 (m, 2H) ppm.  **$^{13}\text{C NMR}$**  (100 MHz,  $\text{CDCl}_3$ ):  $\delta$  151.1, 141.6, 129.4, 124.7, 87.7 (dd,  $J$  = 174.8 Hz,  $J$  = 19.9

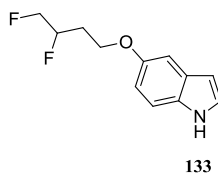
Hz), 83.5 (dd,  $J = 175.4$  Hz,  $J = 22.4$  Hz), 67.0 (d,  $J = 4.5$  Hz), 30.1 (dd,  $J = 21.4$  Hz,  $J = 6.9$  Hz) ppm.  $^{19}\text{F}$  NMR (376 MHz,  $\text{CDCl}_3$ , decoupled):  $\delta$  -193.68 (d,  $J = 12.9$  Hz), -232.06 (d,  $J = 12.9$  Hz) ppm.  $^{19}\text{F}$  NMR (376 MHz,  $\text{CDCl}_3$ , not decoupled):  $\delta$  -193.46 – -193.90 (m), -232.06 (tdd,  $J = 47.2$  Hz,  $J = 22.9$  Hz,  $J = 12.9$  Hz) ppm. IR (thin film):  $\nu$  3111, 2962, 1530, 1365, 1350, 1183, 941, 891, 855, 769, 745, 733, 683, 611, 463  $\text{cm}^{-1}$ . HRMS (EI+): exact mass calculated for  $\text{C}_{10}\text{H}_{11}\text{F}_2\text{NO}_5\text{S}$  ( $[\text{M}]^+$ ), 295.0321; found 295.0312.



### 5-(3,4-Difluorobutoxy)-1-tosyl-1H-indole (**160**):<sup>131</sup>

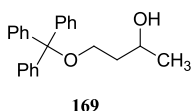
To a solution of 1-tosyl-1H-indol-5-ol (**142**) (1.07 g, 3.74 mmol, 1.20 equiv) and 3,4-difluorobutyl 4-nitrobenzenesulfonate (**158**) (0.920 g, 3.12 mmol, 1.00 equiv) in MeCN (31.2 mL) at rt under inert atmosphere was added potassium carbonate (538 mg, 3.89 mmol, 1.25 equiv). The resulting suspension was then stirred at 80 °C for 24 h, then cooled down to rt, filtered over a pad of Celite<sup>®</sup>, and the filtrate was concentrated *in vacuo*. The resulting crude material was purified by silica gel flash column chromatography (5:1 hexanes/EtOAc) to afford ether **160** (916 mg, 2.41 mmol, 77%) as a pale yellow syrup.

TLC:  $R_f = 0.20$  (10:3 hexanes/EtOAc; UV, CAM, *p*-anisaldehyde,  $\text{KMnO}_4$ ).  $^1\text{H}$  NMR (400 MHz,  $\text{CDCl}_3$ ):  $\delta$  7.88 (d,  $J = 9.0$  Hz, 1H), 7.75–7.70 (m, 2H), 7.52 (d,  $J = 3.6$  Hz, 1H), 7.21 (d,  $J = 8.3$  Hz, 2H), 6.97 (d,  $J = 2.4$  Hz, 1H), 6.91 (dd,  $J = 9.0$  Hz,  $J = 2.5$  Hz, 1H), 6.57 (dd,  $J = 3.6$  Hz,  $J = 0.8$  Hz, 1H), 5.12–4.86 (m, 1H), 4.75–4.41 (m, 2H), 4.12 (dd,  $J = 7.6$  Hz,  $J = 4.9$  Hz, 2H), 2.33 (s, 3H), 2.25–2.02 (m, 2H) ppm.  $^{13}\text{C}$  NMR (100 MHz,  $\text{CDCl}_3$ ):  $\delta$  155.4, 145.0, 135.4, 131.9, 130.0, 127.4, 126.9, 114.6, 114.1, 109.2, 104.7, 89.1 (dd,  $J = 173.0$  Hz,  $J = 19.5$  Hz), 84.3 (dd,  $J = 174.0$  Hz,  $J = 22.1$  Hz), 63.6 (d,  $J = 5.1$  Hz), 30.4 (dd,  $J = 21.2$  Hz,  $J = 6.8$  Hz), 21.7 ppm.  $^{19}\text{F}$  NMR (376 MHz,  $\text{CDCl}_3$ , decoupled):  $\delta$  -191.86 (d,  $J = 12.9$  Hz), -230.24 (d,  $J = 12.9$  Hz) ppm.  $^{19}\text{F}$  NMR (376 MHz,  $\text{CDCl}_3$ , not decoupled):  $\delta$  -191.61 – -192.11 (m), -230.24 (tdd,  $J = 47.7$  Hz,  $J = 22.4$  Hz,  $J = 12.9$  Hz) ppm. IR (thin film):  $\nu$  3144, 2957, 1457, 1368, 1224, 1174, 1155, 1125, 1091, 675, 593, 580, 538  $\text{cm}^{-1}$ . HRMS (ESI+): exact mass calculated for  $\text{C}_{19}\text{H}_{20}\text{F}_2\text{NO}_3\text{S}$  ( $[\text{M}+\text{H}]^+$ ), 380.1126; found 380.1128.

**5-(3,4-Difluorobutoxy)-1H-indole (133):**<sup>116</sup>

To a solution of 5-(3,4-difluorobutoxy)-1-tosyl-1H-indole (**160**) (0.900 g, 2.37 mmol, 1.00 equiv) in MeOH (23.7 mL) at rt were added magnesium turnings (577 mg, 23.7 mmol, 10.0 equiv). The resulting suspension was vigorously stirred at rt for 6 h. The reaction was then quenched with saturated aqueous NH<sub>4</sub>Cl, and the aqueous phase was extracted with EtOAc. The combined organic extracts were washed with brine, dried over Na<sub>2</sub>SO<sub>4</sub>, filtered, and concentrated *in vacuo*. The resulting crude material was purified by silica gel flash column chromatography (10:1 hexanes/EtOAc) to afford indole **133** (0.480 g, 2.13 mmol, 90%) as a yellow oil.

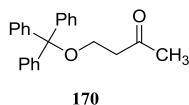
**TLC:**  $R_f$  = 0.34 (5:1 hexanes/EtOAc; UV, CAM, *p*-anisaldehyde). **<sup>1</sup>H NMR** (400 MHz, CDCl<sub>3</sub>): δ 8.06 (bs, 1H), 7.29 (d,  $J$  = 8.7 Hz, 1H), 7.19 (t,  $J$  = 2.8 Hz, 1H), 7.13 (d,  $J$  = 2.4 Hz, 1H), 6.86 (dd,  $J$  = 8.8 Hz,  $J$  = 2.5 Hz, 1H), 6.49 (ddd,  $J$  = 3.1 Hz,  $J$  = 2.0 Hz,  $J$  = 0.9 Hz, 1H), 5.17–4.92 (m, 1H), 4.78–4.44 (m, 2H), 4.18 (dd,  $J$  = 6.8 Hz,  $J$  = 5.1 Hz, 2H), 2.28–2.06 (m, 2H) ppm. **<sup>13</sup>C NMR** (100 MHz, CDCl<sub>3</sub>): δ 153.1, 131.3, 128.5, 125.1, 112.8, 111.9, 103.9, 102.6, 89.5 (dd,  $J$  = 172.8 Hz,  $J$  = 19.4 Hz), 84.4 (dd,  $J$  = 173.7 Hz,  $J$  = 22.0 Hz), 63.9 (d,  $J$  = 5.4 Hz), 30.5 (dd,  $J$  = 21.3 Hz,  $J$  = 6.8 Hz) ppm. **<sup>19</sup>F NMR** (376 MHz, CDCl<sub>3</sub>, decoupled): δ -191.24 (d,  $J$  = 13.0 Hz), -229.91 (d,  $J$  = 13.0 Hz) ppm. **<sup>19</sup>F NMR** (376 MHz, CDCl<sub>3</sub>, not decoupled): δ -190.99 – -191.47 (m), -229.91 (tdd,  $J$  = 47.6 Hz,  $J$  = 22.4 Hz,  $J$  = 12.8 Hz) ppm. **IR** (thin film): ν 3459, 3414, 2957, 2884, 1473, 1455, 1284, 1224, 1157, 1124, 1055, 1017, 758, 726 cm<sup>-1</sup>. **HRMS** (EI<sup>+</sup>): exact mass calculated for C<sub>12</sub>H<sub>13</sub>F<sub>2</sub>NO ([M]<sup>+</sup>), 225.0960; found 225.0954.

**4-(Trityloxy)butan-2-ol (169):**<sup>129</sup>

Trityl chloride (19.4 g, 66.2 mmol, 1.00 equiv) and 4-(*N,N*-dimethylamino)pyridine (327 mg, 2.65 mmol, 4.00 10<sup>-2</sup> equiv) were dissolved in CH<sub>2</sub>Cl<sub>2</sub> (331 mL) at rt under inert atmosphere. The resulting solution was cooled down to 0 °C prior to successively adding butane-1,3-diol

(**168**) (12.0 mL, 132 mmol, 2.00 equiv) and triethylamine (11.2 mL, 79.0 mmol, 1.20 equiv) dropwise. The reaction mixture was then stirred at rt for 2 h before it was quenched with saturated aqueous  $\text{NH}_4\text{Cl}$ . The aqueous phase was extracted with  $\text{CH}_2\text{Cl}_2$  and the combined organic extracts were dried over  $\text{Na}_2\text{SO}_4$ , filtered, and concentrated *in vacuo*. The resulting crude material was purified by silica gel flash column chromatography (5:1 hexanes/EtOAc) to afford alcohol **169** (21.9 g, 65.7 mmol, 99%) as a colorless syrup.

**TLC:**  $R_f = 0.15$  (5:1 hexanes/EtOAc; UV, CAM).  **$^1\text{H}$  NMR** (400 MHz,  $\text{CDCl}_3$ ):  $\delta$  7.47–7.42 (m, 6H), 7.35–7.21 (m, 9H), 4.04–3.94 (m, 1H), 3.42–3.19 (m, 2H), 2.84 (d,  $J = 3.0$  Hz, 1H), 1.87–1.66 (m, 2H), 1.17 (d,  $J = 6.3$  Hz, 3H) ppm.  **$^{13}\text{C}$  NMR** (100 MHz,  $\text{CDCl}_3$ ):  $\delta$  143.9, 128.6, 127.9, 127.1, 87.3, 67.5, 62.5, 38.5, 23.3 ppm. **IR** (thin film):  $\nu$  3393, 3086, 3058, 3032, 2965, 2928, 1490, 1448, 1068, 1032, 1016, 1002, 899, 772, 760, 745, 704, 697, 649, 632  $\text{cm}^{-1}$ . **HRMS** (EI+): exact mass calculated for  $\text{C}_{23}\text{H}_{24}\text{O}_2$  ( $[\text{M}]^+$ ), 332.1771; found 332.1772.

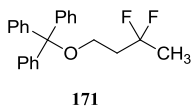


#### 4-(Trityloxy)butan-2-one (**170**):<sup>83</sup>

To a suspension of pyridinium chlorochromate (28.9 g, 131 mmol, 2.00 equiv), sodium acetate (1.63 g, 19.7 mmol, 3.00  $10^{-1}$  equiv), and oven-dried Celite<sup>®</sup> (ca. 3 g) in  $\text{CH}_2\text{Cl}_2$  (164 mL) under inert atmosphere at rt was added a solution of 4-(trityloxy)butan-2-ol (**169**) (21.9 g, 65.7 mmol, 1.00 equiv) in  $\text{CH}_2\text{Cl}_2$  (164 mL) dropwise. After stirring for 2 h at rt, the reaction was diluted with  $\text{Et}_2\text{O}$  (ca. 150 mL) and stirred for 10 min at rt. The resulting suspension was filtered over a pad of Celite<sup>®</sup>, and the filtrate was concentrated *in vacuo*. The crude material was then purified by silica gel flash column chromatography (10:1 hexanes/EtOAc) to afford ketone **170** (16.7 g, 50.5 mmol, 77%) as a white crystalline solid (mp = 86 °C).

**TLC:**  $R_f = 0.35$  (10:3 hexanes/EtOAc; UV, CAM).  **$^1\text{H}$  NMR** (400 MHz,  $\text{CDCl}_3$ ):  $\delta$  7.46–7.41 (m, 6H), 7.34–7.21 (m, 9H), 3.40 (t,  $J = 6.4$  Hz, 2H), 2.68 (t,  $J = 6.4$  Hz, 2H), 2.15 (s, 3H) ppm.  **$^{13}\text{C}$  NMR** (100 MHz,  $\text{CDCl}_3$ ):  $\delta$  207.8, 144.1, 128.8, 128.0, 127.2, 86.9, 59.5, 44.2, 30.4 ppm. **IR** (thin film):  $\nu$  3058, 3032, 2933, 2884, 1715, 1490, 1448, 1072, 1032, 773, 761, 746,

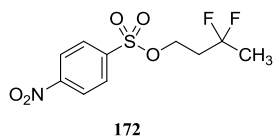
705, 697, 632  $\text{cm}^{-1}$ . **HRMS** (EI+): exact mass calculated for  $\text{C}_{23}\text{H}_{22}\text{O}_2$  ( $[\text{M}]^+$ ), 330.1615; found 330.1608.



**((3,3-Difluorobutoxy)methanetriyl)tribenzene (171):**<sup>84</sup>

To a solution of 4-(trityloxy)butan-2-one (**170**) (8.00 g, 24.2 mmol, 1.00 equiv) in  $\text{CH}_2\text{Cl}_2$  (121 mL) under inert atmosphere at 0 °C was added diethylaminosulfur trifluoride (6.73 mL, 48.4 mmol, 2.00 equiv) dropwise. After stirring for 96 h at rt, the reaction was carefully quenched with saturated aqueous  $\text{NaHCO}_3$ . The aqueous phase was extracted with  $\text{CH}_2\text{Cl}_2$  and the combined organic extracts were dried over  $\text{Na}_2\text{SO}_4$ , filtered, and concentrated *in vacuo*. The resulting crude material was purified by silica gel flash column chromatography (20:1 hexanes/EtOAc) to afford difluoride **171** (3.30 g, 9.35 mmol, 39%) as a colorless syrup that crystallized (mp = 71 °C) upon standing at rt.

**TLC:**  $R_f$  = 0.41 (20:1 hexanes/EtOAc; UV, CAM).  **$^1\text{H}$  NMR** (400 MHz,  $\text{CDCl}_3$ ):  $\delta$  7.48–7.43 (m, 6H), 7.36–7.23 (m, 9H), 3.31 (t,  $J$  = 6.6 Hz, 2H), 2.18 (tt,  $J$  = 15.5 Hz,  $J$  = 6.6 Hz, 2H), 1.61 (t,  $J$  = 18.7 Hz, 3H) ppm.  **$^{13}\text{C}$  NMR** (100 MHz,  $\text{CDCl}_3$ ):  $\delta$  144.1, 128.7, 128.0, 127.2, 123.7 (t,  $J$  = 237.9 Hz), 87.2, 58.3 (t,  $J$  = 6.2 Hz), 38.5 (t,  $J$  = 25.5 Hz), 24.0 (t,  $J$  = 27.5 Hz) ppm.  **$^{19}\text{F}$  NMR** (376 MHz,  $\text{CDCl}_3$ , decoupled):  $\delta$  -88.16 (s) ppm.  **$^{19}\text{F}$  NMR** (376 MHz,  $\text{CDCl}_3$ , not decoupled):  $\delta$  -88.03 – -88.29 (m) ppm. **IR** (thin film):  $\nu$  3059, 3024, 2938, 2888, 1490, 1448, 1391, 1234, 1180, 1138, 1088, 1072, 1032, 1001, 989, 899, 772, 760, 745, 703, 696, 649, 632  $\text{cm}^{-1}$ . **HRMS** (EI+): exact mass calculated for  $\text{C}_{23}\text{H}_{22}\text{F}_2\text{O}$  ( $[\text{M}]^+$ ), 352.1634; found 352.1635.

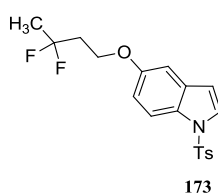


**3,3-Difluorobutyl 4-nitrobenzenesulfonate (172):**<sup>128,130</sup>

((3,3-Difluorobutoxy)methanetriyl)tribenzene (**171**) (2.25 g, 6.37 mmol, 1.00 equiv) was dissolved in  $\text{CH}_2\text{Cl}_2$  (31.9 mL) at rt under inert atmosphere. The resulting solution was cooled down to 0 °C prior to adding hydrochloric acid (4.0 M in dioxane) (3.19 mL, 12.8 mmol, 2.00

equiv) dropwise. The reaction was then stirred at 0 °C for 30 min before triethylamine (3.59 mL, 25.5 mmol, 4.00 equiv) was added dropwise. 4-(*N,N*-Dimethylamino)pyridine (79.0 mg, 6.40 10<sup>-4</sup> mol, 1.00 10<sup>-1</sup> equiv) and 4-nitrobenzene-1-sulfonyl chloride (3.17 g, 14.0 mmol, 2.20 equiv) were successively added, and the resulting solution was stirred at rt for 2 h. The reaction was then quenched with saturated aqueous NH<sub>4</sub>Cl, and the aqueous phase was extracted with CH<sub>2</sub>Cl<sub>2</sub>. The combined organic extracts were dried over Na<sub>2</sub>SO<sub>4</sub>, filtered, and concentrated *in vacuo*. The resulting crude material was purified by silica gel flash column chromatography (10:1 hexanes/EtOAc) to afford nosylate **172** (1.45 g, 4.90 mmol, 77%) as a yellow crystalline solid (mp = 62 °C).

**TLC:** *R<sub>f</sub>* = 0.22 (10:3 hexanes/EtOAc; UV, CAM, KMnO<sub>4</sub>). **<sup>1</sup>H NMR** (400 MHz, CDCl<sub>3</sub>): δ 8.45–8.39 (m, 2H), 8.15–8.10 (m, 2H), 4.33 (t, *J* = 6.5 Hz, 2H), 2.31 (tt, *J* = 15.5 Hz, *J* = 6.6 Hz, 2H), 1.63 (t, *J* = 18.6 Hz, 3H) ppm. **<sup>13</sup>C NMR** (100 MHz, CDCl<sub>3</sub>): δ 151.1, 141.6, 129.4, 124.7, 122.2 (t, *J* = 239.3 Hz), 65.4 (t, *J* = 5.9 Hz), 37.4 (t, *J* = 26.1 Hz), 24.1 (t, *J* = 27.0 Hz) ppm. **<sup>19</sup>F NMR** (376 MHz, CDCl<sub>3</sub>, decoupled): δ -90.91 (s) ppm. **<sup>19</sup>F NMR** (376 MHz, CDCl<sub>3</sub>, not decoupled): δ -90.78 – -91.03 (m) ppm. **IR** (thin film): ν 3111, 1531, 1367, 1350, 1183, 969, 915, 855, 782, 745, 733, 614, 463 cm<sup>-1</sup>. **HRMS** (EI<sup>+</sup>): exact mass calculated for C<sub>10</sub>H<sub>11</sub>F<sub>2</sub>NO<sub>5</sub>S ([M]<sup>+</sup>), 295.0321; found 295.0322.

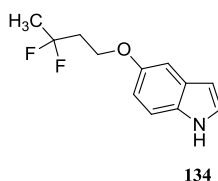


### 5-(3,3-Difluorobutoxy)-1-tosyl-1*H*-indole (**173**):<sup>131</sup>

To a solution of 1-tosyl-1*H*-indol-5-ol (**142**) (782 mg, 2.72 mmol, 1.20 equiv) and 3,3-difluorobutyl 4-nitrobenzenesulfonate (**172**) (0.670 g, 2.27 mmol, 1.00 equiv) in MeCN (22.7 mL) at rt under inert atmosphere was added potassium carbonate (392 mg, 2.84 mmol, 1.25 equiv). The resulting suspension was stirred at 80 °C for 20 h, then cooled down to rt, filtered over a pad of Celite<sup>®</sup>, and the filtrate was concentrated *in vacuo*. The resulting crude material was purified by silica gel flash column chromatography (5:1 hexanes/EtOAc) to afford ether **173** (0.590 g, 1.56 mmol, 69%) as a yellow crystalline solid (mp = 97 °C).

**TLC:** *R<sub>f</sub>* = 0.18 (5:1 hexanes/EtOAc; UV, CAM, *p*-anisaldehyde). **<sup>1</sup>H NMR** (400 MHz, CDCl<sub>3</sub>): δ 7.88 (d, *J* = 9.0 Hz, 1H), 7.75–7.70 (m, 2H), 7.52 (d, *J* = 3.6 Hz, 1H), 7.21 (d, *J* =

8.2 Hz, 2H), 6.97 (d,  $J = 2.4$  Hz, 1H), 6.91 (dd,  $J = 9.0$  Hz,  $J = 2.5$  Hz, 1H), 6.57 (dd,  $J = 3.6$  Hz,  $J = 0.8$  Hz, 1H), 4.15 (t,  $J = 6.5$  Hz, 2H), 2.44–2.30 (m, 5H), 1.69 (t,  $J = 18.8$  Hz, 3H) ppm.  $^{13}\text{C}$  NMR (100 MHz,  $\text{CDCl}_3$ ):  $\delta$  155.3, 145.0, 135.4, 131.9, 130.0, 127.4, 126.9, 123.5 (t,  $J = 238.0$  Hz), 114.6, 114.2, 109.2, 104.7, 62.8 (t,  $J = 6.3$  Hz), 37.9 (t,  $J = 25.9$  Hz), 24.1 (t,  $J = 27.4$  Hz), 21.7 ppm.  $^{19}\text{F}$  NMR (376 MHz,  $\text{CDCl}_3$ , decoupled):  $\delta$  -89.22 (s) ppm.  $^{19}\text{F}$  NMR (376 MHz,  $\text{CDCl}_3$ , not decoupled):  $\delta$  -89.08 – -89.36 (m) ppm. IR (thin film):  $\nu$  3143, 2946, 1457, 1368, 1220, 1173, 1140, 1091, 703, 674, 589, 579, 538  $\text{cm}^{-1}$ . HRMS (ESI+): exact mass calculated for  $\text{C}_{19}\text{H}_{20}\text{F}_2\text{NO}_3\text{S}$  ( $[\text{M}+\text{H}]^+$ ), 380.1126; found 380.1130.

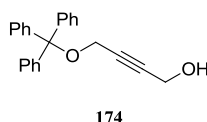


#### 5-(3,3-Difluorobutoxy)-1H-indole (**134**):<sup>116</sup>

To a solution of 5-(3,3-difluorobutoxy)-1-tosyl-1H-indole (**173**) (0.400 g, 1.05 mmol, 1.00 equiv) in MeOH (7.03 mL) at rt were added magnesium turnings (256 mg, 10.5 mmol, 10.0 equiv). The resulting suspension was vigorously stirred at rt for 3 h. The reaction was then quenched with saturated aqueous  $\text{NH}_4\text{Cl}$ , and the aqueous phase was extracted with EtOAc. The combined organic extracts were washed with brine, dried over  $\text{Na}_2\text{SO}_4$ , filtered, and concentrated *in vacuo*. The resulting crude material was purified by silica gel flash column chromatography (5:1 hexanes/EtOAc) to afford indole **134** (233 mg, 1.03 mmol, 98%) as a colorless honey.

**TLC**:  $R_f = 0.17$  (5:1 hexanes/EtOAc; UV, CAM, *p*-anisaldehyde).  $^1\text{H}$  NMR (400 MHz,  $\text{CDCl}_3$ ):  $\delta$  8.05 (bs, 1H), 7.29 (d,  $J = 8.8$  Hz, 1H), 7.19 (t,  $J = 2.8$  Hz, 1H), 7.13 (d,  $J = 2.3$  Hz, 1H), 6.87 (dd,  $J = 8.8$  Hz,  $J = 2.4$  Hz, 1H), 6.52–6.47 (m, 1H), 4.21 (t,  $J = 6.5$  Hz, 2H), 2.41 (tt,  $J = 15.3$  Hz,  $J = 6.5$  Hz, 2H), 1.74 (t,  $J = 18.8$  Hz, 3H) ppm.  $^{13}\text{C}$  NMR (100 MHz,  $\text{CDCl}_3$ ):  $\delta$  153.0, 131.3, 128.4, 125.1, 123.7 (t,  $J = 237.9$  Hz), 112.9, 111.9, 103.8, 102.6, 63.1 (t,  $J = 6.3$  Hz), 38.0 (t,  $J = 25.8$  Hz), 24.0 (t,  $J = 27.4$  Hz) ppm.  $^{19}\text{F}$  NMR (376 MHz,  $\text{CDCl}_3$ , decoupled):  $\delta$  -88.76 (s) ppm.  $^{19}\text{F}$  NMR (376 MHz,  $\text{CDCl}_3$ , not decoupled):  $\delta$  -88.62 – -88.89 (m) ppm. IR (thin film):  $\nu$  3414, 3002, 2944, 2888, 1474, 1455, 1392, 1235, 1219, 1151, 906, 801, 756, 723  $\text{cm}^{-1}$ . HRMS (EI+): exact mass calculated for  $\text{C}_{12}\text{H}_{13}\text{F}_2\text{NO}$  ( $[\text{M}]^+$ ), 225.0960; found 225.0962.

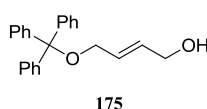




#### 4-(Trityloxy)but-2-yn-1-ol (**174**):<sup>129</sup>

Trityl chloride (18.5 g, 63.2 mmol, 1.00 equiv) and 4-(*N,N*-dimethylamino)pyridine (312 mg, 2.53 mmol, 4.00  $10^{-2}$  equiv) were dissolved in  $\text{CH}_2\text{Cl}_2$  (316 mL) at rt under inert atmosphere. The resulting solution was cooled down to 0 °C prior to successively adding but-2-yne-1,4-diol (**141**) (11.0 g, 126 mmol, 2.00 equiv) and triethylamine (19.6 mL, 139 mmol, 2.20 equiv) dropwise. The reaction mixture was then stirred at rt for 2 h before it was quenched with saturated aqueous  $\text{NH}_4\text{Cl}$ . The aqueous phase was extracted with  $\text{CH}_2\text{Cl}_2$  and the combined organic extracts were dried over  $\text{Na}_2\text{SO}_4$ , filtered, and concentrated *in vacuo*. The resulting crude material was purified by silica gel flash column chromatography (10:1 hexanes/EtOAc) to afford alcohol **174** (14.7 g, 44.7 mmol, 71%) as a white crystalline solid (mp = 83 °C).

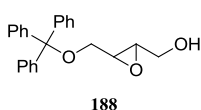
**TLC:**  $R_f$  = 0.10 (5:1 hexanes/EtOAc; UV, CAM).  **$^1\text{H}$  NMR** (400 MHz,  $\text{CDCl}_3$ ):  $\delta$  7.50–7.44 (m, 6H), 7.35–7.22 (m, 9H), 4.26 (dt,  $J$  = 6.2 Hz,  $J$  = 1.8 Hz, 2H), 3.84 (t,  $J$  = 1.8 Hz, 2H), 1.49 (t,  $J$  = 6.2 Hz, 1H) ppm.  **$^{13}\text{C}$  NMR** (100 MHz,  $\text{CDCl}_3$ ):  $\delta$  143.6, 128.8, 128.1, 127.3, 87.7, 83.7, 82.7, 53.2, 51.4 ppm. **IR** (thin film):  $\nu$  3350, 3085, 3058, 3032, 2863, 1490, 1448, 1139, 1053, 1028, 1012, 977, 763, 746, 732, 704, 697, 646, 632  $\text{cm}^{-1}$ . **HRMS** (ESI<sup>+</sup>): exact mass calculated for  $\text{C}_{23}\text{H}_{20}\text{NaO}_2$  ( $[\text{M}+\text{Na}]^+$ ), 351.1356; found 351.1355.



#### (*E*)-4-(Trityloxy)but-2-en-1-ol (**175**):<sup>113</sup>

To a vigorously stirred suspension of lithium aluminium hydride (3.81 g, 98.0 mmol, 2.20 equiv) in THF (223 mL) under inert atmosphere at 0 °C was added a solution of 4-(trityloxy)but-2-yn-1-ol (**174**) (14.7 g, 44.7 mmol, 1.00 equiv) in THF (223 mL) dropwise. The reaction was then stirred at rt for 1 h before it was diluted with additional THF (ca. 250 mL).  $\text{Na}_2\text{SO}_4$  (ca. 50 g) was added to the suspension, and water was then added dropwise until the suspension turned white. After filtration, the filtrate was concentrated *in vacuo* and the resulting crude material was purified by silica gel flash column chromatography (5:1 hexanes/EtOAc) to afford allylic alcohol **175** (12.3 g, 37.2 mmol, 83%) as a colorless syrup that crystallized (mp = 78 °C) upon standing at rt.

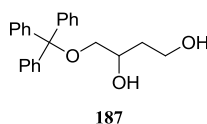
**TLC:**  $R_f = 0.11$  (10:3 hexanes/EtOAc; UV, CAM).  **$^1\text{H NMR}$**  (400 MHz,  $\text{CDCl}_3$ ):  $\delta$  7.50–7.43 (m, 6H), 7.34–7.21 (m, 9H), 6.01 (dtt,  $J = 15.6$  Hz,  $J = 5.5$  Hz,  $J = 1.7$  Hz, 1H), 5.82 (dtt,  $J = 15.4$  Hz,  $J = 4.9$  Hz,  $J = 1.5$  Hz, 1H), 4.18 (tt,  $J = 5.4$  Hz,  $J = 1.4$  Hz, 2H), 3.65 (dq,  $J = 4.7$  Hz,  $J = 1.5$  Hz, 2H), 1.36 (t,  $J = 5.9$  Hz, 1H) ppm.  **$^{13}\text{C NMR}$**  (100 MHz,  $\text{CDCl}_3$ ):  $\delta$  144.3, 130.2, 128.8, 128.0, 127.1, 87.0, 64.2, 63.5 ppm. **IR** (thin film):  $\nu$  3326, 3085, 3057, 3023, 2860, 1490, 1448, 1089, 1054, 1029, 1001, 968, 899, 762, 746, 732, 703, 697, 643, 632  $\text{cm}^{-1}$ . **HRMS** (ESI+): exact mass calculated for  $\text{C}_{23}\text{H}_{22}\text{NaO}_2$  ( $[\text{M}+\text{Na}]^+$ ), 353.1512; found 353.1508.



**(3-((Trityloxy)methyl)oxiran-2-yl)methanol (188):**<sup>132</sup>

To a solution of (*E*)-4-(trityloxy)but-2-en-1-ol (**175**) (5.71 g, 17.3 mmol, 1.00 equiv) in  $\text{CH}_2\text{Cl}_2$  (173 mL) at 0 °C was added *m*-chloroperoxybenzoic acid (6.39 g, 25.9 mmol, 1.50 equiv). The reaction was stirred at rt for 4 h, then quenched with 3 M NaOH (aq), and saturated aqueous  $\text{NaHCO}_3$ . The aqueous phase was extracted with  $\text{CH}_2\text{Cl}_2$ , and the combined organic extracts were dried over  $\text{Na}_2\text{SO}_4$ , filtered, and concentrated *in vacuo*. The resulting crude material was purified by silica gel flash column chromatography (5:2 hexanes/EtOAc) to afford epoxyalcohol **188** (5.02 g, 14.5 mmol, 84%) as a white crystalline solid (mp = 130 °C).

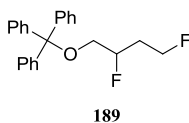
**TLC:**  $R_f = 0.16$  (2:1 hexanes/EtOAc; UV, CAM).  **$^1\text{H NMR}$**  (400 MHz,  $\text{CDCl}_3$ ):  $\delta$  7.50–7.42 (m, 6H), 7.35–7.21 (m, 9H), 3.94 (dd,  $J = 12.7$  Hz,  $J = 2.4$  Hz, 1H), 3.64 (dd,  $J = 12.7$  Hz,  $J = 4.1$  Hz, 1H), 3.39 (dd,  $J = 10.2$  Hz,  $J = 2.2$  Hz, 1H), 3.25–3.10 (m, 3H), 1.80 (bs, 1H) ppm.  **$^{13}\text{C NMR}$**  (100 MHz,  $\text{CDCl}_3$ ):  $\delta$  143.9, 128.8, 128.0, 127.2, 86.9, 63.7, 61.3, 56.0, 54.6 ppm. **IR** (thin film):  $\nu$  3414, 3058, 3023, 2922, 2869, 1490, 1448, 1088, 1031, 1002, 900, 872, 764, 747, 734, 704, 698, 648, 632  $\text{cm}^{-1}$ . **HRMS** (EI+): exact mass calculated for  $\text{C}_{23}\text{H}_{22}\text{O}_3$  ( $[\text{M}]^+$ ), 346.1564; found 346.1569.



#### 4-(Trityloxy)butane-1,3-diol (**187**):<sup>135</sup>

To a stirred solution of (3-((trityloxy)methyl)oxiran-2-yl)methanol (**188**) (4.99 g, 14.4 mmol, 1.00 equiv) in THF (144 mL) under inert atmosphere at 0 °C was added sodium bis(2-methoxyethoxy)aluminumhydride (60% in toluene) (11.7 mL, 36.0 mmol, 2.50 equiv) dropwise. After stirring for 15 min at 0 °C, the reaction was stirred at rt for 2 h. The reaction was then carefully quenched with saturated aqueous Rochelle's salt solution, and vigorous stirring was continued for 1 h at rt. The aqueous phase was then extracted with EtOAc, and the combined organic extracts were washed with brine, dried over Na<sub>2</sub>SO<sub>4</sub>, filtered, and concentrated *in vacuo*. The resulting crude material was purified by silica gel flash column chromatography (1:1 hexanes/EtOAc) to afford diol **187** (5.01 g, 14.4 mmol, 100%) as a white crystalline solid (mp = 97 °C).

**TLC:**  $R_f$  = 0.13 (1:1 hexanes/EtOAc; UV, CAM). **<sup>1</sup>H NMR** (400 MHz, CDCl<sub>3</sub>): δ 7.47–7.41 (m, 6H), 7.35–7.22 (m, 9H), 4.04 (tq,  $J$  = 8.0 Hz,  $J$  = 4.0 Hz, 1H), 3.83–3.75 (m, 2H), 3.20–3.09 (m, 2H), 2.78 (d,  $J$  = 3.4 Hz, 1H), 2.45 (t,  $J$  = 5.3 Hz, 1H), 1.75–1.61 (m, 2H) ppm. **<sup>13</sup>C NMR** (100 MHz, CDCl<sub>3</sub>): δ 143.9, 128.8, 128.0, 127.3, 86.9, 71.0, 67.7, 61.3, 35.1 ppm. **IR** (thin film): ν 3391, 3060, 3033, 2927, 2875, 1448, 1066, 1033, 905, 774, 764, 727, 704, 698, 648, 632 cm<sup>-1</sup>. **HRMS** (ESI<sup>+</sup>): exact mass calculated for C<sub>23</sub>H<sub>24</sub>NaO<sub>3</sub> ([M+Na]<sup>+</sup>), 371.1618; found 371.1610.

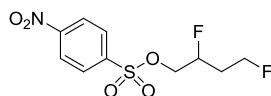


#### ((2,4-Difluorobutoxy)methanetriyl)tribenzene (**189**):<sup>80</sup>

To a solution of 4-(trityloxy)butane-1,3-diol (**187**) (5.01 g, 14.4 mmol, 1.00 equiv) in MeCN (144 mL) under inert atmosphere at 0 °C were successively added *N,N*-diisopropylethylamine (15.2 mL, 86.0 mmol, 6.00 equiv), *N,N*-diisopropylethylamine trihydrofluoride (8.91 mL, 43.2 mmol, 3.00 equiv), and perfluorobutanesulfonyl fluoride (8.44 mL, 43.2 mmol, 3.00 equiv) dropwise. After stirring at 0 °C for 2 h, the reaction was stirred at rt for 1 h, then quenched with saturated aqueous NaHCO<sub>3</sub>. The aqueous phase was extracted with Et<sub>2</sub>O and the combined organic extracts were washed with brine, dried over Na<sub>2</sub>SO<sub>4</sub>, filtered, and

concentrated *in vacuo*. The resulting crude material was purified by silica gel flash column chromatography (20:1 hexanes/EtOAc) to afford difluoride **189** (3.18 g, 9.02 mmol, 63%) as a white crystalline solid (mp = 64 °C).

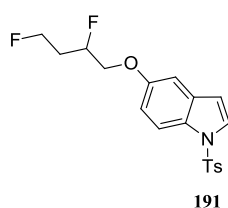
**TLC:**  $R_f$  = 0.30 (20:1 hexanes/EtOAc; UV, CAM).  **$^1\text{H NMR}$**  (400 MHz,  $\text{CDCl}_3$ ):  $\delta$  7.51–7.44 (m, 6H), 7.36–7.22 (m, 9H), 4.83 (dddt,  $J$  = 48.7 Hz,  $J$  = 8.8 Hz,  $J$  = 5.1 Hz,  $J$  = 3.5 Hz, 1H), 4.70–4.43 (m, 2H), 3.38–3.18 (m, 2H), 2.23–1.89 (m, 2H) ppm.  **$^{13}\text{C NMR}$**  (100 MHz,  $\text{CDCl}_3$ ):  $\delta$  143.8, 128.8, 128.0, 127.3, 89.3 (dd,  $J$  = 172.2 Hz,  $J$  = 4.4 Hz), 80.1 (dd,  $J$  = 164.9 Hz,  $J$  = 4.9 Hz), 65.5 (d,  $J$  = 21.8 Hz), 30.0 (t,  $J$  = 20.6 Hz) ppm.  **$^{19}\text{F NMR}$**  (376 MHz,  $\text{CDCl}_3$ , decoupled):  $\delta$  -190.01 (s), -221.83 (s) ppm.  **$^{19}\text{F NMR}$**  (376 MHz,  $\text{CDCl}_3$ , not decoupled):  $\delta$  -189.80 – -190.23 (m), -221.83 (tdd,  $J$  = 47.0 Hz,  $J$  = 31.9 Hz,  $J$  = 20.0 Hz) ppm. **IR** (thin film):  $\nu$  3059, 2970, 2912, 1490, 1448, 1078, 1033, 984, 902, 775, 764, 746, 731, 697, 648, 642, 631  $\text{cm}^{-1}$ . **HRMS** (EI<sup>+</sup>): exact mass calculated for  $\text{C}_{23}\text{H}_{22}\text{F}_2\text{O}$  ( $[\text{M}]^+$ ), 352.1634; found 352.1634.

**190****2,4-Difluorobutyl 4-nitrobenzenesulfonate (190):**<sup>128,130</sup>

((2,4-Difluorobutoxy)methanetriyl)tribenzene (**189**) (3.15 g, 8.93 mmol, 1.00 equiv) was dissolved in  $\text{CH}_2\text{Cl}_2$  (44.7 mL) at rt under inert atmosphere. The resulting solution was cooled down to 0 °C prior to adding hydrochloric acid (4.0 M in dioxane) (4.47 mL, 17.9 mmol, 2.00 equiv) dropwise. The reaction was then stirred at 0 °C for 30 min before triethylamine (5.03 mL, 35.7 mmol, 4.00 equiv) was added dropwise. 4-(*N,N*-Dimethylamino)pyridine (0.110 g, 8.90  $10^{-4}$  mol, 1.00  $10^{-1}$  equiv) and 4-nitrobenzene-1-sulfonyl chloride (4.44 g, 19.7 mmol, 2.20 equiv) were successively added, and the resulting solution was stirred at rt for 2 h. The reaction was then quenched with saturated aqueous  $\text{NH}_4\text{Cl}$ , and the aqueous phase was extracted with  $\text{CH}_2\text{Cl}_2$ . The combined organic extracts were dried over  $\text{Na}_2\text{SO}_4$ , filtered, and concentrated *in vacuo*. The resulting crude material was purified by silica gel flash column chromatography (5:1 hexanes/EtOAc) to afford nosylate **190** (2.16 g, 7.30 mmol, 82%) as a yellow crystalline solid (mp = 98 °C).

**TLC:**  $R_f$  = 0.16 (10:3 hexanes/EtOAc; UV,  $\text{KMnO}_4$ ).  **$^1\text{H NMR}$**  (400 MHz,  $\text{CDCl}_3$ ):  $\delta$  8.44–8.39 (m, 2H), 8.15–8.10 (m, 2H), 4.99–4.80 (m, 1H), 4.66–4.46 (m, 2H), 4.42–4.22 (m, 2H),

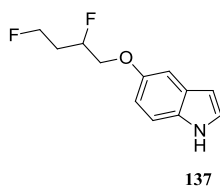
2.13–1.93 (m, 2H) ppm.  $^{13}\text{C}$  NMR (100 MHz,  $\text{CDCl}_3$ ):  $\delta$  151.1, 141.6, 129.5, 124.7, 87.1 (dd,  $J = 176.8$  Hz,  $J = 2.9$  Hz), 79.0 (dd,  $J = 166.2$  Hz,  $J = 5.2$  Hz), 71.6 (dd,  $J = 22.3$  Hz,  $J = 2.1$  Hz), 32.1 (t,  $J = 20.6$  Hz) ppm.  $^{19}\text{F}$  NMR (376 MHz,  $\text{CDCl}_3$ , decoupled):  $\delta$  -190.28 (s), -221.37 (s) ppm.  $^{19}\text{F}$  NMR (376 MHz,  $\text{CDCl}_3$ , not decoupled):  $\delta$  -190.05 – -190.50 (m), -221.12 – -221.61 (m) ppm. IR (thin film):  $\nu$  3110, 2976, 1531, 1369, 1350, 1184, 991, 973, 945, 911, 856, 816, 794, 744, 734, 683, 614, 607  $\text{cm}^{-1}$ . HRMS (EI+): exact mass calculated for  $\text{C}_{10}\text{H}_{11}\text{F}_2\text{NO}_5\text{S}$  ( $[\text{M}]^+$ ), 295.0321; found 295.0326.



**5-(2,4-Difluorobutoxy)-1-tosyl-1H-indole (191):**<sup>131</sup>

To a solution of 1-tosyl-1H-indol-5-ol (**142**) (572 mg, 1.99 mmol, 1.20 equiv) and 2,4-difluorobutyl 4-nitrobenzenesulfonate (**190**) (0.490 g, 1.66 mmol, 1.00 equiv) in MeCN (16.6 mL) at rt under inert atmosphere was added potassium carbonate (287 mg, 2.07 mmol, 1.25 equiv). The resulting suspension was stirred at 80 °C for 72 h, then cooled down to rt, filtered over a pad of Celite<sup>®</sup>, and the filtrate was concentrated *in vacuo*. The resulting crude material was purified by silica gel flash column chromatography (5:1 hexanes/EtOAc) to afford ether **191** (465 mg, 1.23 mmol, 74%) as a yellow honey.

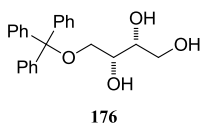
**TLC:**  $R_f = 0.18$  (10:3 hexanes/EtOAc; UV, CAM, *p*-anisaldehyde).  $^1\text{H}$  NMR (400 MHz,  $\text{CDCl}_3$ ):  $\delta$  7.89 (d,  $J = 9.0$  Hz, 1H), 7.76–7.70 (m, 2H), 7.52 (d,  $J = 3.6$  Hz, 1H), 7.20 (d,  $J = 8.2$  Hz, 2H), 6.98 (d,  $J = 2.5$  Hz, 1H), 6.95 (dd,  $J = 9.0$  Hz,  $J = 2.5$  Hz, 1H), 6.57 (d,  $J = 3.6$  Hz, 1H), 5.13–4.93 (m, 1H), 4.77–4.54 (m, 2H), 4.21–4.06 (m, 2H), 2.33 (s, 3H), 2.27–2.07 (m, 2H) ppm.  $^{13}\text{C}$  NMR (100 MHz,  $\text{CDCl}_3$ ):  $\delta$  155.3, 145.0, 135.3, 131.8, 130.1, 130.0, 127.4, 126.9, 114.6, 114.3, 109.2, 105.0, 88.4 (dd,  $J = 173.0$  Hz,  $J = 3.6$  Hz), 79.8 (dd,  $J = 165.4$  Hz,  $J = 5.1$  Hz), 70.2 (d,  $J = 23.1$  Hz), 32.7 (t,  $J = 20.5$  Hz), 21.7 ppm.  $^{19}\text{F}$  NMR (376 MHz,  $\text{CDCl}_3$ , decoupled):  $\delta$  -190.37 (s), -221.44 (s) ppm.  $^{19}\text{F}$  NMR (376 MHz,  $\text{CDCl}_3$ , not decoupled):  $\delta$  -190.14 – -190.60 (m), -221.21 – -221.67 (m) ppm. IR (thin film):  $\nu$  3144, 2924, 1446, 1367, 1223, 1173, 1157, 1142, 1091, 995, 812, 721, 703, 674, 590, 538  $\text{cm}^{-1}$ . HRMS (ESI+): exact mass calculated for  $\text{C}_{19}\text{H}_{20}\text{F}_2\text{NO}_3\text{S}$  ( $[\text{M}+\text{H}]^+$ ), 380.1126; found 380.1127.



### 5-(2,4-Difluorobutoxy)-1*H*-indole (**137**):<sup>116</sup>

To a solution of 5-(2,4-difluorobutoxy)-1-tosyl-1*H*-indole (**191**) (0.320 g, 8.40  $\cdot 10^{-4}$  mol, 1.00 equiv) in MeOH (5.62 mL) at rt were added magnesium turnings (205 mg, 8.43 mmol, 10.0 equiv). The resulting suspension was vigorously stirred at rt for 2 h. The reaction was then quenched with saturated aqueous  $\text{NH}_4\text{Cl}$ , and the aqueous phase was extracted with EtOAc. The combined organic extracts were washed with brine, dried over  $\text{Na}_2\text{SO}_4$ , filtered, and concentrated *in vacuo*. The resulting crude material was purified by silica gel flash column chromatography (5:1 hexanes/EtOAc) to afford indole **137** (175 mg, 7.80  $\cdot 10^{-4}$  mol, 92%) as a colorless oil.

**TLC:**  $R_f = 0.27$  (5:2 hexanes/EtOAc; UV, CAM, *p*-anisaldehyde).  **$^1\text{H}$  NMR** (400 MHz,  $\text{CDCl}_3$ ):  $\delta$  8.08 (bs, 1H), 7.29 (d,  $J = 8.8$  Hz, 1H), 7.19 (t,  $J = 2.8$  Hz, 1H), 7.14 (d,  $J = 2.5$  Hz, 1H), 6.91 (dd,  $J = 8.8$  Hz,  $J = 2.5$  Hz, 1H), 6.49 (td,  $J = 2.1$  Hz,  $J = 1.0$  Hz, 1H), 5.18–4.97 (m, 1H), 4.81–4.56 (m, 2H), 4.26–4.12 (m, 2H), 2.31–2.11 (m, 2H) ppm.  **$^{13}\text{C}$  NMR** (100 MHz,  $\text{CDCl}_3$ ):  $\delta$  153.1, 131.5, 128.4, 125.2, 113.0, 111.9, 104.1, 102.6, 88.7 (dd,  $J = 172.4$  Hz,  $J = 3.9$  Hz), 79.9 (dd,  $J = 165.1$  Hz,  $J = 5.1$  Hz), 70.6 (d,  $J = 22.8$  Hz), 32.8 (t,  $J = 20.5$  Hz) ppm.  **$^{19}\text{F}$  NMR** (376 MHz,  $\text{CDCl}_3$ , decoupled):  $\delta$  -190.36 (s), -221.38 (s) ppm.  **$^{19}\text{F}$  NMR** (376 MHz,  $\text{CDCl}_3$ , not decoupled):  $\delta$  -190.14 – -190.59 (m), -221.14 – -221.63 (m) ppm. **IR** (thin film):  $\nu$  3416, 2971, 2915, 1623, 1582, 1478, 1452, 1285, 1225, 1161, 1123, 1045, 973, 896, 803, 758, 726  $\text{cm}^{-1}$ . **HRMS** (EI+): exact mass calculated for  $\text{C}_{12}\text{H}_{13}\text{F}_2\text{NO}$  ( $[\text{M}]^+$ ), 225.0960; found 225.0963.

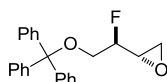


### (±)-*Threo*-4-(Trityloxy)butane-1,2,3-triol (**176**):<sup>109</sup>

To a solution of (*E*)-4-(trityloxy)but-2-en-1-ol (**175**) (12.3 g, 37.1 mmol, 1.00 equiv) in a 4:1 acetone/water mixture (185 mL) at rt were successively added *N*-methylmorpholine *N*-oxide (4.93 g, 40.8 mmol, 1.10 equiv) and osmium tetroxide (4% in water, 2.36 mL, 3.70  $\cdot 10^{-4}$  mol, 1.00  $\cdot 10^{-2}$  equiv). After stirring for 4 h at rt, the reaction was quenched with saturated aqueous

$\text{Na}_2\text{S}_2\text{O}_3$  and stirred for 1 h at rt. The resulting mixture was then extracted with EtOAc, and the combined organic extracts were washed with brine, dried over  $\text{Na}_2\text{SO}_4$ , filtered, and concentrated *in vacuo*. The resulting crude material was purified by silica gel flash column chromatography (100% EtOAc) to afford triol **176** (11.7 g, 32.1 mmol, 87%) as a white crystalline solid (mp = 135 °C).

**TLC:**  $R_f$  = 0.32 (EtOAc; UV,  $\text{KMnO}_4$ ).  **$^1\text{H}$  NMR** (400 MHz,  $\text{CDCl}_3$ ):  $\delta$  7.46–7.40 (m, 6H), 7.35–7.22 (m, 9H), 3.81–3.74 (m, 1H), 3.74–3.68 (m, 1H), 3.68–3.60 (m, 2H), 3.38 (dd,  $J$  = 9.8 Hz,  $J$  = 4.4 Hz, 1H), 3.26 (dd,  $J$  = 9.8 Hz,  $J$  = 5.8 Hz, 1H), 2.86 (d,  $J$  = 5.0 Hz, 1H), 2.76 (d,  $J$  = 5.1 Hz, 1H), 2.27 (dd,  $J$  = 6.6 Hz,  $J$  = 5.2 Hz, 1H) ppm.  **$^{13}\text{C}$  NMR** (100 MHz,  $\text{CDCl}_3$ ):  $\delta$  143.7, 128.7, 128.1, 127.4, 87.3, 71.9, 71.6, 65.5, 64.7 ppm. **IR** (thin film):  $\nu$  3379, 3058, 3032, 2930, 2880, 1490, 1219, 1072, 1032, 1001, 900, 764, 746, 703, 648, 632  $\text{cm}^{-1}$ . **HRMS** (ESI+): exact mass calculated for  $\text{C}_{23}\text{H}_{24}\text{NaO}_4$  ( $[\text{M}+\text{Na}]^+$ ), 387.1567; found 387.1564.



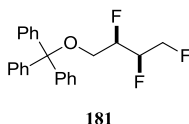
180

(±)-**Anti-Fluoro-2-(trityloxy)ethyl oxirane (180)**:<sup>108,134</sup>

To a vigorously stirred suspension of (±)-*threo*-4-(trityloxy)butane-1,2,3-triol (**176**) (11.7 g, 32.1 mmol, 1.00 equiv) in MeCN (160 mL) under inert atmosphere at rt was added 1,8-diazabicyclo[5.4.0]undec-7-ene (15.8 mL, 103 mmol, 3.20 equiv) dropwise. After complete dissolution of the substrate, the reaction was cooled down to 0 °C, and perfluorobutanesulfonyl fluoride (13.8 mL, 70.6 mmol, 2.20 equiv) was added dropwise. The reaction was stirred at 0 °C for 15 min, followed by 1 h at rt. The reaction was quenched with saturated aqueous  $\text{NaHCO}_3$ , and the aqueous phase was extracted with EtOAc. The combined organic extracts were washed with brine, dried over  $\text{Na}_2\text{SO}_4$ , filtered, and concentrated *in vacuo*. The resulting crude material was purified by silica gel flash column chromatography (20:1 hexanes/EtOAc) to afford fluoroepoxide **180** (6.61 g, 19.0 mmol, 59%) as a white crystalline solid (mp = 90 °C).

**TLC:**  $R_f$  = 0.42 (10:3 hexanes/EtOAc; UV, CAM,  $\text{KMnO}_4$ ).  **$^1\text{H}$  NMR** (400 MHz,  $\text{CDCl}_3$ ):  $\delta$  7.50–7.43 (m, 6H), 7.36–7.22 (m, 9 H), 4.49 (dq,  $J$  = 48.2 Hz,  $J$  = 4.4 Hz, 1H), 3.45–3.36 (m, 2H), 3.22–3.15 (m, 1H), 2.88–2.79 (m, 2H) ppm.  **$^{13}\text{C}$  NMR** (100 MHz,  $\text{CDCl}_3$ ):  $\delta$  143.7, 128.8, 128.1, 127.3, 91.2 (d,  $J$  = 177.6 Hz), 87.0, 63.8 (d,  $J$  = 22.0 Hz), 50.3 (d,  $J$  = 28.9 Hz),

45.1 (d,  $J = 5.3$  Hz) ppm.  $^{19}\text{F}$  NMR (376 MHz,  $\text{CDCl}_3$ , decoupled):  $\delta$  -197.99 (s) ppm.  $^{19}\text{F}$  NMR (376 MHz,  $\text{CDCl}_3$ , not decoupled):  $\delta$  -197.83 – -198.16 (m) ppm. IR (thin film):  $\nu$  3060, 2932, 1490, 1448, 1078, 1033, 934, 906, 774, 763, 728, 697, 648, 632, 533  $\text{cm}^{-1}$ . HRMS (ESI+): exact mass calculated for  $\text{C}_{23}\text{H}_{21}\text{FNO}_2$  ( $[\text{M}+\text{Na}]^+$ ), 371.1418; found 371.1416.

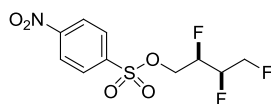


(±)-*Threo*-((2,3,4-Trifluorobutoxy)methanetriyl)tribenzene (**181**):<sup>80,102</sup>

A vigorously stirred mixture of (±)-*anti*-fluoro-2-(trityloxy)ethyl)oxirane (**180**) (1.00 g, 2.87 mmol, 1.00 equiv), *N,N*-diisopropylethylamine (4.56 mL, 25.8 mmol, 9.00 equiv), *N,N*-diisopropylethylamine trihydrofluoride (1.78 mL, 8.61 mmol, 3.00 equiv), and perfluorobutanesulfonyl fluoride (1.12 mL, 5.74 mmol, 2.00 equiv) in a sealed flask was heated at 100 °C for 72 h. After cooling down to rt, the reaction mixture was dissolved in  $\text{CH}_2\text{Cl}_2$ , and quenched with saturated aqueous  $\text{NaHCO}_3$  until any evolution of gas ceased. The aqueous phase was then extracted with  $\text{CH}_2\text{Cl}_2$ , and the combined organic extracts were dried over  $\text{Na}_2\text{SO}_4$ , filtered, and concentrated *in vacuo*. The resulting crude material was purified by silica gel flash column chromatography (40:1 hexanes/EtOAc) to afford trifluoride **181** (797 mg, 2.15 mmol, 75%) as a yellow honey.

TLC:  $R_f = 0.27$  (10:1 hexanes/EtOAc; UV, CAM).  $^1\text{H}$  NMR (400 MHz,  $\text{CDCl}_3$ ):  $\delta$  7.49–7.43 (m, 6H), 7.37–7.24 (m, 9H), 5.14–4.85 (m, 1H), 4.85–4.40 (m, 3H), 3.57 (dddd,  $J = 18.8$  Hz,  $J = 10.9$  Hz,  $J = 4.3$  Hz,  $J = 1.7$  Hz, 1H), 3.35 (dddd,  $J = 23.6$  Hz,  $J = 10.9$ ,  $J = 4.8$  Hz,  $J = 1.0$  Hz, 1H) ppm.  $^{13}\text{C}$  NMR (100 MHz,  $\text{CDCl}_3$ ):  $\delta$  143.4, 128.7, 128.2, 127.5, 91.1–90.6 (m), 89.4–88.8 (m), 87.2, 81.4 (ddd,  $J = 172.1$  Hz,  $J = 24.1$  Hz,  $J = 8.1$  Hz), 61.9 (dd,  $J = 24.1$  Hz,  $J = 6.9$  Hz) ppm.  $^{19}\text{F}$  NMR (376 MHz,  $\text{CDCl}_3$ , decoupled):  $\delta$  -203.25 (d,  $J = 12.6$  Hz), -205.59 (dd,  $J = 14.7$  Hz,  $J = 11.3$  Hz), -233.89 (d,  $J = 14.4$  Hz) ppm.  $^{19}\text{F}$  NMR (376 MHz,  $\text{CDCl}_3$ , not decoupled):  $\delta$  -203.03 – -203.47 (m), -205.35 – -205.83 (m), -233.63 – -234.16 (m) ppm. IR (thin film):  $\nu$  3060, 3034, 2957, 1490, 1449, 1079, 906, 765, 729, 703, 648, 632  $\text{cm}^{-1}$ . HRMS (EI+): exact mass calculated for  $\text{C}_{23}\text{H}_{21}\text{F}_3\text{O}$  ( $[\text{M}]^+$ ), 370.1539; found 370.1543.



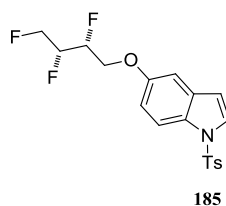


183

**(±)-Threo-2,3,4-Trifluorobutyl 4-nitrobenzenesulfonate (183):**<sup>128,130</sup>

(±)-Threo-((2,3,4-Trifluorobutoxy)methanetriyl)tribenzene (**181**) (1.59 g, 4.30 mmol, 1.00 equiv) was dissolved in CH<sub>2</sub>Cl<sub>2</sub> (21.5 mL) at rt under inert atmosphere. The resulting solution was cooled down to 0 °C prior to adding hydrochloric acid (4.0 M in dioxane) (2.15 mL, 8.60 mmol, 2.00 equiv) dropwise. The reaction was then stirred at 0 °C for 1 h before triethylamine (2.42 mL, 17.2 mmol, 4.00 equiv) was added dropwise. 4-(*N,N*-Dimethylamino)pyridine (53.0 mg, 4.30 10<sup>-4</sup> mol, 1.00 10<sup>-1</sup> equiv) and 4-nitrobenzene-1-sulfonyl chloride (2.14 g, 9.46 mmol, 2.20 equiv) were successively added, and the resulting solution was stirred at rt for 2 h. The reaction was then quenched with saturated aqueous NH<sub>4</sub>Cl, and the aqueous phase was extracted with CH<sub>2</sub>Cl<sub>2</sub>. The combined organic extracts were dried over Na<sub>2</sub>SO<sub>4</sub>, filtered, and concentrated *in vacuo*. The resulting crude material was purified by silica gel flash column chromatography (5:1 hexanes/EtOAc) to afford nosylate **183** (1.24 g, 3.97 mmol, 92%) as a yellow crystalline solid (mp = 91 °C).

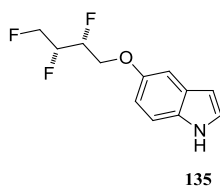
**TLC:**  $R_f$  = 0.18 (10:3 hexanes/EtOAc; UV, KMnO<sub>4</sub>). **<sup>1</sup>H NMR** (400 MHz, CDCl<sub>3</sub>): δ 8.47–8.40 (m, 2H), 8.17–8.10 (m, 2H), 5.04–4.55 (m, 4H), 4.51–4.37 (m, 2H) ppm. **<sup>13</sup>C NMR** (100 MHz, CDCl<sub>3</sub>): δ 151.2, 141.1, 129.5, 124.8, 88.4 (dt,  $J$  = 181.5 Hz,  $J$  = 21.4 Hz), 87.7 (ddd,  $J$  = 183.0 Hz,  $J$  = 21.6 Hz,  $J$  = 6.1 Hz), 80.3 (ddd,  $J$  = 173.3 Hz,  $J$  = 25.5 Hz,  $J$  = 7.0 Hz), 68.1 (ddd,  $J$  = 25.2 Hz,  $J$  = 7.1 Hz,  $J$  = 2.5 Hz) ppm. **<sup>19</sup>F NMR** (376 MHz, CDCl<sub>3</sub>, decoupled): δ -204.55 (d,  $J$  = 11.1 Hz), -207.30 (dd,  $J$  = 14.9 Hz,  $J$  = 11.1 Hz), -233.75 (d,  $J$  = 14.9 Hz) ppm. **<sup>19</sup>F NMR** (376 MHz, CDCl<sub>3</sub>, not decoupled): δ -204.31 – -204.77 (m), -207.07 – -207.56 (m), -233.75 (tdd,  $J$  = 46.9 Hz,  $J$  = 19.7 Hz,  $J$  = 14.9 Hz) ppm. **IR** (thin film): ν 3111, 2963, 1531, 1370, 1350, 1185, 1093, 1078, 978, 856, 801, 744, 737, 683, 611, 463 cm<sup>-1</sup>. **HRMS** (EI<sup>+</sup>): exact mass calculated for C<sub>10</sub>H<sub>10</sub>F<sub>3</sub>NO<sub>5</sub>S ([M]<sup>+</sup>), 313.0227; found 313.0227.



**(±)-Threo-1-Tosyl-5-(2,3,4-trifluorobutoxy)-1H-indole (185).**<sup>131</sup>

To a solution of 1-tosyl-1H-indol-5-ol (**142**) (1.29 g, 4.51 mmol, 1.20 equiv) and (±)-threo-2,3,4-trifluorobutyl 4-nitrobenzenesulfonate (**183**) (1.18 g, 3.75 mmol, 1.00 equiv) in MeCN (37.5 mL) at rt under inert atmosphere was added potassium carbonate (649 mg, 4.69 mmol, 1.25 equiv). The resulting suspension was stirred at 80 °C for 24 h, then cooled down to rt, filtered over a pad of Celite<sup>®</sup>, and the filtrate was concentrated *in vacuo*. The resulting crude material was purified by silica gel flash column chromatography (10:1 hexanes/EtOAc) to afford ether **185** (962 mg, 2.42 mmol, 65%) as a yellow honey.

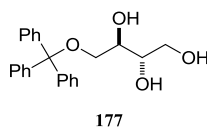
**TLC:**  $R_f = 0.27$  (5:2 hexanes/EtOAc; UV, CAM, *p*-anisaldehyde). **<sup>1</sup>H NMR** (400 MHz, CDCl<sub>3</sub>): δ 7.90 (d,  $J = 9.0$  Hz, 1H), 7.76–7.70 (m, 2H), 7.54 (d,  $J = 3.6$  Hz, 1H), 7.23–7.18 (m, 2H), 7.00 (d,  $J = 2.5$  Hz, 1H), 6.93 (dd,  $J = 9.0$  Hz,  $J = 2.5$  Hz, 1H), 6.58 (dd,  $J = 3.8$  Hz,  $J = 0.8$  Hz, 1H), 5.16–4.88 (m, 2H), 4.86–4.63 (m, 2H), 4.35–4.23 (m, 2H), 2.34 (s, 3H) ppm. **<sup>13</sup>C NMR** (100 MHz, CDCl<sub>3</sub>): δ 154.8, 145.1, 135.3, 131.9, 130.3, 130.0, 127.6, 126.9, 114.7, 114.1, 109.2, 105.1, 89.4 (dt,  $J = 180.2$  Hz,  $J = 20.9$  Hz), 88.9 (ddd,  $J = 179.5$  Hz,  $J = 20.8$  Hz,  $J = 6.7$  Hz), 81.2 (ddd,  $J = 172.3$  Hz,  $J = 24.8$  Hz,  $J = 7.5$  Hz), 66.4 (dd,  $J = 25.4$  Hz,  $J = 6.8$  Hz), 21.7 ppm. **<sup>19</sup>F NMR** (376 MHz, CDCl<sub>3</sub>, decoupled): δ -204.52 (d,  $J = 11.3$  Hz), -206.63 (dd,  $J = 14.6$  Hz,  $J = 11.3$  Hz), -233.42 (d,  $J = 14.6$  Hz) ppm. **<sup>19</sup>F NMR** (376 MHz, CDCl<sub>3</sub>, not decoupled): δ -204.27 – -204.76 (m), -206.37 – -206.91 (m), -233.42 (tdd,  $J = 48.5$  Hz,  $J = 20.9$  Hz,  $J = 14.6$  Hz) ppm. **IR** (thin film): ν 3144, 2958, 1447, 1367, 1222, 1173, 1157, 1142, 1089, 996, 811, 722, 703, 670, 590, 576, 539 cm<sup>-1</sup>. **HRMS** (ESI<sup>+</sup>): exact mass calculated for C<sub>19</sub>H<sub>19</sub>F<sub>3</sub>NO<sub>3</sub>S ([M+H]<sup>+</sup>), 398.1032; found 398.1033.



**(±)-*Threo*-5-(2,3,4-Trifluorobutoxy)-1*H*-indole (135):**<sup>116</sup>

To a solution of (±)-*threo*-1-tosyl-5-(2,3,4-trifluorobutoxy)-1*H*-indole (**185**) (0.930 g, 2.34 mmol, 1.00 equiv) in MeOH (23.4 mL) at rt were added magnesium turnings (569 mg, 23.4 mmol, 10.0 equiv). The resulting suspension was vigorously stirred at rt overnight. The reaction was then quenched with saturated aqueous NH<sub>4</sub>Cl, and the aqueous phase was extracted with EtOAc. The combined organic extracts were washed with brine, dried over Na<sub>2</sub>SO<sub>4</sub>, filtered, and concentrated *in vacuo*. The resulting crude material was purified by silica gel flash column chromatography (5:1 hexanes/EtOAc) to afford indole **135** (544 mg, 2.24 mmol, 96%) as a yellow oil.

**TLC:**  $R_f = 0.27$  (5:2 hexanes/EtOAc; UV, CAM, *p*-anisaldehyde). **<sup>1</sup>H NMR** (400 MHz, CDCl<sub>3</sub>): δ 8.09 (bs, 1H), 7.30 (d,  $J = 8.8$  Hz, 1H), 7.21 (t,  $J = 2.8$  Hz, 1H), 7.15 (d,  $J = 2.4$  Hz, 1H), 6.89 (dd,  $J = 8.8$  Hz,  $J = 2.5$  Hz, 1H), 6.51 (ddd,  $J = 3.1$  Hz,  $J = 2.0$  Hz,  $J = 0.9$  Hz, 1H), 5.19–4.91 (m, 2H), 4.88–4.65 (m, 2H), 4.40–4.29 (m, 2H) ppm. **<sup>13</sup>C NMR** (100 MHz, CDCl<sub>3</sub>): δ 152.6, 131.6, 128.4, 125.4, 112.7, 112.0, 104.2, 102.6, 89.7 (dt,  $J = 179.9$  Hz,  $J = 20.7$  Hz), 89.2 (ddd,  $J = 178.9$  Hz,  $J = 20.6$  Hz,  $J = 6.8$  Hz), 81.4 (ddd,  $J = 172.2$  Hz,  $J = 24.5$  Hz,  $J = 7.8$  Hz), 66.8 (dd,  $J = 25.1$  Hz,  $J = 6.8$  Hz) ppm. **<sup>19</sup>F NMR** (376 MHz, CDCl<sub>3</sub>, decoupled): δ -204.17 (d,  $J = 11.3$  Hz), -206.19 (dd,  $J = 14.6$  Hz,  $J = 11.3$  Hz), -233.40 (d,  $J = 14.6$  Hz) ppm. **<sup>19</sup>F NMR** (376 MHz, CDCl<sub>3</sub>, not decoupled): δ -203.94 – -204.40 (m), -205.95 – -206.44 (m), -233.40 (tdd,  $J = 47.4$  Hz,  $J = 21.1$  Hz,  $J = 14.6$  Hz) ppm. **IR** (thin film): ν 3467, 3417, 2958, 1478, 1452, 1224, 1161, 1124, 1072, 1048, 1002, 908, 895, 854, 803, 757, 724, 604, 472 cm<sup>-1</sup>. **HRMS** (EI+): exact mass calculated for C<sub>12</sub>H<sub>12</sub>F<sub>3</sub>NO ([M]<sup>+</sup>), 243.866; found 243.0872.

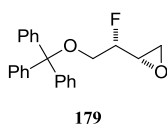


**(±)-*Erythro*-4-(Trityloxy)butane-1,2,3-triol (177):**<sup>143</sup>

A solution of *meso*-erythritol (**178**) (7.50 g, 60.8 mmol, 1.00 equiv), trityl chloride (17.8 g, 60.8 mmol, 1.00 equiv), and 4-(*N,N*-dimethylamino)pyridine (0.300 g, 2.43 mmol, 4.00 10<sup>-2</sup>

equiv) in a 1:4 pyridine/DMF mixture (244 mL) under inert atmosphere was stirred at 50 °C for 24 h. The reaction was then cooled down to rt, concentrated *in vacuo*, and the residue was extracted with EtOAc. The combined organic extracts were successively washed with water, 1 M HCl (aq), saturated aqueous NaHCO<sub>3</sub>, and brine. The organic phase was then dried over Na<sub>2</sub>SO<sub>4</sub>, filtered, and concentrated *in vacuo*. The resulting crude material was purified by silica gel flash column chromatography (100% EtOAc) to afford triol **177** (8.62 g, 23.7 mmol, 39%) as a colorless crystalline solid (mp = 105 °C).

**TLC:**  $R_f$  = 0.33 (EtOAc; UV, CAM). **<sup>1</sup>H NMR** (400 MHz, CDCl<sub>3</sub>): δ 7.46–7.40 (m, 6H), 7.35–7.22 (m, 9H), 3.81 (p,  $J$  = 5.5 Hz, 1H), 3.75–3.61 (m, 3H), 3.34 (qd,  $J$  = 9.8 Hz,  $J$  = 5.2 Hz, 2H), 2.71 (dd,  $J$  = 5.6 Hz,  $J$  = 2.6 Hz, 2H), 2.29 (t,  $J$  = 5.9 Hz, 1H) ppm. **<sup>13</sup>C NMR** (100 MHz, CDCl<sub>3</sub>): δ 143.6, 128.7, 128.1, 127.4, 87.4, 72.5, 71.9, 64.9, 63.8 ppm. **IR** (thin film): ν 3380, 3058, 3032, 2931, 2881, 1490, 1448, 1059, 1033, 1002, 907, 764, 745, 731, 704, 647, 632 cm<sup>-1</sup>. **HRMS** (ESI+): exact mass calculated for C<sub>23</sub>H<sub>24</sub>NaO<sub>4</sub> ([M+Na]<sup>+</sup>), 387.1567; found 387.1563.

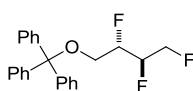


**(±)-Syn-(1-Fluoro-2-(trityloxy)ethyl)oxirane (179):**<sup>108,134</sup>

To a vigorously stirred suspension of (±)-*erythro*-4-(trityloxy)butane-1,2,3-triol (**177**) (8.60 g, 23.6 mmol, 1.00 equiv) in MeCN (118 mL) under inert atmosphere at rt was added 1,8-diazabicyclo[5.4.0]undec-7-ene (11.6 mL, 76.0 mmol, 3.20 equiv) dropwise. After complete dissolution of the substrate, the reaction was cooled down to 0 °C, and perfluorobutanesulfonyl fluoride (10.1 mL, 51.9 mmol, 2.20 equiv) was added dropwise. The reaction was stirred at 0 °C for 15 min, followed by 1 h at rt. The reaction was quenched with saturated aqueous NaHCO<sub>3</sub>, and the aqueous phase was extracted with EtOAc. The combined organic extracts were washed with brine, dried over Na<sub>2</sub>SO<sub>4</sub>, filtered, and concentrated *in vacuo*. The resulting crude material was purified by silica gel flash column chromatography (20:1 hexanes/EtOAc) to afford fluoroepoxide **179** (6.19 g, 17.8 mmol, 75%) as a white crystalline solid (mp = 94 °C).

**TLC:**  $R_f$  = 0.29 (5:1 hexanes/EtOAc; UV, KMnO<sub>4</sub>). **<sup>1</sup>H NMR** (400 MHz, CDCl<sub>3</sub>): δ 7.49–7.43 (m, 6H), 7.36–7.22 (m, 9H), 4.36 (dq,  $J$  = 47.8 Hz,  $J$  = 5.3 Hz, 1H), 3.47–3.34 (m, 2H),

3.25 (dddd,  $J = 12.5$  Hz,  $J = 5.6$  Hz,  $J = 4.3$  Hz,  $J = 2.6$  Hz, 1H), 2.83 (dt,  $J = 5.0$  Hz,  $J = 4.1$  Hz, 1H), 2.66 (ddd,  $J = 4.9$  Hz,  $J = 2.7$  Hz,  $J = 1.3$  Hz, 1H) ppm.  $^{13}\text{C}$  NMR (100 MHz,  $\text{CDCl}_3$ ):  $\delta$  143.6, 128.8, 128.1, 127.4, 92.5 (d,  $J = 176.8$  Hz), 87.1, 63.7 (d,  $J = 25.3$  Hz), 51.4 (d,  $J = 24.1$  Hz), 43.7 (d,  $J = 9.0$  Hz) ppm.  $^{19}\text{F}$  NMR (376 MHz,  $\text{CDCl}_3$ , decoupled):  $\delta$  -194.93 (s) ppm.  $^{19}\text{F}$  NMR (376 MHz,  $\text{CDCl}_3$ , not decoupled):  $\delta$  -194.77 – -195.08 (m) ppm. IR (thin film):  $\nu$  3058, 3023, 2931, 2873, 1448, 1090, 1081, 900, 885, 774, 763, 746, 733, 697, 632  $\text{cm}^{-1}$ . HRMS (EI+): exact mass calculated for  $\text{C}_{23}\text{H}_{21}\text{FO}_2$  ( $[\text{M}]^+$ ), 348.1520; found 348.1518.



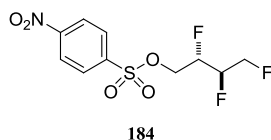
182

(±)-**Erythro-((2,3,4-Trifluorobutoxy)methanetriyl)tribenzene (182)**:<sup>80,102</sup>

A vigorously stirred mixture of (±)-*syn*-(1-fluoro-2-(trityloxy)ethyl)oxirane (**179**) (1.00 g, 2.87 mmol, 1.00 equiv), *N,N*-diisopropylethylamine (4.56 mL, 25.8 mmol, 9.00 equiv), *N,N*-diisopropylethylamine trihydrofluoride (1.78 mL, 8.61 mmol, 3.00 equiv), and perfluorobutanesulfonyl fluoride (1.12 mL, 5.74 mmol, 2.00 equiv) in a sealed flask was heated at 100 °C for 72 h. After cooling down to rt, the reaction mixture was dissolved in  $\text{CH}_2\text{Cl}_2$ , and quenched with saturated aqueous  $\text{NaHCO}_3$  until any evolution of gas ceased. The aqueous phase was then extracted with  $\text{CH}_2\text{Cl}_2$ , and the combined organic extracts were dried over  $\text{Na}_2\text{SO}_4$ , filtered, and concentrated *in vacuo*. The resulting crude material was purified by silica gel flash column chromatography (20:1 hexanes/EtOAc) to afford trifluoride **182** (818 mg, 2.21 mmol, 77%) as a white crystalline solid (mp = 98 °C).

**TLC**:  $R_f = 0.45$  (5:1 hexanes/EtOAc; UV, CAM).  $^1\text{H}$  NMR (400 MHz,  $\text{CDCl}_3$ ):  $\delta$  7.49–7.43 (m, 6H), 7.36–7.23 (m, 9H), 5.09–4.55 (m, 4H), 3.59–3.29 (m, 2H) ppm.  $^{13}\text{C}$  NMR (100 MHz,  $\text{CDCl}_3$ ):  $\delta$  143.5, 128.8, 128.1, 127.4, 89.7–89.2 (m), 87.9–87.4 (m), 87.1, 81.3 (ddd,  $J = 173.7$  Hz,  $J = 20.9$  Hz,  $J = 5.2$  Hz), 62.0 (dd,  $J = 20.2$  Hz,  $J = 4.3$  Hz) ppm.  $^{19}\text{F}$  NMR (376 MHz,  $\text{CDCl}_3$ , decoupled):  $\delta$  -200.62 (d,  $J = 14.2$  Hz), -200.75 (dd,  $J = 14.2$  Hz,  $J = 11.8$  Hz), -235.89 (d,  $J = 11.8$  Hz) ppm.  $^{19}\text{F}$  NMR (376 MHz,  $\text{CDCl}_3$ , not decoupled):  $\delta$  -200.43 – -200.96 (m), -235.89 (tdd,  $J = 47.7$  Hz,  $J = 23.9$  Hz,  $J = 11.8$  Hz) ppm. IR (thin film):  $\nu$  3059, 3033, 2960, 2879, 1490, 1449, 1095, 1069, 1033, 1013, 1002, 980, 901, 884, 776, 765, 747,

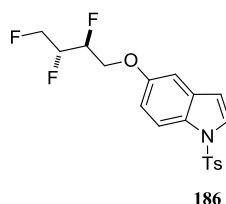
702, 632  $\text{cm}^{-1}$ . **HRMS** (EI+): exact mass calculated for  $\text{C}_{23}\text{H}_{21}\text{F}_3\text{O}$  ( $[\text{M}]^+$ ), 370.1539; found 370.1538.



**(±)-Erythro-2,3,4-Trifluorobutyl 4-nitrobenzenesulfonate (184):**<sup>128,130</sup>

**(±)-Erythro-((2,3,4-Trifluorobutoxy)methanetriyl)tribenzene (182)** (1.47 g, 3.96 mmol, 1.00 equiv) was dissolved in  $\text{CH}_2\text{Cl}_2$  (19.8 mL) at rt under inert atmosphere. The resulting solution was cooled down to 0 °C prior to adding hydrochloric acid (4.0 M in dioxane) (1.98 mL, 7.92 mmol, 2.00 equiv) dropwise. The reaction was then stirred at 0 °C for 1 h before triethylamine (2.23 mL, 15.8 mmol, 4.00 equiv) was added dropwise. 4-(*N,N*-Dimethylamino)pyridine (49.0 mg, 4.00  $10^{-4}$  mol, 1.00  $10^{-1}$  equiv) and 4-nitrobenzene-1-sulfonyl chloride (1.97 g, 8.71 mmol, 2.20 equiv) were successively added, and the resulting solution was stirred at rt for 2 h. The reaction was then quenched with saturated aqueous  $\text{NH}_4\text{Cl}$ , and the aqueous phase was extracted with  $\text{CH}_2\text{Cl}_2$ . The combined organic extracts were dried over  $\text{Na}_2\text{SO}_4$ , filtered, and concentrated *in vacuo*. The resulting crude material was purified by silica gel flash column chromatography (5:1 hexanes/EtOAc) to afford nosylate **184** (1.14 g, 3.65 mmol, 92%) as a yellow crystalline solid (mp = 86 °C).

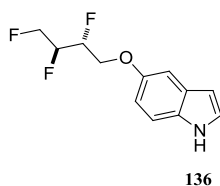
**TLC:**  $R_f$  = 0.20 (10:3 hexanes/EtOAc; UV,  $\text{KMnO}_4$ ).  **$^1\text{H}$  NMR** (400 MHz,  $\text{CDCl}_3$ ):  $\delta$  8.46–8.39 (m, 2H), 8.17–8.10 (m, 2H), 4.99–4.34 (m, 6H) ppm.  **$^{13}\text{C}$  NMR** (100 MHz,  $\text{CDCl}_3$ ):  $\delta$  151.2, 141.3, 129.5, 124.7, 87.2 (ddd,  $J$  = 178.8 Hz,  $J$  = 29.0 Hz,  $J$  = 19.0 Hz), 85.6 (ddd,  $J$  = 180.6 Hz,  $J$  = 29.1 Hz,  $J$  = 6.8 Hz), 80.4 (ddd,  $J$  = 176.1 Hz,  $J$  = 20.7 Hz,  $J$  = 3.1 Hz), 68.3 (ddd,  $J$  = 20.4 Hz,  $J$  = 3.7 Hz,  $J$  = 1.8 Hz) ppm.  **$^{19}\text{F}$  NMR** (376 MHz,  $\text{CDCl}_3$ , decoupled):  $\delta$  -199.57 (d,  $J$  = 15.3 Hz), -203.15 (dd,  $J$  = 15.3 Hz,  $J$  = 11.0 Hz), -237.48 (d,  $J$  = 11.0 Hz) ppm.  **$^{19}\text{F}$  NMR** (376 MHz,  $\text{CDCl}_3$ , not decoupled):  $\delta$  -199.35 – -199.99 (m), -202.92 – -203.39 (m), -237.48 (tdd,  $J$  = 46.8 Hz,  $J$  = 25.4 Hz,  $J$  = 11.0 Hz) ppm. **IR** (thin film):  $\nu$  3110, 2964, 1533, 1350, 1187, 962, 906, 726, 693, 684, 615, 464  $\text{cm}^{-1}$ . **HRMS** (EI+): exact mass calculated for  $\text{C}_{10}\text{H}_{10}\text{F}_3\text{NO}_5\text{S}$  ( $[\text{M}]^+$ ), 313.0227; found 313.0228.



**(±)-Erythro-1-Tosyl-5-(2,3,4-trifluorobutoxy)-1H-indole (186):**<sup>131</sup>

To a solution of 1-tosyl-1H-indol-5-ol (**142**) (1.19 g, 4.15 mmol, 1.20 equiv) and (±)-erythro-2,3,4-trifluorobutyl 4-nitrobenzenesulfonate (**184**) (1.08 g, 3.46 mmol, 1.00 equiv) in MeCN (34.6 mL) at rt under inert atmosphere was added potassium carbonate (597 mg, 4.32 mmol, 1.25 equiv). The resulting suspension was stirred at 80 °C for 24 h, then cooled down to rt, filtered over a pad of Celite<sup>®</sup>, and the filtrate was concentrated *in vacuo*. The resulting crude material was purified by silica gel flash column chromatography (10:1 hexanes/EtOAc) to afford ether **186** (1.02 g, 2.57 mmol, 74%) as a yellow honey.

**TLC:**  $R_f = 0.27$  (5:2 hexanes/EtOAc; UV, CAM, *p*-anisaldehyde). **<sup>1</sup>H NMR** (400 MHz, CDCl<sub>3</sub>): δ 7.90 (d,  $J = 9.0$  Hz, 1H), 7.76–7.70 (m, 2H), 7.54 (d,  $J = 3.6$  Hz, 1H), 7.20 (d,  $J = 8.2$  Hz, 2H), 7.00 (d,  $J = 2.5$  Hz, 1H), 6.96 (dd,  $J = 9.0$  Hz,  $J = 2.5$  Hz, 1H), 6.58 (dd,  $J = 3.6$  Hz,  $J = 0.8$  Hz, 1H), 5.14–4.59 (m, 4H), 4.42–4.17 (m, 2H), 2.33 (s, 3H) ppm. **<sup>13</sup>C NMR** (100 MHz, CDCl<sub>3</sub>): δ 155.0, 145.1, 135.3, 131.9, 130.2, 130.0, 127.5, 126.8, 114.7, 114.2, 109.2, 105.2, 88.1 (ddd,  $J = 177.2$  Hz,  $J = 28.3$  Hz,  $J = 19.3$  Hz), 87.4 (ddd,  $J = 177.3$  Hz,  $J = 28.3$  Hz,  $J = 7.1$  Hz), 81.1 (ddd,  $J = 174.3$  Hz,  $J = 21.1$  Hz,  $J = 4.4$  Hz), 66.7 (dd,  $J = 21.2$  Hz,  $J = 3.7$  Hz), 21.7 ppm. **<sup>19</sup>F NMR** (376 MHz, CDCl<sub>3</sub>, decoupled): δ -200.07 (d,  $J = 14.2$  Hz), -201.90 (dd,  $J = 14.2$  Hz,  $J = 11.6$  Hz), -236.27 (d,  $J = 11.6$  Hz) ppm. **<sup>19</sup>F NMR** (376 MHz, CDCl<sub>3</sub>, not decoupled): δ -199.79 – -200.32 (m), -201.62 – -202.23 (m), -236.27 (tdd,  $J = 47.5$  Hz,  $J = 24.7$  Hz,  $J = 11.6$  Hz) ppm. **IR** (thin film): ν 3145, 2961, 1447, 1368, 1223, 1188, 1174, 1157, 1142, 1125, 1090, 1075, 1035, 993, 907, 811, 760, 724, 703, 671, 650, 589, 538 cm<sup>-1</sup>. **HRMS** (ESI+): exact mass calculated for C<sub>19</sub>H<sub>19</sub>F<sub>3</sub>NO<sub>3</sub>S ([M+H]<sup>+</sup>), 398.1032; found 398.1030.



**(±)-Erythro-5-(2,3,4-Trifluorobutoxy)-1H-indole (136):**<sup>116</sup>

To a solution of (±)-*erythro*-1-tosyl-5-(2,3,4-trifluorobutoxy)-1H-indole (**186**) (0.230 g, 5.80  $10^{-4}$  mol, 1.00 equiv) in MeOH (3.56 mL) at rt were added magnesium turnings (141 mg, 5.79 mmol, 10.0 equiv). The resulting suspension was vigorously stirred at rt overnight. The reaction was then quenched with saturated aqueous  $\text{NH}_4\text{Cl}$ , and the aqueous phase was extracted with EtOAc. The combined organic extracts were washed with brine, dried over  $\text{Na}_2\text{SO}_4$ , filtered, and concentrated *in vacuo*. The resulting crude material was purified by silica gel flash column chromatography (5:1 hexanes/EtOAc) to afford indole **136** (125 mg, 5.10  $10^{-4}$  mol, 89%) as a yellow oil.

**TLC:**  $R_f = 0.27$  (5:2 hexanes/EtOAc; UV, CAM, *p*-anisaldehyde).  **$^1\text{H}$  NMR** (400 MHz,  $\text{CDCl}_3$ ):  $\delta$  8.08 (bs, 1H), 7.30 (d,  $J = 8.8$  Hz, 1H), 7.21 (t,  $J = 2.8$  Hz, 1H), 7.15 (d,  $J = 2.5$  Hz, 1H), 6.90 (dd,  $J = 8.8$  Hz,  $J = 2.5$  Hz, 1H), 6.50 (ddd,  $J = 3.1$  Hz,  $J = 2.0$  Hz,  $J = 0.9$  Hz, 1H), 5.19–4.63 (m, 4H), 4.46–4.22 (m, 2H) ppm.  **$^{13}\text{C}$  NMR** (100 MHz,  $\text{CDCl}_3$ ):  $\delta$  152.9, 131.6, 128.4, 125.3, 112.9, 112.0, 104.4, 102.7, 88.4 (ddd,  $J = 177.0$  Hz,  $J = 27.8$  Hz,  $J = 19.3$  Hz), 87.8 (ddd,  $J = 176.9$  Hz,  $J = 27.9$  Hz,  $J = 7.2$  Hz), 81.2 (ddd,  $J = 173.9$  Hz,  $J = 21.2$  Hz,  $J = 4.8$  Hz), 67.1 (dd,  $J = 21.4$  Hz,  $J = 3.9$  Hz) ppm.  **$^{19}\text{F}$  NMR** (376 MHz,  $\text{CDCl}_3$ , decoupled):  $\delta$  -200.31 (d,  $J = 14.1$  Hz), -201.54 (dd,  $J = 14.1$  Hz,  $J = 12.0$  Hz), -235.93 (d,  $J = 12.0$  Hz) ppm.  **$^{19}\text{F}$  NMR** (376 MHz,  $\text{CDCl}_3$ , not decoupled):  $\delta$  -200.04 – -200.58 (m), -201.30 – -201.82 (m), -235.93 (tdd,  $J = 47.8$  Hz,  $J = 24.2$  Hz,  $J = 12.0$  Hz) ppm. **IR** (thin film):  $\nu$  3465, 3416, 2961, 1478, 1452, 1285, 1225, 1162, 1124, 1068, 1032, 984, 894, 758, 727  $\text{cm}^{-1}$ . **HRMS** (ESI+): exact mass calculated for  $\text{C}_{12}\text{H}_{13}\text{F}_3\text{NO}$  ( $[\text{M}+\text{H}]^+$ ), 244.0944; found 244.0941.



# Appendix

- NMR Spectra

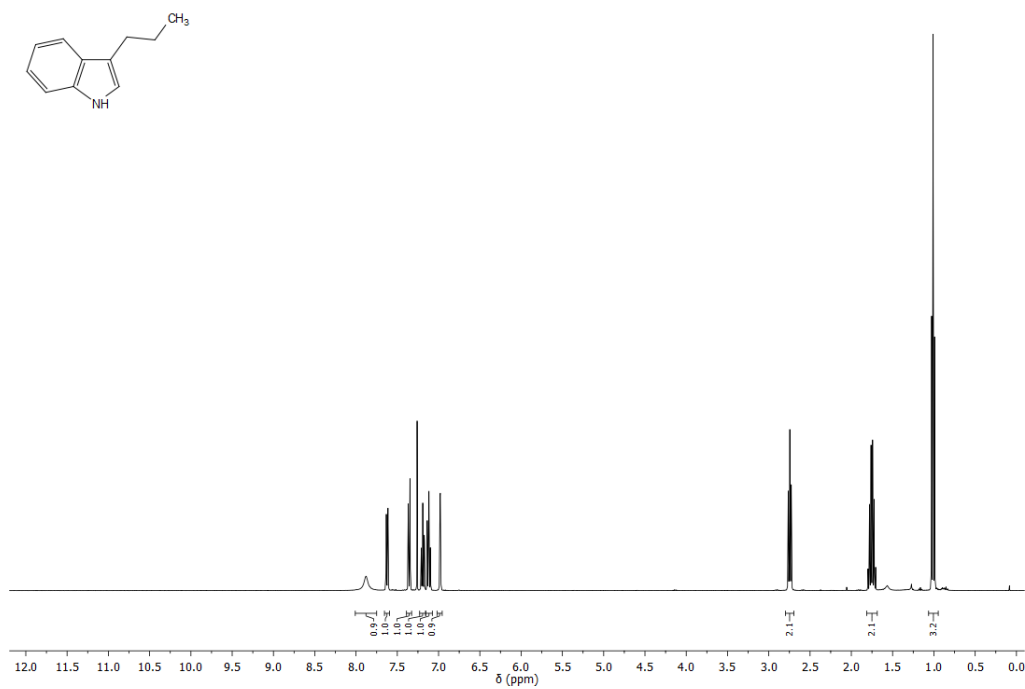


Figure 74. <sup>1</sup>H NMR (400 MHz) spectrum of **23a** in CDCl<sub>3</sub> at 298 K.

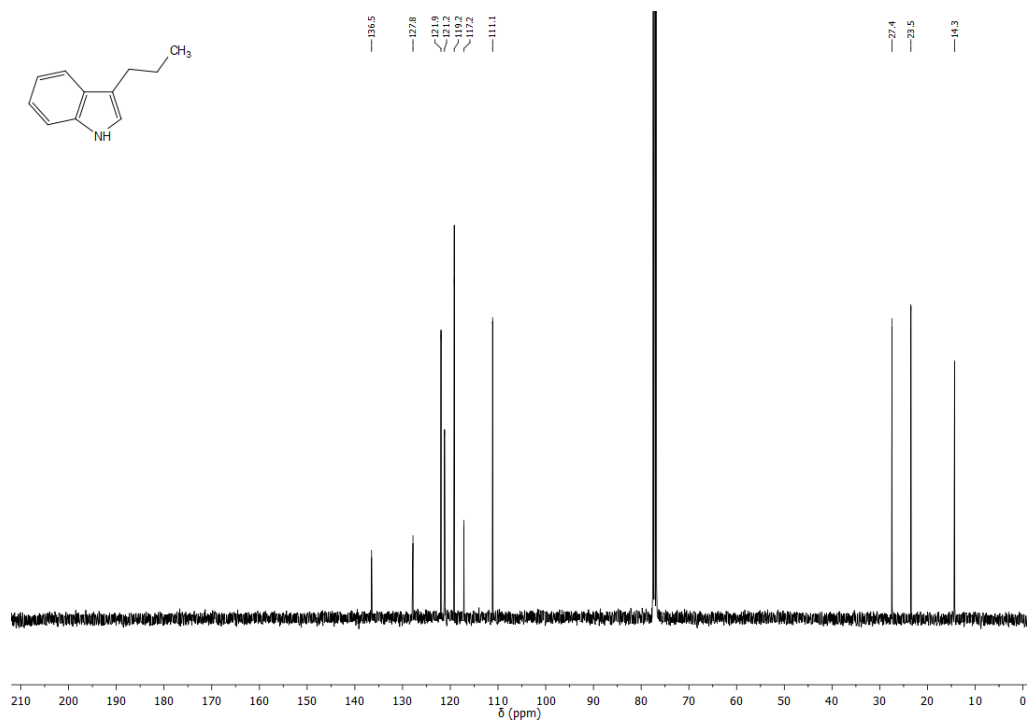
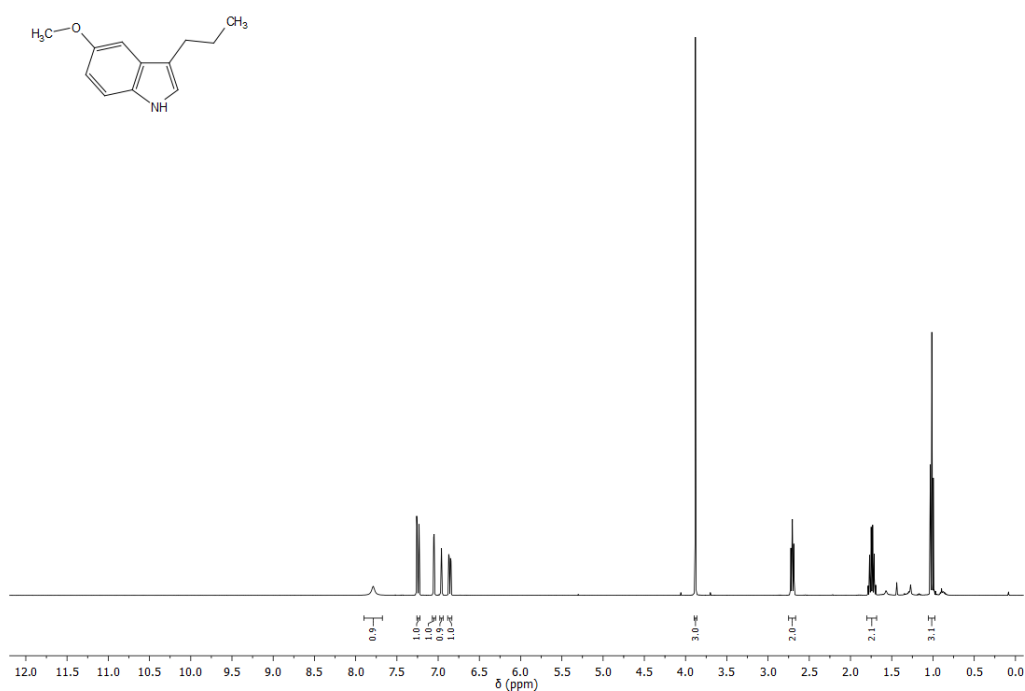
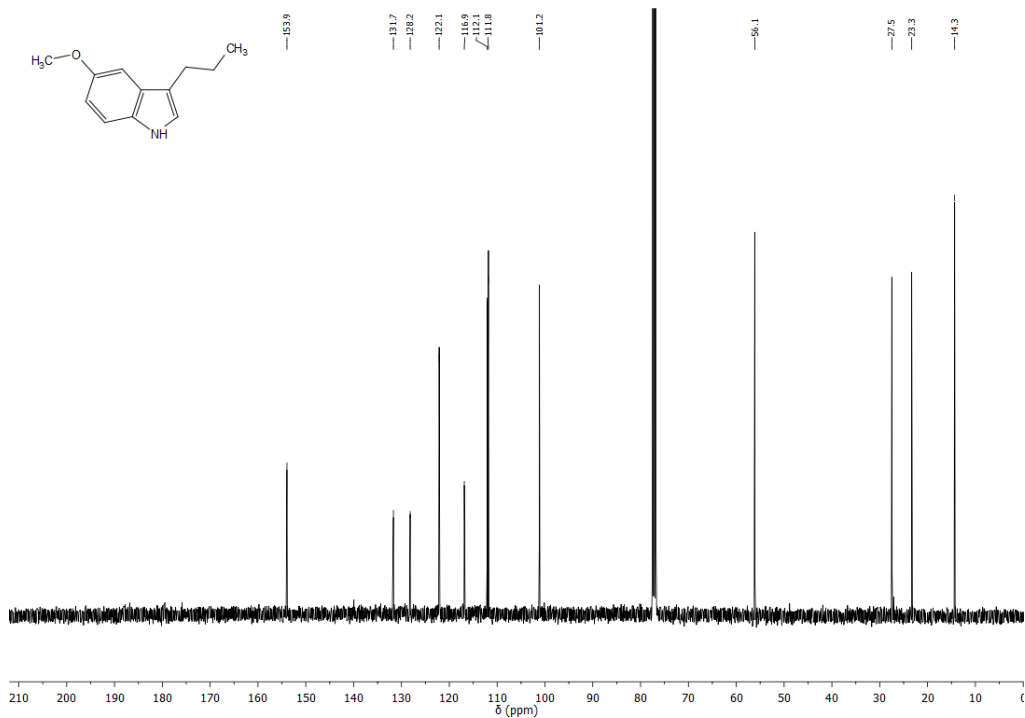


Figure 75. <sup>13</sup>C NMR (100 MHz) spectrum of **23a** in CDCl<sub>3</sub> at 298 K.



**Figure 76.**  $^1\text{H NMR}$  (400 MHz) spectrum of **24a** in  $\text{CDCl}_3$  at 298 K.



**Figure 77.**  $^{13}\text{C NMR}$  (100 MHz) spectrum of **24a** in  $\text{CDCl}_3$  at 298 K.

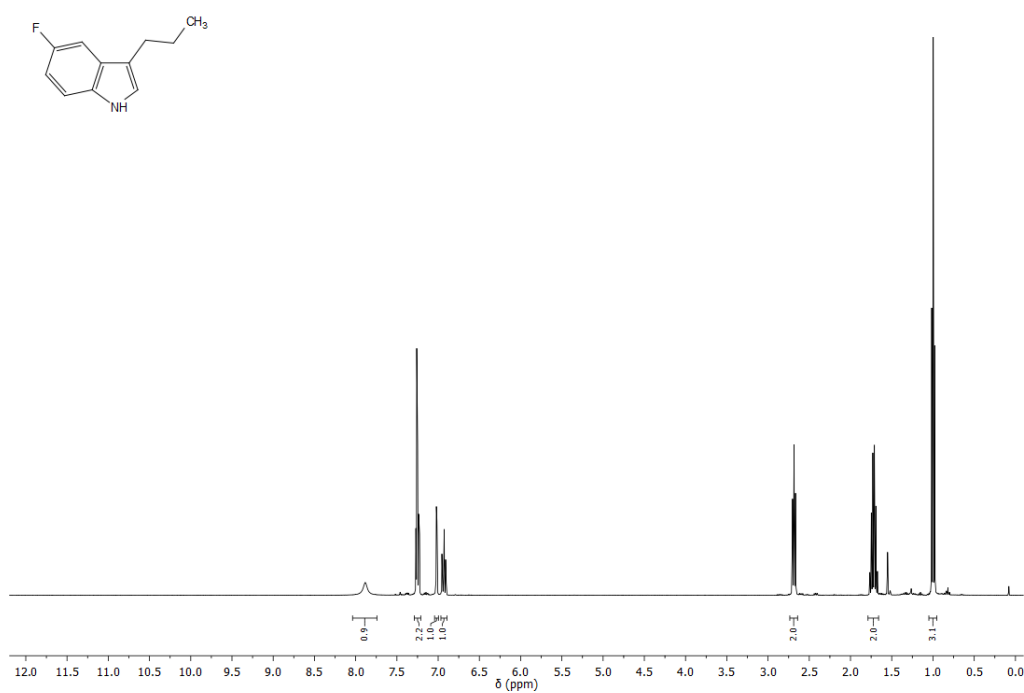


**Figure 78.** <sup>1</sup>H NMR (400 MHz) spectrum of **26a** in CDCl<sub>3</sub> at 298 K.

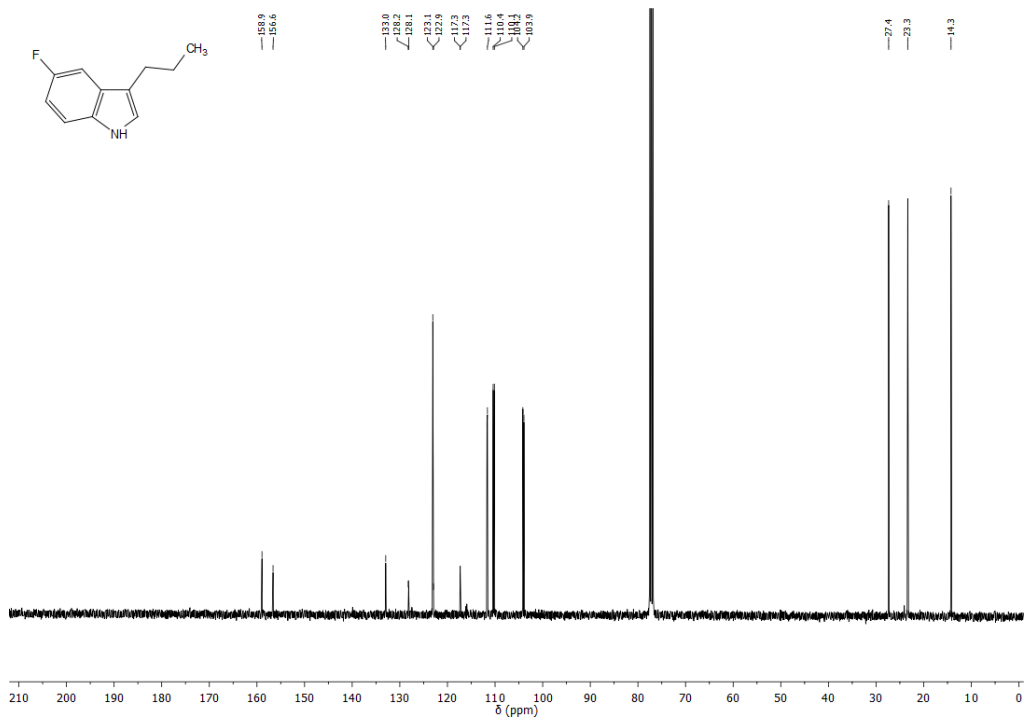


**Figure 79.** <sup>13</sup>C NMR (100 MHz) spectrum of **26a** in CDCl<sub>3</sub> at 298 K.

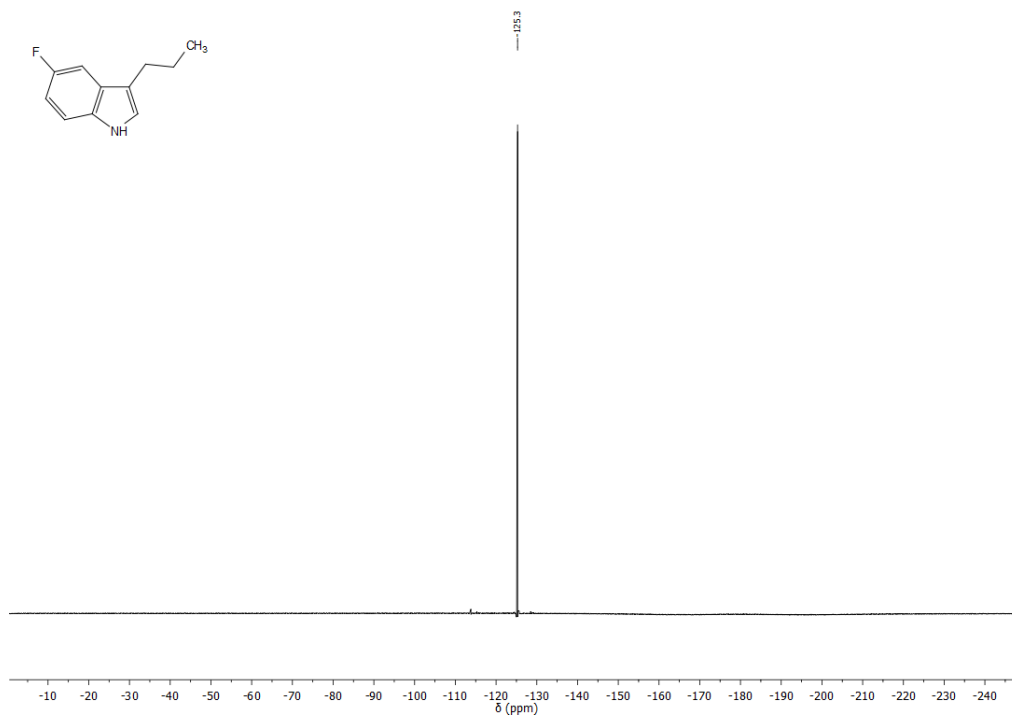


**Figure 80.**  $^{19}\text{F}$  NMR (376 MHz, decoupled) spectrum of **26a** in  $\text{CDCl}_3$  at 298 K.

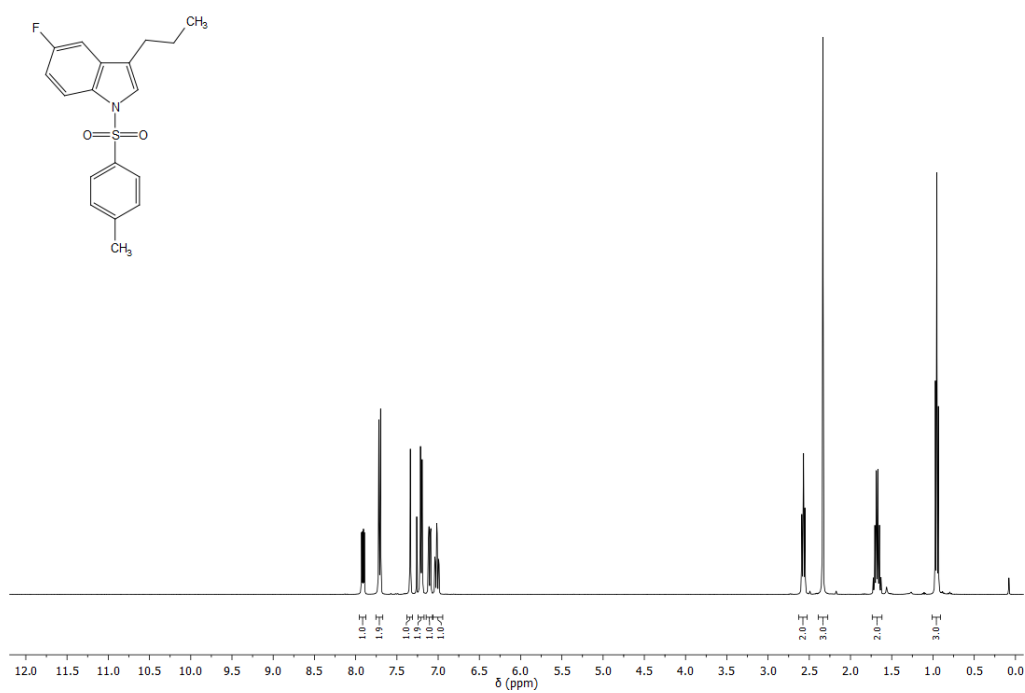


**Figure 81.**  $^1\text{H}$  NMR (400 MHz) spectrum of **25a** in  $\text{CDCl}_3$  at 298 K.

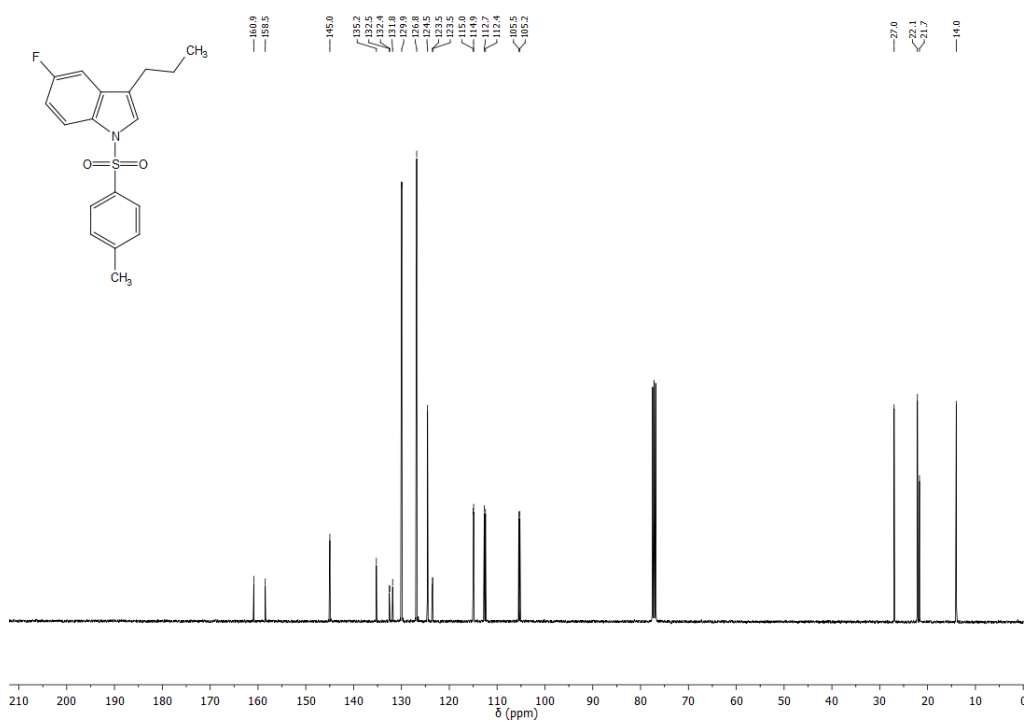


**Figure 82.**  $^{13}\text{C}$  NMR (100 MHz) spectrum of **25a** in  $\text{CDCl}_3$  at 298 K.

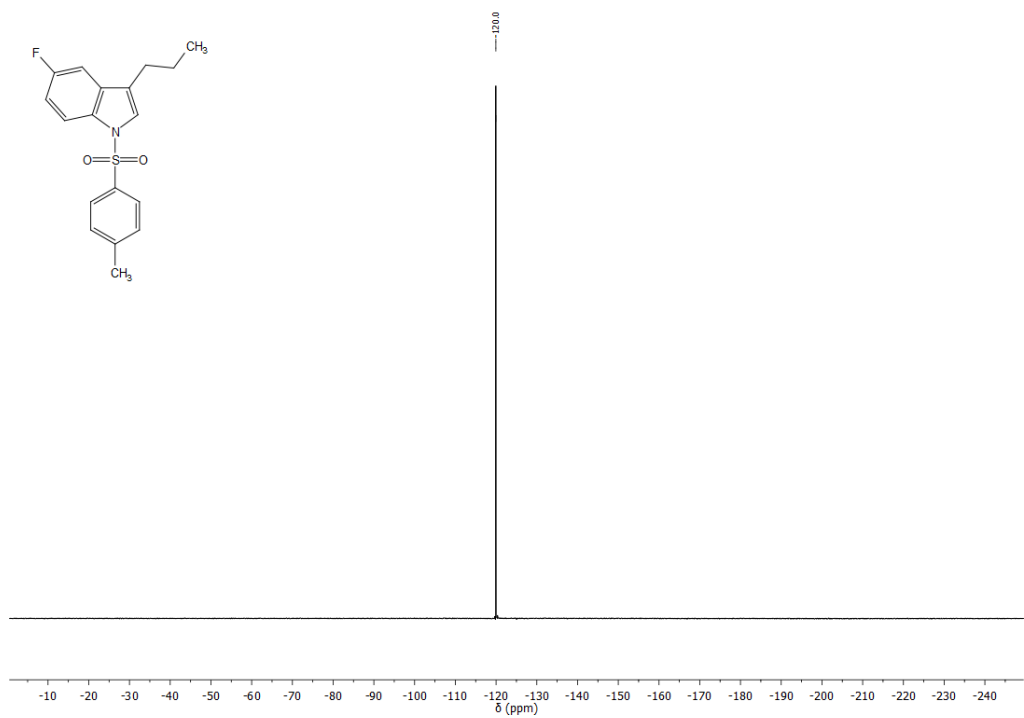


**Figure 83.**  $^{19}\text{F}$  NMR (376 MHz, decoupled) spectrum of **25a** in  $\text{CDCl}_3$  at 298 K.

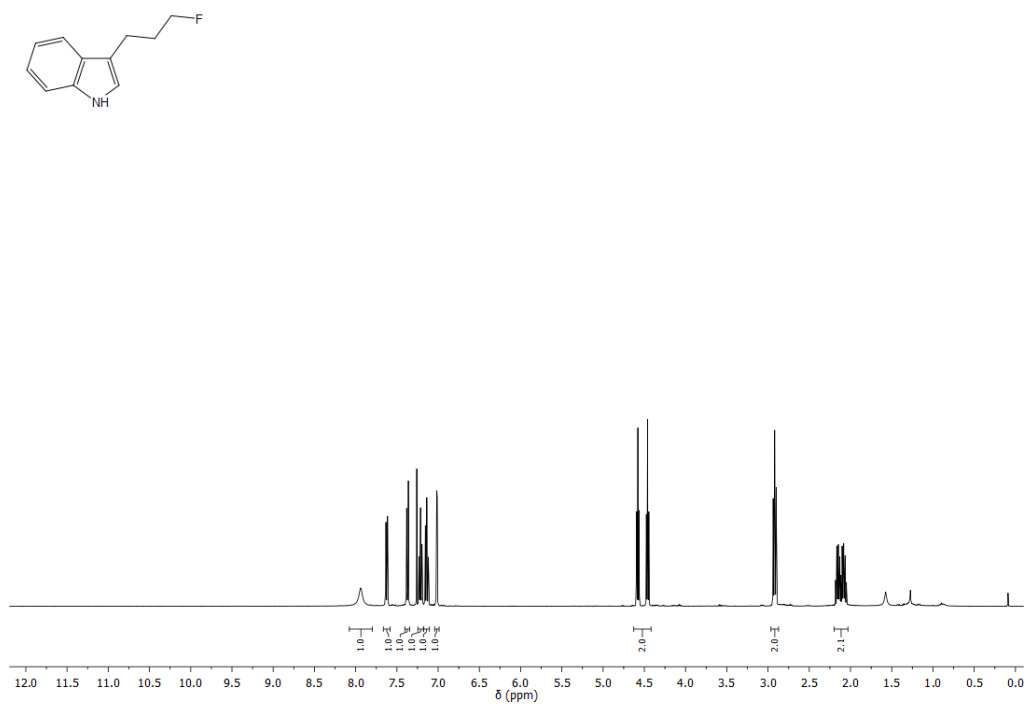


**Figure 84.** <sup>1</sup>H NMR (400 MHz) spectrum of **23b** in CDCl<sub>3</sub> at 298 K.

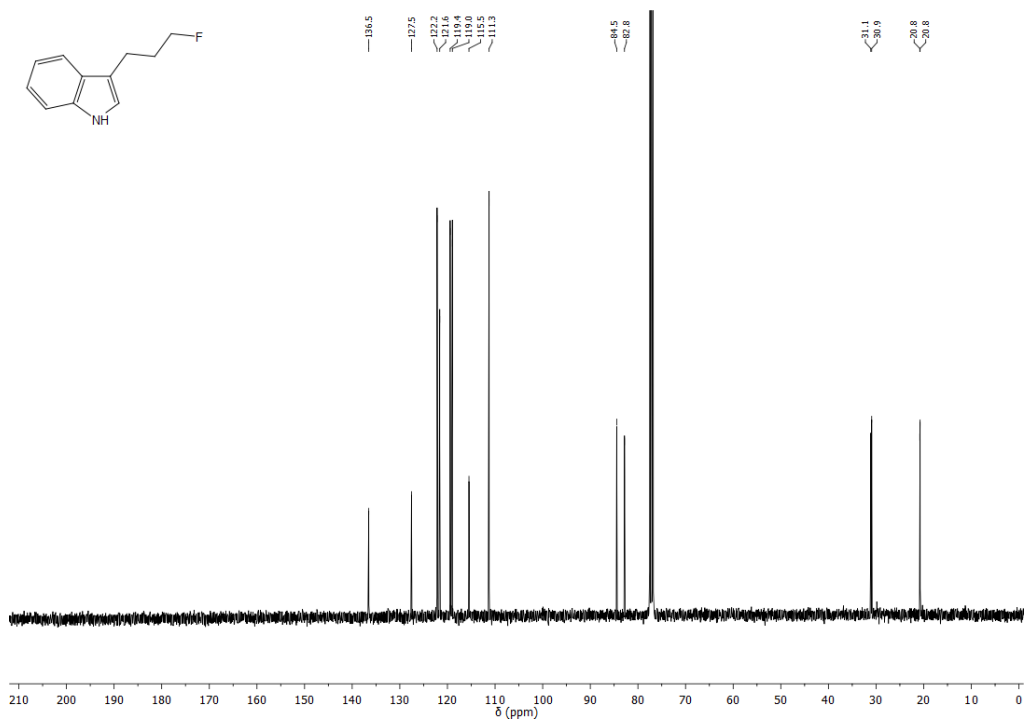


**Figure 85.** <sup>13</sup>C NMR (100 MHz) spectrum of **23b** in CDCl<sub>3</sub> at 298 K.

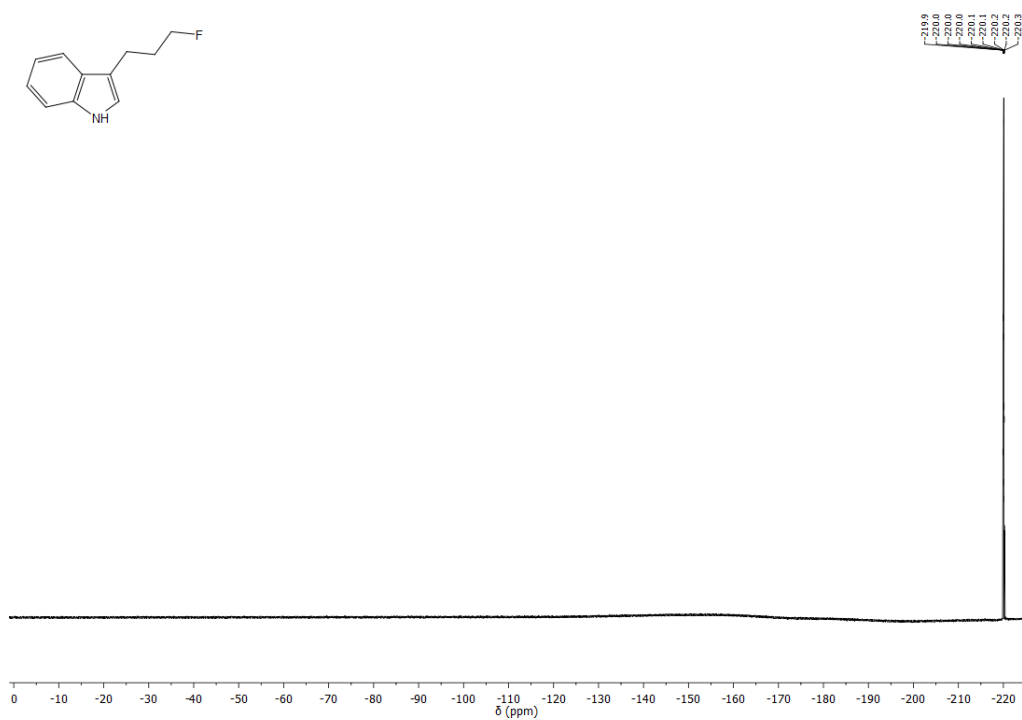


**Figure 86.**  $^{19}\text{F}$  NMR (376 MHz, not decoupled) spectrum of **23b** in  $\text{CDCl}_3$  at 298 K.

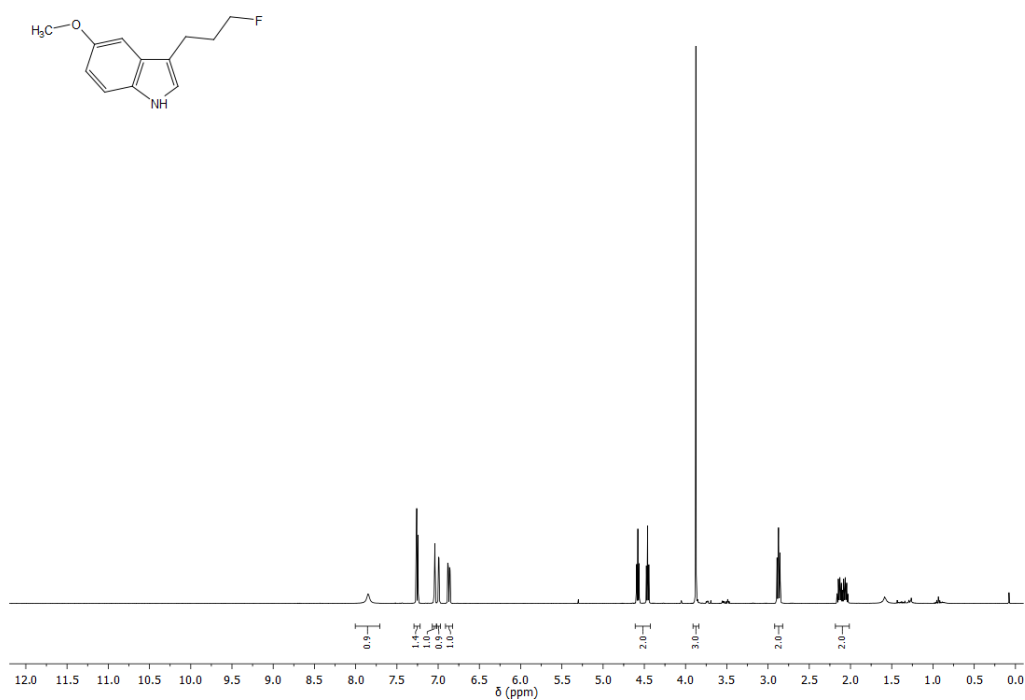


**Figure 87.**  $^1\text{H}$  NMR (400 MHz) spectrum of **24b** in  $\text{CDCl}_3$  at 298 K.

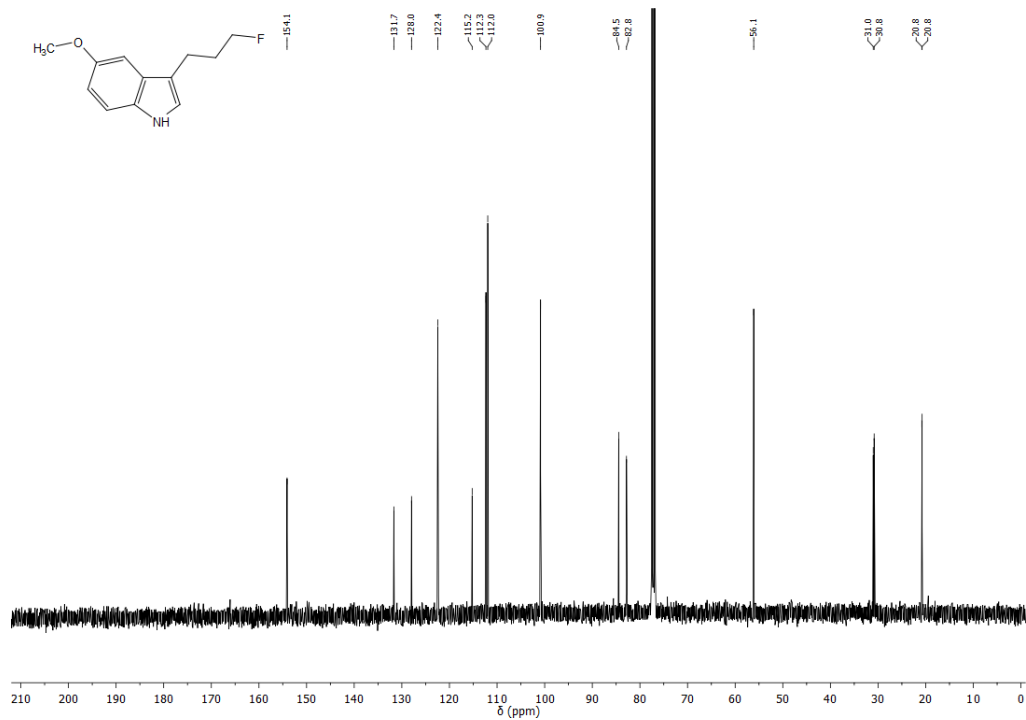


**Figure 88.** <sup>13</sup>C NMR (100 MHz) spectrum of **24b** in CDCl<sub>3</sub> at 298 K.

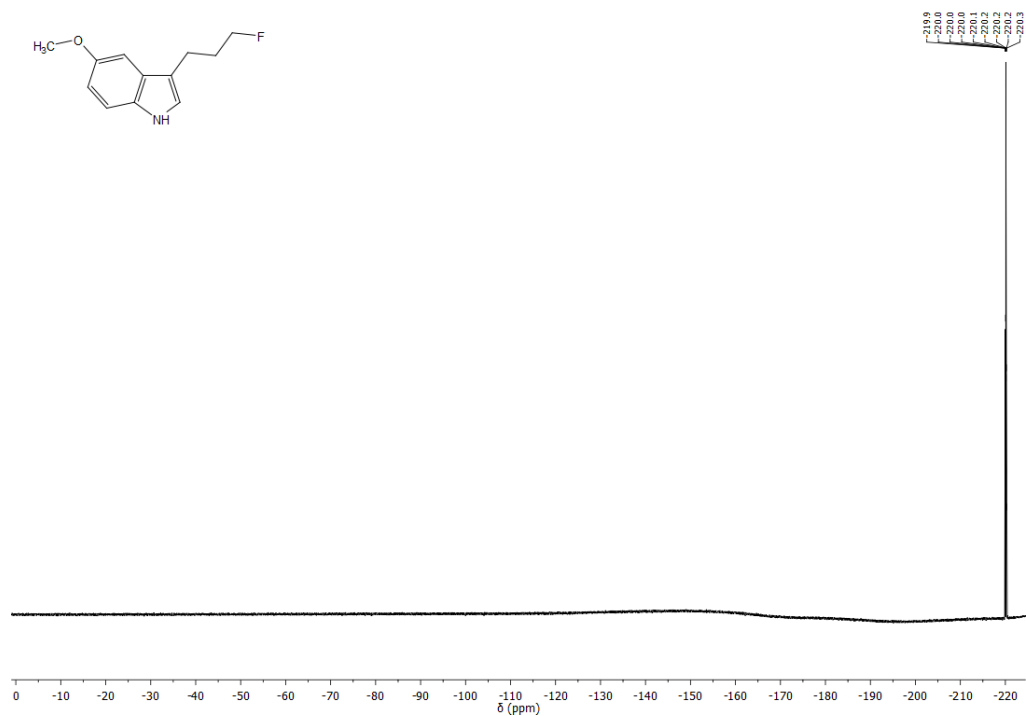


**Figure 89.** <sup>19</sup>F NMR (376 MHz, not decoupled) spectrum of **24b** in CDCl<sub>3</sub> at 298 K.



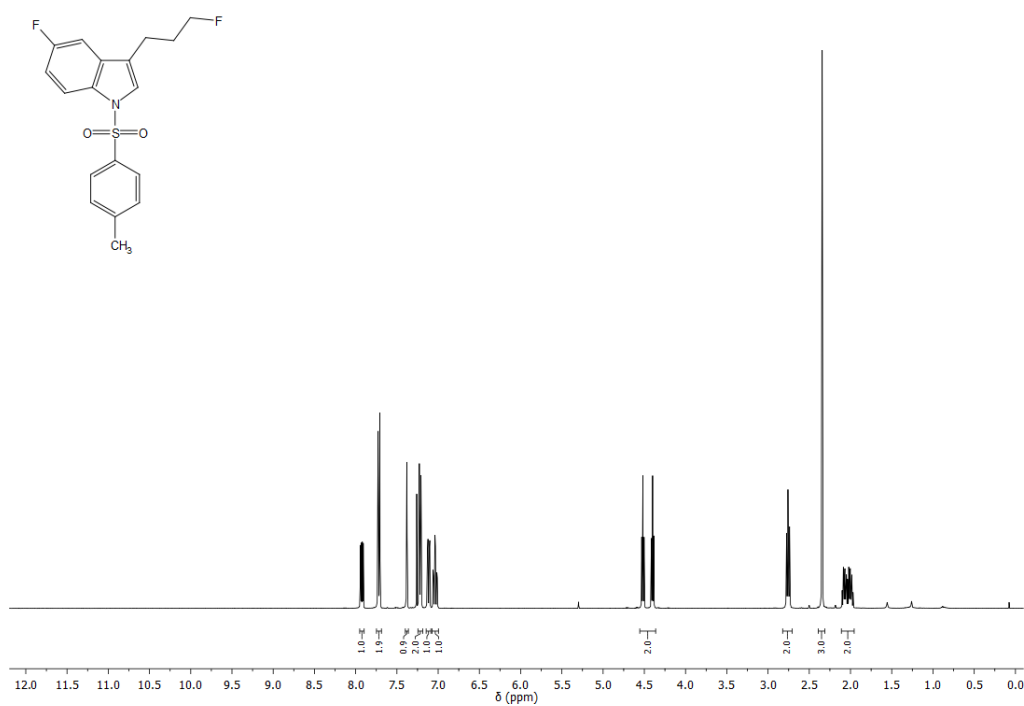


**Figure 90.**  $^1\text{H NMR}$  (400 MHz) spectrum of **25b** in  $\text{CDCl}_3$  at 298 K.

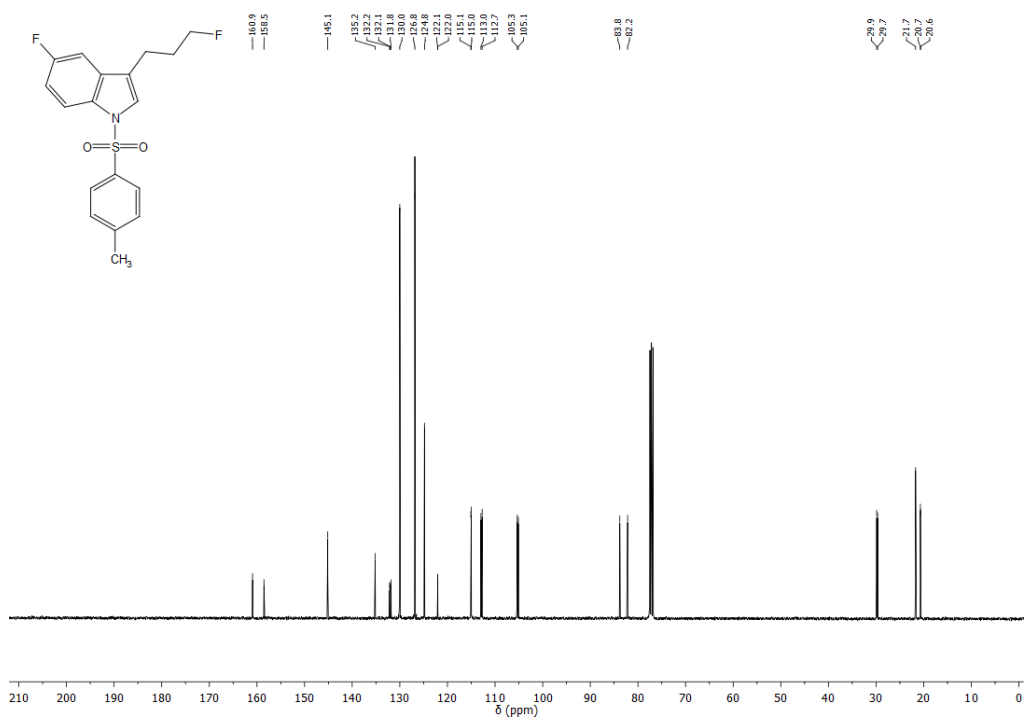


**Figure 91.**  $^{13}\text{C NMR}$  (100 MHz) spectrum of **25b** in  $\text{CDCl}_3$  at 298 K.

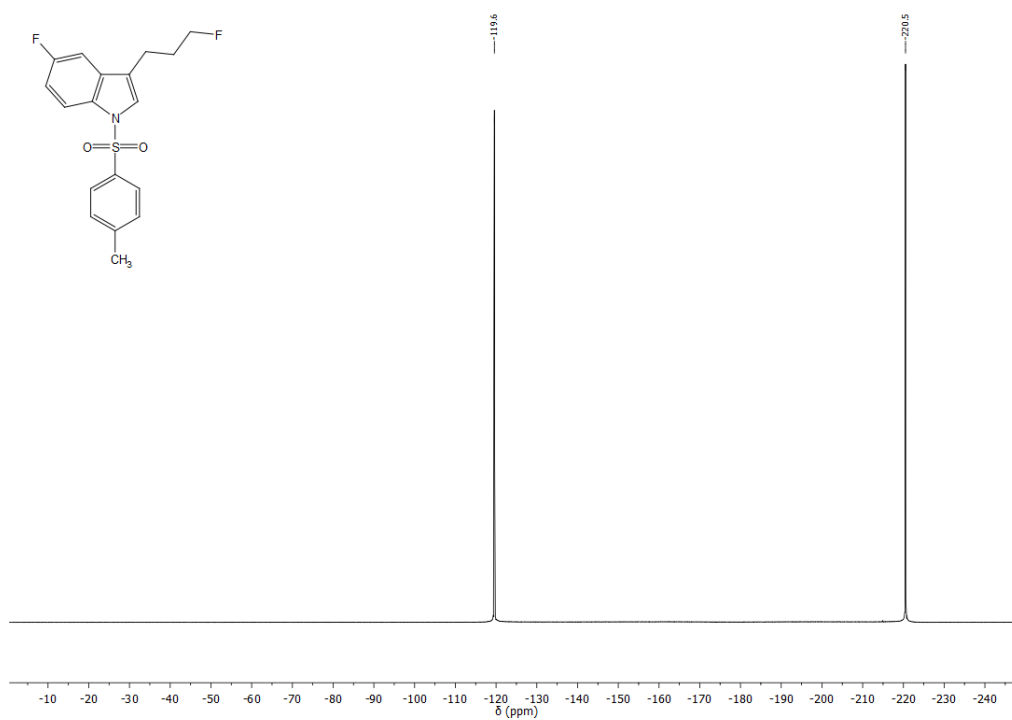


**Figure 92.**  $^{19}\text{F}$  NMR (376 MHz, decoupled) spectrum of **25b** in  $\text{CDCl}_3$  at 298 K.

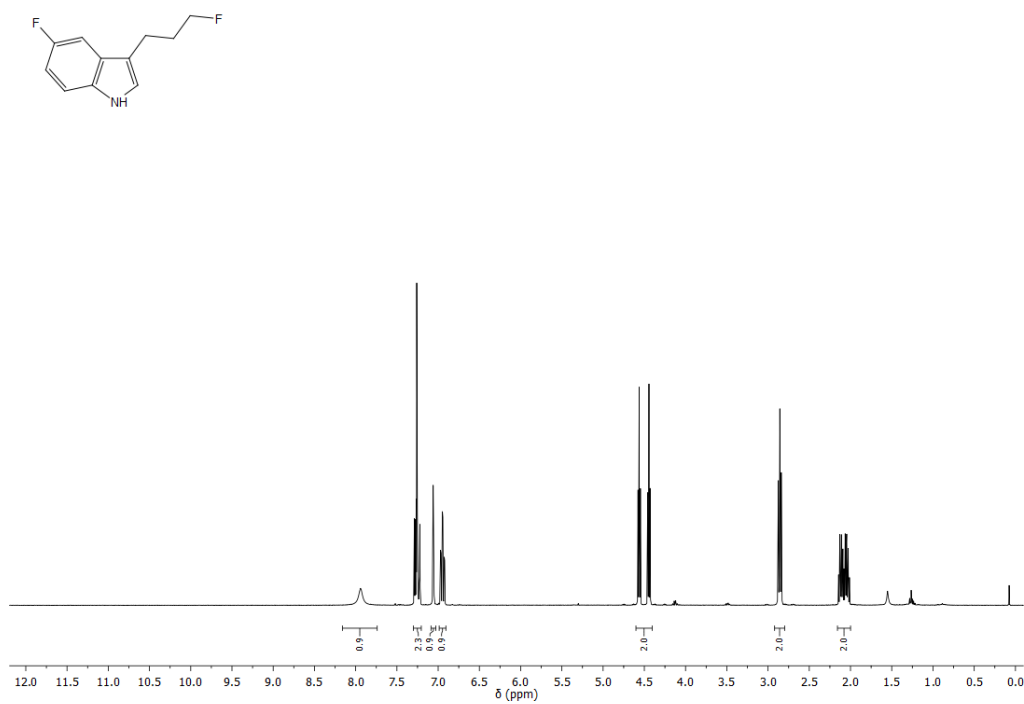


**Figure 93.**  $^1\text{H}$  NMR (400 MHz) spectrum of **26b** in  $\text{CDCl}_3$  at 298 K.

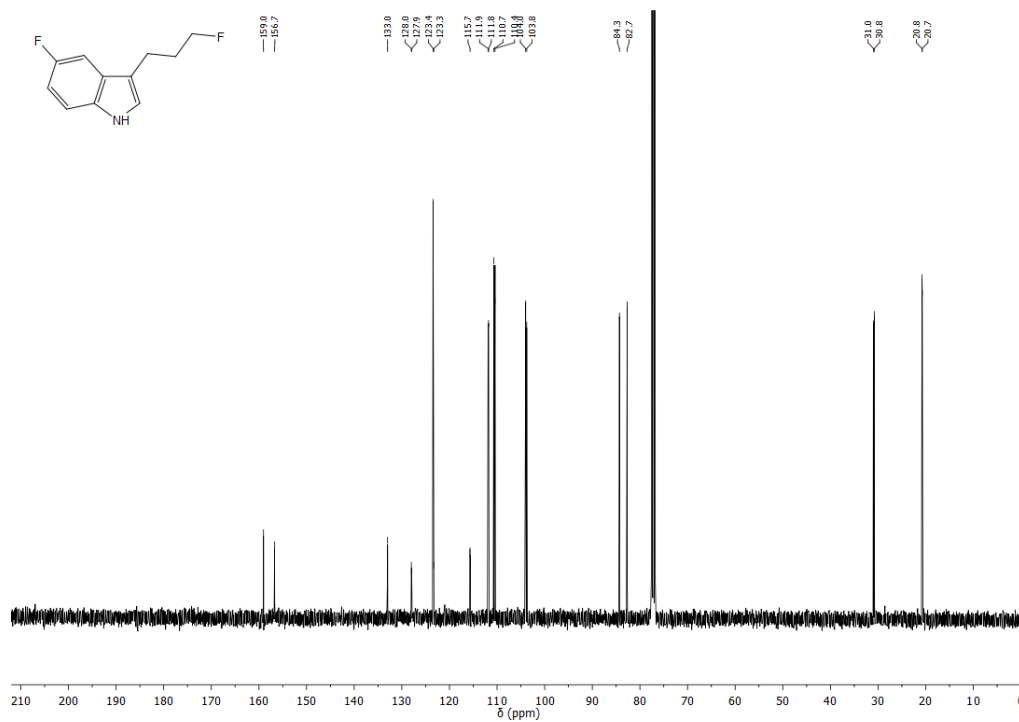


**Figure 94.**  $^{13}\text{C}$  NMR (100 MHz) spectrum of **26b** in  $\text{CDCl}_3$  at 298 K.

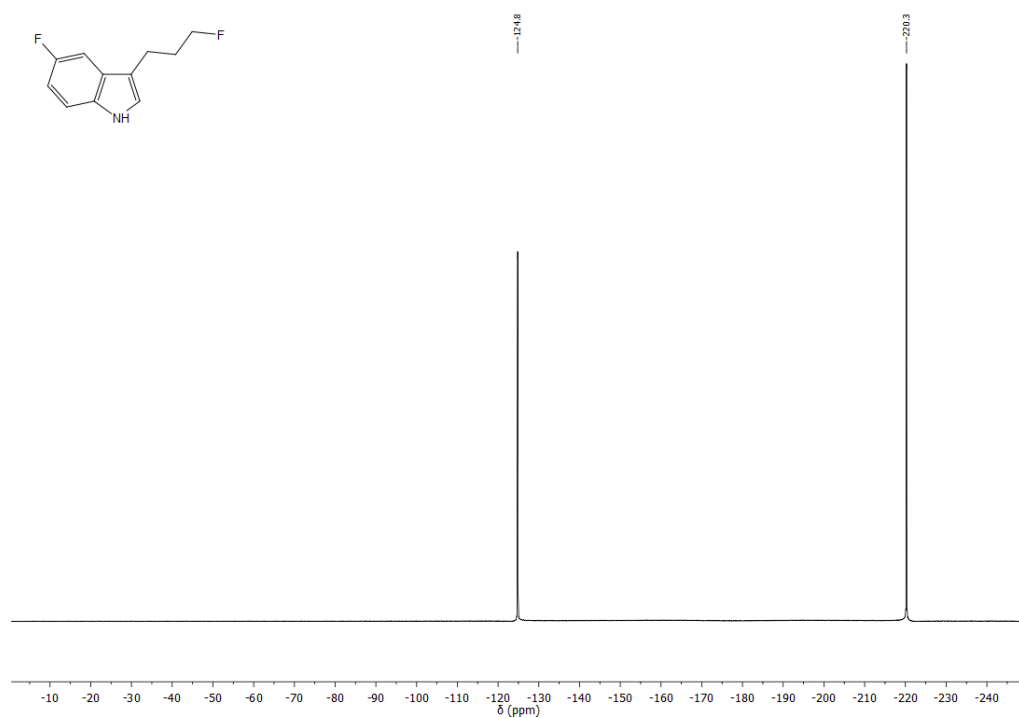


**Figure 95.**  $^{19}\text{F}$  NMR (376 MHz, decoupled) spectrum of **26b** in  $\text{CDCl}_3$  at 298 K.

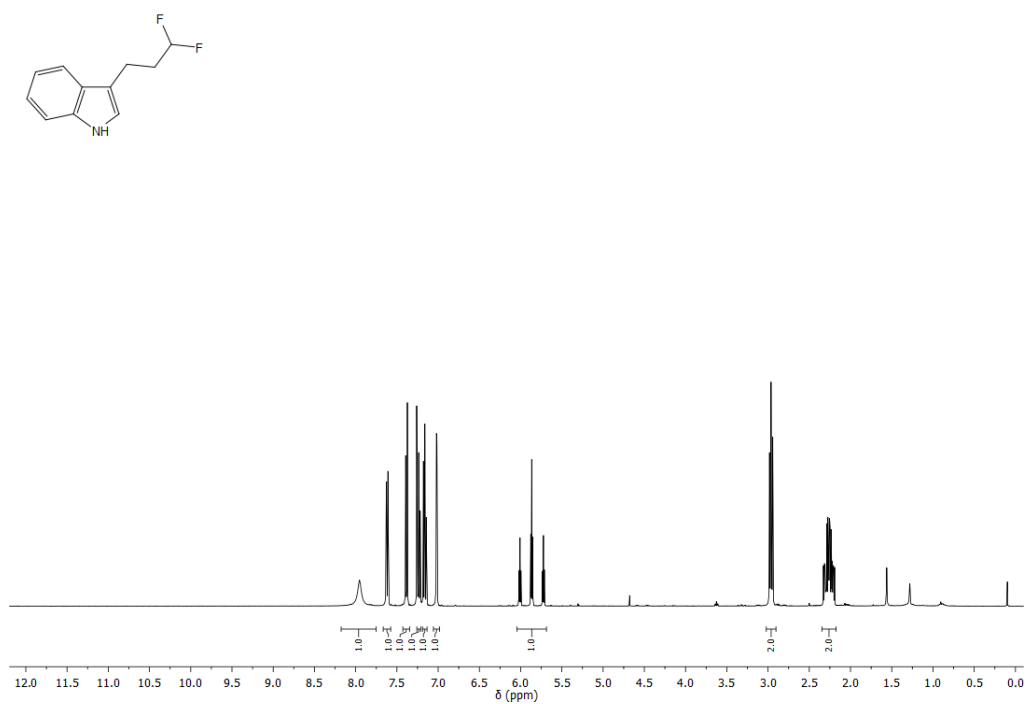


**Figure 96.** <sup>1</sup>H NMR (400 MHz) spectrum of **23c** in CDCl<sub>3</sub> at 298 K.

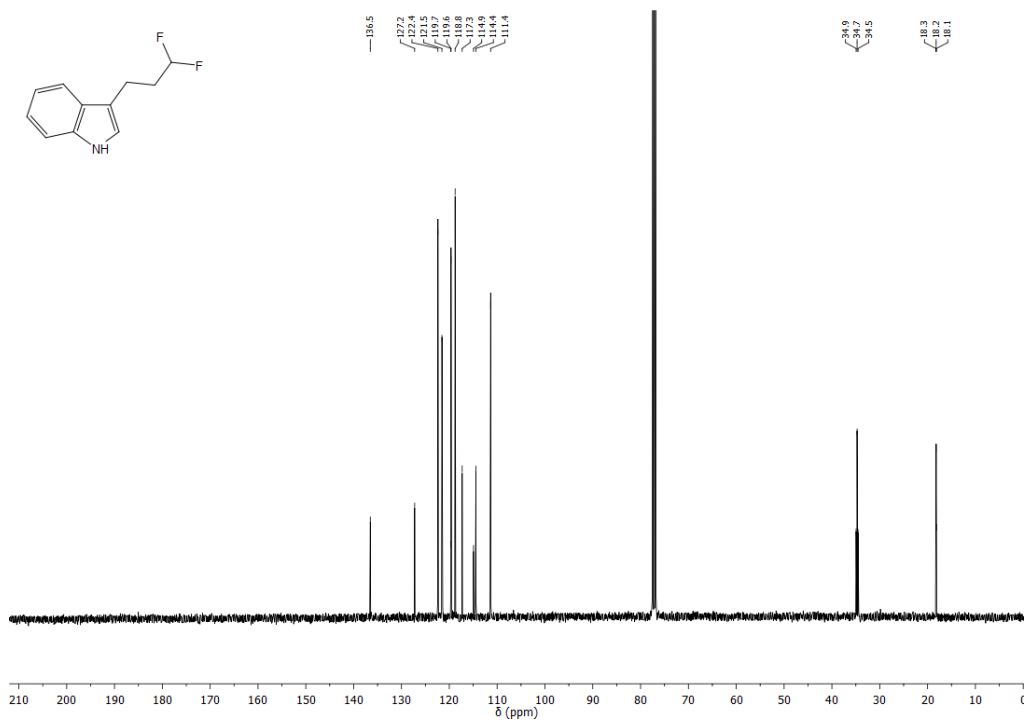


**Figure 97.** <sup>13</sup>C NMR (100 MHz) spectrum of **23c** in CDCl<sub>3</sub> at 298 K.

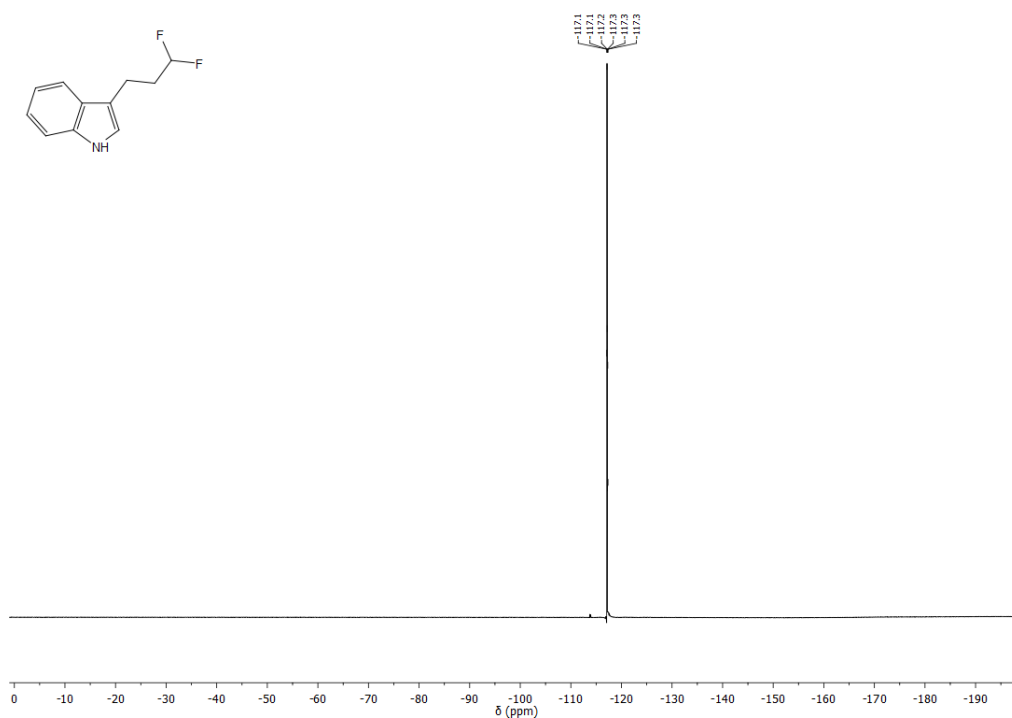


**Figure 98.**  $^{19}\text{F}$  NMR (376 MHz, not decoupled) spectrum of **23c** in  $\text{CDCl}_3$  at 298 K.

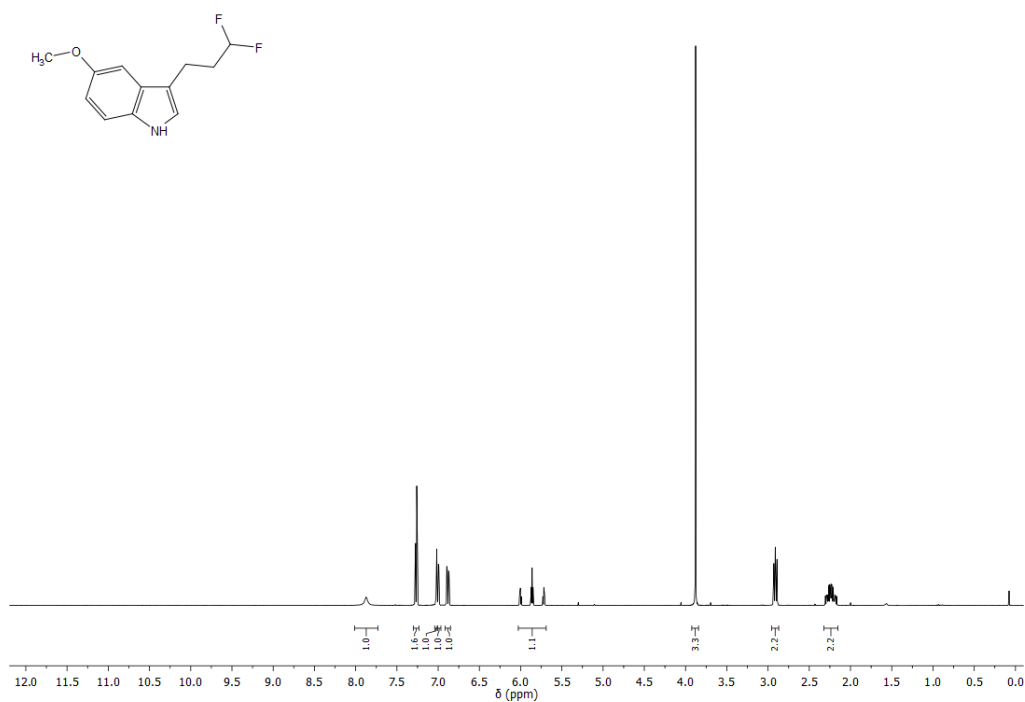


**Figure 99.**  $^1\text{H}$  NMR (400 MHz) spectrum of **24c** in  $\text{CDCl}_3$  at 298 K.

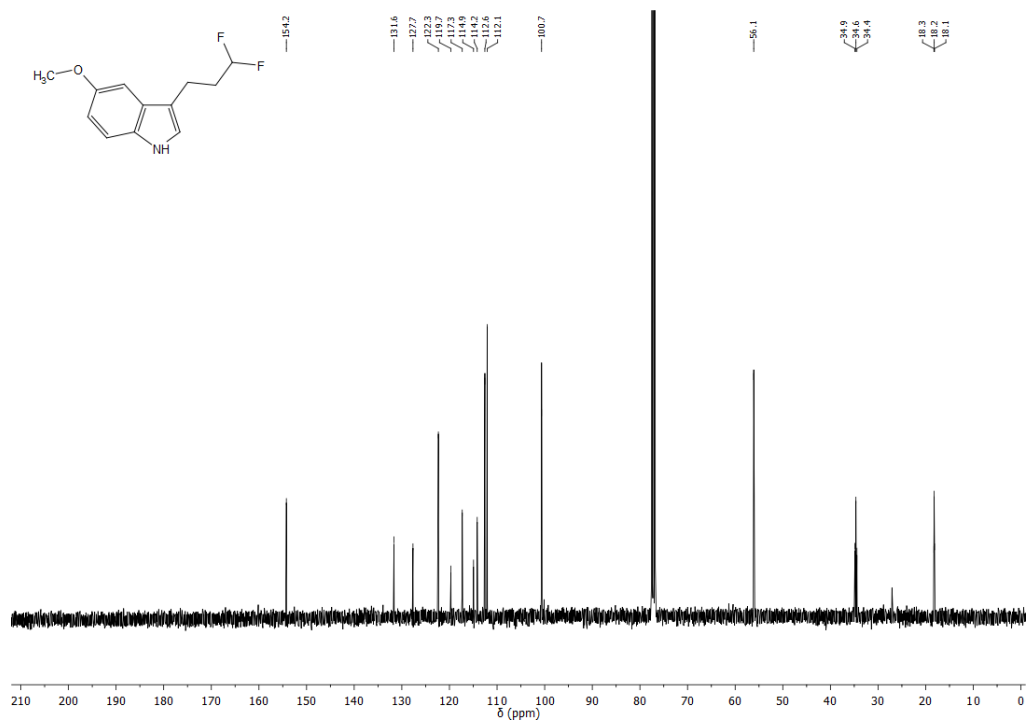


**Figure 100.**  $^{13}\text{C}$  NMR (100 MHz) spectrum of **24c** in  $\text{CDCl}_3$  at 298 K.

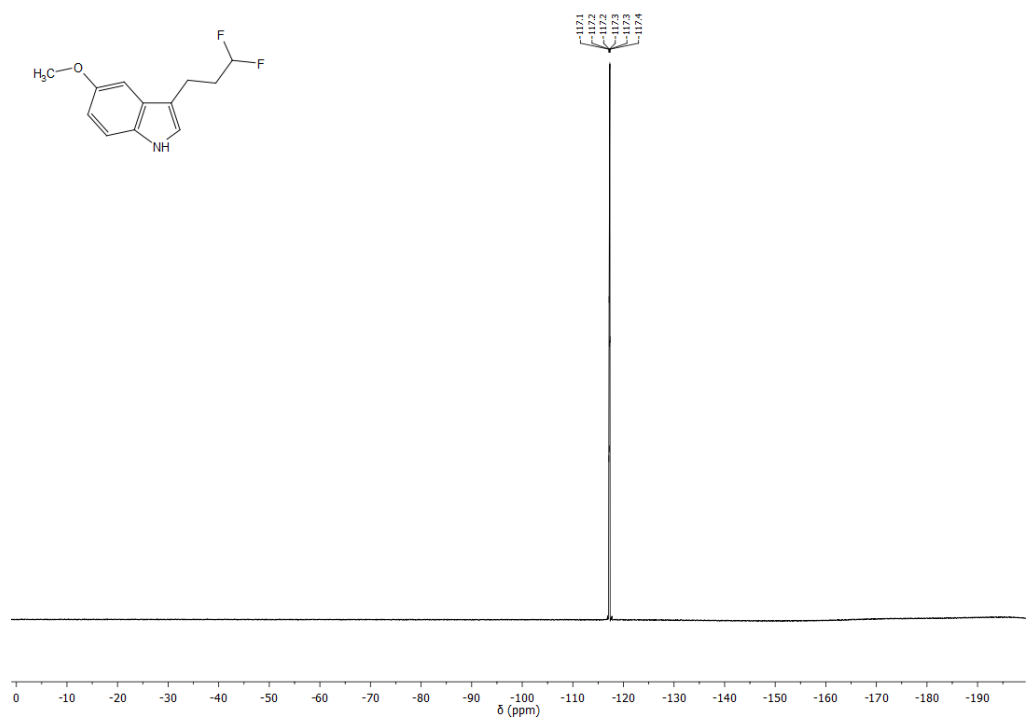


**Figure 101.**  $^{19}\text{F}$  NMR (376 MHz, not decoupled) spectrum of **24c** in  $\text{CDCl}_3$  at 298 K.

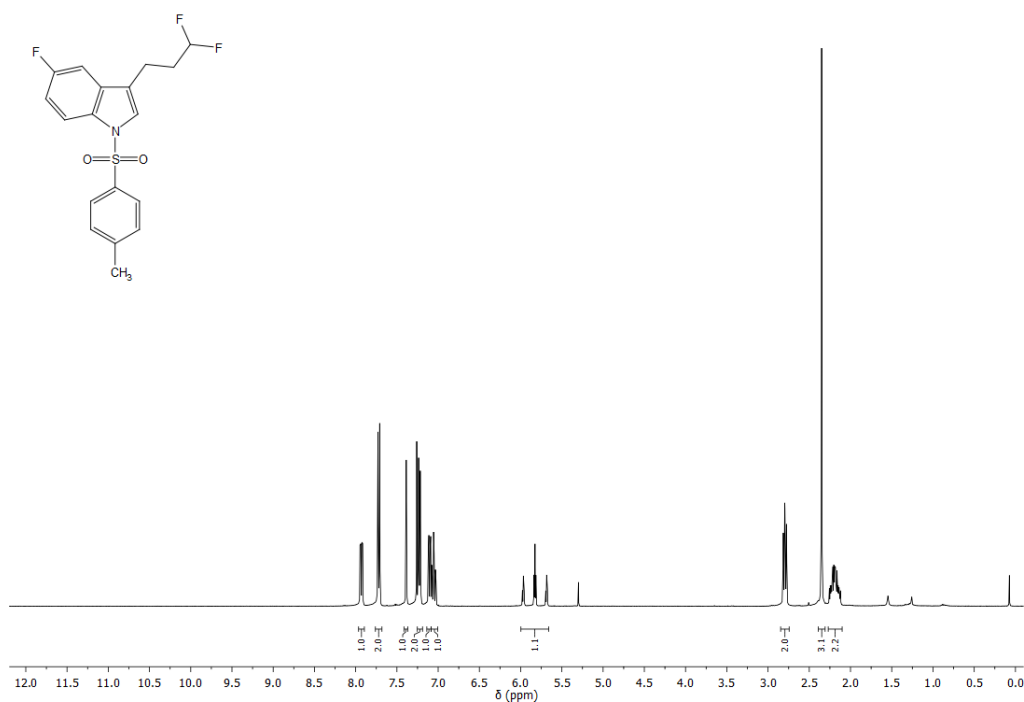


**Figure 102.**  $^1\text{H NMR}$  (400 MHz) spectrum of **25c** in  $\text{CDCl}_3$  at 298 K.

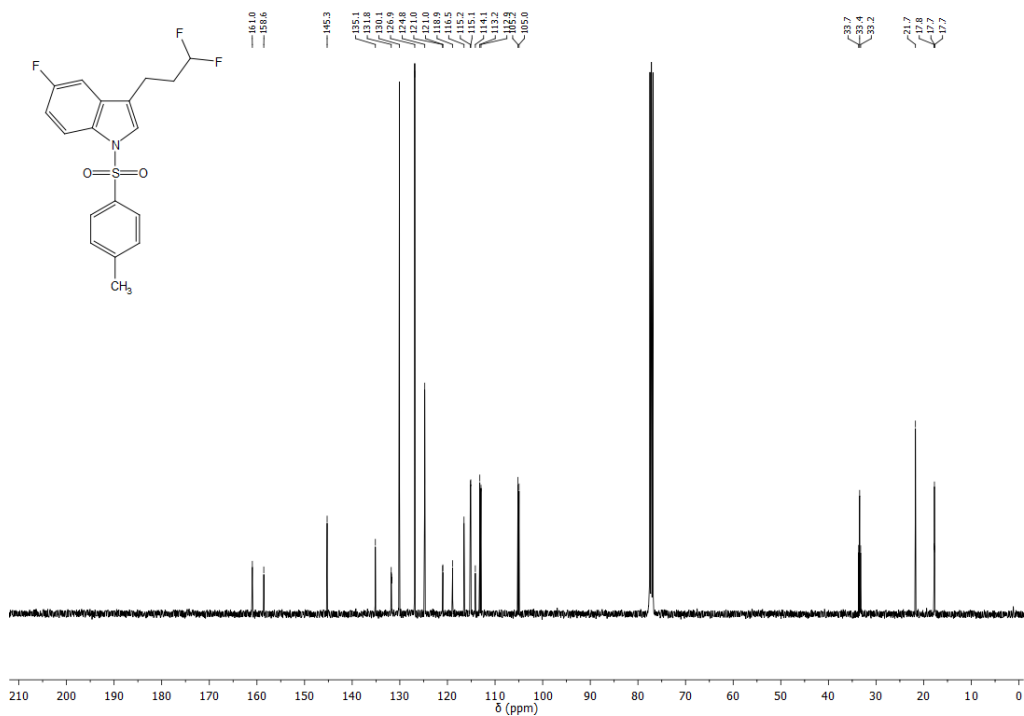


**Figure 103.**  $^{13}\text{C NMR}$  (100 MHz) spectrum of **25c** in  $\text{CDCl}_3$  at 298 K.

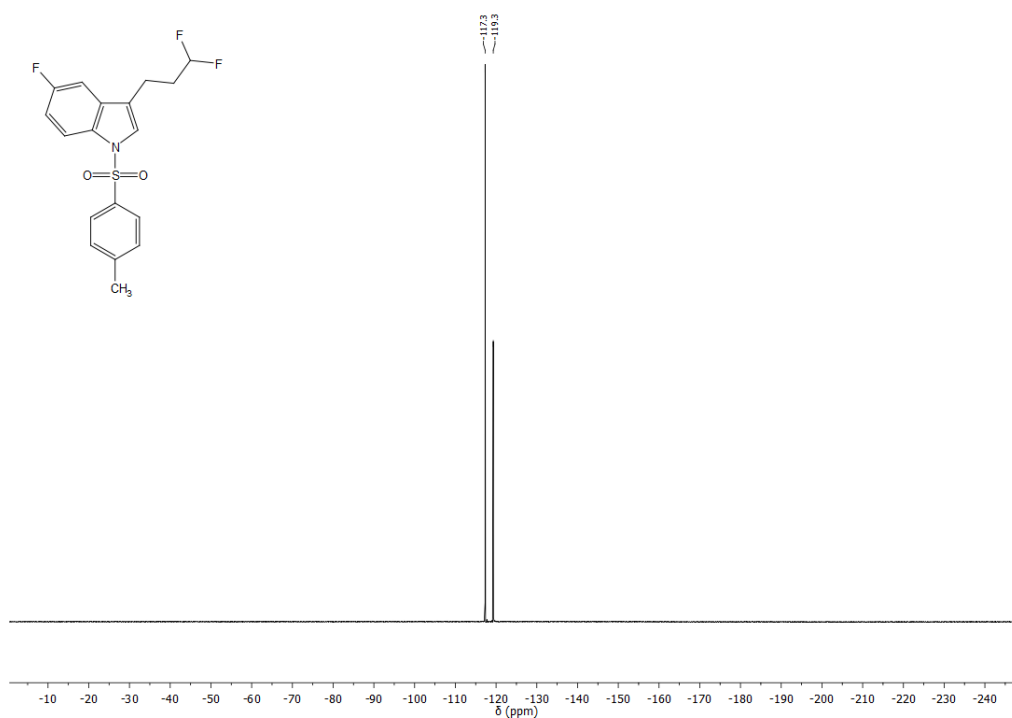


**Figure 104.**  $^{19}\text{F}$  NMR (376 MHz, decoupled) spectrum of **25c** in  $\text{CDCl}_3$  at 298 K.

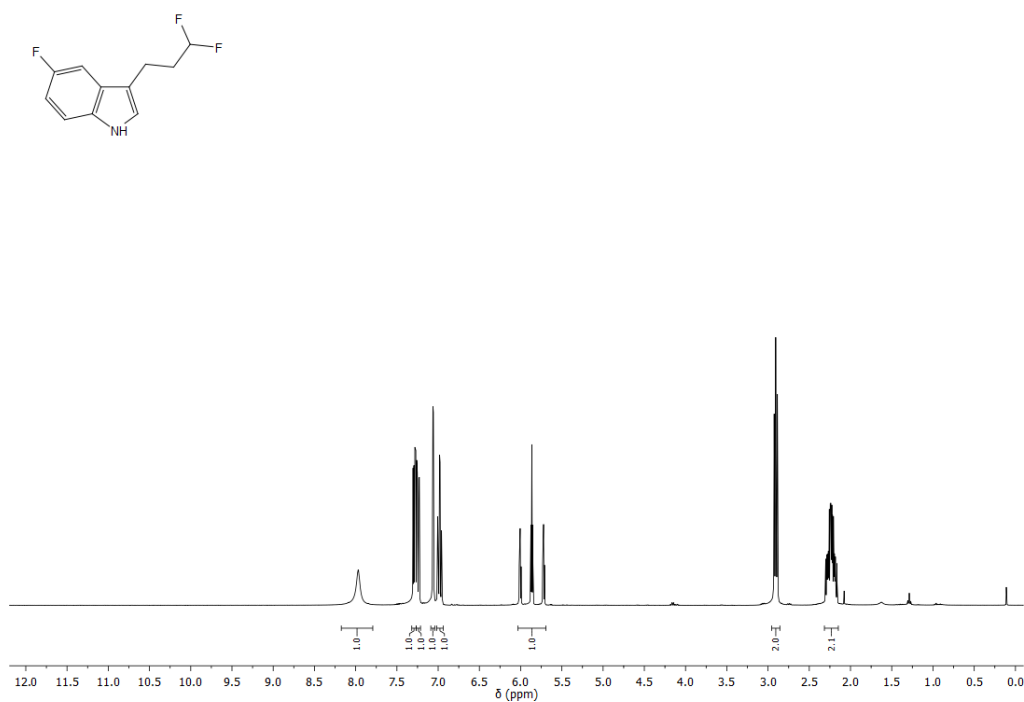


**Figure 105.**  $^1\text{H}$  NMR (400 MHz) spectrum of **26c** in  $\text{CDCl}_3$  at 298 K.



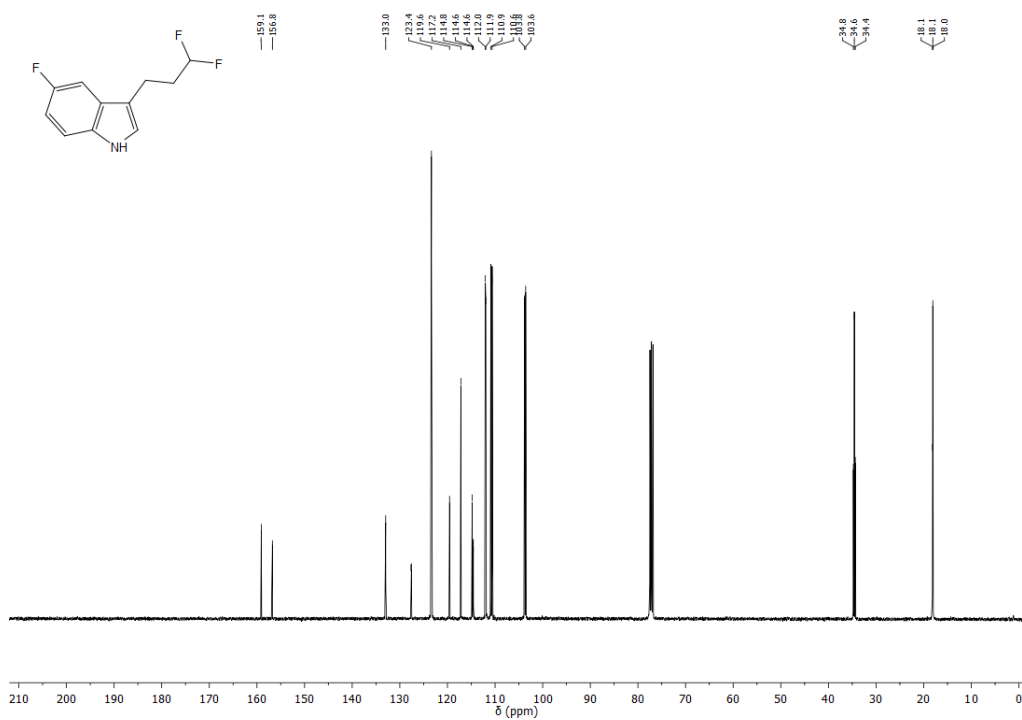


**Figure 106.** <sup>13</sup>C NMR (100 MHz) spectrum of **26c** in CDCl<sub>3</sub> at 298 K.

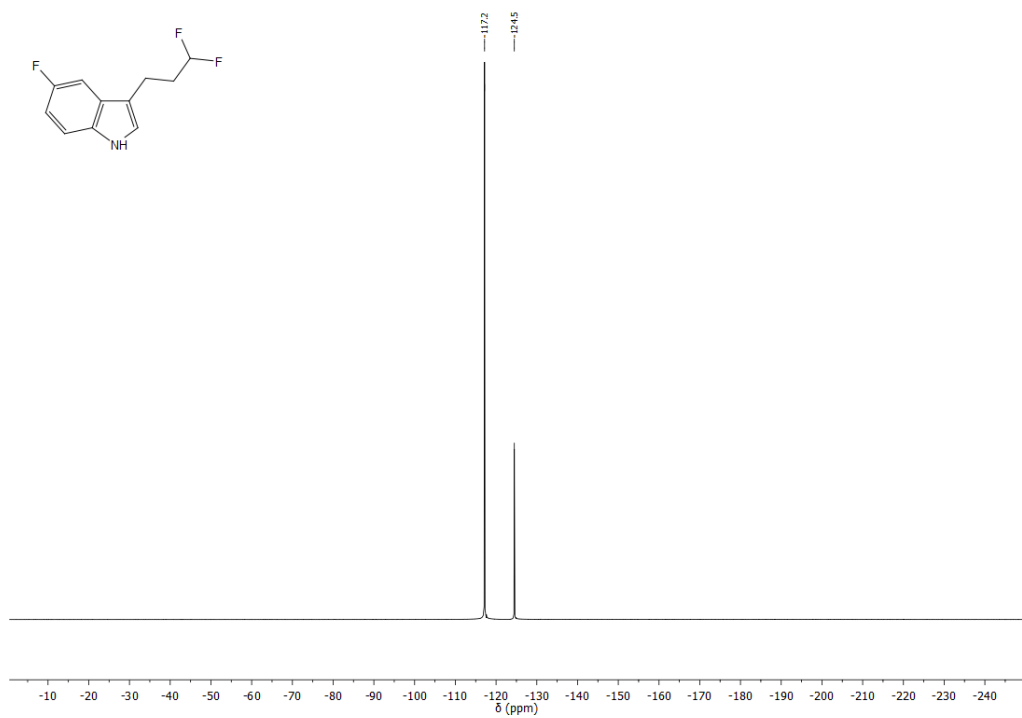


**Figure 107.** <sup>19</sup>F NMR (376 MHz, decoupled) spectrum of **26c** in CDCl<sub>3</sub> at 298 K.

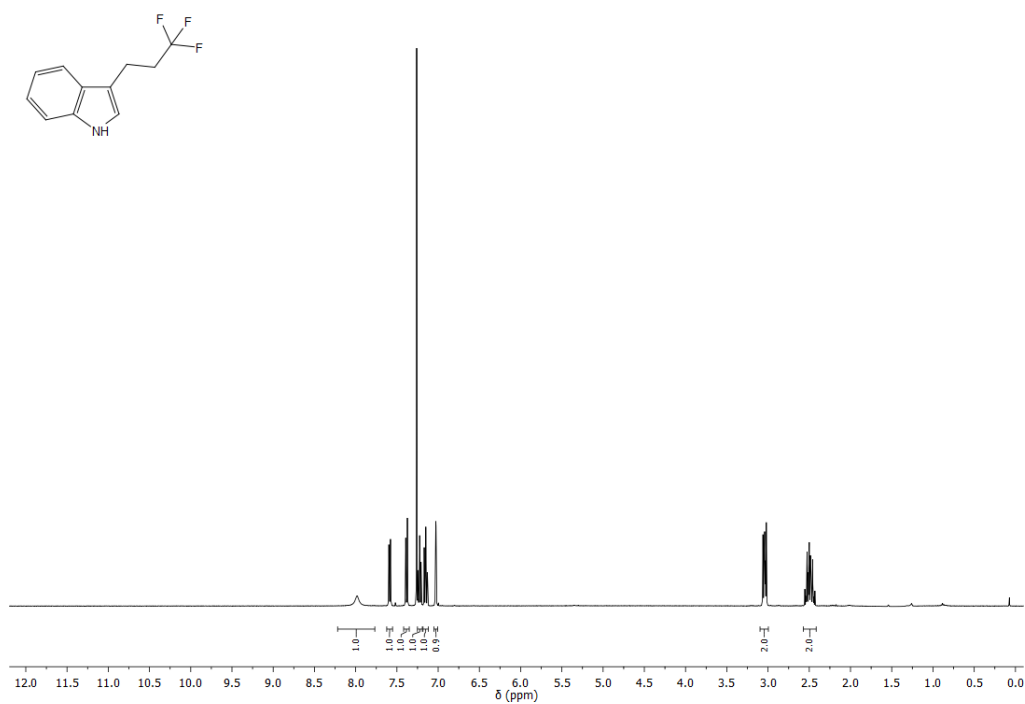


**Figure 108.**  $^1\text{H}$  NMR (400 MHz) spectrum of **23d** in  $\text{CDCl}_3$  at 298 K.

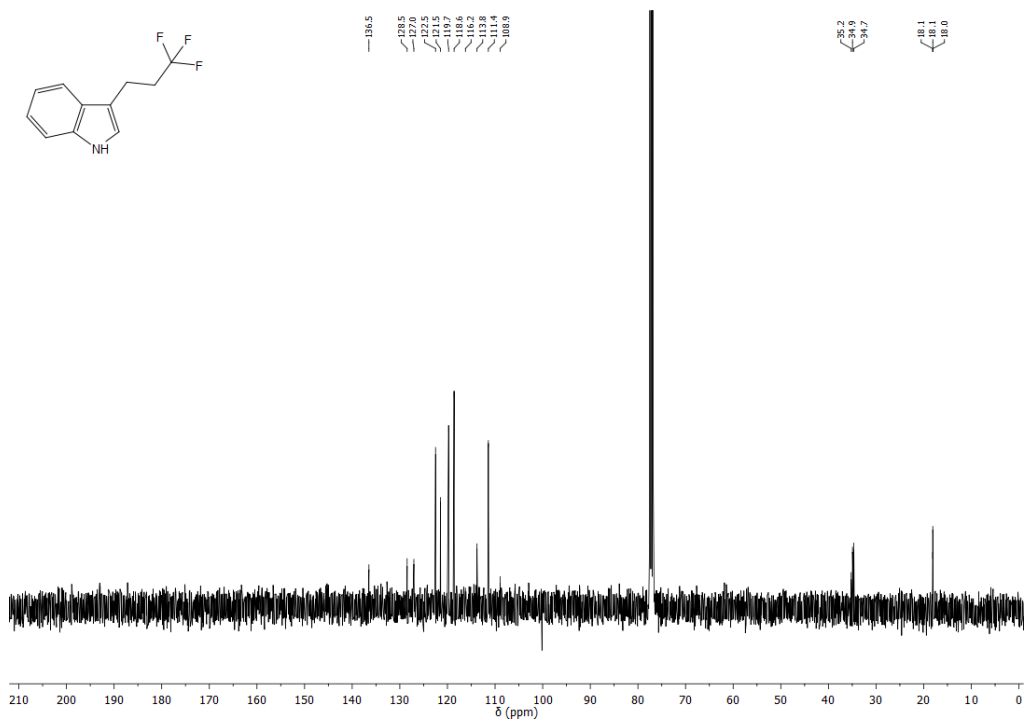


**Figure 109.**  $^{13}\text{C}$  NMR (100 MHz) spectrum of **23d** in  $\text{CDCl}_3$  at 298 K.

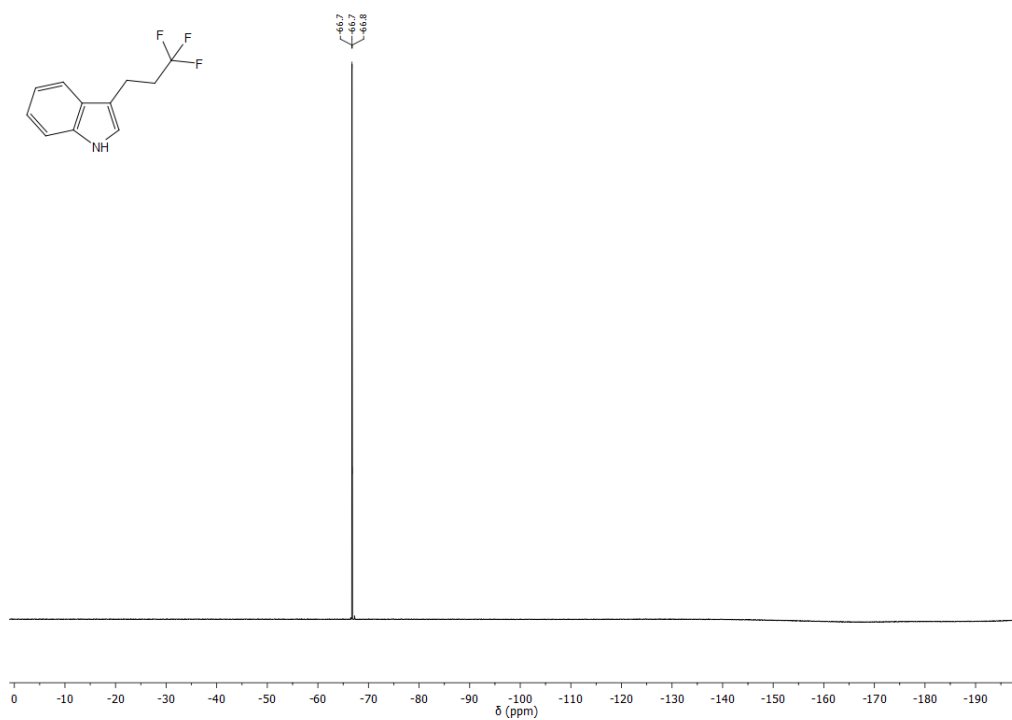


**Figure 110.** <sup>19</sup>F NMR (376 MHz, not decoupled) spectrum of **23d** in CDCl<sub>3</sub> at 298 K.

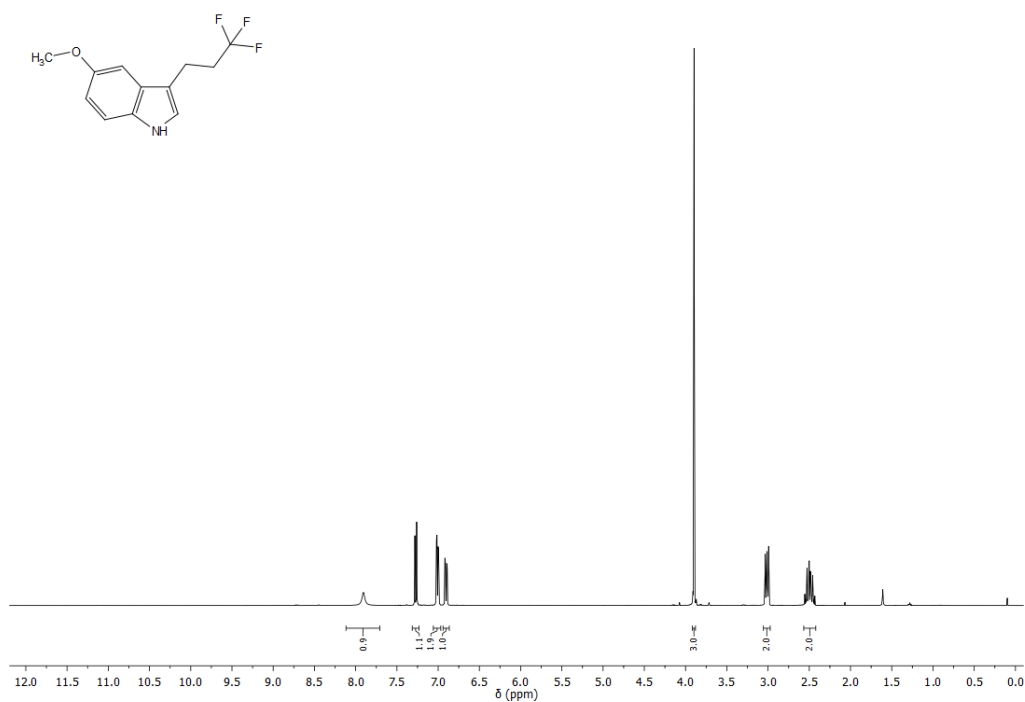


**Figure 111.** <sup>1</sup>H NMR (400 MHz) spectrum of **24d** in CDCl<sub>3</sub> at 298 K.

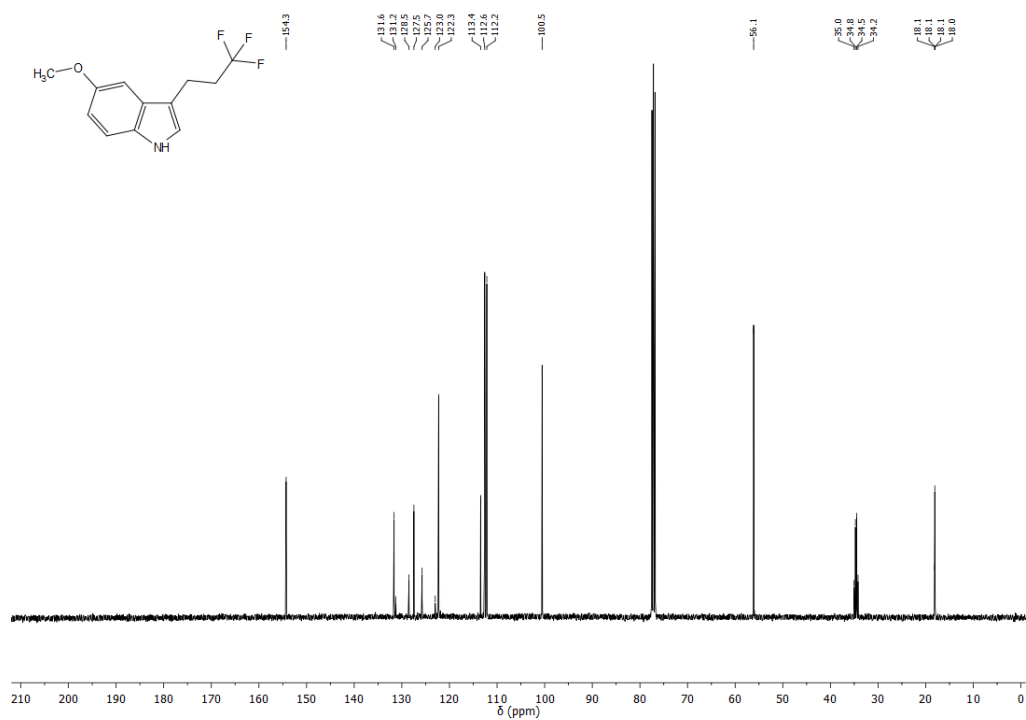


**Figure 112.**  $^{13}\text{C}$  NMR (100 MHz) spectrum of **24d** in  $\text{CDCl}_3$  at 298 K.

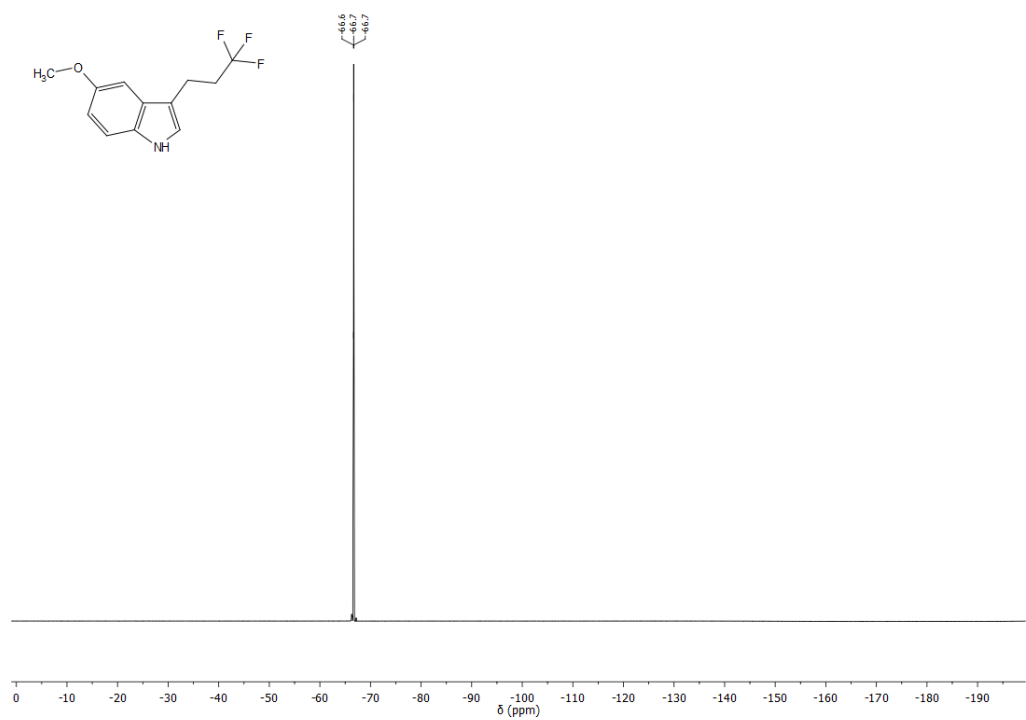


**Figure 113.**  $^{19}\text{F}$  NMR (376 MHz, not decoupled) spectrum of **24d** in  $\text{CDCl}_3$  at 298 K.

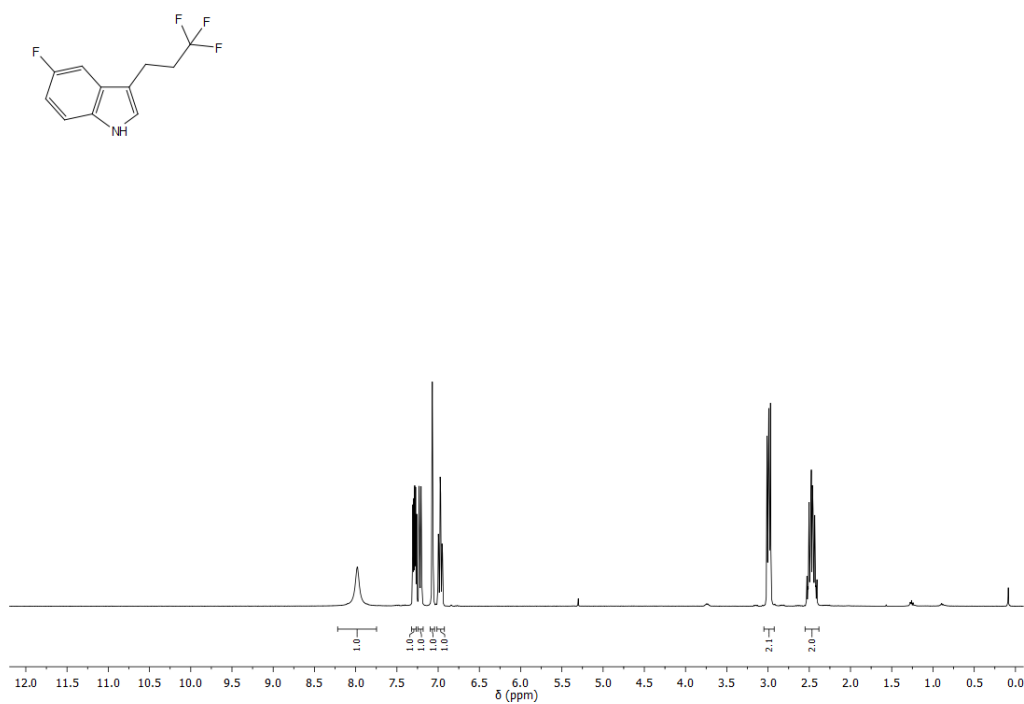


**Figure 114.**  $^1\text{H}$  NMR (400 MHz) spectrum of **26d** in  $\text{CDCl}_3$  at 298 K.

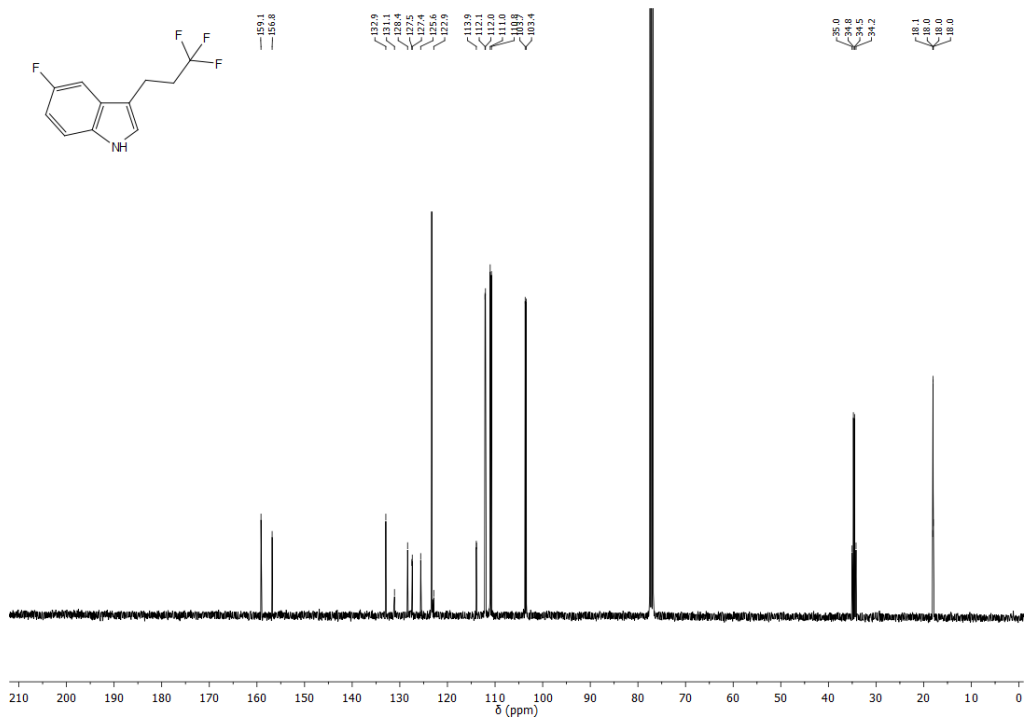


**Figure 115.**  $^{13}\text{C}$  NMR (100 MHz) spectrum of **26d** in  $\text{CDCl}_3$  at 298 K.



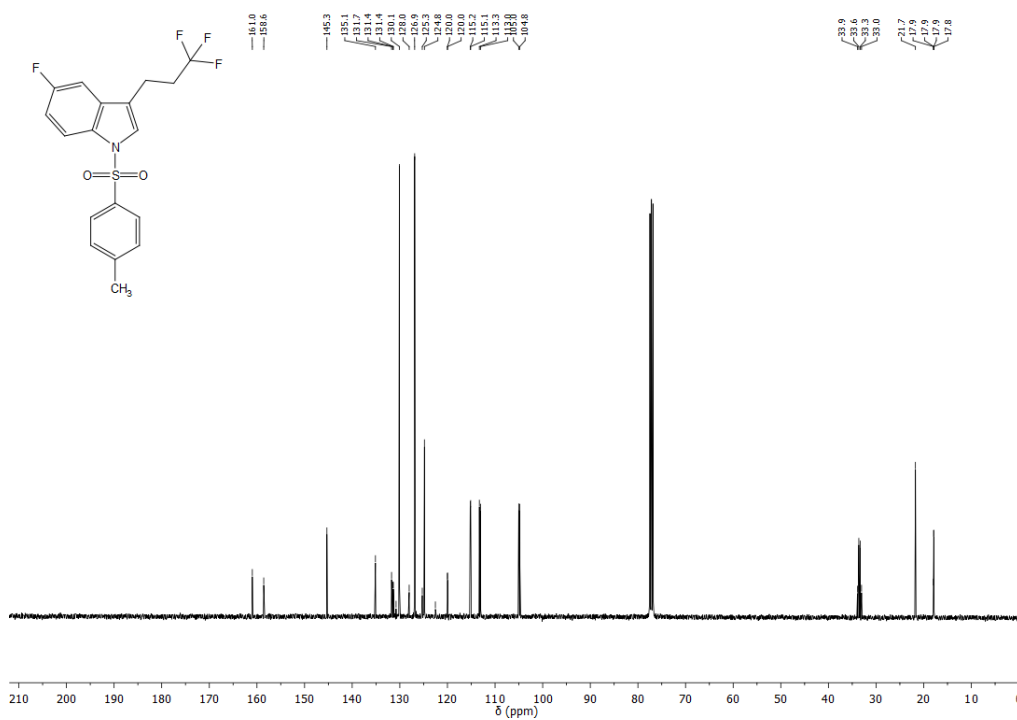


**Figure 118.**  $^{13}\text{C}$  NMR (100 MHz) spectrum of **25d** in  $\text{CDCl}_3$  at 298 K.

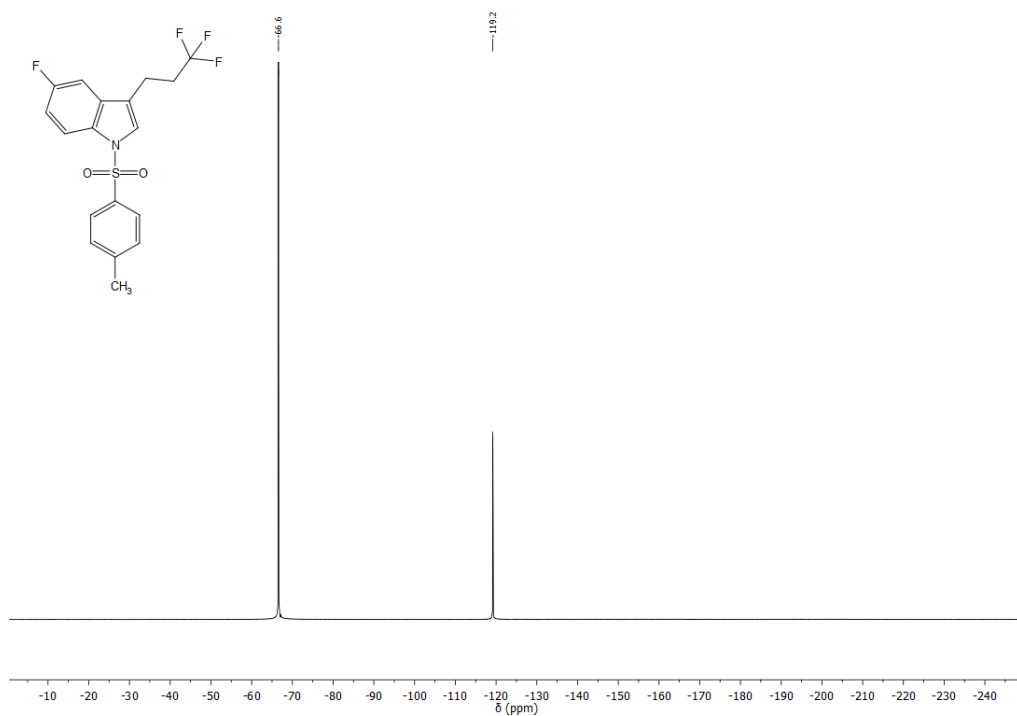


**Figure 119.**  $^{19}\text{F}$  NMR (376 MHz, decoupled) spectrum of **25d** in  $\text{CDCl}_3$  at 298 K.







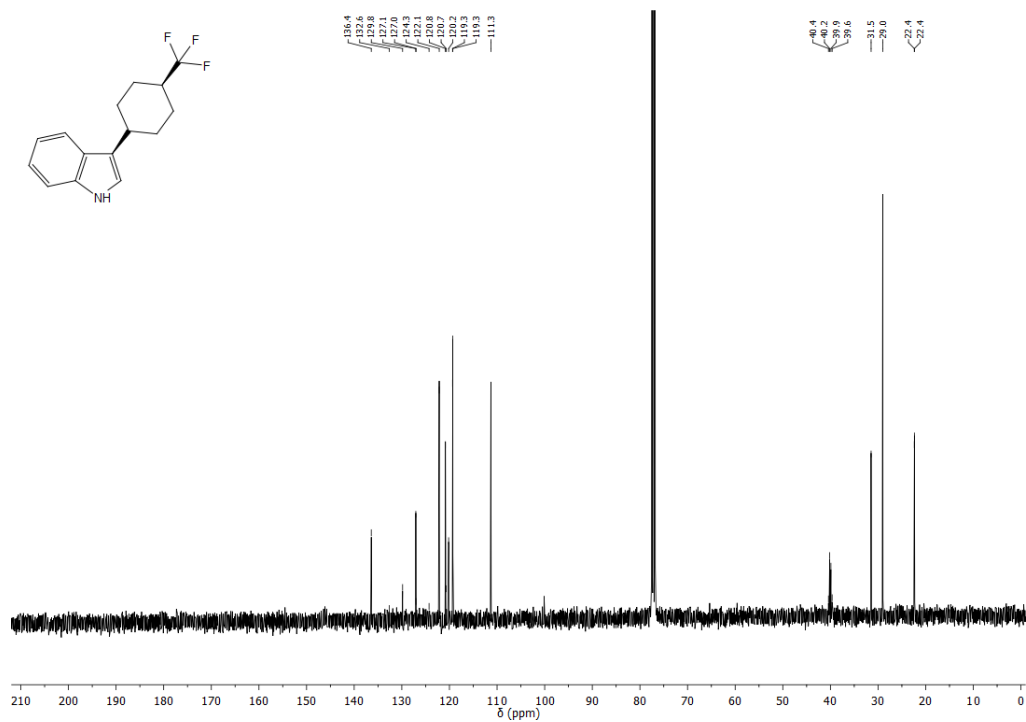


**Figure 124.** <sup>13</sup>C NMR (100 MHz) spectrum of *cis*-45d in CDCl<sub>3</sub> at 298 K.

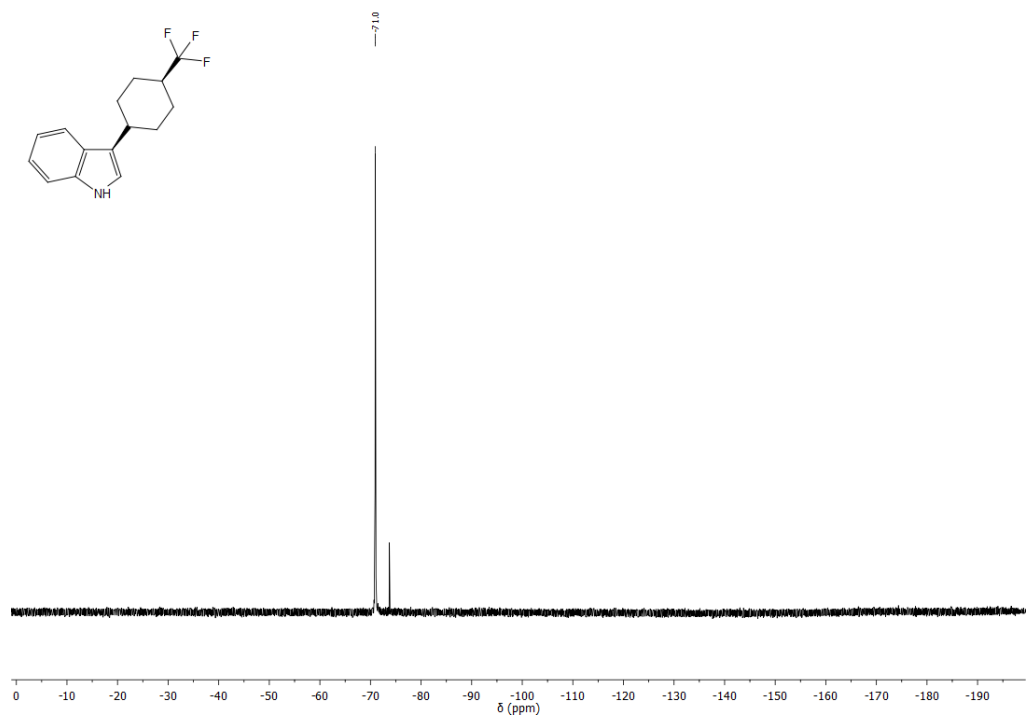


**Figure 125.** <sup>19</sup>F NMR (376 MHz, decoupled) spectrum of *cis*-45d in CDCl<sub>3</sub> at 298 K.

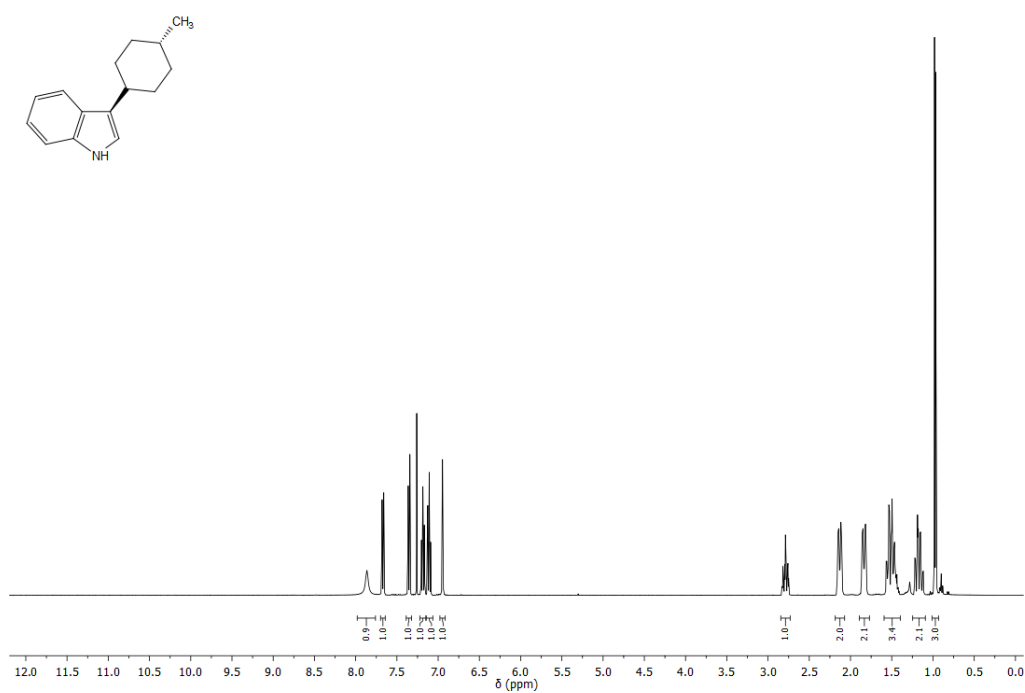


Figure 126. <sup>1</sup>H NMR (400 MHz) spectrum of *trans*-45a in CDCl<sub>3</sub> at 298 K.

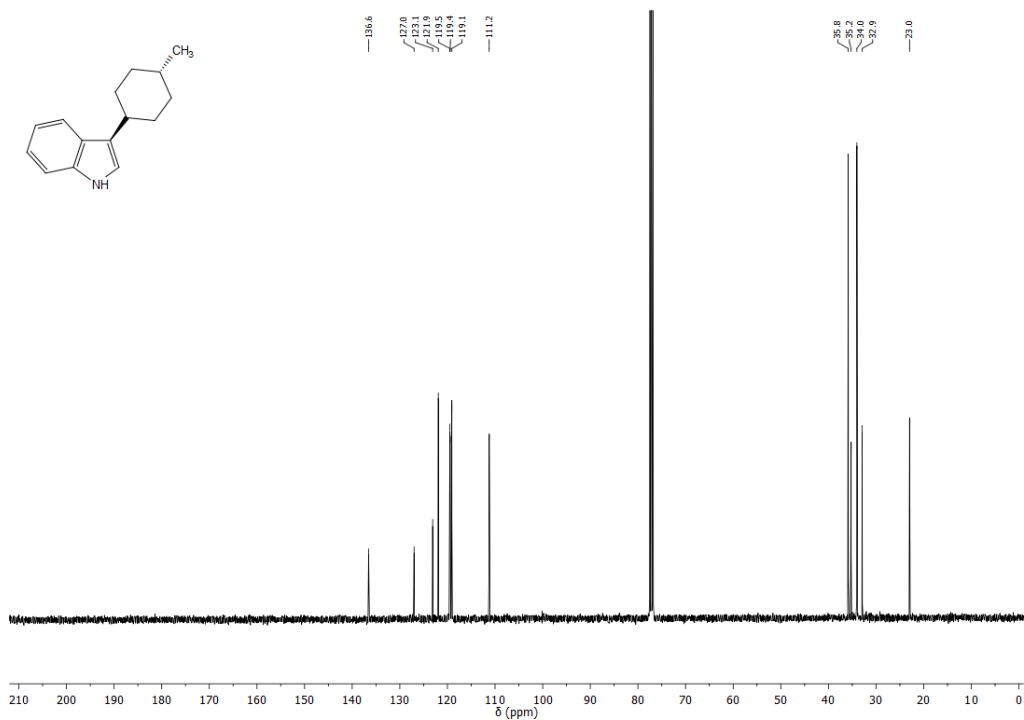


Figure 127. <sup>13</sup>C NMR (100 MHz) spectrum of *trans*-45a in CDCl<sub>3</sub> at 298 K.



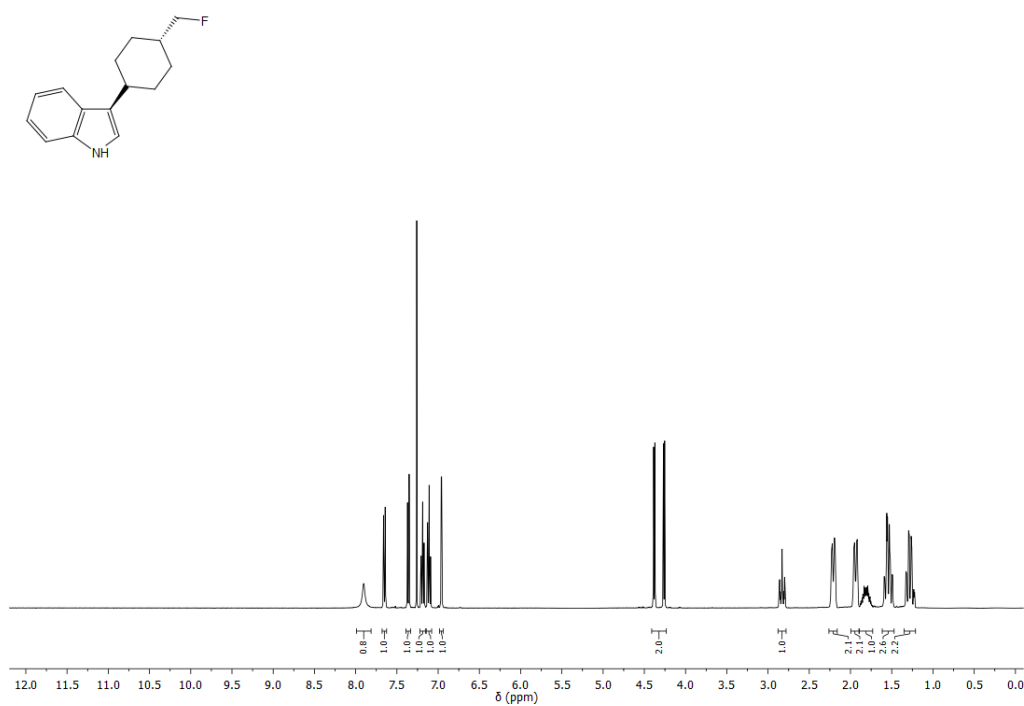


Figure 130. <sup>1</sup>H NMR (400 MHz) spectrum of *trans*-45b in CDCl<sub>3</sub> at 298 K.

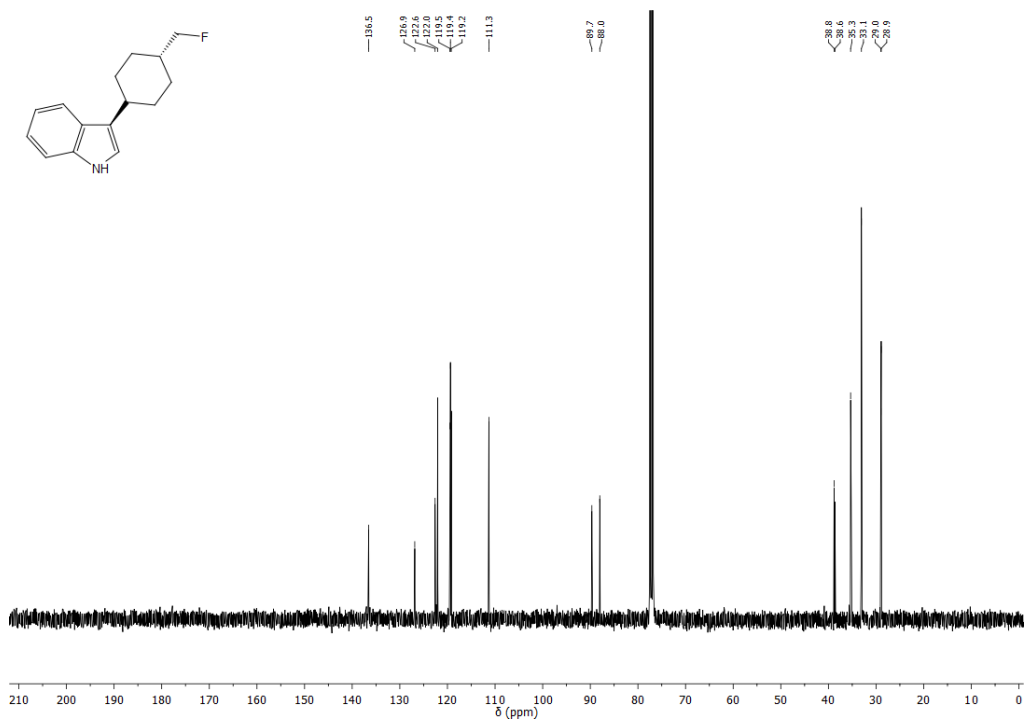
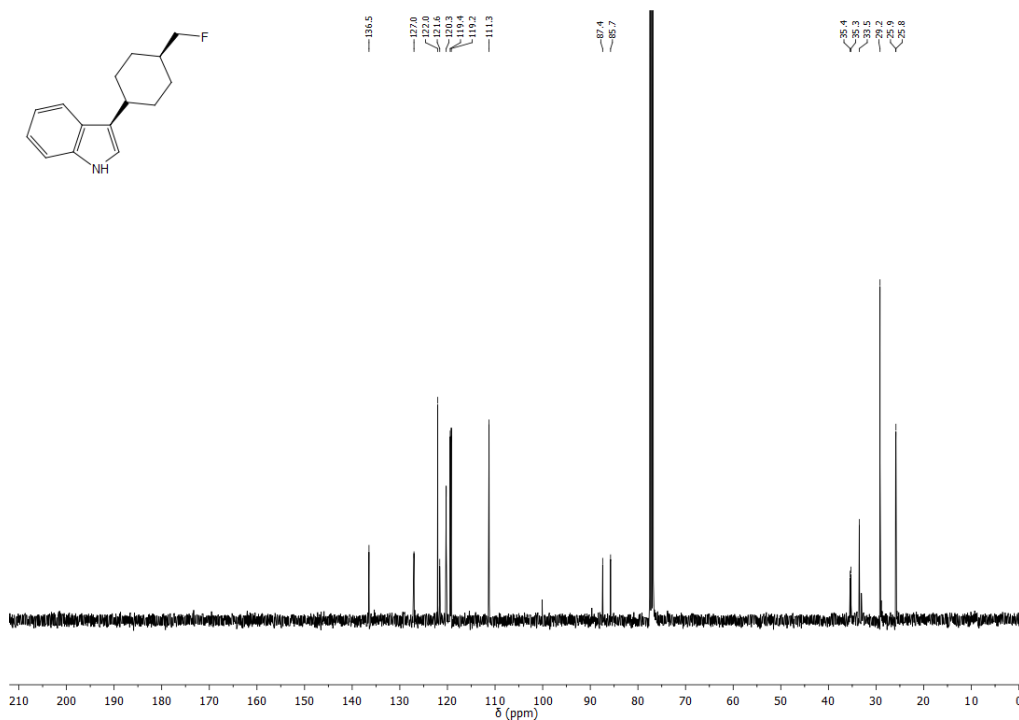
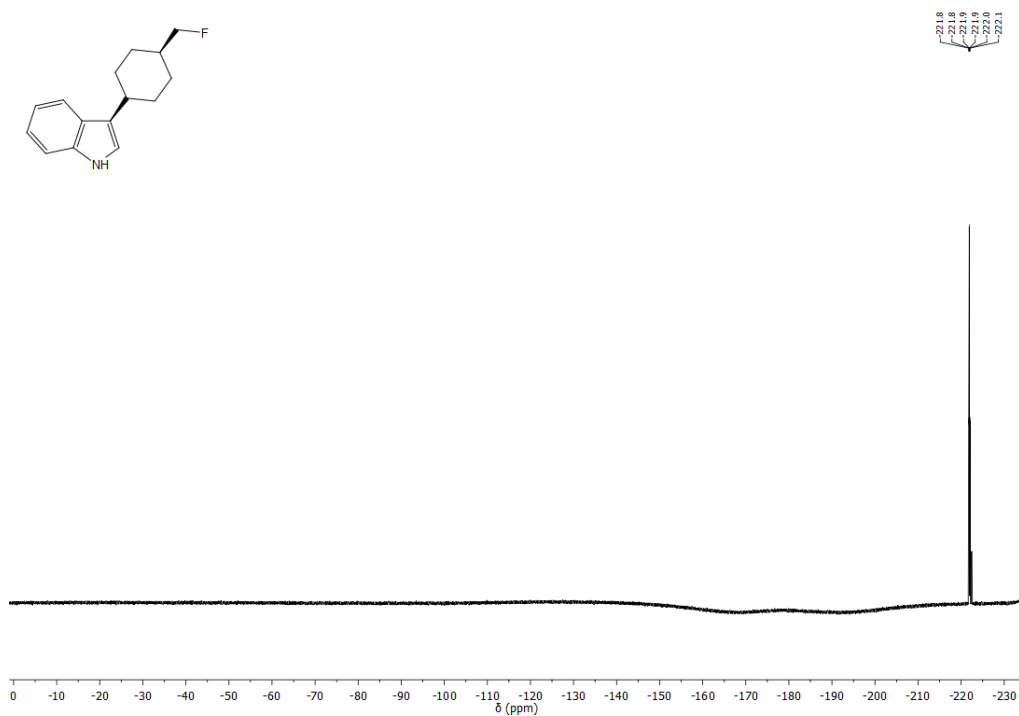


Figure 131. <sup>13</sup>C NMR (100 MHz) spectrum of *trans*-45b in CDCl<sub>3</sub> at 298 K.





**Figure 134.**  $^{13}\text{C}$  NMR (100 MHz) spectrum of *cis*-45b in  $\text{CDCl}_3$  at 298 K.



**Figure 135.**  $^{19}\text{F}$  NMR (376 MHz, not decoupled) spectrum of *cis*-45b in  $\text{CDCl}_3$  at 298 K.

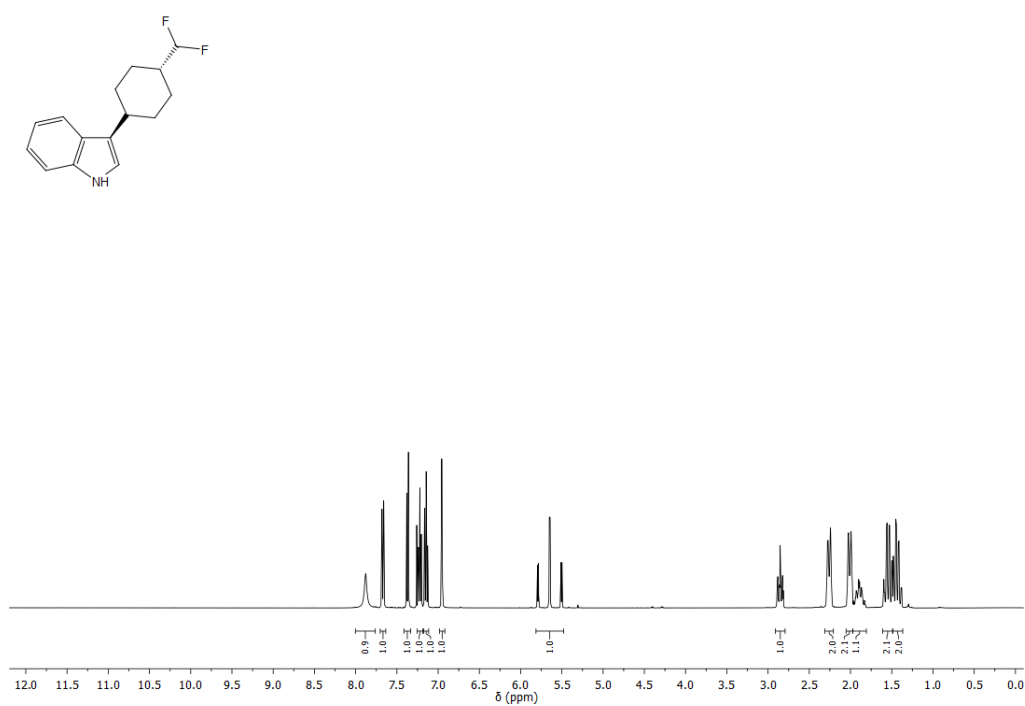


**Figure 136.** <sup>1</sup>H NMR (400 MHz) spectrum of *trans*-45c in CDCl<sub>3</sub> at 298 K.

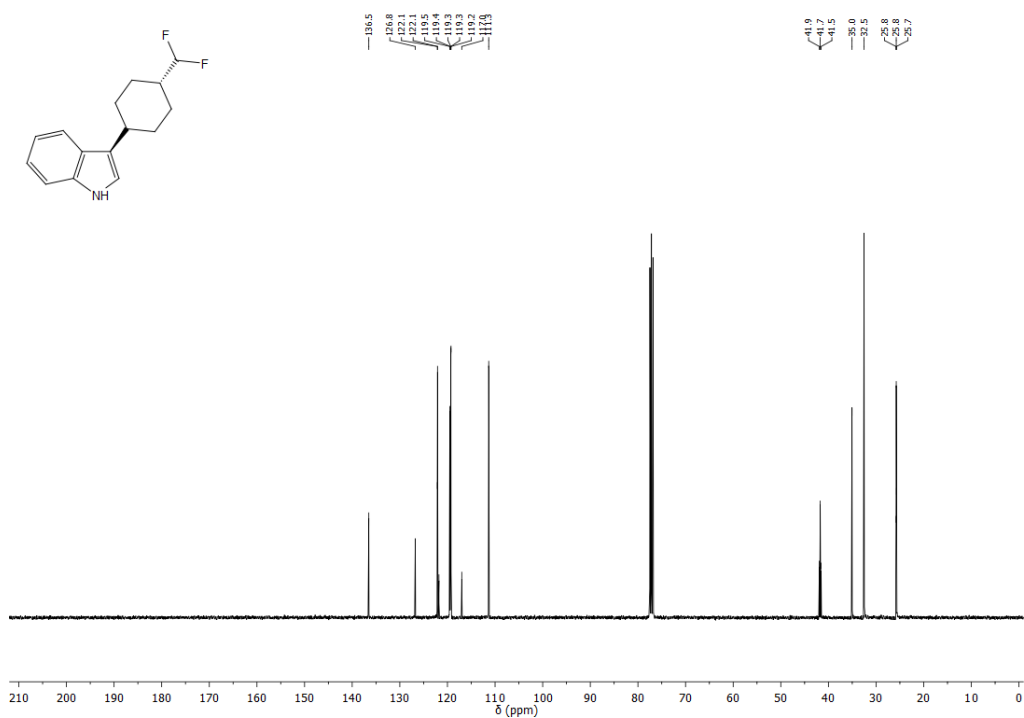


**Figure 137.** <sup>13</sup>C NMR (100 MHz) spectrum of *trans*-45c in CDCl<sub>3</sub> at 298 K.





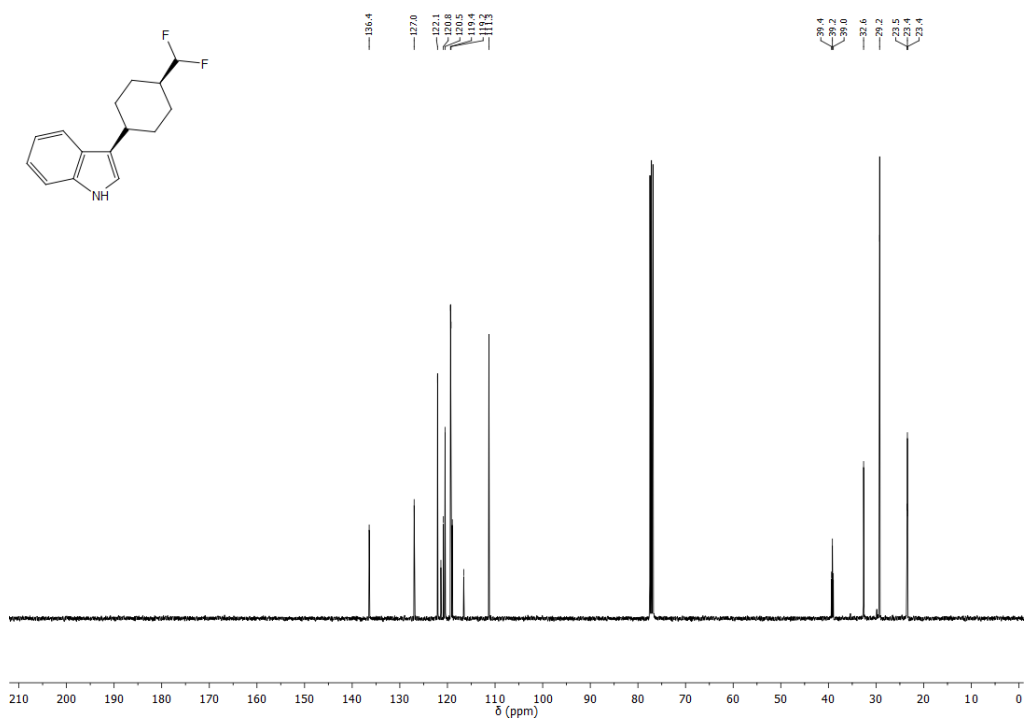


**Figure 140.** <sup>13</sup>C NMR (100 MHz) spectrum of *cis*-45c in CDCl<sub>3</sub> at 298 K.

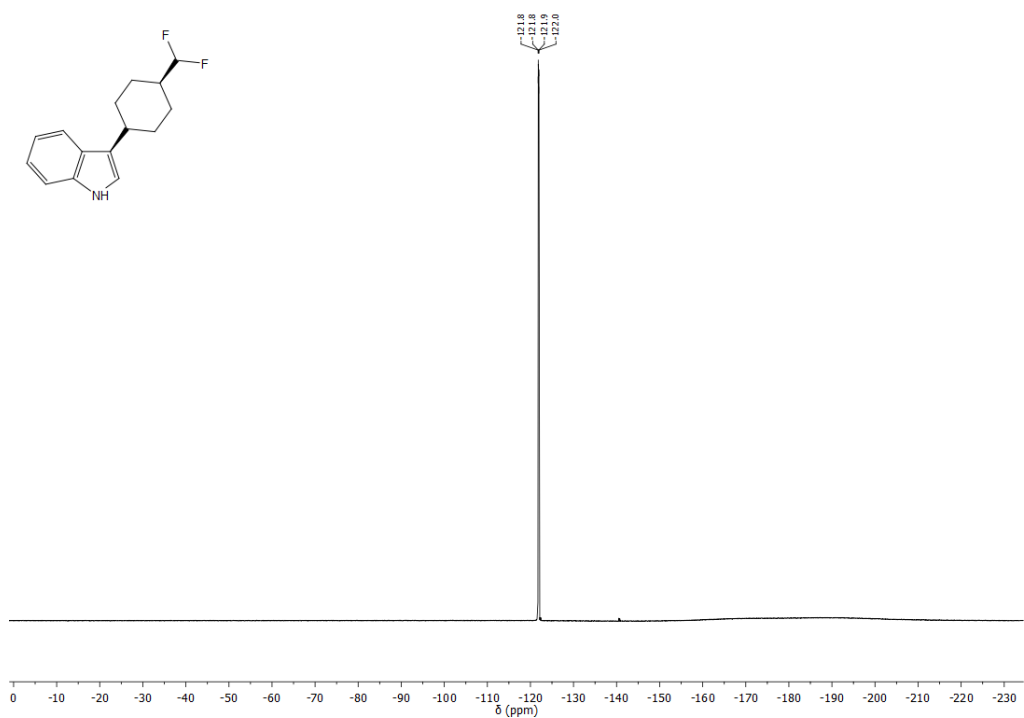


**Figure 141.** <sup>19</sup>F NMR (376 MHz, not decoupled) spectrum of *cis*-45c in CDCl<sub>3</sub> at 298 K.

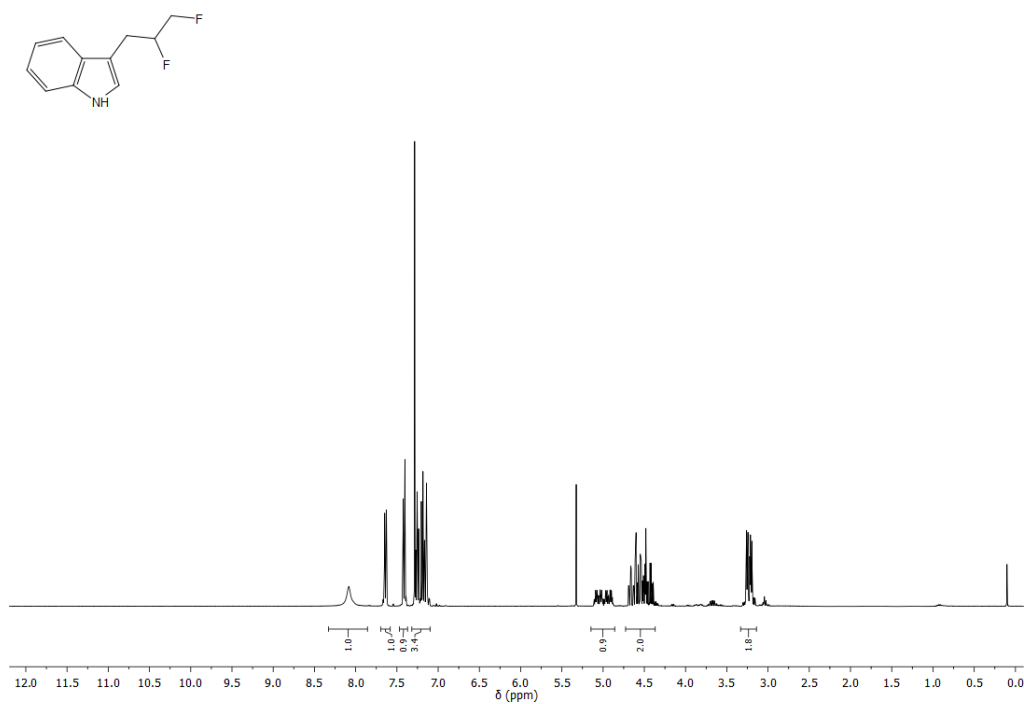


**Figure 142.**  $^1\text{H}$  NMR (400 MHz) spectrum of **60** in  $\text{CDCl}_3$  at 298 K.

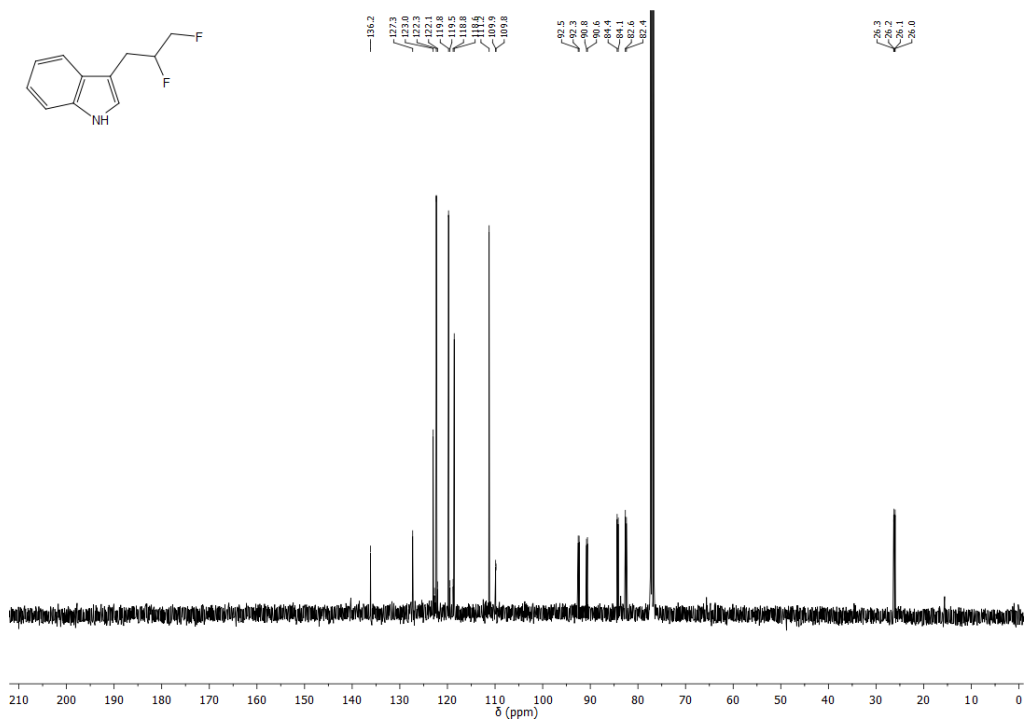


**Figure 143.**  $^{13}\text{C}$  NMR (100 MHz) spectrum of **60** in  $\text{CDCl}_3$  at 298 K.

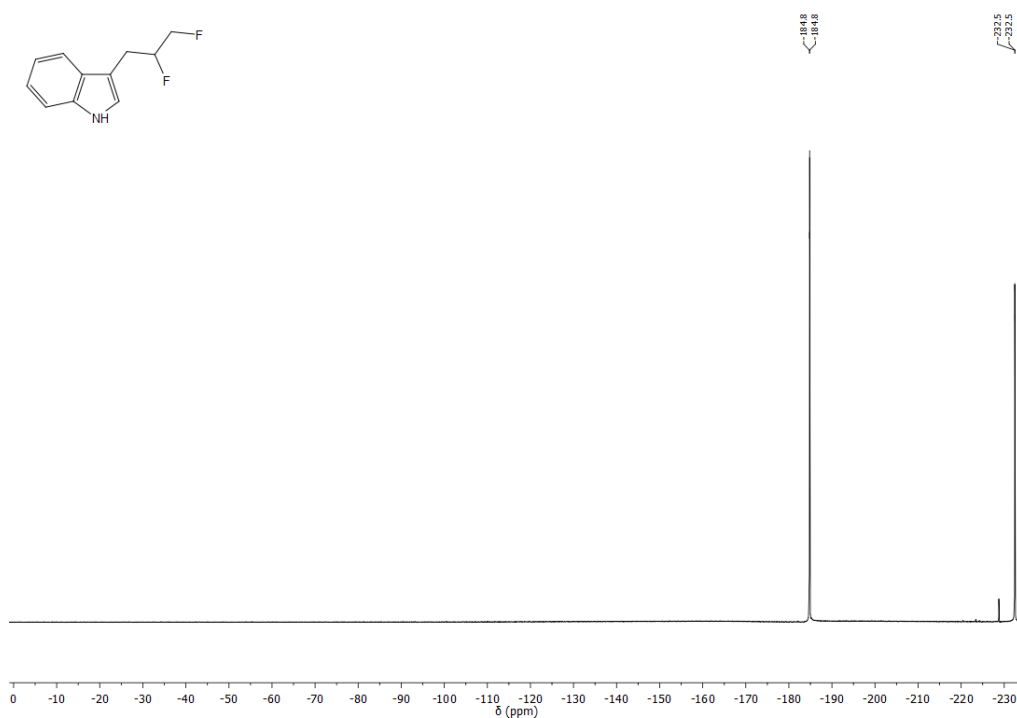


**Figure 144.** <sup>19</sup>F NMR (376 MHz, decoupled) spectrum of **60** in CDCl<sub>3</sub> at 298 K.

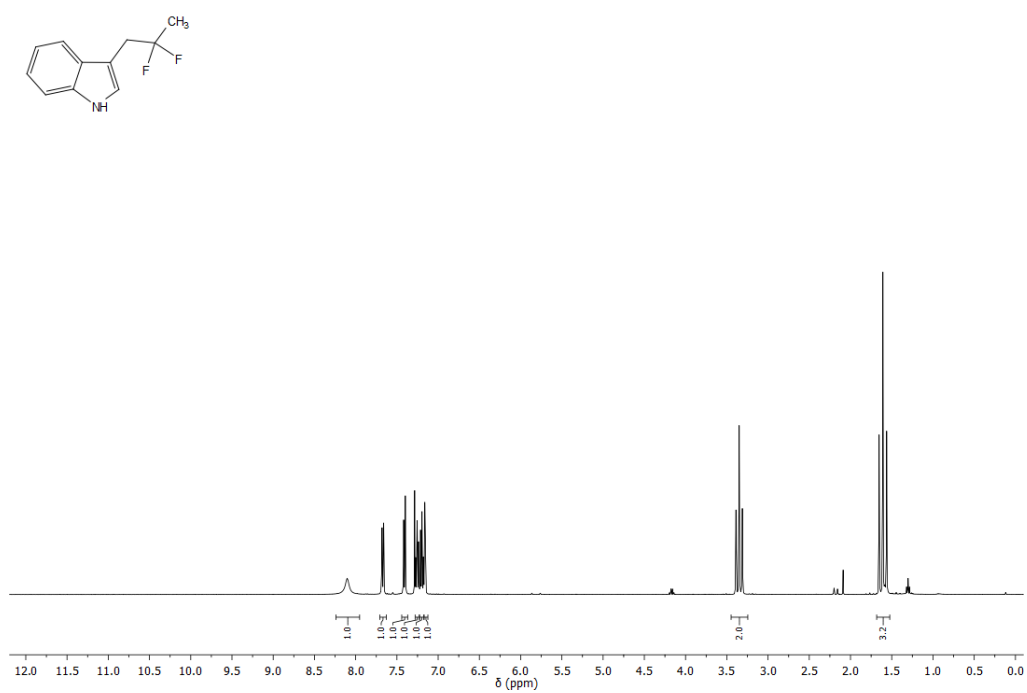


**Figure 145.** <sup>1</sup>H NMR (400 MHz) spectrum of **61** in CDCl<sub>3</sub> at 298 K.

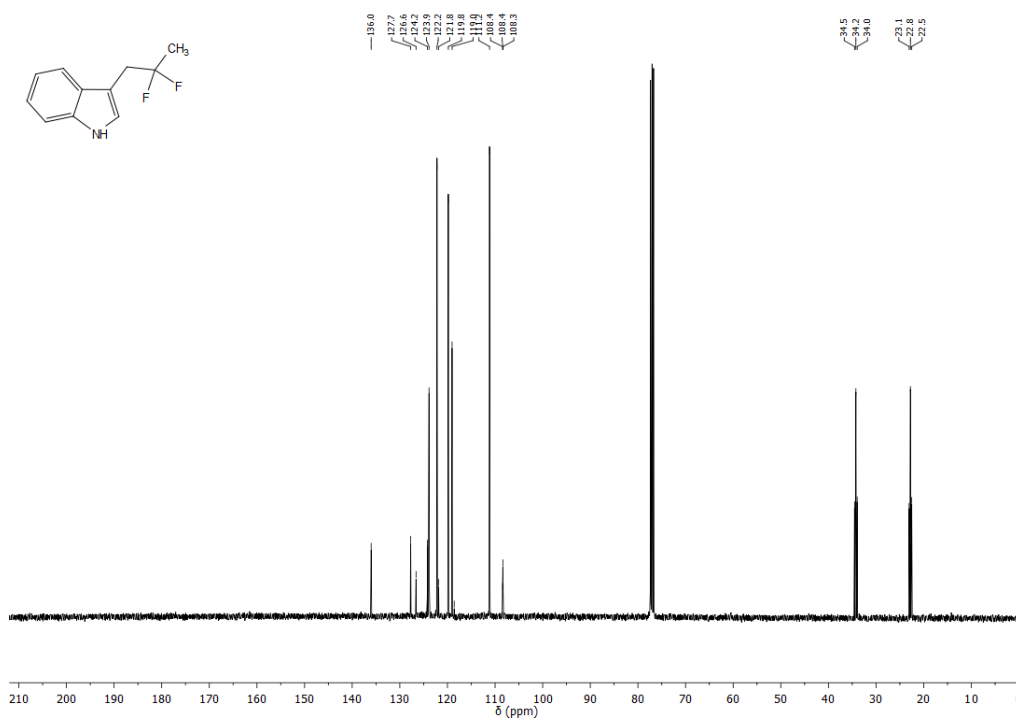


**Figure 146.** <sup>13</sup>C NMR (100 MHz) spectrum of **61** in CDCl<sub>3</sub> at 298 K.

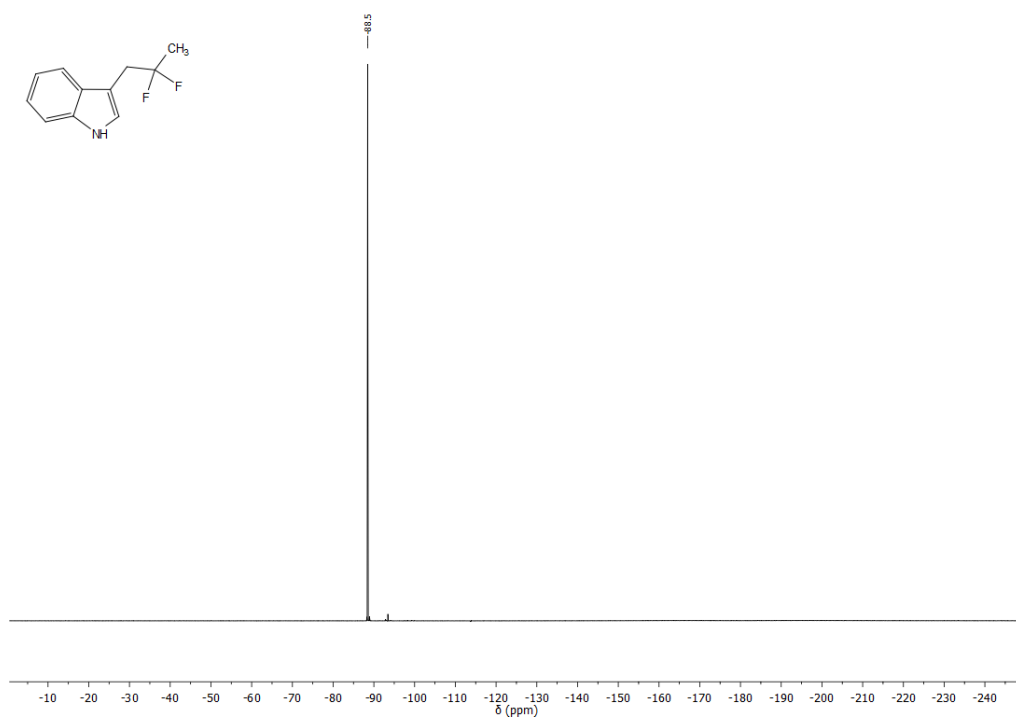


**Figure 147.** <sup>19</sup>F NMR (376 MHz, decoupled) spectrum of **61** in CDCl<sub>3</sub> at 298 K.

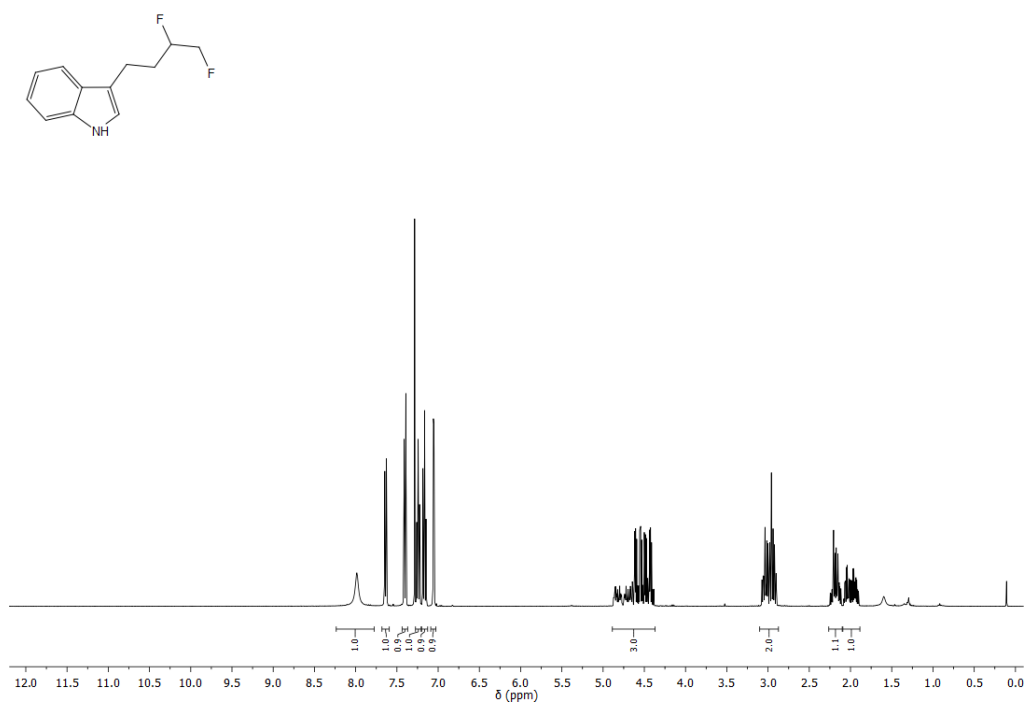


**Figure 148.** <sup>1</sup>H NMR (400 MHz) spectrum of **64** in CDCl<sub>3</sub> at 298 K.

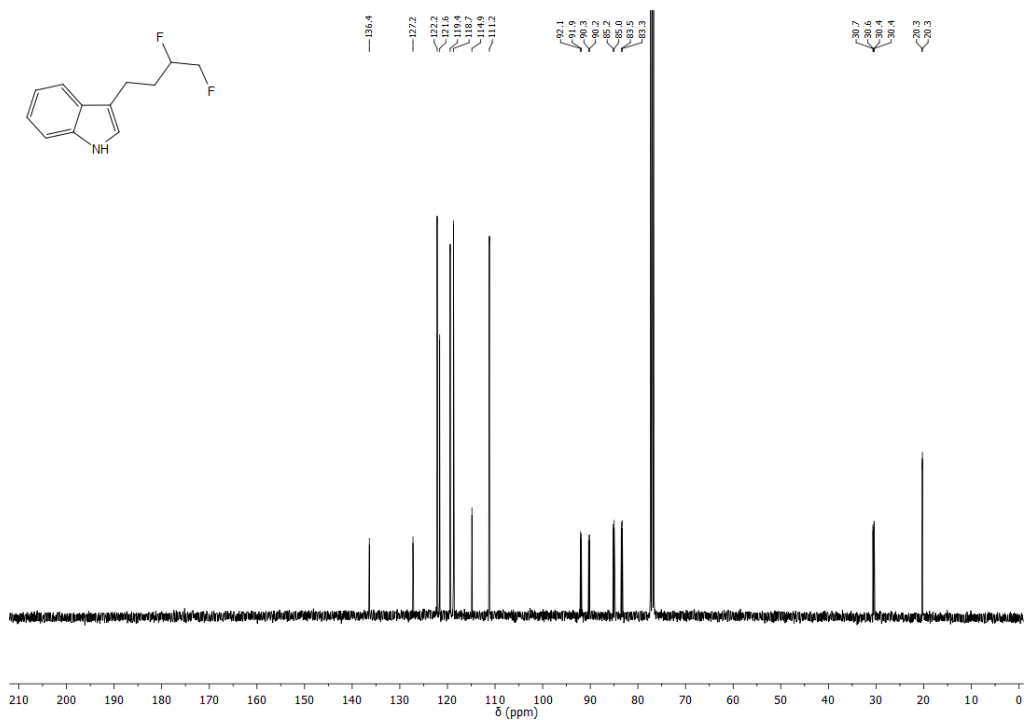


**Figure 149.** <sup>13</sup>C NMR (100 MHz) spectrum of **64** in CDCl<sub>3</sub> at 298 K.

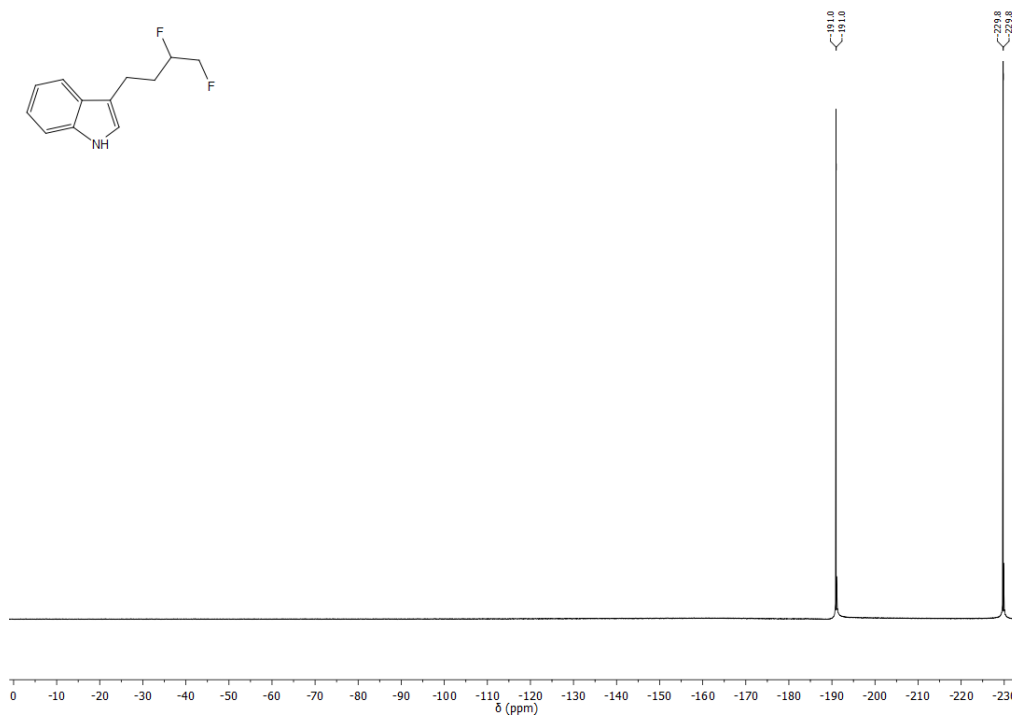


**Figure 150.**  $^{19}\text{F}$  NMR (376 MHz, decoupled) spectrum of **64** in  $\text{CDCl}_3$  at 298 K.

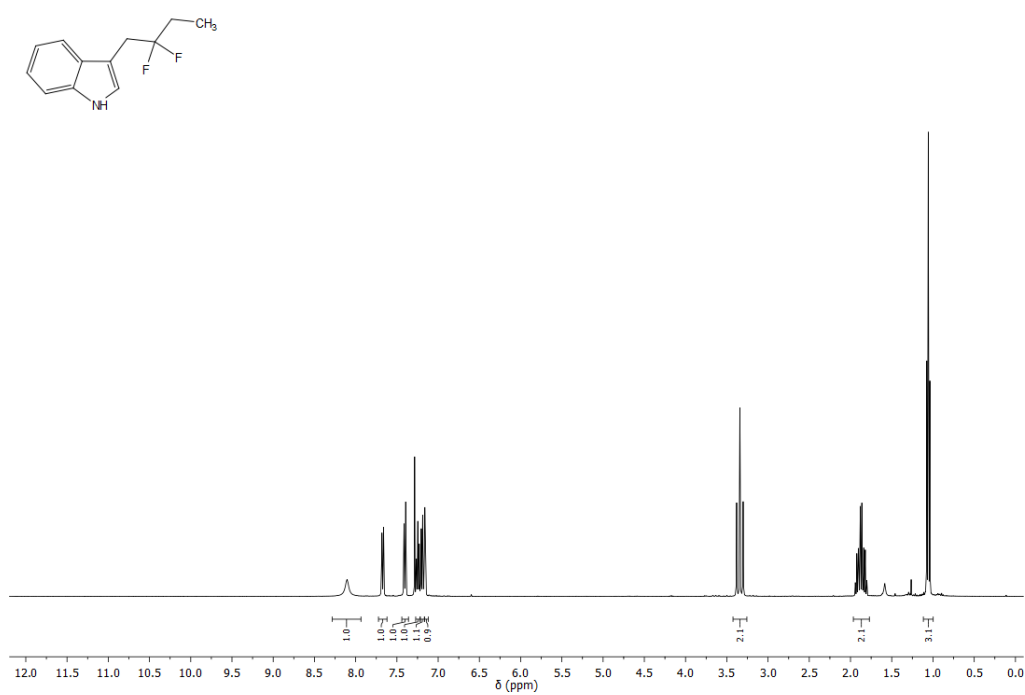


**Figure 151.**  $^1\text{H}$  NMR (400 MHz) spectrum of **62** in  $\text{CDCl}_3$  at 298 K.

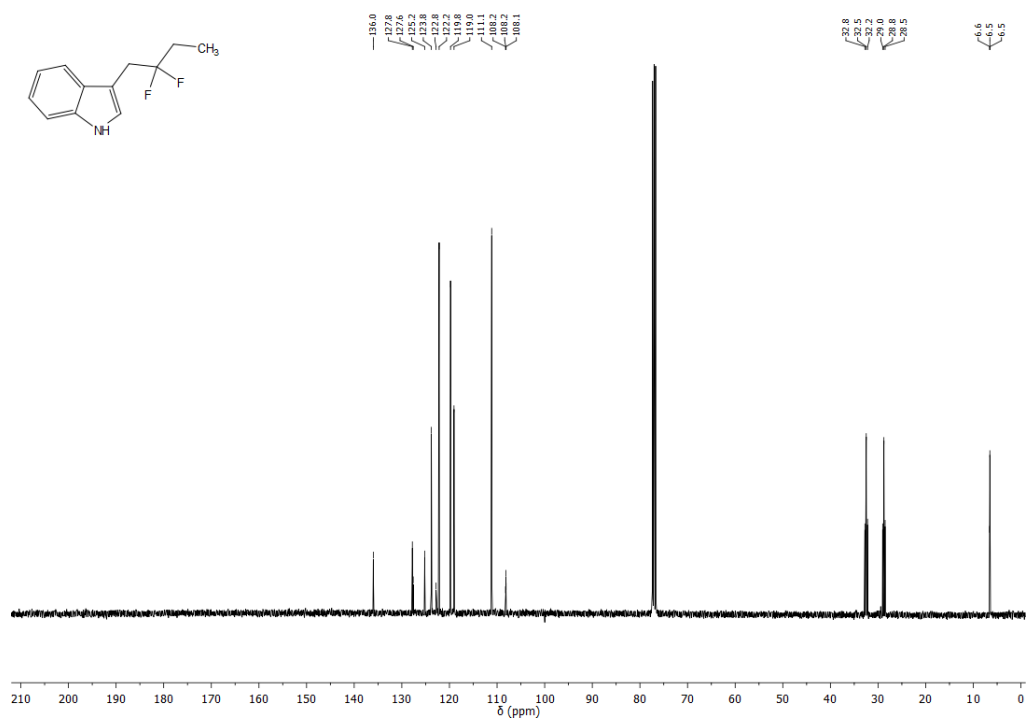


**Figure 152.**  $^{13}\text{C}$  NMR (100 MHz) spectrum of **62** in  $\text{CDCl}_3$  at 298 K.

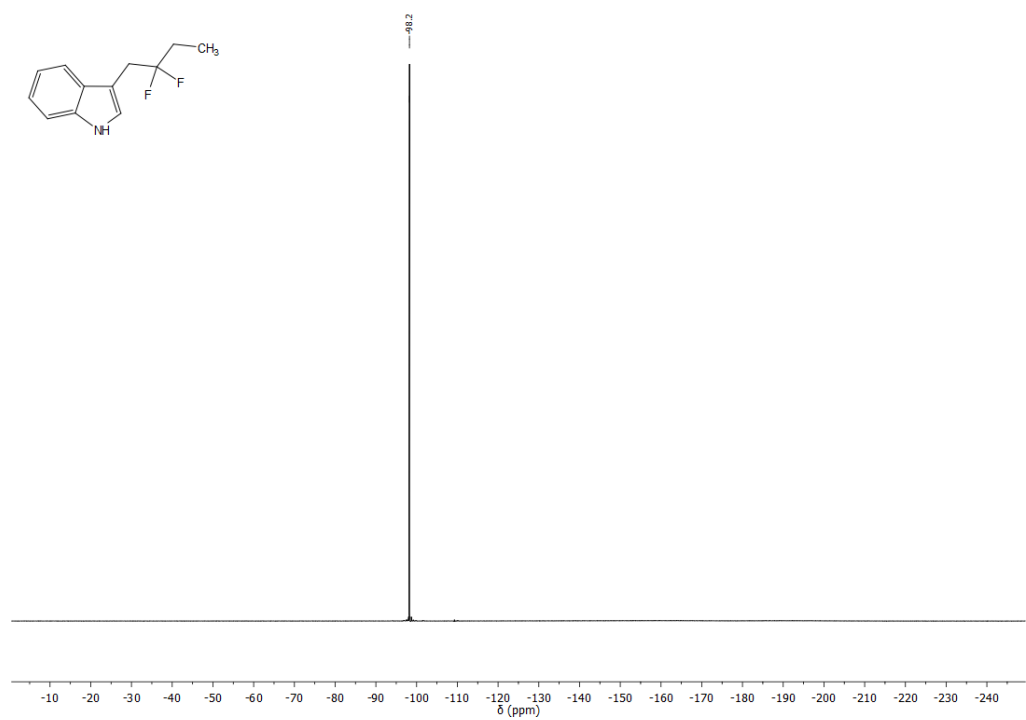


**Figure 153.**  $^{19}\text{F}$  NMR (376 MHz, decoupled) spectrum of **62** in  $\text{CDCl}_3$  at 298 K.



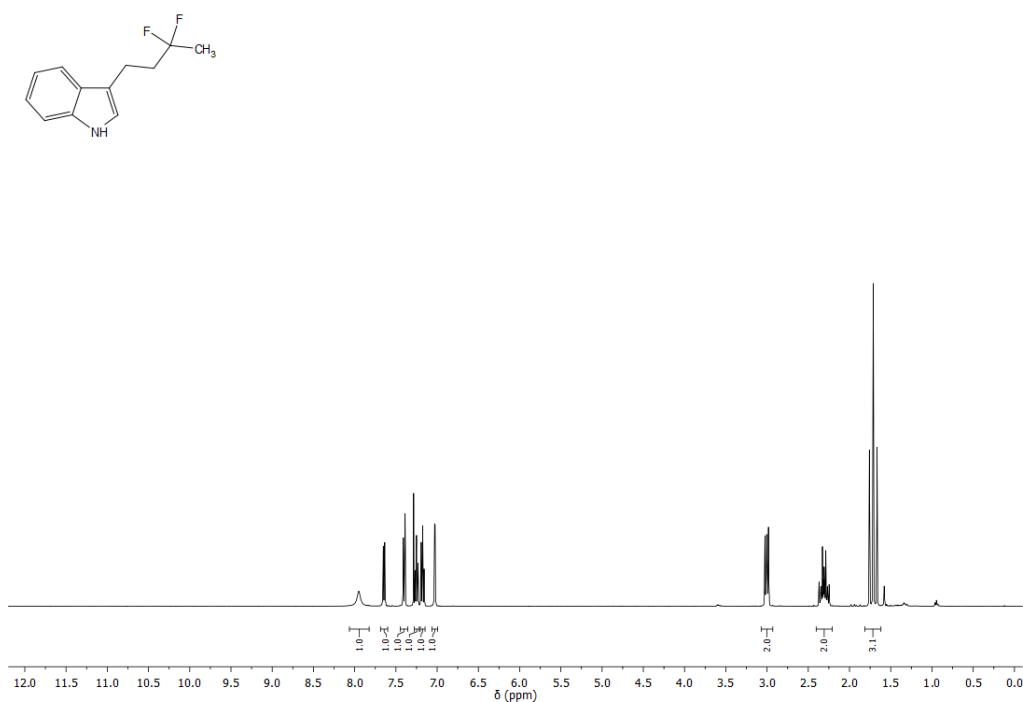


**Figure 154.** <sup>1</sup>H NMR (400 MHz) spectrum of **63** in CDCl<sub>3</sub> at 298 K.

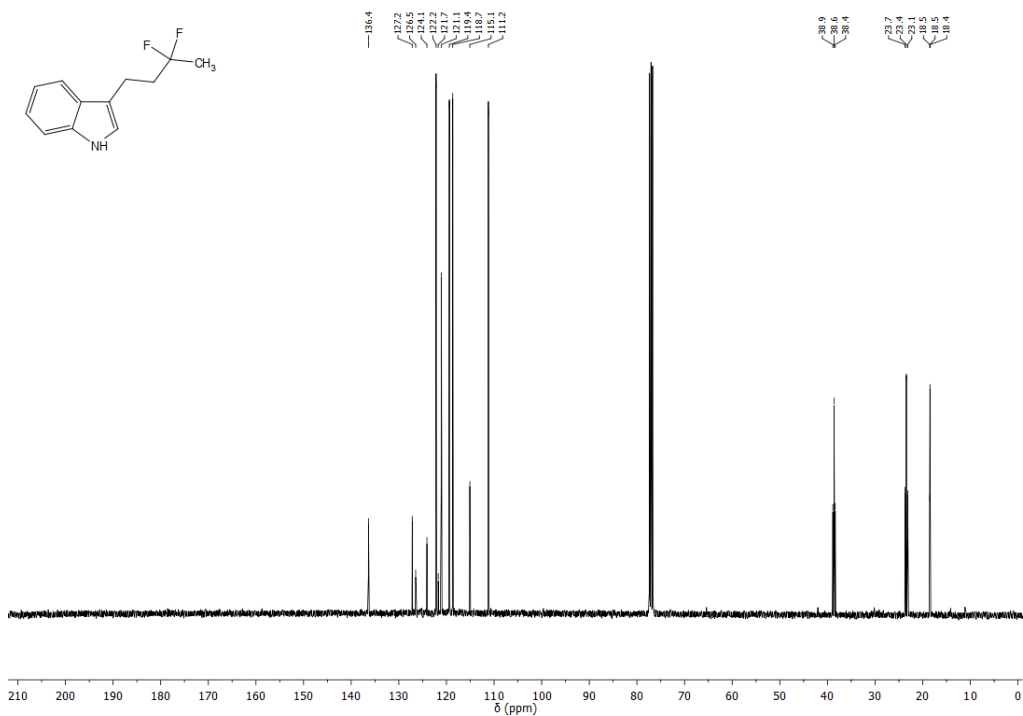


**Figure 155.** <sup>13</sup>C NMR (100 MHz) spectrum of **63** in CDCl<sub>3</sub> at 298 K.

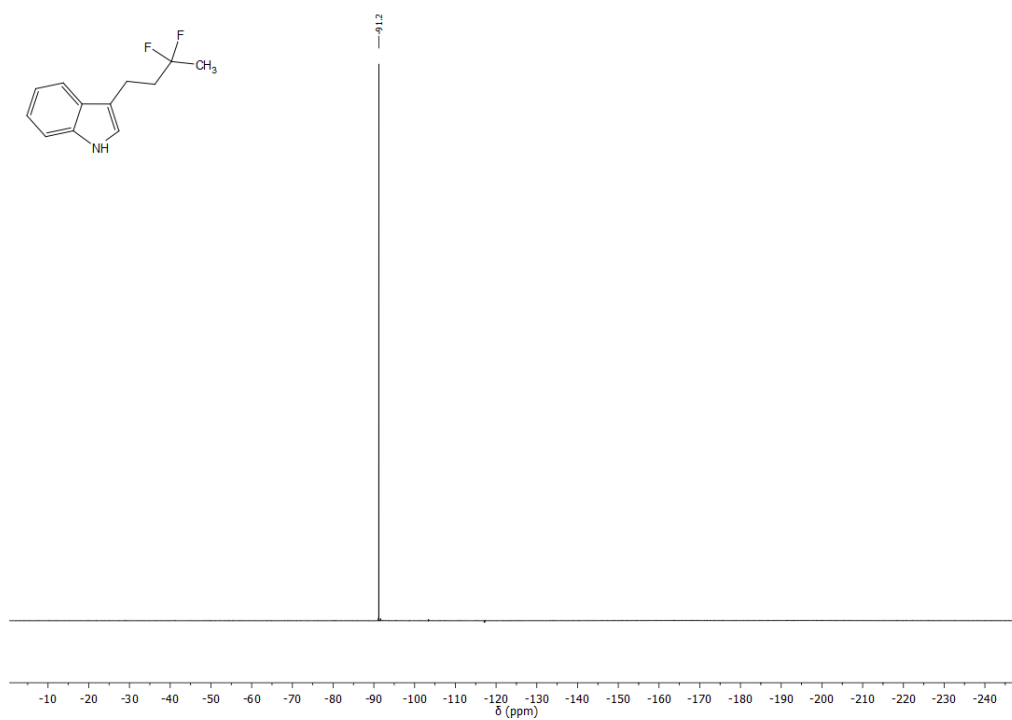


**Figure 156.**  $^{19}\text{F}$  NMR (376 MHz, decoupled) spectrum of **63** in  $\text{CDCl}_3$  at 298 K.

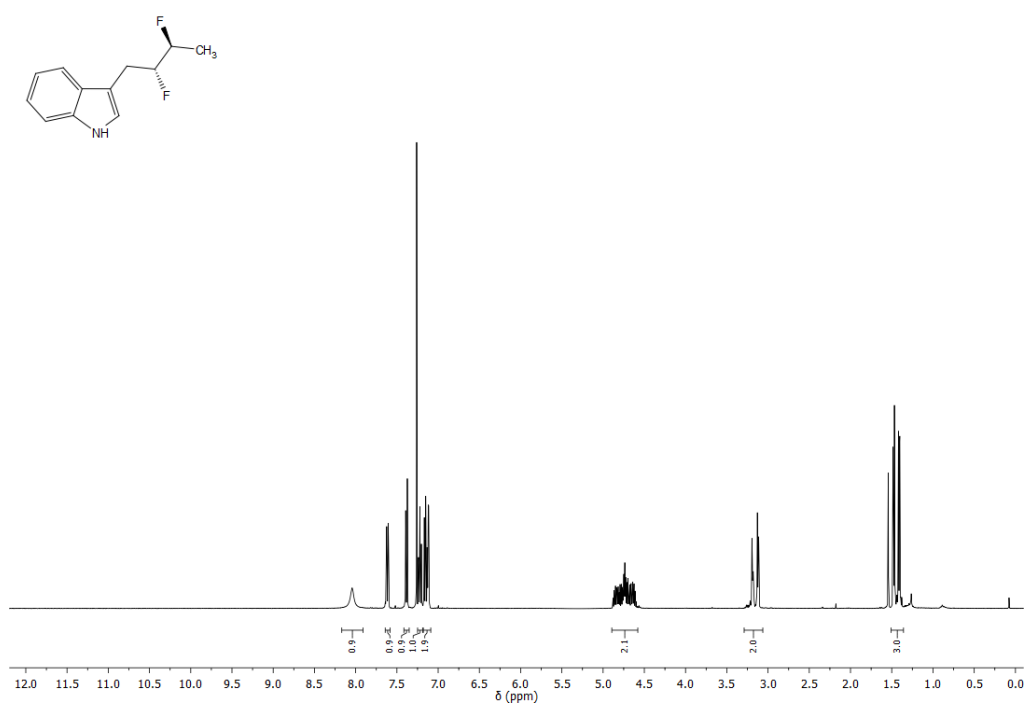


**Figure 157.**  $^1\text{H}$  NMR (400 MHz) spectrum of **66** in  $\text{CDCl}_3$  at 298 K.

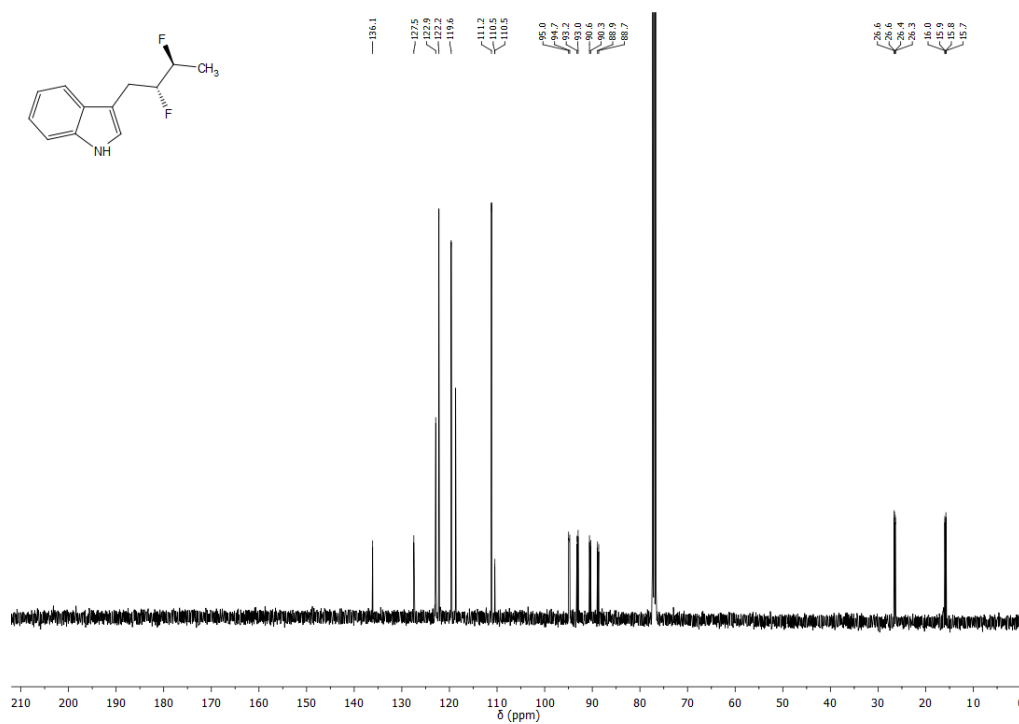


**Figure 158.** <sup>13</sup>C NMR (100 MHz) spectrum of **66** in CDCl<sub>3</sub> at 298 K.

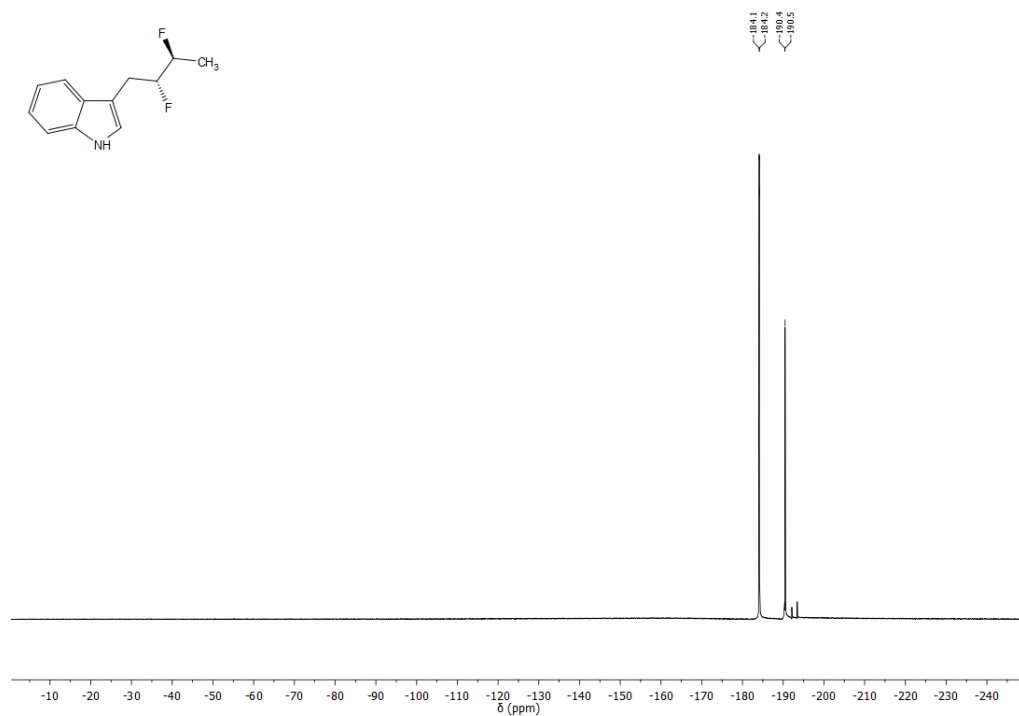


**Figure 159.** <sup>19</sup>F NMR (376 MHz, decoupled) spectrum of **66** in CDCl<sub>3</sub> at 298 K.

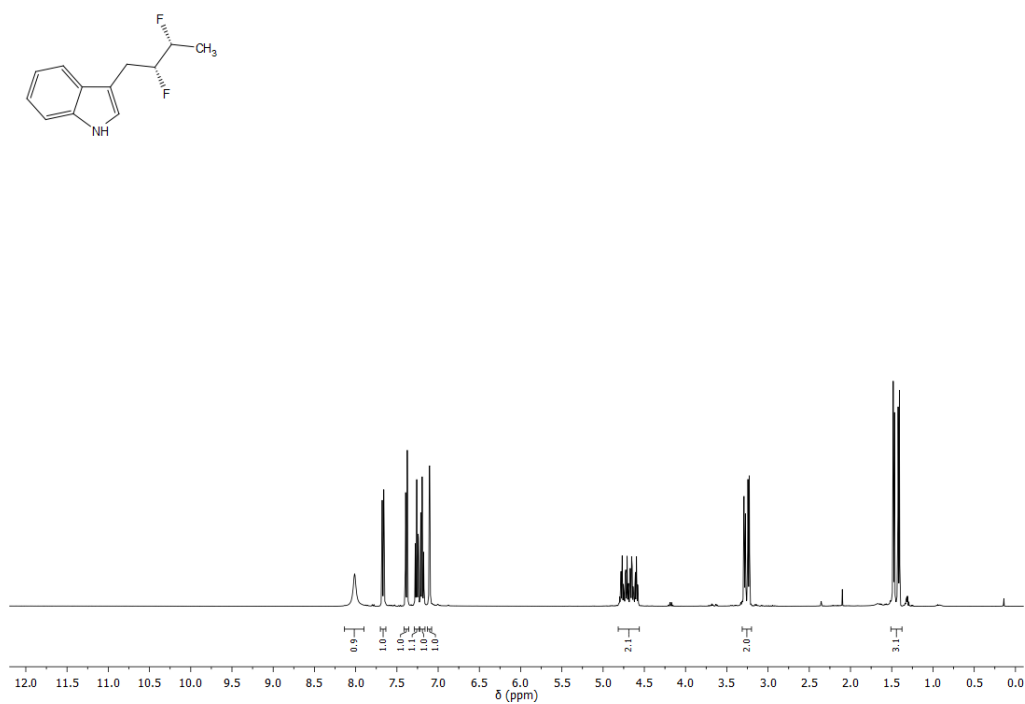


**Figure 160.** <sup>1</sup>H NMR (400 MHz) spectrum of **65** in CDCl<sub>3</sub> at 298 K.

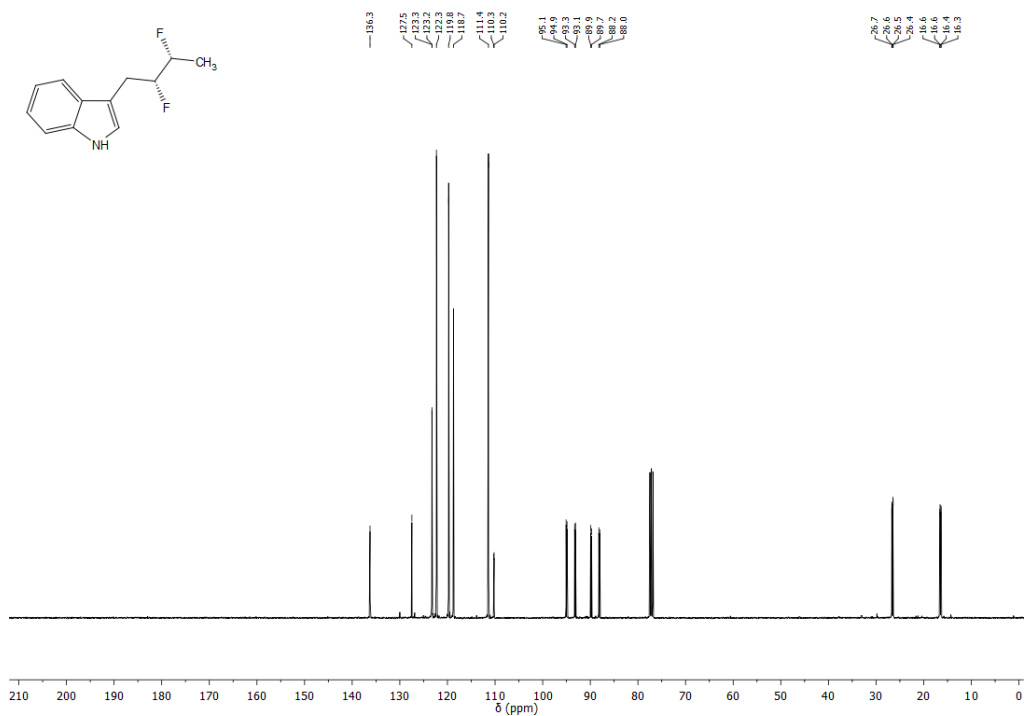


**Figure 161.** <sup>13</sup>C NMR (100 MHz) spectrum of **65** in CDCl<sub>3</sub> at 298 K.

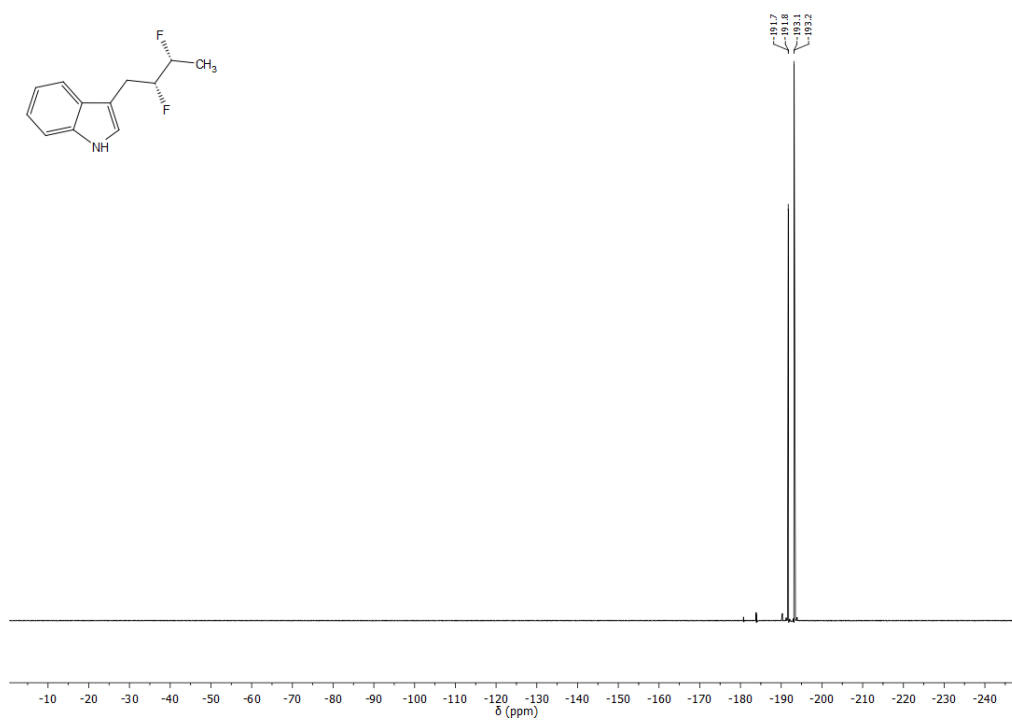


**Figure 162.**  $^{19}\text{F}$  NMR (376 MHz, decoupled) spectrum of **65** in  $\text{CDCl}_3$  at 298 K.

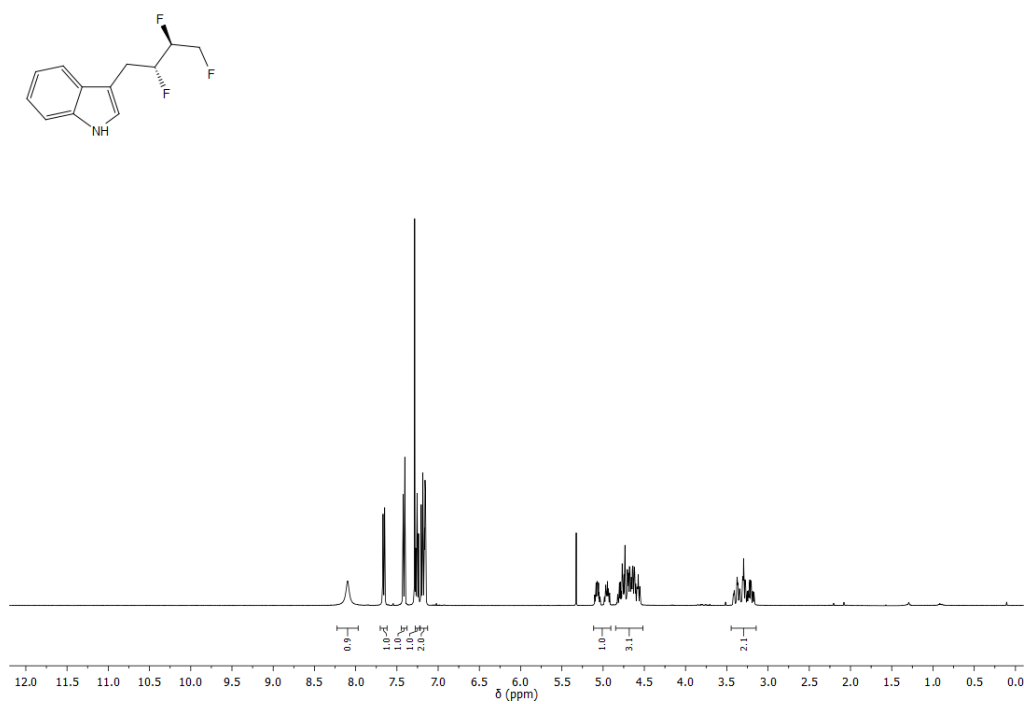


**Figure 163.**  $^1\text{H}$  NMR (400 MHz) spectrum of **68** in  $\text{CDCl}_3$  at 298 K.





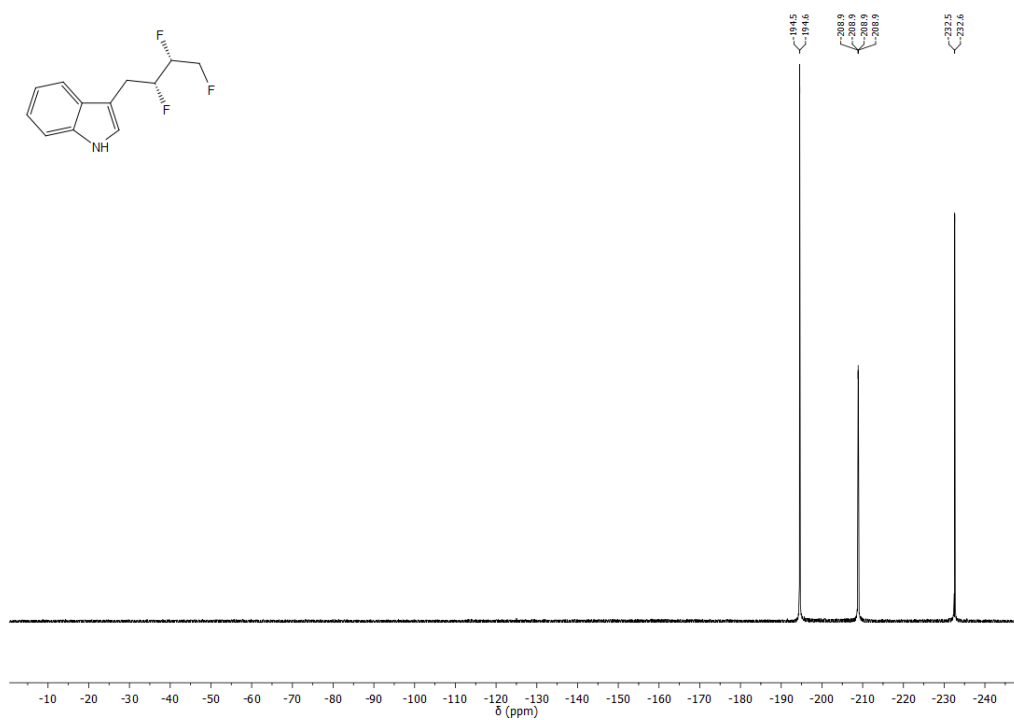


**Figure 168.**  $^{19}\text{F}$  NMR (376 MHz, decoupled) spectrum of **67** in  $\text{CDCl}_3$  at 298 K.

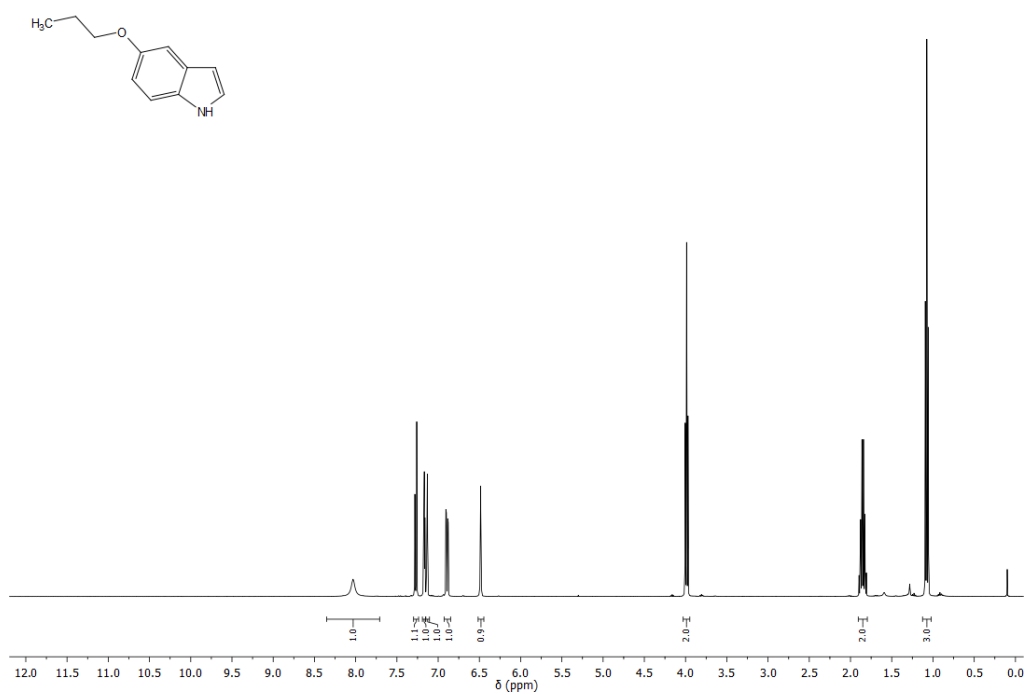


**Figure 169.**  $^1\text{H}$  NMR (400 MHz) spectrum of **130a** in  $\text{CDCl}_3$  at 298 K.



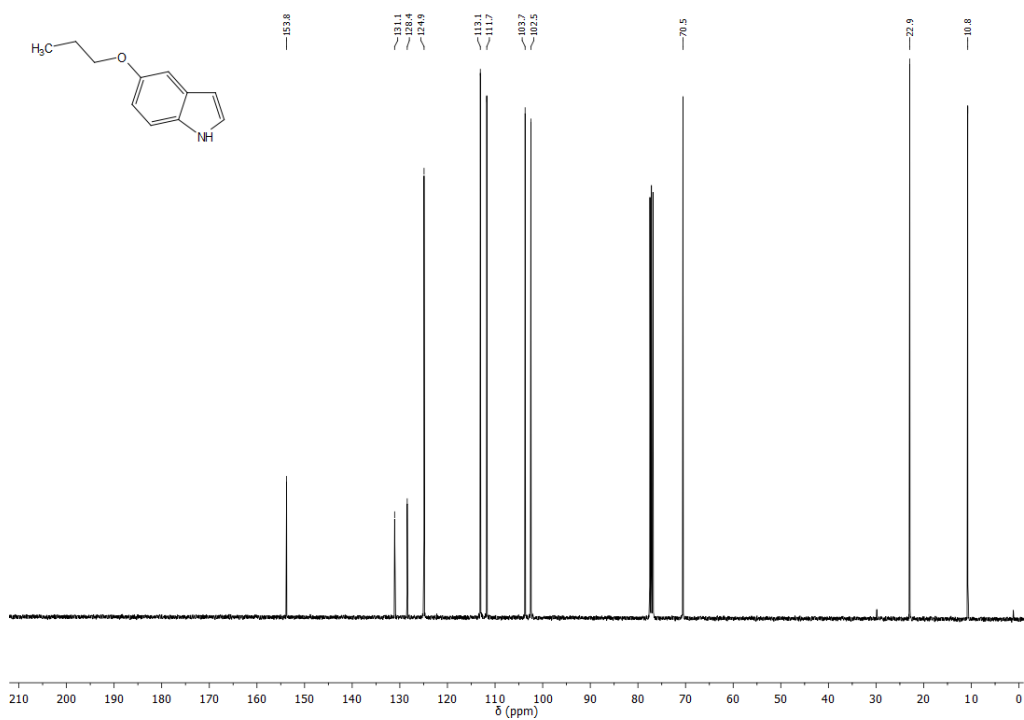


**Figure 170.** <sup>13</sup>C NMR (100 MHz) spectrum of **130a** in CDCl<sub>3</sub> at 298 K.

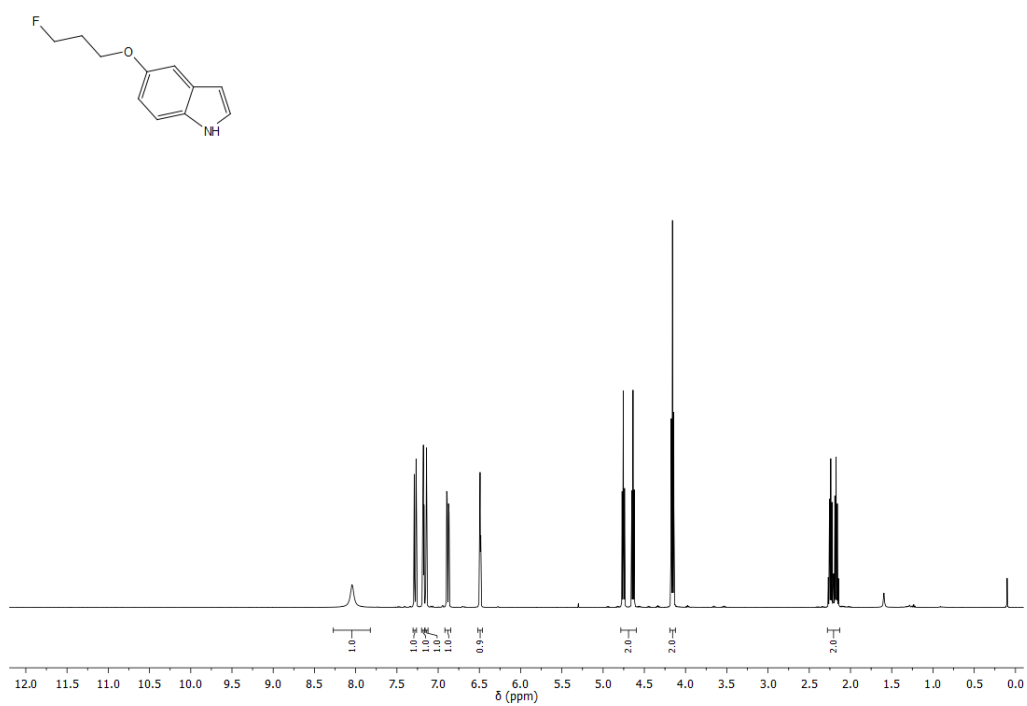


**Figure 171.** <sup>1</sup>H NMR (400 MHz) spectrum of **130b** in CDCl<sub>3</sub> at 298 K.

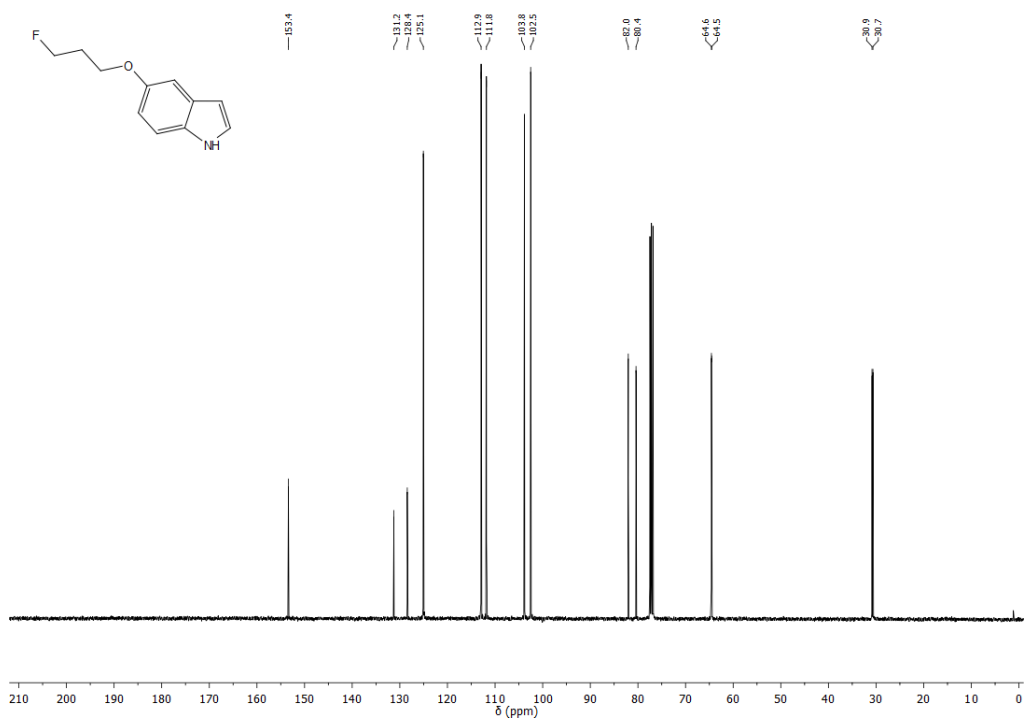


**Figure 172.**  $^{13}\text{C}$  NMR (100 MHz) spectrum of **130b** in  $\text{CDCl}_3$  at 298 K.

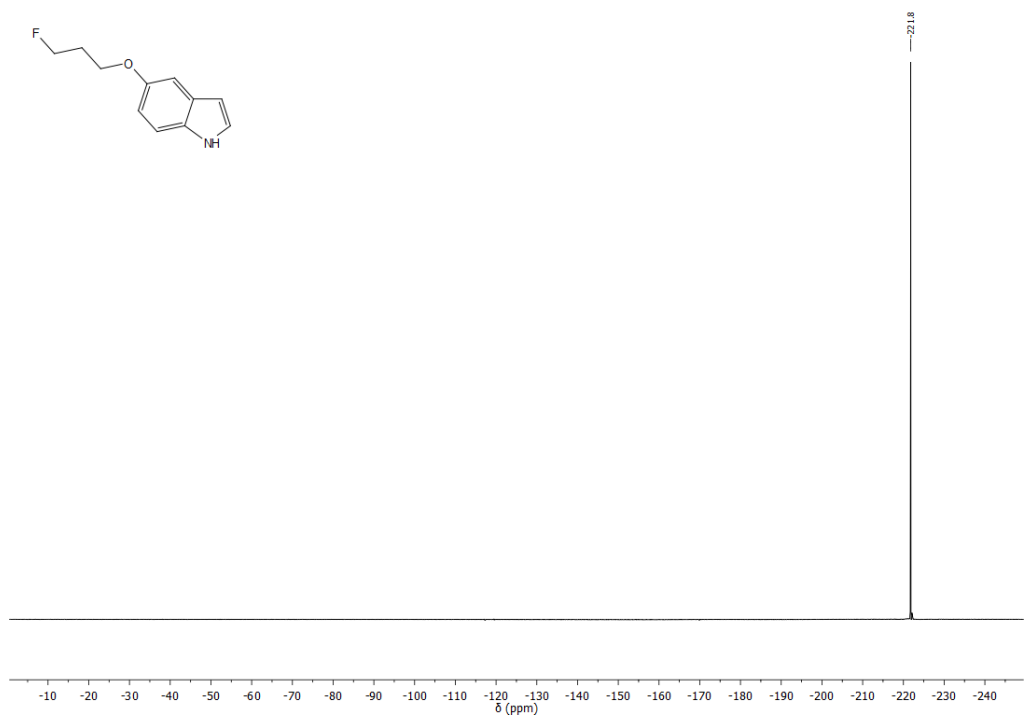


**Figure 173.**  $^{19}\text{F}$  NMR (376 MHz, decoupled) spectrum of **130b** in  $\text{CDCl}_3$  at 298 K.

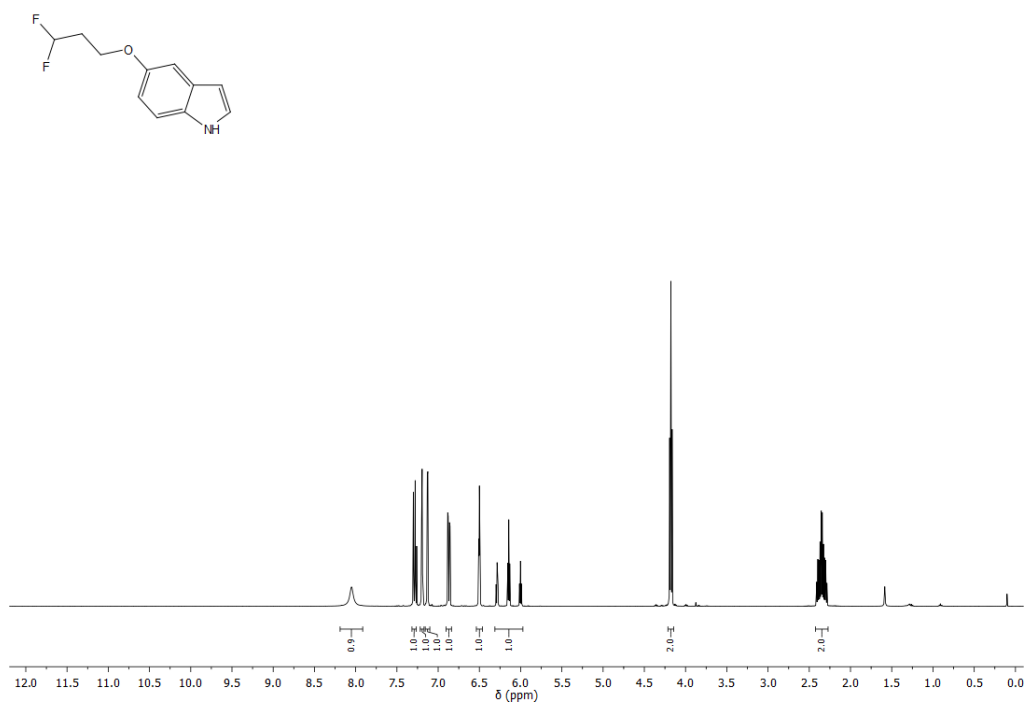


**Figure 174.** <sup>1</sup>H NMR (400 MHz) spectrum of **130c** in CDCl<sub>3</sub> at 298 K.

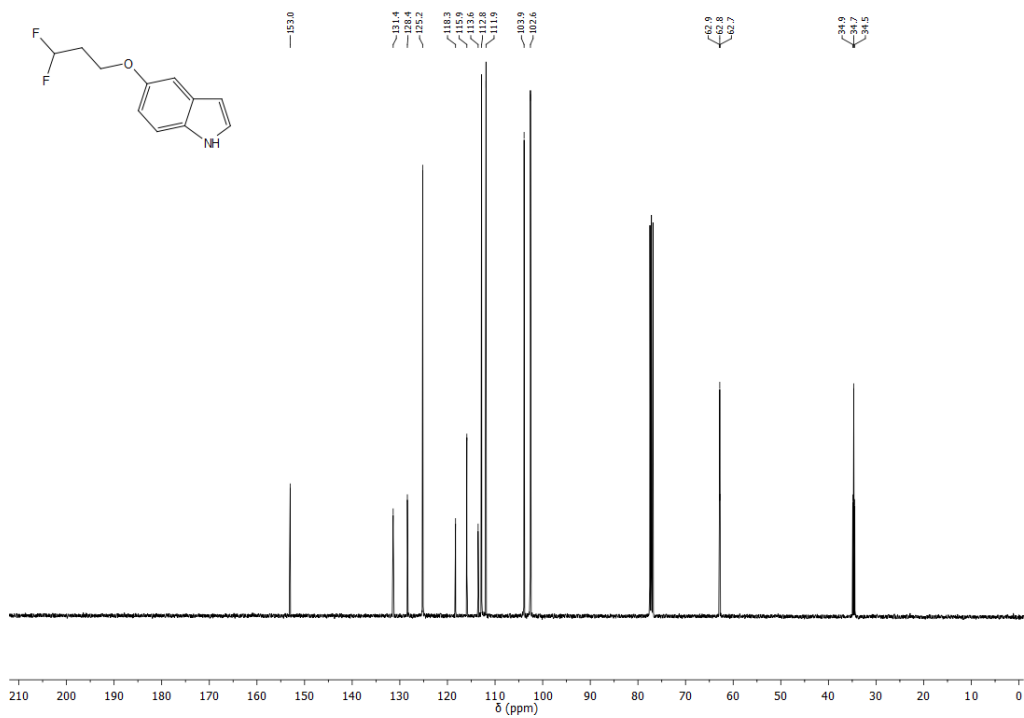


**Figure 175.** <sup>13</sup>C NMR (100 MHz) spectrum of **130c** in CDCl<sub>3</sub> at 298 K.

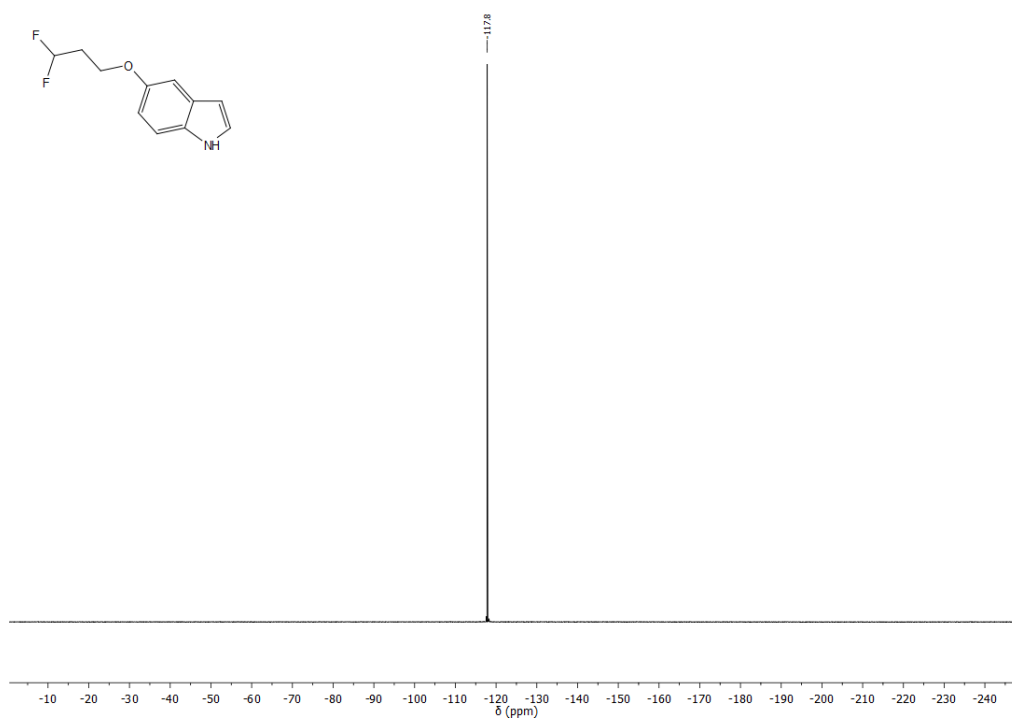


**Figure 176.**  $^{19}\text{F}$  NMR (376 MHz, decoupled) spectrum of **130c** in  $\text{CDCl}_3$  at 298 K.

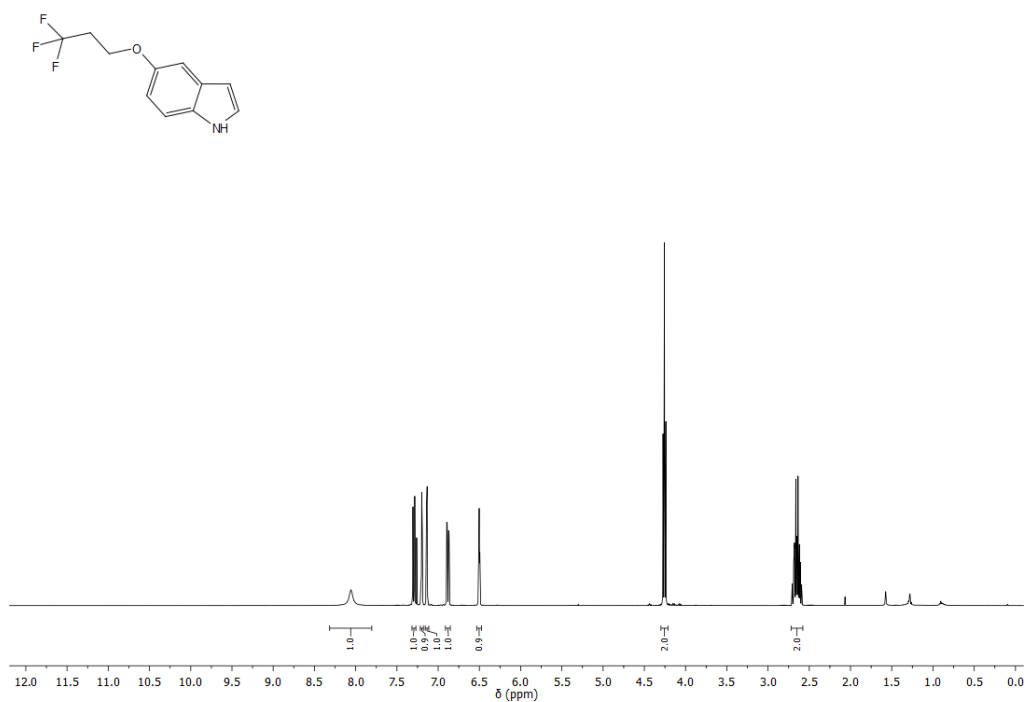


**Figure 177.**  $^1\text{H}$  NMR (400 MHz) spectrum of **130d** in  $\text{CDCl}_3$  at 298 K.

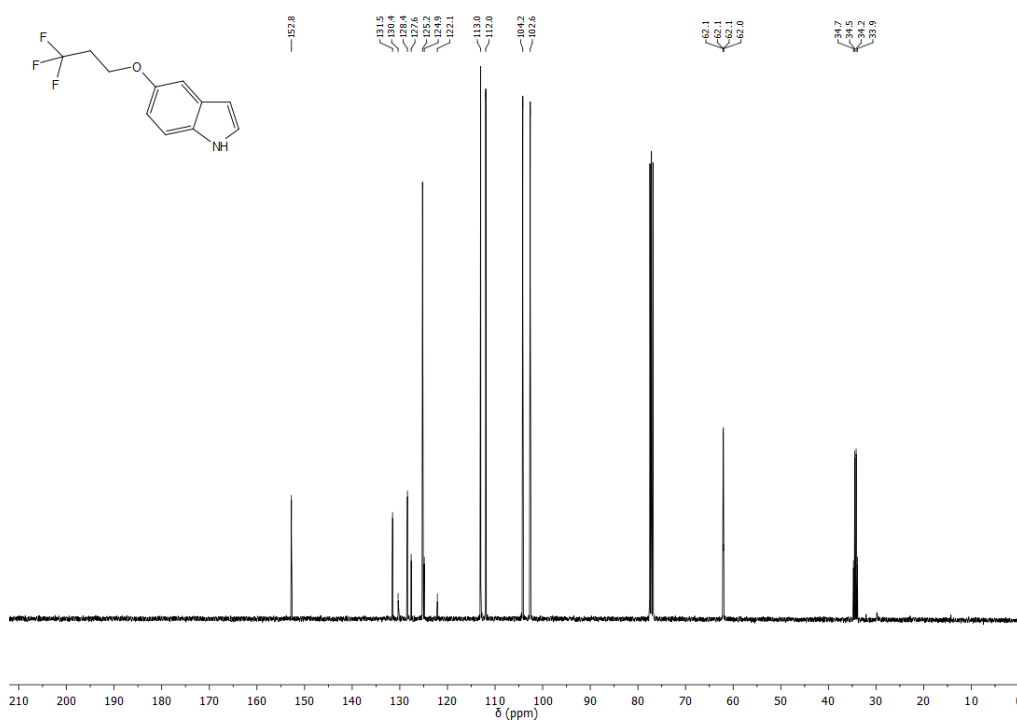


**Figure 178.** <sup>13</sup>C NMR (100 MHz) spectrum of **130d** in CDCl<sub>3</sub> at 298 K.

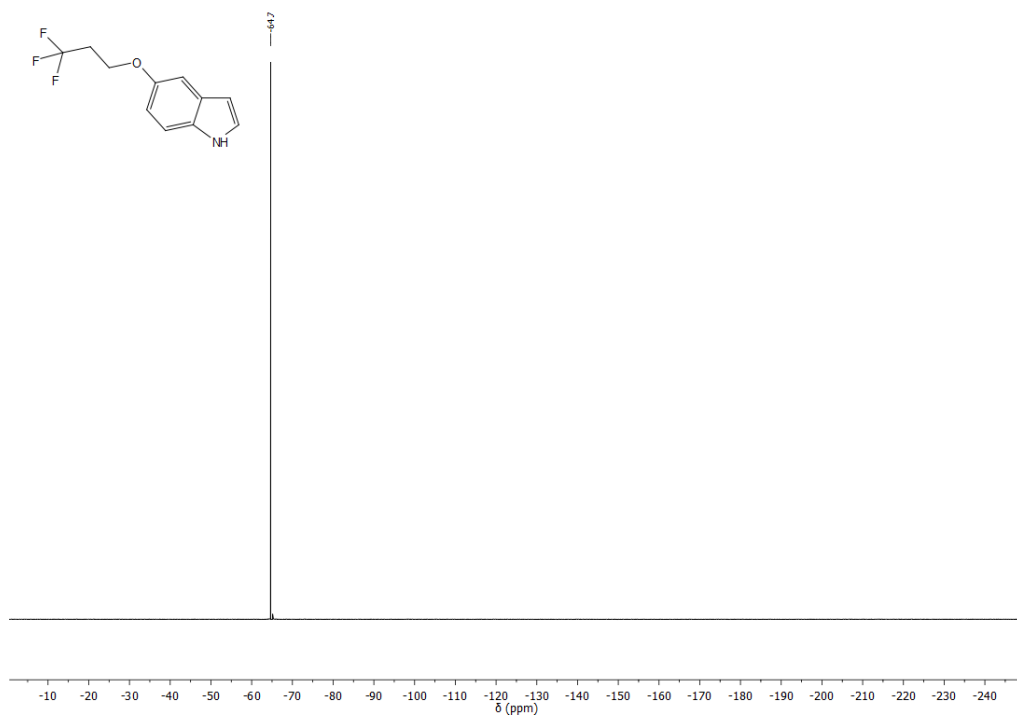


**Figure 179.** <sup>19</sup>F NMR (376 MHz, decoupled) spectrum of **130d** in CDCl<sub>3</sub> at 298 K.

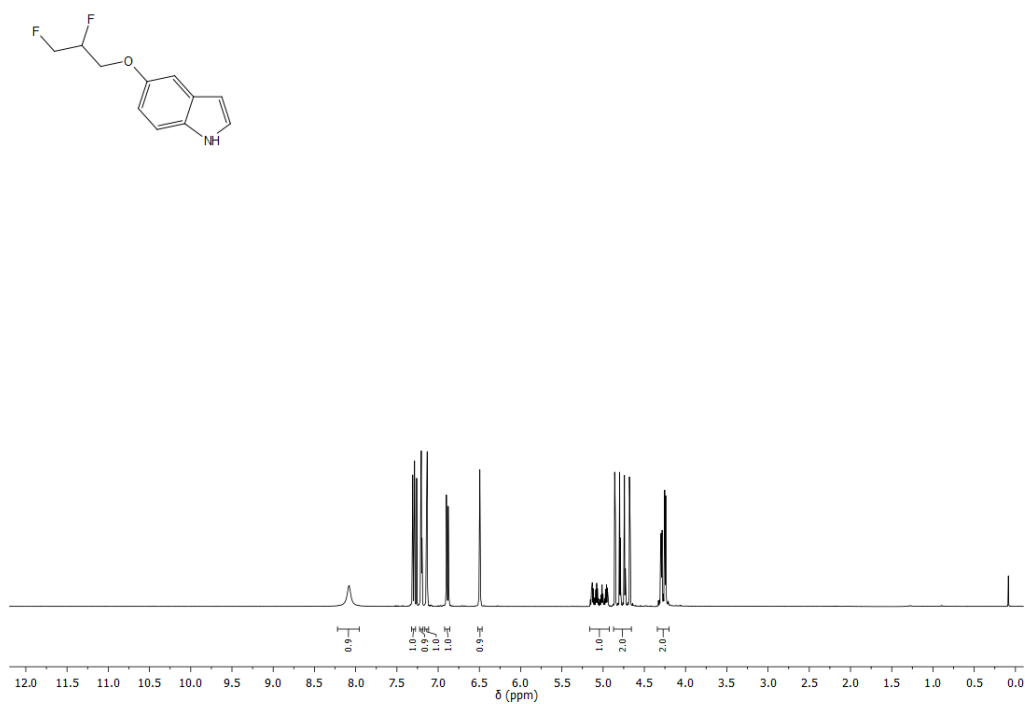


**Figure 180.** <sup>1</sup>H NMR (400 MHz) spectrum of **131** in CDCl<sub>3</sub> at 298 K.

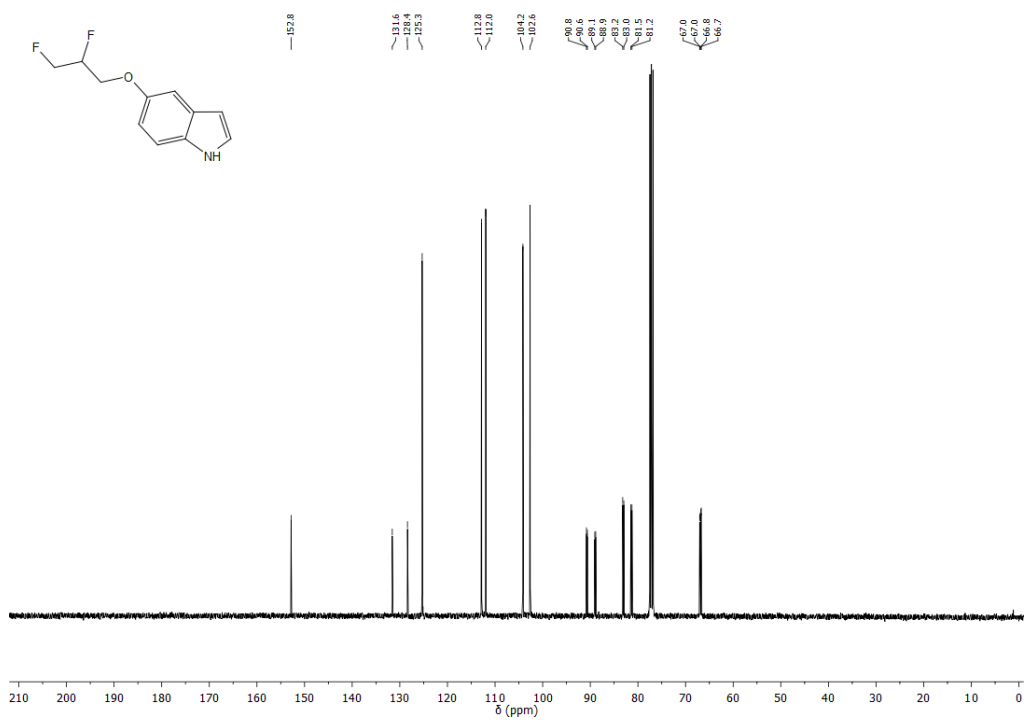


**Figure 181.** <sup>13</sup>C NMR (100 MHz) spectrum of **131** in CDCl<sub>3</sub> at 298 K.

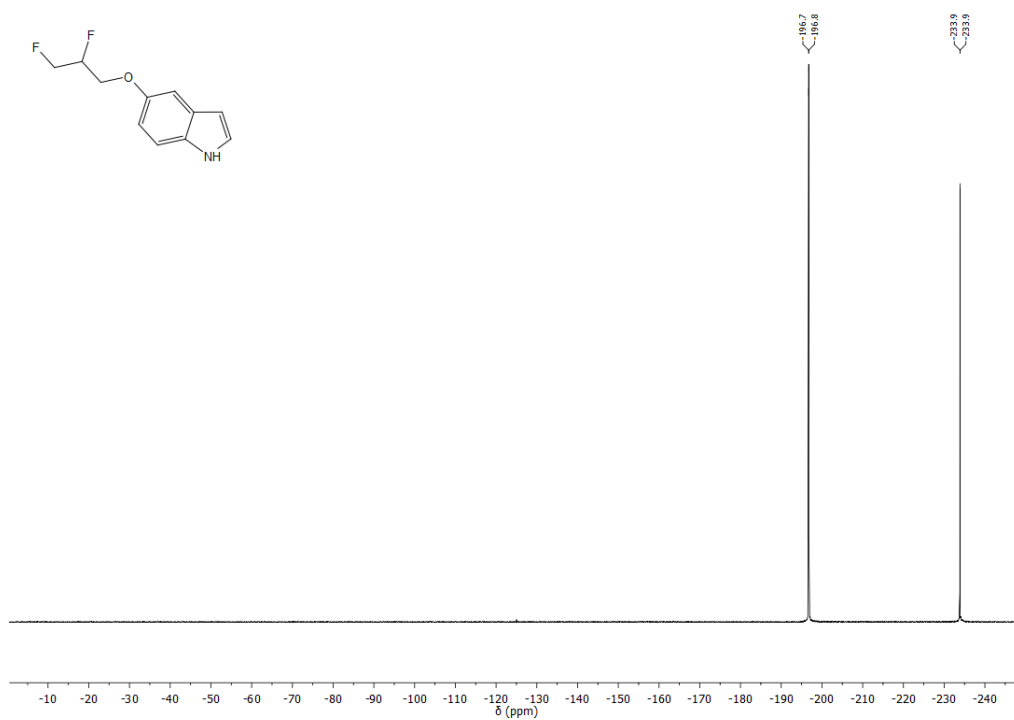


**Figure 182.** <sup>19</sup>F NMR (376 MHz, decoupled) spectrum of **131** in CDCl<sub>3</sub> at 298 K.

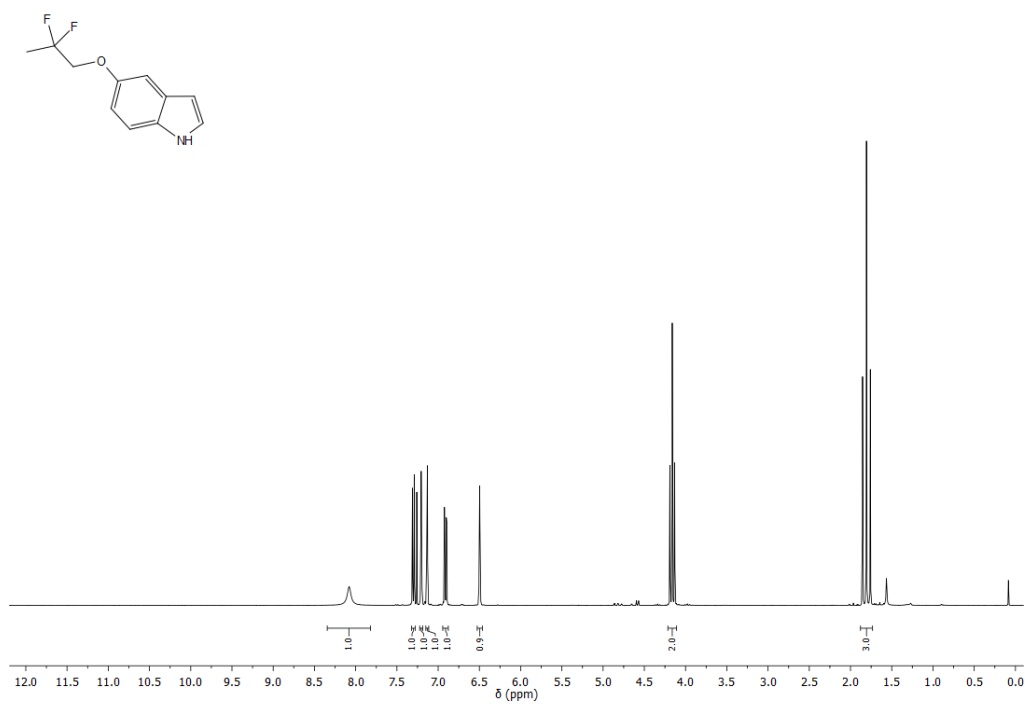


**Figure 183.** <sup>1</sup>H NMR (400 MHz) spectrum of **132** in CDCl<sub>3</sub> at 298 K.

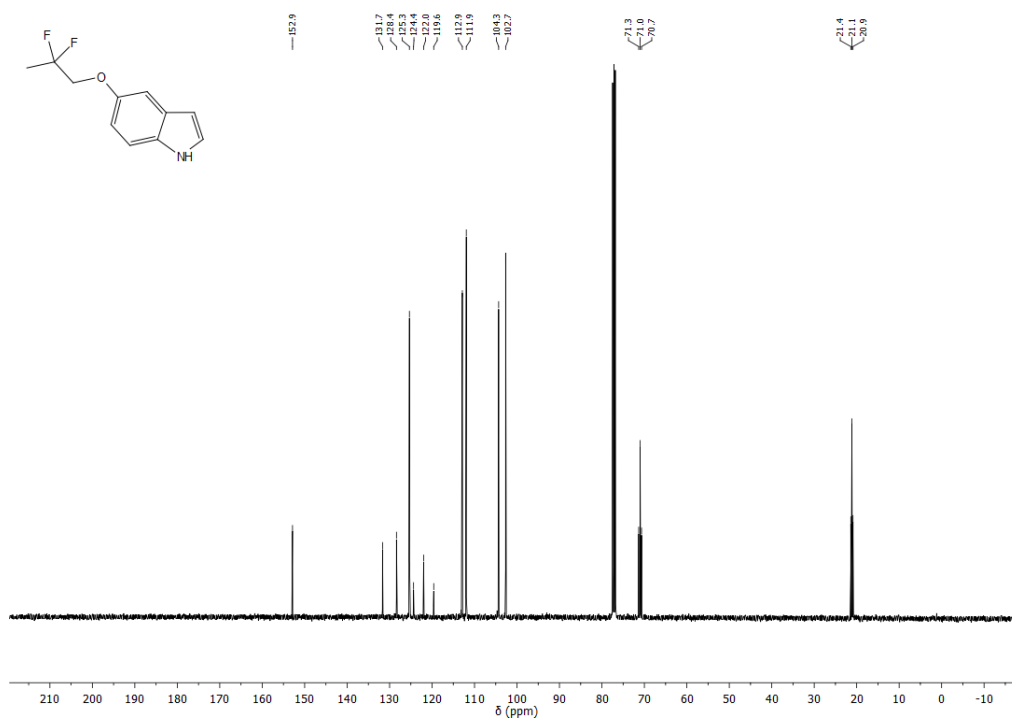


**Figure 184.** <sup>13</sup>C NMR (100 MHz) spectrum of **132** in CDCl<sub>3</sub> at 298 K.

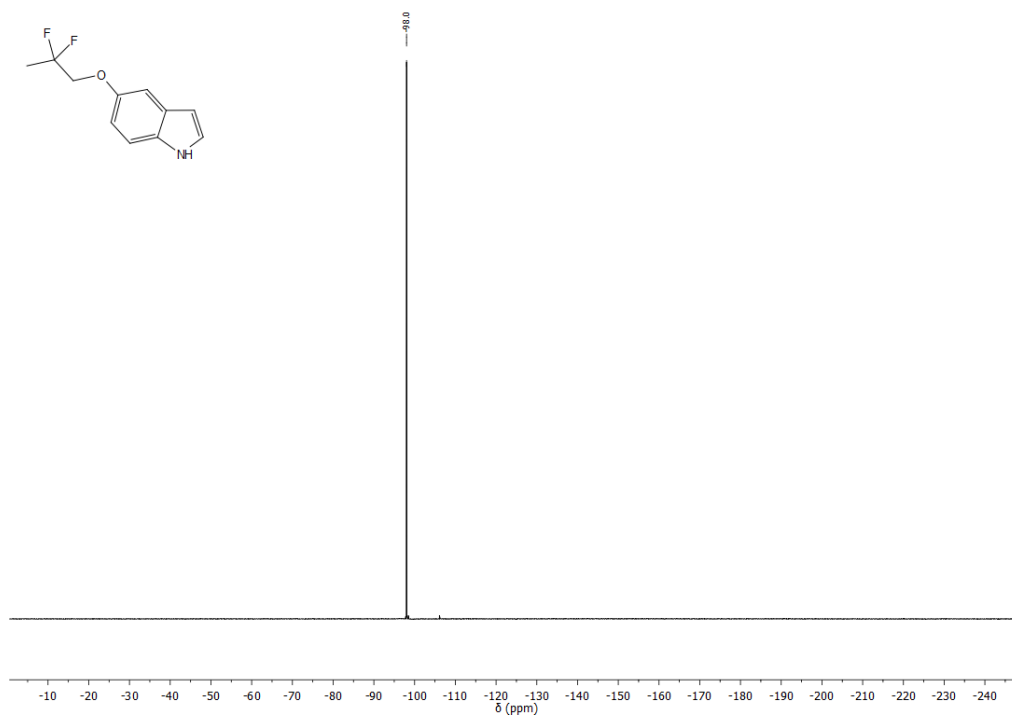


**Figure 185.** <sup>19</sup>F NMR (376 MHz, decoupled) spectrum of **132** in CDCl<sub>3</sub> at 298 K.



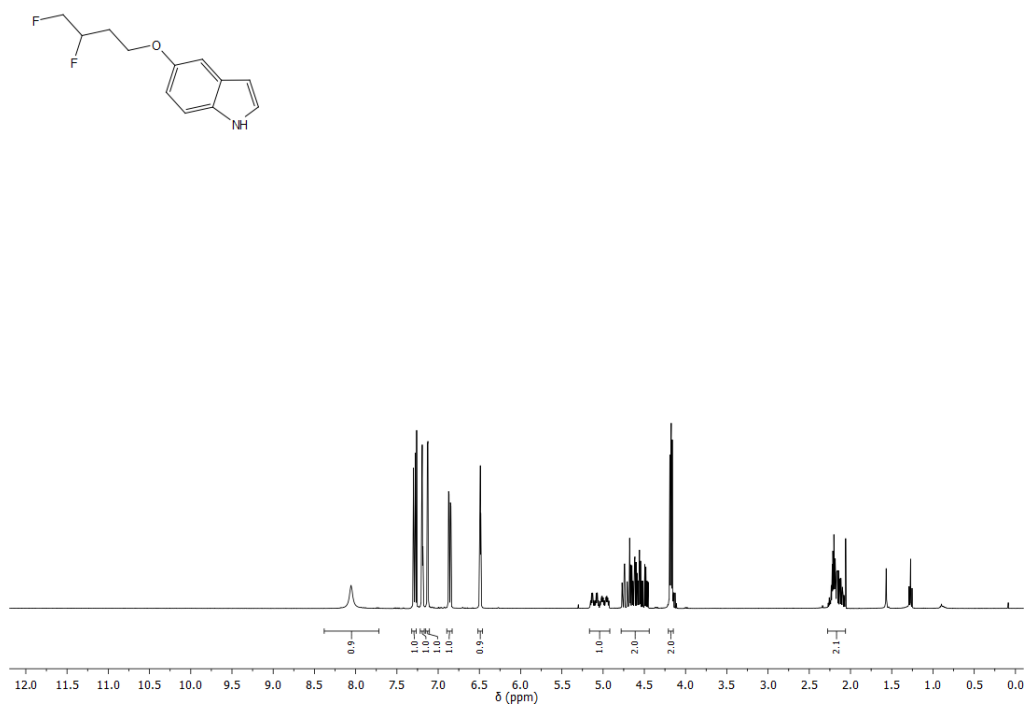


Figure 186.  $^1\text{H}$  NMR (400 MHz) spectrum of **133** in  $\text{CDCl}_3$  at 298 K.

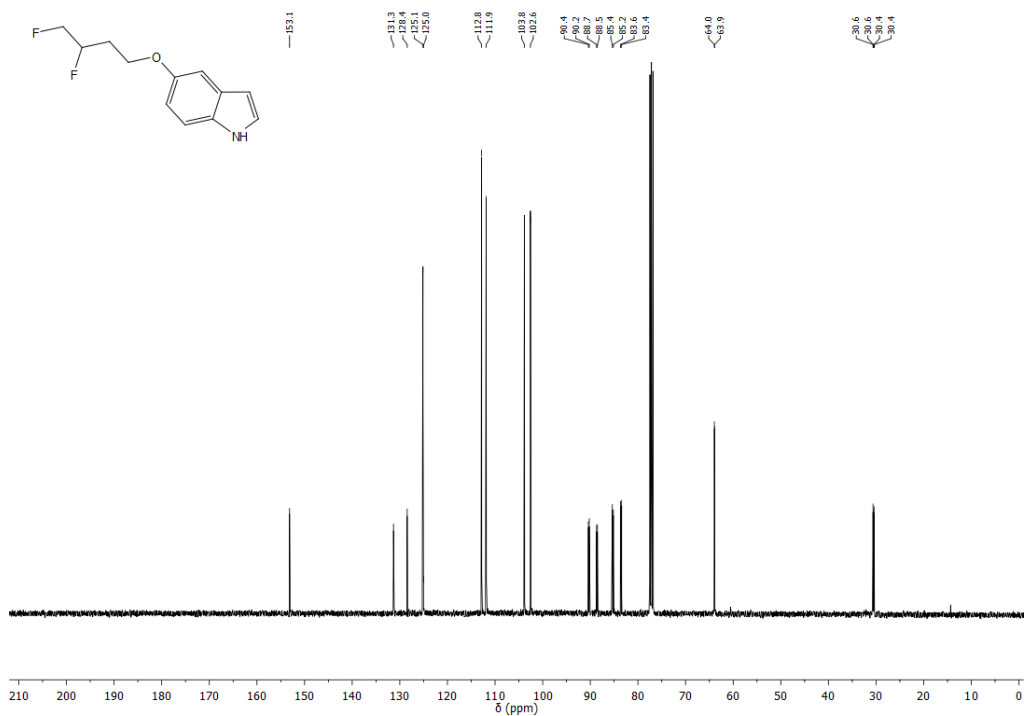
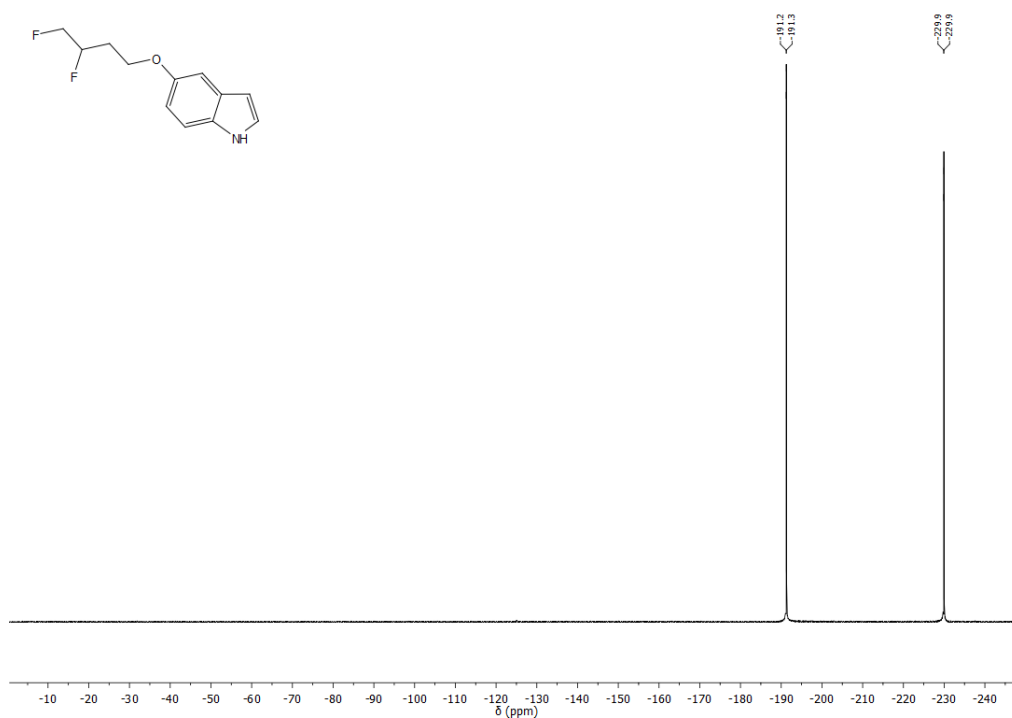
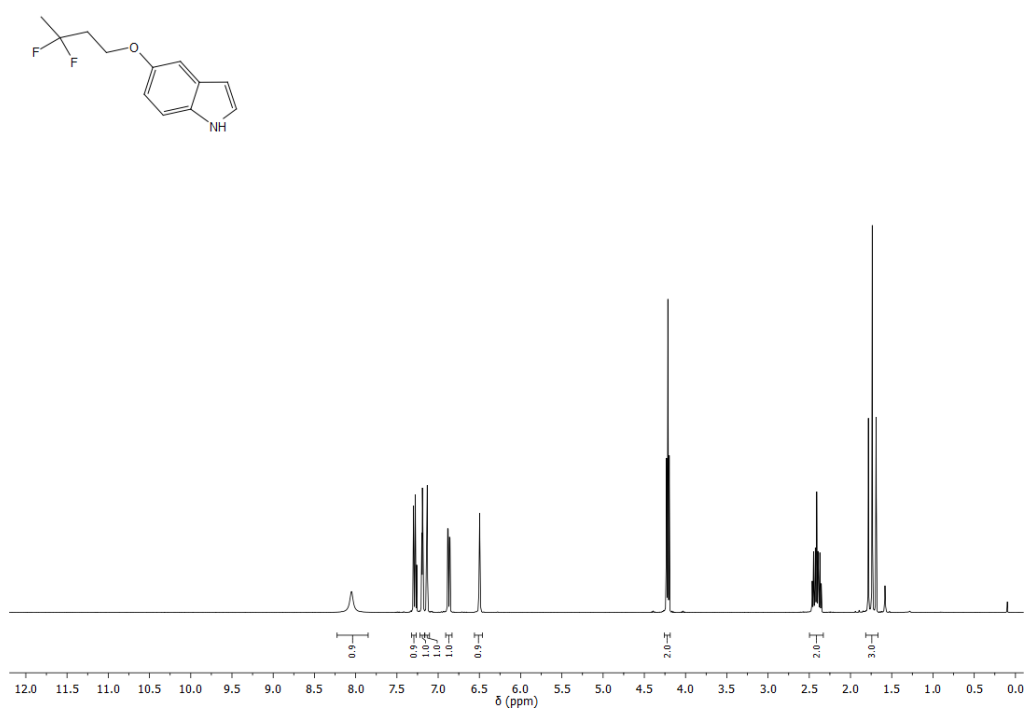


Figure 187.  $^{13}\text{C}$  NMR (100 MHz) spectrum of **133** in  $\text{CDCl}_3$  at 298 K.



**Figure 188.**  $^{19}\text{F}$  NMR (376 MHz, decoupled) spectrum of **133** in  $\text{CDCl}_3$  at 298 K.



**Figure 189.**  $^1\text{H}$  NMR (400 MHz) spectrum of **134** in  $\text{CDCl}_3$  at 298 K.

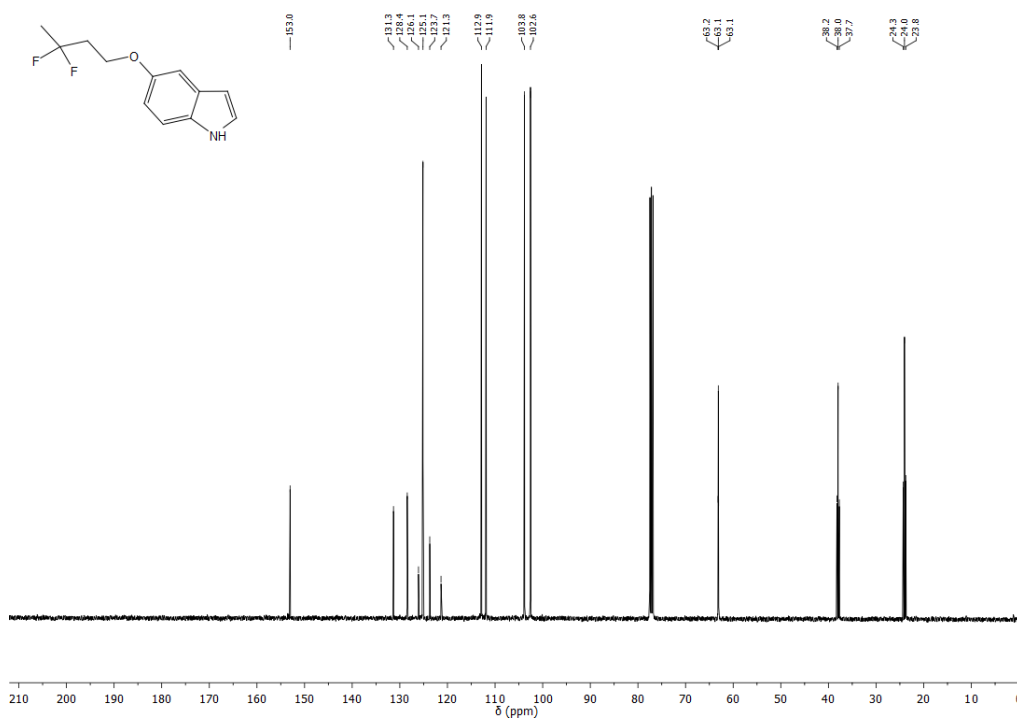


**Figure 190.**  $^{13}\text{C}$  NMR (100 MHz) spectrum of **134** in  $\text{CDCl}_3$  at 298 K.



**Figure 191.**  $^{19}\text{F}$  NMR (376 MHz, decoupled) spectrum of **134** in  $\text{CDCl}_3$  at 298 K.

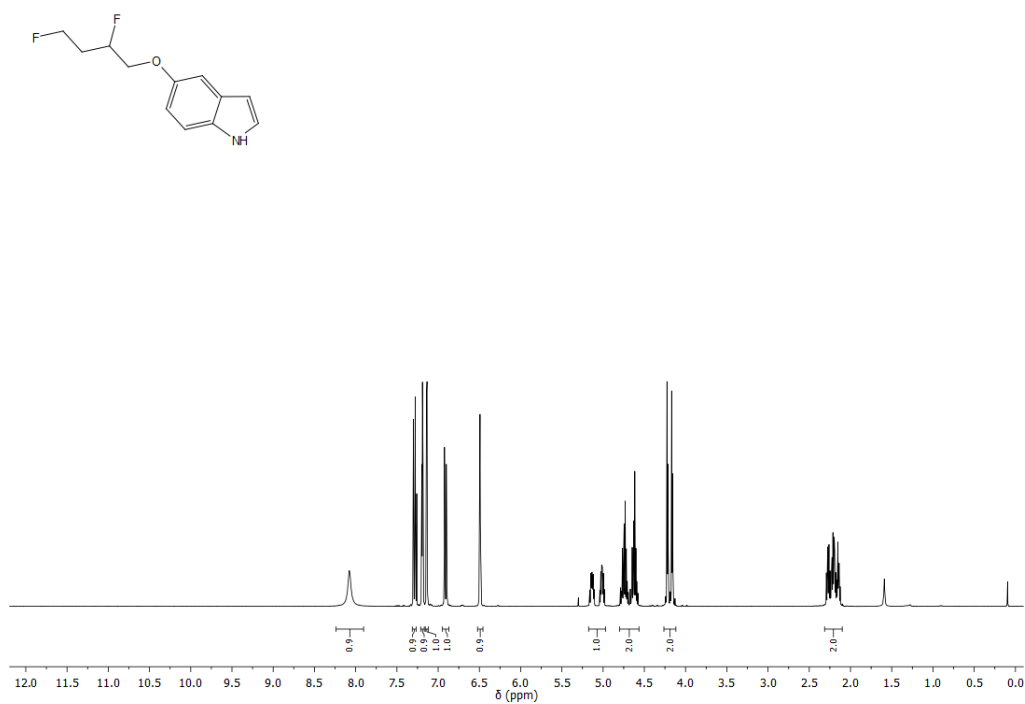


**Figure 192.** <sup>1</sup>H NMR (400 MHz) spectrum of **137** in CDCl<sub>3</sub> at 298 K.

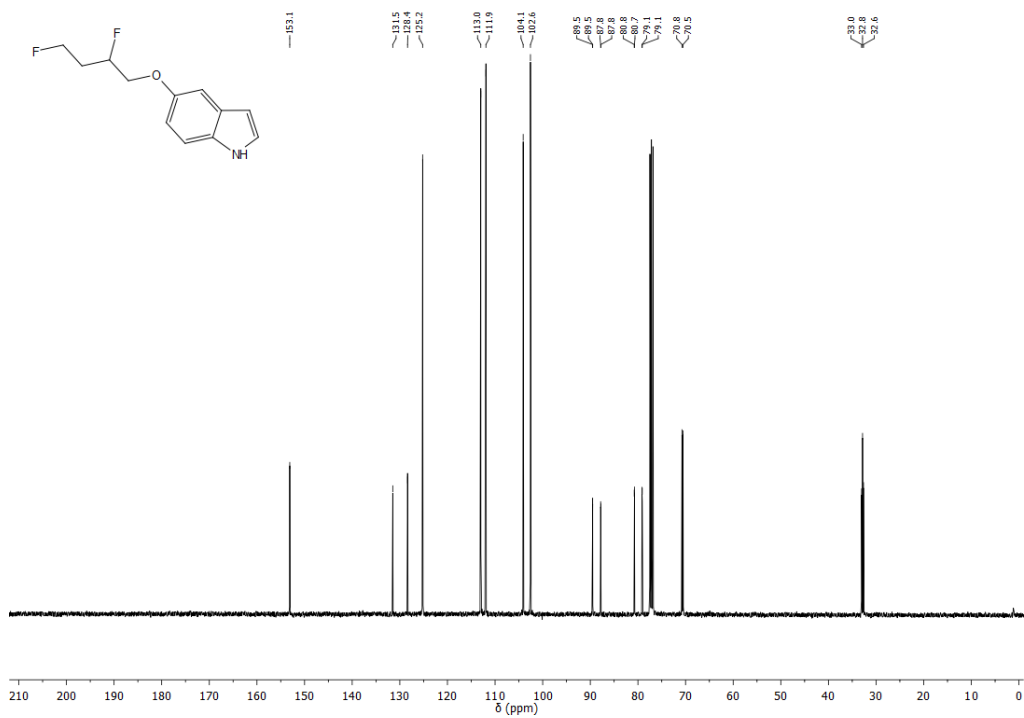


**Figure 193.** <sup>13</sup>C NMR (100 MHz) spectrum of **137** in CDCl<sub>3</sub> at 298 K.

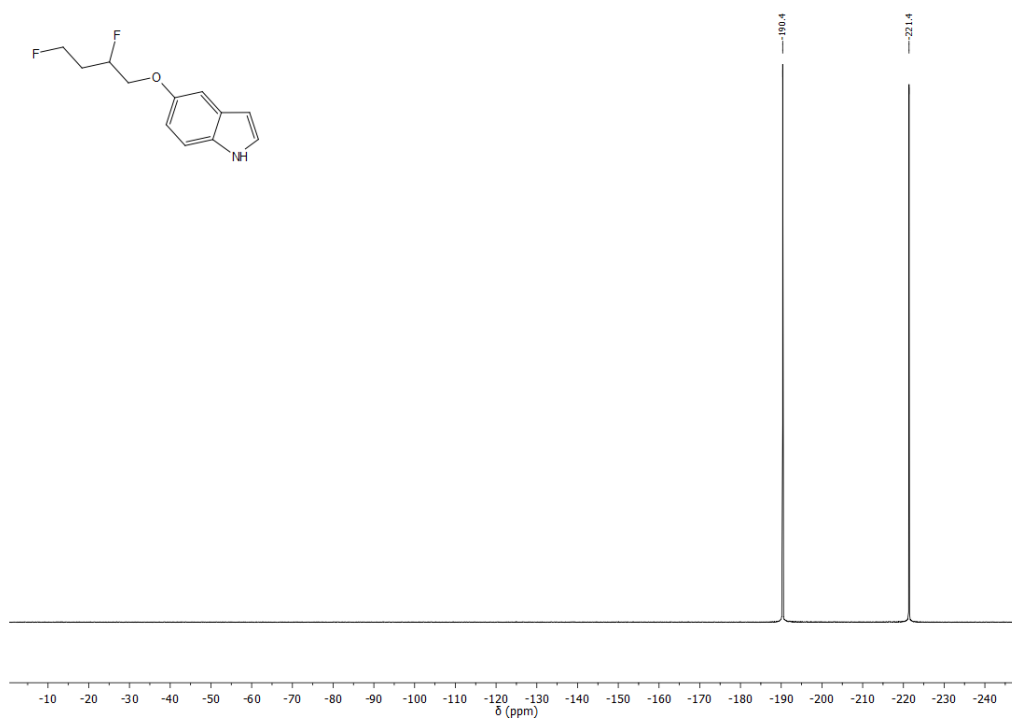


**Figure 194.**  $^{19}\text{F}$  NMR (376 MHz, decoupled) spectrum of **137** in  $\text{CDCl}_3$  at 298 K.

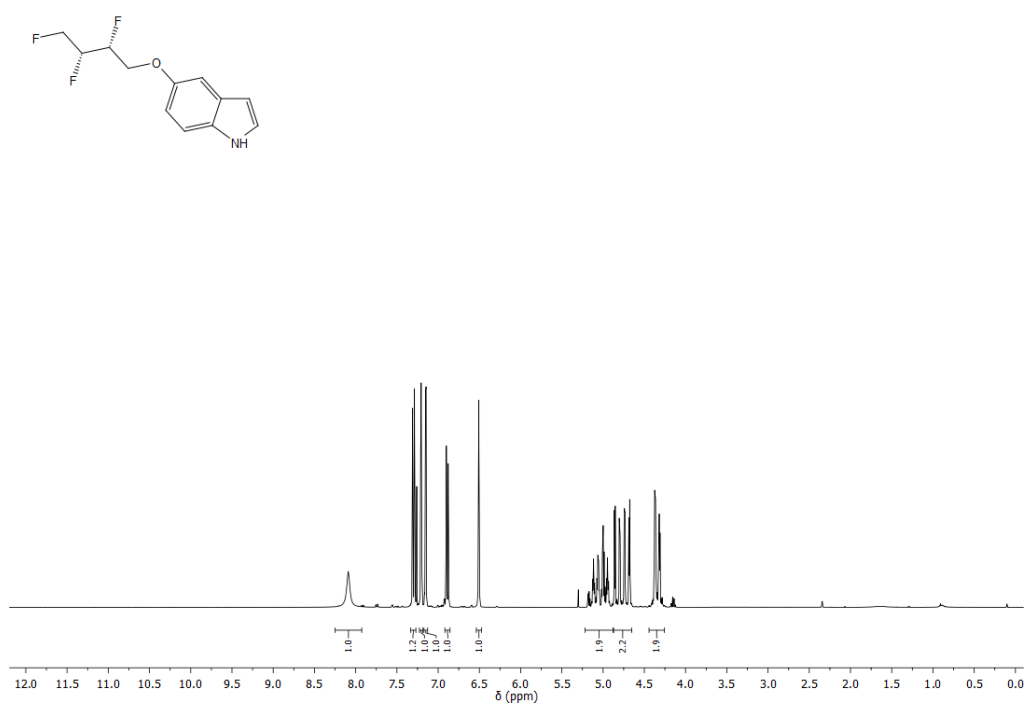


**Figure 195.**  $^1\text{H}$  NMR (400 MHz) spectrum of **135** in  $\text{CDCl}_3$  at 298 K.

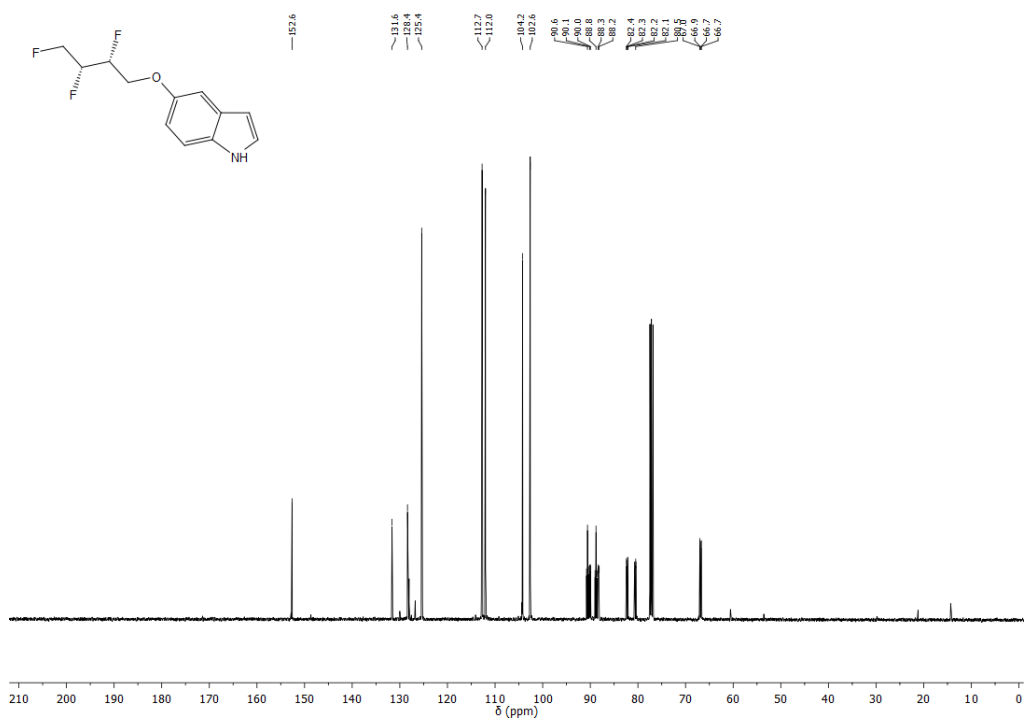


**Figure 196.** <sup>13</sup>C NMR (100 MHz) spectrum of **135** in CDCl<sub>3</sub> at 298 K.

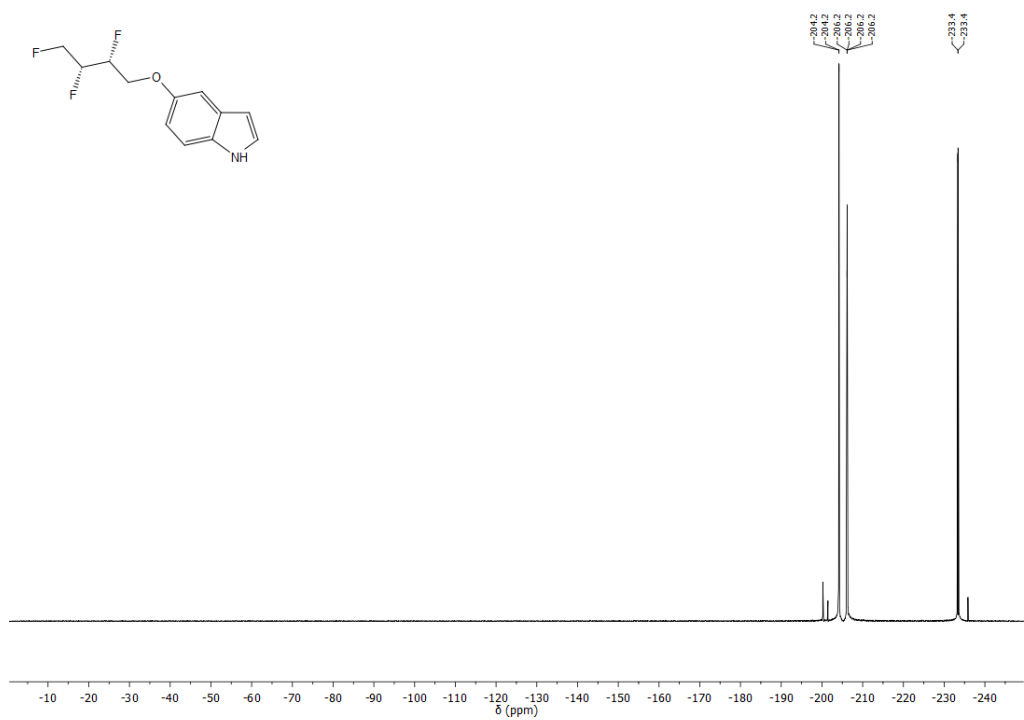


**Figure 197.** <sup>19</sup>F NMR (376 MHz, decoupled) spectrum of **135** in CDCl<sub>3</sub> at 298 K.

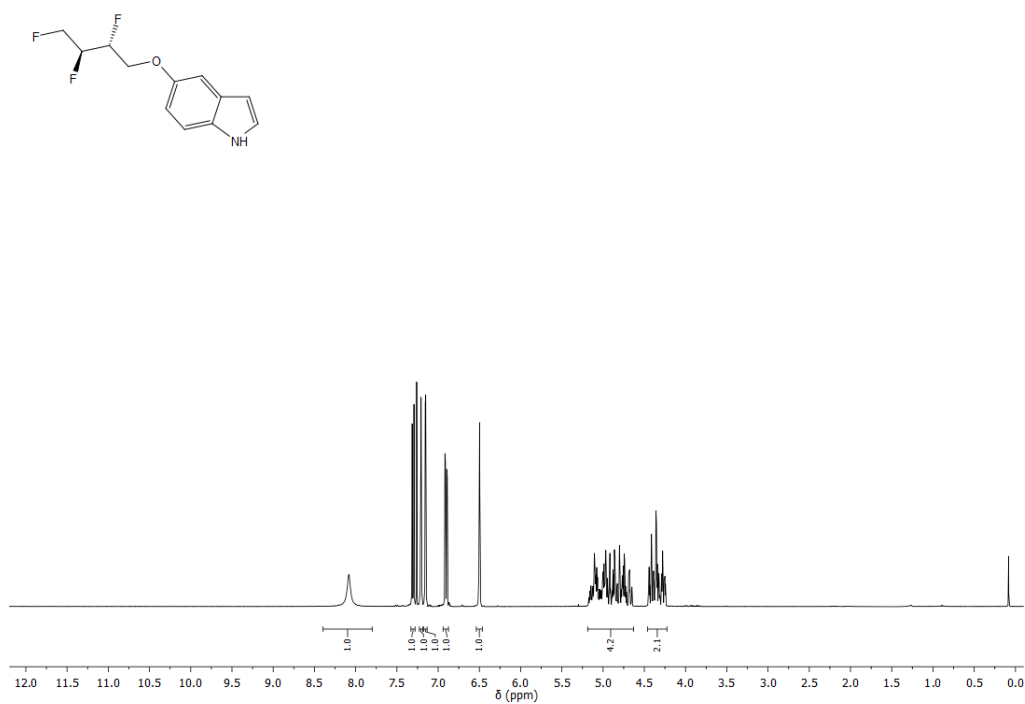


**Figure 198.** <sup>1</sup>H NMR (400 MHz) spectrum of **136** in CDCl<sub>3</sub> at 298 K.

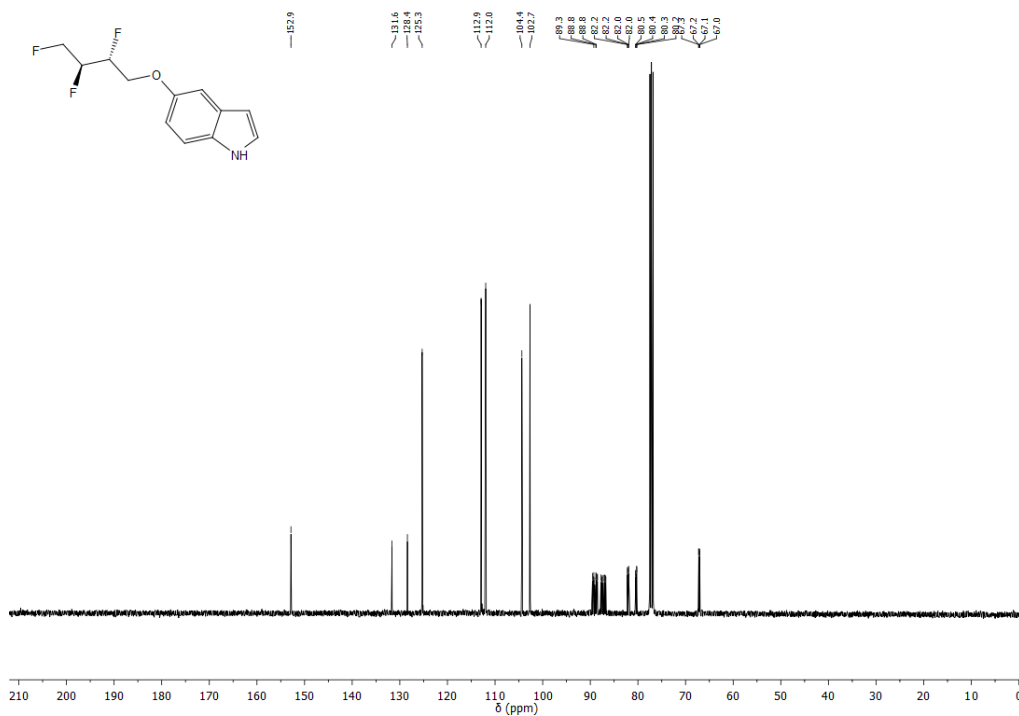


**Figure 199.** <sup>13</sup>C NMR (100 MHz) spectrum of **136** in CDCl<sub>3</sub> at 298 K.

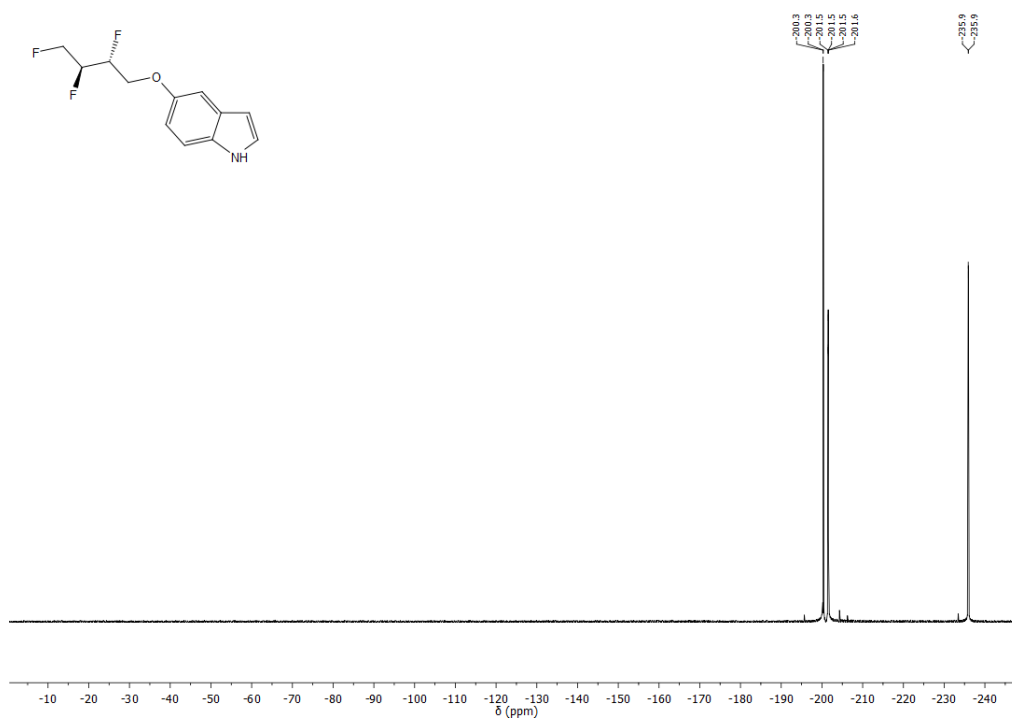


**Figure 200.**  $^{19}\text{F}$  NMR (376 MHz, decoupled) spectrum of **136** in  $\text{CDCl}_3$  at 298 K.



- **X-ray Crystallographic Data**

**General Methods**

Crystals were obtained by slow evaporation from a CH<sub>2</sub>Cl<sub>2</sub>/*n*-hexane mixture at rt. Structures were solved by direct methods and refined by full-matrix least-squares analysis using the OLEX2<sup>138</sup> and Bruker SHELXTL<sup>139</sup> Software Package.

## X-ray Crystal Structure of 25a

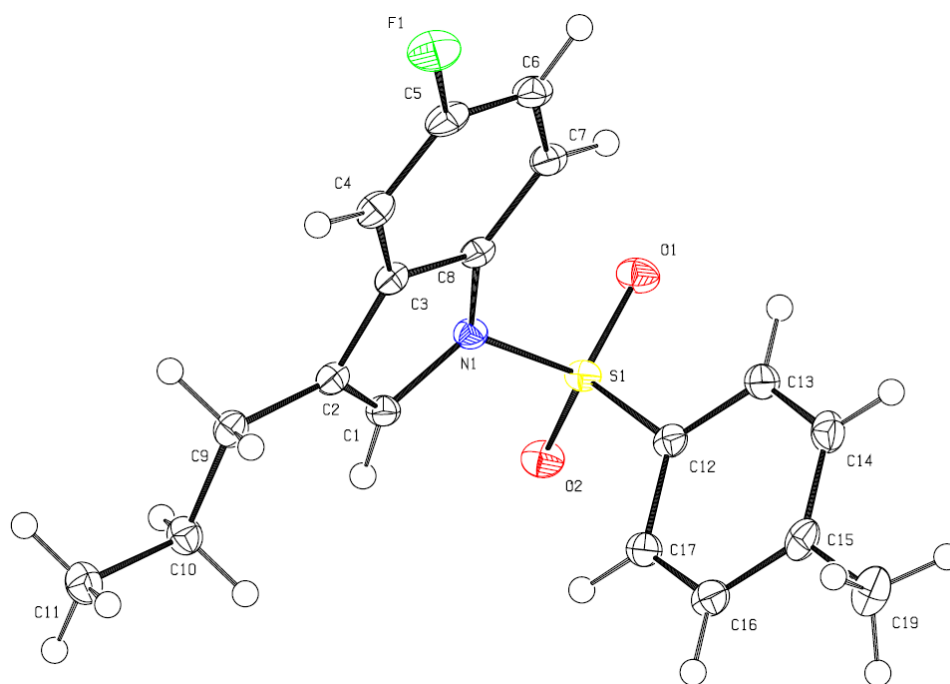


**Figure 201.** ORTEP representation of the structure of **25a** in the crystal. Thermal ellipsoids are represented at 50% probability.

**Table 7.** Crystal data for **25a**.

Chemical Formula	$C_{18}H_{18}NO_2FS$	
$M_r$	331.39 g/mol	
T	99.99 K	
Crystal Dimensions	$0.34 \times 0.26 \times 0.1$ mm	
Crystal System	Triclinic	
Space Group	$P\bar{1}$	
Unit Cell Dimensions	$a = 8.3596(4) \text{ \AA}$	$\alpha = 71.296(2)^\circ$
	$b = 9.0375(5) \text{ \AA}$	$\beta = 71.007(2)^\circ$
	$c = 11.9889(6) \text{ \AA}$	$\gamma = 75.277(2)^\circ$
Unit Cell Volume	$799.79(7) \text{ \AA}^3$	
Z	2	
Density (calcd)	$1.376 \text{ g/cm}^3$	
$\mu$	$0.222 \text{ mm}^{-1}$	

---

$F(000)$  348

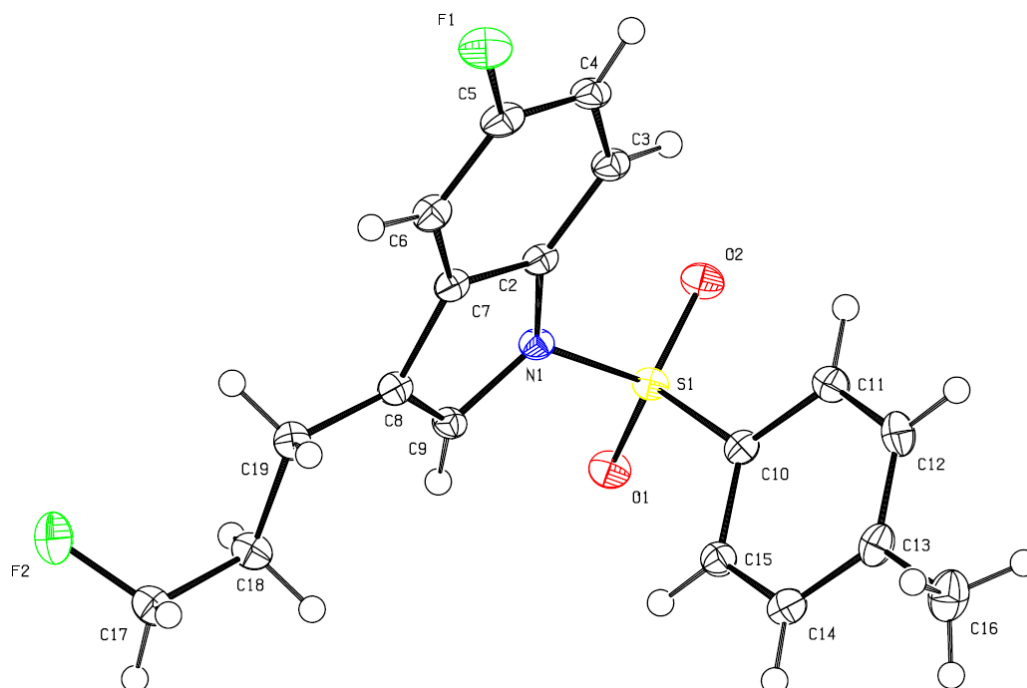
---

**Table 8.** Data collection and structure refinement for **25a**.

---

Diffractometer	Bruker APEX-II CCD
Radiation Source	Incoatec I $\mu$ S microfocus X-ray tube, Cu
Theta Range for Data Collection	$4.826 < \theta < 55.114^\circ$
Reflections Collected	13544
Independent Reflections	3647
Absorption Correction	Multi-scan
Structure Solution Technique	Direct methods
Structure Solution Program	SHELXS-97
Refinement Method	Full-matrix least-squares on $F^2$
Refinement Program	SHELXL-97
Function Minimized	$\Sigma w(F_o^2 - F_c^2)^2$
Data / Restraints / Parameters	3647 / 0 / 210
Goodness-of-Fit on $F^2$	1.043
Final $R$ Indices	$I > 2\sigma(I)$ : $R_1 = 0.0365$ , $wR_2 = 0.0980$ All data: $R_1 = 0.0401$ , $wR_2 = 0.1011$
Largest Diff. Peak and Hole	0.72 and -0.49 e $\text{\AA}^{-3}$

---

X-ray Crystal Structure of **25b**

**Figure 202.** ORTEP representation of the structure of **25b** in the crystal. Thermal ellipsoids are represented at 50% probability.

**Table 9.** Crystal data for **25b**.

Chemical Formula	$C_{18}H_{17}F_2NO_2S$	
$M_r$	349.39 g/mol	
T	100(2) K	
$\lambda$	0.71073 Å	
Crystal Dimensions	0.120 x 0.200 x 0.240 mm	
Crystal Habit	Clear colourless plate	
Crystal System	Triclinic	
Space Group	$P\bar{1}$	
Unit Cell Dimensions	$a = 8.3828(10)$ Å	$\alpha = 72.683(2)^\circ$
	$b = 9.0584(10)$ Å	$\beta = 73.391(2)^\circ$
	$c = 11.9476(14)$ Å	$\gamma = 73.880(2)^\circ$
Unit Cell Volume	$811.38(16)$ Å <sup>3</sup>	
Z	2	

Density (calcd)	1.430 g/cm <sup>3</sup>
$\mu$	0.231 mm <sup>-1</sup>
$F(000)$	364

**Table 10.** Data collection and structure refinement for **25b**.

Diffractometer	Bruker Kappa Apex-II Duo
Radiation Source	Incoatec I $\mu$ S microfocus X-ray tube, Cu
Theta Range for Data Collection	1.83 < $\theta$ < 27.56°
Reflections Collected	7769
Independent Reflections	3725
Absorption Correction	Multi-scan
Max. and Min. Transmission	0.9728 and 0.9466
Structure Solution Technique	Direct methods
Structure Solution Program	SHELXS-97
Refinement Method	Full-matrix least-squares on $F^2$
Refinement Program	SHELXL-97
Function Minimized	$\Sigma w(F_o^2 - F_c^2)^2$
Data / Restraints / Parameters	3725 / 0 / 285
Goodness-of-Fit on $F^2$	1.384
Final $R$ Indices	$I > 2\sigma(I)$ : $R_1 = 0.0389$ , $wR_2 = 0.1223$ All data: $R_1 = 0.0419$ , $wR_2 = 0.1256$
Weighting Scheme	$w = 1/[\sigma^2(F_o^2) + (0.0750P)^2 + 0.0000P]$ where $P = (F_o^2 + 2F_c^2)/3$
Largest Diff. Peak and Hole	0.601 and -0.627 e Å <sup>-3</sup>
R.M.S. Deviation from Mean	0.069 e Å <sup>-3</sup>

## X-ray Crystal Structure of 25c

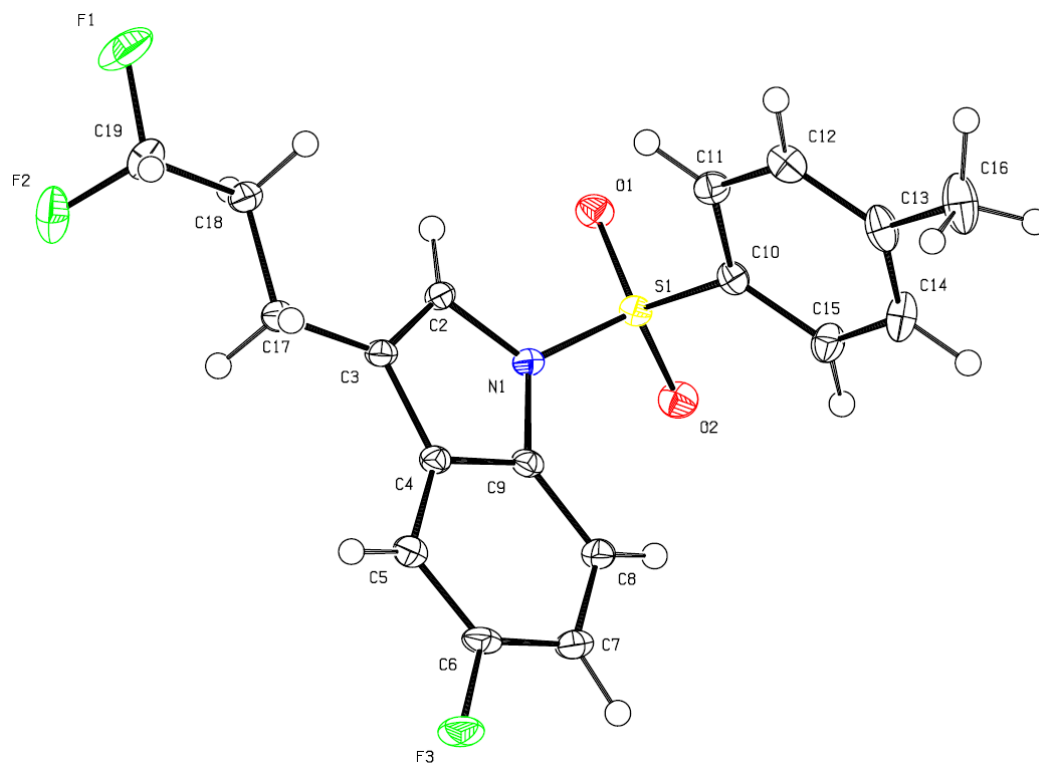


**Figure 203.** ORTEP representation of the structure of **25c** in the crystal. Thermal ellipsoids are represented at 50% probability.

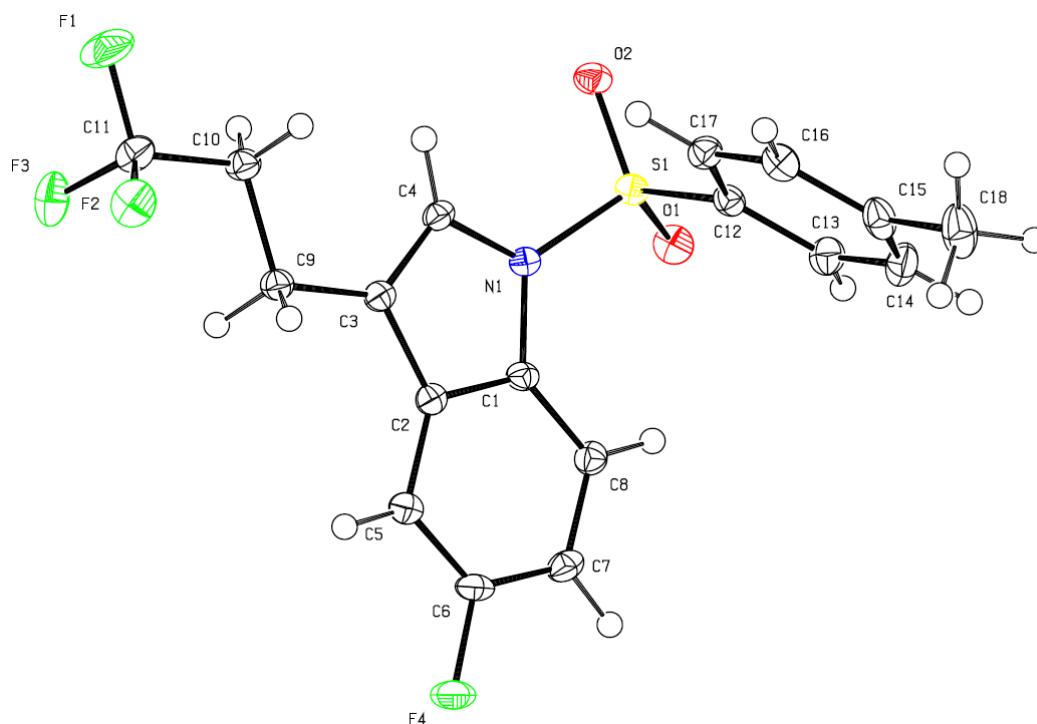
**Table 11.** Crystal data for **25c**.

Chemical Formula	$C_{18}H_{16}F_3NO_2S$	
$M_r$	367.38 g/mol	
T	100(2) K	
$\lambda$	0.71073 Å	
Crystal Dimensions	0.240 x 0.280 x 0.300 mm	
Crystal Habit	Clear colourless plate	
Crystal System	Triclinic	
Space Group	$P\bar{1}$	
Unit Cell Dimensions	$a = 8.0974(5)$ Å	$\alpha = 74.3950(10)^\circ$
	$b = 8.7626(5)$ Å	$\beta = 75.0860(10)^\circ$
	$c = 12.6326(7)$ Å	$\gamma = 76.3800(10)^\circ$
Unit Cell Volume	$820.80(8)$ Å <sup>3</sup>	

$Z$	2
Density (calcd)	1.486 g/cm <sup>3</sup>
$\mu$	0.241 mm <sup>-1</sup>
$F(000)$	380

**Table 12.** Data collection and structure refinement for **25c**.

Diffractometer	Bruker Kappa Apex-II Duo
Radiation Source	Incoatec I $\mu$ S microfocus X-ray tube, Cu
Theta Range for Data Collection	$2.45 < \theta < 27.49^\circ$
Reflections Collected	12727
Independent Reflections	3765
Absorption Correction	Multi-scan
Max. and Min. Transmission	0.9445 and 0.9313
Structure Solution Technique	Direct methods
Structure Solution Program	SHELXS-97
Refinement Method	Full-matrix least-squares on $F^2$
Refinement Program	SHELXL-97
Function Minimized	$\Sigma w(F_o^2 - F_c^2)^2$
Data / Restraints / Parameters	3765 / 0 / 290
Goodness-of-Fit on $F^2$	2.274
Final $R$ Indices	$I > 2\sigma(I)$ : $R_1 = 0.0314$ , $wR_2 = 0.1243$ All data: $R_1 = 0.0326$ , $wR_2 = 0.1258$
Weighting Scheme	$w=1/[\sigma^2(F_o^2)+(0.0500P)^2+0.0000P]$ where $P=(F_o^2+2F_c^2)/3$
Largest Diff. Peak and Hole	0.338 and -0.539 e $\text{\AA}^{-3}$
R.M.S. Deviation from Mean	0.057 e $\text{\AA}^{-3}$

X-ray Crystal Structure of **25d**

**Figure 204.** ORTEP representation of the structure of **25d** in the crystal. Thermal ellipsoids are represented at 50% probability.

**Table 13.** Crystal data for **25d**.

Chemical Formula	$C_{18}H_{15}NO_2F_4S$	
$M_r$	385.37 g/mol	
T	99.98 K	
Crystal Dimensions	$0.26 \times 0.2 \times 0.06$ mm	
Crystal System	Triclinic	
Space Group	$P\bar{1}$	
Unit Cell Dimensions	$a = 8.1453(6)$ Å	$\alpha = 75.566(2)^\circ$
	$b = 8.6857(7)$ Å	$\beta = 76.227(2)^\circ$
	$c = 12.7765(10)$ Å	$\gamma = 76.716(2)^\circ$
Unit Cell Volume	$836.13(11)$ Å <sup>3</sup>	
Z	2	
Density (calcd)	$1.531$ g/cm <sup>3</sup>	
$\mu$	$0.249$ mm <sup>-1</sup>	



---

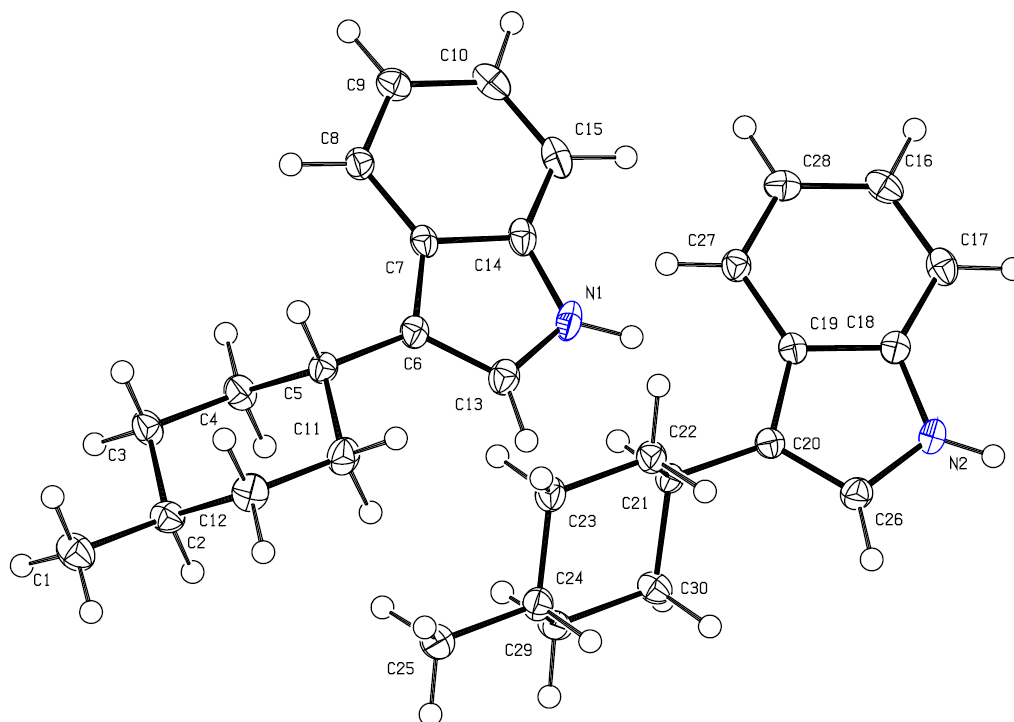
$F(000)$  396

---

**Table 14.** Data collection and structure refinement for **25d**.

Diffractometer	Bruker Nonius Apex II
Radiation Source	Incoatec I $\mu$ S microfocus X-ray tube, Cu
Theta Range for Data Collection	$4.924 < \theta < 55.088^\circ$
Reflections Collected	14026
Independent Reflections	3871
Absorption Correction	Multi-scan
Structure Solution Technique	Direct methods
Structure Solution Program	SHELXS-97
Refinement Method	Full-matrix least-squares on $F^2$
Refinement Program	SHELXL-97
Function Minimized	$\Sigma w(F_o^2 - F_c^2)^2$
Data / Restraints / Parameters	3871 / 0 / 236
Goodness-of-Fit on $F^2$	1.036
Final $R$ Indices	$I > 2\sigma(I)$ : $R_1 = 0.0332$ , $wR_2 = 0.0827$ All data: $R_1 = 0.0403$ , $wR_2 = 0.0870$
Largest Diff. Peak and Hole	0.31 and -0.41 e $\text{\AA}^{-3}$

---

X-ray Crystal Structure of *trans*-45a

**Figure 205.** ORTEP representation of the structure of *trans*-45a in the crystal. Thermal ellipsoids are represented at 50% probability.

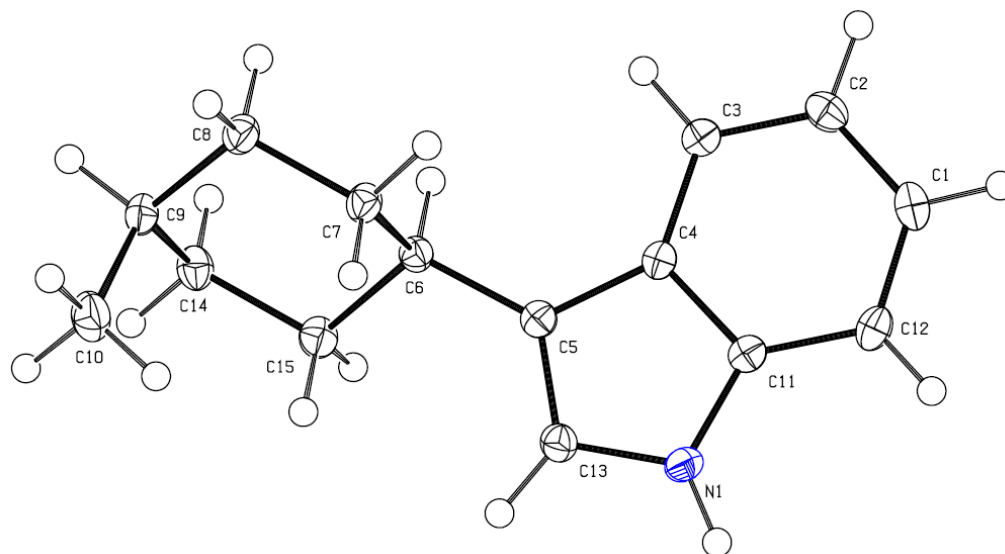
**Table 15.** Crystal data for *trans*-45a.

Chemical Formula	C <sub>15</sub> H <sub>19</sub> N	
$M_r$	213.31 g/mol	
T	100(2) K	
$\lambda$	0.71073 Å	
Crystal Dimensions	0.060 x 0.240 x 0.360 mm	
Crystal Habit	Clear colourless plate	
Crystal System	Monoclinic	
Space Group	$P 2_1/n$	
Unit Cell Dimensions	$a = 12.0463(7)$ Å	$\alpha = 90^\circ$
	$b = 7.7632(4)$ Å	$\beta = 102.760(2)^\circ$
	$c = 26.7445(15)$ Å	$\gamma = 90^\circ$
Unit Cell Volume	$2439.3(2)$ Å <sup>3</sup>	
Z	8	

Density (calcd)	1.162 g/cm <sup>3</sup>
$\mu$	0.067 mm <sup>-1</sup>
$F(000)$	928

**Table 16.** Data collection and structure refinement for *trans*-45a.

Diffractometer	Bruker Nonius APEX II
Radiation Source	Incoatec I $\mu$ S microfocus X-ray tube, Cu
Theta Range for Data Collection	$2.59 < \theta < 27.53^\circ$
Reflections Collected	20847
Independent Reflections	5612
Absorption Correction	Multi-scan
Max. and Min. Transmission	0.9960 and 0.9763
Structure Solution Technique	Direct methods
Structure Solution Program	SHELXS-97
Refinement Method	Full-matrix least-squares on $F^2$
Refinement Program	SHELXL-97
Function Minimized	$\Sigma w(F_o^2 - F_c^2)^2$
Data / Restraints / Parameters	5612 / 0 / 441
Goodness-of-Fit on $F^2$	1.111
Final $R$ Indices	$I > 2\sigma(I)$ : $R_1 = 0.0451$ , $wR_2 = 0.0979$ All data: $R_1 = 0.0718$ , $wR_2 = 0.1087$
Weighting Scheme	$w = 1/[\sigma^2(F_o^2) + (0.0500P)^2 + 0.0000P]$ where $P = (F_o^2 + 2F_c^2)/3$
Largest Diff. Peak and Hole	0.228 and -0.246 e $\text{\AA}^{-3}$
R.M.S. Deviation from Mean	0.044 e $\text{\AA}^{-3}$

X-ray Crystal Structure of *cis-45a*

**Figure 206.** ORTEP representation of the structure of *cis-45a* in the crystal. Thermal ellipsoids are represented at 50% probability.

**Table 17.** Crystal data for *cis-45a*.

Chemical Formula	C <sub>15</sub> H <sub>19</sub> N	
$M_r$	213.31 g/mol	
T	100(2) K	
$\lambda$	0.71073 Å	
Crystal Dimensions	0.090 x 0.100 x 0.220 mm	
Crystal Habit	Clear pale colourless-purple prism	
Crystal System	Monoclinic	
Space Group	$P 2_1/n$	
Unit Cell Dimensions	$a = 10.8971(8)$ Å	$\alpha = 90^\circ$
	$b = 5.4955(4)$ Å	$\beta = 93.565(3)^\circ$
	$c = 19.8152(16)$ Å	$\gamma = 90^\circ$
Unit Cell Volume	1184.34(16) Å <sup>3</sup>	
$Z$	4	
Density (calcd)	1.196 g/cm <sup>3</sup>	
$\mu$	0.069 mm <sup>-1</sup>	

---

$F(000)$  464

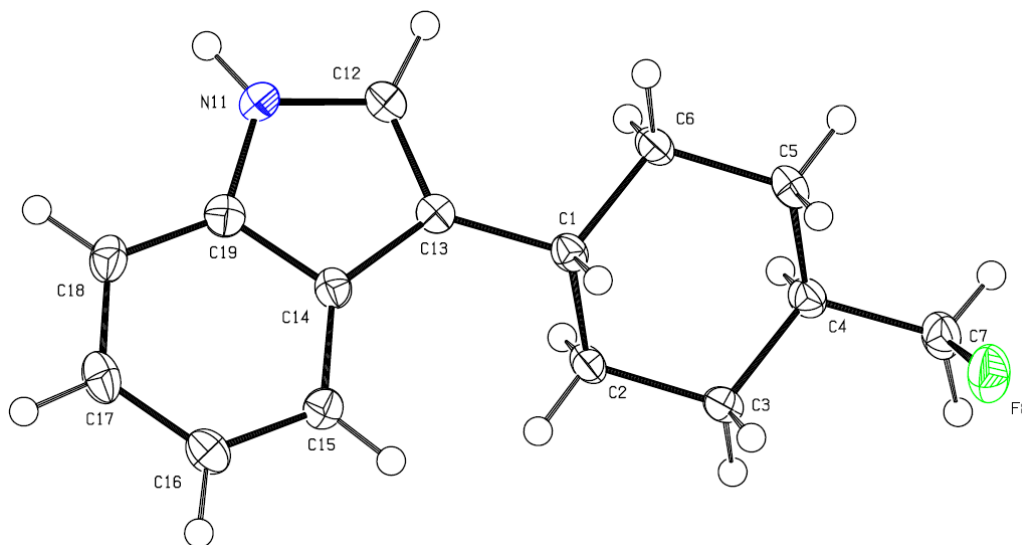
---

**Table 18.** Data collection and structure refinement for *cis-45a*.

---

Diffractometer	Bruker Kappa Apex-II Duo
Radiation Source	Incoatec I $\mu$ S microfocus X-ray tube, Cu
Theta Range for Data Collection	$2.06 < \theta < 27.53^\circ$
Reflections Collected	7464
Independent Reflections	2673
Absorption Correction	Multi-scan
Max. and Min. Transmission	0.9938 and 0.9850
Structure Solution Technique	Direct methods
Structure Solution Program	SHELXS-97
Refinement Method	Full-matrix least-squares on $F^2$
Refinement Program	SHELXL-97
Function Minimized	$\Sigma w(F_o^2 - F_c^2)^2$
Data / Restraints / Parameters	2673 / 0 / 221
Goodness-of-Fit on $F^2$	1.523
Final $R$ Indices	$I > 2\sigma(I)$ : $R_1 = 0.0388$ , $wR_2 = 0.1040$ All data: $R_1 = 0.0469$ , $wR_2 = 0.1078$
Weighting Scheme	$w = 1/[\sigma^2(F_o^2) + (0.0500P)^2 + 0.0000P]$ where $P = (F_o^2 + 2F_c^2)/3$
Largest Diff. Peak and Hole	0.318 and -0.277 e $\text{\AA}^{-3}$
R.M.S. Deviation from Mean	0.040 e $\text{\AA}^{-3}$

---

X-ray Crystal Structure of *trans*-45b

**Figure 207.** ORTEP representation of the structure of *trans*-45b in the crystal. Thermal ellipsoids are represented at 50% probability.

**Table 19.** Crystal data for *trans*-45b.

Chemical Formula	$C_{15}H_{18}FN$
$M_r$	231.30 g/mol
T	100(2) K
$\lambda$	0.71073 Å
Crystal Dimensions	0.03 x 0.04 x 0.26 mm
Crystal Habit	Clear colourless rod
Crystal System	Monoclinic
Space Group	$P 2_1/n$
Unit Cell Dimensions	$a = 11.8535(13)$ Å $\alpha = 90^\circ$ $b = 5.5451(5)$ Å $\beta = 99.327(4)^\circ$ $c = 18.727(2)$ Å $\gamma = 90^\circ$
Unit Cell Volume	$1214.6(2)$ Å <sup>3</sup>
Z	4
Density (calcd)	$1.265$ g/cm <sup>3</sup>
$\mu$	$0.084$ mm <sup>-1</sup>

---

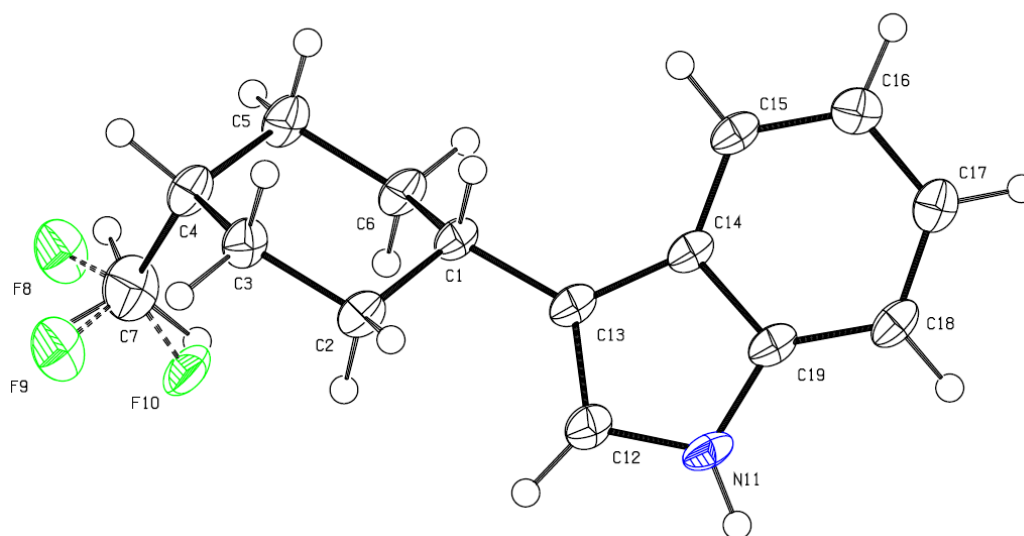
 $F(000)$ 496

---

**Table 20.** Data collection and structure refinement for *trans*-**45b**.

Diffractometer	Bruker Nonius APEX II
Radiation Source	Incoatec I $\mu$ S microfocus X-ray tube, Cu
Theta Range for Data Collection	$1.90 < \theta < 27.50^\circ$
Reflections Collected	5792
Independent Reflections	2720
Absorption Correction	Multi-scan
Structure Solution Technique	Direct methods
Structure Solution Program	SHELXS-97
Refinement Method	Full-matrix least-squares on $F^2$
Refinement Program	SHELXL-97
Function Minimized	$\Sigma w(F_o^2 - F_c^2)^2$
Data / Restraints / Parameters	2720 / 0 / 226
Goodness-of-Fit on $F^2$	0.975
Final $R$ Indices	$I > 2\sigma(I)$ : $R_1 = 0.0531$ , $wR_2 = 0.1241$ All data: $R_1 = 0.1146$ , $wR_2 = 0.1785$
Weighting Scheme	$w = 1/[\sigma^2(F_o^2) + (0.1000P)^2 + 0.0000P]$ where $P = (F_o^2 + 2F_c^2)/3$
Largest Diff. Peak and Hole	0.341 and -0.318 e $\text{\AA}^{-3}$
R.M.S. Deviation from Mean	0.080 e $\text{\AA}^{-3}$

---

X-ray Crystal Structure of *cis-45b*

**Figure 208.** ORTEP representation of the structure of *cis-45b* in the crystal. Thermal ellipsoids are represented at 50% probability.

**Table 21.** Crystal data for *cis-45b*.

Chemical Formula	$C_{15}H_{18}FN$
$M_r$	231.30 g/mol
T	100(2) K
$\lambda$	0.71073 Å
Crystal Dimensions	0.03 x 0.10 x 0.26 mm
Crystal Habit	Clear colourless rod
Crystal System	Monoclinic
Space Group	$P 2_1/n$
Unit Cell Dimensions	$a = 10.8815(11)$ Å $\alpha = 90^\circ$ $b = 5.4827(5)$ Å $\beta = 93.907(3)^\circ$ $c = 20.161(2)$ Å $\gamma = 90^\circ$
Unit Cell Volume	1200.0(2) Å <sup>3</sup>
Z	4
Density (calcd)	1.280 g/cm <sup>3</sup>
$\mu$	0.085 mm <sup>-1</sup>



---

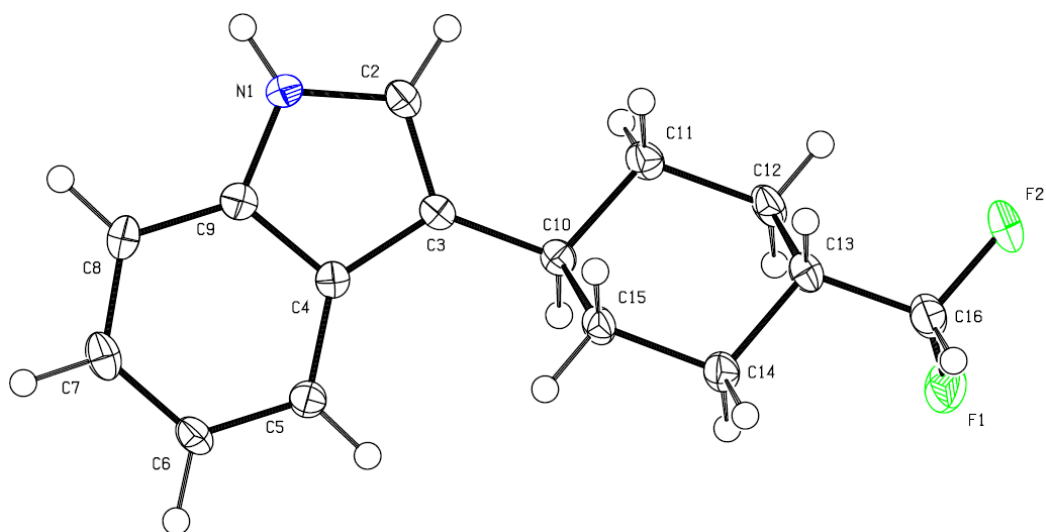
 $F(000)$ 496

---

**Table 22.** Data collection and structure refinement for *cis-45b*.

Diffractometer	Bruker Nonius APEX II
Radiation Source	Incoatec I $\mu$ S microfocus X-ray tube, Cu
Theta Range for Data Collection	$3.46 < \theta < 25.48^\circ$
Reflections Collected	10437
Independent Reflections	2222
Absorption Correction	Multi-scan
Structure Solution Technique	Direct methods
Structure Solution Program	SHELXS-97
Refinement Method	Full-matrix least-squares on $F^2$
Refinement Program	SHELXL-97
Function Minimized	$\Sigma w(F_o^2 - F_c^2)^2$
Data / Restraints / Parameters	2222 / 4 / 242
Goodness-of-Fit on $F^2$	0.935
Final $R$ Indices	$I > 2\sigma(I)$ : $R_1 = 0.0482$ , $wR_2 = 0.1207$ All data: $R_1 = 0.0829$ , $wR_2 = 0.1440$
Weighting Scheme	$w = 1/[\sigma^2(F_o^2) + (0.1000P)^2 + 0.0000P]$ where $P = (F_o^2 + 2F_c^2)/3$
Largest Diff. Peak and Hole	0.238 and -0.218 e $\text{\AA}^{-3}$
R.M.S. Deviation from Mean	0.050 e $\text{\AA}^{-3}$

---

X-ray Crystal Structure of *trans*-45c

**Figure 209.** ORTEP representation of the structure of *trans*-45c in the crystal. Thermal ellipsoids are represented at 50% probability.

**Table 23.** Crystal data for *trans*-45c.

Chemical Formula	C <sub>15</sub> H <sub>17</sub> F <sub>2</sub> N	
$M_r$	249.30 g/mol	
T	100(2) K	
$\lambda$	0.71073 Å	
Crystal Dimensions	0.020 x 0.030 x 0.030 mm	
Crystal Habit	Clear colourless rod	
Crystal System	Monoclinic	
Space Group	$P 2_1/n$	
Unit Cell Dimensions	$a = 12.163(2)$ Å	$\alpha = 90^\circ$
	$b = 5.8157(10)$ Å	$\beta = 97.959(8)^\circ$
	$c = 17.850(3)$ Å	$\gamma = 90^\circ$
Unit Cell Volume	1250.5(4) Å <sup>3</sup>	
Z	4	
Density (calcd)	1.324 g/cm <sup>3</sup>	
$\mu$	0.098 mm <sup>-1</sup>	

---

$F(000)$  528

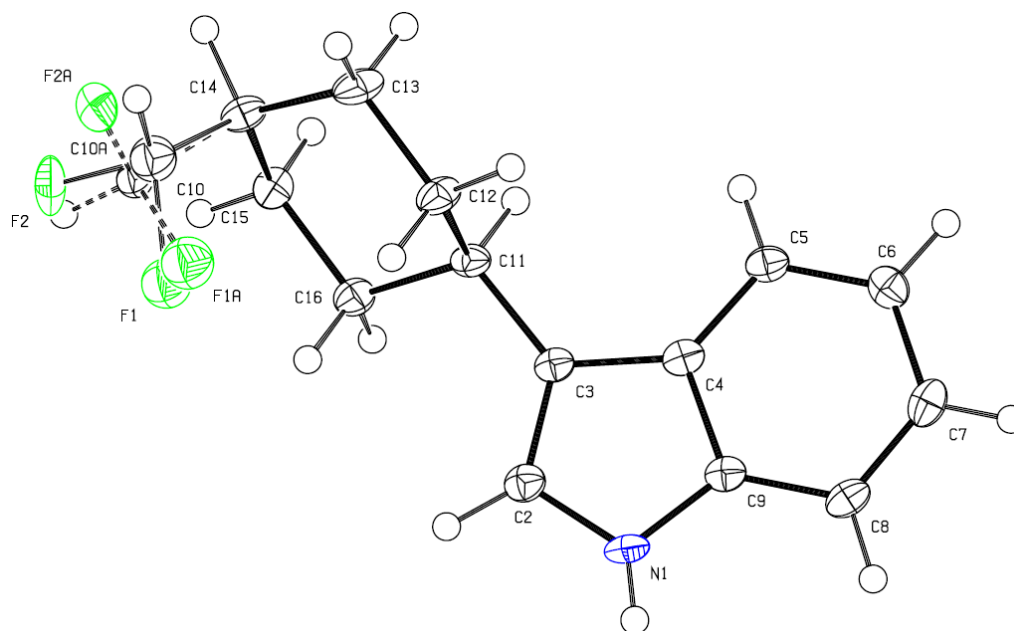
---

**Table 24.** Data collection and structure refinement for *trans*-45c.

---

Diffractometer	Bruker Nonius APEX-II
Radiation Source	Incoatec I $\mu$ S microfocus X-ray tube, Cu
Theta Range for Data Collection	$3.38 < \theta < 26.40^\circ$
Reflections Collected	9335
Independent Reflections	2565
Absorption Correction	Multi-scan
Max. and Min. Transmission	0.9985 and 0.9971
Structure Solution Technique	Direct methods
Structure Solution Program	SHELXS-97
Refinement Method	Full-matrix least-squares on $F^2$
Refinement Program	SHELXL-97
Function Minimized	$\Sigma w(F_o^2 - F_c^2)^2$
Data / Restraints / Parameters	2565 / 0 / 231
Goodness-of-Fit on $F^2$	0.989
Final $R$ Indices	$I > 2\sigma(I)$ : $R_1 = 0.0486$ , $wR_2 = 0.0990$ All data: $R_1 = 0.1038$ , $wR_2 = 0.1184$
Weighting Scheme	$w = 1/[\sigma^2(F_o^2) + (0.0576P)^2 + 0.0000P]$ where $P = (F_o^2 + 2F_c^2)/3$
Largest Diff. Peak and Hole	0.194 and -0.258 e $\text{\AA}^{-3}$
R.M.S. Deviation from Mean	0.054 e $\text{\AA}^{-3}$

---

X-ray Crystal Structure of *cis-45c*

**Figure 210.** ORTEP representation of the structure of *cis-45c* in the crystal. Thermal ellipsoids are represented at 50% probability.

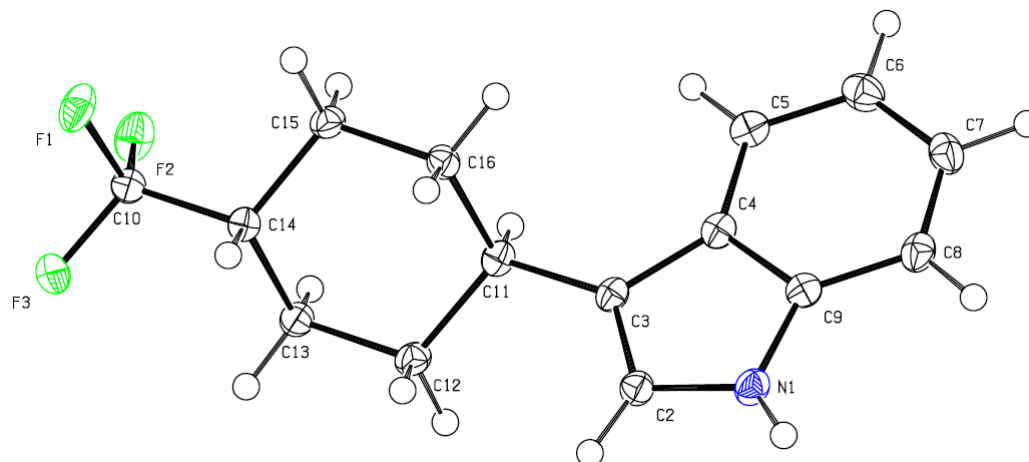
**Table 25.** Crystal data for *cis-45c*.

Chemical Formula	$C_{15}H_{17}F_2N$
$M_r$	249.30 g/mol
T	100(2) K
$\lambda$	0.71073 Å
Crystal Dimensions	0.010 x 0.060 x 0.120 mm
Crystal Habit	Clear yellow needle
Crystal System	Monoclinic
Space Group	$P 2_1/n$
Unit Cell Dimensions	$a = 10.8409(16)$ Å $\alpha = 90^\circ$ $b = 5.5650(8)$ Å $\beta = 94.831(11)^\circ$ $c = 20.420(3)$ Å $\gamma = 90^\circ$
Unit Cell Volume	$1227.6(3)$ Å <sup>3</sup>
Z	4
Density (calcd)	$1.349$ g/cm <sup>3</sup>

$\mu$	0.100 mm <sup>-1</sup>
$F(000)$	528

**Table 26.** Data collection and structure refinement for *cis-45c*.

Diffractometer	Bruker Kappa Apex-II Duo
Radiation Source	Incoatec I $\mu$ S microfocus X-ray tube, Cu
Theta Range for Data Collection	2.00 < $\theta$ < 27.49°
Reflections Collected	8129
Independent Reflections	2802
Absorption Correction	Multi-scan
Max. and Min. Transmission	0.9988 and 0.9881
Structure Solution Technique	Direct methods
Structure Solution Program	SHELXS-97
Refinement Method	Full-matrix least-squares on $F^2$
Refinement Program	SHELXL-97
Function Minimized	$\Sigma w(F_o^2 - F_c^2)^2$
Data / Restraints / Parameters	2802 / 0 / 235
Goodness-of-Fit on $F^2$	1.009
Final $R$ Indices	$I > 2\sigma(I)$ : $R_1 = 0.0566$ , $wR_2 = 0.1276$ All data: $R_1 = 0.1079$ , $wR_2 = 0.1491$
Weighting Scheme	$w=1/[\sigma^2(F_o^2)+(0.0800P)^2+0.0000P]$ where $P=(F_o^2+2F_c^2)/3$
Largest Diff. Peak and Hole	0.234 and -0.494 e Å <sup>-3</sup>
R.M.S. Deviation from Mean	0.058 e Å <sup>-3</sup>

X-ray Crystal Structure of *trans*-45d

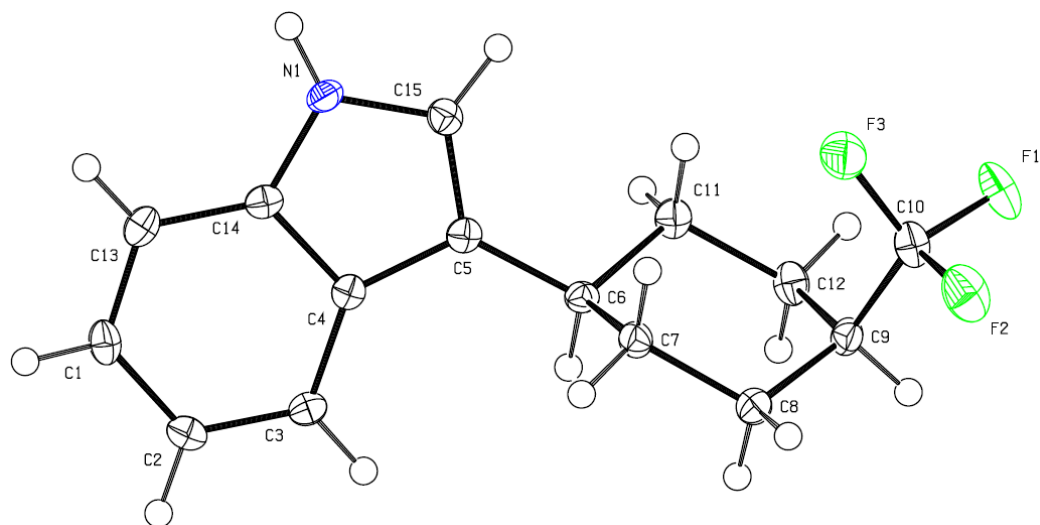
**Figure 211.** ORTEP representation of the structure of *trans*-45d in the crystal. Thermal ellipsoids are represented at 50% probability.

**Table 27.** Crystal data for *trans*-45d.

Chemical Formula	C <sub>15</sub> H <sub>16</sub> F <sub>3</sub> N	
<i>M<sub>r</sub></i>	267.29 g/mol	
T	100(2) K	
$\lambda$	0.71073 Å	
Crystal Dimensions	0.020 x 0.160 x 0.240 mm	
Crystal Habit	Clear pale colourless-bronze plate	
Crystal System	Monoclinic	
Space Group	<i>P</i> 2 <sub>1</sub> / <i>c</i>	
Unit Cell Dimensions	<i>a</i> = 9.5949(5) Å	$\alpha$ = 90°
	<i>b</i> = 5.3436(3) Å	$\beta$ = 92.645(2)°
	<i>c</i> = 24.3405(14) Å	$\gamma$ = 90°
Unit Cell Volume	1246.64(12) Å <sup>3</sup>	
<i>Z</i>	4	
Density (calcd)	1.424 g/cm <sup>3</sup>	
$\mu$	0.114 mm <sup>-1</sup>	
<i>F</i> (000)	560	

**Table 28.** Data collection and structure refinement for *trans*-45d.

Diffractometer	Bruker Kappa Apex-II Duo
Radiation Source	Incoatec I $\mu$ S microfocus X-ray tube, Cu
Theta Range for Data Collection	$1.68 < \theta < 27.51^\circ$
Reflections Collected	7916
Independent Reflections	2794
Absorption Correction	Multi-scan
Max. and Min. Transmission	0.9983 and 0.9731
Structure Solution Technique	Direct methods
Structure Solution Program	SHELXS-97
Refinement Method	Full-matrix least-squares on $F^2$
Refinement Program	SHELXL-97
Function Minimized	$\Sigma w(F_o^2 - F_c^2)^2$
Data / Restraints / Parameters	2794 / 0 / 236
Goodness-of-Fit on $F^2$	0.873
Final $R$ Indices	$I > 2\sigma(I)$ : $R_1 = 0.0388$ , $wR_2 = 0.1100$ All data: $R_1 = 0.0600$ , $wR_2 = 0.1264$
Weighting Scheme	$w = 1/[\sigma^2(F_o^2) + (0.1000P)^2 + 0.0000P]$ where $P = (F_o^2 + 2F_c^2)/3$
Largest Diff. Peak and Hole	0.261 and -0.259 e $\text{\AA}^{-3}$
R.M.S. Deviation from Mean	0.047 e $\text{\AA}^{-3}$

X-ray Crystal Structure of *cis-45d*

**Figure 212.** ORTEP representation of the structure of *cis-45d* in the crystal. Thermal ellipsoids are represented at 50% probability.

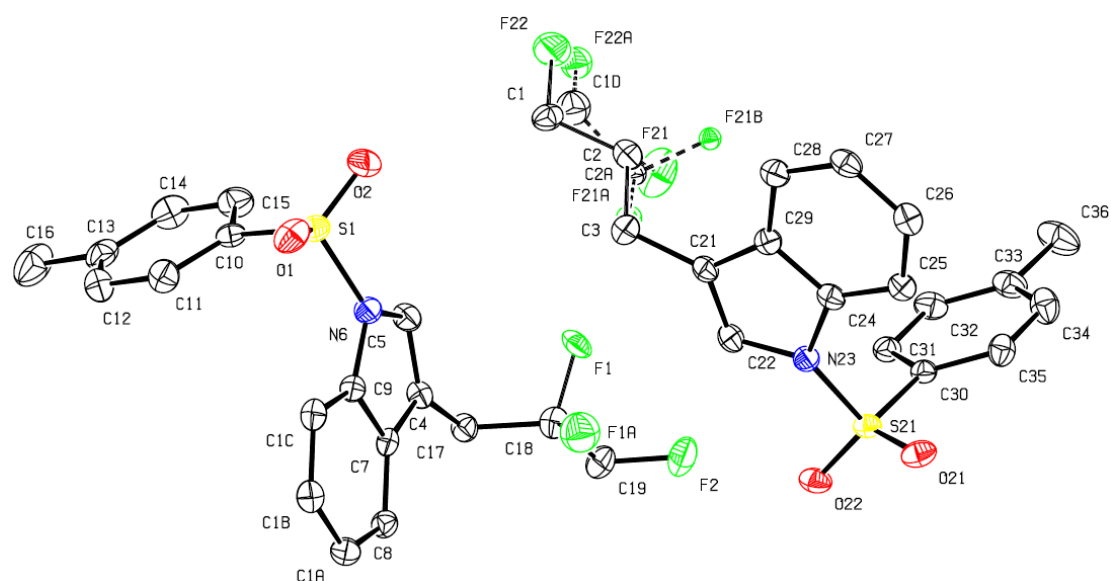
**Table 29.** Crystal data for *cis-45d*.

Chemical Formula	C <sub>15</sub> H <sub>16</sub> F <sub>3</sub> N	
<i>M<sub>r</sub></i>	267.29 g/mol	
T	100(2) K	
$\lambda$	0.71073 Å	
Crystal Dimensions	0.080 x 0.260 x 0.340 mm	
Crystal Habit	Clear colourless rod	
Crystal System	Orthorhombic	
Space Group	<i>P</i> 2 <sub>1</sub> 2 <sub>1</sub> 2 <sub>1</sub>	
Unit Cell Dimensions	<i>a</i> = 5.5516(3) Å	$\alpha$ = 90°
	<i>b</i> = 10.6975(5) Å	$\beta$ = 90°
	<i>c</i> = 21.3575(12) Å	$\gamma$ = 90°
Unit Cell Volume	1268.38(12) Å <sup>3</sup>	
<i>Z</i>	4	
Density (calcd)	1.400 g/cm <sup>3</sup>	
$\mu$	0.112 mm <sup>-1</sup>	
<i>F</i> (000)	560	



**Table 30.** Data collection and structure refinement for *cis-45d*.

Diffractometer	Bruker Nonius APEX-II
Radiation Source	Incoatec I $\mu$ S microfocus X-ray tube, Cu
Theta Range for Data Collection	$2.70 < \theta < 27.57^\circ$
Reflections Collected	5832
Independent Reflections	2818
Absorption Correction	Multi-scan
Max. and Min. Transmission	0.9911 and 0.9628
Structure Solution Technique	Direct methods
Structure Solution Program	SHELXS-97
Refinement Method	Full-matrix least-squares on $F^2$
Refinement Program	SHELXL-97
Function Minimized	$\Sigma w(F_o^2 - F_c^2)^2$
Data / Restraints / Parameters	2818 / 0 / 236
Goodness-of-Fit on $F^2$	1.325
Final $R$ Indices	$I > 2\sigma(I)$ : $R_1 = 0.0315$ , $wR_2 = 0.0689$ All data: $R_1 = 0.0352$ , $wR_2 = 0.0703$
Weighting Scheme	$w = 1/[\sigma^2(F_o^2) + (0.0300P)^2 + 0.0000P]$ where $P = (F_o^2 + 2F_c^2)/3$
Largest Diff. Peak and Hole	0.221 and -0.215 e $\text{\AA}^{-3}$
R.M.S. Deviation from Mean	0.038 e $\text{\AA}^{-3}$

X-ray Crystal Structure of **83**

**Figure 213.** ORTEP representation of the structure of **83** in the crystal. Thermal ellipsoids are represented at 50% probability. Hydrogen atoms have been removed for clarity.

**Table 31.** Crystal data for **83**.

Chemical Formula	$C_{36}H_{34}F_4N_2O_4S_2$	
$M_r$	698.77 g/mol	
T	100(2) K	
$\lambda$	0.71073 Å	
Crystal Dimensions	0.120 x 0.240 x 0.360 mm	
Crystal Habit	Clear colourless prism	
Crystal System	Tetragonal	
Space Group	$P 4_3$	
Unit Cell Dimensions	$a = 10.0259(5)$ Å	$\alpha = 90^\circ$
	$b = 10.0259(5)$ Å	$\beta = 90^\circ$
	$c = 32.393(3)$ Å	$\gamma = 90^\circ$
Unit Cell Volume	3256.1(4) Å <sup>3</sup>	
Z	4	
Density (calcd)	1.425 g/cm <sup>3</sup>	
$\mu$	0.230 mm <sup>-1</sup>	

---

$F(000)$  1456

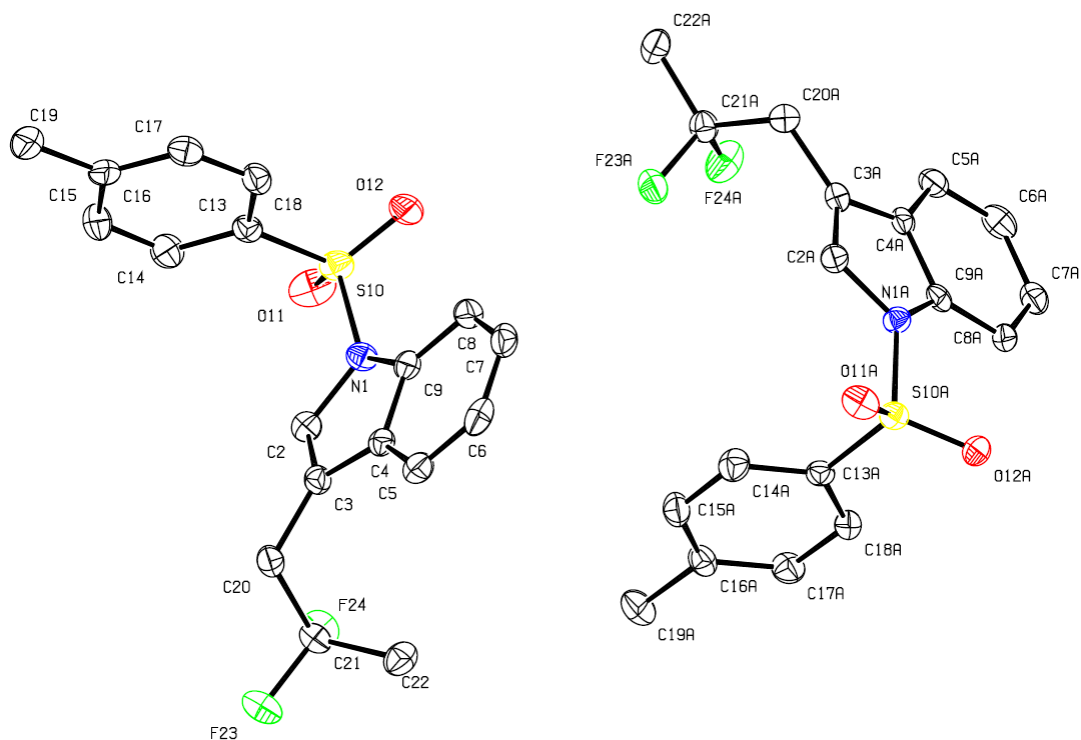
---

**Table 32.** Data collection and structure refinement for **83**.

---

Diffractometer	Bruker Nonius APEX-II
Radiation Source	Incoatec I $\mu$ S microfocus X-ray tube, Cu
Theta Range for Data Collection	$1.89 < \theta < 27.71^\circ$
Reflections Collected	39282
Independent Reflections	7589
Absorption Correction	Multi-scan
Max. and Min. Transmission	0.9729 and 0.9217
Structure Solution Technique	Direct methods
Structure Solution Program	SHELXS-97
Refinement Method	Full-matrix least-squares on $F^2$
Refinement Program	SHELXL-97
Function Minimized	$\Sigma w(F_o^2 - F_c^2)^2$
Data / Restraints / Parameters	7589 / 8 / 461
Goodness-of-Fit on $F^2$	0.813
Final $R$ Indices	$I > 2\sigma(I)$ : $R_1 = 0.0364$ , $wR_2 = 0.0976$ All data: $R_1 = 0.0423$ , $wR_2 = 0.1061$
Weighting Scheme	$w = 1/[\sigma^2(F_o^2) + (0.1000P)^2 + 0.0000P]$ where $P = (F_o^2 + 2F_c^2)/3$
Largest Diff. Peak and Hole	0.226 and -0.279 e $\text{\AA}^{-3}$
R.M.S. Deviation from Mean	0.046 e $\text{\AA}^{-3}$

---

X-ray Crystal Structure of **72**

**Figure 214.** ORTEP representation of the structure of **72** in the crystal. Thermal ellipsoids are represented at 50% probability. Hydrogen atoms have been removed for clarity.

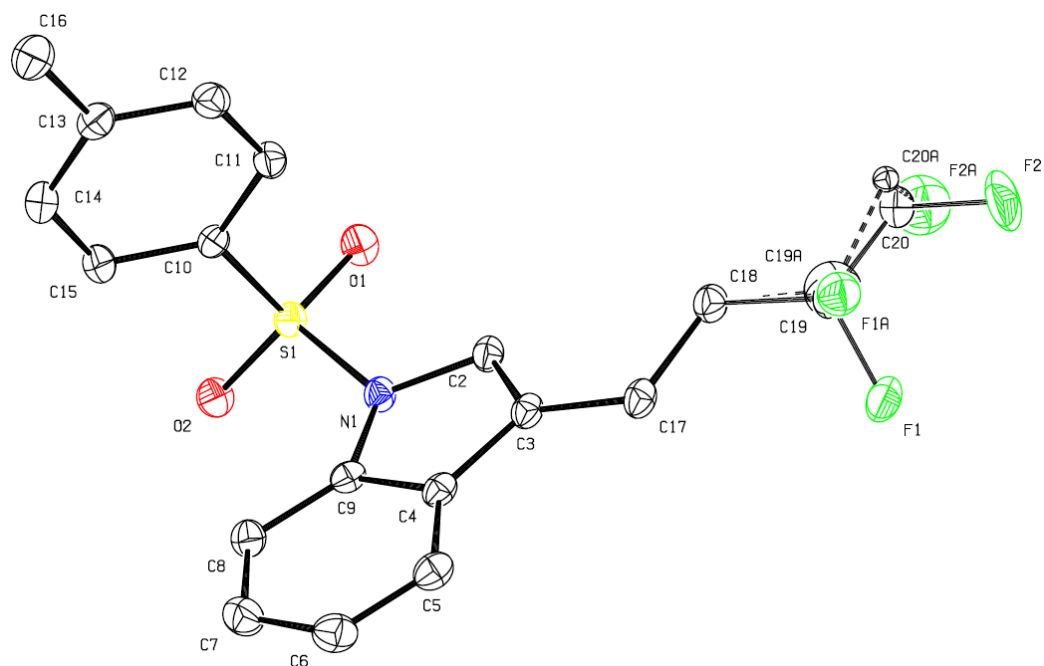
**Table 33.** Crystal data for **72**.

Chemical Formula	$C_{18}H_{17}F_2NO_2S$	
$M_r$	349.39 g/mol	
T	100(2) K	
$\lambda$	0.71073 Å	
Crystal Dimensions	0.080 x 0.100 x 0.140 mm	
Crystal Habit	Clear colourless rod	
Crystal System	Triclinic	
Space Group	$P\bar{1}$	
Unit Cell Dimensions	$a = 9.8246(5)$ Å	$\alpha = 106.6497(19)^\circ$
	$b = 10.2117(5)$ Å	$\beta = 97.5951(19)^\circ$
	$c = 17.3979(9)$ Å	$\gamma = 96.5909(19)^\circ$
Unit Cell Volume	1636.05(14) Å <sup>3</sup>	
Z	4	

Density (calcd)	1.418 g/cm <sup>3</sup>
$\mu$	0.229 mm <sup>-1</sup>
$F(000)$	728

**Table 34.** Data collection and structure refinement for **72**.

Diffractometer	Bruker Nonius APEX-II
Radiation Source	Incoatec I $\mu$ S microfocus X-ray tube, Cu
Theta Range for Data Collection	$1.24 < \theta < 27.72^\circ$
Reflections Collected	25536
Independent Reflections	7423
Absorption Correction	Multi-scan
Max. and Min. Transmission	0.9819 and 0.9686
Structure Solution Technique	Direct methods
Structure Solution Program	SHELXS-97
Refinement Method	Full-matrix least-squares on $F^2$
Refinement Program	SHELXL-97
Function Minimized	$\Sigma w(F_o^2 - F_c^2)^2$
Data / Restraints / Parameters	7423 / 0 / 569
Goodness-of-Fit on $F^2$	1.308
Final $R$ Indices	$I > 2\sigma(I)$ : $R_1 = 0.0547$ , $wR_2 = 0.1205$ All data: $R_1 = 0.0900$ , $wR_2 = 0.1304$
Weighting Scheme	$w = 1/[\sigma^2(F_o^2) + (0.0500P)^2 + 0.0000P]$ where $P = (F_o^2 + 2F_c^2)/3$
Largest Diff. Peak and Hole	0.343 and -0.370 e $\text{\AA}^{-3}$
R.M.S. Deviation from Mean	0.067 e $\text{\AA}^{-3}$

X-ray Crystal Structure of **84**

**Figure 215.** ORTEP representation of the structure of **84** in the crystal. Thermal ellipsoids are represented at 50% probability. Hydrogen atoms have been removed for clarity.

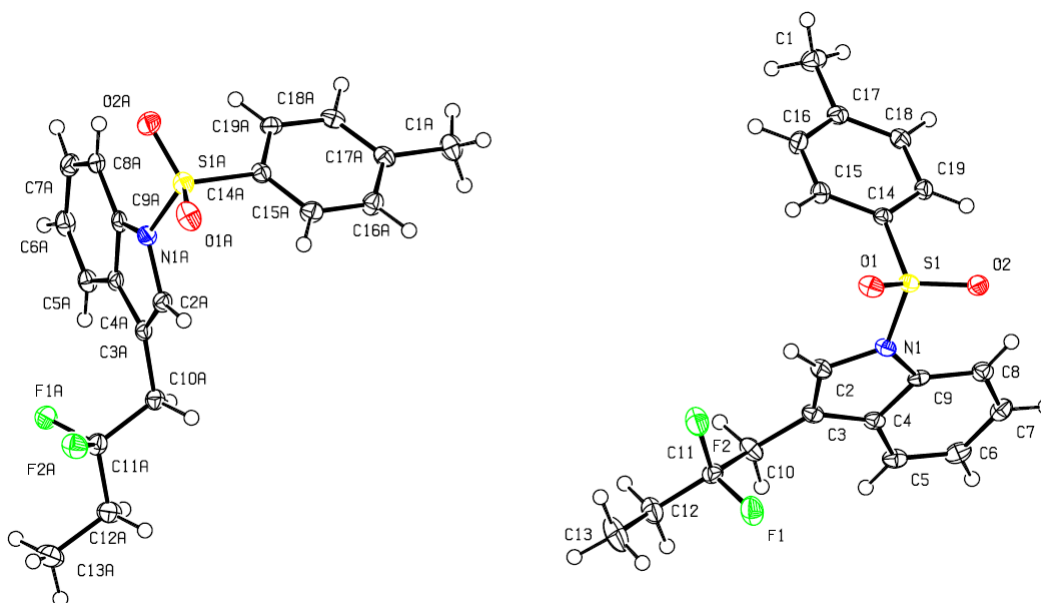
**Table 35.** Crystal data for **84**.

Chemical Formula	$C_{19}H_{19}F_2NO_2S$	
$M_r$	363.41 g/mol	
T	100(2) K	
$\lambda$	0.71073 Å	
Crystal Dimensions	0.240 x 0.300 x 0.360 mm	
Crystal Habit	Clear colourless prism	
Crystal System	Triclinic	
Space Group	$P\bar{1}$	
Unit Cell Dimensions	$a = 8.3500(3)$ Å	$\alpha = 101.9950(10)^\circ$
	$b = 8.9257(3)$ Å	$\beta = 98.2960(10)^\circ$
	$c = 12.5352(4)$ Å	$\gamma = 106.3350(10)^\circ$
Unit Cell Volume	$856.26(5)$ Å <sup>3</sup>	
Z	2	
Density (calcd)	$1.410$ g/cm <sup>3</sup>	

$\mu$	0.222 mm <sup>-1</sup>
$F(000)$	380

**Table 36.** Data collection and structure refinement for **84**.

Diffractometer	Bruker Nonius APEX-II
Radiation Source	Incoatec I $\mu$ S microfocus X-ray tube, Cu
Theta Range for Data Collection	2.46 < $\theta$ < 27.56°
Reflections Collected	7252
Independent Reflections	3894
Absorption Correction	Multi-scan
Max. and Min. Transmission	0.9487 and 0.9244
Structure Solution Technique	Direct methods
Structure Solution Program	SHELXS-97
Refinement Method	Full-matrix least-squares on $F^2$
Refinement Program	SHELXL-97
Function Minimized	$\Sigma w(F_o^2 - F_c^2)^2$
Data / Restraints / Parameters	3894 / 2 / 307
Goodness-of-Fit on $F^2$	1.733
Final $R$ Indices	$I > 2\sigma(I)$ : $R_1 = 0.0341$ , $wR_2 = 0.1058$ all data: $R_1 = 0.0377$ , $wR_2 = 0.1079$
Weighting Scheme	$w = 1/[\sigma^2(F_o^2) + (0.0450P)^2 + 0.0000P]$ where $P = (F_o^2 + 2F_c^2)/3$
Largest Diff. Peak and Hole	0.357 and -0.393 e Å <sup>-3</sup>
R.M.S. Deviation from Mean	0.048 e Å <sup>-3</sup>

X-ray Crystal Structure of **73**

**Figure 216.** ORTEP representation of the structure of **73** in the crystal. Thermal ellipsoids are represented at 50% probability.

**Table 37.** Crystal data for **73**.

Chemical Formula	$C_{38}H_{38}F_4N_2O_4S_2$	
$M_r$	726.82 g/mol	
T	100(2) K	
$\lambda$	0.71073 Å	
Crystal Dimensions	0.100 x 0.140 x 0.280 mm	
Crystal Habit	Clear colourless prism	
Crystal System	Triclinic	
Space Group	$P\bar{1}$	
Unit Cell Dimensions	$a = 9.8408(2)$ Å	$\alpha = 110.7270(10)^\circ$
	$b = 13.5966(2)$ Å	$\beta = 102.2540(10)^\circ$
	$c = 14.3307(3)$ Å	$\gamma = 97.3240(10)^\circ$
Unit Cell Volume	1708.91(6) Å <sup>3</sup>	
Z	2	
Density (calcd)	1.413 g/cm <sup>3</sup>	
$\mu$	0.222 mm <sup>-1</sup>	



---

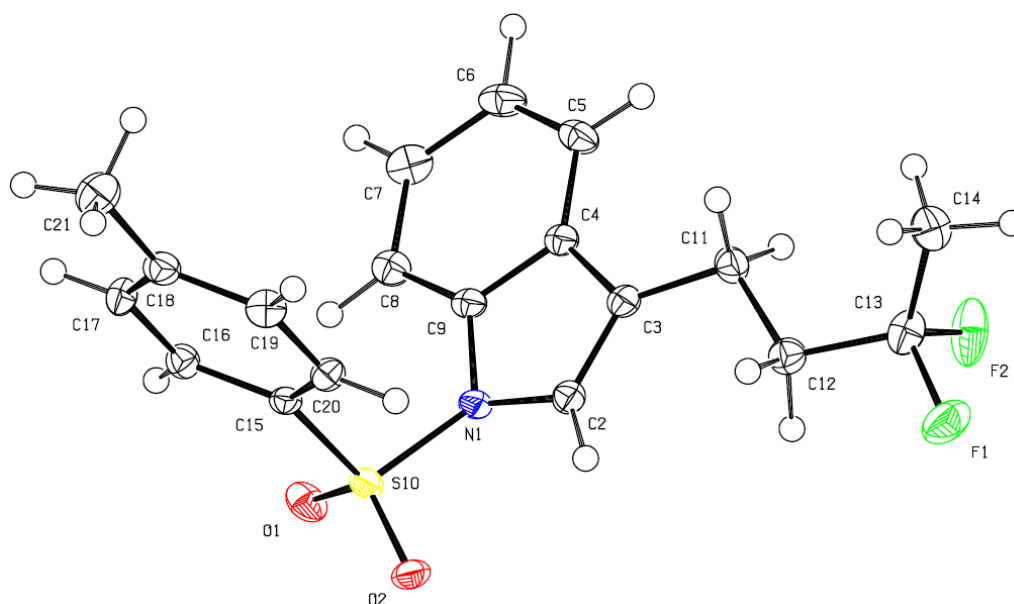
$F(000)$  760

---

**Table 38.** Data collection and structure refinement for **73**.

Diffractometer	Bruker Kappa Apex-II Duo
Radiation Source	Incoatec I $\mu$ S microfocus X-ray tube, Cu
Theta Range for Data Collection	$1.78 < \theta < 27.55^\circ$
Reflections Collected	11976
Independent Reflections	7776
Absorption Correction	Multi-scan
Max. and Min. Transmission	0.9781 and 0.9404
Structure Solution Technique	Direct methods
Structure Solution Program	SHELXS-97
Refinement Method	Full-matrix least-squares on $F^2$
Refinement Program	SHELXL-97
Function Minimized	$\Sigma w(F_o^2 - F_c^2)^2$
Data / Restraints / Parameters	7776 / 0 / 603
Goodness-of-Fit on $F^2$	1.475
Final $R$ Indices	$I > 2\sigma(I)$ : $R_1 = 0.0355$ , $wR_2 = 0.0970$ all data: $R_1 = 0.0435$ , $wR_2 = 0.1009$
Weighting Scheme	$w = 1/[\sigma^2(F_o^2) + (0.0450P)^2 + 0.0000P]$ where $P = (F_o^2 + 2F_c^2)/3$
Largest Diff. Peak and Hole	0.461 and -0.408 e $\text{\AA}^{-3}$
R.M.S. Deviation from Mean	0.050 e $\text{\AA}^{-3}$

---

X-ray Crystal Structure of **74**

**Figure 217.** ORTEP representation of the structure of **74** in the crystal. Thermal ellipsoids are represented at 50% probability.

**Table 39.** Crystal data for **74**.

Chemical Formula	$C_{19}H_{19}F_2NO_2S$	
$M_r$	363.41 g/mol	
T	100(2) K	
$\lambda$	0.71073 Å	
Crystal Dimensions	0.020 x 0.120 x 0.130 mm	
Crystal Habit	Clear colourless plate	
Crystal System	Monoclinic	
Space Group	$P 2_1/n$	
Unit Cell Dimensions	$a = 13.6341(7)$ Å	$\alpha = 90^\circ$
	$b = 8.4875(4)$ Å	$\beta = 104.312(2)^\circ$
	$c = 15.5303(7)$ Å	$\gamma = 90^\circ$
Unit Cell Volume	$1741.38(14)$ Å <sup>3</sup>	
Z	4	
Density (calcd)	$1.386$ g/cm <sup>3</sup>	
$\mu$	$0.218$ mm <sup>-1</sup>	

---

$F(000)$  760

---

**Table 40.** Data collection and structure refinement for **74**.

---

Diffractometer	Bruker Nonius APEX-II
Radiation Source	Incoatec I $\mu$ S microfocus X-ray tube, Cu
Theta Range for Data Collection	$1.78 < \theta < 27.61^\circ$
Reflections Collected	23857
Independent Reflections	4020
Absorption Correction	Multi-scan
Max. and Min. Transmission	0.9956 and 0.9722
Structure Solution Technique	Direct methods
Structure Solution Program	SHELXS-97
Refinement Method	Full-matrix least-squares on $F^2$
Refinement Program	SHELXL-97
Function Minimized	$\Sigma w(F_o^2 - F_c^2)^2$
Data / Restraints / Parameters	4020 / 0 / 302
Goodness-of-Fit on $F^2$	1.079
Final $R$ Indices	$I > 2\sigma(I)$ : $R_1 = 0.0448$ , $wR_2 = 0.0958$ All data: $R_1 = 0.0831$ , $wR_2 = 0.1195$
Weighting Scheme	$w = 1/[\sigma^2(F_o^2) + (0.0600P)^2 + 0.0000P]$ where $P = (F_o^2 + 2F_c^2)/3$
Largest Diff. Peak and Hole	0.300 and -0.408 e $\text{\AA}^{-3}$
R.M.S. Deviation from Mean	0.081 e $\text{\AA}^{-3}$

---

## X-ray Crystal Structure of 150a

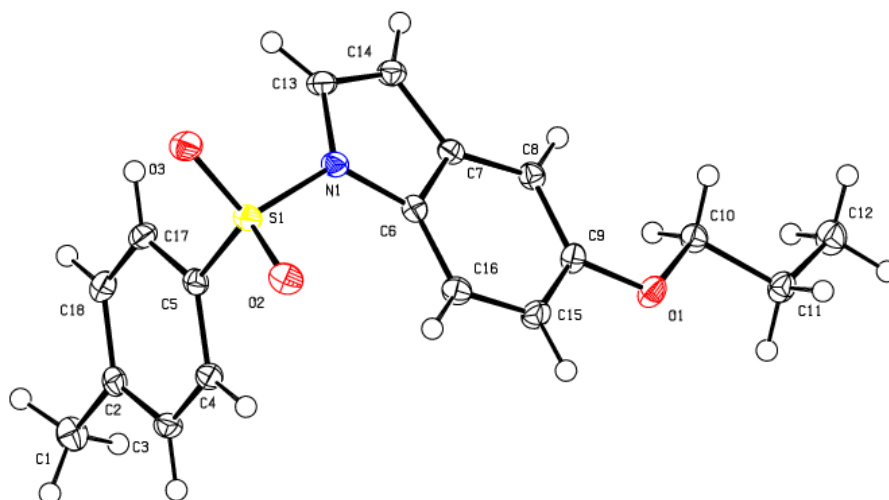


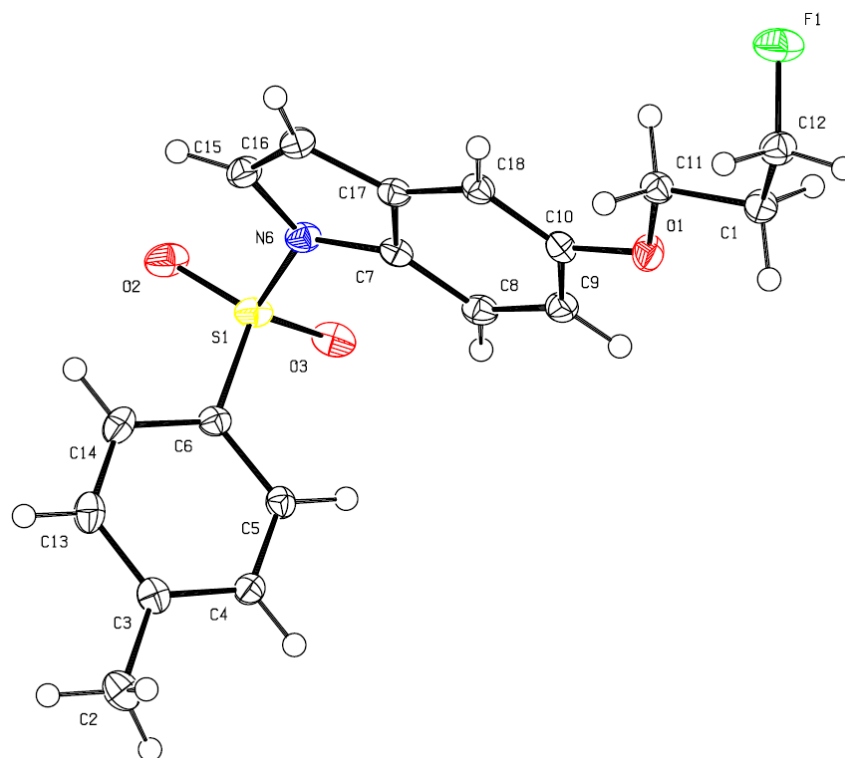
**Figure 218.** ORTEP representation of the structure of **150a** in the crystal. Thermal ellipsoids are represented at 50% probability.

**Table 41.** Crystal data for **150a**.

Chemical Formula	$C_{18}H_{19}NO_3S$	
$M_r$	329.40 g/mol	
T	99.99 K	
Crystal Dimensions	$0.2 \times 0.1 \times 0.06$ mm	
Crystal System	Triclinic	
Space Group	$P\bar{1}$	
Unit Cell Dimensions	$a = 8.1678(6)$ Å	$\alpha = 84.4570(10)^\circ$
	$b = 8.8858(7)$ Å	$\beta = 74.2680(10)^\circ$
	$c = 12.6178(10)$ Å	$\gamma = 66.1630(10)^\circ$
Unit Cell Volume	$806.19(11)$ Å <sup>3</sup>	
Z	2	
Density (calcd)	$1.357$ g/cm <sup>3</sup>	
$\mu$	$0.215$ mm <sup>-1</sup>	
$F(000)$	348	

**Table 42.** Data collection and structure refinement for **150a**.

Diffractometer	Bruker APEX-II CCD
Radiation Source	Incoatec I $\mu$ S microfocus X-ray tube, Cu
Theta Range for Data Collection	$3.36 < \theta < 55.1^\circ$
Reflections Collected	13618
Independent Reflections	3686
Absorption Correction	Multi-scan
Structure Solution Technique	Direct methods
Structure Solution Program	SHELXS-97
Refinement Method	Full-matrix least-squares on $F^2$
Refinement Program	SHELXL-97
Function Minimized	$\Sigma w(F_o^2 - F_c^2)^2$
Data / Restraints / Parameters	3686 / 0 / 210
Goodness-of-Fit on $F^2$	1.035
Final $R$ Indices	$I > 2\sigma(I)$ : $R_1 = 0.0300$ , $wR_2 = 0.0805$ All data: $R_1 = 0.0343$ , $wR_2 = 0.0837$
Largest Diff. Peak and Hole	0.39 and -0.41 e $\text{\AA}^{-3}$

X-ray Crystal Structure of **150b**

**Figure 219.** ORTEP representation of the structure of **150b** in the crystal. Thermal ellipsoids are represented at 50% probability.

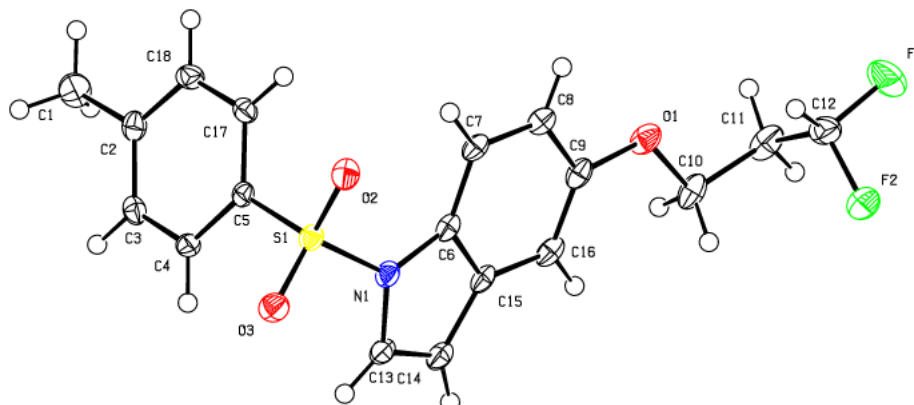
**Table 43.** Crystal data for **150b**.

Chemical Formula	$C_{72}H_{72}F_4N_4O_{12}S_4$	
$M_r$	347.40 g/mol	
T	100.15 K	
Crystal Dimensions	0.19 × 0.13 × 0.06 mm	
Crystal System	Monoclinic	
Space Group	$P 2_1/c$	
Unit Cell Dimensions	$a = 8.1835(5) \text{ \AA}$	$\alpha = 90^\circ$
	$b = 24.7104(17) \text{ \AA}$	$\beta = 128.346(3)^\circ$
	$c = 10.3001(5) \text{ \AA}$	$\gamma = 90^\circ$
Unit Cell Volume	$1633.54(17) \text{ \AA}^3$	
Z	1	
Density (calcd)	$1.413 \text{ g/cm}^3$	

$\mu$	0.225 mm <sup>-1</sup>
$F(000)$	728

**Table 44.** Data collection and structure refinement for **150b**.

Diffractometer	Bruker Apex-II Nonius
Radiation Source	Incoatec I $\mu$ S microfocus X-ray tube, Cu
Theta Range for Data Collection	5.3 < $\theta$ < 55.12°
Reflections Collected	26250
Independent Reflections	3763
Absorption Correction	Multi-scan
Structure Solution Technique	Direct methods
Structure Solution Program	SHELXS-97
Refinement Method	Full-matrix least-squares on $F^2$
Refinement Program	SHELXL-97
Function Minimized	$\Sigma w(F_o^2 - F_c^2)^2$
Data / Restraints / Parameters	3763 / 0 / 218
Goodness-of-Fit on $F^2$	1.027
Final $R$ Indices	$I > 2\sigma(I)$ : $R_1 = 0.0339$ , $wR_2 = 0.0819$ all data: $R_1 = 0.0443$ , $wR_2 = 0.0876$
Largest Diff. Peak and Hole	0.43 and -0.36 e Å <sup>-3</sup>

X-ray Crystal Structure of **150c**

**Figure 220.** ORTEP representation of the structure of **150c** in the crystal. Thermal ellipsoids are represented at 50% probability.

**Table 45.** Crystal data for **150c**.

Chemical Formula	$C_{72}H_{68}F_8N_4O_{12}S_4$
$M_r$	365.40 g/mol
T	100.15 K
Crystal Dimensions	$0.36 \times 0.1 \times 0.04$ mm
Crystal System	Monoclinic
Space Group	$P 2_1/c$
Unit Cell Dimensions	$a = 6.0892(4)$ Å $\alpha = 90^\circ$ $b = 19.1847(12)$ Å $\beta = 112.844(2)^\circ$ $c = 15.4617(8)$ Å $\gamma = 90^\circ$
Unit Cell Volume	$1664.56(17)$ Å <sup>3</sup>
Z	1
Density (calcd)	$1.458$ g/cm <sup>3</sup>
$\mu$	$0.233$ mm <sup>-1</sup>
$F(000)$	760

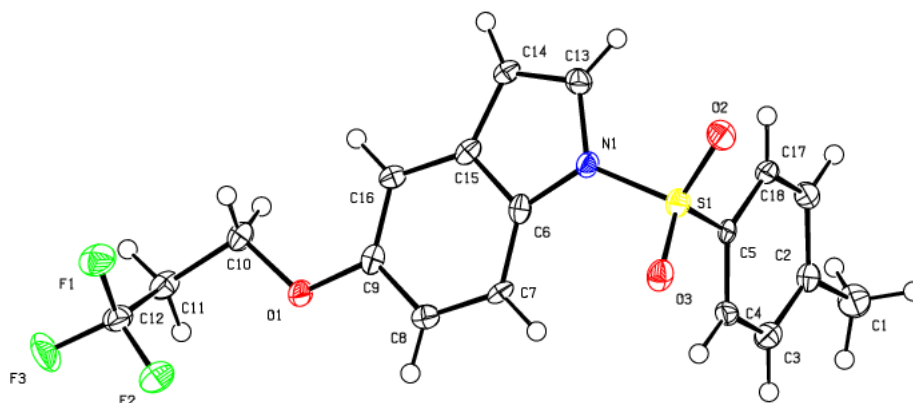


**Table 46.** Data collection and structure refinement for **150c**.

---

Diffractometer	Bruker Apex-II D8
Radiation Source	Incoatec I $\mu$ S microfocus X-ray tube, Cu
Theta Range for Data Collection	$3.56 < \theta < 55^\circ$
Reflections Collected	10409
Independent Reflections	3796
Absorption Correction	Multi-scan
Structure Solution Technique	Direct methods
Structure Solution Program	SHELXS-97
Refinement Method	Full-matrix least-squares on $F^2$
Refinement Program	SHELXL-97
Function Minimized	$\Sigma w(F_o^2 - F_c^2)^2$
Data / Restraints / Parameters	3796 / 0 / 227
Goodness-of-Fit on $F^2$	1.012
Final $R$ Indices	$I > 2\sigma(I)$ : $R_1 = 0.0343$ , $wR_2 = 0.0800$ All data: $R_1 = 0.0519$ , $wR_2 = 0.0878$
Largest Diff. Peak and Hole	0.34 and -0.35 e $\text{\AA}^{-3}$

---

X-ray Crystal Structure of **150d**

**Figure 221.** ORTEP representation of the structure of **150d** in the crystal. Thermal ellipsoids are represented at 50% probability.

**Table 47.** Crystal data for **150d**.

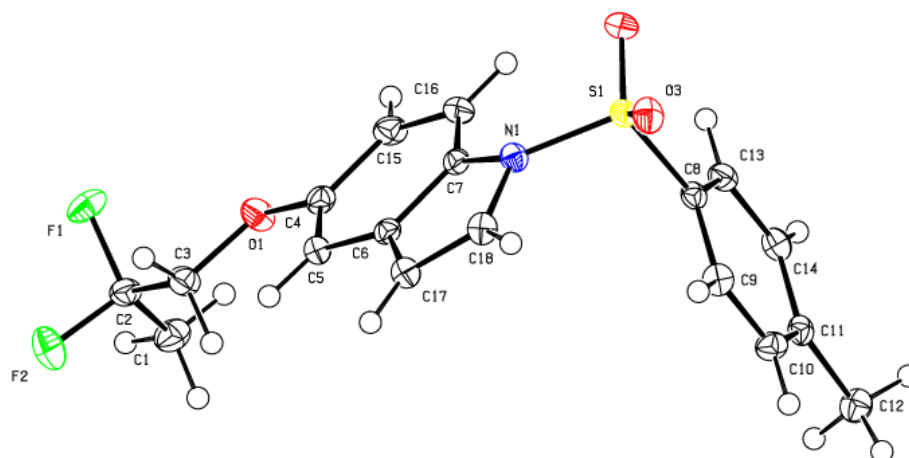
Chemical Formula	$C_{18}H_{16}F_3NO_3S$	
$M_r$	383.38 g/mol	
T	100.15 K	
Crystal Dimensions	$0.17 \times 0.05 \times 0.01$ mm	
Crystal System	Monoclinic	
Space Group	$P 2_1/c$	
Unit Cell Dimensions	$a = 5.9937(9)$ Å	$\alpha = 90^\circ$
	$b = 19.675(4)$ Å	$\beta = 110.827(8)^\circ$
	$c = 15.196(3)$ Å	$\gamma = 90^\circ$
Unit Cell Volume	$1674.9(5)$ Å <sup>3</sup>	
Z	4	
Density (calcd)	$1.520$ g/cm <sup>3</sup>	
$\mu$	$0.244$ mm <sup>-1</sup>	
$F(000)$	792	

**Table 48.** Data collection and structure refinement for **150d**.

---

Diffractometer	Bruker Apex-II Nonius
Radiation Source	Incoatec I $\mu$ S microfocus X-ray tube, Cu
Theta Range for Data Collection	$5.04 < \theta < 49.42^\circ$
Reflections Collected	13250
Independent Reflections	2848
Absorption Correction	Multi-scan
Structure Solution Technique	Direct methods
Structure Solution Program	SHELXS-97
Refinement Method	Full-matrix least-squares on $F^2$
Refinement Program	SHELXL-97
Function Minimized	$\Sigma w(F_o^2 - F_c^2)^2$
Data / Restraints / Parameters	2848 / 0 / 236
Goodness-of-Fit on $F^2$	1.000
Final $R$ Indices	$I > 2\sigma(I)$ : $R_1 = 0.0469$ , $wR_2 = 0.0881$ All data: $R_1 = 0.0935$ , $wR_2 = 0.1012$
Largest Diff. Peak and Hole	0.26 and -0.43 e $\text{\AA}^{-3}$

---

X-ray Crystal Structure of **167**

**Figure 222.** ORTEP representation of the structure of **167** in the crystal. Thermal ellipsoids are represented at 50% probability.

**Table 49.** Crystal data for **167**.

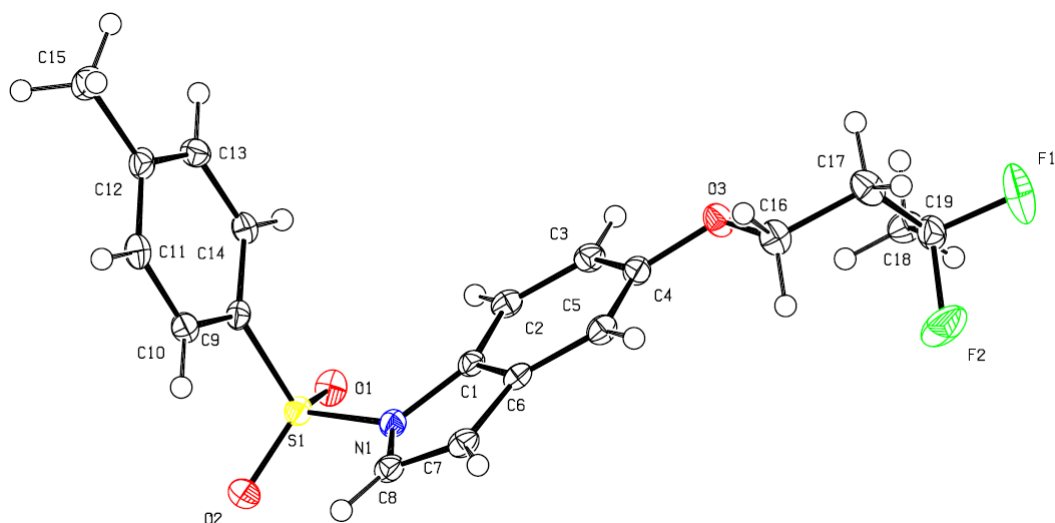
Chemical Formula	$C_{18}H_{17}NO_3F_2S$	
$M_r$	365.38 g/mol	
T	100.02 K	
$\lambda$	0.71073 Å	
Crystal Dimensions	0.24 × 0.18 × 0.1 mm	
Crystal System	Triclinic	
Space Group	$P\bar{1}$	
Unit Cell Dimensions	$a = 7.7010(2)$ Å	$\alpha = 81.3390(10)^\circ$
	$b = 9.2801(3)$ Å	$\beta = 72.9800(10)^\circ$
	$c = 13.0373(5)$ Å	$\gamma = 68.410(2)^\circ$
Unit Cell Volume	827.45(5) Å <sup>3</sup>	
Z	2	
Density (calcd)	1.467 g/cm <sup>3</sup>	
$\mu$	0.234 mm <sup>-1</sup>	
$F(000)$	380	

**Table 50.** Data collection and structure refinement for **167**.

---

Diffractometer	Bruker Apex-II Nonius
Radiation Source	Incoatec I $\mu$ S microfocus X-ray tube, Cu
Theta Range for Data Collection	$4.726 < \theta < 54.96^\circ$
Reflections Collected	6469
Independent Reflections	3653
Absorption Correction	Multi-scan
Structure Solution Technique	Direct methods
Structure Solution Program	SHELXS-97
Refinement Method	Full-matrix least-squares on $F^2$
Refinement Program	SHELXL-97
Function Minimized	$\Sigma w(F_o^2 - F_c^2)^2$
Data / Restraints / Parameters	3653 / 0 / 228
Goodness-of-Fit on $F^2$	1.035
Final $R$ Indices	$I > 2\sigma(I)$ : $R_1 = 0.0366$ , $wR_2 = 0.0886$ All data: $R_1 = 0.0448$ , $wR_2 = 0.0938$
Largest Diff. Peak and Hole	0.30 and -0.38 e $\text{\AA}^{-3}$

---

X-ray Crystal Structure of **173**

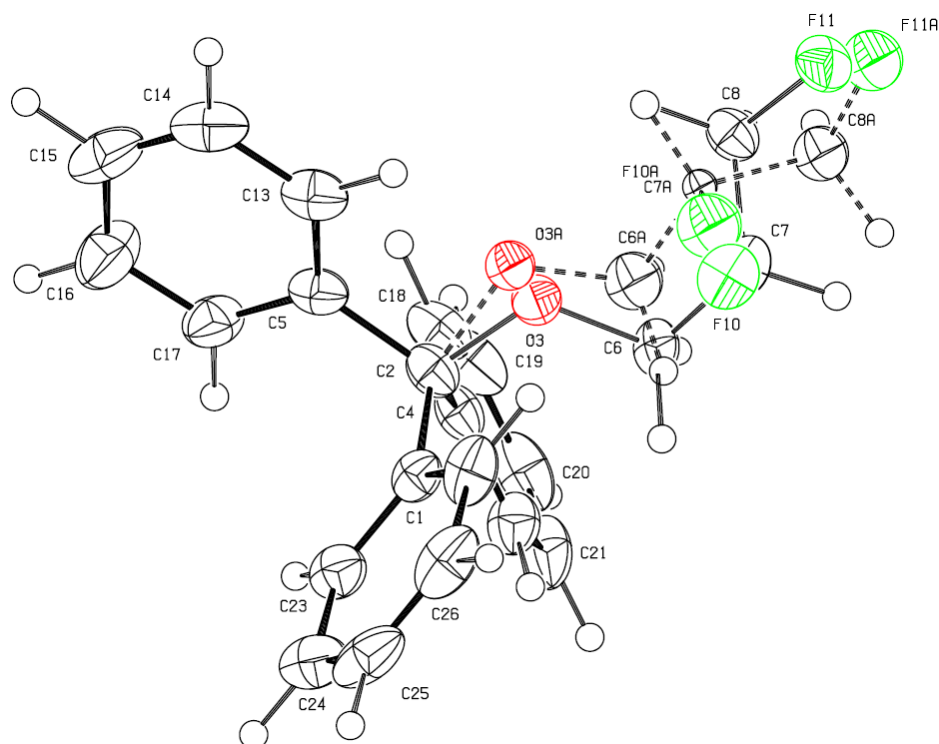
**Figure 223.** ORTEP representation of the structure of **173** in the crystal. Thermal ellipsoids are represented at 50% probability.

**Table 51.** Crystal data for **173**.

Chemical Formula	$C_{19}H_{19}F_2NO_3S$	
$M_r$	379.41 g/mol	
T	100.0 K	
$\lambda$	0.71073 Å	
Crystal Dimensions	0.18 × 0.13 × 0.05 mm	
Crystal System	Monoclinic	
Space Group	$P 2_1/n$	
Unit Cell Dimensions	$a = 6.1713(2)$ Å	$\alpha = 90^\circ$
	$b = 19.8855(7)$ Å	$\beta = 92.1590(10)^\circ$
	$c = 14.2787(5)$ Å	$\gamma = 90^\circ$
Unit Cell Volume	1751.03(10) Å <sup>3</sup>	
Z	4	
Density (calcd)	1.439 g/cm <sup>3</sup>	
$\mu$	0.224 mm <sup>-1</sup>	
$F(000)$	792	

**Table 52.** Data collection and structure refinement for **173**.

Diffractometer	Bruker Nonius Apex-II
Radiation Source	Incoatec I $\mu$ S microfocus X-ray tube, Cu
Theta Range for Data Collection	$4.994 < \theta < 55.218^\circ$
Reflections Collected	17833
Independent Reflections	4023
Absorption Correction	Multi-scan
Structure Solution Technique	Direct methods
Structure Solution Program	SHELXS-97
Refinement Method	Full-matrix least-squares on $F^2$
Refinement Program	SHELXL-97
Function Minimized	$\Sigma w(F_o^2 - F_c^2)^2$
Data / Restraints / Parameters	4023 / 0 / 237
Goodness-of-Fit on $F^2$	1.019
Final $R$ Indices	$I > 2\sigma(I)$ : $R_1 = 0.0379$ , $wR_2 = 0.0872$ All data: $R_1 = 0.0516$ , $wR_2 = 0.0944$
Largest Diff. Peak and Hole	0.59 and -0.40 e $\text{\AA}^{-3}$

X-ray Crystal Structure of **155**

**Figure 224.** ORTEP representation of the structure of **155** in the crystal. Thermal ellipsoids are represented at 50% probability.

**Table 53.** Crystal data for **155**.

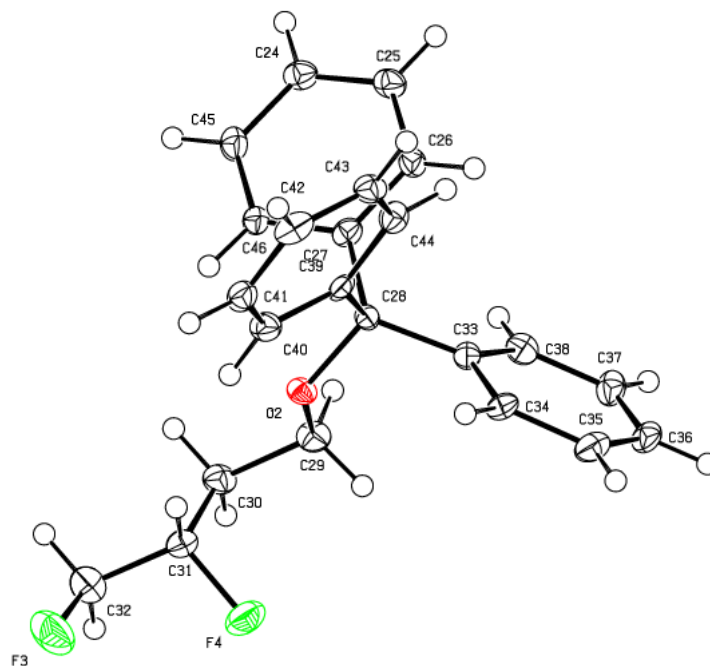
Chemical Formula	$C_{22}H_{20}F_2O$	
$M_r$	338.38 g/mol	
T	100(2) K	
$\lambda$	0.71073 Å	
Crystal Dimensions	0.020 x 0.160 x 0.240 mm	
Crystal Habit	Clear colourless plate	
Crystal System	Triclinic	
Space Group	$P\bar{1}$	
Unit Cell Dimensions	$a = 8.8314(8)$ Å	$\alpha = 90.189(3)^\circ$
	$b = 11.2354(10)$ Å	$\beta = 92.110(3)^\circ$
	$c = 17.4532(17)$ Å	$\gamma = 90.131(3)^\circ$
Unit Cell Volume	$1730.6(3)$ Å <sup>3</sup>	



<i>Z</i>	4
Density (calcd)	1.299 g/cm <sup>3</sup>
$\mu$	0.093 mm <sup>-1</sup>
<i>F</i> (000)	712

**Table 54.** Data collection and structure refinement for **155**.

Diffractometer	Bruker Nonius APEX II
Radiation Source	Incoatec I $\mu$ S microfocus X-ray tube, Cu
Theta Range for Data Collection	1.81 < $\theta$ < 24.67°
Reflections Collected	14100
Independent Reflections	5578
Absorption Correction	Multi-scan
Max. and Min. Transmission	0.9986 and 0.9781
Structure Solution Technique	Direct methods
Structure Solution Program	SHELXS-97
Refinement Method	Full-matrix least-squares on $F^2$
Refinement Program	SHELXL-97
Function Minimized	$\Sigma w(F_o^2 - F_c^2)^2$
Data / Restraints / Parameters	5578 / 0 / 502
Goodness-of-Fit on $F^2$	1.164
Final <i>R</i> Indices	$I > 2\sigma(I)$ : $R_1 = 0.0666$ , $wR_2 = 0.1422$ All data: $R_1 = 0.1338$ , $wR_2 = 0.1622$
Weighting Scheme	$w = 1/[\sigma^2(F_o^2) + (0.0650P)^2 + 0.0000P]$ where $P = (F_o^2 + 2F_c^2)/3$
Largest Diff. Peak and Hole	0.255 and -0.282 e Å <sup>-3</sup>
R.M.S. Deviation from Mean	0.064 e Å <sup>-3</sup>

X-ray Crystal Structure of **156**

**Figure 225.** ORTEP representation of the structure of **156** in the crystal. Thermal ellipsoids are represented at 50% probability.

**Table 55.** Crystal data for **156**.

Chemical Formula	$C_{23}H_{22}OF_2$	
$M_r$	352.40 g/mol	
T	100.02 K	
$\lambda$	1.54178 Å	
Crystal Dimensions	0.08 × 0.05 × 0.03 mm	
Crystal System	Monoclinic	
Space Group	$Pc$	
Unit Cell Dimensions	$a = 10.5114(3)$ Å	$\alpha = 90^\circ$
	$b = 8.6268(3)$ Å	$\beta = 90.534(2)^\circ$
	$c = 60.352(2)$ Å	$\gamma = 90^\circ$
Unit Cell Volume	$5472.5(3)$ Å <sup>3</sup>	
Z	12	
Density (calcd)	1.283 g/cm <sup>3</sup>	
$\mu$	0.742 mm <sup>-1</sup>	

---

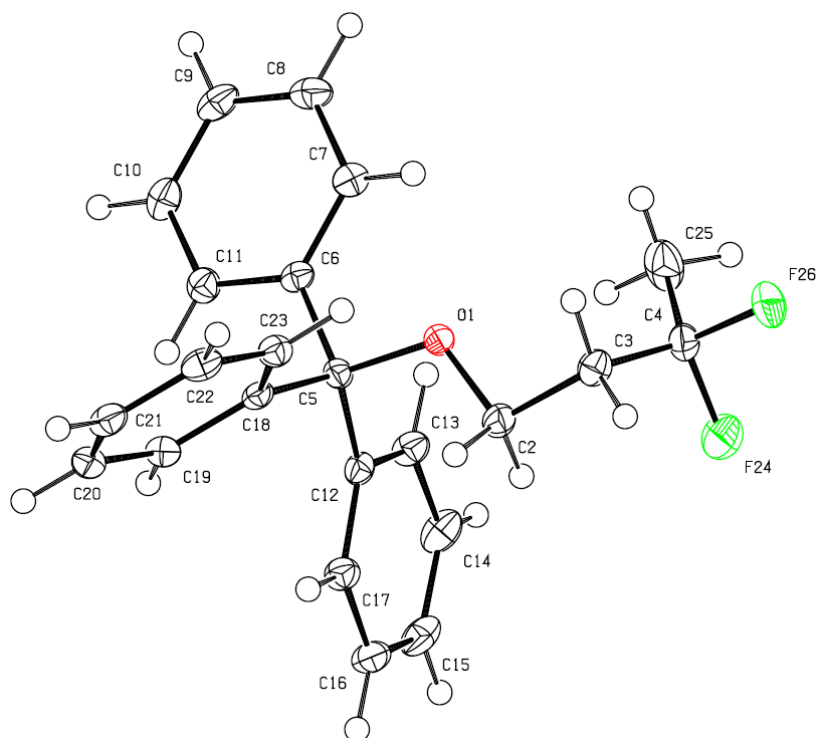
 $F(000)$ 2232

---

**Table 56.** Data collection and structure refinement for **156**.

Diffractometer	Bruker Apex-II D8
Radiation Source	Incoatec I $\mu$ S microfocus X-ray tube, Cu
Theta Range for Data Collection	$8.412 < \theta < 133.068^\circ$
Reflections Collected	32549
Independent Reflections	14788
Absorption Correction	Multi-scan
Structure Solution Technique	Direct methods
Structure Solution Program	SHELXS-97
Refinement Method	Full-matrix least-squares on $F^2$
Refinement Program	SHELXL-97
Function Minimized	$\Sigma w(F_o^2 - F_c^2)^2$
Data / Restraints / Parameters	14788 / 2 / 1405
Goodness-of-Fit on $F^2$	1.061
Final $R$ Indices	$I > 2\sigma(I)$ : $R_1 = 0.0565$ , $wR_2 = 0.1426$ All data: $R_1 = 0.0609$ , $wR_2 = 0.1458$
Largest Diff. Peak and Hole	1.00 and -0.44 e $\text{\AA}^{-3}$

---

X-ray Crystal Structure of **171**

**Figure 226.** ORTEP representation of the structure of **171** in the crystal. Thermal ellipsoids are represented at 50% probability.

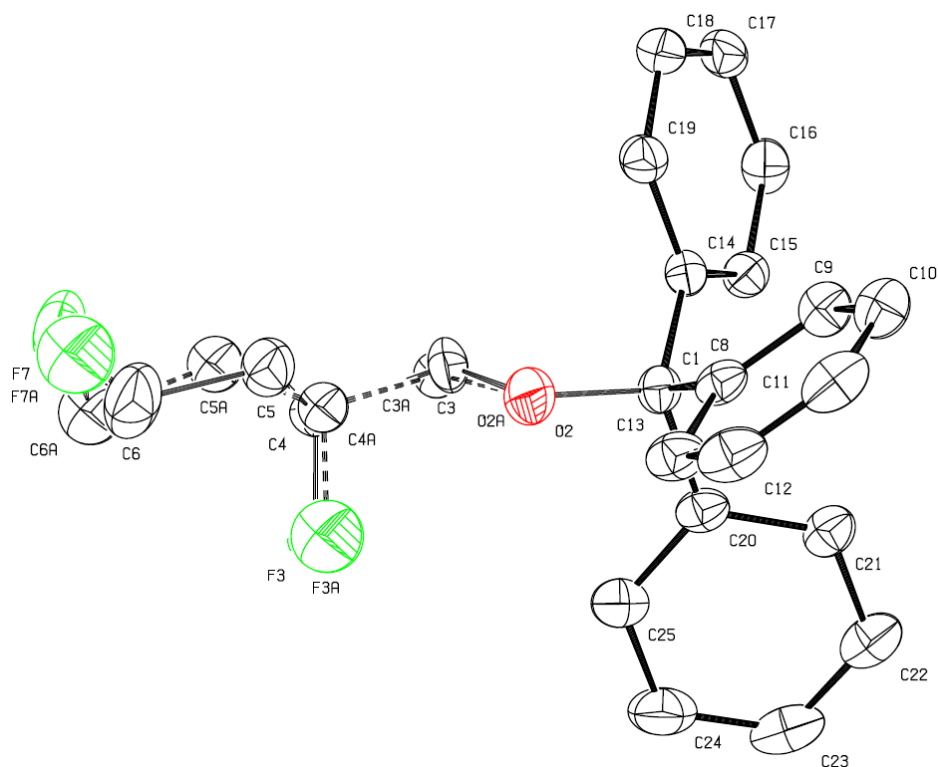
**Table 57.** Crystal data for **171**.

Chemical Formula	$C_{23}H_{22}F_2O$	
$M_r$	352.41 g/mol	
T	100(2) K	
$\lambda$	0.71073 Å	
Crystal Dimensions	0.200 x 0.220 x 0.260 mm	
Crystal Habit	Clear colourless rod	
Crystal System	Orthorhombic	
Space Group	$P bca$	
Unit Cell Dimensions	$a = 11.0380(4)$ Å	$\alpha = 90^\circ$
	$b = 13.9144(5)$ Å	$\beta = 90^\circ$
	$c = 23.9773(9)$ Å	$\gamma = 90^\circ$
Unit Cell Volume	$3682.6(2)$ Å <sup>3</sup>	

<i>Z</i>	8
Density (calcd)	1.271 g/cm <sup>3</sup>
$\mu$	0.090 mm <sup>-1</sup>
<i>F</i> (000)	1488

**Table 58.** Data collection and structure refinement for **171**.

Diffractometer	Bruker Nonius APEX-II
Radiation Source	Incoatec I $\mu$ S microfocus X-ray tube, Cu
Theta Range for Data Collection	2.50 < $\theta$ < 27.57°
Reflections Collected	31641
Independent Reflections	4242
Absorption Correction	Multi-scan
Max. and Min. Transmission	0.9822 and 0.9770
Structure Solution Technique	Direct methods
Structure Solution Program	SHELXS-97
Refinement Method	Full-matrix least-squares on $F^2$
Refinement Program	SHELXL-97
Function Minimized	$\Sigma w(F_o^2 - F_c^2)^2$
Data / Restraints / Parameters	4242 / 0 / 324
Goodness-of-Fit on $F^2$	1.424
Final <i>R</i> Indices	$I > 2\sigma(I)$ : $R_1 = 0.0398$ , $wR_2 = 0.0861$ All data: $R_1 = 0.0599$ , $wR_2 = 0.0920$
Weighting Scheme	$w = 1/[\sigma^2(F_o^2) + (0.0350P)^2 + 0.0000P]$ where $P = (F_o^2 + 2F_c^2)/3$
Largest Diff. Peak and Hole	0.261 and -0.270 e Å <sup>-3</sup>
R.M.S. Deviation from Mean	0.049 e Å <sup>-3</sup>

X-ray Crystal Structure of **189**

**Figure 227.** ORTEP representation of the structure of **189** in the crystal. Thermal ellipsoids are represented at 50% probability. Hydrogen atoms have been removed for clarity.

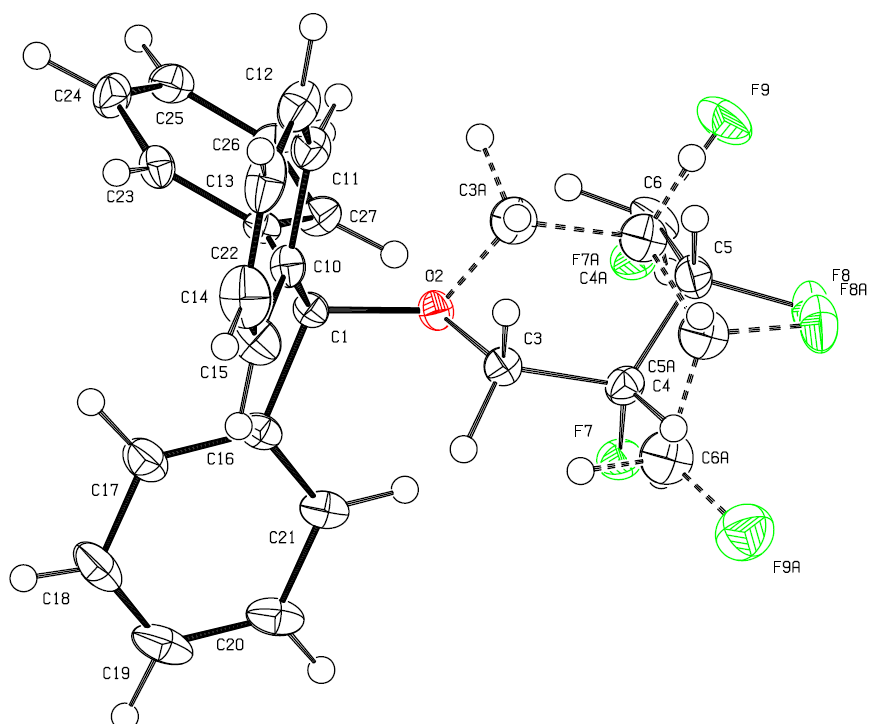
**Table 59.** Crystal data for **189**.

Chemical Formula	$C_{23}H_{22}F_2O$
$M_r$	352.41 g/mol
T	100(2) K
$\lambda$	0.71073 Å
Crystal Dimensions	0.050 x 0.090 x 0.170 mm
Crystal Habit	Clear colourless plate
Crystal System	Orthorhombic
Space Group	$P\ ccn$
Unit Cell Dimensions	$a = 14.7196(12)$ Å $\alpha = 90^\circ$ $b = 33.963(3)$ Å $\beta = 90^\circ$ $c = 7.2254(5)$ Å $\gamma = 90^\circ$
Unit Cell Volume	$3612.1(5)$ Å <sup>3</sup>

<i>Z</i>	8
Density (calcd)	1.296 g/cm <sup>3</sup>
$\mu$	0.092 mm <sup>-1</sup>
<i>F</i> (000)	1488

**Table 60.** Data collection and structure refinement for **189**.

Diffractometer	Bruker Nonius APEX-II
Radiation Source	Incoatec I $\mu$ S microfocus X-ray tube, Cu
Theta Range for Data Collection	$2.77 < \theta < 27.61^\circ$
Reflections Collected	40924
Independent Reflections	4200
Absorption Correction	Multi-scan
Max. and Min. Transmission	0.9954 and 0.9846
Structure Solution Technique	Direct methods
Structure Solution Program	SHELXS-97
Refinement Method	Full-matrix least-squares on $F^2$
Refinement Program	SHELXL-97
Function Minimized	$\Sigma w(F_o^2 - F_c^2)^2$
Data / Restraints / Parameters	4200 / 8 / 304
Goodness-of-Fit on $F^2$	1.152
Final <i>R</i> Indices	$I > 2\sigma(I)$ : $R_1 = 0.0537$ , $wR_2 = 0.1170$ All data: $R_1 = 0.1060$ , $wR_2 = 0.1345$
Weighting Scheme	$w = 1/[\sigma^2(F_o^2) + (0.0600P)^2 + 0.0000P]$ where $P = (F_o^2 + 2F_c^2)/3$
Largest Diff. Peak and Hole	0.243 and -0.294 e $\text{\AA}^{-3}$
R.M.S. Deviation from Mean	0.044 e $\text{\AA}^{-3}$

X-ray Crystal Structure of **182**

**Figure 228.** ORTEP representation of the structure of **182** in the crystal. Thermal ellipsoids are represented at 50% probability.

**Table 61.** Crystal data for **182**.

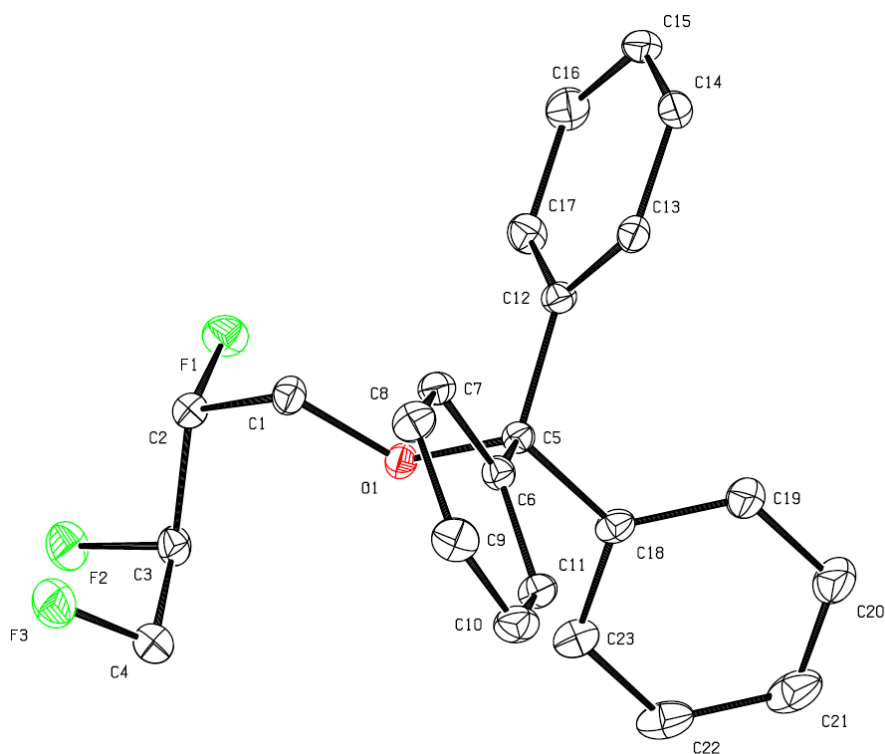
Chemical Formula	$C_{23}H_{21}F_3O$	
$M_r$	370.40 g/mol	
T	273(2) K	
$\lambda$	0.71073 Å	
Crystal Dimensions	0.140 x 0.220 x 0.280 mm	
Crystal Habit	Clear colourless prism	
Crystal System	Monoclinic	
Space Group	$P 2_1/n$	
Unit Cell Dimensions	$a = 8.6890(2)$ Å	$\alpha = 90^\circ$
	$b = 17.7460(3)$ Å	$\beta = 102.3550(10)^\circ$
	$c = 12.2941(2)$ Å	$\gamma = 90^\circ$
Unit Cell Volume	$1851.79(6)$ Å <sup>3</sup>	
Z	4	



Density (calcd)	1.329 g/cm <sup>3</sup>
$\mu$	0.100 mm <sup>-1</sup>
$F(000)$	776

**Table 62.** Data collection and structure refinement for **182**.

Diffractometer	Bruker Kappa Apex-II Duo
Radiation Source	Incoatec I $\mu$ S microfocus X-ray tube, Cu
Theta Range for Data Collection	2.30 < $\theta$ < 29.16°
Reflections Collected	18303
Independent Reflections	4974
Absorption Correction	Multi-scan
Structure Solution Technique	Direct methods
Structure Solution Program	SHELXS-97
Refinement Method	Full-matrix least-squares on $F^2$
Refinement Program	SHELXL-97
Function Minimized	$\Sigma w(F_o^2 - F_c^2)^2$
Data / Restraints / Parameters	4974 / 8 / 351
Goodness-of-Fit on $F^2$	1.320
Final $R$ Indices	$I > 2\sigma(I)$ : $R_1 = 0.0463$ , $wR_2 = 0.1646$ All data: $R_1 = 0.0544$ , $wR_2 = 0.1699$
Weighting Scheme	$w = 1/[\sigma^2(F_o^2) + (0.1000P)^2 + 0.0000P]$ where $P = (F_o^2 + 2F_c^2)/3$
Largest Diff. Peak and Hole	0.389 and -0.296 e Å <sup>-3</sup>
R.M.S. Deviation from Mean	0.046 e Å <sup>-3</sup>

X-ray Crystal Structure of **181**

**Figure 229.** ORTEP representation of the structure of **181** in the crystal. Thermal ellipsoids are represented at 50% probability. Hydrogen atoms have been removed for clarity.

**Table 63.** Crystal data for **181**.

Chemical Formula	$C_{23}H_{21}F_3O$	
$M_r$	370.40 g/mol	
T	100(2) K	
$\lambda$	0.71073 Å	
Crystal Dimensions	0.200 x 0.280 x 0.360 mm	
Crystal Habit	Clear colourless prism	
Crystal System	Monoclinic	
Space Group	$P 2_1$	
Unit Cell Dimensions	$a = 8.5877(9)$ Å	$\alpha = 90^\circ$
	$b = 11.4668(11)$ Å	$\beta = 92.568(4)^\circ$
	$c = 9.4810(10)$ Å	$\gamma = 90^\circ$
Unit Cell Volume	932.69(17) Å <sup>3</sup>	

$Z$	2
Density (calcd)	1.319 g/cm <sup>3</sup>
$\mu$	0.100 mm <sup>-1</sup>
$F(000)$	388

**Table 64.** Data collection and structure refinement for **181**.

Diffractometer	Bruker Nonius APEX-II
Radiation Source	Incoatec I $\mu$ S microfocus X-ray tube, Cu
Theta Range for Data Collection	2.15 < $\theta$ < 27.63°
Reflections Collected	7637
Independent Reflections	4161
Absorption Correction	Multi-scan
Max. and Min. Transmission	0.9803 and 0.9650
Structure Solution Technique	Direct methods
Structure Solution Program	SHELXS-97
Refinement Method	Full-matrix least-squares on $F^2$
Refinement Program	SHELXL-97
Function Minimized	$\Sigma w(F_o^2 - F_c^2)^2$
Data / Restraints / Parameters	4161 / 1 / 328
Goodness-of-Fit on $F^2$	1.345
Final $R$ Indices	$I > 2\sigma(I)$ : $R_1 = 0.0291$ , $wR_2 = 0.0832$ All data: $R_1 = 0.0309$ , $wR_2 = 0.0843$
Weighting Scheme	$w = 1/[\sigma^2(F_o^2) + (0.0450P)^2 + 0.0000P]$ where $P = (F_o^2 + 2F_c^2)/3$
Largest Diff. Peak and Hole	0.285 and -0.202 e Å <sup>-3</sup>
R.M.S. Deviation from Mean	0.040 e Å <sup>-3</sup>



# Abbreviations

atm	atmosphere
ADMET	absorption, distribution, metabolism, excretion, toxicity
AIBN	2,2'-azobis(2-methylpropionitrile)
aq	aqueous
ax	axial
b	broad
B	base
Bn	benzyl
bs	broad singlet
Bu	butyl
ca.	circa, approximately
c.a.	commercially available
CAM	ceric ammonium molybdate
calcd	calculated
cat.	catalytic
CDI	1,1'-carbonyldiimidazole
$Cl_{int}$	intrinsic clearance rate
$c \log P$	calculated $\log P$
CYP	cytochrome P-450
$\Delta$	difference; heating
d	day(s)
DAST	diethylaminosulfur trifluoride
DBH	1,3-dibromo-5,5-dimethylhydantoin
DBU	1,8-diazabicyclo[5.4.0]undec-7-ene
DCM	dichloromethane

DFT	density functional theory
DIBAL-H	diisobutylaluminum hydride
DIPEA	<i>N,N</i> -diisopropylethylamine
DMAP	<i>N,N</i> -dimethylpyridin-4-amine
DMF	<i>N,N</i> -dimethylformamide
DMSO	dimethyl sulfoxide
dr	diastereoisomeric ratio
ee	enantiomeric excess
EC <sub>50</sub>	half maximal (50%) effective concentration
EI	electron impact ionization
eq	equatorial
equiv	stoichiometric equivalents
ESI	electron-spray ionization
<i>et al.</i>	<i>et alii</i> , and others
Et <sub>2</sub> O	diethyl ether
EtOAc	ethyl acetate
exp	experimental
FG	functional group
<i>g</i>	<i>gauche</i>
<i>gem</i>	geminal
HF	hydrofluoric acid
HPLC	high performance liquid chromatography
HRMS	high resolution mass spectrometry
HTS	high throughput screening
<i>i</i>	<i>iso</i>
IC <sub>50</sub>	half maximal (50%) inhibitory concentration

---

IV	intravenous
LG	leaving group
$\log D$	logarithm of the 1-octanol/H <sub>2</sub> O distribution coefficient
$\log P$	logarithm of the 1-octanol/H <sub>2</sub> O partition coefficient
<i>m</i>	<i>meta</i>
M	molecular ion; molar
Me	methyl
MeCN	acetonitrile
MeI	iodomethane
<i>m</i> -CPBA	<i>meta</i> -chloroperoxybenzoic acid
MMPA	matched molecular pair analysis
MS	mass spectrometry
n.a.	not available
NBS	<i>N</i> -bromosuccinimide
<i>n</i> -BuLi	<i>n</i> -butyllithium
NfF	perfluorobutanesulfonyl fluoride; nonafllyl fluoride
NMO	<i>N</i> -methylnmorpholine- <i>N</i> -oxide
NMR	nuclear magnetic resonance
Ns	4-nitrobenzenesulfonyl; nosyl
<i>o</i>	<i>ortho</i>
ORTEP	Oak Ridge Thermal Ellipsoid Plot
<i>p</i>	<i>para</i>
PG	protecting group
pH	negative logarithm of proton concentration, $-\log_{10}([H^+])$
PK	pharmacokinetics
$pK_a$	negative logarithm of the acid dissociation constant

---

PO	<i>per os</i>
ppm	parts per million
quant.	quantitative
rac	racemic
rel	relative
$R_f$	retention factor
rt	room temperature
<i>Sol.</i>	aqueous solubility
<i>t</i>	<i>trans, tert</i>
$t_{1/2}$	half-life
TBAF	tetrabutylammonium fluoride
TBAI	tetrabutylammonium iodide
TBS	<i>t</i> -butyldimethylsilyl
TEA	triethylamine
Tf	trifluoromethanesulfonyl
TfOH	trifluoromethanesulfonic acid
THF	tetrahydrofuran
TLC	thin-layer chromatography
TMEDA	<i>N,N,N',N'</i> -tetramethylethane-1,2-diamine
Tr	trityl
Ts	tosyl, 4-methylbenzenesulfonyl
UV	ultraviolet
<i>vic</i>	vicinal



---

## References

- (1) Harper, D. B.; O'Hagan, D.; Murphy, C. D. In *Natural Production of Organohalogen Compounds*; Gribble, G., Ed.; The Handbook of Environmental Chemistry; Springer Berlin Heidelberg, 2003; pp. 141–169.
- (2) Greenwood, N. N.; Earnshaw, A. *Chemistry of the elements*; Butterworth Heinemann, 1998.
- (3) Kirsch, P. *Modern Fluoroorganic Chemistry*; Wiley-VCH, Weinheim, Germany, 2006.
- (4) Moissan, H. *Le fluor et ses composés*; 1900.
- (5) Weeks, M. E. *J. Chem. Educ.* **1932**, 9, 1915.
- (6) Bégué, J.-P.; Bonnet-Delpon, D. *Bioorganic and Medicinal Chemistry of Fluorine*; John Wiley & Sons, Inc., Hoboken, New Jersey, 2007.
- (7) Wang, J.; Sánchez-Roselló, M.; Aceña, J. L.; del Pozo, C.; Sorochinsky, A. E.; Fustero, S.; Soloshonok, V. A.; Liu, H. *Chem. Rev.* **2013**.
- (8) Fried, J.; Sabo, E. F. *J. Am. Chem. Soc.* **1953**, 75, 2273.
- (9) Fried, J.; Sabo, E. F. *J. Am. Chem. Soc.* **1954**, 76, 1455.
- (10) Heidelberger, C.; Chaudhuri, N. K.; Danneberg, P.; Mooren, D.; Griesbach, L.; Duschinsky, R.; Schnitzer, R. J.; Plevin, E.; Scheiner, J. *Nature* **1957**, 179, 663.
- (11) *Fluorine in Medicinal Chemistry and Chemical Biology*; Ojima, I., Ed.; 2009.
- (12) Smart, B. E. *J. Fluor. Chem.* **2001**, 109, 3.
- (13) Biffinger, J. C.; Kim, H. W.; DiMagno, S. G. *ChemBioChem* **2004**, 5, 622.
- (14) Cametti, M.; Crousse, B.; Metrangolo, P.; Milani, R.; Resnati, G. *Chem. Soc. Rev.* **2011**, 41, 31.
- (15) Dolbier Jr., W. R. *J. Fluor. Chem.* **2005**, 126, 157.
- (16) Wang, P.; Fichera, A.; Kumar, K.; Tirrell, D. A. *Angew. Chem. Int. Ed.* **2004**, 43, 3664.
- (17) Bott, G.; Field, L. D.; Sternhell, S. *J. Am. Chem. Soc.* **1980**, 102, 5618.
- (18) Nagai, T.; Nishioka, G.; Koyama, M.; Ando, A.; Miki, T.; Kumadaki, I. *Chem. Pharm. Bull. (Tokyo)* **1991**, 39, 233.
- (19) Leroux, F. *ChemBioChem* **2004**, 5, 644.
- (20) Schlosser, M.; Michel, D. *Tetrahedron* **1996**, 52, 99.
- (21) Götzö, S. P.; Seebach, D.; Sanglier, J.-J. *Eur. J. Org. Chem.* **1999**, 1999, 2533.

- (22) Betageri, R.; Zhang, Y.; Zindell, R. M.; Kuzmich, D.; Kirrane, T. M.; Bentzien, J.; Cardozo, M.; Capolino, A. J.; Fadra, T. N.; Nelson, R. M.; Paw, Z.; Shih, D.-T.; Shih, C.-K.; Zuvella-Jelaska, L.; Nabozny, G.; Thomson, D. S. *Bioorg. Med. Chem. Lett.* **2005**, *15*, 4761.
- (23) O'Hagan, D. *Chem. Soc. Rev.* **2008**, *37*, 308.
- (24) Briggs, C. R. S.; O'Hagan, D.; Howard, J. A. K.; Yufit, D. S. *J. Fluor. Chem.* **2003**, *119*, 9.
- (25) Briggs, C. R. S.; O'Hagan, D.; Rzepa, H. S.; Slawin, A. M. Z. *J. Fluor. Chem.* **2004**, *125*, 19.
- (26) Briggs, C. R. S.; Allen, M. J.; O'Hagan, D.; Tozer, D. J.; Slawin, A. M. Z.; Goeta, A. E.; Howard, J. A. K. *Org. Biomol. Chem.* **2004**, *2*, 732.
- (27) Imori, T.; Murai, Y.; Wakizawa, Y.; Ohtsuka, Y.; Ohuchi, S.; Kodama, Y.; Oishi, T. *Chem. Pharm. Bull. (Tokyo)* **1993**, *41*, 775.
- (28) Kerns, E. H.; Di, L. *Drug-like Properties: Concepts, Structure Design and Methods*; Academic Press: San Diego, 2008.
- (29) Dunitz, J. D.; Taylor, R. *Chem. – Eur. J.* **1997**, *3*, 89.
- (30) O'Hagan, D.; Rzepa, H. S. *Chem. Commun.* **1997**, 645.
- (31) Howard, J. A. K.; Hoy, V. J.; O'Hagan, D.; Smith, G. T. *Tetrahedron* **1996**, *52*, 12613.
- (32) Murray-Rust, P.; Stallings, W. C.; Monti, C. T.; Preston, R. K.; Glusker, J. P. *J. Am. Chem. Soc.* **1983**, *105*, 3206.
- (33) Carosati, E.; Sciabola, S.; Cruciani, G. *J. Med. Chem.* **2004**, *47*, 5114.
- (34) Takahashi, L. H.; Radhakrishnan, R.; Rosenfield, R. E.; Meyer, E. F.; Trainor, D. A. *J. Am. Chem. Soc.* **1989**, *111*, 3368.
- (35) Groves, M. R.; Yao, Z.-J.; Roller, P. P.; Burke, Terrence R.; Barford, D. *Biochemistry (Mosc.)* **1998**, *37*, 17773.
- (36) Abraham, M. H.; Duce, P. P.; Prior, D. V.; Barratt, D. G.; Morris, J. J.; Taylor, P. J. *J. Chem. Soc. Perkin Trans. 2* **1989**, 1355.
- (37) Ouvrard, C.; Berthelot, M.; Laurence, C. *J. Chem. Soc. Perkin Trans. 2* **1999**, 1357.
- (38) Donetti, A.; Cereda, E.; Ezhaya, A.; Micheletti, R. *J. Med. Chem.* **1989**, *32*, 957.
- (39) Grunewald, G. L.; Seim, M. R.; Lu, J.; Makboul, M.; Criscione, K. R. *J. Med. Chem.* **2006**, *49*, 2939.
- (40) Gung, B. W.; Amicangelo, J. C. *J. Org. Chem.* **2006**, *71*, 9261.
- (41) El-azizi, Y.; Schmitzer, A.; Collins, S. K. *Angew. Chem. Int. Ed.* **2006**, *45*, 968.

- 
- (42) Razgulin, A. V.; Mecozzi, S. *J. Med. Chem.* **2006**, *49*, 7902.
- (43) Lai, J. S.; Kool, E. T. *Chem. – Eur. J.* **2005**, *11*, 2966.
- (44) Gerebtzoff, G.; Li-Blatter, X.; Fischer, H.; Frentzel, A.; Seelig, A. *ChemBioChem* **2004**, *5*, 676.
- (45) Huchet, Q. A.; Kuhn, B.; Wagner, B.; Fischer, H.; Kansy, M.; Zimmerli, D.; Carreira, E. M.; Müller, K. *J. Fluor. Chem.* **2013**, *152*, 119.
- (46) Müller, K.; Faeh, C.; Diederich, F. *Science* **2007**, *317*, 1881.
- (47) Morgenthaler, M.; Schweizer, E.; Hoffmann-Röder, A.; Benini, F.; Martin, R. E.; Jaeschke, G.; Wagner, B.; Fischer, H.; Bendels, S.; Zimmerli, D.; Schneider, J.; Diederich, F.; Kansy, M.; Müller, K. *ChemMedChem* **2007**, *2*, 1100.
- (48) Jacobs, R. T.; Bernstein, P. R.; Cronk, L. A.; Vacek, E. P.; Newcomb, L. F.; Aharony, D.; Buckner, C. K.; Kusner, E. J. *J. Med. Chem.* **1994**, *37*, 1282.
- (49) Pliška, V.; Testa, B.; Waterbeemd, P.-D. H. van de. *Lipophilicity in Drug Action and Toxicology*; Wiley-VCH Verlag GmbH, 2008.
- (50) Böhm, H.-J.; Banner, D.; Bendels, S.; Kansy, M.; Kuhn, B.; Müller, K.; Obst-Sander, U.; Stahl, M. *ChemBioChem* **2004**, *5*, 637.
- (51) Van Niel, M. B.; Collins, I.; Beer, M. S.; Broughton, H. B.; Cheng, S. K. F.; Goodacre, S. C.; Heald, A.; Locker, K. L.; MacLeod, A. M.; Morrison, D.; Moyes, C. R.; O'Connor, D.; Pike, A.; Rowley, M.; Russell, M. G. N.; Sohal, B.; Stanton, J. A.; Thomas, S.; Verrier, H.; Watt, A. P.; Castro, J. L. *J. Med. Chem.* **1999**, *42*, 2087.
- (52) Park, B. K.; Kitteringham, N. R.; O'Neill, P. M. *Annu. Rev. Pharmacol. Toxicol.* **2001**, *41*, 443.
- (53) Legros, J.; Crousse, B.; Bonnet-Delpon, D.; Bégué, J.-P.; Maruta, M. *Tetrahedron* **2002**, *58*, 4067.
- (54) Bird, T. G. C.; Fredericks, P. M.; Jones, E. R. H.; Meakins, G. D. *J. Chem. Soc. [Perkin 1]* **1980**, 750.
- (55) Haufe, G.; Wölker, D. *Eur. J. Org. Chem.* **2003**, *2003*, 2159.
- (56) Ford, H.; Siddiqui, M.; Driscoll, J. S.; Marquez, V. E.; Kelley, J. A.; Mitsuya, H.; Shirasaka, T. *J. Med. Chem.* **1995**, *38*, 1189.
- (57) Jeannot, F.; Mathé, C.; Gosselin, G. *Nucleosides Nucleotides Nucleic Acids* **2001**, *20*, 755.
- (58) Chang, C.-S.; Negishi, M.; Nakano, T.; Morizawa, Y.; Matsumura, Y.; Ichikawa, A. *Prostaglandins* **1997**, *53*, 83.
- (59) Bleicher, K. H.; Böhm, H.-J.; Müller, K.; Alanine, A. I. *Nat. Rev. Drug Discov.* **2003**, *2*, 369.
-

- (60) Van de Waterbeemd, H.; Smith, D. A.; Beaumont, K.; Walker, D. K. *J. Med. Chem.* **2001**, *44*, 1313.
- (61) Pinder, R. M.; Burger, A. *J. Med. Chem.* **1968**, *11*, 267.
- (62) Hussain, J.; Rea, C. *J. Chem. Inf. Model.* **2010**, *50*, 339.
- (63) Wuitschik, G.; Carreira, E. M.; Wagner, B.; Fischer, H.; Parrilla, I.; Schuler, F.; Rogers-Evans, M.; Müller, K. *J. Med. Chem.* **2010**, *53*, 3227.
- (64) Iwasa, J.; Fujita, T.; Hansch, C. *J. Med. Chem.* **1965**, *8*, 150.
- (65) O'Hagan, D.; Wang, Y.; Skibinski, M.; Slawin, A. M. Z. *Pure Appl. Chem.* **2012**, *84*, 1587.
- (66) Nelson, R. D.; Lide Jr., D. R.; Maryott, A. A. In *Handbook of Chemistry and Physics*; CRC Press: Cleveland, OH, 1977; p. E64.
- (67) Meyer, C. W.; Morrison, G. *J. Phys. Chem.* **1991**, *95*, 3860.
- (68) Hirota, E. *J. Phys. Chem.* **1962**, *37*, 283.
- (69) Hayashi, M.; Ikeda, C. *J. Mol. Struct.* **1990**, *223*, 207.
- (70) Durig, J. R.; Guirgis, G. A.; Li, Y. S. *J. Chem. Phys.* **1981**, *74*, 5946.
- (71) Sharma, V.; Kumar, P.; Pathak, D. *J. Heterocycl. Chem.* **2010**, *47*, 491.
- (72) Singh, R. P.; Shreeve, J. M. *Synthesis* **2002**, 2561.
- (73) Liang, T.; Neumann, C. N.; Ritter, T. *Angew. Chem. Int. Ed.* **2013**, n/a.
- (74) Umemoto, T.; Singh, R. P.; Xu, Y.; Saito, N. *J. Am. Chem. Soc.* **2010**, *132*, 18199.
- (75) Vicente, R. *Org. Biomol. Chem.* **2011**, *9*, 6469.
- (76) Angelovski, G.; Keränen, M. D.; Linnepe, P.; Grudzielanek, S.; Eilbracht, P. *Adv. Synth. Catal.* **2006**, *348*, 1193.
- (77) Wang, K.; Liu, Z. *Synth. Commun.* **2009**, *40*, 144.
- (78) Hirschmann, R.; Nicolaou, K. C.; Pietranico, S.; Leahy, E. M.; Salvino, J.; Arison, B.; Cichy, M. A.; Spoor, P. G.; Shakespeare, W. C. *J. Am. Chem. Soc.* **1993**, *115*, 12550.
- (79) Beaulieu, F.; Beauregard, L.-P.; Courchesne, G.; Couturier, M.; LaFlamme, F.; L'Heureux, A. *Org. Lett.* **2009**, *11*, 5050.
- (80) Yin, J.; Zarkowsky, D. S.; Thomas, D. W.; Zhao, M. M.; Huffman, M. A. *Org. Lett.* **2004**, *6*, 1465.
- (81) MacKay, J. A.; Bishop, R. L.; Rawal, V. H. *Org. Lett.* **2005**, *7*, 3421.
- (82) Taber, D. F.; Amedio, J. C.; Jung, K. Y. *J. Org. Chem.* **1987**, *52*, 5621.

- 
- (83) Mueller, K.; Leukel, P.; Ziereis, K.; Gawlik, I. *J. Med. Chem.* **1994**, *37*, 1660.
- (84) Dow, R. L.; Carpino, P. A.; Hadcock, J. R.; Black, S. C.; Iredale, P. A.; DaSilva-Jardine, P.; Schneider, S. R.; Paight, E. S.; Griffith, D. A.; Scott, D. O.; O'Connor, R. E.; Nduaka, C. I. *J. Med. Chem.* **2009**, *52*, 2652.
- (85) Amat, M.; Hadida, S.; Sathyanarayana, S.; Bosch, J. *J. Org. Chem.* **1994**, *59*, 10.
- (86) Nakamura, M.; Matsuo, K.; Ito, S.; Nakamura, E. *J. Am. Chem. Soc.* **2004**, *126*, 3686.
- (87) Thompson, T. N. *Med. Res. Rev.* **2001**, *21*, 412.
- (88) Weiler-Feilchenfeld, H.; Pullman, A.; Berthod, H.; Giessner-Prettre, C. *J. Mol. Struct.* **1970**, *6*, 297.
- (89) Tannor, D. J.; Marten, B.; Murphy, R.; Friesner, R. A.; Sitkoff, D.; Nicholls, A.; Honig, B.; Ringnalda, M.; Goddard, W. A. *J. Am. Chem. Soc.* **1994**, *116*, 11875.
- (90) Rizzo, J. R.; Alt, C. A.; Zhang, T. Y. *Tetrahedron Lett.* **2008**, *49*, 6749.
- (91) Denton, J. *Synthesis* **2009**, *2010*, 775.
- (92) Pearson, A. J.; Fang, X. *J. Org. Chem.* **1997**, *62*, 5284.
- (93) Booth, H.; Everett, J. R. *J. Chem. Soc. Perkin Trans. 2* **1980**, 255.
- (94) Carcenac, Y.; Diter, P.; Wakselman, C.; Tordeux, M. *New J. Chem.* **2006**, *30*, 442.
- (95) Carcenac, Y.; Tordeux, M.; Wakselman, C.; Diter, P. *New J. Chem.* **2006**, *30*, 447.
- (96) Craig, N. C.; Chen, A.; Suh, K. H.; Klee, S.; Mellau, G. C.; Winnewisser, B. P.; Winnewisser, M. *J. Am. Chem. Soc.* **1997**, *119*, 4789.
- (97) Wiberg, K. B. *Acc. Chem. Res.* **1996**, *29*, 229.
- (98) Rablen, P. R.; Hoffmann, R. W.; Hrovat, D. A.; Borden, W. T. *J. Chem. Soc. Perkin Trans. 2* **1999**, 1719.
- (99) Durig, J. R.; Liu, J.; Little, T. S.; Kalasinsky, V. F. *J. Phys. Chem.* **1992**, *96*, 8224.
- (100) Muir, M. *Mol. Phys.* **1996**, *89*, 211.
- (101) O'Hagan, D.; Rzepa, H. S.; Schüler, M.; Slawin, A. M. Z. *Beilstein J. Org. Chem.* **2006**, *2*, 19.
- (102) Hamatani, T.; Matsubara, S.; Matsuda, H.; Schlosser, M. *Tetrahedron* **1988**, *44*, 2875.
- (103) Nicoletti, M.; Bremer, M.; Kirsch, P.; O'Hagan, D. *Chem. Commun.* **2007**, 5075.
- (104) Farran, D.; Slawin, A. M. Z.; Kirsch, P.; O'Hagan, D. *J. Org. Chem.* **2009**, *74*, 7168.
- (105) Hunter, L.; Slawin, A. M. Z.; Kirsch, P.; O'Hagan, D. *Angew. Chem. Int. Ed.* **2007**, *46*, 7887.
-

- (106) Kimura, M.; Futamata, M.; Mukai, R.; Tamaru, Y. *J. Am. Chem. Soc.* **2005**, *127*, 4592.
- (107) Colombo, F.; Cravotto, G.; Palmisano, G.; Penoni, A.; Sisti, M. *Eur. J. Org. Chem.* **2008**, *2008*, 2801.
- (108) Klar, U.; Neef, G.; Vorbrüggen, H. *Tetrahedron Lett.* **1996**, *37*, 7497.
- (109) Koizumi, Y.; Kobayashi, H.; Wakimoto, T.; Furuta, T.; Fukuyama, T.; Kan, T. *J. Am. Chem. Soc.* **2008**, *130*, 16854.
- (110) Duval, E.; Cuny, G. D. *Tetrahedron Lett.* **2004**, *45*, 5411.
- (111) Le, B. M.; Na, Y. M.; Pagniez, F.; Le, B. G.; Le, P. P.; Abdala, H. Antifungal and/or antiparasitic pharmaceutical composition and novel indole derivatives as active principle of such a composition. US2004067998 (A1), April 8, 2004.
- (112) Davies, K. A.; Abel, R. C.; Wulff, J. E. *J. Org. Chem.* **2009**, *74*, 3997.
- (113) Barker, S. A.; Foster, A. B.; Lamb, D. C.; Jackman, L. M. *Tetrahedron* **1962**, *18*, 177.
- (114) Keck, G. E.; Dougherty, S. M.; Savin, K. A. *J. Am. Chem. Soc.* **1995**, *117*, 6210.
- (115) Concellón, J. M.; Bernad, P. L.; del Solar, V.; Suárez, J. R.; García-Granda, S.; Díaz, M. R. *J. Org. Chem.* **2006**, *71*, 6420.
- (116) Goswami, K.; Paul, S.; Bugde, S. T.; Sinha, S. *Tetrahedron* **2012**, *68*, 280.
- (117) Dorsey, B. D.; Levin, R. B.; McDaniel, S. L.; Vacca, J. P.; Guare, J. P.; Darke, P. L.; Zugay, J. A.; Emini, E. A.; Schleif, W. A. *J. Med. Chem.* **1994**, *37*, 3443.
- (118) Van de Waterbeemd, H. *Eur. J. Pharm. Sci.* **1998**, *7*, 1.
- (119) Li, Y.; Zhu, Y.-M.; Jiang, H.-J.; Pan, J.-P.; Wu, G.-S.; Wu, J.-M.; Shi, Y.-L.; Yang, J.-D.; Wu, B.-A. *J. Med. Chem.* **2000**, *43*, 1635.
- (120) Dressman, J. B.; Amidon, G. L.; Reppas, C.; Shah, V. P. *Pharm. Res.* **1998**, *15*, 11.
- (121) French, A. N.; Napolitano, E.; VanBrocklin, H. F.; Brodack, J. W.; Hanson, R. N.; Welch, M. J.; Katzenellenbogen, J. A. *J. Label. Compd. Radiopharm.* **1991**, *30*, 431.
- (122) French, A. N.; Napolitano, E.; Vanbrocklin, H. F.; Hanson, R. N.; Welch, M. J.; Katzenellenbogen, J. A. *Nucl. Med. Biol.* **1993**, *20*, 31.
- (123) Kuroboshi, M.; Suzuki, K.; Hiyama, T. *Tetrahedron Lett.* **1992**, *33*, 4173.
- (124) Fuss, A.; Koch, V. *Synthesis* **1990**, *1990*, 681.
- (125) Iurre Jr., J.; Casas, J.; Messeguer, A. *Bioorg. Med. Chem. Lett.* **1993**, *3*, 179.
- (126) Ito, F.; Shudo, K.; Yamaguchi, K. *Tetrahedron* **2011**, *67*, 1805.
- (127) Trogden, B. G.; Kim, S. H.; Lee, S.; Katzenellenbogen, J. A. *Bioorg. Med. Chem. Lett.* **2009**, *19*, 485.

- 
- (128) Koudih, R.; Gilbert, G.; Dhilly, M.; Abbas, A.; Barré, L.; Debruyne, D.; Sobrio, F. *Eur. J. Med. Chem.* **2012**, *53*, 408.
- (129) Petursson, S.; Jonsdottir, S. *Tetrahedron Asymmetry* **2011**, *22*, 1809.
- (130) Lenagh-Snow, G. M. J.; Araújo, N.; Jenkinson, S. F.; Martínez, R. F.; Shimada, Y.; Yu, C.-Y.; Kato, A.; Fleet, G. W. J. *Org. Lett.* **2012**, *14*, 2142.
- (131) Chiummiento, L.; Funicello, M.; Lupattelli, P.; Tramutola, F.; Campaner, P. *Tetrahedron* **2009**, *65*, 5984.
- (132) Albert, B. J.; Koide, K. *J. Org. Chem.* **2008**, *73*, 1093.
- (133) Wang, T.-C.; Chen, I.-L.; Kuo, D.-H.; Liao, C.-H. *Helv. Chim. Acta* **2004**, *87*, 983.
- (134) Vorbrüggen, H. *Synthesis* **2008**, *2008*, 1165.
- (135) Viti, S. M. *Tetrahedron Lett.* **1982**, *23*, 4541.
- (136) Nicoletti, M.; O'Hagan, D.; Slawin, A. M. Z. *J. Am. Chem. Soc.* **2005**, *127*, 482.
- (137) Burke, M. D.; Thompson, S.; Weaver, R. J.; Wolf, C. R.; Mayers, R. T. *Biochem. Pharmacol.* **1994**, *48*, 923.
- (138) Dolomanov, O. V.; Bourhis, L. J.; Gildea, R. J.; Howard, J. A. K.; Puschmann, H. *J. Appl. Crystallogr.* **2009**, *42*, 339.
- (139) Sheldrick, G. M. *Acta Crystallogr. A* **2007**, *64*, 112.
- (140) Krasovskiy, A.; Knochel, P. *Synthesis* **2006**, *2006*, 0890.
- (141) Hirsch, J. A.; Vu Chi Truc. *J. Org. Chem.* **1986**, *51*, 2218.
- (142) Morwick, T.; Hrapchak, M.; DeTuri, M.; Campbell, S. *Org. Lett.* **2002**, *4*, 2665.
- (143) Mizuno, M.; Kitazawa, S.; Goto, K. *J. Fluor. Chem.* **2008**, *129*, 955.





# Curriculum Vitae

Born December 13<sup>th</sup> 1986 in Dakar, Senegal.

**09/2010 – 04/2014** Doctoral studies in the group of Prof. Dr. *Erick M. Carreira*, **ETH Zurich**, Switzerland.

Title: *Design, Synthesis, and Evaluation of Novel Partially Fluorinated Alkyl Groups*.

**02/2010 – 07/2010** Master thesis in the group of Prof. Dr. *Jack E. Baldwin*, **University of Oxford**, England.

Title: *Study Towards the Total Synthesis of Frondosin A and B*.

**09/2009 – 08/2010** Master of Science in Organic Chemistry at the **University of Rouen**, France.

**09/2008 – 08/2009** Research internship in Medicinal Chemistry, **Pierre Fabre Research Institute**, Castres, France.

Title: *Study Towards the Total Synthesis of Natural Product Analogs*.

**07/2008 – 08/2008** Research internship in the group of Prof. Dr. *Antonio Togni*, **ETH Zurich**, Switzerland.

Title: *Study on the Trifluoromethylation of Sulfonic Acids*.

**09/2004 – 08/2010** Chemical engineering studies at the **National Institute of Applied Sciences**, Rouen, France.

**07/2004** Scientific French Baccalaureate

During my doctoral studies, I was twice teaching assistant for an introductory-level organic chemistry laboratory course, and responsible for seven undergraduate students in the context of their research projects.

Zurich, April 2014

Quentin A. Huchet